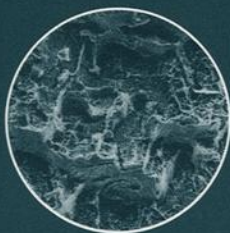


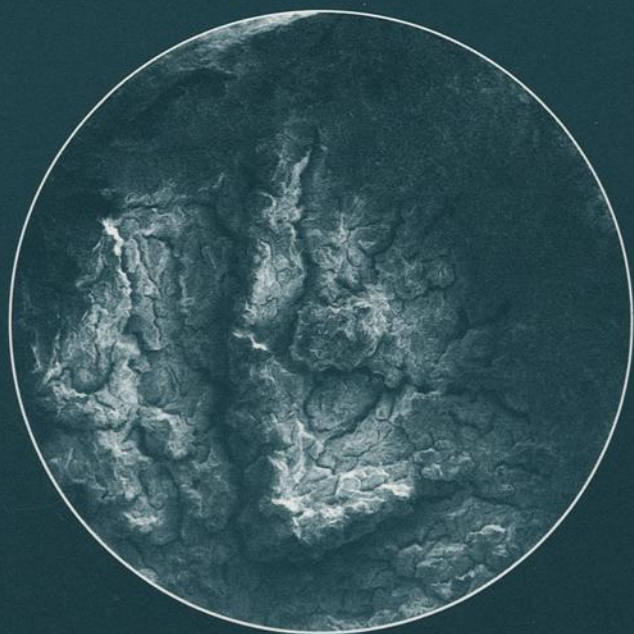
# Slow Strain Rate Testing *for the* Evaluation *of* Environmentally Induced Cracking

*Research and Engineering Applications*



**RUSSELL D. KANE** EDITOR

**ASTM** STP 1210



**STP 1210**

***Slow Strain Rate Testing for the  
Evaluation of Environmentally  
Induced Cracking: Research and  
Engineering Applications***

*Russell D. Kane, editor*

ASTM Publication Code Number (PCN)  
04-012100-27



ASTM  
1916 Race Street  
Philadelphia, PA 19103

## Library of Congress Cataloging-in-Publication Data

Slow strain rate testing for the evaluation of environmentally induced cracking : research and engineering applications / Russell D. Kane, editor.

(STP ; 1210)

Includes bibliographical references and index.

ISBN 0-8031-1870-8

1. Stress corrosion—Testing. 2. Alloys—Fatigue—Testing.

I. Kane, R. D. II. Series: ASTM special technical publication ; 1210.

TA462.S565 1993

620.1'63—dc20

93-19461

CIP

Copyright ©1993 AMERICAN SOCIETY FOR TESTING AND MATERIALS, Philadelphia, PA. All rights reserved. This material may not be reproduced or copied, in whole or in part, in any printed, mechanical, electronic, film, or other distribution and storage media, without the written consent of the publisher.

### Photocopy Rights

Authorization to photocopy items for internal or personal use, or the internal or personal use of specific clients, is granted by the AMERICAN SOCIETY FOR TESTING AND MATERIALS for users registered with the Copyright Clearance Center (CCC) Transactional Reporting Service, provided that the base fee of \$2.50 per copy, plus \$0.50 per page is paid directly to CCC, 27 Congress St., Salem, MA 01970; (508) 744-3350. For those organizations that have been granted a photocopy license by CCC, a separate system of payment has been arranged. The fee code for users of the Transactional Reporting Service is 0-8031-1870-8/93 \$2.50 + .50.

### Peer Review Policy

Each paper published in this volume was evaluated by three peer reviewers. The authors addressed all of the reviewers' comments to the satisfaction of both the technical editor(s) and the ASTM Committee on Publications.

The quality of the papers in this publication reflects not only the obvious efforts of the authors and the technical editor(s), but also the work of these peer reviewers. The ASTM Committee on Publications acknowledges with appreciation their dedication and contribution to time and effort on behalf of ASTM.

Printed in Baltimore, MD

July 1993

# Foreword

This publication, *Slow Strain Rate Testing for the Evaluation of Environmentally Induced Cracking: Research and Engineering Applications*, contains papers presented at the symposium of the same name, held in Pittsburgh, PA on 18–19 May 1992. The symposium was sponsored by ASTM Committee G-1 on Corrosion of Metals. Russell D. Kane, Cortest Laboratories, Inc., presided as symposium chairman and is editor of the resulting publication.

# Contents

<b>Overview</b>	1
DEVELOPMENT AND APPLICATION OF SLOW STRAIN RATE TESTING TECHNIQUES	
<b>Slow Strain Rate Testing—25 Years Experience—R. N. PARKINS</b>	7
<b>Limitations of the Slow Strain Rate Test Technique—J. A. BEAVERS AND G. H. KOCH</b>	22
<b>Status of Standardization Activities on Slow Strain Rate Testing Techniques— R. D. KANE AND S. M. WILHELM</b>	40
Discussion	47
USES OF SLOW STRAIN RATE SCC TESTING TO CONTROL OR MONITOR INDUSTRIAL PROCESSES: APPLICATIONS IN NUCLEAR POWER	
<b>SSRT for Hydrogen Water Chemistry Verification in BWRs—M. E. INDIG</b>	51
<b>Applications of Slow Strain Rate Testing in the Nuclear Power Industry— M. T. MIGLIN AND B. P. MIGLIN</b>	65
<b>Measurement of the Deformability of Austenitic Stainless Steels and Nickel-Base Alloys in Light Water Reactor Cores—P. DEWES, D. ALTER, F. GARZAROLLI, R. HAHN, AND J. L. NELSON</b>	83
RESEARCH APPLICATIONS AND DEVELOPMENTS IN SLOW STRAIN RATE TESTING TECHNIQUES	
<b>The Use of Precracked and Notched Slow Strain Rate Specimens—J. TORIBIO</b>	105
<b>Environmental Slow Strain Rate <i>J</i>-Integral Testing of Ni-Cu Alloy K-500— M. G. VASSILAROS, R. L. JUERS, M. E. NATISHAN, AND A. K. VASUDEVAN</b>	123

<b>Application of the Rising Displacement Test to SCC Investigations—</b> W. DIETZEL AND K.-H. SCHWALBE	134
<b>Slow Strain Rate Fracture of High-Strength Steel at Controlled Electrochemical Potentials in Ammonium Chloride, Potassium Chloride, and Ammonium Nitrate Solutions—</b> D. T. NGUYEN, D. E. NICHOLS, AND R. D. DANIELS	149
<b>Slow Strain Rate Testing of Precracked Titanium Alloys in Salt Water and Inert Environments—</b> D. A. MEYN AND P. S. PAO	158
INDUSTRIAL APPLICATIONS OF SLOW STRAIN RATE TESTING TO EVALUATE ENVIRONMENTALLY INDUCED CRACKING	
<b>Case Histories Using the Slow Strain Rate Test—</b> K. L. BAUMERT AND W. R. WATKINS, JR.	173
<b>Use of Slow Strain Rate Tests to Evaluate the Embrittlement of Aluminum and Stainless Alloys in Process Environments Containing Mercury—</b> R. D. KANE, D. WU, AND S. M. WILHELM	181
<b>Effect of Heat Treatment on Liquid Metal-Induced Cracking of Austenitic Alloys—</b> J. J. KRUPOWICZ	193
<b>Hydrogen Cracking Initiation of a High-Strength Steel Weldment—</b> P. A. KLEIN, R. A. HAYS, P. J. MORAN, AND J. R. SCULLY	202
USE OF SLOW STRAIN RATE TESTING FOR QUALIFICATION OF SCC RESISTANCE OF CORROSION RESISTANT ALLOYS: CASE HISTORIES IN PETROLEUM PRODUCTION	
<b>Problems Associated with Slow Strain Rate Quality Assurance Testing of Nickel-Base Corrosion Resistant Alloy Tubulars in Hydrogen Sulfide Environments—</b> H. S. AHLUWALIA	225
<b>The Role of Slow Strain Rate Testing on Evaluation of Corrosion Resistant Alloys for Hostile Hot Sour Gas Production—</b> A. IKEDA, M. UEDA, AND H. OKAMOTO	240
<b>Relationship of Localized Corrosion and SCC in Oil and Gas Production Environments—</b> S. M. WILHELM AND D. M. CURRIE	263
<b>Improved SSR Test for Lot Acceptance Criterion—</b> E. L. HIBNER	290
<b>Author Index</b>	295
<b>Subject Index</b>	297

# Overview

---

## Background

In the past 40 to 50 years, there has been an increased awareness of the effects of service environments on the performance of engineering materials of construction. Of particular concern is the susceptibility of these materials to environmentally induced cracking. Environmentally induced cracking is a "catch-all" term that refers to a number of different modes of corrosive degradation involving brittle cracking through the combined action of an environment, tensile stress (either applied or residual), and a susceptible material. These types of failures can oftentimes occur unexpectedly at stresses that are below normal design stresses and without substantial deformation. Examples of such types of cracking are chloride stress corrosion cracking (SCC), caustic cracking, hydrogen embrittlement, and liquid metal embrittlement.

Any material may be subject to environmentally induced cracking under the right (or wrong) environment and enough stress. Environmental induced cracking is a major concern particularly as larger, more sophisticated and costly equipment, components, and structures are being fabricated. The economic, safety, environmental, and legal impact of failures in these systems are, in many cases, paramount considerations.

Due to the aforementioned concerns for environmentally induced cracking, corrosion and materials specialists have worked consistently for the development of better and more predictive laboratory tests for this phenomenon. The activities of ASTM G-1 (Corrosion of Metals) has been largely directed at standardization of corrosion testing methods and procedures including those for environmentally induced cracking. These methods have historically involved exposure of statically stressed specimens (i.e., tension, C-ring, bent beam, or fracture mechanics specimens) of a material to a particular corrosive environment. Oftentimes, such tests are conducted over a range of applied stress levels while monitoring for time-to-failure. These types of tests are described in many ASTM standards.

One problem often associated with tests for environmentally induced cracking conducted in the aforementioned manner is the amount of testing time required to initiate cracking and, in turn, the amount of time needed to conduct a proper evaluation of these types of phenomena. In some cases, the initiation time needed to produce cracking in some material/environment situations is in excess of 10 000 hours (>1 year). In order to reduce this initiation time, many investigators use aggressive, artificial solutions to chemically accelerate these tests. However, the problem often associated with tests conducted in these environments is one of producing test results that relate to real-world situations. These methods can often be used to screen one material from another, but their predictive capabilities are often in doubt.

Approximately 20 years ago, a new testing technique referred to as slow strain rate testing was first applied to the investigation of environmentally induced cracking of metals and alloys. In this test method, the specimen is not held at a constant load or deflection during the period of exposure. The slow strain rate test uses the application of *dynamic* straining of the specimen in the form of a slow, monotonically increasing strain to failure. The apparent advantage of slow strain rate testing over conventional techniques is the use of the dynamic straining to mechanically accelerate cracking. It is hoped that this technique will allow the use of more realistic environments and also reduce the total time requirement for evaluating various metallurgical or environmental parameters.

### **Previous ASTM Symposium on Slow Strain Rate Testing**

In 1979, ASTM Committee G-1 sponsored its first symposium on slow strain rate testing techniques resulting in the publication of *STP 665* (G. M. Ugiansky and J. H. Payer, editors). In that symposium, many papers were presented on the new technique which, at that time, was largely restricted to fundamental studies and research investigations. In general, the conclusions made by many investigators at the first symposium was that this new test method offered many advantages to conventional testing techniques for investigating environmentally induced cracking. In many cases, correlations were obtained between slow strain rate test results and operating experience that were not predicted by conventional corrosion testing techniques. However, more experience would be required before the true benefit of slow strain rate testing would be realized.

During the decade since the previous symposium, use of the slow strain rate symposium has expanded and been used for a number of different purposes, from fundamental research studies to material lot release testing and monitoring of corrosive severity of service environments. Additional experience has been gained in many material/environment situations using a variety of test specimens and loading procedures.

### **The Current Symposium**

On 18-19 May 1992, ASTM Committee G-1 sponsored a second slow strain rate symposium. The goal of this second symposium was to highlight some of the new directions in testing for environmentally induced cracking using a variety of slow strain rate techniques. At this symposium, presentations were made that described both fundamental research studies and more practical engineering applications. These presentations centered on the developments that have been made in the understanding of slow strain rate test data and extensions in this testing technique that have occurred over the past ten years.

The slow strain rate symposium involved researchers for industry, government agencies, and universities from the United States, England, Germany, Spain, and Japan. Focused sessions were held on the use of slow strain rate testing techniques for the evaluation of environmentally induced cracking in nuclear power, oil and gas production, chemical process, and marine service.

### **Development and Application of Slow Strain Rate Testing Techniques**

The symposium contained keynote and plenary lectures as well as sessions that focused on specific applications of slow strain rate testing. In keeping with the historical perspective, a presentation was made by Dr. Redvers Parkins (Emeritus Professor, University of Newcastle Upon Tyne) that summarized 25 years of experience with the slow strain rate testing technique. Dr. Parkins, who has played a key role in the inception and development of this testing technique, provides an excellent review of this subject in this section.

Additionally, this section contains a critical assessment of the limits of the slow strain rate technique as applied to the evaluation of stress corrosion cracking. This assessment was conducted through the review of the published literature and through a survey of user experience. In general, slow strain rate testing provided results that were predictive for stress corrosion cracking. However, if focused attention on the need to use consideration of electrochemical potential in the evaluation of test data in order to relate laboratory and field behavior.

### **Uses of Slow Strain Rate Testing to Control or Monitor Industrial Processes: Applications in Nuclear Power**

This section highlighted the results from both laboratory studies and in-plant tests related to the serviceability of stainless steels and nickel base alloys in nuclear power applications. Specific emphasis was on the role of slow strain rate test data in the evaluation of materials for service in various types of reactor environments of varying environmental severity.

The application of slow strain rate testing to the study of environmentally induced cracking in high-temperature, high-purity water environments highlights the benefits of this testing technique. In many cases, it was difficult to simulate actual service experience using conventional statically stressed specimens under laboratory conditions that simulated those producing in-service failures. However, when slow strain rate testing was employed, better correlation between laboratory and plant experience was obtained.

The sensitivity of the slow strain rate testing technique to environmental and metallurgical parameters is highlighted. In tests conducted in boiling water reactor environments, it was possible to verify reactor water chemistry requirements and to minimize cracking problems using tests on materials of known susceptibility. This work illustrates the benefits of slow strain rate testing outside of the laboratory.

### **Research Applications and Developments in Slow Strain Rate Testing Techniques**

This section focuses on developments of modified slow strain rate test techniques. These modified techniques incorporate a conventional, slowly increasing load with fracture mechanics test methods and precracked specimens. They are applied to the evaluation of hydrogen embrittlement and SCC in steels and nickel alloys. While shortening the testing time required for evaluation of material or environmental variables, it is hoped that the combination of these techniques also provides fracture mechanics data usable in design of equipment, components, and structures. This is a new area for slow strain rate testing and further work and development will be needed.

Also examined in this section are fundamental studies of SCC of high-strength steels and titanium alloys in various aqueous environments. The advantages of the slow strain rate technique are highlighted. In the case of high-strength steels, rapid evaluation of these materials to many environmental conditions and electrochemical potentials can be easily accomplished, thus aiding in the identification of cracking mechanisms. In the case of titanium alloys, the use of slow strain rate techniques provides for more consistent test results through minimizing the effects of crack initiation on the test results. However, the effects of strain rate on the test results in titanium alloys requires further work.

### **Industrial Applications of Slow Strain Rate Testing to Evaluate Environmentally Induced Cracking**

This section contains papers that have used slow strain rate testing techniques to evaluate the compatibility of environments and materials of construction in various chemical process environments. Case histories are presented that show the benefits of slow strain rate data in the materials selection process. Additionally, they show the use of this test technique in the development of (1) process control parameters to limit the aggressiveness of chemical process environment on materials of construction, and (2) hydrogen content limits for high-strength steel weldments.

Specific emphasis is placed on the use of slow strain rate techniques for the evaluation of liquid metal embrittlement (LME) of aluminum and stainless alloys in contact with

mercury. The data present in these papers show the applicability of this corrosion testing technique for the evaluation of LME. It overcomes the problems of surface tension and crack initiation commonly observed in statically stressed specimens.

### **Use of Slow Strain Rate Testing for Qualification of SCC Resistance of Corrosion Resistant Alloys (CRAs)**

This section presents a case study that highlights the application of slow strain rate testing techniques to the lot release testing of commercial heats of nickel-base alloys. The case study specifically focuses on the use of this testing technique and related experiences found in the petroleum industry to obtain nickel-base alloys with adequate resistance to SCC in severe hydrocarbon production environments containing chloride, hydrogen sulfide, and elemental sulfur. This industry has found that in order for slow strain rate testing techniques to be truly predictive of alloy performance strict adherence to standardized procedures must be obtained. The test results from interlaboratory studies and the effects of heat-to-heat variations are discussed along with the effects of various environmental and metallurgical parameters on SCC performance.

The results presented in this section indicate the degree of control and standardization required for slow strain rate tests to be predictive. The lessons learned from this petroleum industry experience will most likely apply to other practical applications of slow strain rate testing in the future. It is hoped that through the presentation of this case study, the development effort required for future use of this testing technique will be minimized.

#### *Acknowledgments*

As symposium chairman, I hope that this STP benefits both fundamental researchers and practical engineers. The authors of the various papers in this volume have worked diligently in the application and development of new corrosion testing techniques and, in some cases, have dedicated their careers to this task. I would like to acknowledge their personal and technical efforts in this regard. Additionally, I wish to gratefully thank the ASTM staff that has worked so hard to make this publication possible.

*Dr. Russell D. Kane*

Cortest Laboratories, Inc.  
P.O. Box 691505  
Houston, TX 77269-1505;  
symposium chairman and editor

# **Development and Application of Slow Strain Rate Testing Techniques**

# Slow Strain Rate Testing—25 Years Experience

---

**REFERENCE:** Parkins, R. N., “**Slow Strain Rate Testing—25 Years Experience,**” *Slow Strain Rate Testing for the Evaluation of Environmentally Induced Cracking: Research and Engineering Applications*, ASTM STP 1210, R. D. Kane, Ed., American Society for Testing and Materials, Philadelphia, 1993, pp. 7–21.

**ABSTRACT:** The development of slow strain rate testing for environment sensitive cracking over the last 25 years is reviewed. In its original form, in which specimens are continuously strained to total failure, the method is still valuable, especially as a rapid sorting approach to the effects of metallurgical or environmental changes in systems, and examples are given of such. The importance of employing an appropriate strain rate for the particular system being studied is emphasized, after which consideration is given to applying variations on the method to determining threshold stresses for cracking.

**KEYWORDS:** stress corrosion cracking (SCC), strain rate, threshold stresses, interrupted tests, tapered specimen tests, cyclic loading

The form in which slow strain rate stress corrosion cracking tests were initially developed and used, essentially as a go-no go sorting test, remains as one of its attractions for some applications. However, a considerable volume of laboratory data is now available that demonstrates the importance of surface or crack tip strain rates in the incidence and growth of environment sensitive cracks, i.e., strain rate plays an important mechanistic role in stress corrosion cracking (SCC). This is because of the synergistic effects of the time dependences of corrosion-related reactions and of film rupture, the frequency of the latter determined by the strain rate. Since engineering structures are mostly designed to a maximum allowable stress that is some fraction of the yield stress and slow strain rate tests (SSRTs) can involve much higher stresses, there is sometimes reluctance to accept the relevance of the results they provide in relation to operating structures. However, SSRTs do not have to involve high stresses or high plastic strains, as indicated in the following, and when they are conducted in one or other of these modified forms the data they provide are at least as relevant to industrial application as that from any other type of SCC test. (Unless stated otherwise, strain rate herein refers to the initial strain rate calculated from the initial gage length and its deflection rate.)

## Monotonic SSRTs

This expression is used here to indicate tests in which straining is continued monotonically until the test specimen displays total fracture, and is the form in which SSRTs were initially designed and is still most frequently employed. In this form they are attractive because they give a definitive answer in a relatively short time to the question of whether or not a given

---

<sup>1</sup> Emeritus professor of metallurgy, University of Newcastle upon Tyne, Newcastle upon Tyne NE1 7RU, England.

alloy-environment combination displays susceptibility to SCC, assuming that appropriate test conditions have been chosen, as indicated in the following. Where susceptibility is indicated, usually by the generation of cracks of appropriate morphology, some measure of the extent of that susceptibility is usually required and that can take various forms [1]. The easiest quantities to use, because they are usually measured during the SSRT, are the time to failure, often normalized with respect to the time to failure in the absence of the potent environment, or the maximum load or stress achieved during the test. Ductility parameters, such as % reduction in area or elongation, are easily measured after completion of the test and also constitute useful means of providing relative measures of susceptibility. Although somewhat less easily measured than those quantities previously mentioned, average crack velocity, from measurement of the deepest crack on the fracture surface or the deepest secondary crack in a microsection divided by the time to failure, is a parameter that often has more direct relevance to defining SCC susceptibility than some of the alternatives, most of which are employed in the data presented.

SSRTs are perhaps at their most useful for conducting rapid sorting of the effects of metallurgical changes or defining the potency of an environment in terms of its composition. Figure 1 shows the effects of various nickel additions to a ferritic steel upon cracking susceptibility in a sodium hydroxide solution at various controlled potentials [2]. The time to failure ratio (time to failure in the cracking environment/time to failure in an inert environment—oil—at the same temperature) is used as a measure of susceptibility and clearly is capable of distinguishing the marked differences in cracking propensity of the various nickel steels over a range of controlled potentials.

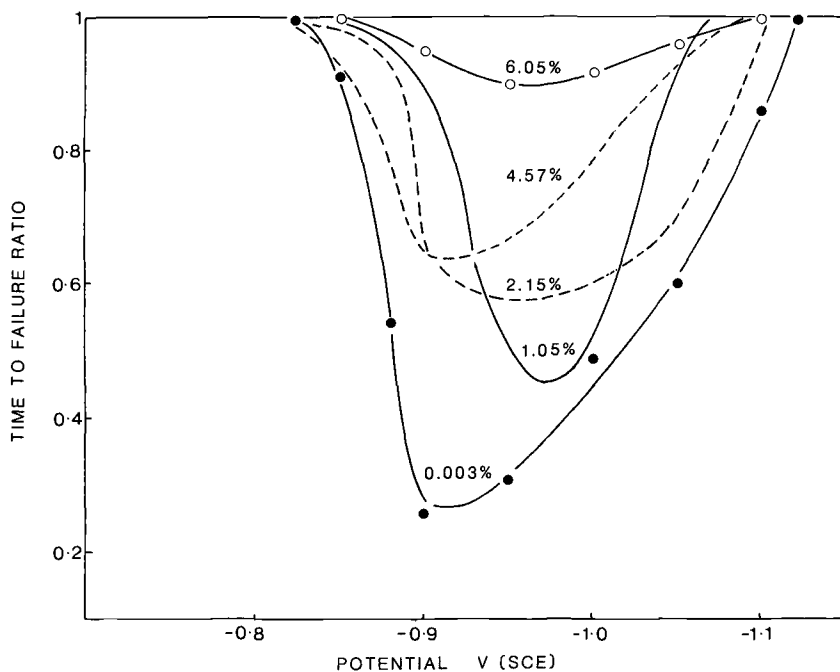


FIG. 1—Time to failure ratios from slow strain rate test ( $10^{-6} \text{ s}^{-1}$ ) on various nickel-containing ferritic steels exposed to boiling 8.75 M NaOH at various potentials. (The Ni contents of the various steels are appended to the curves) [2].

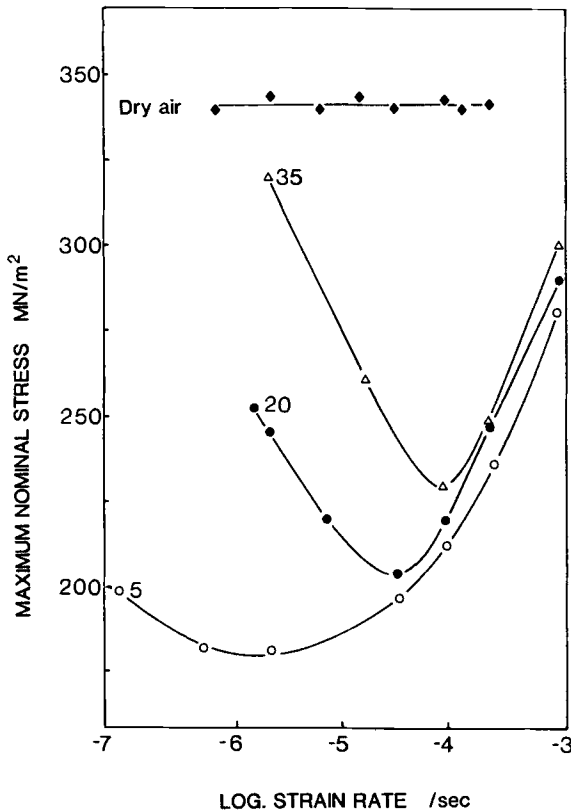


FIG. 2—The effect of strain rate upon the maximum nominal stress to fracture initially plain specimens of Mg-8.8% Al alloy exposed to dry air or solutions containing 5 g/L NaCl and various amounts of  $K_2CrO_4$  (appended to curves in g/L) [3].

Figure 2 shows the influence of potassium chromate ( $K_2CrO_4$ ) additions to a sodium chloride (NaCl) solution on the SCC of a Mg-Al alloy over a range of strain rates, using the maximum nominal stress as a measure of cracking susceptibility [3], and again the differences are readily recognizable. However, such measures of susceptibility are not invariably sufficiently discriminating and especially so when crack growth rates are relatively low. In those cases measurement of the maximum crack depth, possibly supplemented with data on the number of cracks per unit length or area, may provide a better means of distinguishing degrees of susceptibility. Moreover, metallographic assessment of specimens after any SCC test is likely to be useful especially after SSRTs where the number of cracks is often an indication of whether or not they are the result of environmental influence. Thus, one or two very small cracks in the necked region of a specimen may be the consequence of the presence of near-surface inclusions, whereas SCC is usually associated with the formation of a relatively large number of cracks not just confined to the necked region.

#### Importance of Choosing an Appropriate Strain Rate

Figure 2 shows that the maximum susceptibility to cracking occurs at different strain rates depending upon the chromate concentration of the solution and indeed suggests that at

sufficiently high and low strain rates SCC would not be observed, at least in the highest chromate-containing solution. It is not surprising that at relatively high strain rates SCC may not be displayed, since the reactions involved in the growth of environment sensitive cracks proceed at a rate that is slower than that at which ductile cracking may propagate. However, the rate controlling step in SCC will vary according to the metal-environment combination involved and so the upper limit of strain rate to display SCC will vary. Thus, Fig. 3 shows results from tests at various strain rates on a very low strength mild steel exposed to a sodium dihydrogen phosphate ( $\text{NaH}_2\text{PO}_4$ ) solution at the controlled potential of  $-1.0$  V (SCE) and indicates that even at a strain rate of  $10^{-3} \text{ s}^{-1}$  a significant fall in the % reduction in area (RA%) to fracture, by comparison with the value for a test in air, was measured. On the other hand, Fig. 4 shows that, for the same strain rate, aluminum alloy 7179 tested in tap water at open circuit gave the same RA% as when tested in a vacuum, and that it was not until a strain rate approaching  $10^{-5} \text{ s}^{-1}$  was applied that a change in cracking response approximating that shown in Fig. 3 at  $10^{-3} \text{ s}^{-1}$  was detected [4]. Clearly the choice of the strain rate to be applied is critical and, since in many cases it will not be desired to go through the type of data collecting shown in Figs. 2 through 4, it may be helpful to have some guidance as to appropriate strain rates to use for systems for which there is no prior experience. For steels, copper, nickel, and aluminum based alloys,  $10^{-6} \text{ s}^{-1}$  will often be found useful, followed by tests at  $10^{-7} \text{ s}^{-1}$  or  $10^{-5} \text{ s}^{-1}$ , or both, if SCC does not occur in the initial test. Figure 2 suggests for magnesium based alloys, and titanium based materials often behave similarly,  $10^{-5} \text{ s}^{-1}$  would be a suitable initial choice, followed by  $10^{-6} \text{ s}^{-1}$  or  $10^{-4} \text{ s}^{-1}$ , or both, if SCC is not promoted in the initial test. It needs to be remembered that, quite apart from the time dependence of strain, there are other time dependent aspects to environment sensitive fracture that may interact with tests for such and particularly SSRTs. Thus, in some alloys, particularly at elevated temperatures, aging processes may occur that influence cracking response, or changes in environment composition may similarly take place and affect results. Such changes have sometimes been reflected

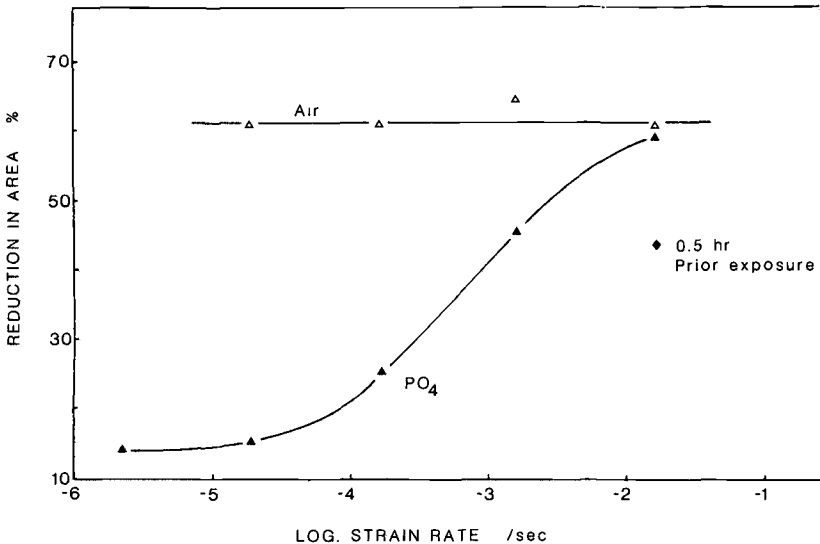


FIG. 3—Reduction in area in slow strain rate tests on dead soft mild steel in air and in  $1 \text{ M NaH}_2\text{PO}_4$  at  $-1.0$  V (SCE) as a function of initial strain rate.

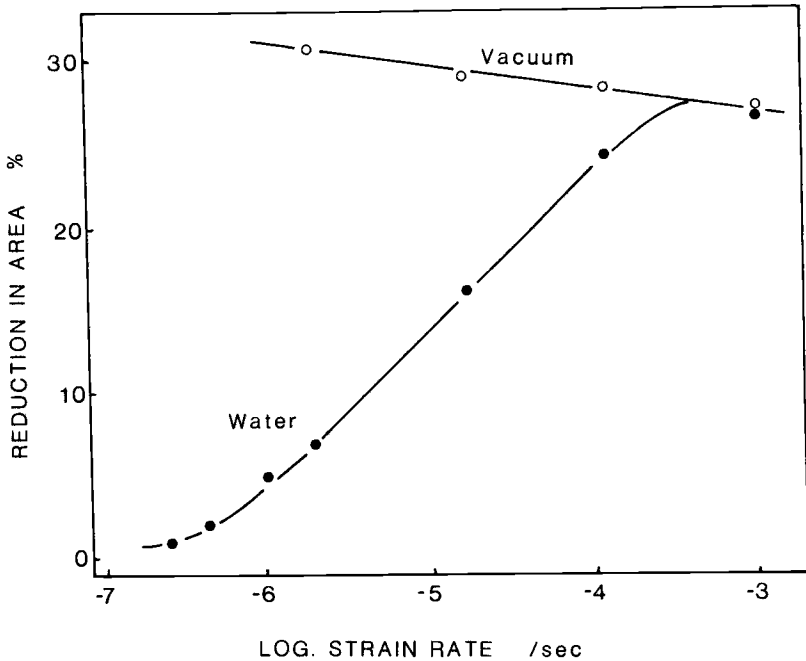


FIG. 4—Variation of reduction in area at fracture with strain rate for aluminum alloy 7179 tested in tap water at room temperature and open circuit potential, and under vacuum [4].

in extremely low ( $10^{-8} \text{ s}^{-1}$ ) strain rates having to be applied to promote cracking. In those cases it may not be the strain rate as such that is important, but the time that such strain rates allow for the changes in alloy or environment that engender cracking. Moreover, with such low applied strain rates the question arises as to whether such tests are the most appropriate, since constant strain or constant load tests are likely to provide strain or creep rates of that order.

Figure 2 indicates that there may be a lower limiting strain rate for cracking, just as there is an upper limit. Similar trends have been observed in other systems and also with precracked specimens, rather than the initially plain specimens that develop many cracks and to which Fig. 2 refers. Experiments on two magnesium based alloys in chloride-chromate solutions employed precracked specimens that were subjected to a constant rate of displacement, the latter being varied from test to test [5]. Relevant measurements were made to provide  $J$ -contour integral versus crack extension plots, with  $J$  defined in incremental form [6] by

$$dJ = (2/b) Pdu - (1/b) Gda \quad (1)$$

where

- $P$  = load/unit thickness,
- $u$  = displacement rate,
- $G$  = energy release rate,
- $b$  = uncracked ligament length, and
- $a$  = crack length beyond load line.

Equation 1 shows the essential form of the expression for calculating  $J$ , but modifications are introduced according to the type of specimen used.  $J$  is calculated by integrating the

expression during the course of a test but its usefulness may sometimes be extended by the use of the tearing modulus [7], a dimensionless parameter that measures resistance to crack growth and relates to the initial slope of the  $J$ - $a$  curve, and expressed as

$$T = (E/\sigma_y^2) dJ/da \quad (2)$$

where

$E$  = Young's Modulus, and  
 $\sigma_y$  = yield stress.

Figure 5 shows the tearing modulus as a function of displacement rate for two magnesium alloys exposed to a chromate-chloride solution and both indicate an increasing tearing modulus as the displacement rate, scaled with crack length, is reduced below about  $10^{-6} \text{ s}^{-1}$  [5]. This reflects a decreasing crack velocity, after an initial increase, as the displacement rate is progressively reduced and at slow enough displacement rates the value of  $dJ/da$  approaches that for tests in dry air, i.e., the tearing resistance approximates that for purely mechanical crack growth. Similar results have been obtained with other systems, Fig. 6 showing that SCC only occurred within a certain range of crack tip strain rates for precracked specimens of a C-Mn steel exposed to a carbonate-bicarbonate solution [8]. In those tests the cantilever beam specimens were initially loaded to the same deflection, after which the specimens were allowed to creep under noncracking conditions until the creep rate fell below that which was subsequently applied when the potential was moved to a value at which SCC would occur. By restricting the total deflection during the cracking phase of the experiments, the effective load changes during the tests were contained within a few percent of the initial load. The explanation of such lower limiting strain rates, below which SCC does not occur, is probably the same for most systems, that a passivating film remains present and is not sufficiently frequently disrupted to allow those reactions that result in crack growth to occur. That may be so when the mechanism of crack growth involves hydrogen ingress into the metal, as with the magnesium alloys referred to previously, as well as when the primary feature of growth is by dissolution. Thus, with the magnesium alloys a film of  $\text{Mg}(\text{OH})_2$  forms and prevents the passage of hydrogen to the metal, while with ferritic steels exposed to carbonate-bicarbonate solution a film of  $\text{Fe}_3\text{O}_4$  and  $\text{FeCO}_3$  will prevent dissolution so long as it remains intact.

While there will invariably be an upper limit of strain rate above which SCC will not be observed, a lower bound for cracking will not always be observed. The reason for this is apparent from consideration of an expression for the crack tip strain rate in specimens containing many cracks such as are most often involved in SSRTs. Using elastic-plastic fracture mechanics the following expression was derived [9]

$$\epsilon_{ct} = (75/N) \epsilon_{app} + (CV/5) \log_e (1000/N) \quad (3)$$

where

$\epsilon_{ct}$  = crack tip strain rate,  
 $N$  = number of cracks along gage length,  
 $\epsilon_{app}$  = applied strain rate, and  
 $CV$  = crack velocity.

(The constants in Eq 3 will depend on the material involved and test specimen size.)

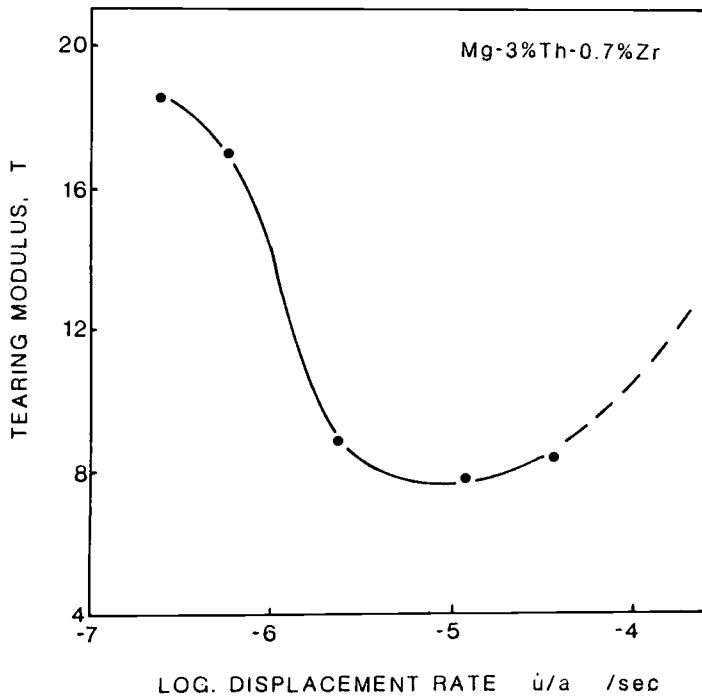
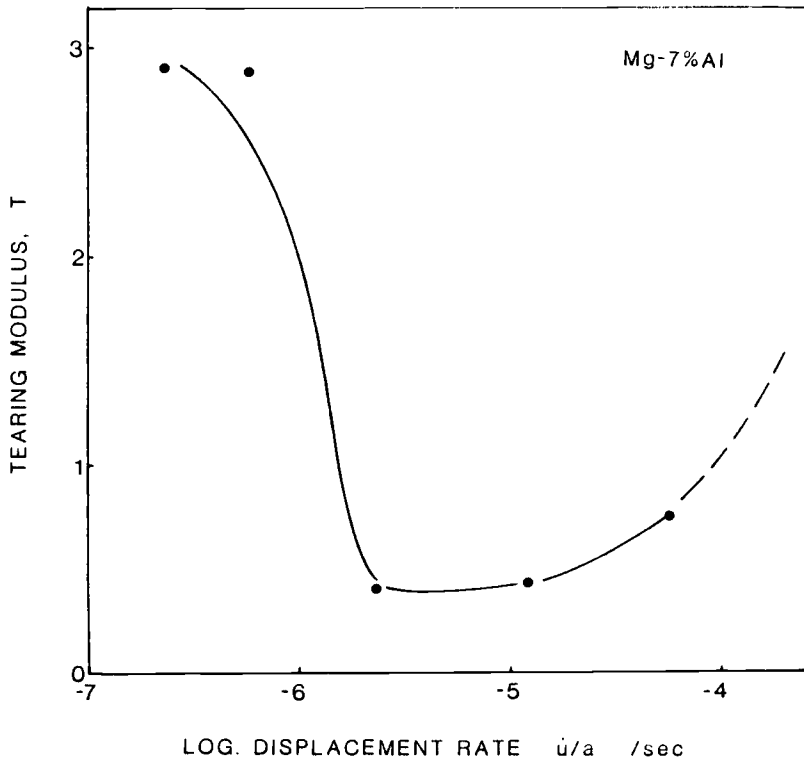


FIG. 5—Tearing modulus as a function of applied displacement rate (scaled with crack length) for a Mg-7Al and a Mg-3Th-0.7Zr alloy exposed to a solution containing 5 g/L NaCl and 20 g/L  $K_2CrO_4$  [5].

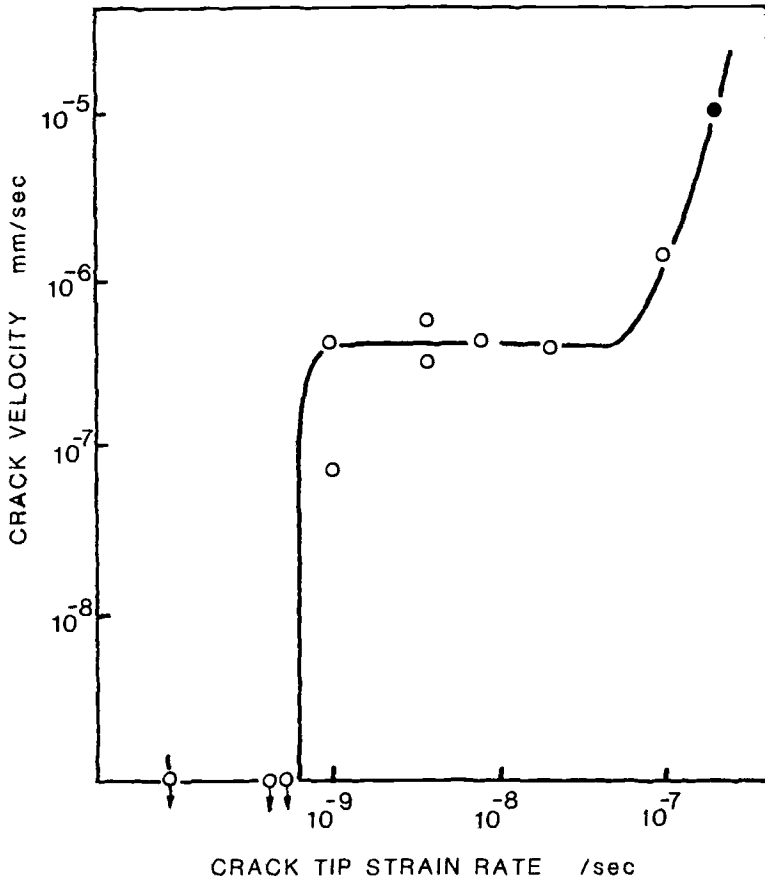


FIG. 6—Intergranular stress corrosion crack velocities for various applied crack tip strain rates in C-Mn steel exposed to 0.5 M  $\text{Na}_2\text{CO}_3$  + 1.0 M  $\text{NaHCO}_3$  solution at 75°C and -0.65 V (SCE).

If some appropriate values for the applied strain rate, crack velocity and number of cracks are put into Eq 3, the results can be expressed graphically as in Fig. 7. Because the first term in Eq 3 dominates at high applied strain rates and the second term at low applied rates, there is little effect of crack velocity at high applied rates, i.e., the crack growth contributes little to the crack tip strain rate. However, at low applied strain rates, the SCC growth maintains the crack tip strain rate at values that are appreciably higher than would be obtained if the crack growth had been ignored. Thus, it may be expected that in those systems that display relatively high crack growth rates no lower limiting applied strain rate will be observed, because the crack growth will itself sustain a relatively high crack tip strain rate.

### Threshold Stresses from SSRTs

One of the commonest complaints relating to SSRTs is that they do not provide threshold stresses for use in engineering design [10]. Quite apart from whether SCC threshold stresses are ever used in design, it is the case that monotonic SSRTs do not give threshold stresses,

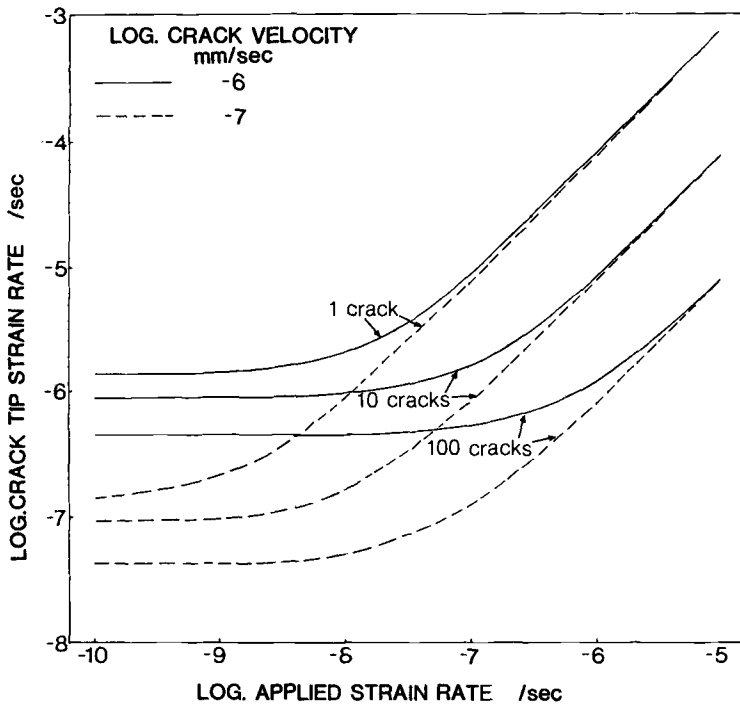


FIG. 7—Effects of crack velocity and number of cracks on the crack tip strain rate calculated from Eq 3.

since they were not designed for such, but it is possible to conduct tests in such a way as to provide that information. Three approaches are indicated.

#### *Interrupted SSRTs*

Obviously SSRTs may be stopped at any time during the loading cycle and examined for cracks, so that by terminating tests at different maximum stresses some indication of the magnitude of the latter to initiate cracking can be obtained. The variability of the microplastic deformation rate in a load cycle that starts at a relatively low level in the elastic range leaves some doubts associated with such an approach, especially in view of the strain rate dependence of threshold stresses. Consequently, a better approach may be to preload the specimens to various initial stresses in the absence of the cracking environment or at a potential that prevents cracking, after which they are allowed to creep until the rate of the latter falls below the strain rate to be applied. The environmental conditions for cracking are established at the start of the applied strain rate part of the test, straining being continued for a sufficient time, but no more, to allow accurate measurement of the depths of any cracks formed, so that the test is interrupted after a restricted stress range has been traversed. During straining, the stress upon the specimen varies over a range dependent upon the magnitude of the applied strain rate, hence the importance of restricting the test time to no longer than that necessary to produce measurable cracks. The cracks are measured by microscopy on longitudinal sections of the gage length, the deepest crack being used to calculate an average crack velocity by division of its length by the time for which the strain rate was applied.

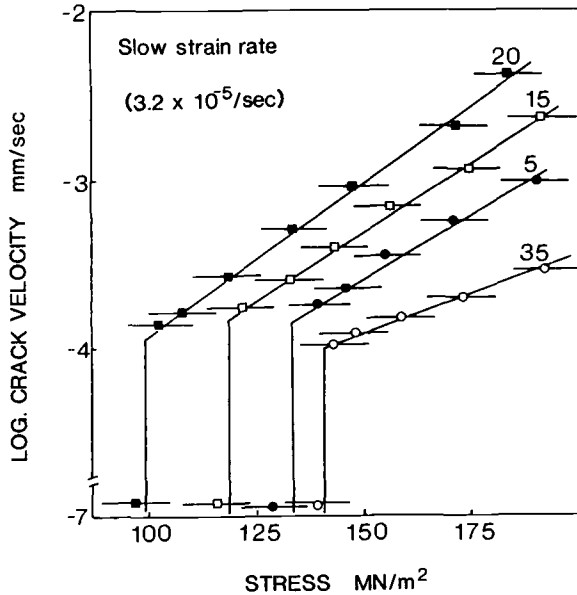


FIG. 8—Effects of  $K_2CrO_4$  content (appended to curves as g/L) of solutions containing 35 g/L NaCl upon stress corrosion crack velocity in specimens of Mg-8.8Al alloy subjected to slow strain rate tests over restricted stress ranges [3].

Figure 8 shows results from such tests on a magnesium-aluminum alloy in NaCl solution with various additions of  $K_2CrO_4$ , where the lengths of the bars indicate the stress ranges for each test [3]. A threshold stress is indicated for each solution, the value of which varies with the chromate content of the solution, although not in a proportional manner. (In this system, minimal threshold stresses and maximal crack velocities occur at intermediate chloride-chromate ratios of 1:2. Increasing the chloride-chromate concentration ratio of solutions facilitates discharge of hydrogen and also increases the frequency of pitting. Up to chloride-chromate ratios of 1:2 these trends result in increased susceptibility to cracking. At ratios higher than 2 cracking susceptibility diminishes again, despite the enhanced discharge of hydrogen. However, the greater dissolution at such ratios results in blunting of the cracks or their disappearance, so that cracking susceptibility decreases at the higher chloride-chromate ratios.) The threshold stresses in Fig. 8 refer to an applied strain rate of  $3.2 \times 10^{-5} \text{ s}^{-1}$  and, just as the values depend upon solution composition, they may be expected to be influenced by strain rate because of the interaction of the latter with film growth rate. The point may be illustrated by results from a different system involving the exposure of nickel-aluminum bronze specimens to seawater [11]. Using the same approach as that involved with the results indicated in Fig. 8, the threshold stresses determined are shown in Fig. 9 as a function of applied strain rate. At strain rates of about  $10^{-6} \text{ s}^{-1}$  or higher the threshold stresses are in the region of 60% of the 0.2% proof stress, but as the strain rate is reduced the threshold for SCC increases until at the slowest rate it approaches the tensile strength of the alloy. That result conforms with those shown in Figs. 2, 5, and 6 for quite different systems, in showing that at slow enough strain rates SCC does not occur even though the stresses or stress intensity factors are very high. Notwithstanding these demonstrations that threshold stresses are not just a function of alloy composition or struc-

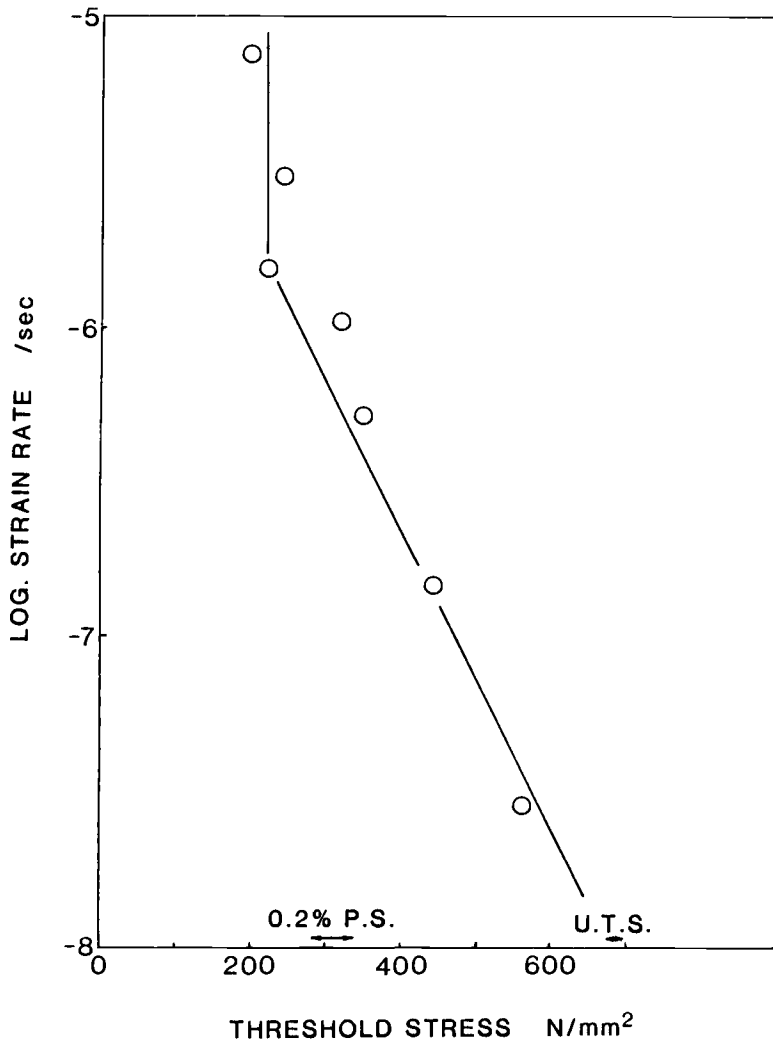


FIG. 9—Threshold stresses at different initial strain rates from interrupted slow strain rate tests on cast Ni-Al bronze specimens exposed to seawater at  $-0.15$  V (SCE) [11].

ture, but are dependent upon environmental factors and strain rate, it is clear that SSRTs can be used to determine threshold stresses.

#### *Tapered Specimen Tests*

When interrupted SSRTs are used for determining a threshold stress several specimens loaded to different initial stresses are required, as with constant strain or constant load tests aimed at determining threshold stresses. It is possible however to use a single specimen for threshold stress determination, by incorporating a tapered gage length [12]. The taper creates a variation in stress along the gage length and from examination of a longitudinal section of the tested specimen the position at which cracks can just be detected allows the stress at

that position to be defined. The semi-angle of the taper should be minimized to avoid large resolved components of the tensile load. A further obvious requirement is that cracks should be restricted to the gage length and it is readily shown [13] that that requirement will be met when

$$L \tan \theta > (D_0/2)[(\sigma_{\max}/\sigma_i)^{0.5} - 1] \quad (4)$$

and

$$\sigma_{\max}/\sigma_i < 2.6$$

where

- $L$  = gage length,
- $\theta$  = semi-angle of taper,
- $D_0$  = minimum diameter in gage length,
- $\sigma_{\max}$  = maximum stress at narrow end of taper, and
- $\sigma_i$  = crack initiation stress.

For  $L = 28.6$  mm and  $D = 5$  mm, as in the tests with results given below,  $\theta = 3^\circ$  and the error in the resolved principle tensile stress is only 0.2%, which is negligible. The measured variation in strain rate along the gage length amounts to a factor of about 2, well within the reproducibility limits for the effect of strain rate upon SCC initiation.

The method has been applied to several systems and the results [12] are given in Tables 1 and 2. In Table 1, the crack initiation stresses from tapered specimen tests are compared with published data obtained by different test methods for the same systems, where such data are available; in Table 2, the results from tapered specimen tests are compared with those from interrupted SSRTs and from constant load tests for the five systems studied. The results in Table 2 show that there is reasonable agreement between the three methods of measuring the stress for crack initiation, while Table 1 shows that published data, even though for different steels and involving different test methods, indicate similar trends with respect to changes in the test environment to those obtained from the SSRTs on tapered specimens. A point worthy of mention concerns the maximum load to which specimens should be taken. Clearly,  $\sigma_{\max} > \sigma_i$  if cracking is to be observed and it was indicated earlier that  $\sigma_{\max}/\sigma_i < 2.6$  if cracking is to be contained within the gage length. However, in some cases if specimens are strained to total failure  $\sigma_{UTS}/\sigma_i > 2.6$  and it may be prudent to stop tests before the maximum load is exceeded.

TABLE 1—Crack initiation stresses ( $\sigma_i$ ) and  $\sigma_i/\sigma_{ys}$  ratios from slow strain rate tests on tapered specimens and from static test data in the publications referenced in the final column [12].

System	$\sigma_i$ (MPa)	$\sigma_i/\sigma_{ys}$ (tapered specimens)	$\sigma_i/\sigma_{ys}$ (published static test data)
Brass in Mattsson's soln.	58	0.62	—
Copper in $\text{NaNO}_2$	80	2.06	—
C-Mn steel in $\text{CO}_3/\text{HCO}_3$	214	0.92	0.93 (14)
C-Mn steel in NaOH	268	1.15	1.02 (15)
C-Mn steel in $\text{NaNO}_3$	190	0.81	0.74 (16)

TABLE 2—Results from tests on nontapered specimens subjected to constant load tests or slow strain rate tests ( $3.2 \times 10^{-6} \text{ s}^{-1}$ ) with the latter stopped at various maximum stresses quoted in relation to the values of  $\sigma$ , given in Table 1 [12].

System	Interrupted SSRT		Constant Load Test	
	$\sigma/\sigma_t$	Cracking	$\sigma/\sigma_t$	Cracking
Brass in Mattsson's soln.	1.19	Yes	1.21	Yes
	0.98	No	1.00	No
	0.86	No	0.86	No
Copper in $\text{NaNO}_2$	1.19	Yes	1.50	Yes
	0.95	No	1.23	Yes
	0.94	No	1.00	No
C-Mn steel in $\text{CO}_3/\text{HCO}_3$	0.88	No		
	1.73	Yes	1.34	Yes
	1.46	Yes	0.99	No
C-Mn steel in $\text{NaOH}$	0.96	No		
	1.18	Yes	1.17	Yes
	0.96	No	0.86	No
C-Mn steel in $\text{NaNO}_3$			0.86	No
	1.10	Yes	1.10	Yes
	0.85	No	0.85	No

### Cyclic Loading

With interrupted SSRTs, or even when tapered specimens are monotonically strained, to determine threshold stresses there are possible problems because of the limited time for which cracking conditions may exist. This is likely to be more of a problem in systems that display relatively low crack velocities, where the time for growth may be such that crack depths are too small for accurate detection or measurement. A possible solution to this problem is to employ cyclic loading, where strain rate effects are still involved because of the strain hysteresis associated with cyclic loading, although the strain rate is less readily quantified as a result of its variability over different parts of the load cycle. A discussion of this or of the distinctions between SCC and corrosion fatigue, if the latter is assumed to refer to cyclic loading and the former not, is beyond the scope of the present paper. However, for present purposes it is convenient to present some results in terms of stressing rate, rather than strain rate, although some of the data to be replotted is that from SSRTs shown in Fig. 9. Just as it is not possible to define a single value strain rate for cyclic loading tests, so also is it impossible to provide a single value stressing rate for interrupted SSRTs. During the tests that produced the data shown in Fig. 9, the loads were continuously recorded and from those the range of stressing rates involved in determining each threshold stress were calculated. Those are shown in Fig. 10, together with threshold stresses determined in cyclic loading tests; for the latter, the threshold stresses are shown as a range extending between the highest stress that did not produce cracking and the lowest stress that gave cracking [11]. It is apparent from Fig. 10 that the threshold stress reaches a lower limiting value of about 60% of the 0.2% proof stress for the faster monotonic loading conditions and for cyclic loading, involving a variety of stress ranges, over a wide range of frequencies. Moreover, where the stressing rates for the two types of loading were similar the threshold stresses were effectively the same. It is difficult to escape the conclusion that essentially the same phenomenon is occurring under both monotonic and cyclic loading conditions. This view is

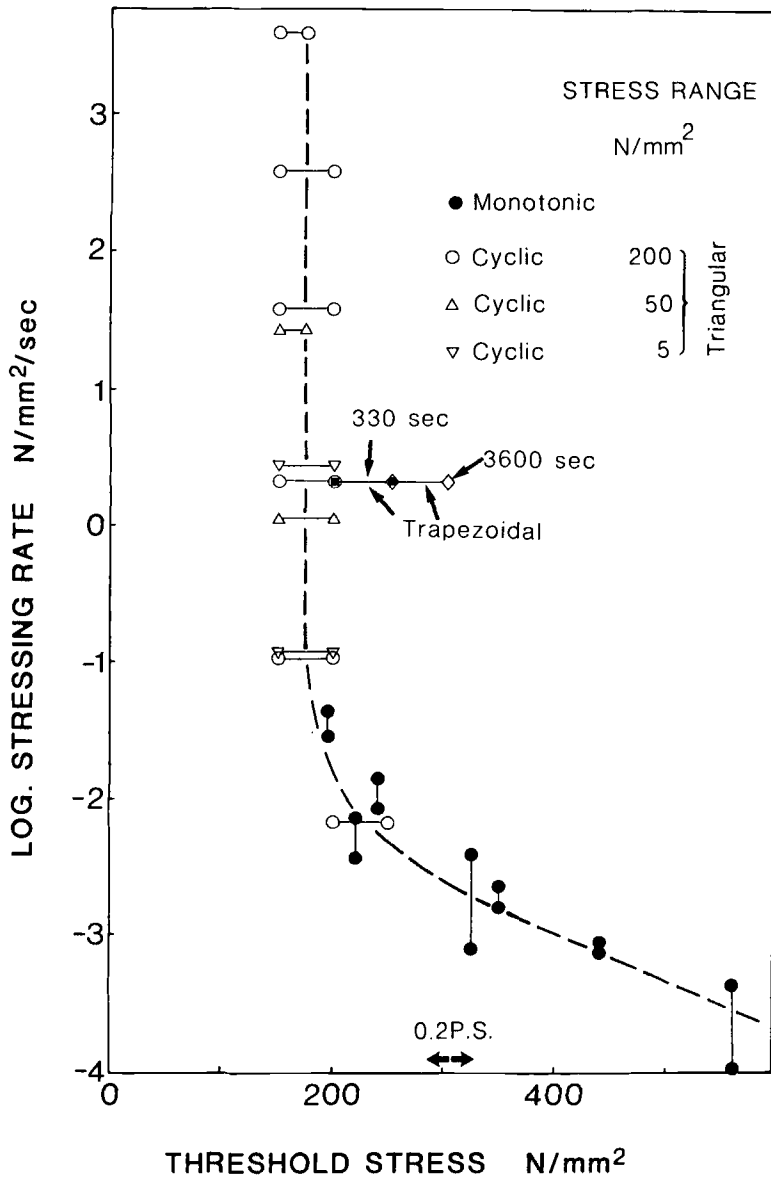


FIG. 10—Threshold stresses as a function of stressing rate for interrupted slow strain rate and cyclic loading tests on cast Ni-Al bronze specimens exposed to seawater at  $-0.15$  V (SCE) [11].

supported by the fractographic characteristics being indistinguishable from both types of test in the vicinity of the thresholds.

**Conclusion**

Twenty-five years of use of slow strain rate testing has seen the method lose much of the skepticism that surrounded it in its early days, although some reservations remain centered

upon the high stresses and plastic strains that are often a consequence of taking specimens monotonically to total failure. The method does not need to involve such conditions if they are not acceptable, since tests can be stopped at any desired maximum stress or strain. The method can be used to define a threshold stress for cracking by restricting the stresses to which a series of specimens are subjected, or a single specimen with an appropriately tapered gage length may be used for the same purpose. The mechanistic importance of strain rate in environment sensitive cracking manifests itself in similar threshold conditions for cracking in both monotonic and cyclic loading tests and that can sometimes be useful in conducting laboratory tests.

## References

- [1] Parkins, R. N., "Development of Strain-Rate Testing and Its Implications," *Stress Corrosion Cracking: The Slow Strain Rate Technique, ASTM STP 665*, G. M. Ugiansky and J. H. Payer, Eds., American Society for Testing and Materials, Philadelphia, 1979, pp. 5-25.
- [2] Parkins, R. N., Slattery, P. W., and Poulson, B. S., "The Effects of Alloying Additions to Ferritic Steels upon Stress Corrosion Cracking Resistance," *Corrosion*, Vol. 37, No. 11, Nov. 1981, pp. 650-664.
- [3] Ebtehaj, K., Hardie, D., and Parkins, R. N., "The Influence of Chloride-Chromate Solution Composition on the Stress Corrosion Cracking of a Mg-Al Alloy," *Corrosion Science*, Vol. 28, No. 8, 1988, pp. 811-829.
- [4] Hardie, D., Holroyd, N. J. H., and Parkins, R. N., "Reduced Ductility of High-Strength Aluminum Alloy During or After Exposure to Water," *Metal Science*, Vol. 13, Nov. 1979, pp. 603-610.
- [5] Abramson, G., Evans, J. T., and Parkins, R. N., "Investigation of Stress Corrosion Crack Growth in Mg Alloys Using *J*-Integral Estimations," *Metallurgical Transactions A*, Vol. 16A, Jan. 1985, pp. 101-108.
- [6] Hermann, L. and Rice, J. R., "Comparison of Theory and Experiment for Elastic-Plastic Plane-Strain Crack Growth," *Metal Science*, Vol. 14, 1980, pp. 285-291.
- [7] Paris, P. C., Tada, H., Zahoor, A., and Ernst, H., "A Treatment of the Subject of Tearing Instability," *U.S. Nuclear Regulatory Commission Report NUREG-0311*, Aug. 1977.
- [8] Parkins, R. N., Marsh, G. P., and Evans, J. T., "Strain Rate Effects in Environment Sensitive Fracture," *Predictive Methods for Assessing Corrosion Damage to BWR Piping and PWR Steam Generators*, H. Okada and R. W. Staehle, Eds., National Association of Corrosion Engineers, Houston, 1982, pp. 249-260.
- [9] Congleton, J., Shoji, T., and Parkins, R. N., "The Stress Corrosion Cracking of Reactor Pressure Vessel Steel in High Temperature Water," *Corrosion Science*, Vol. 25, No. 8/9, 1985, pp. 633-650.
- [10] Eriksson, H. and Bernhardsson, S., "The Applicability of Duplex Stainless Steels in Sour Environments," *Corrosion*, Vol. 47, No. 8, 1991, pp. 719-727.
- [11] Parkins, R. N. and Suzuki, Y., "Environment Sensitive Cracking of a Nickel-Aluminium Bronze Under Monotonic and Cyclic Loading Conditions," *Corrosion Science*, Vol. 23, No. 6, 1983, pp. 577-599.
- [12] Yu, J., Xue, L. J., Zhao, Z. J., Chi, G. X., and Parkins, R. N., "Determination of Stress Corrosion Crack Initiation Stress and Crack Velocities Using Slowly Strained Tapered Specimens," *Fatigue and Fracture of Engineering Materials and Structures*, Vol. 12, No. 6, 1989, pp. 481-493.
- [13] Yu, J., Holroyd, N. J. H., and Parkins, R. N., "Application of Slow-Strain-Rate Tests to Defining the Stress for Stress Corrosion Crack Initiation in 70/30 Brass," *Environment-Sensitive Fracture: Evaluation and Comparison of Test Methods, ASTM STP 821*, S. W. Dean, E. N. Pugh, and G. M. Ugiansky, Eds., American Society for Testing and Materials, Philadelphia, 1984, pp. 288-309.
- [14] Parkins, R. N., "The Controlling Parameters in Stress Corrosion Cracking," *Fifth Symposium on Line Pipe Research*, American Gas Association, Arlington, VA, 197, Catalog No. L30174, pp. U1-40.
- [15] Bohnenkamp, K., "Caustic Cracking of Mild Steel," *Proceedings, Conference on Fundamental Aspects of Stress Corrosion Cracking*, R. W. Staehle, A. J. Forty, and D. Van Rooyen, Eds., National Association of Corrosion Engineers, Houston, 1969, pp. 374-383.
- [16] Parkins, R. N. and Usher, R., "The Effect of Nitrate Solutions in Producing Stress Corrosion Cracking in Mild Steel," *First International Congress on Metallic Corrosion*, Butterworth's, London, 1961, pp. 289-295.

## Limitations of the Slow Strain Rate Test Technique

---

**REFERENCE:** Beavers, J. A. and Koch, G. H. "Limitations of the Slow Strain Rate Test Technique," *Slow Strain Rate Testing for the Evaluation of Environmentally Induced Cracking: Research and Engineering Applications*, ASTM STP 1210, R. D. Kane, Ed., American Society for Testing and Materials, Philadelphia, 1993, pp. 22–39.

**ABSTRACT:** A state-of-the-art survey was performed on slow strain rate (SSR) testing methods for the Materials Technology Institute of the Chemical Process Industries, Inc. (MTI). The goal of the survey was to determine if SSR testing methods yield useful data in predicting stress-corrosion cracking (SCC) susceptibility of metals used in the chemical process industry (CPI). The information was obtained by searching the literature and by sending out questionnaires to relevant sources. It was concluded that most reported cases of anomalous behavior with the SSR test technique can be attributed to inadequate control or measurement of strain rate or potential, which are the major controlling parameters for a specific material-environment combination.

**KEYWORDS:** stress-corrosion cracking (SCC), slow strain rate (SSR), chemical process industry (CPI), strain rate, potential, stainless steels, nickel-base alloys, copper alloys, carbon steels, aluminum alloys, titanium alloys, zirconium alloys

In recent years, the slow strain rate (SSR) test technique has become widely used and accepted for stress-corrosion cracking (SCC) evaluations by companies in a variety of industries. It is being used by many chemical process industries (CPI) to screen alloys for new process equipment applications, to identify alloys that should not experience SCC in service, and to verify that existing plant equipment should not fail by SCC when placed into new service conditions.

Briefly, the SSR technique involves the slow straining of a specimen of the alloy of interest in a possible cracking environment. Typically, a strain rate of the order of  $10^{-6} \text{ s}^{-1}$  is used, which is about four orders-of-magnitude slower than that used in a standard tensile test. Cracking susceptibility is indicated by a decrease in mechanical properties (e.g., strain to failure, ultimate tensile strength, reduction in area) over those observed in an inert environment and, in some cases, the presence of secondary cracking along the gage length of the specimen. A major advantage of the SSR technique over constant load or constant deflection techniques is that the test period is generally shorter with the SSR technique. The SSR technique also avoids the problem of specifying a test time. For example, if cracking is not observed in a 1000-hour test period with U-bend specimens, would it occur in 1500 hours? With the SSR technique, the specimen is generally strained to failure and the test duration itself provides an indication of cracking susceptibility. The SSR technique is also generally much less costly than fracture-mechanics crack-propagation tests since the specimen geometry and test procedures are simpler with the SSR technique.

---

<sup>1</sup> Vice president, Research, and senior group leader, respectively, CORTEST COLUMBUS TECHNOLOGIES, INC. (CC Technologies), Columbus, OH 43235.

In the literature, several terms and associated acronyms have been used to describe the SSR technique. These include constant extension rate (CER), constant extension rate test (CERT), slow extension rate test or technique (SERT), constant strain rate (CSR), slow strain rate (SSR), and slow strain rate test (SSRT). The terms containing constant extension rate or constant strain rate have generally fallen out of favor because neither are constant in a test. Both vary somewhat during a test depending on factors such as the stiffness of the load frame, specimen dimensions and strength, the number of secondary cracks that initiate, and the time of their initiation. In this report, the single term SSR is used to describe this test technique.

While the SSR technique has been shown to be a useful tool for SCC testing, recent laboratory results may indicate problems with the technique for at least some alloy-environment systems. Specifically, it has been discovered that results from some SSR tests do not display cracking in environments where SCC is known to occur in field conditions or with other SCC test methods, such as U-bend tests. There are a number of possible explanations for the apparent discrepancy between SSR and constant load and constant strain test results. These include incubation time effects, potential range effects, and strain rate effects.

A state-of-the-art survey was performed on SSR testing methods for the Materials Technology Institute of the Chemical Process Industries, Inc. (MTI). The overall goal of this survey was to determine if SSR testing methods yield useful data in predicting SCC susceptibility of metals used in the CPI. The specific objectives of the state-of-the-art survey were:

- (1) to identify the alloy-environment systems in which the SSR technique produces anomalous SCC results,
- (2) to identify which test variables must be controlled to make the SSR test results applicable to the CPI, and
- (3) to identify the limitations of the SSR test technique.

A summary of the results of the survey was presented at CORROSION/91 [1]. This paper updates the original work to include more recent articles from the literature.

### **Approach**

The open literature from 1982–1991 was searched using the NACE CORAB computer program. This program is commercially available through the National Association of Corrosion Engineers (NACE) and is Corrosion Abstracts on a CD ROM. More recent NACE literature was hand searched. Literature prior to 1982 was searched through NTIS and Corrosion Abstracts. Several hundred articles were found on the SSR test technique. Abstracts for each of these articles were obtained and reviewed. It was not within the scope of this program to review and summarize this extensive literature. A few criteria were used to select articles for inclusion in the report, based on a review of the abstract:

- (1) an indication of problems with the SSR test technique,
- (2) a good comparison of the SSR test technique with other test techniques,
- (3) data on strain rate effects and,
- (4) data that were relevant to problems with the technique identified either from the literature or from the questionnaire.

In order to obtain the unpublished work on anomalous SSR behavior, questionnaires were sent out to MTI, NACE, and ASTM members. Follow-up telephone contacts were made with sources providing relevant data.

The paper is subdivided into sections on the major alloy systems of interest to the chemical process industry. Each section contains discussions on the questionnaire results and the major factors affecting the SSR results for the particular alloy system. For the alloy systems in which no anomalous behavior was identified, a discussion on strain rate effects was included. Strain rate is the single parameter that is unique to the SSR test technique.

## Results and Discussion

Approximately 300 questionnaires were mailed to MTI, NACE, and ASTM members and 34 responses were received. Of the 34 responses, 13 described cases of anomalous behavior for the SSR technique. Eight of the responses indicated good experience with the SSR technique with no anomalous behavior observed. Two of the responses described general problems with the technique while the remaining responses indicated they had not used the technique. A summary of the questionnaires indicating anomalous behavior with the SSR technique is given in Table 1. These data show that over 75% of the responses were associated with stainless steels and nickel-base alloys. This may reflect the more extensive research performed on these alloys but also suggests that the problems are more prevalent in these systems.

The two general responses were interesting and informative. Garner [2] described problems associated with SSR testing of welded specimens. He indicated that the SSR test strains the softest part of the microstructure preferentially and thereby leads to SCC in that part of the specimen; whereas, in practice, the hardest part of the microstructure is often the site where cracking occurs.

Silverman [3] indicated that his company has stopped using the SSR technique because of its lack of predictive capability. Both false positives and false negatives can occur with the technique because of the difficulty of accurately reproducing field conditions. However, their primary concern is the SSR test results producing false negatives, where cracking may occur in the field but no cracking is observed in SSR tests. Silverman indicated that similar problems can occur with U-bend or other SCC tests, but U-bend tests are less expensive to run than are SSR tests.

Discussions of questionnaire responses and relevant literature for the major alloy systems are given.

### *Stainless Steels*

There were six responses to the questionnaire indicating anomalous behavior with stainless steels. The effects reported by Demo [4] are clearly a reflection of the strain rate dependence of the SCC in the stainless steel-chloride system. In boiling acidified 26% NaCl, cracking occurred in the shoulder of the Type 316 specimen at a strain rate of  $1 \times 10^{-6} \text{ s}^{-1}$ ; whereas, at a slower strain rate ( $1 \times 10^{-7} \text{ s}^{-1}$ ), or in a more concentrated  $\text{CaCl}_2$  solution, cracking occurred in the gage section. These results are consistent with those of Daniels [5] who found that the maximum strain rate, in which cracking was observed, in SSR tests decreased with decreasing chloride concentration. His data, while not complete, predict a strain rate of less than  $1 \times 10^{-6} \text{ s}^{-1}$  for cracking to occur in the boiling 26% solution, as shown in Fig. 1.

The anomalous behavior reported by Baumert [6] also may be associated with strain rate effects. He performed SSR tests on three stainless steels (Type 304, Type 316 and Nitronic 50) in two known cracking environments; aqueous 15% NaCl and high-temperature caustic. The former were performed under aerated conditions at 99°C at a strain rate of  $1.14 \times 10^{-6} \text{ s}^{-1}$  while the latter were performed under deaerated conditions at 177°C and a strain

rate of  $2.8 \times 10^{-6} \text{ s}^{-1}$ . No cracking was observed in the chloride environment while incipient cracks were observed in the necked region of some specimens tested in the caustic environment. In the chloride environment, the strain rate used was probably too high, based on the work of Daniels [5]. A similar argument may be applicable to the caustic environment, although data were not found in the literature on strain rate effects in that system.

The behavior reported by Bruemmer [7] is also associated with strain rate effects. He reported that the SSR test technique, at strain rates greater than or equal to  $10^{-7} \text{ s}^{-1}$ , was less sensitive than constant-load tests in detecting intergranular SCC (IG-SCC) of sensitized Type 304 in low-temperature water with or without additions.

The anomalous behavior reported by Frechem [8] may be associated with potential effects. In neutral 15% aqueous NaCl at  $95^\circ\text{C}$ , he found that U-bend specimens of Type 304 and Type 316 cracked readily while SSR tests did not produce cracking at strain rates of  $10^{-6}$  to  $10^{-8} \text{ s}^{-1}$ . All testing was performed under freely corroding conditions. Shibata [9] performed SCC tests at the free-corrosion potential and at controlled potentials on Type 304 in  $\text{CaCl}_2$  solutions at  $100^\circ\text{C}$  using constant load and SSR test techniques. Under freely corroding conditions, SCC was more severe in the constant load tests. It also was found that the free corrosion potentials in the SSR tests were generally more negative than those found in the constant load tests. When the potentials in the SSR tests were held at the potentials measured in the constant load tests, better agreement was obtained between the two techniques.

The remaining two responses to the questionnaire for stainless steels were associated with over-sensitivity where the SSR technique detected cracking under conditions where field experience did not indicate a problem. The authors of this report do not consider this to be a serious problem with the technique. A desirable feature of a test technique is to provide an early warning to potential problems. The fact that only the SSR test results indicated cracking suggests that the field conditions may be somewhat less aggressive than those used in the laboratory. Nevertheless, these results suggest that a problem may exist in the field.

Reports of anomalous SSR behavior for the stainless steels in the open literature were quite limited. In most cases, the SSR technique compared favorably with other test techniques. Furthermore, in some cases, the SSR technique was found to be superior to other test techniques in sensitivity. For example, Daniels [5] and Takaku [10] reported that the constant-load test technique was less effective than the SSR for indicating SCC. In the former study, U-bend tests also were more sensitive to cracking than constant-load tests while Takaku [10] found cyclic-load tests superior to constant-load tests. On the other hand, Bruemmer [11] reported that the constant load technique gave a better simulation of a service failure and produced cracking over a wider range of conditions than either SSR or U-bend techniques. Bruemmer [11] suggested that the strain rate used in his testing was probably too high for the low temperature, relatively benign, environment. Thus, his criticism of the technique can probably be attributed to a strain-rate effect.

A more common criticism of the technique is associated with fracture mode behavior. In some cases, the fracture mode reported for the SSR test technique was different than that reported for other techniques. For example, Daniels [5] reported that the SSR technique produced intergranular cracking while mixed intergranular and transgranular cracking was observed for U-bend tests on alloy 304 in concentrated chloride solutions at near-boiling temperatures. Yamanaka [12] reported that SSR and constant load tests produced mixed mode cracking while U-bend and decreasing stress intensity ( $K$ ) tests produced transgranular cracking in tests on several austenitic stainless steels in boiling concentrated  $\text{MgCl}_2$ . Andresen [13] reported that the extent of intergranular cracking was greater in SSR test specimens than in compact tension specimens in SCC tests performed on stainless steels in  $288^\circ\text{C}$  water. These tests suggest that the SSR technique may favor intergranular cracking but it is also

TABLE 1—Summary of responses to the questionnaire in which anomalous SSR behavior was reported.

Reference	Alloy	Environment	Temperature, °C	Strain Rate S <sup>-1</sup>	Potential	Comment
4	Alloy 316	Acidified 26% NaCl	Boiling	10 <sup>-6</sup>	FCP <sup>a</sup>	Cracking in shoulder of specimen.
6	Alloy 304	Aerated 15% NaCl	99	1.14 × 10 <sup>-6</sup>	FCP	No cracking.
6	Alloy 316	Aerated 15% NaCl	99	1.14 × 10 <sup>-6</sup>	FCP	No cracking.
6	Nitronic 50	Aerated 15% NaCl	99	1.14 × 10 <sup>-6</sup>	FCP	No cracking.
6	Alloy 304	Concentrated Caustic	177	2.8 × 10 <sup>-6</sup>	FCP	Incipient cracking.
6	Alloy 316	Concentrated Caustic	177	2.8 × 10 <sup>-6</sup>	FCP	Incipient cracking.
6	Nitronic 50	Concentrated Caustic	177	2.8 × 10 <sup>-6</sup>	FCP	Incipient cracking.
8	Alloy 316	Neutral 15% NaCl	95	10 <sup>-8</sup> –10 <sup>-6</sup>	FCP	No cracking.
8	Alloy 304	Neutral 15% NaCl	95	10 <sup>-8</sup> –10 <sup>-6</sup>	FCP	No cracking.
7	Alloy 304	Pure water with Cl <sup>-</sup> .	Low	≥10 <sup>-7</sup>	FCP	No cracking.
15	Alloy G3	F <sup>-</sup> and S <sub>2</sub> O <sub>3</sub> <sup>-2</sup> NaCl—H <sub>2</sub> S—S <sup>0</sup>	High	ND	FCP	No cracking.

15	Alloy 825	NaCl—H <sub>2</sub> S—S <sup>a</sup>	High	ND	FCP	No cracking.
16	Alloy G3	CO <sub>2</sub> —H <sub>2</sub> S	High	2 × 10 <sup>-6</sup>	FCP	No cracking.
16	Alloy 825	CO <sub>2</sub> —H <sub>2</sub> S	High	2 × 10 <sup>-6</sup>	FCP	No cracking.
20	Alloy 600	Deaerated high-purity water	High	ND	FCP	No cracking.
20	Alloy 690	Deaerated high-purity water	High	ND	FCP	No cracking.
20	Alloy 750	Deaerated high-purity water	High	ND	FCP	No cracking.
21	Alloy 600	Pure water	High	10 <sup>-8</sup> –10 <sup>-6</sup>	FCP	No cracking at faster strain rate.
30	C Steel	NaOH—S <sup>a</sup>	93–138	ND	—	Narrow potential range for SCC.
35	3.5% Ni turbine rotor steel	Pure water	High	ND	—	Different fracture mode from service.
37	Low-alloy steel	Organic liquid & formic acid	ND <sup>b</sup>	ND	—	No cracking with smooth specimen.
44	Duplex SS	H <sub>2</sub> S/Cl <sup>-</sup>	80	ND <sup>b</sup>	FCP	Extensive cracking.
45	Alloy 316 NG	Pure water + 0.2 ppm O <sub>2</sub>	288	ND	FCP	Extensive cracking.

<sup>a</sup> FCP—Free Corrosion Potential.

<sup>b</sup> ND—Not defined.

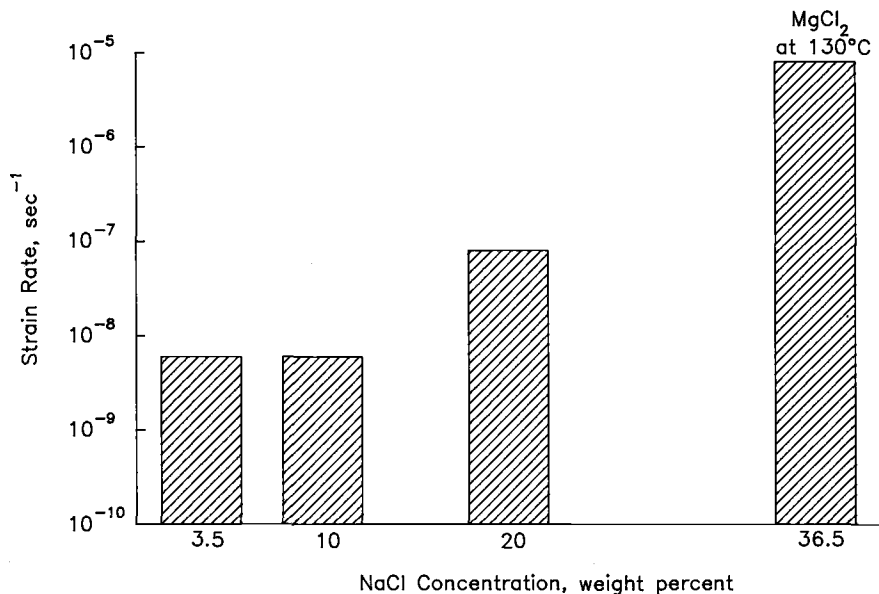


FIG. 1—Maximum strain rate in which cracking was observed in SSR tests on alloy 304 in NaCl solutions at 100°C (after Daniels [5]).

clear that peculiar effects of test technique on fracture mode are not limited to the SSR test technique.

A significant paper with regard to understanding the SSR test technique was authored by Shibata [9]. As previously described, he performed SCC tests at the free-corrosion potential and at controlled potentials on Type 304 in CaCl<sub>2</sub> solutions at 100°C using constant load and SSR test techniques. Under freely corroding conditions, SCC was more severe in the constant load tests. It also was found that the free corrosion potentials in the SSR tests generally were more negative than those found in the constant load tests, as shown in Fig. 2. The potentials plotted in Fig. 2 are the peak (maximum) free corrosion potentials measured in each test. The data show that, with the exception of the constant load test in 30% CaCl<sub>2</sub>, all of the free corrosion potentials measured in the SSR tests were equal to or more negative than those measured in the constant load tests in solutions of similar concentration. The observed effect was attributed to the production of fresh surface in the SSR tests, which would tend to depress the free corrosion potential. When the potentials in the SSR tests were held at the free corrosion potentials measured in the constant load tests, better agreement was obtained between the two techniques.

Shibata [9] also concluded that the SSR test technique was not effective at reproducing the cracking observed in constant load tests in lower concentration (CaCl<sub>2</sub> concentrations below 25%) solutions. However, comparison of his test results with those of Daniels [5] suggests that the strain rate used by Shibata was too fast for the low concentration solutions. The study by Shibata demonstrates the two most important parameters affecting cracking, namely, potential and strain rate.

Potential and strain rate effects may not account for all of the discrepancies in the data between the SSR test technique and other SCC test techniques. Yang [14] evaluated the effects of temperature, chloride content, and dissolved oxygen content on the susceptibility to SCC of slightly sensitized alloy 304 in high-temperature water. U-bend and SSR test

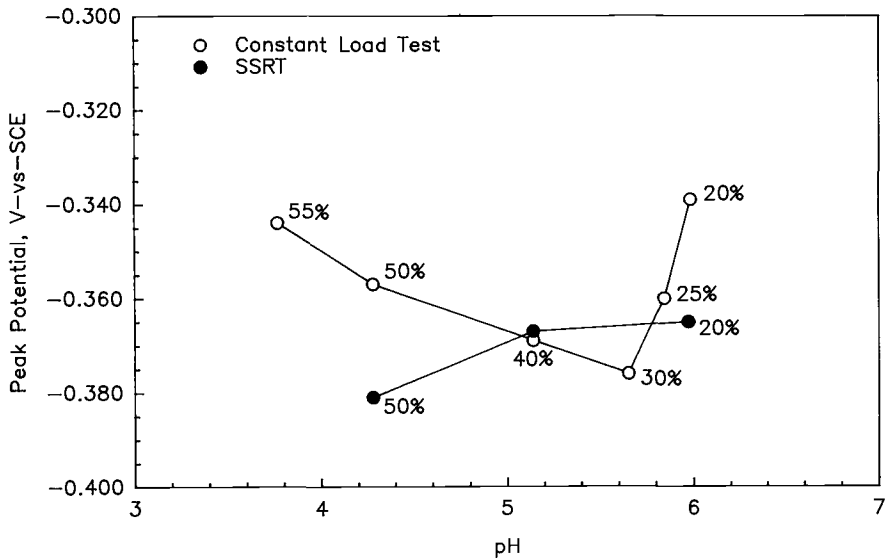


FIG. 2—Relation between peak potential and pH for alloy 304 in  $\text{CaCl}_2$  solutions of different concentrations (after Shibata [9]).

techniques were used and the testing was performed under freely corroding conditions. Oxide film thickness and composition were measured using Auger Electron Spectroscopy (AES). In water containing 100 ppm  $\text{Cl}^-$  and 8 ppm  $\text{O}_2$  over the temperature range of 200 to 300°C, the U-bend specimens showed a decreasing susceptibility to cracking with increasing temperature while the SSR specimens exhibited a maximum in susceptibility to cracking at 250°C (see Fig. 3).

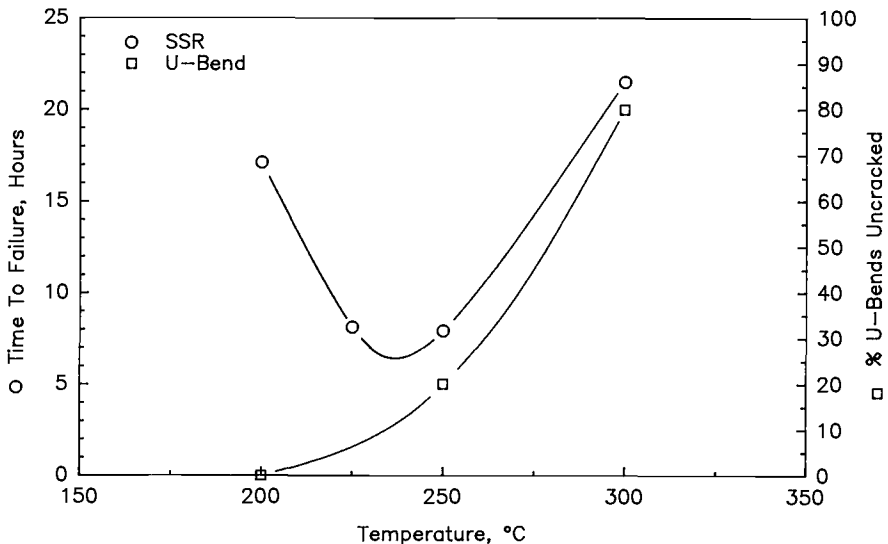


FIG. 3—Time to failure of alloy 304 in high-temperature water for U-bend and SSR tests as a function of temperature (after Yang [14]).

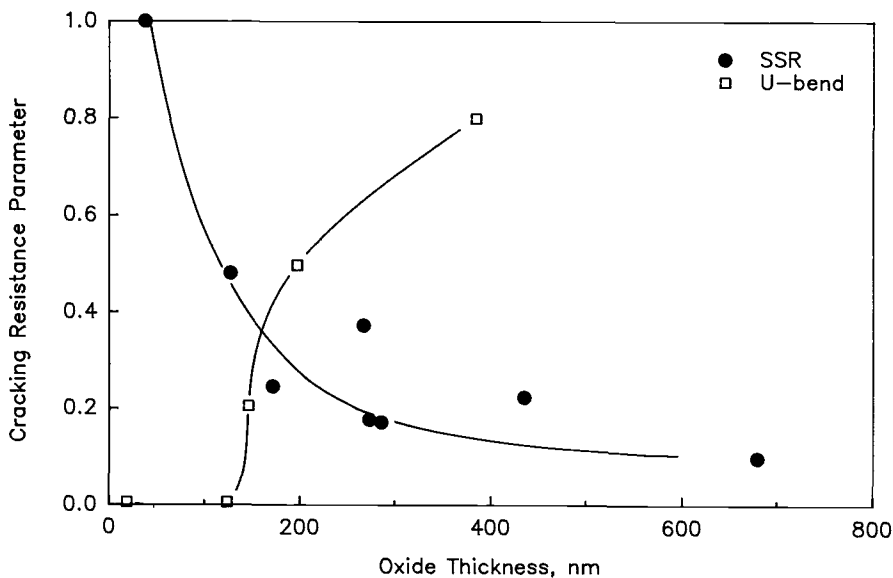


FIG. 4—Resistance to SCC of alloy 304 in high-temperature water as a function of oxide thickness for U-bend and SSR tests. The resistance to cracking for U-bend is expressed as the fraction of specimens remaining uncracked after the test period. Cracking resistance for the SSR tests is equated to time-to-failure in water/time-to-failure in argon (after Yang [14]).

The difference in the behavior for the two test techniques was attributed to a difference in response to the thicker films formed at higher temperatures. Resistance to SCC was found to increase with increasing film thickness for the U-bend tests while the opposite effect was observed for the SSR tests; see Fig. 4. In Fig. 4, the cracking resistance parameter for U-bends is expressed as the fraction of specimens remaining uncracked after the test period. The cracking resistance parameter for the SSR tests is equated to time-to-failure in water/time-to-failure in argon. While these cracking resistance parameters are calculated differently for the two test techniques, they provide similar conclusions at the limits of behavior; a cracking resistance parameter of 1 indicates negligible cracking.

It was also noted in the study by Yang [14] that the composition of the films formed on the SSR test specimens was enhanced with respect to nickel while no such enhancement was observed for the films on the U-bend specimens. Only limited free corrosion potential data were given for the SSR specimens and no potential data were given for U-bend specimens. It is tempting to attribute the difference in composition of the films on the two types of specimens to differences in potential during testing. However, this interpretation does not account for the effects of film thickness on cracking behavior for the two test techniques. From a mechanistic standpoint, the film thickness effects also are reasonable. Under SSR test conditions, a thick film may fracture more readily than a thin film, while a thick film may be more protective for a specimen tested under constant strain.

#### Nickel-Base Alloys

Four responses to the questionnaire survey indicated anomalous behavior for the nickel-base alloys. Sridhar [15] and Kolts [16] reported on the anomalous behavior of alloy G-3 and alloy 825 in  $H_2S$  environments. In the research by Sridhar [15], the behavior clearly can

be attributed to solution chemistry effects. He reported that alloy G-3 and alloy 825 cracked in C-ring tests in a NaCl-H<sub>2</sub>S-S<sup>o</sup> environment in several hundred hours while, under the same conditions, no cracking was observed in the SSR tests. SSR tests performed by Wilhelm [17] under similar conditions produced cracking of these alloys. A close comparison of the test procedures at the two laboratories indicated that Wilhelm agitated the autoclave following H<sub>2</sub>S addition to more rapidly reach equilibrium. When Sridhar followed this test procedure, he also observed cracking in SSR tests in these alloy-environment systems. Wilhelm attributed the anomalous SSR behavior to the difficulty in achieving the proper H<sub>2</sub>S concentration in the solution in the short time period of the SSR test.

It also has been reported that the deaeration procedure used in SSR testing of nickel-base alloys in H<sub>2</sub>S environments can significantly affect the results. Ikeda [18] found that SCC susceptibility of several nickel-base alloys was much greater when only N<sub>2</sub> sparging, as opposed to vacuum deaeration, was used to deaerate the autoclave prior to SSR testing in H<sub>2</sub>S-CO<sub>2</sub>-Cl<sup>-</sup> environments at 150 to 175°C.

Kolts [16] reported anomalous behavior in SSR tests on alloy 825 and alloy G-3 in high-temperature CO<sub>2</sub>-H<sub>2</sub>S environments. In long-term (over one year) tests, C-ring specimens of alloy 825 cracked but no cracking was observed in SSR tests at a strain rate of  $2 \times 10^{-6}$  s<sup>-1</sup>. The C-ring and SSR tests also gave reverse rankings for the two alloys. The C-ring specimens were prepared from sheet and had a total applied strain of about 6%. The tests were performed on the two alloys at the same strength level, which resulted in a higher degree of cold work for the alloy 825 specimens. Typically the alloy 825 specimens had an elongation to failure in standard mechanical tests in air of only 7% whereas the alloy G-3 specimens had an elongation of 25%. As a result of this difference in ductility, the SSR test times for the alloy 825 specimens were considerably shorter than those for the alloy G-3 specimens. Kolts speculated that this difference in time in the test solution may account for the anomalous behavior observed.

Asphahani [19] reported similar anomalous behavior for the SSR test technique in SCC studies of alloy C-276 and alloy MP35N in 50% NaOH at 147°C. Constant strain (C-ring) tests of these alloys indicated that the 50% cold-worked specimens were more susceptible to SCC than solution annealed specimens, based on the maximum depth of cracking. On the other hand, SSR tests of the same materials indicated that the annealed material was more susceptible to SCC. Asphahani [19] attributed this behavior to the fact that the cold-worked C-ring specimens experienced much higher stresses than the annealed specimens. In these tests, the total strain was about 6%, which corresponded to a stress of 200 ksi (1380 MPa) for the cold-worked specimens and 70 ksi (483 MPa) for the annealed specimens of alloy C-276. Strain rate and test time effects were considered but rejected as an explanation for the behavior. In the SSR tests, the failure times for the cold-worked material were shorter than the annealed material because of the lower ductility of the former. However, the cold-worked specimens exhibited shallower cracks than the annealed specimens even when the strain rate of the tests on the cold-worked material was reduced in order to achieve comparable failure times for the two metallurgical conditions.

In both studies, the cold-worked specimens exhibited higher susceptibility in the C-ring tests than in the SSR tests. In the former, the behavior was attributed to a test-time effect (cold-worked specimens failed in a shorter test time than annealed specimens because of the reduced ductility) while in the latter, the behavior was attributed to a strength level effect. One could argue that the test-time effect is a deficiency of the SSR test technique. On the other hand, one could equally argue that strength-level effects on failure times are an inherent deficiency of constant-strain techniques such as the U-bend technique. When several alloys of different strength levels are plastically strained to the same value, the higher strength materials will experience a higher stress assuming similar rates of work hardening.

This problem can be avoided in C-ring tests by controlling the stress level rather than the strain level. The most appropriate test technique depends on the loading conditions in service.

Was [20] reported anomalous behavior in SSR tests on alloys 600, 690, and X750 in deaerated high-purity water at elevated temperatures. Constant load and U-bend tests exhibited SCC while SSR tests did not show significant cracking. The questionnaire response by Payer [21] may provide an explanation for the anomalous behavior reported by Was [20]. Payer reported that alloy 600 has failed by SCC in primary-side water in pressurized water reactors while it is difficult to reproduce the cracking in SSR tests in the laboratory unless very slow strain rates ( $10^{-7}$  to  $10^{-8}$  s $^{-1}$ ) are used. The strain rates used by Was were not indicated in the response but it is likely that they were faster than those indicated by Payer. Bandy [22] also reported, in SSR studies of nickel-base alloys in deaerated high-temperature water, that it was found to be necessary to decrease the strain rate in the range of  $1 \times 10^{-6}$  to  $3 \times 10^{-8}$  s $^{-1}$  in order to see SCC of more resistant alloys; details of the testing or actual data were not given in the reference.

Studies by Page [23] are contradictory to the behavior reported by Was [20]. He investigated the use of creviced and uncreviced SSR specimens for the study of the SCC of alloy 600 in partially deoxygenated (200 ppb) and oxygenated (8 to 16 ppm) pure water at 288°C. Smooth constant-load test specimens were evaluated for comparison purposes. It was found that the specimens cracked, regardless of heat treatment, in the SSR tests under oxygenated conditions only when crevices were present. No cracking was observed under partially deoxygenated conditions or in the constant load tests under any of the test conditions. The reasons for the discrepancy between the researchers is not readily apparent but may be attributable to environmental factors such as oxygen content or water purity.

Reports of anomalous behavior from the open literature were limited and, in most cases, the root cause was confirmed or speculated by the authors. Examples include the cold work effect described by Asphahani [19] and previously discussed and the effects of multiple cracking on the specimen potential, as reported by Newman [24]. SSR and interrupted SSR testing were performed on alloy 600 in 0.21 M boric acid containing lithium hydroxide, sodium thiosulfate, and sodium tetrathionate at 40°C. It was found that the corrosion potential of the specimen was depressed by the initiation of the stress-corrosion cracks in the gage section, which reduced the cracking velocity. The addition of the lithium ion to the test solution greatly reduced the number of cracks in the specimen, which promoted an increase in the potential and the cracking velocity. At still higher lithium ion concentrations, the inhibiting effect of the ion dominated and the cracking velocity decreased; see Figs. 5 and 6. One might speculate that these deleterious effects could be avoided by performing SSR tests under potential control, but, as described by Newman [24], this approach may not be effective in highly resistive solutions. A similar effect of SSR testing on corrosion potentials was previously reported for stainless steels.

Asphahani [19] also reported that the SSR technique could not distinguish between intergranular attack (IGA) and intergranular SCC of nickel-base alloys. In SSR tests on sensitized alloy C-276, intergranular cracking was observed on anodically polarized specimens in a chloride environment. Under similar test conditions, IGA was found on both the tension and compression faces of C-ring specimens. As described by Asphahani [19], both phenomena are capable of causing service failures and the SSR technique is capable of revealing each.

In other work related to the SSR test technique, Asphahani [19] investigated the parameters used to assess SCC susceptibility in a SSR test. It was found that the mechanical properties parameters often used to measure susceptibility, such as percent elongation, percent reduction in area, load at failure, and the total time to failure, were not always

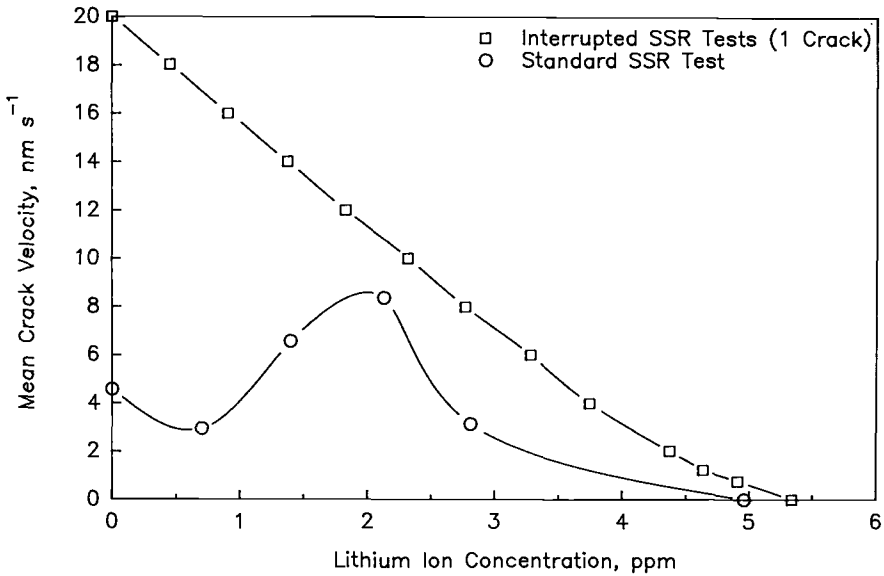


FIG. 5—Effect of LiOH addition on the mean crack velocity of solution-annealed and sensitized Inconel 600 in air-saturated 1.3%  $H_3BO_3$  + 0.7 ppm sulfur as  $Na_2S_2O_3$ . The mean crack velocity is shown for SSR-tests at  $3 \times 10^{-6} s^{-1}$  strain rate. For the interrupted SSR test, the crack velocity was estimated visually and from the load decay at constant deflection (after Newman [24]).

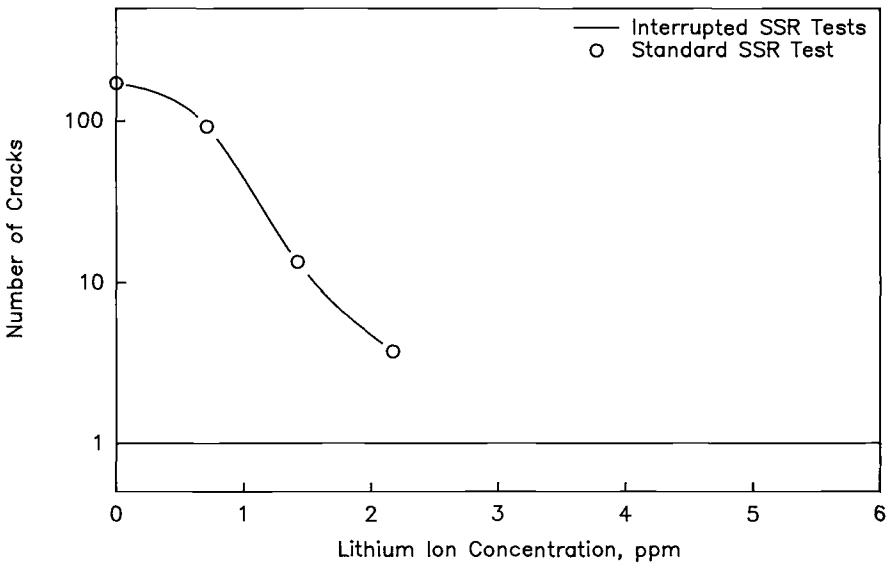


FIG. 6—Effect of LiOH addition on the number of cracks in solution-annealed and sensitized Inconel 600 in air-saturated 1.3  $H_3BO_3$  + 0.7 ppm sulfur as  $Na_2S_2O_3$ . The strain rate was  $3 \times 10^{-6} s^{-1}$  (after Newman [24]).

consistent indicators of SCC of nickel-base alloys. It was concluded that the metallographic measurement of secondary crack depth is the most reliable technique for the determination of SCC of nickel-base alloys. Payer [25] reached a similar conclusion for the general application of the SSR technique "Metallography or fractography is essential to confirm the presence or absence of SCC."

### *Copper Alloys*

No responses to the questionnaire indicating anomalous behavior of SSR tests on copper alloys were received. However, effects of strain rate, potential, and metallurgy, which could produce anomalous results, were reported in the literature. Bradford [26], Birley [27], and Yu [28] found that, in different SCC inducing environments, cracking occurs only below a certain strain rate ( $10^{-4} \text{ s}^{-1}$ ). It should be noted that a minimum strain rate below which SCC would not occur was not detected. Scully [29] further showed that a narrow range of potentials exist around the free corrosion potential for brass in a 15 N ammoniacal solution, where there was maximum susceptibility to SCC.

Finally, various metallurgical parameters such as grain size and degree of work-hardening were reported to affect the results of SSR testing. Yu [28] demonstrated that grain size could affect the various SSR parameters such as crack velocity, frequency of cracking, and percent reduction in area. The effect of work-hardening of copper alloys on SSR testing was demonstrated by Scully [29]. It can be hypothesized that metallurgical factors influence the measured SSR parameters by affecting the strain or stressing rate at the crack tip.

### *Carbon Steels*

There were three responses to the questionnaire indicating anomalous or potentially anomalous behavior with SSR testing of carbon steels. The effect of electrochemical potential on SCC reported by Clayton [30] clearly indicated that if close attention is not paid to the potential at which the SSR test is conducted, the SSR test may exhibit anomalous behavior. He showed that SCC in continuous digesters occurs in a very narrow potential range and that, for SSR testing in this environment to be meaningful, the tests must be performed within this range. This strong potential dependence was supported by Singbeil [31,32] in tests on carbon steel in typical kraft digester liquors (see Fig. 7), by Sriram [33] who conducted potentiostatically controlled SSR tests in various caustic environments, and by Parkins [34] who studied potential dependence of cracking of carbon steel in carbonate-bicarbonate solutions. In these environments, carbon steel exhibits active-passive behavior in the potentiodynamic polarization curves and the potential range for SCC is associated with the potential range in which the active-passive transitions occur.

Speidel [35] reported on anomalies in the fracture mode of a 3.5% nickel turbine rotor steel in high-temperature pure water. The cracking mode during SSR testing was found to be transgranular while service failures were intergranular. He also reported that cracking was intergranular in fracture mechanics tests performed under constant stress intensity conditions. This apparent anomaly may be attributed to strain-rate effects. Several authors are in agreement that the SSR test is generally more severe than actual field conditions because of the high stresses generated at the crack tip. Also different fracture mechanisms may predominate at different strain rates. For example, Kim [36] showed that, while on one hand intergranular SCC in sodium carbonate/bicarbonate solutions occurs in a very narrow range of strain rates, transgranular hydrogen induced cracking is less strain rate dependent and will thus occur at a much broader range of strain rates.

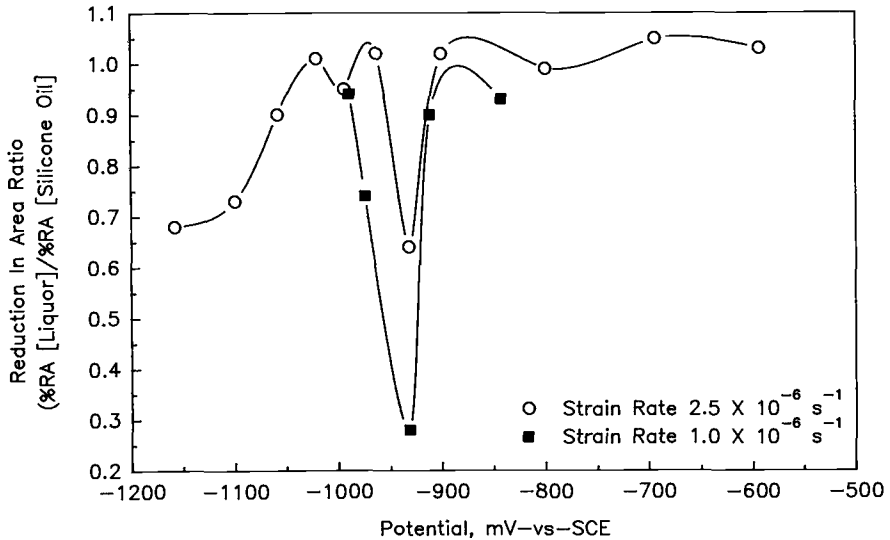


FIG. 7—Effects of potential and strain rate on the reduction in area ratio for SSR tests performed on A516 Grade 70 steel in an impregnation zone liquor containing 20–70 g/l NaOH and 20–25 g/l  $\text{Na}_2\text{S}$  at  $110^\circ\text{C}$  (after Singbeil [31]).

Murata [37] reported difficulty in reproducing SCC of a carbon steel in an organic liquid using a conventional SSR test on a specimen with a smooth gage section. However, he could reproduce SCC when using a slow bending rate test technique on prenotched specimens. In a conventional SSR test, multiple stress-corrosion cracks generally initiate in the gage section of the specimen. Thus, the crack tip strain rate varies during the test and is ill-defined. On the other hand, the strain rate can be more accurately controlled in a precracked or prenotched specimen tested at a constant deflection rate under bending or at a constant cross head speed under tension. Thus, the observation by Murata [37] suggests that stresses at the crack tip and the resulting strain rate played an important role in this material-environment system. The differences in cracking susceptibilities that were reported in the literature for the various test techniques and other environments may also relate to differences in strain rate at the crack tip.

### Aluminum Alloys

Experience with the SSR test technique for studying SCC of aluminum alloys has been good. Negative responses, indicating problems with the technique, for this alloy system, were not received from the questionnaire survey. Moreover, several researchers have reported favorable comparisons between the SSR technique and other SCC test techniques for aluminum alloys. As has been reported for other alloy systems, the optimum strain rate for SSR testing was found to be a function of the specific alloy. Thus one must exercise care in comparing SCC susceptibility for different alloys at a given strain rate.

Two articles by Buhl [38,39] were the only references in which the validity of the SSR technique was questioned for application to aluminum alloys. He performed SSR tests on three aluminum alloys in aqueous NaCl under potentiostatic control and found a ranking of SCC resistance of 7075 > 2014 > 2024 where alloy 7075 was the most resistant. On the other hand, Brown [40] performed constant load and constant strain SCC tests and found

a resistance ranking of  $2014 > 7075 > 2024$ . Based on these data, Buhl [38] concluded that the applicability of the SSR technique is doubtful for aluminum alloys. Scamans [41] attributed the discrepancy in Buhl's work to strain rate effects. However, an examination of the article by Buhl [38] suggests that the strain rate effects were taken into consideration. Buhl [39] attributed the discrepancy to differences in potential control (freely corroding versus potentiostated at the free corrosion potential). In any case, it is the reviewers' opinion that the conclusions about problems with the technique for this alloy system are based on very limited data.

### *Titanium Alloys*

A limited number of references was found in the literature on the use of the SSR technique for SCC testing of titanium base alloys [29,38,39]. For those references examined, the performance of the SSR technique has been good. In addition, negative responses, indicating problems with the technique, were not received from the questionnaire for this alloy system. Good data on strain rate effects on cracking were not found in the literature and thus care should be used in the selection of a strain rate for this system and in the application of the SSR technique.

### *Zirconium Alloys*

Negative responses, indicating problems with the SSR technique, were not received from the questionnaire for this alloy system. With one exception, the SSR technique also has compared favorably with constant load and constant strain SCC tests on zirconium alloys. The single exception involved a situation where the SSR technique appeared to be a more sensitive indicator of cracking than constant load and U-bend tests and was based on limited data.

However, as is the case for other alloy systems, aspects of the SSR technique and peculiarities of zirconium alloys make interpretation of the test results difficult in some cases. Beavers [42] and Yau [43] observed a strong orientation dependence of SCC of zirconium in nitric and hydrochloric acids, respectively. Thus, comparison of SSR results for different orientations without taking this information into consideration may lead to erroneous conclusions.

As is the case for other alloy systems, a strong dependence of cracking on strain rate also has been observed for zirconium alloys. This strain rate dependence of SCC susceptibility is more typical of stainless steels and carbon steels than of titanium alloys. The strain rate dependence was found to be a function of specimen geometry as well as environment.

## **Discussion and Conclusions**

The review of the literature and the responses to the questioning indicate that, for a specific material-environment combination, the two most important parameters controlling the SSR test are strain rate and electrochemical potential. Most reported cases of anomalous behavior can therefore be attributed to inadequate control or measurement of one or both of these parameters. In some cases, discrepancies between the SSR technique and more conventional test technique could be attributed to limitation of the latter.

When comparing different materials or environments, SSR testing at a single strain rate could produce erroneous results because of the specific material-environment dependency of the critical strain rate for cracking. Similarly, comparison of different materials or environment at a single potential could produce erroneous results because of the specific

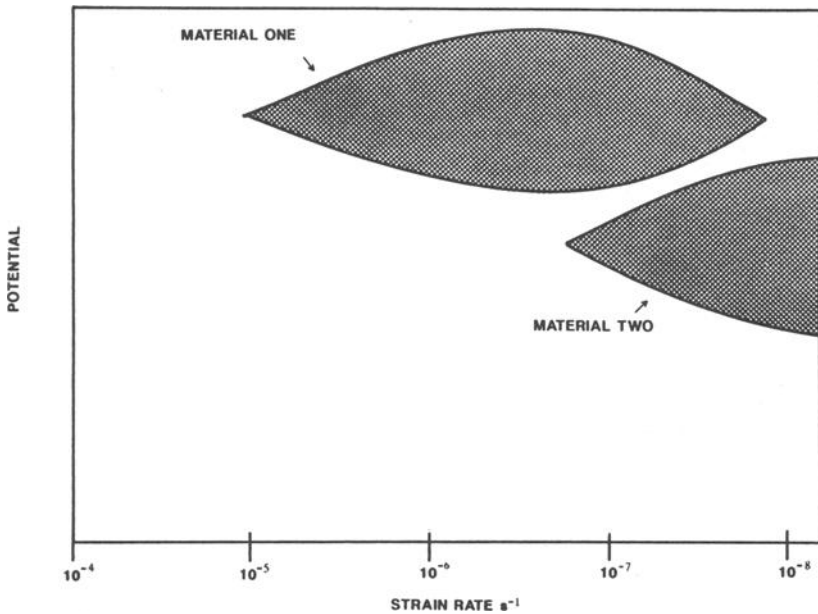


FIG. 8—Schematic diagram showing regions of electrochemical potential and strain rate in which SSR test can be conducted for specific materials.

material-environment dependency of the critical potential for cracking. Also, for environments that do not cause severe cracking or for SCC resistant materials, the SSR technique may not be practicable because very slow strain rates are required for cracking to occur.

From the review it can be concluded that the electrochemical potential should be controlled or monitored in all SSR tests. Where the critical potential range is not known, a range of SSR tests, at different potentials, should be conducted. Also, the critical strain-rate for cracking should be identified for the specific alloy-environment system under investigation. Based on the result of these preliminary SSR tests, potential-strain rate diagrams such as Fig. 8, can be constructed that will provide guidelines for SSR testing of specific alloys in specific environments.

Finally, it should be noted that extreme care needs to be taken in comparing alloys or environment for cracking susceptibility because of the specific nature of the strain rate and potential dependence.

#### Acknowledgments

The authors would like to thank MTI for sponsoring the research and R. W. Ross and the members of the resource group of MTI for their valuable input and guidance on the research. The unabridged report of the research will be available through NACE in the near future.

#### References

- [1] Beavers, J. A. and Koch, G. H. "Limitations of the Slow Strain Rate Test For Stress-Corrosion Cracking Testing," *Corrosion/91*, Paper 477.

- [2] Garner, A., Pulp and Paper Research Institute of Canada, Vancouver, B. C., Private communication, questionnaire response, 1990.
- [3] Silverman, D. C., Monsanto, St. Louis, MO, Private communication, questionnaire response, 1990.
- [4] Demo, J. J., E. I. Du Pont De Nemours and Co., Newark, DE, Private communication, MTI questionnaire response, 1990.
- [5] Daniels, W. J., "Comparative Findings Using the Slow-Strain-Rate, Constant Flow Stress, and U-Bend Stress Corrosion Cracking Techniques," *Stress Corrosion Cracking: The Slow Strain-Rate Technique*, ASTM STP 665, G. M. Ugiansky and J. H. Payer, Eds., American Society for Testing and Materials, Philadelphia, 1979, p. 347.
- [6] Baumert, K. L., Air Products and Chemicals, Inc., Allentown, PA, Private communication, MTI questionnaire response, 1990.
- [7] Bruemmer, S. M., Battelle Northwest, Richland, WA, Private communication, MTI questionnaire response, 1990.
- [8] Frechem, B. S., Rohm and Haas Co., Spring House, PA, Private communication, MTI questionnaire response, 1990.
- [9] Shibata, T., Asada, A., and Fujimoto, S., "Controlled-Potential SSRT Evaluation of Stress Corrosion Tendency in Type 304 Stainless Steel," *Corrosion Engineering*, Vol. 37, No. 9, 1988, p. 113.
- [10] Takaku, H., Kuwabara, K., and Kushiashi, M., "Susceptibility to SCC of High Nitrogen Forged Stainless Steel Pipe," *Materials Performance*, Vol. 21, No. 5, 1982, p. 36.
- [11] Bruemmer, S. M., Jones, R. H., Divine, J. R., and Johnson, Jr., A. B., "Evaluating the Intergranular SCC Resistance of Sensitized Type 304 Stainless Steel in Low-Temperature Water Environments," *Environment-Sensitive Fracture: Evaluation and Comparison of Test Methods*, ASTM STP 821, S. W. Dean, E. N. Pugh, and G. M. Ugiansky, Eds., American Society for Testing and Materials, Philadelphia, 1984, p. 256.
- [12] Yamanaka, K. and Kowaka, M., "Characteristics of the Estimation of the Susceptibility to Stress Corrosion Cracking with Different Testing Methods for Austenitic Stainless Steels," *The Sumitomo Search*, Vol. 27, No. 12, 1982, p. 23.
- [13] Andresen, P. L. and Briant, C. L., "Environmentally Assisted Cracking of Types 304L/316L/316NG Stainless Steel in 288°C Water," *Corrosion*, Vol. 45, No. 6, 1989, p. 448.
- [14] Yang, W., Zhang, M., Zhao, G., and Congleton, J., "A Comparison of U-bend and Slow Strain Rate Procedures for Assessing the SCC Resistance of Type 304 Stainless Steel in High-Temperature Water," *Corrosion*, Vol. 47, No. 4, April 1981, p. 226.
- [15] Shridhar, N. and Hodge, G., Haynes International Inc., Kokomo, IN, Private communication, MTI questionnaire response, 1990.
- [16] Kolts, J., Conoco Inc., Ponca City, OK, Private communication, MTI questionnaire response, 1990.
- [17] Wilhelm, M., Cortest Laboratories, Houston, TX, Private communication, May 1990.
- [18] Ikeda, A., Ueda, M., Okamoto, H., and Yamamoto, E., "Examination of Test Condition in SSRT Evaluation of High Alloys in Hostile Environments," *Corrosion/90*, Paper No. 272.
- [19] Asphahani, A. I., "Slow Strain-Rate Technique and Its Applications to the Environmental Stress Cracking of Nickel-Base and Cobalt-Base Alloys," *Stress Corrosion Cracking: The Slow Strain-Rate Technique*, ASTM STP 665, G. M. Ugiansky and J. H. Payer, Eds., American Society for Testing and Materials, Philadelphia, 1979, p. 279.
- [20] Was, G. S. and Crawford, D., University of Michigan, Ann Arbor, MI, Private communication, MTI questionnaire response, 1990.
- [21] Payer, J. H., Case Western Reserve University, Cleveland, OH, Private communication, MTI questionnaire response, 1990.
- [22] Bandy, R. and Van Rooyen, D., "Tests with Inconel 600 to Obtain Quantitative Stress-Corrosion Cracking Data for Evaluating Service Performance," U.S. Nuclear Regulatory Commission, BNL-NUREG-31814, 10, 1982.
- [23] Page, R. A., "Stress Corrosion Cracking of Alloys 600 and 690 and Nos. 82 and 182 Weld Metals in High Temperature Water," *Corrosion*, Vol. 39, No. 10, 1983, p. 409.
- [24] Newman, R. C., Roberge, R., and Bandy, R., "Evaluation of SCC Test Methods for Inconel 600 in Low-Temperature Aqueous Solutions," *Environment-Sensitive Fracture: Evaluation and Comparison of Test Methods*, ASTM STP 821, S. W. Dean, E. N. Pugh, and G. M. Ugiansky, Eds., American Society for Testing and Materials, Philadelphia, 1984, p. 310.
- [25] Payer, J. H., Berry, W. E., and Parkins, R. N., "Application of Slow Strain Rate Technique to Stress Corrosion Cracking of Pipeline Steel," *Stress Corrosion Cracking: The Slow Strain-Rate*

- Technique, *ASTM STP 665*, G. M. Ugiansky and J. H. Payer, Eds., American Society for Testing and Materials, Philadelphia, 1979, p. 222.
- [26] Bradford, S. A. and Lee, T., "Effect of Strain Rate on Stress Corrosion Cracking of Brass," *Corrosion*, Vol. 34, No. 3, 1978, p. 96.
- [27] Birley, S. S. and Tromans, D., "Stress Corrosion Cracking of Beta-Brasses in Water," *Metallurgical Transactions A*, Vol. 12A, No. 7, 1981, p. 1215.
- [28] Yu, J., Holroyd, N. J. H., and Parkins, R. N., "Application of Slow Strain-Rate Tests to Defining the Stress for Stress Corrosion Crack Initiation in 70/30 Brass," *Environment-Sensitive Fracture: Evaluation and Comparison of Test Methods*, *ASTM STP 821*, S. W. Dean, E. N. Pugh, and G. M. Ugiansky, Eds., American Society for Testing and Materials, Philadelphia, 1984, p. 288.
- [29] Scully, J. C., "Propagation of Stress Corrosion Cracks Under Constant Strain-Rate Conditions," *Stress Corrosion Cracking: The Slow Strain-Rate Technique*, *ASTM STP 665*, G. M. Ugiansky and J. H. Payer, Eds., American Society for Testing and Materials, Philadelphia, 1979, p. 237.
- [30] Clayton, W. E., The Procter and Gamble Co., Cincinnati, OH, Private communication, MTI questionnaire response, 1990.
- [31] Singbeil, D. L. and Garner, A., "Stress Corrosion Cracking of Kraft Continuous Digesters," *International Congress on Metallic Corrosion*, Vol. 1, No. 6, 1984, p. 187.
- [32] Singbeil, D. and Tromans, D., "Effect of Sulfide Ions on Caustic Cracking of Mild Steel," *Electrochemical Science and Technology*, Electrochemical Society, Vol. 128, No. 10, 1981, p. 2065.
- [33] Sriram, R. and Tromans, D., "Stress Corrosion Cracking of Carbon Steel in Caustic Aluminate Solutions-Slow Strain Rate Studies," *Corrosion*, Vol. 1, No. 7, 1985, p. 381.
- [34] Parkins, R. N., "Development of Strain-Rate Testing and Its Implications," *Stress Corrosion Cracking: The Slow Strain-Rate Technique*, *ASTM STP 665*, G. M. Ugiansky and J. H. Payer, Eds., American Society for Testing and Materials, Philadelphia, 1979, p. 5.
- [35] Speidel, M. O., Institute of Metallurgy, Zurich, Switzerland, Private communication, MTI questionnaire response, 1990.
- [36] Kim, C. D. and Wilde, B. E., "A Review of the Constant Strain-Rate Stress Corrosion Cracking Test," *Stress Corrosion Cracking: The Slow Strain-Rate Technique*, *ASTM STP 665*, G. M. Ugiansky and J. H. Payer, Eds., American Society for Testing and Materials, Philadelphia, 1979, p. 97.
- [37] Murata, T., Nippon Steel Corporation, Tokyo, Japan, Private communication, MTI questionnaire response, 1990.
- [38] Buhl, H., "Validity of the Slow Straining Test Method in the Stress Corrosion Cracking Research Compared with Conventional Testing Techniques," *Stress Corrosion Cracking: The Slow Strain-Rate Technique*, *ASTM STP 665*, G. M. Ugiansky and J. H. Payer, Eds., American Society for Testing and Materials, Philadelphia, 1979, p. 333.
- [39] Buhl, H., "The Validity of the Constant Straining Test Method in the SCC-Research Compared with Conventional Testing Techniques," German Institute for Aerospace Materials Research (DFVLR), *Technical Report DLR-FB 76-89*, 1976.
- [40] Brown, A. R. G. and Gray, J. A., "A Comparison of RAE Stress Corrosion Test Data on Aluminum Alloys Including the Merits of the Test Techniques," *Royal Aircraft Establishment Technical Report 74153*, 1974.
- [41] Scamans, G. M., "Correlation of Stress Corrosion Resistance with Heat Treatment of Aluminum Alloys," *Aluminum*, Vol. 57, No. 4, 1981, p. 268.
- [42] Beavers, J. A., Griess, J. C., and Boyd, W. K., "Stress Corrosion Cracking of Zirconium in Nitric Acid," *Corrosion*, Vol. 36, No. 5, 1981, p. 292.
- [43] Yau, T. and Maguire, M., "Electrochemical Protection of Zr Against SCC by Oxidizing HCl Solutions," *Corrosion*, Vol. 41, No. 7, 1985, p. 397.
- [44] Eriksson, H., AB Sandvik Steel Co., Sandviken, Sweden, Private communication, MTI questionnaire response, 1990.
- [45] McMinn, A., Failure Analysis Associates, Alexandria, VA, Private communication, MTI questionnaire response, 1990.

# Status of Standardization Activities on Slow Strain Rate Testing Techniques

---

**REFERENCE:** Kane, R. D. and Wilhelm, S. M., "Status of Standardization Activities on Slow Strain Rate Testing Techniques," *Slow Strain Rate Testing for the Evaluation of Environmentally Induced Cracking: Research and Engineering Applications*, ASTM STP 1210, R. D. Kane, Ed., American Society for Testing and Materials, Philadelphia, 1993, pp. 40-47.

**ABSTRACT:** A brief review of current test method standardization activities for slow strain rate testing will be given. This presentation will include activities involving ASTM Committee G-1.06.05 (Corrosion of Metals/SCC Test Methods/Dynamic Testing) and NACE Task Group T-1F-9 (Metallic Materials Testing Techniques for Sulfide Corrosion Cracking).

**KEYWORDS:** slow strain rate (SSR) testing, stress corrosion cracking (SCC), hydrogen embrittlement (HEC), liquid metal embrittlement (LME), test method, standardization

Over the past two decades, the slow strain rate (SSR) testing technique has emerged as a rapid and simple method that can be used for the evaluation of metals and alloys for resistance to a variety of environmental assisted cracking phenomena. These phenomena include stress corrosion cracking (SCC), hydrogen embrittlement (HEC), and liquid metal embrittlement (LME). During this time, the use of SSR testing techniques has graduated from a procedure for the development of fundamental research data to a tool for the qualification of performance properties of materials and the assessment of environmental parameters of service applications.

SSR testing uses the application of an externally applied constant extension rate typically in the range of  $10^{-4}$  to  $10^{-6}$  m/s. The dynamic straining of the specimen commonly provides an acceleration of environmentally assisted crack initiation over that typically obtained in statically stressed specimens. The benefits of this acceleration are the reduction in testing time and fewer discrepancies in test results caused by variation in crack initiation.

The benefit of reduced testing time required for SSR tests over conventional techniques has been found to be extremely useful in the evaluation of metals and alloys on a heat lot basis for use in the qualification of their cracking performance for specific service applications. In some cases, literally thousands of hours of exposure under static stress conditions can be reduced to less than a few days through the use of SSR testing techniques [1,2]. Additionally, the short testing time associated with SSR testing has promoted its use as a way to monitor service environments for conditions that will promote environmentally assisted cracking [3].

## Standardization Activities

In an effort to achieve more uniformity in SSR testing techniques, efforts have been directed toward industry standardization of the methodologies employed in SSR testing.

---

<sup>1</sup> Cortest Laboratories, Inc., Houston, TX 77269.

Three major efforts are known and documented herein. These include activities in ASTM, NACE (National Association of Corrosion Engineers), and ISO (International Standards Organization). In 1979, ASTM held a symposium entitled, "Stress Corrosion Cracking: The Slow Strain Rate Technique" sponsored by Committee G-1. The proceedings of this symposium were published as *ASTM STP 665* and contain the results of many investigations that used the SSR testing technique to develop fundamental information on environmentally assisted cracking of metals and alloys [4]. This STP has served as the principal reference in this area of testing technology for over the past ten years. The publication has helped to guide investigators and promote acceptance of the SSR test methodologies described in the results of the various studies presented in that symposium.

Through the activities of ASTM G-1.06.05 Task Group on Dynamic Test Methods for SCC, work has taken place to standardize the SSR testing technique. This effort has taken several years to develop a consensus of opinion on the scope and style of its standard activity. It has taken the form of a standard practice and ASTM G.01.06.05 is currently working on a draft of this document. It is entitled, "ASTM Practice for Slow Strain Rate Testing to Evaluate Susceptibility of Metallic Materials to Environmentally Assisted Cracking (EAC)." NACE Committee T-1 through its task group T1F9 has also been working for the past several years on a SSR testing procedure. This work has focused specifically on the evaluation of corrosion resistant alloys for oil and gas applications. It currently has a draft document entitled "Slow Strain Rate Test Method for Screening Corrosion Resistant Alloys (CRAs) for Sour Oilfield Service."

The only consensus standard that has been issued by a recognized national or international standards organization has been developed through ISO. It is presented as one part of a seven-part document entitled "Stress Corrosion Testing" (ISO 7539) which represents a general guide for several SCC testing methods.

For purposes of highlighting each of these activities, a brief overview of each will be presented here. This review should offer a better understanding of these activities. Furthermore, it is hoped that this review will promote greater interest and involvement of researchers, engineers, and their companies in the application of SSR testing techniques and the benefits derived from the standardization process. This document was also issued as a British standard.

### **ISO 7539 Part 7: Method for SSR Testing**

This SSR document is the only currently referenceable standard that addresses specific guidelines for conducting SSR tests. It was issued in 1989 as one part of a multipart document, entitled "Stress Corrosion Testing," issued by ISO. It was also ratified and issued as a part of British Standard (BS) 6980 in 1990. It is directed specifically at investigating the susceptibility of metals to SCC and hydrogen-induced failures.

The ISO standard describes the methods to be followed in conducting SSR tests by subjecting specimens to increasing strain while exposed to a specified environment. The enhanced deterioration of the test specimen resulting from the exposure conditions is usually due to the formation and growth of cracks in the gage section of the specimen. In the ISO SSR test standard, the specimen is not specifically defined. Smooth, notched, and precracked specimens may be employed. In all cases, it is recommended that a comparative evaluation be performed in which tests are conducted in both a corrosive environment and in an inert environment.

Most of the verbiage in ISO 7539 Part 7 relates to guiding the person conducting the test in the procedural aspects of SSR testing. For example, a range of strain rates to be considered ( $10^{-3}$  to  $10^{-7}$  s<sup>-1</sup>) is given along with suggested strain rates for specific metal-environment

TABLE 1—*Recommended initial strain rates for SCC.*

System	Initial Strain Rate, $s^{-1}$
Aluminum alloys in chloride solutions	$10^{-6}$
Copper alloys in ammoniacal solutions	$10^{-6}$
Ferritic steels in carbonate, hydroxide, or nitrate solutions	$10^{-6}$
Magnesium alloys in chromate/chloride solutions	$10^{-5}$
Nickel based alloys in high-temperature water	$10^{-7}$
Stainless steels in chloride solutions	$10^{-6}$
Stainless steels in pure water	$10^{-6}$
Titanium alloys in chloride solutions	$10^{-5}$

combinations (see Table 1). Information on several factors that can affect SSR test results is noted which include galvanic corrosion and crevice corrosion. Information is also given regarding the assessment and reporting of SSR test data. Ratios of the SSR data (i.e., environment versus inert) are recommended which use time-to-failure, ductility, maximum load, fracture energy, and percentage SCC on the fracture surface. Visual examination of the gage section of the specimen is also encouraged. Cases have occurred where a reduction in properties can be experienced without any evidence of cracking in the gage section of the specimen.

### **ASTM G.01.06.05: Standard Practice for SSR Testing**

#### *Background*

The current version of the draft standard practice being developed by ASTM G.01.06.05 describes the procedures for the design, preparation, and use of tension specimens for application in SSR tests used in the evaluation of the susceptibility of metals and alloys to environmentally assisted cracking. Since many of the procedures employed in many cracking phenomena are very similar, the focus of the draft practice is for evaluation of SCC, HEC, and LME. Therefore, it is not specific with regard to the nature of the chemical environment present. These test environments may contain aqueous and nonaqueous fluids and gaseous components either singularly or in combination.

The standard practice resulting from these standardization activities is intended to be used for the accelerated screening of EAC resistance of metallic materials in various exposure environments. In some cases, these environments may be intended merely for purposes of laboratory evaluation of fundamental properties. In such cases, the results may not be representative of actual service performance but may be intended only for screening or comparative evaluation of materials. Most commonly, these types of SSR tests are used in the investigation of either metallurgical or environmental variables on sensitivity to EAC. However, provisions are also given for actual simulation of service environments. In these cases, the test conditions may contain high temperatures and high pressures and exposure to potentially hazardous materials and chemicals.

### *Summary of Draft Standard Practice*

This practice describes the use of tension specimens for evaluation of resistance to EAC. In this practice, a slow constant extension rate is applied to the specimen ( $\leq 10^{-3}$  m/s). In terms of an initial strain rate on conventional specimens this relates to  $\leq 10^{-4}$  s<sup>-1</sup>. It uses a comparative evaluation of the results from a tension specimen tested in the environment of interest with that of a similarly tested specimen in a chemically inert environment. Specific information is given to the intended person performing SSR testing that this procedure should be conducted over a range of extension rates to determine the effect of the tension rate on cracking susceptibility. Furthermore, the results of SSR tests should be compared with those of constant load or constant strain tests and actual service experience, if available, to obtain a more complete understanding of the relationship of SSR data to the results from these other conventional test methods and actual service performance.

Several other ASTM standards are referenced in this draft practice document. The aim is to guide the user of SSR test methods to previously standardized procedures. Examples of these reference documents are those used to prepare and test tension test specimens in air and for SCC (ASTM E 8, Test Methods of Tension Testing of Metallic Materials, and G 49, Recommended Practice for Preparation and Use of Direct Tension Stress Corrosion Test Specimens) and for calibration of testing machines (ASTM E 6, Definitions of Terms Relating to Methods of Mechanical Testing).

A range of specimen sizes is allowed. However, care should be given to explore the effect of specimen geometry. Additionally, comparisons between SSR tests conducted in test environments and inert environments should be made using similar specimens and test methods.

The draft standard practice provides for the evaluation of cracking performance based on the comparative evaluation mentioned previously using the following parameters: (1) Time-to-Failure Ratio (RTTF), (2) Elongation Ratio (RE), and (3) Reduction in Area Ratio (RRA). One or more of these parameters may be used for qualifying materials performance. The relevance of each parameter is specific to each material and environment under consideration. Typically, values of these ratios that approach unity indicate high resistance to EAC while lower values denote increasing susceptibility to cracking.

Additionally, visual examination of the test specimens after exposure and testing is recommended since the nature of the specimen fracture and gage section can be extremely helpful in more fully documenting and understanding the specific material behavior. Provisions are also included to advise the user of SSR tests to consider other parameters as potential measures of performance. These are: (1) fracture energy (i.e., area under the stress-strain curve), (2) ultimate tensile strength, (3) strain to crack initiation, and (4) crack velocity assessment.

### **NACE T1F9: Draft SSR Test Method for CRAs in Sour Oilfield Environments**

The current draft document is concerned with the testing of CRA materials (i.e., stainless steels and nickel-base alloys) specifically subjected to tensile stress and dynamic strain in combination with low pH aqueous environments which contain hydrogen sulfide, carbon dioxide, and chloride. The purpose of the test method is to facilitate the screening of these materials for resistance to SCC at elevated temperatures in oilfield production service.

NACE T1F9 has also worked on and standardized methods for the evaluation of materials for sulfide stress cracking (SSC) which is a form of HEC. These previous efforts resulted in NACE Standard Test Method TM0177 which now incorporates constant load and deflection specimens and fracture mechanics double cantilever beam (DCB) specimens for SSC evaluation. However, it was found that such methods did not work effectively for the

evaluation of CRAs under conditions where SCC was possible (i.e.,  $>60^{\circ}\text{C}$  in acidic solutions containing both sulfide and chloride species). As indicated previously, these conditions sometimes required exposure times in excess of six months to adequately evaluate for SCC. Therefore, alternate approaches have shown the benefit of SSR testing techniques for reproducible and predictable acceleration of SCC tests.

As in the case of the ASTM G.01.06.05 standard practice, the NACE T1F9 draft test method provides for a comparative evaluation through the application of a constant extension (cross-head deflection) rate on tension specimens exposed to a test environment and compared to corresponding results obtained in an inert environment. The data from these tests are compared based on the same ratios of time-to-failure, elongation, and reduction in area as given in the draft ASTM G.01.06.05 standard practice.

Guidelines are provided for visual examination of the gage section of the tension specimen after SSR testing. Specimens are categorized according to the following classifications: (1) Class 1—Normal ductile behavior with no indication of SCC on the primary fracture surface of secondary cracking, (2) Class 2—Ductile behavior but with some shallow fissuring limited to the highly cold-worked (necked) region of the gage section immediately adjacent to the primary fracture surface, and (3) Class 3—Evidence of EAC in the gage section either resulting from cracking on the primary fracture surface or secondary cracking elsewhere, or both, in the gage section.

The major difference between the NACE and ASTM efforts is that the NACE effort is specifically directed toward the screening of particular alloys for particular service applications. Consequently, it contains procedures to obtain specific test conditions that simulate oil and gas production environments. Several suggested environments are cited. These are intended to assist in selecting test conditions that will provide relevant and comparative information on particular alloys under a particular set of environmental conditions.

For martensitic and duplex stainless steels, environments are suggested that contain 800 to 1200 psia (5.5 to 8.3 MPa) partial pressure carbon dioxide gas and 0 to 15 psia (0 to 0.1 MPa) partial pressure hydrogen sulfide with a solution containing 25 weight percent NaCl. Tests on martensitic stainless steels are conducted at  $23^{\circ}\text{C}$  around which SSC is found to be most severe. Tests on duplex stainless steels are suggested to be conducted at  $93^{\circ}\text{C}$  around which SCC is most severe for these materials. These environments are based on conditions that should differentiate materials with varying degrees of susceptibility to cracking.

The suggested environment for austenitic stainless steels and intermediate nickel base alloys (i.e., 35% to 42% nickel with approximately 20% iron) consists of 200 to 400 psia (1.4 to 2.8 MPa) hydrogen sulfide and 200 to 800 psia (1.4 to 5.5 MPa) carbon dioxide with a solution containing 25% NaCl at  $177^{\circ}\text{C}$ . For very highly alloyed nickel base alloys (i.e.,  $>50\%$  nickel and  $<20\%$  iron), the suggested environment consists of 800 to 1200 psia (5.5 to 8.3 MPa) hydrogen sulfide and 600 to 800 psia (4.1 to 5.5 MPa) carbon dioxide with a solution containing 25% NaCl to be tested at  $232^{\circ}\text{C}$ . Optionally, an additional 1 g/L elemental sulfur can be added to the test environment to simulate the increase in SCC susceptibility often found.

A round robin test program was initiated by NACE T1F9 to evaluate the variability in the test method. The program examined SCC susceptibility of a nickel base alloy (UNS N08825) in several test environments. Approximately eight test laboratories participated. The major findings were that substantial variation was reported in the absolute value of ductility parameters (elongation, reduction in area, time-to-failure); however, ductility ratios exhibited considerably less variance from laboratory to laboratory. Cracking susceptibility correlated strongly with specimen surface finish but less so with environmental simulation procedure.

### Technical Issues in Standardizing SSR Testing

SSR testing differs fundamentally from mechanical tension testing in several respects. In the first case, the strain rate and the extension rate are the same, merely slow. Figure 1 shows the variation in extension relative to cross-head displacement for a typical apparatus. The criteria for standardization on the monitoring of the extension rate are that the cross-head displacement rate can be controlled and held constant over time and varying load. Extensometers cannot be easily employed because the test specimen is usually exposed to a corrosive environment. Also, because environmental exposure is required, smaller (sub-size) tensile specimens are often employed so they can be contained in test cells and autoclaves. This often translates into smaller testing machines that generally have a greater compliance than standard mechanical property tensile test instruments. This presents some difficulty in obtaining reproducibility between test frames. Some test procedures (NACE) require the citation of the slope of the load/time (load/displacement) plot as a measure of machine compliance.

Standardization of environmental simulation procedures is usually outside the scope of most SSR test procedure documents. Many test procedures, however, require temperature control; hence reference to thermocouple and temperature calibration is required. Load measurement is a critical component of SSR testing and therefore rigorous calibration and documentation is necessary to ensure accuracy.

Specimen surface finish can be critical to the outcome of an SSR experiment. For materials that can be work hardened or that are susceptible to localized corrosion, or both, the initiation of cracking can be significantly affected by surface finish. A specimen fabricated by turning on a lathe is often subjected to localized cold work and can exhibit grooves that serve as initiation sites for localized corrosion. For these reasons, specimen fabrication practice needs

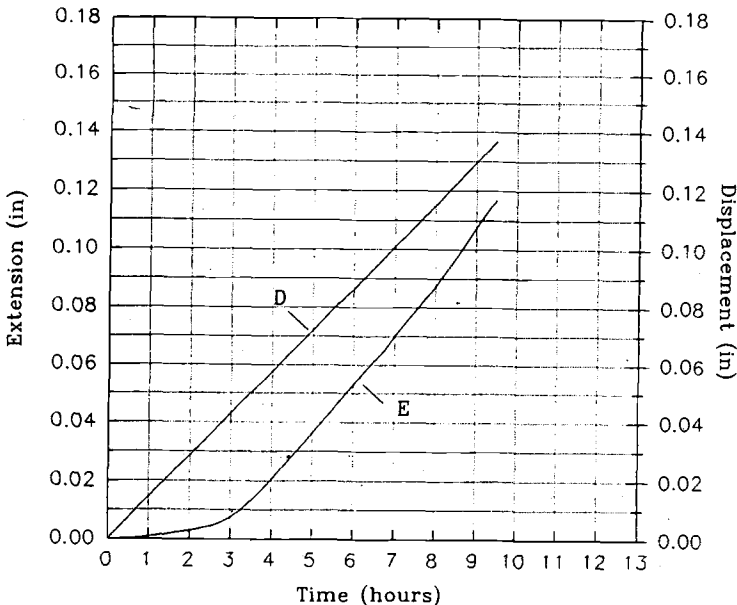


FIG. 1—Variation in specimen extension to cross-head displacement.

to be specified and closely controlled. The NACE SSR document requires a ground specimen surface with final polish to 10  $\mu\text{in. RMS}$  (0.25  $\mu\text{ RMS}$ ) or better.

A common concern for SSR standardization is that the environmental exposure should not interfere with the measurement of mechanical tensile properties. Seal friction in pressure vessels, pressure loading, and the alignment of loading relative to containment vessels are areas of concern and should be minimized through proper selection. Similarly, the test specimen is required to be electrically isolated from the test vessel and grips which might induce galvanic interactions. Galvanic interactions have been shown to substantially affect SCC susceptibility.

The main result of an SSR test is the diagnosis of cracking susceptibility, or conversely, cracking resistance. This is usually accomplished by measuring the ratio of a ductility parameter (elongation, time-to-failure, or reduction in area) to that measured in an inert environment (i.e., air, inert gas, or oil). Pass/fail criteria, where needed, are usually based on minimum acceptable values of these ratios and upon visual observations of SSC or secondary cracking (i.e., visible SCC on the gage section of the test specimen), or both. In many situations, the requirement for an unambiguous designation of susceptibility may necessitate careful scrutiny of the fracture surface by SEM and quantitative fractography. Quantitative criteria for pass/fail based on fracture surface morphology have yet to be incorporated into the test standards developed by ASTM, NACE, or ISO, as discussed herein. However, individual companies have developed their own SSR testing acceptance criteria based on service experience and extensive laboratory testing. For most applications, SSR test ratios of at least 0.80 to 0.90 have been required based on time to failure, elongation, or reduction in area, or a combination thereof, with no evidence of environmentally assisted cracking in the gage section of the specimen.

## Conclusion

As discussed herein, over the past two decades the SSR test technique has been evolving from a laboratory research tool to a standardized test for use in materials screening, heat lot qualification, and environment monitoring. Standardization efforts such as those found in ASTM, NACE, and ISO are helping to build a consensus of opinion from which consistent and accurate data can be obtained. Additionally, these activities allow researchers and engineers operating in different laboratories around the world to compare test results on a common basis.

## References

- [1] McIntyre, D. R., Kane, R. D., and Wilhelm, S. M., "Slow Strain Rate Testing for Materials Evaluation in High Temperature  $\text{H}_2\text{S}$  Environments," *Corrosion*, Vol. 44, No. 12, November 1988, pp. 920–926.
- [2] Kane, R. D., Greer, J., and Jacobs, D., "Stress Corrosion Cracking of Nickel Base Alloys in Chloride Containing Environments," *CORROSION/79*, Paper No. 174, NACE, Atlanta, GA, April 1979.
- [3] Indig, M. E., "SSRT for Hydrogen Water Chemistry Verification in BWRs," *Slow Strain Rate Testing for the Evaluation of Environmentally Induced Cracking: Research and Engineering Applications*, ASTM STP 1210, R. D. Kane, Ed., American Society for Testing and Materials, Philadelphia, 1993 (this publication).
- [4] *Stress Corrosion Cracking: The Slow Strain Rate Technique*, ASTM STP 665, G. M. Ugiansky and J. H. Payer, Eds., American Society for Testing and Materials, Philadelphia, 1979.

## DISCUSSION

---

*D. A. Jones<sup>1</sup> (written discussion)*—Is it possible to compare SCC behavior of different alloys or the same alloy at different initial strength/ductility levels in the same corrosive environment by SSRT?

*R. D. Kane and S. M. Wilhelm (authors' closure)*—Yes. However, it requires comparing SSR test data in the environment to data in an inert (SCC-free) environment for each material. Therefore, each material condition's SCC behavior is compared to its baseline properties. This comparison is usually based on ductility parameters such as elongation or reduction in area.

---

<sup>1</sup> University of Nevada, Reno, Mackay School of Mines, Reno, NV 89557.

**Uses of Slow Strain Rate SCC Testing to  
Control or Monitor Industrial Processes:  
Applications in Nuclear Power**

## SSRT for Hydrogen Water Chemistry Verification in BWRs

---

**REFERENCE:** Indig, M. E., "SSRT for Hydrogen Water Chemistry Verification in BWRs," *Slow Strain Rate Testing for the Evaluation of Environmentally Induced Cracking: Research and Engineering Applications*, ASTM STP 1210, R. D. Kane, Ed., American Society for Testing and Materials, Philadelphia, 1993, pp. 51–64.

**ABSTRACT:** The slow strain rate test (SSRT) has been used as a laboratory tool to investigate the susceptibility of austenitic stainless steels and other materials to intergranular stress corrosion cracking (IGSCC). During operation, IGSCC has occurred in the recirculation piping of Boiling Water Reactors (BWRs). The SSRT has demonstrated that weld or thermally sensitized T-304 stainless is susceptible to IGSCC in simulated BWR environments.

On the other hand, it has also been demonstrated that if the BWR environment can be modified, such that the electrochemical potential (ECP) is lowered sufficiently, IGSCC can be mitigated. A data base was developed indicating that the protection potential for T-304 stainless steel is  $\leq -0.230$  V(SHE).

In application to operating BWR power plants hydrogen is injected into the reactor feedwater system, which eventually decreases the ECP in the recirculation system. The effect in the recirculation piping water is measured by delivering water from the piping to an external test system. The test system often consists of two autoclaves, one of which measures the ECP, and the second where SSRT is performed. Typically, highly sensitized T-304 stainless steel is tested in the SSRT autoclave before hydrogen addition. In the normal BWR water chemistry ( $\sim 270^\circ\text{C}$ , 200 ppb  $\text{O}_2$ ) IGSCC occurs usually after  $>100$  h of testing. Subsequently, a second SSRT is performed when the target ECP is achieved in the BWR water, now modified with hydrogen. This second SSRT verifies that indeed IGSCC mitigation has been achieved. Results from a number of operating BWRs show that ECP control verified by SSRT provides reactor operators with criteria for IGSCC control.

**KEYWORDS:** slow strain rate techniques, intergranular stress corrosion cracking (IGSCC), Boiling Water Reactor (BWR), electrochemical potential (ECP)

The slow strain rate test (SSRT) was developed to investigate the susceptibility of materials to stress corrosion cracking (SCC) in specific environments. This paper is a historical review of how the SSRT was applied to investigate the environmental cause of intergranular stress corrosion cracking (IGSCC) in the recirculation piping in operating Boiling Water Reactors (BWRs) and eventually provide an environmental method for mitigation of the cracking phenomenon. This application required the development of SSRTs, test systems and reference electrodes capable of operation in aqueous systems that approach  $300^\circ\text{C}$ .

During BWR shutdown inspections, cracks due to IGSCC were identified in the weld heat affected zones (HAZ) of some of the austenitic stainless steel pipes in the reactor recirculation system. The cracks occurred after some period of operation in the BWR environment. This environment in the reactor recirculation system is high-purity water at about  $275^\circ\text{C}$ , with 200 to 300 ppb dissolved oxygen, some hydrogen peroxide, and about 5

---

<sup>1</sup> GE Company, Vallecitos Nuclear Center, Pleasanton, CA 94566.

## *GE BWRs* Reactor Water Conductivity

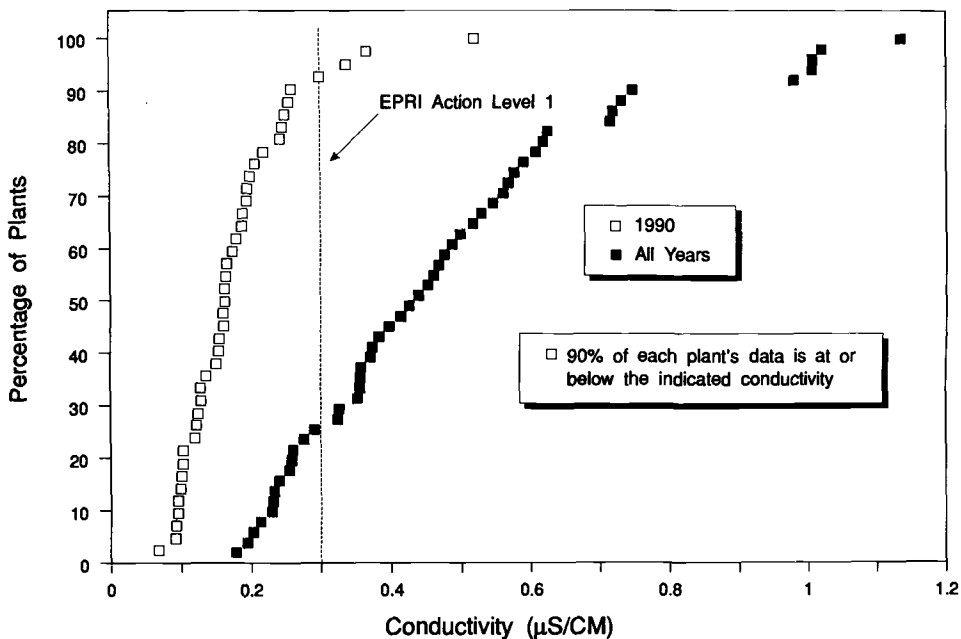


FIG. 1—Reactor water conductivity improvement over the years.

to 10 ppb dissolved hydrogen. The particular mixture of  $O_2$ ,  $H_2O_2$ , and  $H_2$  results from radiolytic reactions of water in the reactor core. The purity of the water is unaffected by the radiation and is measured by the conductivity of samples of the reactor water cooled to ambient temperature. Over the years improved power plant practices have resulted in a decrease in reactor water conductivity from about  $1.0 \mu\text{S}/\text{cm}$  to  $<0.3 \mu\text{S}/\text{cm}$  in today's operating BWRs (Fig. 1). While this improvement in water purity has undoubtedly decreased IGSCC crack growth rates of the austenitic stainless steels, the improvement has not been sufficient to eliminate the cracking. To eliminate cracking, it is possible to replace the piping system with newer austenitic stainless steels that are resistant to IGSCC. Another approach is to alter the aqueous environment within the piping system, such that the altered environment would either decrease or eliminate initiation and propagation of IGSCC in the HAZs of the pipe weldments. It is the latter approach that concerns this paper. More specifically, this paper will present how the use of the SSRT, together with electrochemical measurements, led to the original qualification of an environmental control for IGSCC mitigation and then describe the inplant testing that allowed each BWR to determine the proper environmental IGSCC mitigation procedure.

### The SSRT Developed for BWR Environments

The first high-temperature SSRT was developed some years ago by Indig and Vermilyea [1]. The device (Fig. 2) was used to study IGSCC at controlled potentials during a relatively

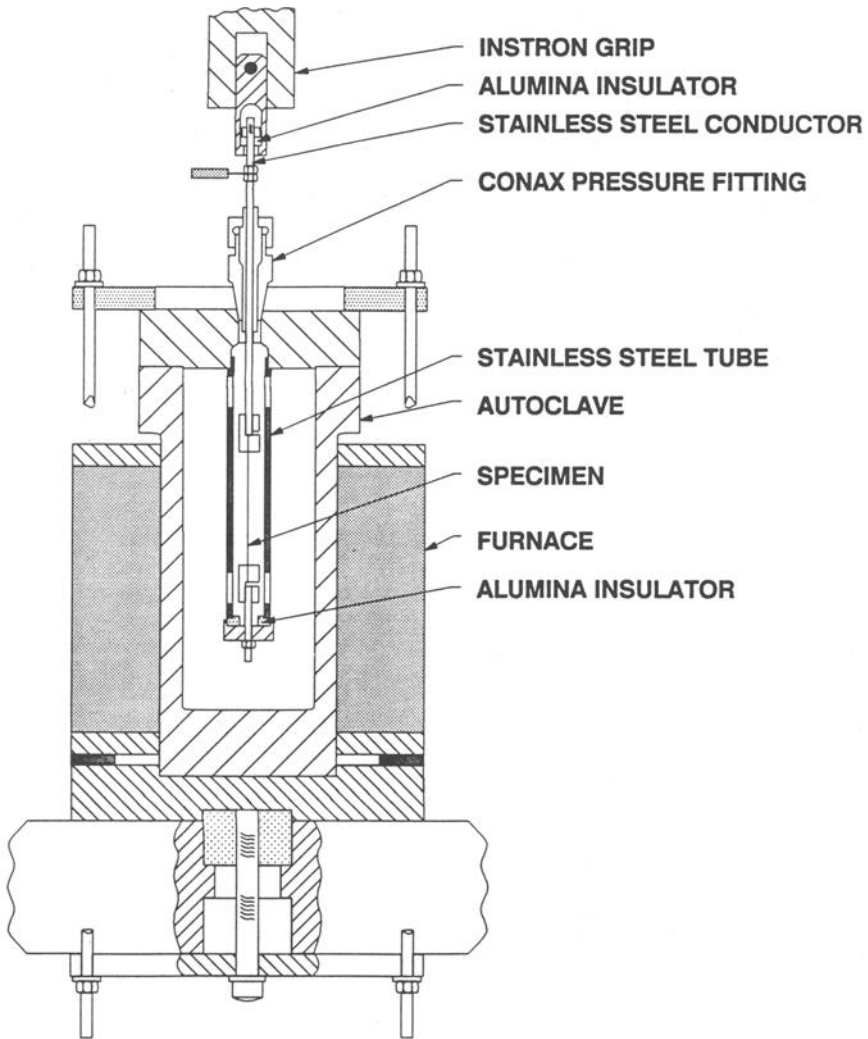


FIG. 2—First high-temperature SSRT facility.

short testing period. Furnace sensitized, austenitic stainless steel wires within a 1-L stainless steel autoclave were the SSRT specimens. In the autoclave the wires were held taut within grips. A stainless steel conductor rod, which also functioned as the pull rod, was screwed into the upper grip. The pull rod passed out of the autoclave through a Teflon® seal in a sealing gland. Above the autoclave the pull rod was linked to the drive system of the Instron machine. At the linkage the rod was insulated from ground with a shouldered alumina insulator, as indicated in Fig. 2. The concept of coupling a specimen within an autoclave to an external drive system by passing the pull rod through a low-friction Teflon seal was the basis of the subsequent SSRT device to be described in this paper.

In this first device, the potential of the stainless steel wire inside the autoclave was controlled by applying potentials to the conductor/pull rod outside the autoclave with a potentiostat. Inside the autoclave the electrolyte, 0.01 N  $\text{Na}_2\text{SO}_4$ , was heated to 289°C. It

was found that at potentials from 0.0 to 0.25 V(SHE) IGSCC occurred. When no potential was applied,  $E_{\text{corr}} = -0.54$  V(SHE), the wire specimen was eventually pulled to failure by ductile rupture. At constant applied potential, the amount of IGSCC fracture was controlled by the degree of sensitization and the extension rate (cross-head speed) of the Instron machine. The higher the sensitization and the slower the extension, the greater the percent of IGSCC on the fracture surface.

At the time of these experiments, the potential of stainless steel within an operating BWR had not been measured, nor was the effect of varying the electrochemical potential on IGSCC known in a quantitative manner.

### Electrochemical Measurements

The electrochemical potential (ECP) of T-304 stainless steel was determined in a number of operating BWRs during the years that followed. In general, high-temperature water samples were piped from the reactor recirculation piping to an autoclave outside the reactor pressure vessel, where there was a series of monitoring and reference electrodes. The sensor end of the monitoring electrode was a cylindrical electrode of T-304 stainless steel and the usual reference electrode was a silver/silver chloride electrode (Fig. 3). To deliver water samples to the autoclave with minimum loss of sample quality, a number of factors had been considered. Minimizing sample line length, maximizing the internal diameters in the sample line to minimize the internal surface area-to-volume ratio, and maximizing flow rates all contributed to maintaining water sample integrity. The results of autoclave measurements from a number of operating BWRs indicated that the steady state BWR ECP of the piping was  $0.080 \pm 0.050$  V(SHE) in the normal BWR water chemistry [2].

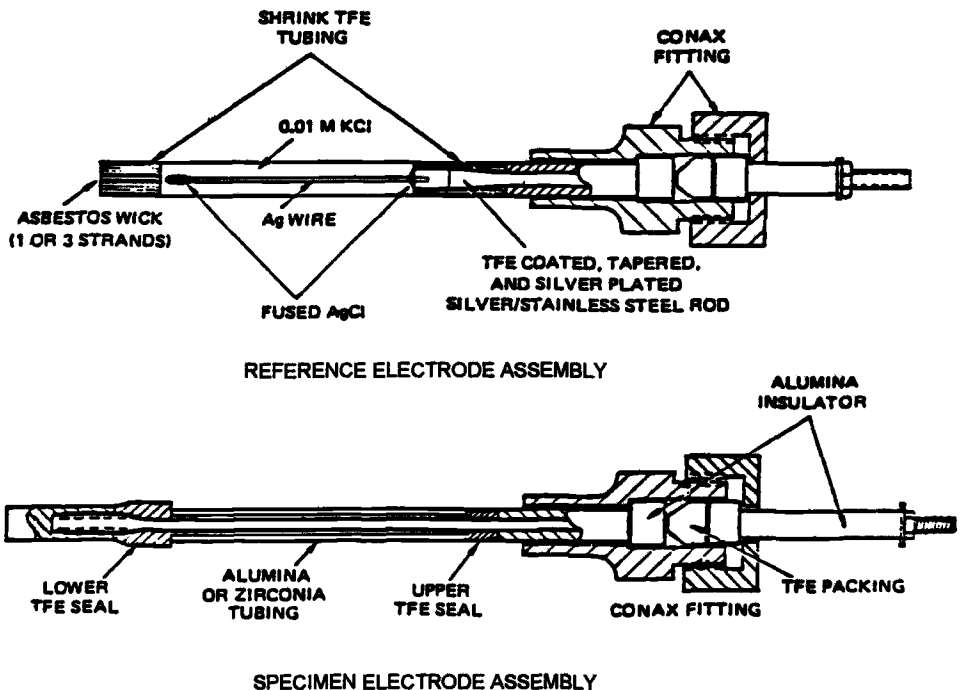


FIG. 3—Silver/silver chloride and stainless steel electrodes.

Once the BWR baseline electrochemical potential was established, meaningful experiments could be performed to determine the effect of varying the ECP on IGSCC. The major goal of this approach was to determine the potential where IGSCC could be effectively mitigated. For these studies the SSRT facility was effectively used.

### SSRT for Laboratory and In-Plant Studies

The SSRT used for most of these studies was originally developed for the study of the SCC behavior of materials considered for the steam generator of the liquid metal fast breeder reactor (LMFBR). Unlike studies for the BWR, the LMFBR steam generator studies were performed in 5 and 10% NaOH at 316°C. The SSRT facility and the test results were reported in a previous ASTM publications [3].

The SSRT facility is shown in Fig. 4. Rather than an Instron machine, the drive system consisted of a variable speed motor, variable and fixed gear reducers, and a worm gear which transformed the rotary motion of the motor into a vertical movement of the pull rod. As in the first device described in this paper, the pull rod linked to the test specimen within the autoclave was passed from inside the autoclave to the ambient through a Teflon seal in the top sealing gland. By adjusting the tightness of the sealing gland, it was possible to withdraw the pull rod from the autoclave without significant frictional losses or causing a water/steam leak. As the pull rod was withdrawn, the test specimen in the autoclave was slowly strained. The rate of extension of the test specimen for these studies was  $7.06 \times 10^{-7}$  cm/s (0.001 in./h). In these SSRTs, dog-bone tension specimens, shown in Fig. 5, were the test specimens. For the specific gage length of 1.91 cm (0.75 in.) the strain rate was  $3.7 \times 10^{-7}$  s<sup>-1</sup>. The initial laboratory tests were conducted under potentiostatic control in 0.01 N Na<sub>2</sub>SO<sub>4</sub> at 275°C by Indig and McIlree [4]. One of their major findings was that decreasing the control potential decreased the tendency for IGSCC. For T-304 stainless steel tension samples with a weld in the center of the gage, an apparent threshold potential of -0.400 V(SHE) was identified. The cracking occurred in the HAZs on either side of the weld. If the degree of sensitization was increased, a lower potential was required to eliminate IGSCC.

In these potentiostatic controlled SSRTs a silver/silver chloride electrode was used as the reference electrode. The design of the reference included an asbestos wick in the end plug that served as the liquid junction, shown in figure 3 of Ref 4. Some years later, it was determined that the asbestos wick contributed a sizable liquid junction potential of ~0.160 V [5]. If the 0.160 V correction is applied to the earlier data of Indig and McIlree [4], the -0.400 V(SHE) becomes -0.240 V(SHE), in surprising agreement with later data when this error was eliminated.

The relationship of the potentiostatically controlled electrochemical tests by Indig and McIlree to the actual BWR environment was not precisely known. For example, the use of Na<sub>2</sub>SO<sub>4</sub> not only increased the conductivity, which was required for potentiostatic control, but also resulted in an elevated pH [4], which decreases the corrosion potential. The sulfate anion has also been found to be a severe accelerator of the IGSCC of sensitized austenitic stainless steel in high-temperature water [6]. Other effects that must be considered are the resulting separation of anodic and cathodic reactions on different surfaces which occur during experiments under potentiostatic control. For example, if it is necessary to polarize the test surface anodically, a local acid condition will develop on the specimens which can accelerate crack initiation and propagation. However, SSRTs under potential control did indicate that IGSCC was directly related to the ECP. The final determination of the role of electrochemical potential and the identification of environment/potential where IGSCC could be eliminated awaited tests in actual BWR systems.

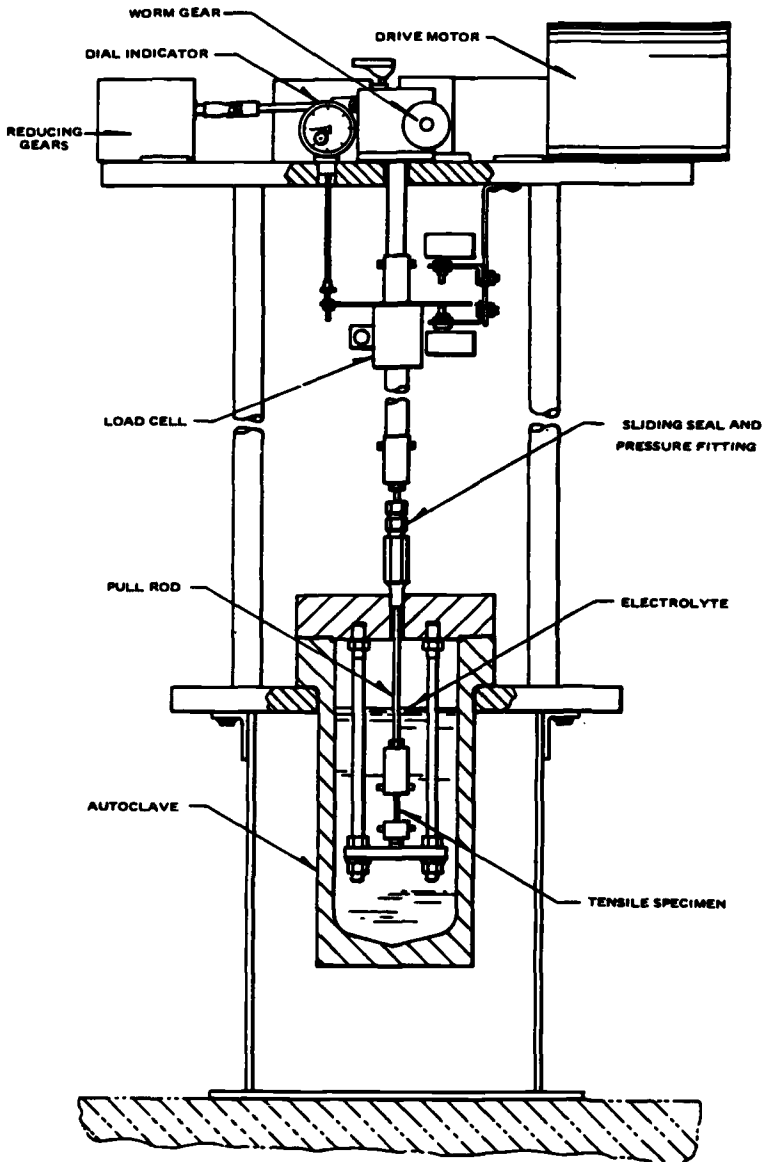


FIG. 4—SSRT facility for steam generator studies.

### SSRTs in High-Purity and BWR Waters

Electrochemical measurements performed by Indig and McIlree had shown the relationship of dissolved oxygen to the corrosion potential of T-304 stainless steel [4]. If the dissolved oxygen in BWR water, and thus the corrosion potential, could be lowered to a suitable value, the SSRTs performed under potential control indicated that IGSCC could be mitigated. A decrease of the dissolved oxygen concentration in the recirculation piping of a

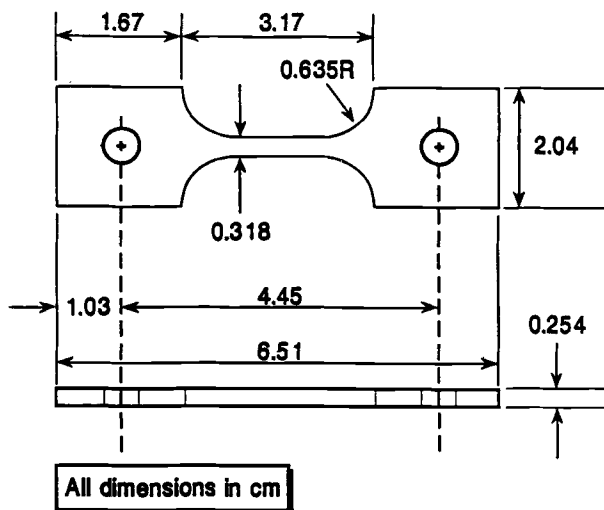
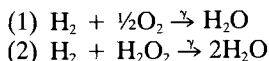


FIG. 5—Stress corrosion tension sample.

BWR could be accomplished by hydrogen addition to the feedwater system. Just as radiation had produced excess oxygen in recirculation piping, hydrogen addition with high levels of radiation could lower the dissolved oxygen and hydrogen peroxide, which is also produced, according to the following reactions:



Reactions 1 and 2 are the overall reactions in simplified form. A more detailed listing of the reactions that result in 1 and 2 are given by Burns and Marsh [7].

The reaction of excess hydrogen with the radiolytic oxidizing species occurs in the BWR downcomer region, shown in Fig. 6, where radiation dose rates are high. All of the water from the downcomer discharges to recirculation piping where IGSCC of the HAZ of pipe welds had occurred. Thus, the addition of hydrogen to the feedwater system could result in a decrease of total oxidizing species and the decrease of ECP in the recirculation piping, which should result in the mitigation of IGSCC.

This concept was tested at the Dresden-2 Nuclear Power Station, Morris, Illinois, in 1982–1983 [5]. Addition of hydrogen to the reactor feedwater was performed and the resulting ECPs were measured in an external autoclave with a sample delivery system described earlier. The SSRT facility, shown in Fig. 4, was installed in parallel with the electrochemical monitoring system. SSRTs were performed with furnace sensitized T-304 stainless steel and constant hydrogen addition to control the ECP. The major finding of these first demonstration tests clearly indicated that IGSCC could be avoided at low enough potentials. This finding, shown in Fig. 7, from Ref 5, indicates that IGSCC was eliminated at potential  $\leq -0.230$  V(SHE). While it appeared the ECP control could eliminate IGSCC, it was necessary to determine whether the potential  $-0.230$  V(SHE) was plant specific or universal.

### Application of SSRTs in HWC in Operating BWRs

A number of HWC programs were performed in operating BWRs to determine the variation of dissolved oxygen and ECP from the recirculation system with hydrogen additions

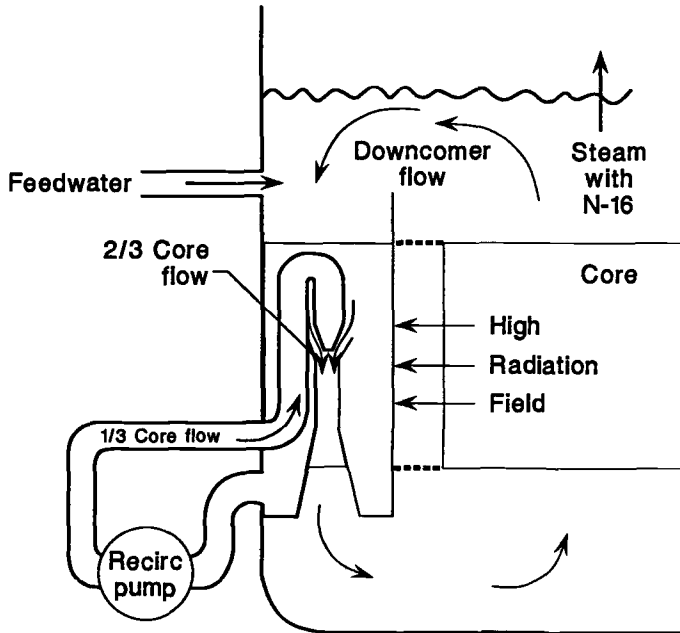
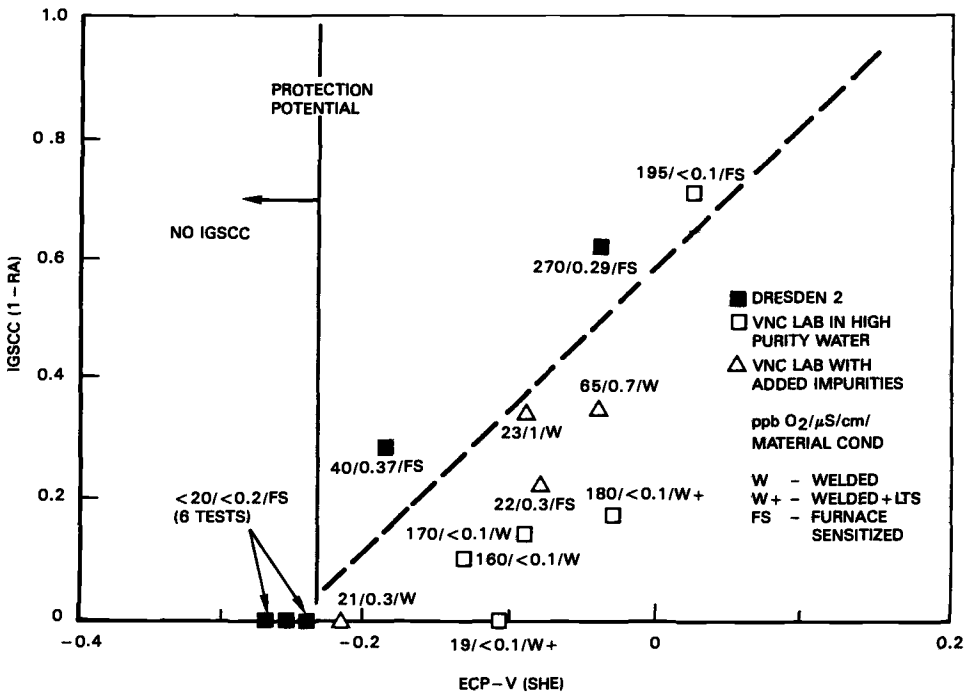


FIG. 6—Schematic of downcomer region for a jet pump boiling water reactor plant.



304SS ECP vs IGSCC INDEX - PLANT AND LAB RESULTS

FIG. 7—IGSCC of sensitized T-304SS versus ECP.

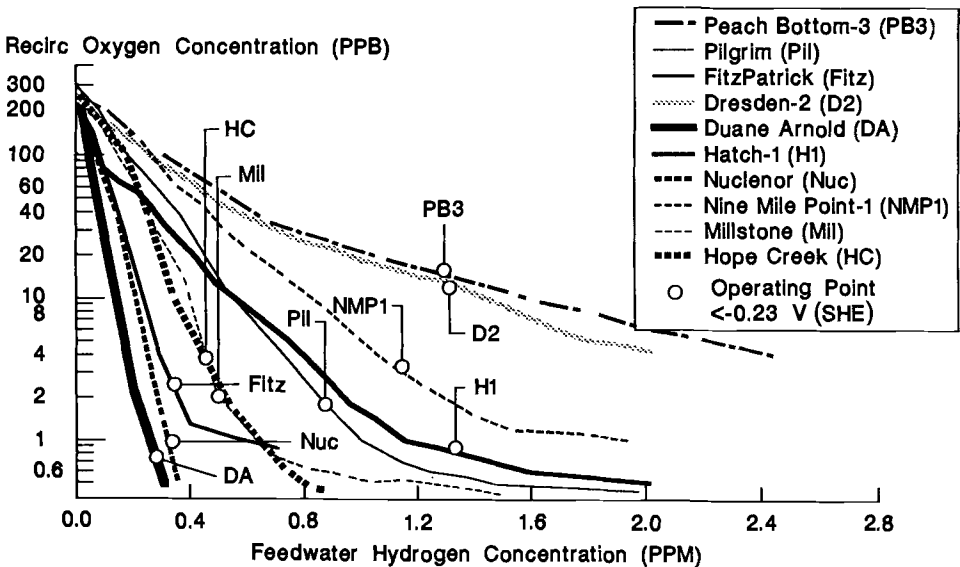


FIG. 8—Recirculation water dissolved oxygen versus feedwater hydrogen injection in BWRs; pointers indicate hydrogen requirements for IGSCC mitigation.

to the feedwater system. Figure 8 indicates that the combination of hydrogen addition to the feedwater and oxygen concentration from the recirculation system required to produce the target potential of  $-0.230$  V(SHE) on austenitic stainless steel varies among plants and is not easily predicted. From these measurements it was apparent that the dissolved oxygen concentration from the reactor recirculation water could not be used as the parameter to predict IGSCC mitigation.

SSRTs on furnace sensitized T-304 stainless steel were also conducted in the operating BWRs during the HWCs. To determine baseline behavior, SSRTs were conducted in the usual oxygenated water chemistry developed from the BWR recirculation system. In these baseline SSRTs, SCC always occurred. However, the time of sample failure by IGSCC was dependent on the water purity from the BWR. Figure 9 shows that the lower the water conductivity, the longer the failure time. The point from BWR C illustrates the effect of the mechanical condition of the tension sample on SSRT results. According to the conductivity of BWR C during the SSRT, the failure time of the furnace sensitized tension sample should have been about 140 h. However, during sample fabrication cold-work was introduced into the sample. Although the sample failure was primarily due to IGSCC, there was some transgranular brittle cleavage associated with the cold work, which decreased the SSRT failure time to less than 100 h. Thus, for comparison of SSRT results, the mechanical condition, the specific heat and test parameters should be maintained constant.

From the SSRTs, it was not possible to determine whether the increased failure times were the result of delayed time for crack initiation times or slower propagation rates. The Ford-Andresen crack growth algorithm [8] predicts that the lower the conductivity, the lower the crack growth rate. The SSRT conducted at BWR A where the conductivity was the lowest, 0.085 to 0.10  $\mu\text{S}/\text{cm}$  in normal water chemistry, was terminated after one week without sample failure. However, examination of the tension sample showed IGSCC had indeed initiated. The load-time curve during the SSRT showed load drops prior to the termination of the test (Fig. 10), which may indicate the onset of cracking. In this case, it appears that the major effect of the high-purity water was the delay of crack initiation. It

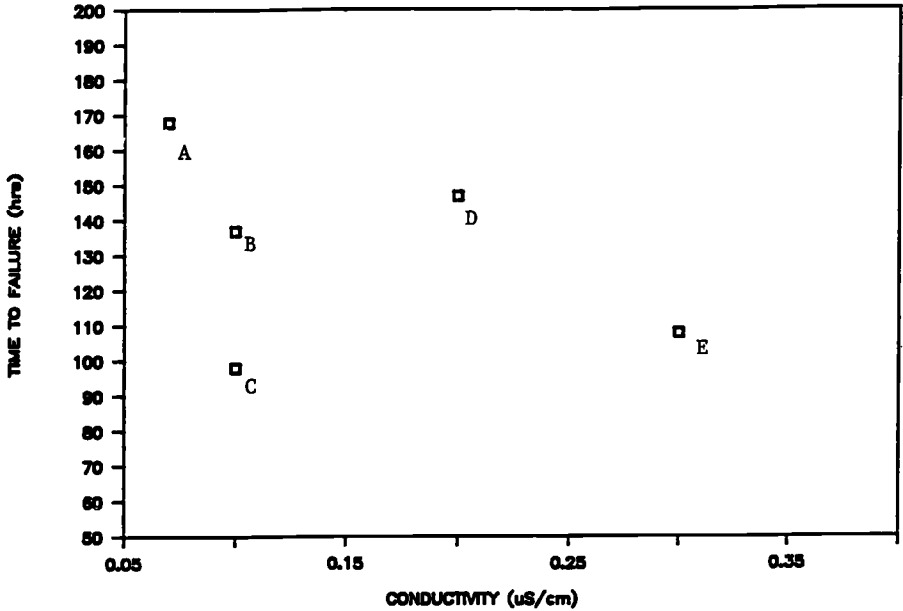


FIG. 9—Time to failure in SSRTs by IGSCC versus conductivity in BWRs.

is postulated that cracking eventually initiated at the extremely high stress of ~345 MPa (50 ksi), and after a calculated strain on the tension specimen of about 20%. The strain approximation was obtained from the load-time curve, where every ten hours on the time axis is equal to 1.3% strain.

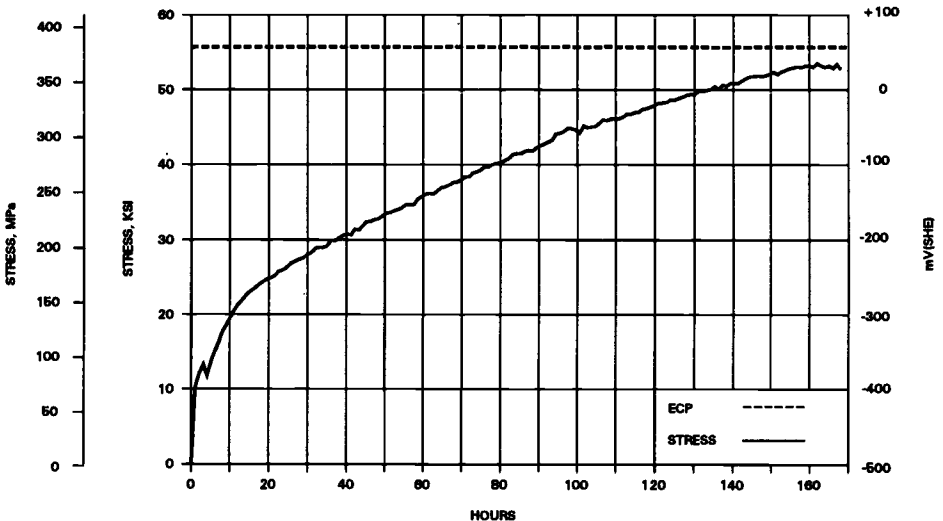


FIG. 10—Load-time curve during SSRTs in normal BWR water chemistry.

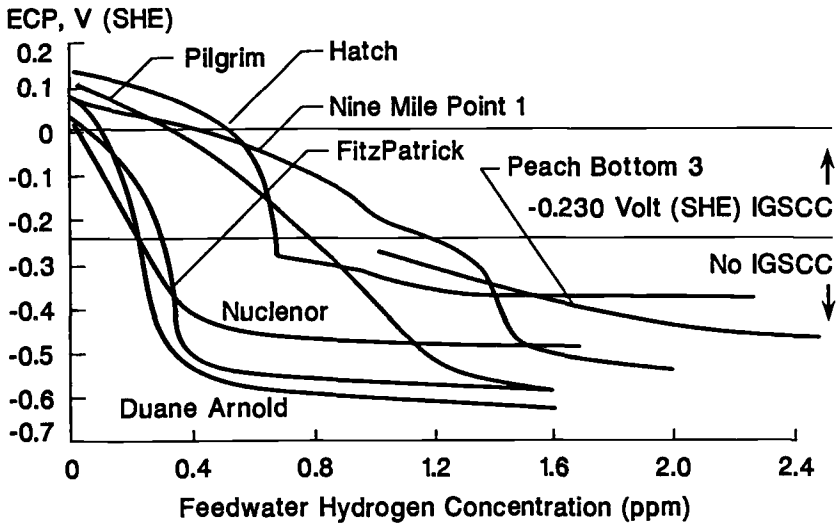


FIG. 11—Comparison of T-304SS ECPs in recirculation water sampling system versus feedwater hydrogen injection concentrations from seven BWRs.

Electrochemical Potential (V,SHE)

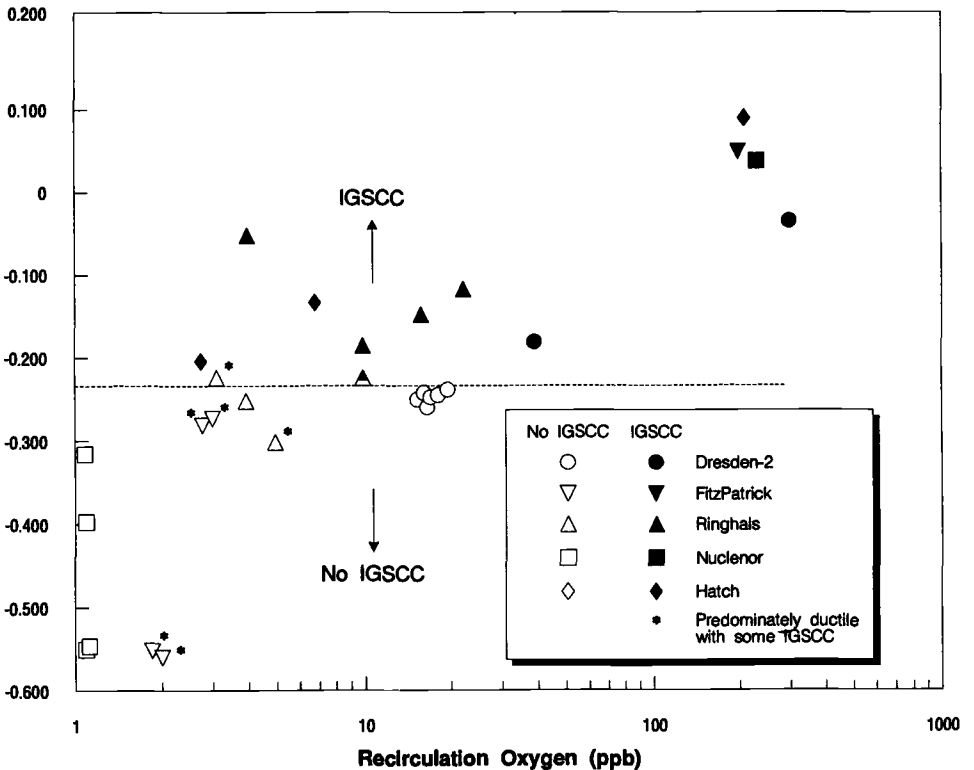
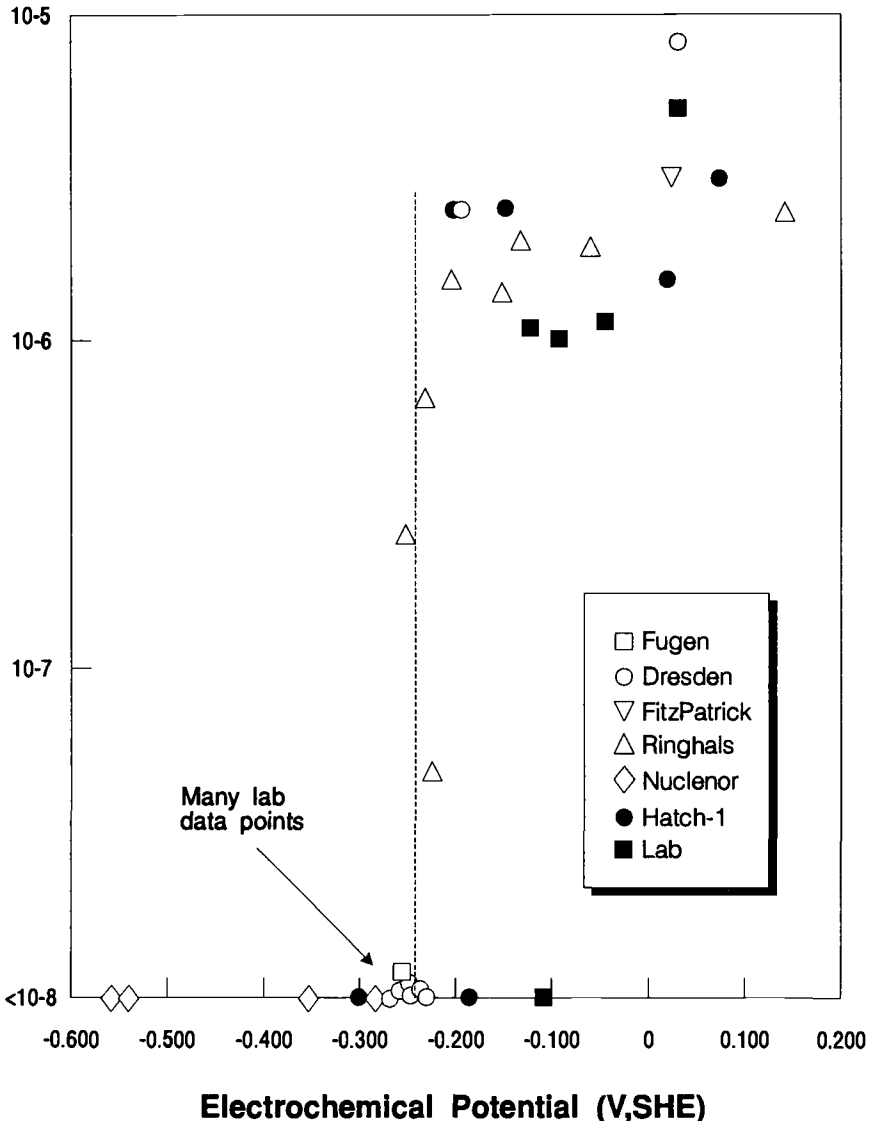


FIG. 12—SSRT results as a function of ECP and dissolved oxygen from BWR recirculation water sampling systems.

Figure 11 shows the empirical relationship of T-304SS ECP versus hydrogen injection for a number of BWRs. Once the hydrogen addition rate that resulted in a decrease of potential to  $-0.230$  V(SHE) or below was determined, the SSRT was performed. During the SSRT the ECP was continuously monitored. If the monitored stainless steel potential rose above the desired potential, the hydrogen addition rate to feedwater was re-adjusted so that the potential remained at or below  $-0.230$  V(SHE).

**Average IGSCC Crack Propagation Rate (mm/sec)**



The SSRT was run until either the tension sample failed or the test was terminated at seven days. In either case, the sample was examined for IGSCC initiation by microscopy. Figure 12 presents a summary of SSRT results as a function of ECP and dissolved oxygen. IGSCC occurred over a fairly wide range of dissolved oxygen concentration, but there were no failures below  $-0.230$  V(SHE). The major point from Fig. 12 is that ECP rather than dissolved oxygen is the controlling environmental parameter. Figure 13 presents average crack growth rates calculated from the length of cracks and the test times. The major feature of this curve is the very sharp drop-off of crack growth rates at  $-0.230$  V(SHE).

The SSRTs showed conclusively that IGSCC could be effectively mitigated in BWR recirculation systems if the potential could be controlled at or below  $-0.230$  V(SHE). Today the main emphasis is to monitor in-reactor ECP *in-situ*, rather than monitoring ECP of water samples delivered to external autoclaves. For this reason, the main application of the SSRT to BWR plant work is completed. Where direct monitoring of crack growth is required, techniques other than the SSRT are used.

The SSRT continues to be a useful laboratory technique for characterizing the environmental aspect of SCC. A recent successful application has been in the identification of a protection potential for irradiation assisted stress corrosion cracking (IASCC) [9].

## Summary

This paper presents a historical review of one application of the SSRT. In this application the SSRT was used together with ECP measurements to identify the environmental condition where IGSCC could be mitigated in BWR recirculation piping systems. The initial studies were performed in the laboratory and subsequently SSRTs were performed in operating plants. In the first application of the SSRT in an operating BWR, it was found that when the corrosion potential of T-304 stainless steel was reduced from about 0.1 V to  $-0.230$  V(SHE), IGSCC of furnace sensitized T-304 stainless steel was mitigated. Subsequently, SSRTs performed in other BWRs verified that the potential of  $-0.230$  V(SHE) did mitigate IGSCC. Crack growth calculations from SSRT tests in operating plants also yielded powerful confirmation for the electrochemical criteria. On the other hand, the SSRT showed that the relationship between IGSCC and the dissolved oxygen concentration in the recirculation water varied significantly among plants. Thus, the dissolved oxygen concentration was not useful as a control parameter for IGSCC. While in-plant SSRTs for BWRs have served their purpose, the technique continues to be useful for materials evaluation and in studies of irradiation assisted stress corrosion cracking.

## References

- [1] Indig, M. E. and Vermilyea, D. A., "The Straining Electrode Around 300°C," *Proceedings, High Temperature, High Pressure Electrochemistry in Aqueous Solutions*, National Association of Corrosion Engineers, Houston, TX, University of Surrey, England, January 1973, pp. 558-567.
- [2] Lin, C. C., Cowan, R. L., and Pathania, R. S., to be published, *Corrosion/93*, #93619, NACE, New Orleans, LA, March 1993.
- [3] Indig, M. E., "Slow Strain Rate Stress Corrosion Testing for Liquid Metal Fast Breeder Reactor Steam Generator Applications," *Stress Corrosion Cracking: The Slow Strain Rate Technique*, ASTM STP 665, American Society for Testing and Materials, Philadelphia, G. M. Ugiansky and J. H. Payer, Eds., May 1977, pp. 170-202.
- [4] Indig, M. E. and McIlree, A. R., *Corrosion*, Vol. 38, 1977, pp. 289-295.
- [5] Indig, M. E., Gordon, B. M., Davis, R. B. and Weber, J. E., "Evaluation of Inreactor Intergranular Stress Corrosion Cracking Via Electrochemical Measurements," *Proceedings of the 2nd International Symposium on Environmental Degradation of Material in Nuclear Power Systems—Water Reactors*, American Nuclear Society, LaGrange Park, IL, Monterey, CA, September 9, 1985, pp. 411-418.

- [6] Indig, M. E., Gordon, G. M., and Davis, R. B., "The Role of Water Purity on Stress Corrosion Cracking," *Proceedings, Environmental Degradation of Materials in Nuclear Power Systems—Water Reactors*, National Association of Corrosion Engineers, Houston, TX, Myrtle Beach, SC, August 22, 1983, pp. 506–531.
- [7] Burns, W. G. and Marsh, W. R., *Journal of the Chemical Society Faraday Transactions, I*, Vol. 77, No. 197, 1981.
- [8] Ford, F. P. and Andresen, P. L., "Development and Use of a Predictive Model of Crack Propagation in 304/316L, A533/A508 and Inconel 600/182 Alloys in 288°C Water," *Proceedings of the 3rd International Conference on Degradation of Materials in Nuclear Power Systems—Water Reactors*, TMS-AIME, Warrendale, PA, Traverse City, MI, 1988.
- [9] Indig, M. E., Nelson, J. L., and Wozadlo, G. P., "Investigation of the Protection Potential Against IASCC," *Proceedings of the 5th International Symposium on Environmental Degradation of Materials in Nuclear Power Systems—Water Reactors*, American Nuclear Society, LaGrange Park, IL, Monterey, CA, August 25, 1991, pp. 941–947.

# Applications of Slow Strain Rate Testing in the Nuclear Power Industry

---

**REFERENCE:** Miglin, M. T. and Miglin, B. P., “Applications of Slow Strain Rate Testing in the Nuclear Power Industry,” *Slow Strain Rate Testing for the Evaluation of Environmentally Induced Cracking: Research and Engineering Applications*, ASTM STP 1210, R. D. Kane, Ed., American Society for Testing and Materials, Philadelphia, 1993, pp. 65–82.

**ABSTRACT:** Slow strain rate (SSR) tests are widely used to evaluate materials for service in the nuclear power industry. The slow strain rate method is used to select new materials and to qualify heats of existing materials for use in components exposed to reactor coolant.

Several different modifications of the SSR test have been developed over the years to meet the demands of specific reactor applications. For testing the nickel-base superalloys used in reactor core internals, tensile bars may be notched or fatigue-precracked to accelerate crack initiation. A precracked fracture mechanics specimen may be substituted for a tensile bar. Three-point-bend loading, rather than tensile loading, is used for evaluating material resistance to cracking during the intermediate temperatures associated with reactor heat-up and cool-down transients.

For testing thin-walled steam generator tubing, tube tensile specimens or single-ligament tensile bars are used. Rather than testing in a typical steam generator environment, a high-temperature caustic environment may be chosen, with an anodic potential applied to the specimen to accelerate cracking.

The SSR test method is also applied to reactor pressure vessel steels and weldments. Tests conducted in reactor coolant environment have established the importance of maintaining low oxygen levels in preventing stress corrosion cracking (SCC).

**KEYWORDS:** nuclear power, pressurized water reactor (PWR), boiling water reactor (BWR), light water reactor (LWR), slow strain rate (SSR) test, constant extension rate test, stress corrosion cracking (SCC), stainless steel, inconel, nickel-base alloy, pressure vessel steel, steam generator

Corrosion in light water reactors (LWRs) for commercial power generation has caused losses in generating capacity from 5 to 18%. Figure 1 [1] shows the capacity losses for the two types of water-cooled reactors used for generating electricity in the United States, the pressurized water reactor (PWR) and the boiling water reactor (BWR). Most of the capacity losses in PWRs have resulted and continue to result from corrosion of steam generator tubing, and the mid-1980s peak in capacity loss in BWRs was due to stress corrosion cracking (SCC) of austenitic piping.

Figure 2 is a schematic drawing of a PWR. Heat is generated by nuclear fission in the core of the reactor, contained in the reactor pressure vessel. The primary-side coolant carries heat from the reactor core to the steam generator, where it courses through thousands of steam generator tubes, then back to the reactor vessel via the reactor coolant pumps. A pressurizer (not shown in Fig. 2) maintains the reactor coolant at operating pressure to

---

<sup>1</sup> Research specialist and section manager, respectively, Babcock & Wilcox, a McDermott Co., Research and Development Division, Alliance, OH 44601.

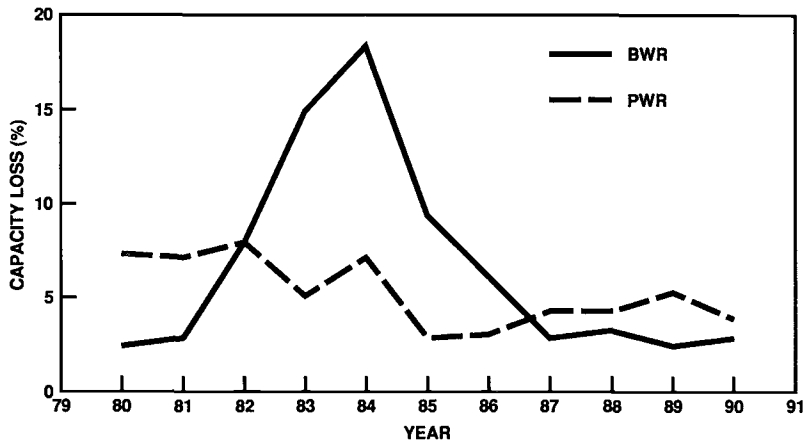


FIG. 1—Corrosion-related capacity factor losses in U.S. light water reactors [1].

prevent conversion to steam. Steam is formed from the secondary-side coolant in the steam generator, from which it is piped to the turbines for electric power generation. After passing over condensing tubes to return to the water phase, the secondary coolant is pumped back into the steam generator. The primary coolant is radioactive whereas the secondary coolant is not.

The operation of a BWR differs from a PWR in that the steam is generated directly in the reactor vessel of a BWR. There is only one coolant loop, and there are no steam generators. Radioactive steam is piped directly to the turbines and condensers, and then back to the reactor vessel.

The slow strain rate (SSR) test method has been adapted to address many of the SCC problems that occur in PWRs and BWRs. While steam generator problems are unique to PWRs and austenitic piping cracking is unique to BWRs, the two types of reactors share similar SCC problems with reactor core internals, reactor vessels, and coolant pumps. Many

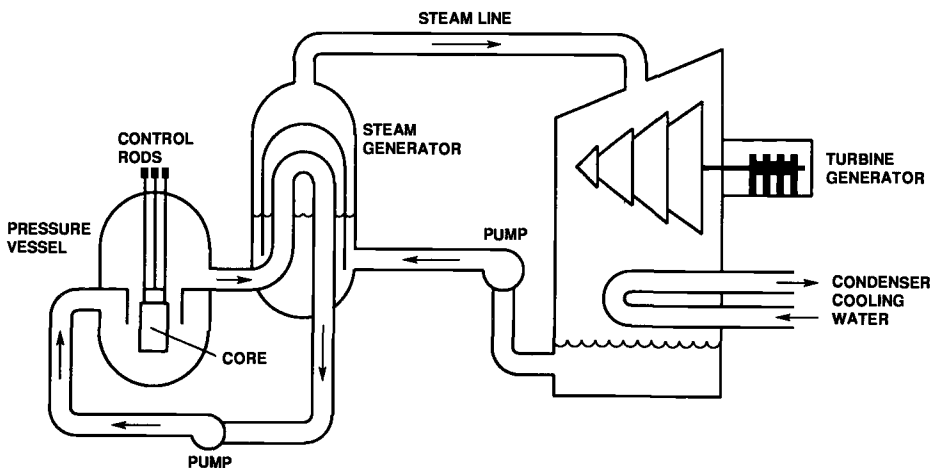


FIG. 2—Schematic drawing of a pressurized water reactor.

of these problems have been technically challenging and have inspired the development of sophisticated forms of SSR testing that go well beyond the simple pulling of tensile bars to rank material susceptibility.

### Core Internals

Core internals alloys which are susceptible to SCC fall into two categories, the precipitation-hardenable alloys and the stainless steels. The precipitation-hardenable alloys include the nickel-base alloys X-750 and 718, and the iron-base alloy A-286. These alloys are widely used for components requiring high strength, relaxation resistance, and corrosion resistance in LWR environments. Alloy A-286 experienced SCC problems early on, and has been widely replaced by either of the two nickel-base alloys. The stainless steels present in the core are comprised primarily of alloy 304 and 316, used for a wide variety of components requiring lower strengths, but good corrosion resistance. Corrosion problems have been more common for alloy 304, with radiation effects contributing to the failure process.

#### *Nickel-base Alloys*

Alloy X-750 is susceptible to two types of cracking in LWR environments. High-temperature cracking occurs near 300°C, and can be studied using conventional SSR techniques. Low-temperature cracking occurs near 100°C, and is believed to result from hydrogen embrittlement, and must be studied using precracked bend specimens.

While studies of the high-temperature cracking phenomenon in alloy X-750 have used conventional SSR techniques, they have provided useful information for students of the SSR test technique. Typically the SCC susceptibility of a material in the SSR test is evaluated by time to failure, elongation at failure, and the percent of intergranular cracking on the fracture surface. For alloy X-750 tested in reactor coolant environments, a completely intergranular fracture surface can be produced in the *absence* of SCC. Figure 3 shows the fracture surface of a SSR specimen tested in the PWR primary-side environment (~320°C deaerated water with pH adjusted by controlled additions of LiOH and H<sub>3</sub>BO<sub>3</sub>). The fracture is intergranular, but examination at higher magnification shows that failure occurred by dimpled rupture, not SCC. The fracture surface appearance is indistinguishable from that of a tensile specimen tested in air at the same temperature [2]. An SCC failure of alloy X-750 shows intergranular facets with no dimples.

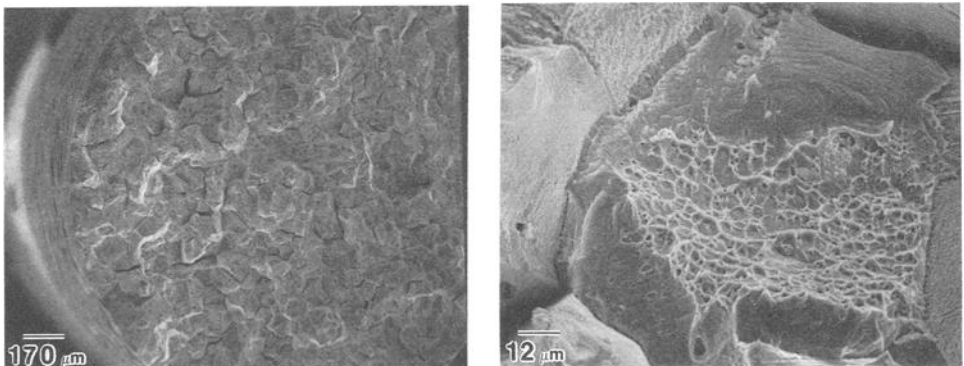


FIG. 3—Scanning electron micrographs of an alloy X-750 (1107°C/1h/AC + 704°C/20h/AC) specimen pulled until failure in 288°C PWR primary-side water [2].

Conventional SSR testing verified that a high-temperature anneal ( $\sim 1100^{\circ}\text{C}$ ) followed by a single aging treatment ( $700^{\circ}\text{C}/20\text{h}$ ) imparts good SCC resistance to alloy X-750 in high-temperature aqueous service. Previous heat treatments used in LWRs were borrowed from the jet engine industry. These heat treatments, which were developed to produce optimum creep strength, included a lower annealing temperature to minimize grain growth, and an intermediate hardening step ( $\sim 900^{\circ}\text{C}$ ) to form acicular grain boundary  $\eta$  phase to decrease grain boundary migration in service. Grain boundary  $\eta$  phase is deleterious to SCC resistance and is eliminated by a high-temperature annealing treatment. A single age near  $700^{\circ}\text{C}$  precipitates  $\gamma$  prime for high strength, while also forming globular grain boundary  $\text{Cr}_{23}\text{C}_6$ . The grain boundary chromium carbides do not have the deleterious effect on SCC resistance that  $\eta$  phase does [2].

Alloy X-750 is also susceptible to low-temperature ( $\sim 100^{\circ}\text{C}$ ) cracking, which is of concern during reactor startup and cooldown. The low-temperature cracking mechanism is probably hydrogen embrittlement. To study low-temperature cracking of alloy X-750, a SSR type of test is used, but with a precracked specimen loaded in three-point-bending. Figure 4 shows the apparatus in which the specimen is loaded. For simulation of low-temperature cracking in reactor coolant, the specimen is tested in deaerated water at  $100^{\circ}\text{C}$  by applying a constant displacement rate of  $0.005\text{ cm/min}$ . Typical test results are shown in Fig. 5. Brittle behavior is indicative of sensitivity to low-temperature cracking, and ductile behavior signifies immunity. As for high-temperature cracking, heat treatments with a high annealing temperature and a single age near  $700^{\circ}\text{C}$  show improved resistance to cracking [2].

Alloy 718 has a history similar to alloy X-750 in the commercial power industry. Until recently, the alloy has been given heat treatments developed by the jet engine industry for optimal creep resistance. These heat treatments rely on the precipitation of an acicular grain

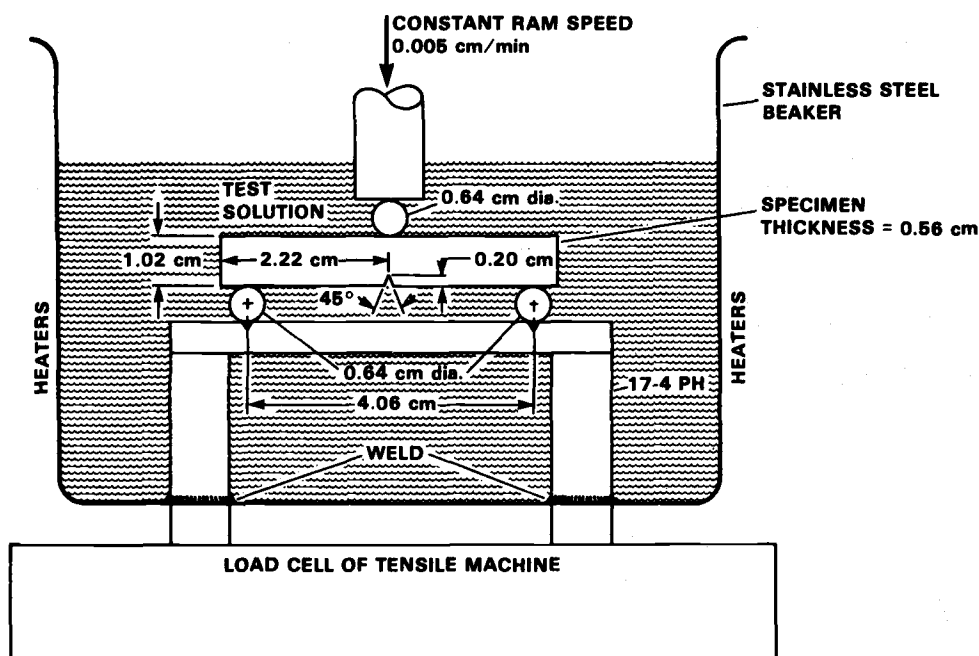


FIG. 4—Schematic drawing of apparatus for testing resistance to low-temperature cracking of alloy X-750.

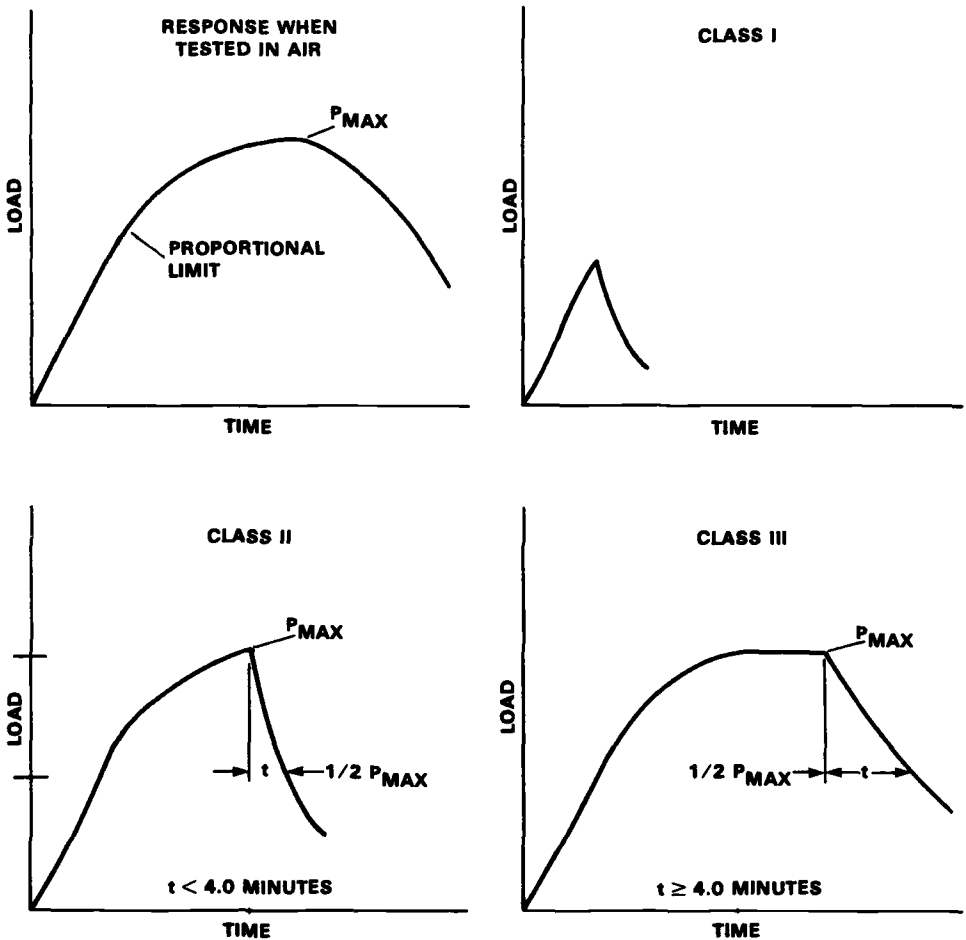


FIG. 5—Schematic diagram of low-temperature cracking test results showing: (a) load-time curve typical of an air test; (b) Class I behavior—specimen fails before the proportional limit is reached; (c) Class II behavior—load drops from  $P_{max}$  to  $1/2 P_{max}$  in less than 4 min; and (d) Class III behavior—load drops from  $P_{max}$  to  $1/2 P_{max}$  in greater than 4 min. Class I or II behavior indicates significant susceptibility to low-temperature cracking in reactor environments.

boundary phase,  $\delta$  phase, for grain boundary pinning in service.  $\delta$  phase is deleterious to SCC resistance in LWRs, and its elimination has proven beneficial for SCC resistance in LWR environments.

In the SSR test, however, alloy 718 differs from alloy X-750 in that initiation of SCC is very difficult. The same is true for statically loaded SCC specimens, except for those which have been fatigue precracked. Notching and fatigue precracking are necessary to initiate SCC in a reasonable timeframe in the laboratory, although the material initiates SCC on as-machined surfaces in service, possibly because of differences in surface finish between laboratory specimens and field components. Figure 6 is a drawing of a notched and fatigue precracked SSR specimen used to study SCC of alloy 718 plate used for fuel assembly holddown springs [3].

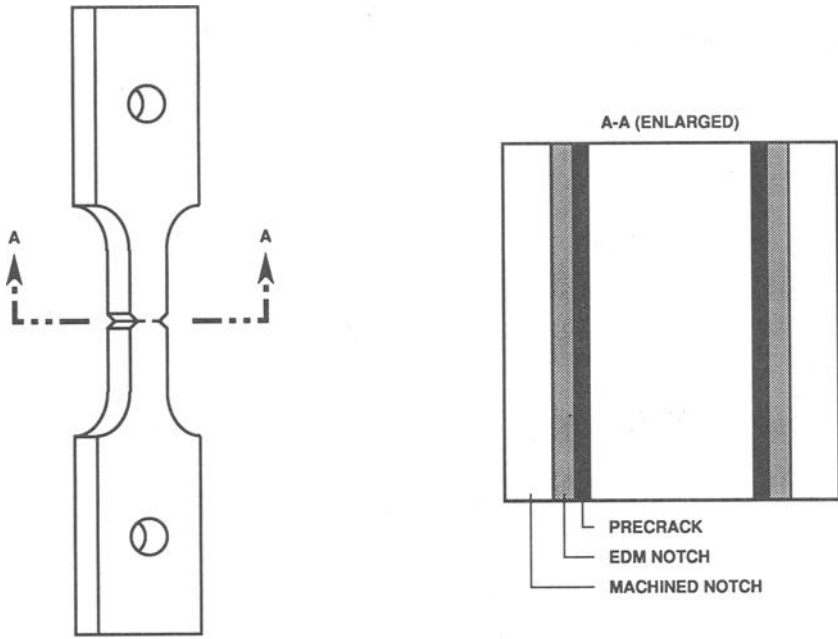


FIG. 6—Diagram of a fatigue-precracked SSR specimen.

Fatigue precracking a tensile specimen for SSR testing is tedious, and where precracking is necessary, it is advantageous to use a larger, fracture mechanics specimen such as the compact specimen in Fig. 7. Besides being easier to precrack, the compact specimen can be used to provide fracture mechanics data useful in component design and analysis. It is first necessary to instrument the specimen for measurement of the crack length during testing. When testing in high-temperature aqueous environments, reversing direct current potential

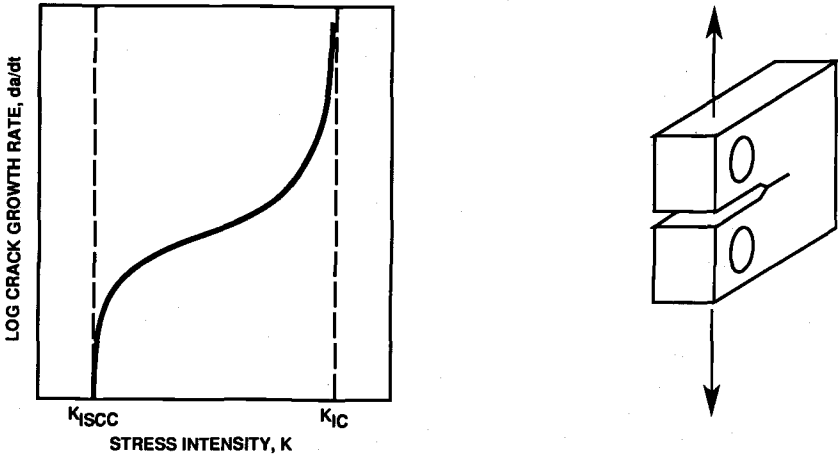


FIG. 7—Fracture mechanics approach to SCC testing. At left is a diagram of typical test results, and at right is a compact fracture specimen.

drop (DCPD) is useful for monitoring crack length. A constant current is input into the specimen sufficient to provide a small ( $\sim 100 \mu\text{V}$ ) voltage drop across the crack mouth. The voltage drop can be converted into a crack length value. Details of this procedure are in Refs 4 and 5. Electrical isolation of the specimen is required for reliable voltage readings. Zirconia, Teflon<sup>®</sup>, or oxidized zircaloy insulators can be used, depending on test temperature and environment. An apparatus in which five such specimens can be tested simultaneously is shown in Fig. 8 [6].

As with the conventional SSR test, the SSR test with the compact specimen requires an appropriate choice of strain rate. For nickel-base alloys such as alloy 718 tested in relatively benign environments such as PWR primary-side water, the critical strain rate for maximum SCC susceptibility can be as low as  $5 \times 10^{-8} \text{ s}^{-1}$  or lower [7]. SSR tests using compact specimens of alloy 718 in PWR primary-side environment at  $5 \times 10^{-8} \text{ s}^{-1}$  last several weeks. Testing at such slow rates can present schedule or budget difficulties, or both. However, for material/environment combinations such as alloy 718 in PWR primary-side environment, the alternatives are few. Static tests of precracked specimens require many months, and acceleration of the test using environmental contaminants can provide misleading results.

The SSR test using the compact specimen has been used to refine the heat treatment for alloy 718. As for alloy X-750, heat treatments which avoid the formation of the high-temperature grain-boundary pinning precipitate,  $\delta$  phase in the case of alloy 718, provide

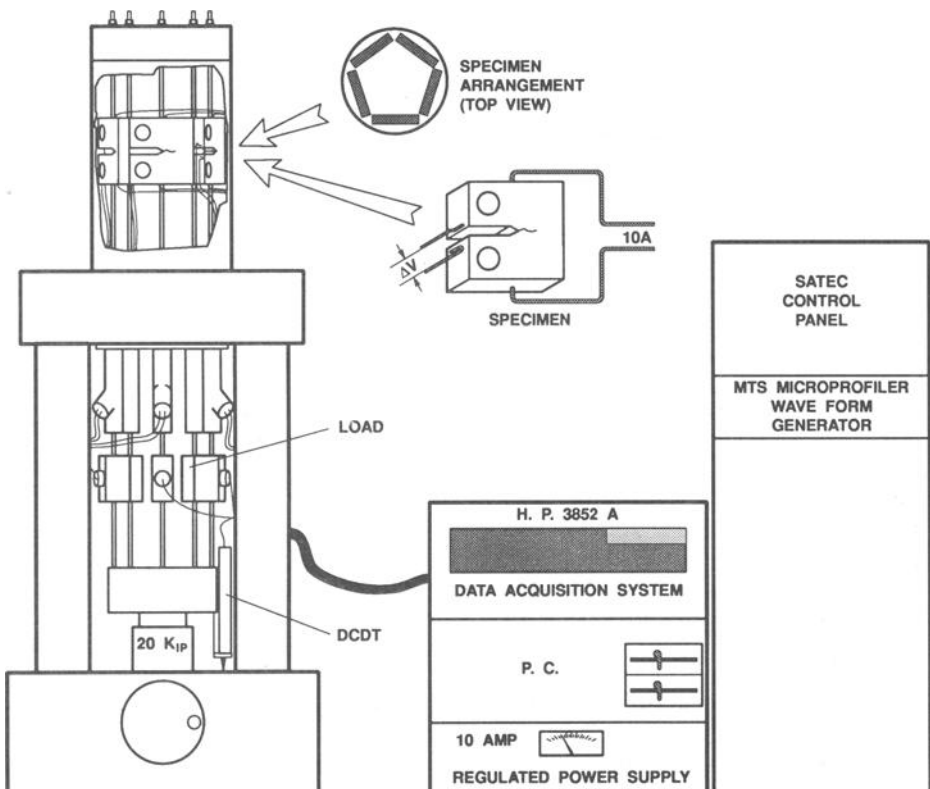


FIG. 8—Diagram of apparatus for SSR testing of five compact fracture specimens simultaneously [6].

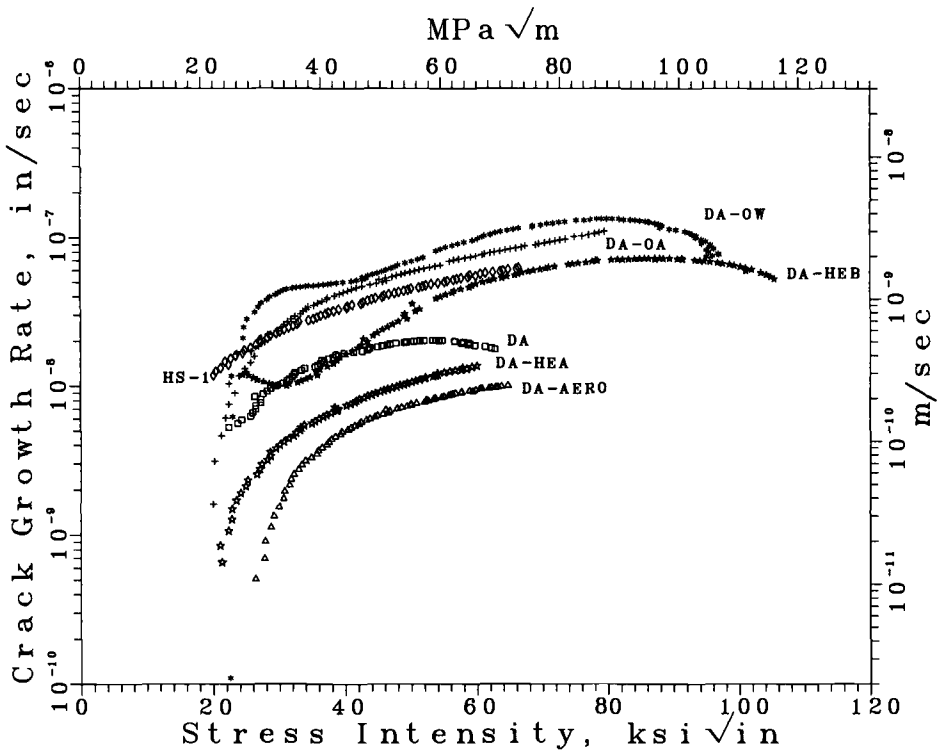


FIG. 9—Composite graph showing results of SSR tests of alloy 718 in several heat treatment conditions tested in apparatus from Fig. 8 [6].

good resistance to SCC in the PWR primary-side environment. Figure 9 shows results for alloy 718 in various heat treatment conditions [6].

### Stainless Steels

The primary challenge when using the SSR test to simulate SCC failures of in-core stainless steel components has been the simulation of radiation effects. While it has been hypothesized that radiation contributes to SCC failures of in-core high-strength nickel-base alloys, for stainless steels there is no doubt. Data of Jacobs and Kodama from SSR testing of preirradiated specimens in  $288^{\circ}\text{C}$  water show that the percent intergranular fracture increases as a function of neutron fluence, with a threshold fluence below which failure is purely ductile [8,9]. These specimens were tested in a conventional SSR test machine located in a hot cell.

Testing pre-irradiated specimens recreates the neutron damage to the material, but does not provide for radiation effects on the environment. Gamma radiation decomposes water, generating free oxygen and hydroxide and raising the electrochemical potential of the in-core components. This has been simulated in SSR testing of pre-irradiated 304SS specimens with electrochemical potential controlled by addition of oxygen to the environment [8–10]. This simulation requires the addition of a high-temperature reference electrode to monitor specimen potential, and the corresponding electrical isolation. The results demonstrated that there is a threshold electrochemical potential for irradiation-assisted SCC (IASCC),

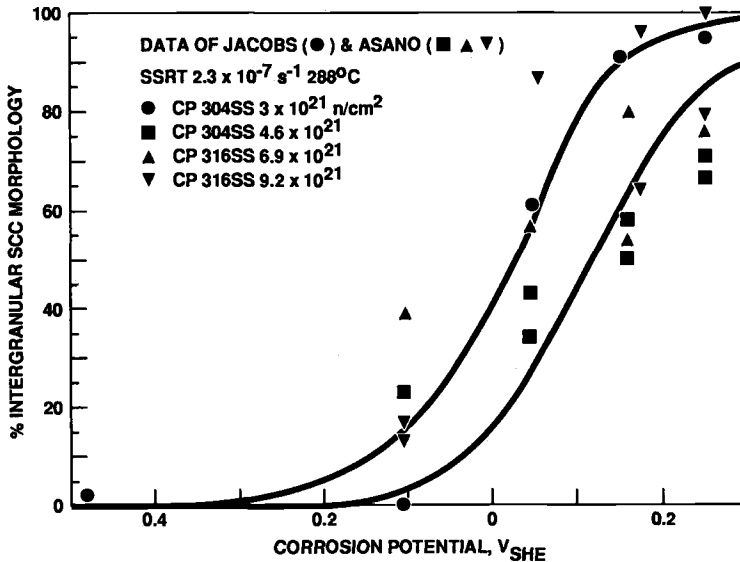


FIG. 10—Graph showing data of Jacobs [8] and Kodama [9] for pre-irradiated SS304 and 316 tested in 288°C water.

and that below the threshold potential, IASCC does not occur even if the neutron fluence is above the threshold value (see Fig. 10).

The SSR test providing the best representation of radiation effects on the material and the environment is conducted in the core of a nuclear reactor. The expanding mandrel SSR test uses a thin tube fabricated from the alloy under study, filled with  $\text{Al}_2\text{O}_3$  and  $\text{B}_4\text{C}$  (see Fig. 11). The doped alumina swells in the radiation field, straining the tube. The tubes are extracted from the reactor periodically and examined in a hot cell for cracking. Results of expanding mandrel tests have been used to confirm laboratory simulations of IASCC [11].

### Steam Generators

Although there are a number of corrosion problems in PWR nuclear steam generators, the main concern is stress corrosion cracking of the tubing. The tubing in these units provides

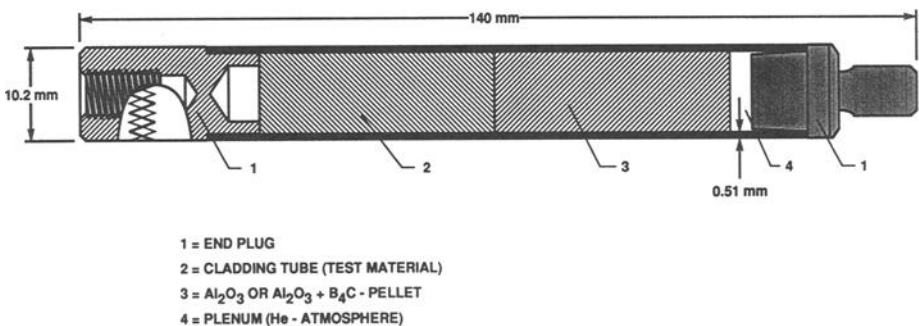


FIG. 11—Expanding mandrel specimen for in-reactor testing.

the physical barrier between the radioactive primary-side environment and the nonradioactive secondary-side water. To prevent radioactivity transport from the primary to secondary coolant, tubing leaks must be avoided.

When a leaking tube is discovered during a plant outage, the leak is repaired by either removing the tube from service or repairing the tube. Removal of the tube from service usually entails plugging the tube. Tube repair requires insertion of a sleeve to bridge the leak and hence to serve as a new pressure boundary. These tube repairs are costly both in maintenance expenses and in general thermal degradation of the unit from loss of heat transfer surface when tubes are plugged. As more plugs are installed, the unit may be derated, resulting in the utility facing the necessity of finding another source of power. Many utilities today are seriously considering steam generator replacements well before reaching the intended design life. The single cause for these replacements is corrosion, especially stress corrosion cracking of alloy 600 tubing.

Figure 12 [12] shows two of the regions of a nuclear steam generator that are susceptible to stress corrosion; U-bends and tube or support plates. In these regions, the material is highly stressed. On the secondary side, SCC occurs in tubesheet or support plate crevices where contaminants can concentrate. Thus, simulation of PWR steam generator cracking conditions in the laboratory requires the ability to stress the material while exposed to either prototypic (primary-side) or upset (secondary-side) chemistry conditions. For nuclear steam generator SCC concerns, the slow strain rate technique has been used as an accelerated test method to screen materials for environmental compatibility. These test programs generally fall into one of two categories: either deterministic in nature as to specific environmental problems, or more basic in nature in order to elucidate mechanisms. The following sections describe several of these two types of programs.

### *Deterministic SCC Programs*

Deterministic programs strive to achieve prototypic conditions to simulate nuclear steam generator conditions. These may include the test materials, the test environments, or both. For example, nuclear steam generator tubing material is highly worked. Tubing which is on the order of 19 mm in diameter with a wall thickness of 1.1 mm typically starts as a tube hollow 90 mm in diameter with a 13 mm wall thickness. To allow testing of actual tubing materials in the SSR test, double window tensile specimens have been used [13]. Figure 13 illustrates the double window tensile specimen. This specimen geometry meets the needs of the SSR test and also has the same metallurgical condition as tubing used in the power plant.

Caustic contamination is often of concern on the secondary side, especially in tubesheet or support plate crevices. Caustic attack is known to cause intergranular corrosion [14] and also SCC [15] of alloy 600. Since caustic is a known secondary-side SCC agent, electrochemical studies have been performed to define the electrochemical potential regime in which SCC occurs [15,16]. The SSR test can be further accelerated by application of electrochemical potentials that place the tubing material in a SCC susceptible region. SCC and various other degradation modes are possible, depending upon the value of the electrochemical potential.

Sensitized alloy 600 is susceptible to SCC in acid sulfur environments at low temperatures (i.e.,  $<100^{\circ}\text{C}$ ). SSR tests were performed to examine the material and environmental factors relevant to a low-temperature SCC problem of once through steam generators at Three Mile Island which were inadvertently exposed to thiosulfate on the primary side [17]. The results from this program confirmed that thiosulfate produced SCC. However, the SSR tests

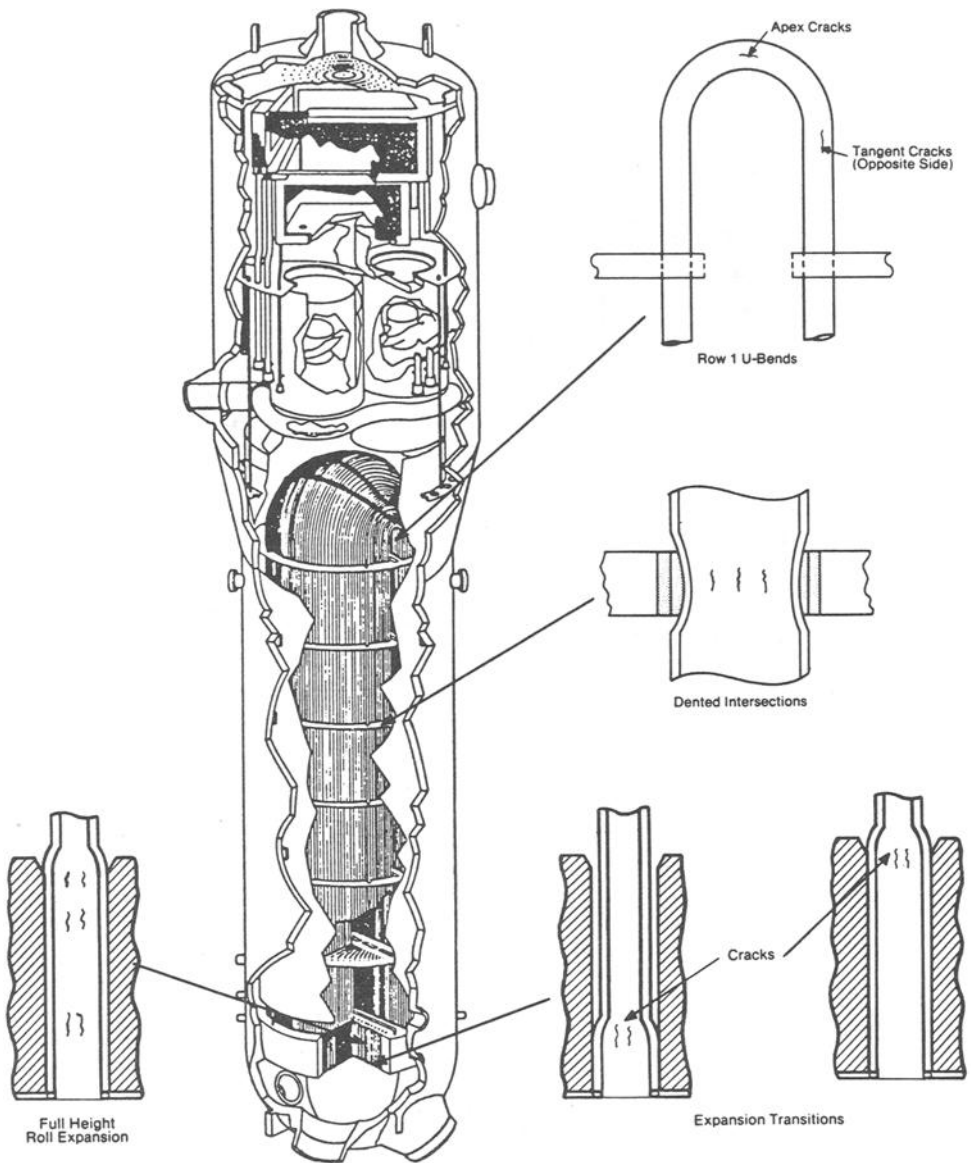


FIG. 12—Typical locations of SCC in steam generators [12].

also demonstrated that addition of lithium hydroxide mitigated the severity of attack, indicating that this SCC process could be alleviated by pH control.

SSR tests have also been used to determine the critical cracking potentials of sensitized alloy 600 [18]. These experiments were designed to compare the material behavior in creviced and bulk water environments.

SSR tests have been used to study materials for other steam generator components. In one study [19], the SSR technique was used to demonstrate the acceptability of 410 stainless

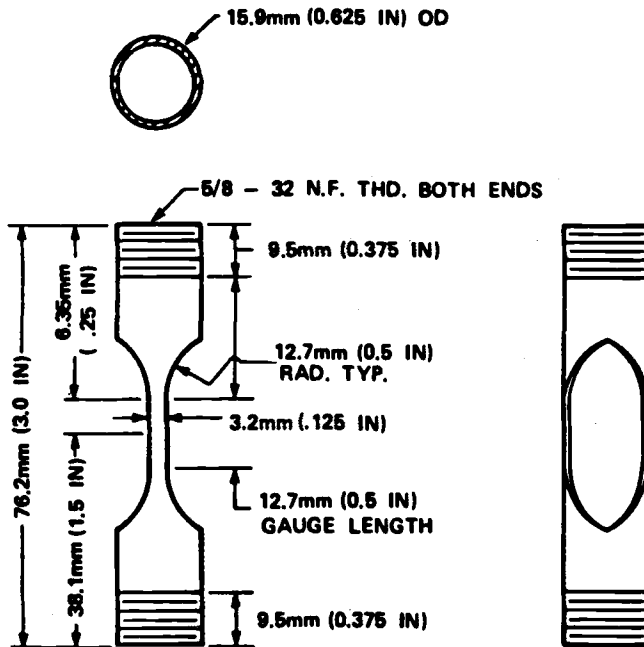


FIG. 13—Double window SSR specimen for testing steam generator tubing.

steel as lattice bar support material. Another study [20] demonstrated that welded 316 stainless steel was susceptible to SCC in environments that simulated water treatment resin intrusion.

#### *Mechanistic SCC Programs*

The SSR technique has been used to elucidate mechanistic information about SCC of steam generator tubing material. References 21 and 22 are illustrative of these programs. The former study investigated the role of grain boundary chemistries on pure water cracking of high purity heats of alloy 600. The authors concluded the creep plays a significant role in the intergranular cracking process since this form of attack was observed in SSR tests conducted in both water and argon environments at 360°C.

The latter study [22] also investigated the SCC behavior of high-purity heats of alloy 600. In this study the degree of grain boundary misorientation was studied and correlated to SCC performance. The results of SSR tests suggested to the authors that the SCC performance could be enhanced by increasing the proportions of coincident boundaries and low-angle boundaries. The authors further speculated that this enhanced SCC performance may be due to enhanced slip and hence decreasing strain energy density.

#### **Pressure Vessels**

While the primary concern with reactor pressure vessels is irradiation-induced loss in fracture toughness, SCC is a problem if it allows crack propagation to the critical flaw size for overload fracture. Limited, isolated incidents of SCC in pressure vessels have been

observed in service. Environmentally assisted cracking, encompassing both corrosion fatigue and SCC, has been studied extensively for the low-alloy pressure vessel steels A533GrB and A508Cl2. SCC of pressure vessel steels in nuclear service is influenced greatly by electrochemical potential and steel sulfur content.

SSR tests with an electrochemical potential applied to the specimen have demonstrated that there is a critical minimal potential required to induce SCC. The value of this electrochemical potential depends upon the sulfur content of the steel. Figure 14 presents the results of SSR tests conducted at  $4 \times 10^{-6} \text{ s}^{-1}$  illustrating the dependence of critical potential on sulfur content [23].

There are various hypotheses to explain the mechanism by which sulfur degrades the SCC resistance of pressure vessel steels. One of these hypotheses was investigated by monitoring the anodic current density during SSR tests of A533GrB with controlled additions of sulfide to the environment. Cathodic current due to water or sulfate reduction was eliminated by imposing a potential 50 to 100 mV above the free corrosion potential. Specimens were electrically isolated and a Ag/AgCl reference electrode and nickel-base alloy counter electrode were employed. Sulfur was added as  $\text{H}_2\text{S}$  to the deaerated water environment, with  $\text{H}_3\text{BO}_4$  and LiOH for pH control. High dissolution currents were observed when the concentration of sulfides was in excess of a threshold value, as is apparent in Fig. 15. Absorbed sulfur inhibits the nucleation of protective magnetite, raising the metal dissolution rate and hence the anodic current. Figure 16 is an illustration of this proposed mechanism. When a slip step intersects the metal surface, a small area of bare metal is exposed and magnetite grows laterally to cover it. When an MnS inclusion decoheres ahead of crack tip, sulfur

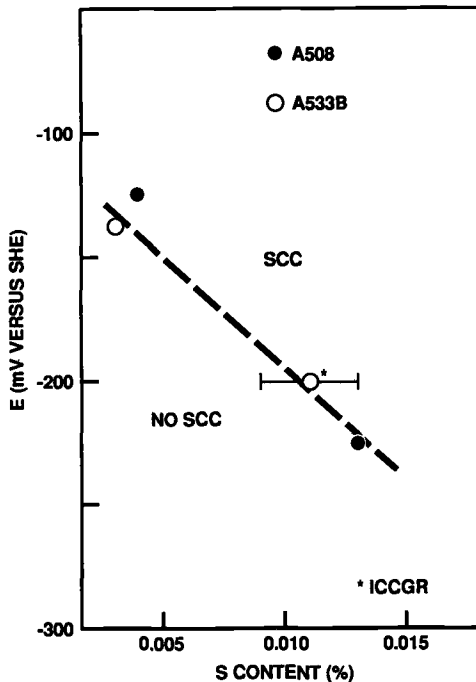


FIG. 14—Critical electrochemical potential for SCC versus sulfur content for pressure vessel steels tested in  $288^\circ\text{C}$  water [23].

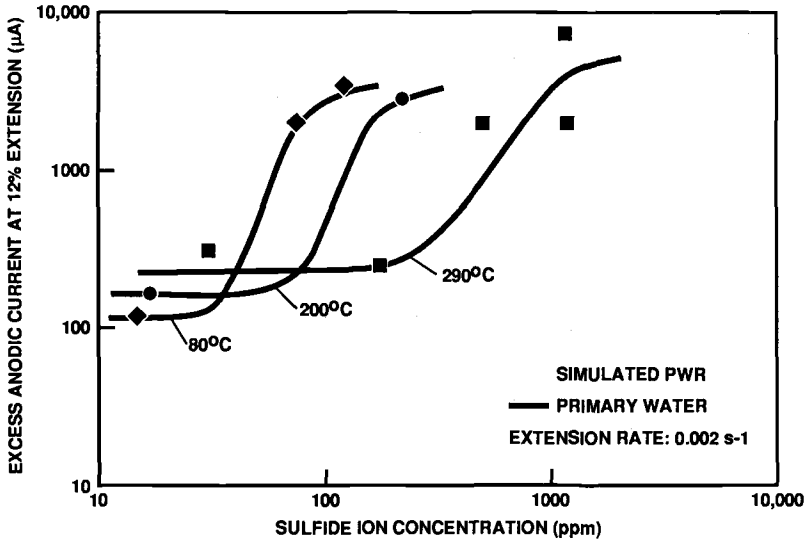


FIG. 15—SSR tests of A533GrB in simulated PWR primary-side water with sulfide additions. The specimens were polarized at 50 mV above free corrosion potential to suppress stray cathodic currents [24].

adsorbs on the bare metal surface surrounding the inclusion. When the crack tip reaches the void, a large bare metal area with adsorbed sulfur is exposed to the environment. The area is too great to be covered by lateral growth of magnetite, and nucleation of a protective magnetite layer is inhibited by adsorbed sulfur. Instead, a thick, porous, and poorly protective magnetite layer forms that does not prevent dissolution of the metal [24].

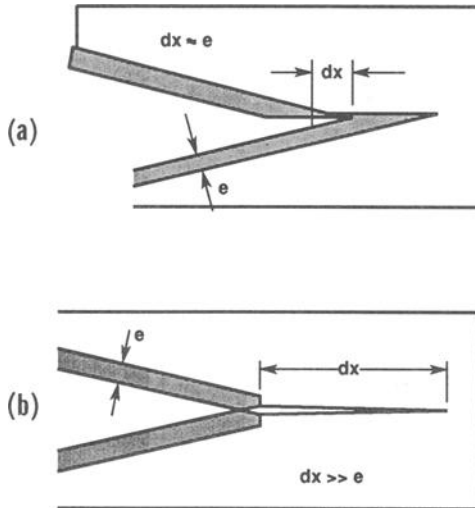


FIG. 16—Model for SCC crack advance: (a) In the absence of MnS, slip steps intersect the material surface and film repair occurs by magnetite growth. (b) Mechanical decohesion of an MnS particle (not shown) ahead of the crack tip creates a large area of bare metal surface. Adsorbed sulfide inhibits nucleation of magnetite [24].

## Pumps

Reactor coolant pumps in PWRs and recirculation pumps in BWRs have experienced shaft failures resulting from thermal fatigue with possible corrosion assistance. SSR testing of pump shaft materials includes testing of prototypical weldments. SSR testing of weldments is complicated by the differences in strength between the base metal, heat-affected zone (HAZ) and weld metal. A cross-weld specimen containing all of these three constituents in the gage section will usually fail in the weakest zone, generally the base metal, regardless of its corrosion resistance. To allow testing of all three zones simultaneously, it is preferable to use a longitudinal specimen, as shown in Fig. 17 for a prototype weld of Nitronic 50 and 308L. The results of these tests demonstrated the superior SCC resistance of Nitronic 50/308L weldments to welded alloy A-286 for reactor coolant pump shafts [25].

### Austenitic Piping

SCC of weld heat-affected zones in sensitized 304SS piping has caused greater capacity loss in the 1980s in BWRs than all other corrosion problems combined. The SSR test has played an important role in understanding this problem, and continues to play a role in mitigating the problem. The SSR test was used to define the critical electrochemical potential region for SCC, and the SSR test is used for on-line monitoring of reactor conditions to prevent SCC. Prevention of IASCC is achieved by injecting hydrogen into the feedwater. Controlled hydrogen injections prevent the buildup of  $O_2$  and  $H_2O_2$  which lead to elevated electrochemical potential values. The water chemistry is monitored on-line using the SSR test by diverting coolant into an autoclave located on-site and conducting periodic SSR tests using sensitized 304SS specimens. The details of this procedure are presented by Indig [26].

## Summary

The SSR test has had many applications in the commercial nuclear power industry, and these applications have led to several modifications of the basic SSR test method. Perhaps

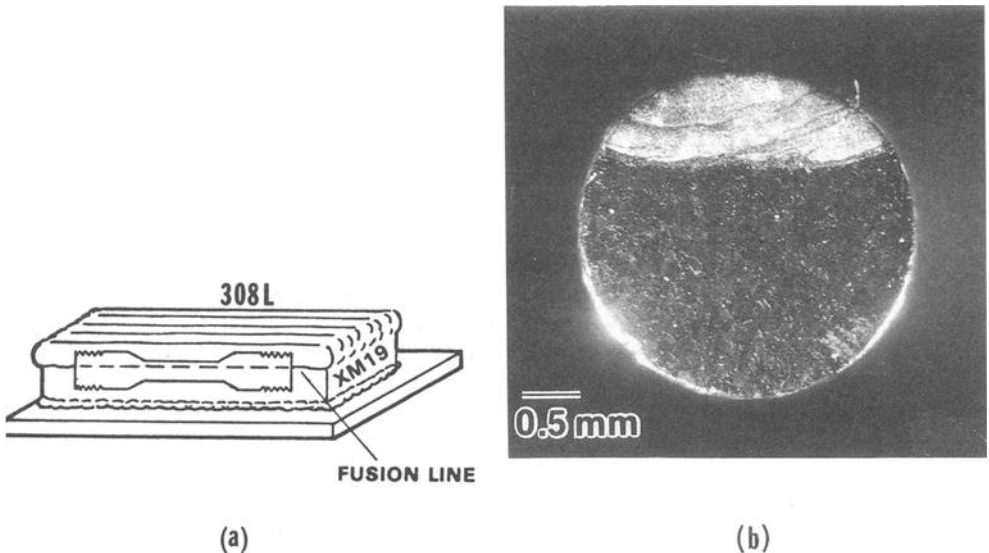


FIG. 17—SSR specimen orientation for Nitronic 50 (XM19)/308L prototypical weldment [25].

the most dramatic modifications have been developed for testing core internals alloys. For assessing high-temperature cracking resistance of precipitation-hardenable alloys, precracked compact fracture specimens are preferred because the presence of a fatigue precrack greatly increases the ease of SCC initiation in some of these alloys. With a compact fracture specimen, crack growth can be monitored during testing and results can be obtained in the form of SCC growth rate as a function of applied stress intensity factor. For measuring low-temperature cracking resistance, a precracked bend bar is used in a simpler test which does not require use of an autoclave or crack length monitoring.

Testing of stainless steels for resistance to IASCC occurring in-core presents unique challenges, which have been met by a variety of means. Radiation effects on both the environment and the material must be simulated to accurately reproduce the IASCC that occurs in-core. This has been accomplished by testing pre-irradiated specimens in a hot cell with controlled additions of oxygen to raise the electrochemical potential of the specimen to that of the alloy in-core. Radiation effects are duplicated precisely with the expanding mandrel test, in which a tubular specimen is strained in-core by the radiation-induced expansion of doped alumina inside the tube.

Testing of steam generator tubing inspired the development of the double-window specimen, which can be fabricated using production tubing to achieve the same microstructure and surface condition as steam generator tubing in the plant. The use of caustic environments with an electrochemical potential applied to the specimen accelerates the test to provide rapid information on susceptibility to failure in contaminated PWR secondary-side environments.

The SSR test has been used to identify the critical parameters in environmentally assisted cracking of pressure vessel steels. The critical electrochemical potential for cracking was defined, as well as the critical sulfur content of the material. SSR tests with applied potential and intentional additions of sulfide to the environment have been used to elucidate the mechanism by which sulfur enhances susceptibility to environmentally assisted cracking.

SSR testing of welded materials used for reactor coolant pump shafts necessitated the development of a "composite" specimen containing weld metal, HAZ, and base metal in a longitudinal arrangement such that each component experiences the same strain and strain rate during testing. This is important when testing welded materials for which the yield strengths of the base metal, weld metal, and HAZ vary significantly.

The SSR test is in use as a plant monitoring device for BWRs. To monitor the effectiveness of feedwater hydrogen injections, coolant is channeled from the plant into an autoclave, in which SSR tests of sensitized stainless steel are conducted. Appropriate feedwater hydrogen levels prevent SCC in the slipstream SSR tests.

### *Acknowledgments*

The authors would like to acknowledge the support of the Babcock & Wilcox Co. in the preparation of this document. The support of the authors' SCC research by the Electric Power Research Institute is also gratefully acknowledged.

### **References**

- [1] Marston, T. U. and Jones, R. L., "Materials Degradation Problems in the Advanced Light Water Reactors," *Proceedings of the Fifth International Symposium on Environmental Degradation of Materials in Nuclear Power Systems—Water Reactors*, ANS, LaGrange, IL, 1991, pp. 3–9.
- [2] Miglin, M. T. and Domian, H. A., "Microstructure and Stress Corrosion Resistance of Alloys X750, 718, and A-286 in Light-Water Reactor Environments," *Journal of Materials Engineering*, Vol. 9, No. 2, June 1987, pp. 113–132.

- [3] Miglin, B. P., Miglin, M. T., Monter, J. V., Sato, T., and Aoki, K., "Stress Corrosion Cracking of Commercial Grade Alloy 718 in Pressurized-Water-Reactor Primary Water," *Proceedings of the Fourth International Symposium on Environmental Degradation of Materials in Nuclear Power Systems—Water Reactors*, NACE, 1990, pp. 11-32-11-44.
- [4] Mayville, R. A., Warren, T. J., and Hilton, P. D., "Determination of the Loading Rate Needed to Obtain Environmentally Assisted Cracking in Rising Load Tests," *Journal of Testing and Evaluation*, Vol. 17, No. 4, July 1989, pp. 203-211.
- [5] Dietzel, W. and Schwalbe, K.-H., *Materialpruefung*, Vol. 28, No. 11, Nov. 1986, pp. 368-372.
- [6] Miglin, M. T., Monter, J. V., Wade, C. S., and Nelson, J. L., "Effect of Heat Treatment on Stress Corrosion of Alloy 718 in Pressurized-Water-Reactor Primary Water," *Proceedings of the Fifth International Symposium on Environmental Degradation of Materials in Nuclear Power Systems—Water Reactors*, ANS, LaGrange, IL, 1991.
- [7] Miglin, M. T. and Nelson, J. L., "Strain Rate Sensitivity of Alloy 718 Stress Corrosion Cracking," *Superalloys 718, 625 and Various Derivatives*, E. A. Loria, Ed., TMS-AIME, Warrendale, PA, 1991, pp. 695-704.
- [8] Was, G. S. and Andresen, P. L., "Irradiation-Assisted Stress-Corrosion Cracking in Austenitic Alloys," *Journal of Metals*, April, 1992, pp. 8-13.
- [9] Kodama, M., Nishimura, S., Morisawa, J., Suzuki, S., Shima, S., and Yamamoto, M., "Effect of Fluence and Dissolved Oxygen on IASCC in Austenitic Stainless Steel," *Proceedings of the Fifth International Symposium on Environmental Degradation of Materials in Nuclear Power Systems—Water Reactors*, ANS, LaGrange, IL, 1991.
- [10] Indig, M. E., Nelson, J. L., and Wozadlo, G. P., "Investigation of the Protection Potential Against IGSCC," *Proceedings of the Fifth International Symposium on Environmental Degradation of Materials in Nuclear Power Systems—Water Reactors*, ANS, LaGrange, IL, 1991.
- [11] Garzarolli, F., Alter, D., and Dewes, P., "Deformability of Austenitic Stainless Steels and Nickel-Base Alloys in the Core of a Boiling and a Pressurized Water Reactor," *Proceedings of the International Symposium on Environmental Degradation of Materials in Nuclear Power Systems—Water Reactors*, Monterey, CA, Sept. 9-12, 1985, ANS, 1986, pp. 131-138.
- [12] "Workshop Proceedings: U-Bend Tube Cracking in Steam Generators," C. E. Shoemaker, Ed., *Report No. EPRI WS-80-136*, Electric Power Research Institute, Palo Alto, CA, June 1981.
- [13] Theus, G. J. and Cels, J. R., "Slow Strain Rate Technique: Application to Caustic Stress Corrosion Cracking Studies," *Proceedings of the ASTM Symposium on Stress Corrosion Cracking—The Constant Strain Rate Technique*, Toronto, Canada, May 1977.
- [14] Miglin, B. P. and Sarver, L. W., "Mechanism of Intergranular Corrosion of Alloy 600 at Elevated Temperatures," NACE Paper No. 89 presented at Corrosion/85, Boston, MA, March 1985.
- [15] Theus, G. J., "Caustic Stress Corrosion Cracking of Inconel 600, Incoloy 800, and Type 304 Stainless Steel," *Proceedings of the International Conference on Materials for Nuclear Steam Generators*, Gatlinburg, TN, September 1975.
- [16] Bandy, R., Roberge, R., and van Rooyen, D., "Intergranular Failures of Alloy 600 in High Temperature Caustic Environments," *Proceedings of the EPRI Workshop on Primary Side SCC and Secondary Side SCC and IGC in PWR Steam Generator Tubing*, Clearwater Beach, FL, November 1983.
- [17] Bandy, R. and Kelly, K., "Electrochemical and Metallurgical Aspects of Stress Corrosion Cracking of Sensitized Alloy 600 in Simulated Primary Water Containing Sulfur Contamination," *Proceedings of the Second International Symposium on the Environmental Degradation of Materials in Nuclear Power Systems—Water Reactors*, Monterey, CA, September 1985.
- [18] Anzai, H., Kuniya, J., Shoji, T., and Yoshida, K., "Effects of Sensitization and Crevices on Critical Cracking Potential for SCC of Alloy 600," *Proceedings of the Fifth International Symposium on Environmental Degradation of Materials in Nuclear Power Systems—Water Reactors*, ANS, LaGrange, IL, 1991.
- [19] Sarver, J. M., Seelye, R. R., and Lees, M. D., "Assessment of Autogenous Type 410S Stainless Steel Welds in Replacement Steam Generator Tube Support Structures," *Proceedings of the Fifth International Symposium on Environmental Degradation of Materials in Nuclear Power Systems—Water Reactors*, ANS, LaGrange, IL, 1991.
- [20] Zhang, W., Lin, F., Gao, F., Zhou, H., and Cao, X., "Stress Corrosion Cracking of 316SS and Incoloy 800 in High Temperature Aqueous Containing Sulfate and Chloride," *Proceedings of the Fifth International Symposium on Environmental Degradation of Materials in Nuclear Power Systems—Water Reactors*, ANS, LaGrange, IL, 1991.
- [21] Sung, J. K. and Was, G. S., "The Role of Grain Boundary Chemistry in Pure Water Intergranular Stress Corrosion Cracking of Ni-16Cr-9Fe Alloys," *Proceedings of the Fifth International Symposium on Environmental Degradation of Materials in Nuclear Power Systems—Water Reactors*, ANS, LaGrange, IL, 1991.

- [22] Crawford, D. C. and Was, G. S., "The Effect of Grain Boundary Misorientation on Intergranular Cracking in Ni-16Cr-9Fe in 360°C Argon and High Purity Water," *Proceedings of the Fifth International Symposium on Environmental Degradation of Materials in Nuclear Power Systems—Water Reactors*, ANS, LaGrange, IL, 1991.
- [23] Shoji, T., Takahashi, H., Aizawa, S., and Saito, M., "Effects of Sulfate Contamination, Sulfur in Steel and Strain Rate on Critical Cracking Potential for SCC of Pressure Vessel Steels in Pressurized High Temperature Water," *Proceedings of the Third International Conference on Environmental Degradation of Materials in Nuclear Power Systems—Water Reactors*, TMS, Warrendale, PA, 1988, pp. 251–259.
- [24] Combrade, P. and Foucault, M., "Crack Tip Conditions Related to Environmentally Assisted Cracking in Pressure Vessel Steels: Effect of Temperature," *Proceedings of the Fifth International Symposium on Environmental Degradation of Materials in Nuclear Power Systems—Water Reactors*, ANS, LaGrange, IL, 1991.
- [25] Miglin, M. T., *Babcock & Wilcox Internal Report No. RDD:87:5356-01:01*, June 15, 1986.
- [26] Indig, M. E., "SSRT for Hydrogen Water Chemistry Verification in BWRs," *Slow Strain Rate Testing for the Evaluation of Environmentally Induced Cracking: Research and Engineering Applications*, ASTM STP 1210, R. D. Kane, Ed., American Society for Testing and Materials, Philadelphia, (this publication).

## Measurement of the Deformability of Austenitic Stainless Steels and Nickel-Base Alloys in Light Water Reactor Cores

---

**REFERENCE:** Dewes, P., Alter, D., Garzarolli, F., Hahn, R., and Nelson, J. L., "Measurement of the Deformability of Austenitic Stainless Steels and Nickel-Base Alloys in Light Water Reactor Cores," *Slow Strain Rate Testing for the Evaluation of Environmentally Induced Cracking: Research and Engineering Applications, ASTM STP 1210*, R. D. Kane, Ed., American Society for Testing and Materials, Philadelphia, 1993, pp. 83–101.

**ABSTRACT:** The deformability of austenitic stainless steels and nickel-base alloys was studied in an experimental program combining the influence of irradiation in a light water reactor (LWR) core environment and high stresses and strains. Tubular specimens filled with ceramic mandrels were inserted into fuel elements of both a BWR and a PWR where they were exposed to the neutron flux and coolant water of the core. The ceramic mandrels swelled under irradiation and applied high stresses to the cladding tube specimens; hence, in case of sensitive material, this led to intergranular stress corrosion cracking. The strain was varied by choosing different ceramic materials and by the axial position of the specimens in the reactor core. During the refueling shutdown of the reactor, the specimens were examined by integrity testing and diameter measurements.

The experimental setup, irradiation conditions, examination methods, and deduced stresses will be described and the status of the experiments outlined. Many materials failed by brittle cracking under the conditions applied. In the first program phase only a low phosphorus and silicon stainless steel and an Inconel alloy 718 with a special heat treatment were found to be resistant. In the second phase, when other material charges were used to verify the first results, the good performance of alloy 718 was confirmed. High purity austenitic stainless steels, however, failed during Phase 2 at the same low strain level as commercial purity material. In the case of alloy X-750, it was found that the material surface condition had a significant influence on the resistance to stress corrosion cracking.

**KEYWORDS:** stainless steel, nickel-base alloy, stress corrosion cracking, irradiation, in-pile test, light water reactor (LWR), slow strain rate testing

In the core of water cooled reactors there are components, made of austenitic stainless steels or nickel-base alloys, which are highly loaded. The experience with these components has, in general, been good. However, not enough is known of the long-term deformability of the various materials. In the high flux region of BWRs and PWRs, both austenitic stainless steels and nickel-base alloys have been observed to experience intergranular stress corrosion cracking.

It is commonly accepted that for stainless steels, irradiation, besides stress and strain, has an essential influence on the in-pile behavior, with respect to cracking of structural core parts during their reactor life. The damage phenomenon is called Irradiation Assisted Stress

---

<sup>1</sup> Research engineers, senior research engineer, and research engineer, respectively, Siemens AG, Power Generation Group (KWU), 8520 Erlangen, Federal Republic of Germany.

<sup>2</sup> Project manager, Electric Power Research Institute, Palo Alto, CA 94304.

Corrosion Cracking (IASCC). For nickel-base alloys, no information exists on whether irradiation has an additional effect on Intergranular Stress Corrosion Cracking (IGSCC) caused by the LWR coolant as a relatively pure water.

In order to close some of the gaps in the knowledge, an irradiation program was initiated in the cores of both a BWR and a PWR. In the first phase of that program the deformability of various austenitic stainless steels and nickel-base alloys was studied under irradiation at high stresses and strains in both BWR and PWR environments. The results have been reported in [1]. It was concluded that

- (1) for stainless steels, high purity with respect to phosphorus and silicon is a means of achieving high ductility during irradiation, thus avoiding damage by IASCC. For example, high-purity AISI 348 stainless steel withstood strains up to about 3% without failure, whereas commercial stainless steels failed at strains of 0.2 to 1% by intergranular cracking.
- (2) for nickel-base alloys, heat treatment is important in controlling IGSCC and, in particular, for alloy 718 a low-temperature solution anneal plus a two-step aging process seems to be required.

After that, the experimental program was continued in order to verify these findings and to broaden the experimental basis by testing other high-purity stainless steels and nickel-base alloys in various conditions. The results of the second phase of this program (Phase 2) will be reported here and the experimental setup, the irradiation conditions, and the examination methods will be described.

### **Experimental Program**

The objective of the Phase 2 program was to determine the deformability of high-purity stainless steels and nickel-base alloys in typical LWR environments. In particular, the program consisted of the following objective items

- (1) Three different types of austenitic stainless steels, all of high purity with respect to silicon and phosphorus, were tested. Additionally, one melt of commercial purity of one of these alloys was included into the test program as a control, forming a connection to the preceding program, Phase 1.
- (2) Two different nickel-base alloys were tested in altogether five variants with respect to manufacturing process and alloy purity. The variations included:
  - Alloy 718: the benefit of a proper heat treatment should be verified with two different melts of commercial and of high purity,
  - Alloy X-750; the beneficial effect of a special heat treatment found to be resistant to IGSCC in laboratory tests should be verified and the knowledge on the effect of the fabrication sequence on the behavior of alloy X-750 should be extended.
- (3) Testing was done in two different environments, in hydrogenated water in the PWR and in oxygenated water in the BWR.
- (4) The accumulated strains and the straining rates were varied by use of different swelling mandrels.

The materials were tested in the form of tubular specimens that were internally stressed by swelling mandrels consisting of sintered  $\text{Al}_2\text{O}_3$  material or  $\text{Al}_2\text{O}_3$  mixed with 3% or 5%  $\text{B}_4\text{C}$  in order to obtain different irradiation induced swelling rates.

## Test Materials

The chemical composition of the test materials is given in Table 1. The data were taken either from suppliers' certificates or have been specially measured on the final products. Table 2 lists the tensile properties at room temperature and the grain size data of the test materials. For stainless steels, the high-purity variants have reduced strength with considerable ductility, compared to standard stainless steels. For the nickel-base alloys, there is a large influence of the solution annealing temperature on strength. Alloys 718 and 1.4981 were fine-grained, the other materials had a rather coarse grain size. All materials were tested in the form of tubes that were either produced by drawing (1.4981), or manufactured by drilling and machining from bar stock. The tubes of alloy 1.4981 were solution-annealed and one of them (b) was subsequently cold-worked to about 8%. The nickel-base tubes were age-hardened. The materials have the following features:

- AISI 304 is a nonstabilized CrNi austenitic steel; one high-purity heat with respect to silicon and phosphorus and one commercial purity heat were tested.
- AISI 316 is a nonstabilized CrNiMo austenitic stainless steel. It was tested in the high-purity (Si,P) version.
- DIN 1.4981 is a stabilized CrNiMo austenitic stainless steel. It was tested in the high-purity, solution-annealed, and cold-worked condition.
- Alloy X-750 is an age hardenable high nickel-containing alloy. The variants tested differed in purity and in their manufacturing sequence.
- Alloy 718 is an age hardenable medium nickel alloy. There was one high-purity and one commercial purity variant tested in Phase 2.

For alloy X-750, the two different fabrication routines chosen ("machined-aged" and "aged-machined") yielded different surface conditions which were characterized by metallography. Microscopic inspection showed deformation lines 15- $\mu\text{m}$  deep below the surface of the "aged-machined" specimen, whereas the "machined-aged" specimen had a surface layer of 15  $\mu\text{m}$  which was heavily covered with precipitates (Fig. 1).

All materials were tested in boiling 5N  $\text{HNO}_3$  with the addition of 5g  $\text{Cr}^{6+}$  per liter which is believed to yield a ranking of the susceptibility to IGSCC in the core of LWRs. The rate of intergranular attack was determined by metallography after 24 h exposure. The results are included in Table 2.

## Experimental Setup

### *Test Specimens*

The test specimens used in this experimental program consisted of tubes made from the various materials to be tested, sealed with end plugs. The tubes were filled with ceramic mandrels which swell under neutron irradiation thus straining the tubes when the initial gap between mandrels and cladding tube was closed. The design of the specimens is shown in Fig. 2. In Phase 2, four different types of swelling mandrels were used:

- $\text{Al}_2\text{O}_3$  or  $\text{Al}_2\text{O}_3$  with addition of 3% or 5%  $\text{B}_4\text{C}$  in the form of two hot-pressed pellets per specimen, each pellet being 50 mm long,
- Two 16-mm-long  $\text{B}_4\text{C}$  pellets per specimen; these short pellets are axially fixed in place inside the specimen by an  $\text{Al}_2\text{O}_3$  filler pellet and a support tube.

The initial gap between pellets and tubes has been made as small as technically feasible. For that purpose the tubes have been heated up in a furnace to about 220°C prior to filling in order to open the gap for loading the "zero-gap" pellets. All specimens were filled with

TABLE 1—Chemical composition of the test materials.

Alloy UNS No. Element	304a S30400	304b S30400	316b S31603	1.4981a*	1.4981b*	X750d N07750	X750e* N07750	X750f* N07750	718c N07718	718d N07718
	wt%									
C	0.043	<0.01	<0.01	0.015	0.015	0.041	0.043	0.059	0.064	0.03
Si	0.43	0.056	0.074	0.05	0.05	0.09	0.15	0.15	0.23	0.06
Mn	0.27	0.04*	0.050*	0.05*	0.05*	0.04*	0.13*	0.04*	0.20*	0.03
Mn	1.64	1.71	1.62	1.61	1.61	0.08	0.25	0.25	0.15	0.03
P	0.032	0.007	0.009	<0.005*	<0.005*	0.002	0.007	0.007	0.015	0.0026
S	0.017	0.001*	0.001*	0.005*	0.005*	0.001	0.001	0.001	0.001	0.0015
Fe	Bal.	0.004*	0.006*	<0.003	<0.003	0.001	0.001	0.001	0.012*	—
Cr	18.60	Bal.	Bal.	Bal.	Bal.	8.19	7.92	7.92	Bal.	19.57
Ni	8.90	18.5	17.6	16.0	16.0	15.4	14.6	14.6	18.1	18.0
Ni	—	10.5	13.9	15.8	15.8	71.8	72.2	72.2	52.0	52.7
Mo	—	—	2.14	1.83	1.83	—	—	—	3.12	2.99
Nb	—	—	—	0.42	0.42	—	—	—	—	—
Ta	—	0.042	<0.005	—	—	—	—	—	—	—
Nb + Ta	—	—	—	—	—	1.01	0.85	0.85	5.30	5.14
Cu	0.26*	0.001*	0.12*	0.006*	0.006*	0.04	0.06	0.06	0.04	0.01
N	—	0.084	0.082	0.042	0.042	0.02*	0.02*	0.02*	0.10*	0.08*
Ti	—	0.079*	0.090*	0.042*	0.042*	—	—	—	—	—
Al	—	<0.005	0.013	0.008	0.008	2.64	2.46	2.46	0.96	0.97
V	—	<0.001*	0.030*	0.031*	0.031*	0.66	0.59	0.59	0.55	0.57
V	—	0.002*	—	—	—	0.69*	0.56*	0.56*	—	—
B	—	<0.001	<0.001	0.001*	0.001*	0.2	0.04	0.04	—	—
B	—	0.001*	0.001*	0.001*	0.001*	—	0.002	0.002	0.006	0.006
Co	—	—	—	<0.01	<0.01	0.01	0.07	0.07	0.24	0.01
Ca	<0.0001*	<0.0001*	<0.001	<0.0001*	<0.0001*	<0.001	<0.0001*	<0.0001*	<0.0001*	<0.0001*

\* check analysis.

\* same heat.

TABLE 2—Mechanical and microstructural properties.

Alloy	Condition	Mechanical Properties at RT				Microstructure Grain Size (ASTM-No)	Corrosion Rate <sup>a</sup> , μm/h
		Yield Strength (N/mm <sup>2</sup> )	Tensile Strength (N/mm <sup>2</sup> )	Elong., %			
AISI 304 a	commercial, mill-annealed	256	627	64.0	4	7.4	
AISI 304 b	high-purity, 1066°C/1h	207	544	73.0	3	7.2	
AISI 316 b	high-purity, 1066°C/1h	223	555	65.0	3	12.5	
1.4981 a	high-purity, 25% CW	710	831	14.0	10	1.5	
1.4981 b	high-purity, 1050°C/10 min	267	591	44.0	7-8	1.3	
Inc. X750 d	1093°C/1h + 704°C/20h + mach.				2	27.0	
Inc. X750 e	1110°C/1h + 704°C/20h + mach.	730	1141	3.0	4	27.0	
Inc. X750 f	1110°C/1h + mach. + 704°C/20h				3-4	33.0	
Inc. 718 c	954°C/1h + mach. + 718°C/8h + 621°C/8h	1196	1391	17.1	7-8	1.4	
Inc. 718 d	954°C/1h + mach. + 718°C/8h + 621°C/8h	1217	1450	21.2	8	3.6	

<sup>a</sup> in boiling HNO<sub>3</sub> + Cr<sup>6+</sup>

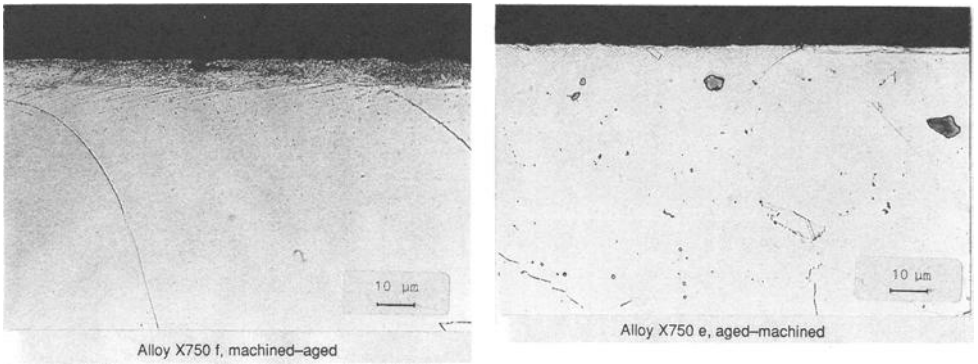
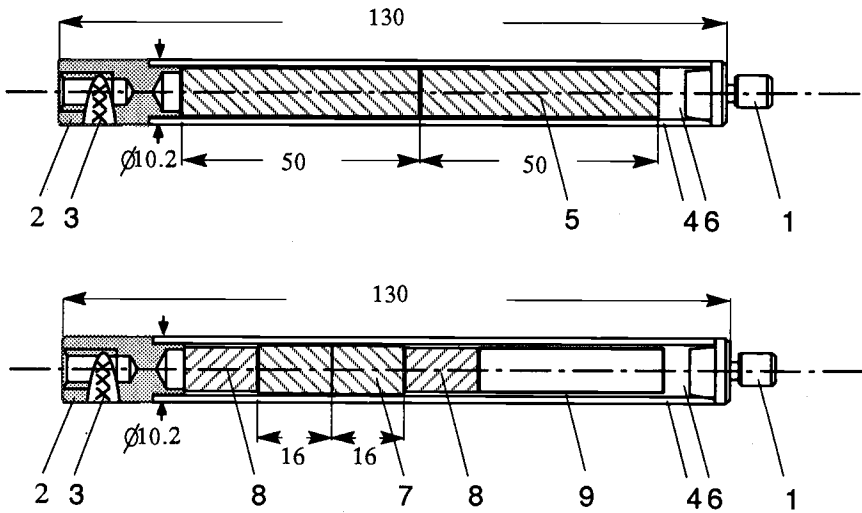


FIG. 1—Microstructure near the outer surface of alloy X750 after different manufacturing sequences.



- |   |  |   |  |
|---|--|---|--|
| 1 | Top end plug   | 6 | Plenum (filled with He)                      |
| 2 | Bottom end plug  | 7 | B <sub>4</sub> C pellet                      |
| 3 | Identification No.                                       | 8 | Al <sub>2</sub> O <sub>3</sub> filler pellet |
| 4 | Clad (test material)                                     | 9 | support tube                                 |
| 5 | Al <sub>2</sub> O <sub>3</sub> + B <sub>4</sub> C pellet |   |  |

all dimensions in mm

FIG. 2—Design of the test specimens.

helium at normal atmospheric pressure. The diameter of the finished specimens was measured by means of a laboratory profilometer along a spiral trace with about 8 mm pitch distance.

### Arrangement of the Test Specimens in the Carrier Fuel Assembly

Within this program irradiation of the test specimens was done in the region of the highest neutron flux prevailing in the core of commercial power reactors that is inside normal fuel assemblies in the inner core region. In the BWR the water rods of an 8 by 8 fuel assembly were used as test facilities (Fig. 3a). These water rods were perforated with holes over the length in order to allow direct access of the coolant water to the specimen surface. In the PWR the test specimens were inserted into control rod guide tubes of a standard fuel assembly

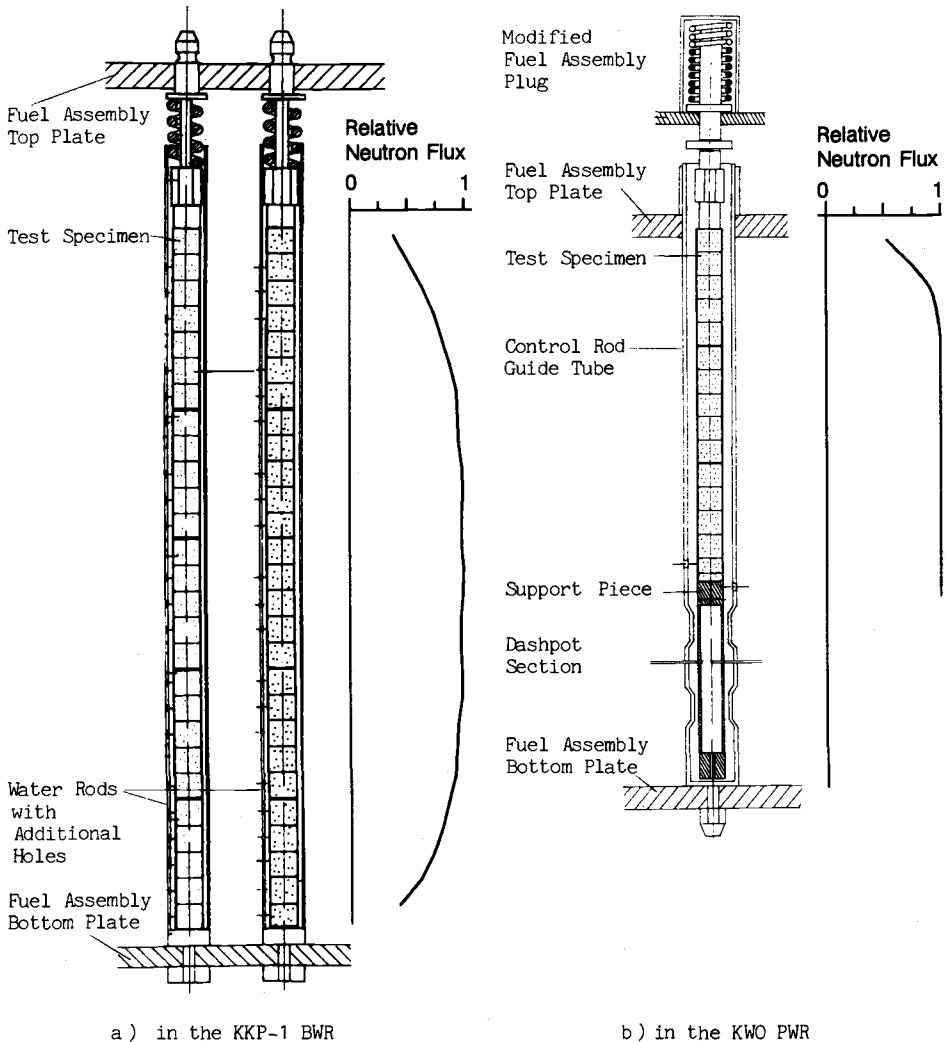


FIG. 3—Irradiation setup.

(Fig. 3b). A modified assembly plug was used to secure the specimen stringers in place and to allow for an adequate coolant flow.

The individual test specimens have been assembled into specimen stringers by screw connections in order to facilitate handling in the reactor pool during examination of the specimens. Defective specimens, however, are normally to be restrained from further exposure. Reassembling of stringers, which contain single defective specimens, cannot be done during the refueling shutdown period because of time constraints. Therefore, only a small number of five to seven specimens have been tightly connected into stringers. Several such stringers were stacked one upon another and fitted together by proper end fittings.

In the BWR the specimen stack reaches down to the bottom of the active zone of the core, whereas in the PWR the specimen stack rests upon a special supporting piece located in the dashpot part of the guide thimble. In both cases the uppermost specimen is positioned near the upper core periphery.

### Irradiation

Irradiation of the Phase 2 specimens was performed in the Philippsburg BWR (KKP-1) in continuation of the Phase 1 experiment. PWR irradiation was done in the Biblis-B PWR in Phase 1 and has been continued in the Obrigheim PWR (KWO) for Phase 2. Irradiation of the Phase 2 specimens was planned for two consecutive reactor cycles. After the first cycle, however, only 22 out of a total of 54 specimens in the BWR and only one stringer with five specimens in the PWR could be reinserted for a second cycle, because many specimens had cracked. During the subsequent operation cycle of the KWO PWR, 15 sound specimens were reassembled into new stringers and reinserted at the next refueling shutdown. A few PWR specimens have been exposed even for a third cycle resulting in 957 effective full power days (EFPD) total duration of irradiation. The main irradiation data are summarized in Table 3.

The neutron flux level of the specimens varied according to their axial position in the reactor core. Therefore, some specimens located in the neutron flux gradient near the top and the bottom (in BWR only) of the core achieved lower fluences than the majority. Typical flux profiles for both the BWR and the PWR irradiations are shown in Fig. 3.

### Examination

After each cycle of irradiation, the specimen stringers were examined in the spent fuel pool of the reactors for IGSCC. Diameter measurements were used to determine the accumulated diametral strain of the test specimens, whereas the tube integrity or crack formation was examined by eddy current (EC) and visual inspection with a video camera.

TABLE 3—Main irradiation data.

Reactor	Irradiation		Accumulated Neutron Fluence ( $E > 1\text{MeV}$ ) ( $10^{21} \text{ cm}^{-2}$ )
	Cycle	Duration (EFPD)	
BWR KKP-1	1	243	0.6–1.5
	2	309	1.2–3.2
PWR KWO	1	316	1.2–2.3
	2	322	2.4–4.5
	3	319	6.8

### Measuring Device

Multiple measuring devices, similar in KKP-1 and in KWO, and, which have been developed in the course of fuel service activities for examination of fuel rods, were used for these measurements (Fig. 4). The measuring device provides precision guidance for the test specimen stringer to be measured and is equipped with an encircling coil for EC defect testing, a gage head with linear variable differential transformer for diameter profilometry, and a video camera for visual examination. The specimen stringer to be measured is handled by a special handling tool, which allows for axial and rotational movement of the stringer through the measuring device.

### Eddy Current Testing

EC testing was performed with an encircling double coil system operated at a frequency of 330 kHz. The system was calibrated to tube standards of both stainless steel and Inconel material containing test holes at three axial planes (1, 2, and 4 holes per plane).

### Diameter Measurements

In diameter profilometry, the specimen stringer was traced by two opposite parallel feelers (knife edges) on the gage head, and the specimen diameter is measured by one LVDT. The system was calibrated against a standard with different diameter steps. The accuracy of the diameter measurement was within  $\pm 0.005$  mm. For each specimen stringer linear diameter traces were taken at four angular orientations.

### Visual Inspection

The video system consisted of an underwater camera (black and white), monitor and video recorder. The resolution of the viewing system was 480 lines for the full screen. At

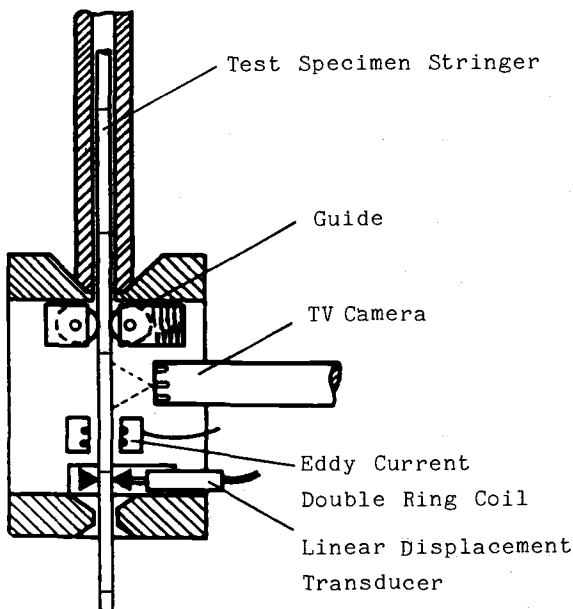


FIG. 4—Multi-purpose measuring and examination gage.

maximum viewing magnification, a test specimen of normal size (diameter 10.2 mm) filled the entire monitor screen.

## Results

### *Diametral Strain*

Typical axial profiles of the diameter changes measured after irradiation for the different types of swelling mandrels used are shown in Fig. 5. In addition to  $\text{Al}_2\text{O}_3$  base pellets, which proved to be very appropriate in Phase 1 [1],  $\text{B}_4\text{C}$  pellets were used in Phase 2 in order to obtain sufficient swelling rates even at high fluences ( $>2$  cycles) when the  $^{10}\text{B}$  is burned out in the  $\text{Al}_2\text{O}_3 + \text{B}_4\text{C}$  pellets. Figure 6 shows the diametral swelling of the various pellet types as derived from the measured diameter increase of the clad and the known initial gap. The swelling rate of the  $\text{Al}_2\text{O}_3$  base material increased with increasing  $\text{B}_4\text{C}$  content and showed a tendency to saturate with increasing neutron fluence. In the strongly absorbing  $\text{B}_4\text{C}$  pellets,  $^{10}\text{B}$  burns out only in an outer rim. The resulting interaction with the cladding is affected by the behavior of this rim, which probably detached from the inner part of the pellet and possibly cracked under the "back forces" of the strained cladding. Therefore, some second cycle specimens filled with  $\text{B}_4\text{C}$  pellets showed little or even a negative diameter change.

Defective specimens quite often exhibited much larger, and over the circumference, more irregular diameter increases than intact ones due to crack opening. In Fig. 7, the diameter profiles, EC traces, and photographs of defective specimens are shown. In such cases the diametral strains were estimated from the swelling data measured on comparable intact specimens. Visual inspection showed the cracks to be of brittle appearance, with no signs of necking. The cracks were often branched and preferentially in the axial direction.

### *BWR Results*

In the BWR environment (Fig. 8), both alloy 718 variants showed excellent behavior, with all specimens being intact after the second cycle where they achieved strains up to 1.1% and 0.7% irrespective of their different impurity content.

All alloy X-750 behaved only moderately well with strains to failure between 0.3% and 0.5%. Only specimens with  $\text{Al}_2\text{O}_3 + \text{B}_4\text{C}$  failed, whereas all specimens with  $\text{Al}_2\text{O}_3$  pellets remained intact. The "aged + machined" materials were slightly better. They survived the first cycle, in which the "machined + aged" specimen already failed.

All stainless steels behaved rather poorly even in the case of the high-purity alloys. All specimens failed in the first cycle when strained to more than 0.45%. There are no significant differences due to their different alloying elements and purity.

### *PWR Results*

Due to higher exposure (higher neutron flux level and longer exposure time), higher strains were imposed on PWR specimens than on BWR specimens with the same pellet types.

In the PWR environment (Fig. 9), again both alloy 718 variants exhibited excellent behavior, reaching the highest achievable strains of 2.0 and 1.5% without defects. The defects at 1 and 1.2% diameter change of alloys 718c and 718d are attributed to manufacturing imperfections. Figure 10 shows a picture of an intact specimen of material 718c, reconstructed by interpolation of the measured diameter profiles after irradiation in comparison to normal appearance. It shows several ridges, which reflect the uneven inner tube surface formed by

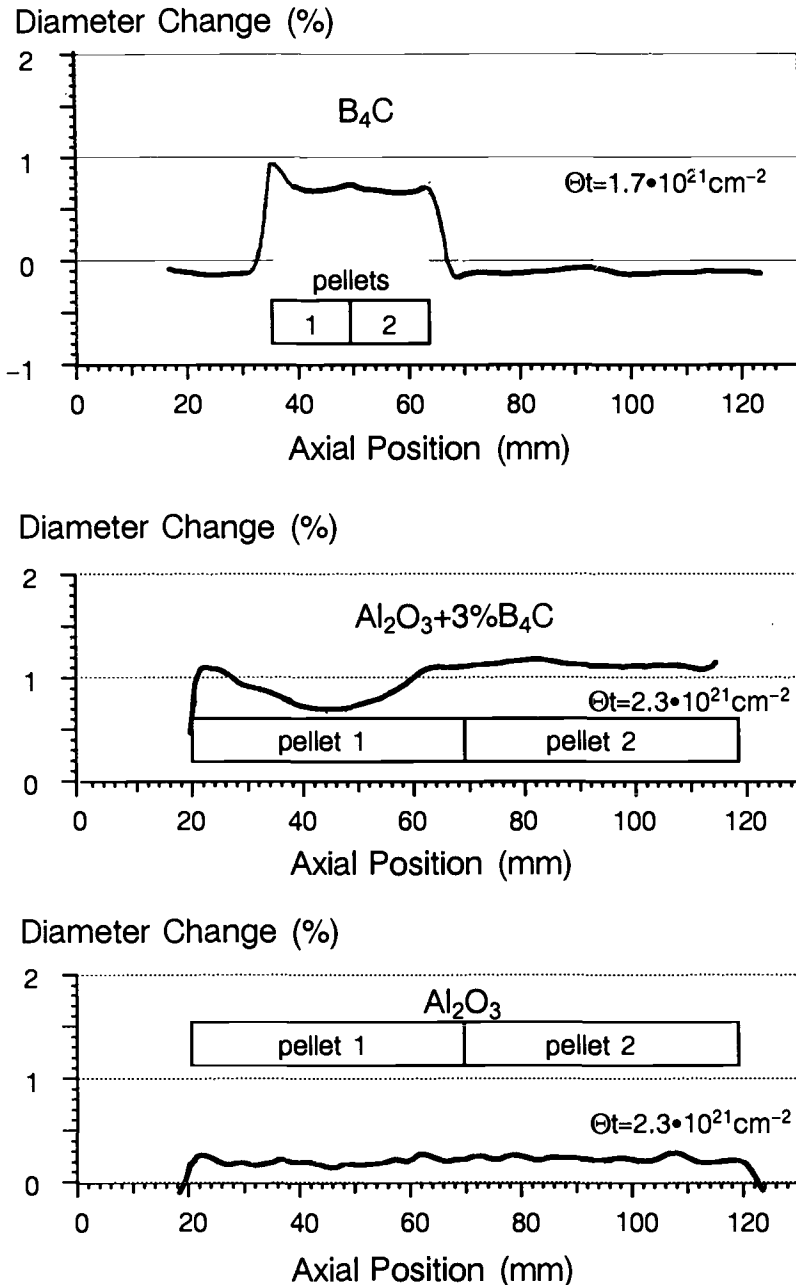


FIG. 5—Typical diameter change profiles of intact specimens with various swelling mandrels.

drilling from bar stock. The unevenness of the inner surface was transferred to the outside when the ground and smooth swelling mandrel expanded and strained the cladding tube. Such features were observed in several of those specimens that were machined from bar stock. Therefore, it has to be considered that these imperfections of the tube inner surface

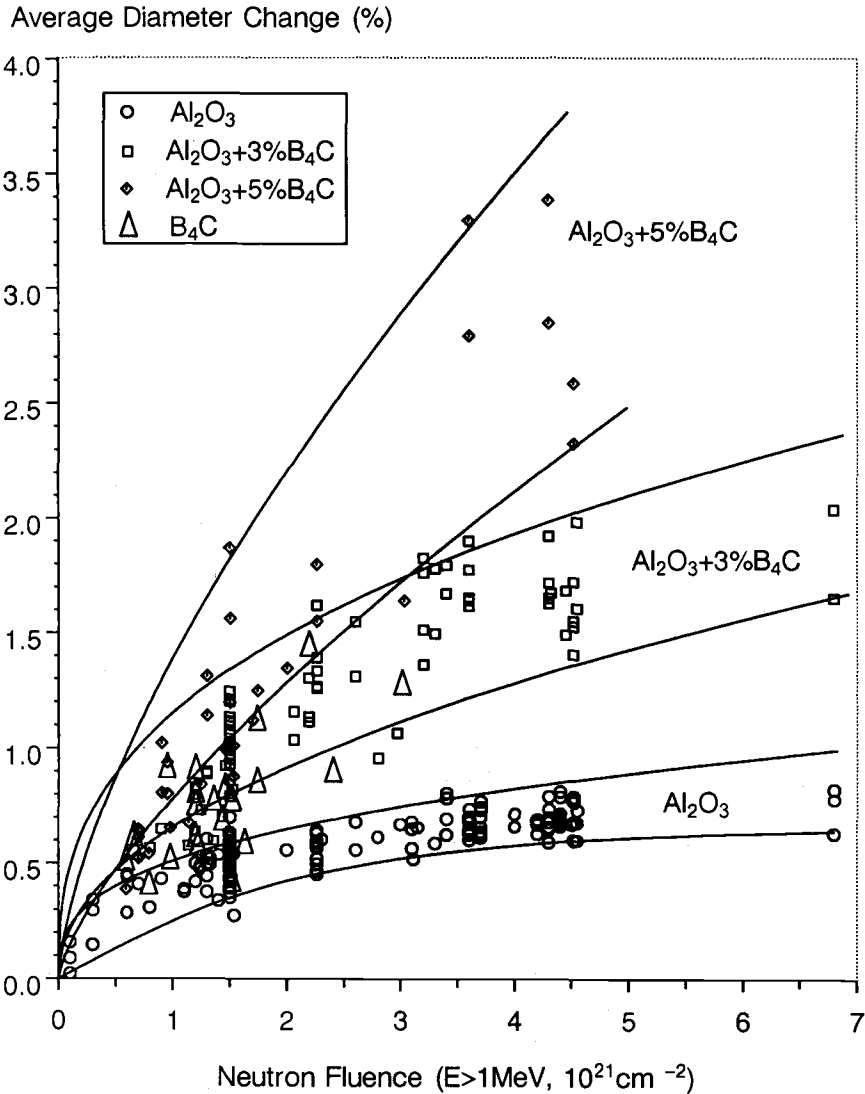


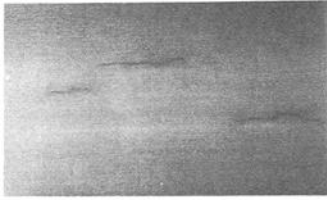
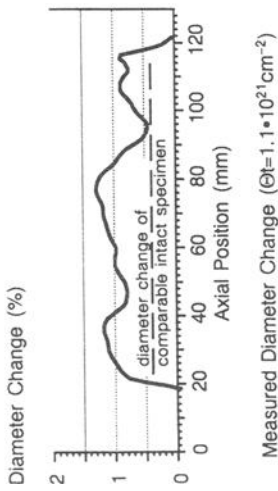
FIG. 6—Swelling of ceramic mandrels as a function of neutron fluence.

originating from the manufacturing process may have caused early failures (cracking of specimens at low strain levels exceeded by intact specimens of the same material).

All alloy X-750 d specimens (high-purity, aged-machined) did not fail up to the highest strains of 2%. Alloy X-750 e (commercial purity, aged-machined) failed at 1.4%. Reversing the fabrication sequence (machined-aged), the same heat failed at 0.7%.

The different variants of the stainless steels all showed rather poor behavior (strains to failure between 0.1% and 0.8%) with the following features:

- the high-purity version of AISI 304 has only a slightly higher ductility than the commercial purity version
- the solution-annealed DIN 1.4981 has a slightly higher ductility than the cold-worked variant.



a) BWR Specimen No. 118, 304a  
 $\text{Al}_2\text{O}_3+5\%\text{B}_4\text{C}$  pellets,  
 neutron fluence  $1.1 \cdot 10^{21} \text{cm}^{-2}$



b) BWR Specimen No. 223, 1.4981b  
 $\text{Al}_2\text{O}_3+5\%\text{B}_4\text{C}$  pellets,  
 neutron fluence  $1.5 \cdot 10^{21} \text{cm}^{-2}$   
 (Diameter out of measuring range)



EC test record (large, overrided defect signals)

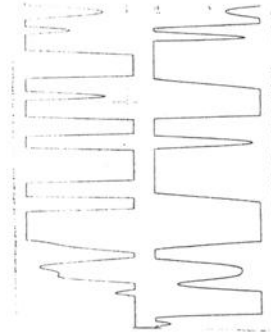


FIG. 7—Typical appearance of defective specimens.

Average Diameter Change (%)

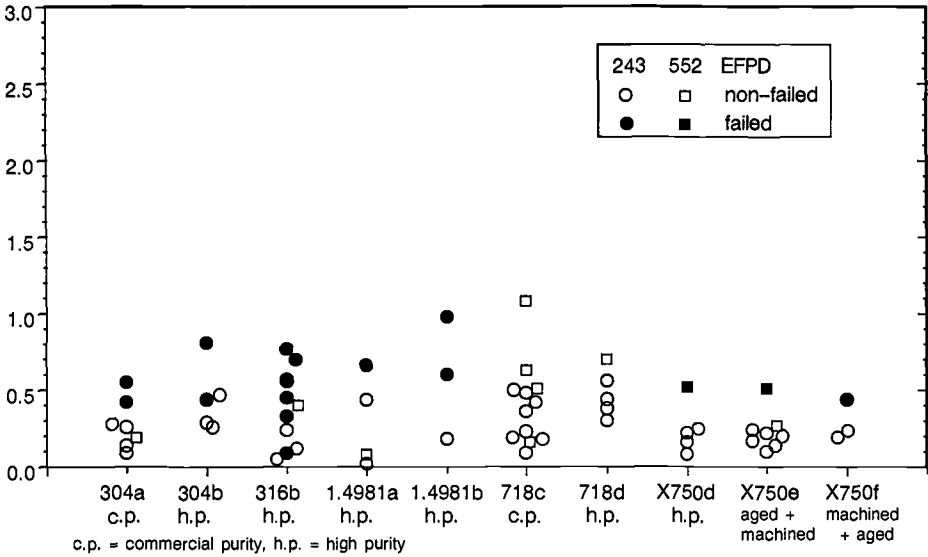


FIG. 8—Failure results for swelling mandrel experiments in BWR environment.

The behavior of AISI 316 was, again, confusing, with a defective specimen at 0.1% and two unfailed specimens at 0.3 and 0.5%. With all specimens defective for strains >0.7%, this high-purity steel showed, as in the BWR, poor behavior. The one defective specimen that failed at very low strain was probably affected also by imperfections of the inner tube surface due to drilling as previously suggested.

All 1.4981 specimens failed within the first cycle at strains between 0.4% and 0.8%.

Average Diameter Change (%)

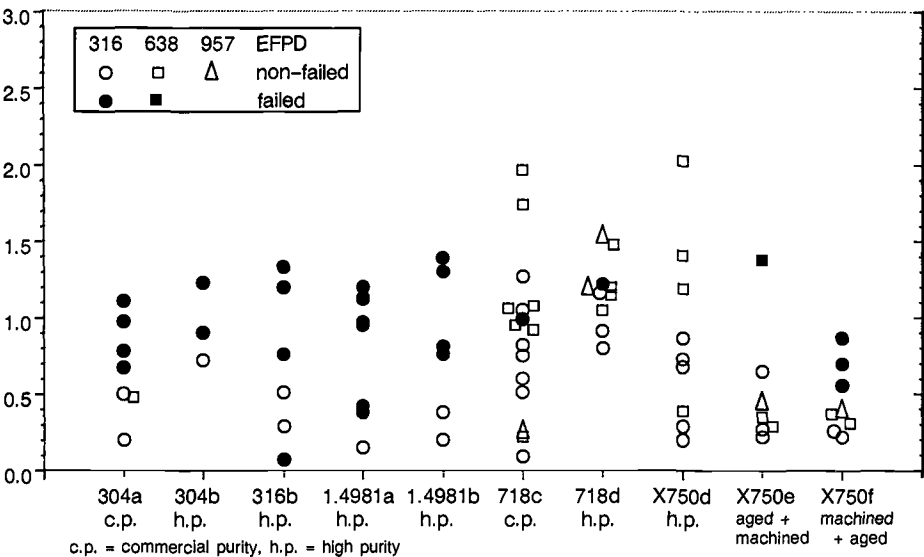


FIG. 9—Failure results for swelling mandrel experiments in PWR environment.

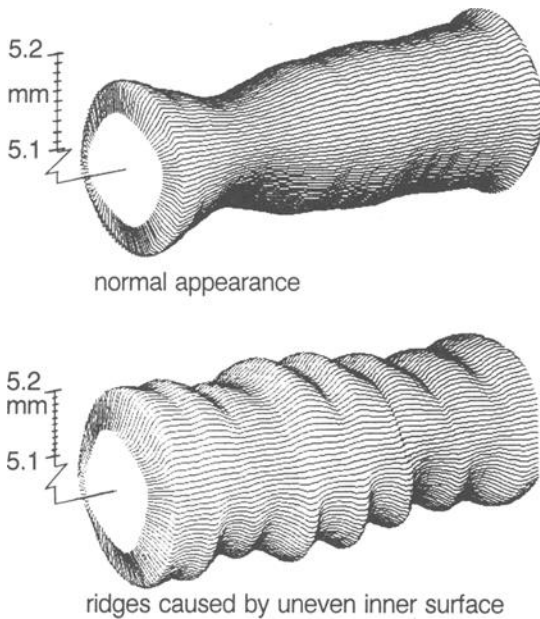


FIG. 10—Interpolated diameter profiles of the outer surface of irradiated specimens.

## Discussion

The experimental results of the Phase 2 materials and some comparable Phase 1 materials are shown in Table 4 together with relevant material characteristics.

### *Comparison of Out-Pile Corrosion and In-Pile Deformability*

There is obviously no clear correlation between the corrosion rate in boiling  $\text{HNO}_3 + \text{Cr}^{6+}$  and the strain to failure measured in the BWR and the PWR. The superior stainless steel 348b of Phase 1 showed almost no corrosion attack in the laboratory test thus indicating an existing correlation. But the high-purity steels of Phase 2, 304b and 316b, which also showed a low corrosion rate in boiling  $\text{HNO}_3 + \text{Cr}^{6+}$ , behaved in reactor no better than other materials with high corrosion rates in boiling  $\text{HNO}_3 + \text{Cr}^{6+}$ . Good behavior in the  $\text{HNO}_3 + \text{Cr}^{6+}$  test is obviously not a guarantee for good IASCC resistance.

### *BWR versus PWR Environment*

As in Phase 1, no significant difference in the behavior in BWR environment (oxygenated water) and PWR environment (hydrogenated water, higher temperature) could be detected in Phase 2. The only clear difference is the better behavior of alloy X-750 in the PWR than in the BWR.

### *Effect of Material Properties*

*Nickel-base alloys*—Alloy 718 did not fail in the BWR and reached high strains in the PWR in both variants. The conclusion made from Phase 1 that alloy 718, mill-annealed and hardened by a two-stage aging, all at rather low temperatures, has an excellent in-pile behavior, could thus be verified. Since the impurity content (silicon, phosphorus, sulfur,

TABLE 4—Comparison of in-BWR and in-PWR failure threshold and material characteristics.

Program Phase No.	Material	Corr. Rate in HNO <sub>3</sub> + Cr <sup>6+</sup> (mm/h)	Chemical Composition					Average Diametral Strain <sup>a</sup>				
			C (ppm)	Si (ppm)	P (ppm)	S (ppm)	N (ppm)	in BWR		in PWR		
							NF, %	F, %	NF, %	F, %		
1	348 a	6.0	740	3400	70	90	420	0.4	0.7	0.6	0.6	0.6
	348 b	0.8	410	190	20	70	80	1.6	—	2.8	—	—
2	304 a	12.5	430	2700	320	170	—	0.3	0.4	0.5	0.7	0.7
	304 b	1.5	<100	400	10	40	790	0.5	0.4	0.7	0.9	0.9
	316 b	1.3	<100	500	10	50	900	0.4	0.1	0.5	0.1 <sup>b</sup>	0.1 <sup>b</sup>
	1-4981 a	7.4	150	500	50	20	420	0.4	0.7	0.2	0.4	0.4
	1-4981 b	7.2	150	500	50	<30	420	0.2	0.6	0.4	0.8	0.8
1	718 a	3.2	300	1000	80	30	60	1.5	—	1.0	—	—
2	718 c	1.4	640	2000	150	120	—	1.1	—	2.0	1.0 <sup>b</sup>	1.0 <sup>b</sup>
	718 d	3.6	300	300	26	15	—	0.7	—	1.5	1.2 <sup>b</sup>	1.2 <sup>b</sup>
1	X750 c	6.9	400	1400	70	20	50	0.4	0.6	0.5	0.5	0.5
2	X750 d	27.0	410	400	20	10	—	0.3	0.5	2.0	—	—
	X750 e	27.0	430	1300	70	10	—	0.3	0.5	0.7	1.4	1.4
	X750 f	33.0	590	1500	70	10	—	0.2	0.4	0.4	0.4	0.6

<sup>a</sup> NF = maximum of nonfailed specimens, F = minimum of failed specimens.<sup>b</sup> probably affected by tube ID imperfections.

carbon) of the two heats differed substantially, it can be concluded that these impurities obviously have no major influence on the IGSCC behavior of this particular alloy.

Alloy X-750 did not fail in the PWR tests, if treated properly and having a high purity. A proper heat treatment is characterized by high solution-annealing temperature followed by aging at rather low temperatures, in the right fabrication sequence ("aged-machined"). Higher impurity content as well as a "machined-aged" sequence reduced the in-pile deformability. The BWR environment for alloy X-750, and does not discriminate between different chemistries of the two heats (especially in silicon and phosphorus).

Thus, for nickel-base alloys, the major conclusions from Phase 1 could be confirmed.

*Stainless Steels*—All stainless steel variants failed in both the BWR and the PWR at rather low strains. Thus the conclusion from Phase 1, that reduction of impurities eliminates IASCC, could not be verified. Obviously, low phosphorus and silicon content alone is not enough to eliminate IASCC. The high-purity steel 304b was found to be only slightly better than the commercial purity version, and both 1.4981 high-purity variants never reached the excellent IASCC behavior of the high-purity material 348b of Phase 1. For AISI 316, the high-purity version, b, of Phase 2 was even worse than the commercial purity version tested in Phase 1.

Comparing the stainless steels of Phase 1 to those of Phase 2, it was found that the latter had significantly higher nitrogen content (Table 4). Thus it is necessary to check whether the high nitrogen level is the reason for the poor behavior of the high-purity steels of Phase 2. This is being investigated in a subsequent program phase.

### *Stress History of the Test Specimens*

It is a characteristic of this experiment that only strain, in terms of diameter changes of the tubular test material, can be measured directly in the room temperature condition. For many applications and for modeling, however, stresses are of importance. As outlined in Ref 1, the stress that occurred in the test specimens during irradiation can be estimated on the basis of:

- (a) the swelling characteristics of the ceramic mandrels known from diameter measurements,
- (b) the as-fabricated geometry data—inner and outer diameter of the cladding tube and diameter of the mandrels, and
- (c) the irradiation creep properties of the cladding material.

After a preliminary period of irradiation, when the initial gap between mandrels and cladding is closed, the specimen will experience an increasing tensile stress. The stress will be reduced by irradiation induced creep, which increases linearly with both stress and fast neutron fluence [2]. Knowing the irradiation creep constants for the various materials tested, the stress at each time of irradiation can easily be calculated assuming uniform expansion of the tubular specimen in the radial direction. The calculated tensile stress in a Phase 2 specimen of material 304a is shown in Fig. 11. Failure occurred at a stress somewhat below 500 N/mm<sup>2</sup>.

High-purity materials have a reduced creep strength [3,4]. The stress histories of a Phase 1 specimen of the superior material 348b, calculated for two different creep constants, are shown in Fig. 12. In any case high stress levels close to or even above the yield strength were reached, in the case of this high-purity material, without failure. Above the yield strength, which increases with irradiation, plastic straining has to be expected in addition

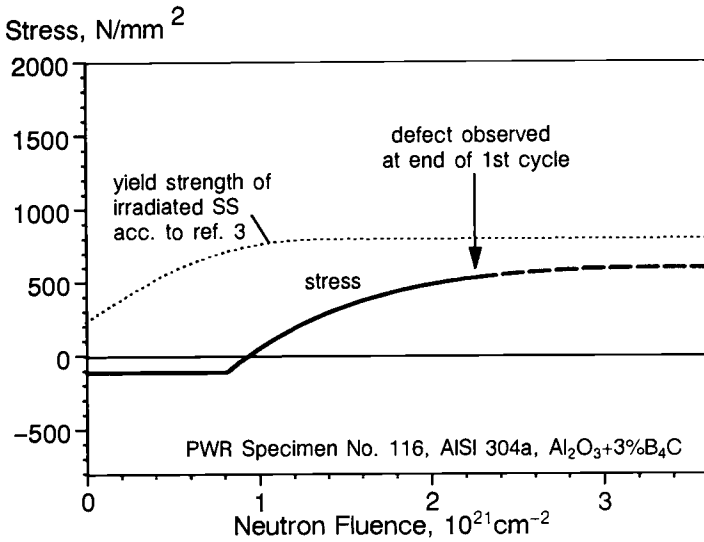


FIG. 11—Calculated stress of a defective Phase 2 specimen with commercial stainless steel clad as a function of neutron fluence.

to irradiation creep which also contributes to the deformation of the specimen and leads to a reduction of the predicted stresses.

By knowledge of the creep properties of the materials tested, this method does allow the experimental results to be expressed also in terms of critical stress levels.

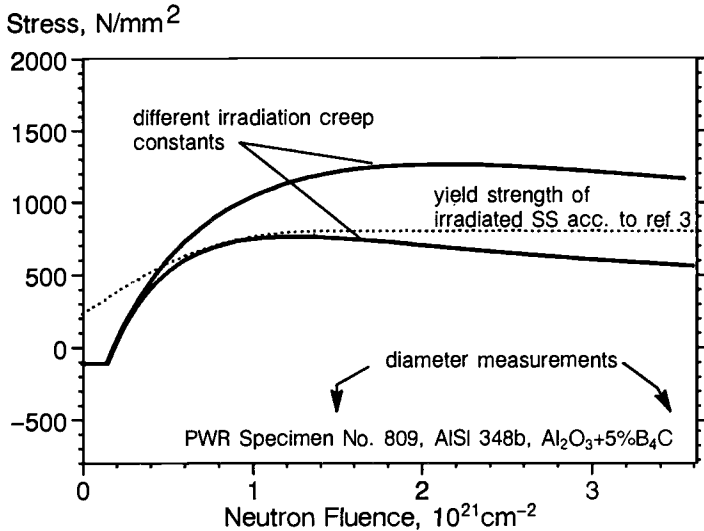


FIG. 12—Calculated stress of an intact Phase 1 specimen with high-purity stainless steel clad as a function of neutron fluence.

## Conclusions

- (1) Good performance of alloy 718 with annealing at 950°C was confirmed.
- (2) Alloy X-750 behaved better in the PWR than in the BWR. Aging before machining resulted in lower sensitivity to in-reactor brittle failure than aging after machining.
- (3) The beneficial effect of high purity for stainless steels deduced from Phase 1 could not be verified. A major difference between the high-purity stainless steels of Phase 1 and the high-purity stainless steels of Phase 2 was the nitrogen content. The influence of nitrogen is being studied in the subsequent program phase.
- (4) Sensitive stainless steels fail below yield strength. Insensitive stainless steels can withstand stresses at or even above yield strength.

## References

- [1] Garzarolli, F., Alter, D., Dewes, P., and Nelson, J. L., "Deformability of Austenitic Stainless Steels and Ni-Base Alloys in the Core of a Boiling and a Pressurized Water Reactor," *Proceedings of the Third International Symposium on Environmental Degradation of Materials in Nuclear Power Systems—Water Reactors*, G. J. Theus and J. R. Weeks, Eds., Traverse City, MI, August 30–September 3, 1987, pp. 657–664.
- [2] McElroy, W. M., Dahl, R. E. Jr., and Gilbert, E. R., "Neutron Energy-Dependent Damage Function for Analysis of Austenitic Steel Creep Data," *Nuclear Engineering and Design* 14, 1970, pp. 319–331.
- [3] Beeston, J. M. and Thomas, L. E., "Creep and Swelling of Type 348 Stainless Steel at Temperatures up to 700 K and Comparison with Fast Reactor Data," *Effects of Radiation on Materials: Eleventh Conference, ASTM STP 782*, H. R. Brager and J. S. Perrin, Eds., American Society for Testing and Materials, Philadelphia, 1982, pp. 71–91.
- [4] Bates, J. F., Powell, R. W., and Gilbert, E. R., "Reduction of Irradiation-Induced Creep and Swelling in AISI 316 by Compositional Modifications," *Effects of Radiation on Materials: Tenth Conference, ASTM STP 725*, D. Kramer, H. R. Brager, and J. S. Perrin, Eds., American Society for Testing and Materials, Philadelphia, 1981, pp. 713–734.

**Research Applications and  
Developments in Slow Strain Rate  
Testing Techniques**

## The Use of Precracked and Notched Slow Strain Rate Specimens

---

**REFERENCE:** Toribio, J., “The Use of Precracked and Notched Slow Strain Rate Specimens,” *Slow Strain Rate Testing for the Evaluation of Environmentally Induced Cracking: Research and Engineering Applications, ASTM STP 1210*, R. D. Kane, Ed., American Society for Testing and Materials, Philadelphia, 1993, pp. 105–122.

**ABSTRACT:** The use of precracked and notched specimens in slow strain rate testing (SSRT) has important advantages, the main one being the localization of the environmental effect in the vicinity of the crack or notch tip. There is, however, an important difficulty in interpretation of results: the local strain rate at the crack or notch tip—and not the externally applied displacement rate—is the variable that controls the environmental cracking. In this paper, results from SSRT of a wide range of notched geometries are compared, showing the interest of presenting the results as a function of local strain rate at the notch tip.

**KEYWORDS:** slow strain rate testing (SSRT), precracked specimens, notched specimens, local strain rate, global strain rate, environmentally induced cracking (EIC), stress corrosion cracking (SCC), hydrogen assisted cracking (HAC)

A well-known technique for the evaluation of environmentally induced cracking (EIC) is the performance of slow strain rate tests (SSRT) on initially smooth, precracked, or notched specimens, in which a constant displacement rate is externally applied on the specimen ends up to fracture. The intrinsic advantages of this technique have been profusely outlined in previous works [1–3], and they become even more important when compared to those of constant load or constant strain tests [4].

The primary conceptual advantage of the SSRT technique is the use of the strain rate as the main test variable, which allows an analysis of the very relevant transient processes in EIC phenomena. Constant load and constant strain tests represent, thus limit, cases of SSRT when the strain rate tends to zero and does not represent a tests variable. Final fracture is always reached in SSRT more rapidly than in the constant load or constant strain tests, since in the former the environmental process is accelerated by imposing an increasing external load up to final fracture. A higher stress level is thus applied in SSRT in a more rapid and aggressive manner.

Using the SSRT technique provides other relevant benefits, e.g., the realistic approach to service failures [1], the establishment of an electrochemically dependent range of strain rates within which EIC occurs [1], the rapid identification of environment/metal combinations which produce EIC [2], and the establishment of quantitative rankings of EIC properties of metals and alloys having similar microstructures [2].

---

<sup>1</sup> Professor, Department of Engineering, University of La Coruña, 15141 Arteixo, La Coruña, Spain.

### The Use of Precracked and Notched Specimens in Slow Strain Rate Testing

The use of precracked or notched specimens favors the localization of the environmental attack just at the crack or notch tip, thus decreasing experimental scatter. Precracked specimens can be prepared by fatigue, whereas notched specimens require previous machining, more expensive in general. That is one of the reasons of the fact that precracked specimen testing has become more widespread in the last 20 years or so. However, the use of notched specimens has been strongly recommended more recently for experimental research on EIC using SSRT [5]. In addition, recent work has revived interest in the use of notched specimens for fundamental studies of hydrogen embrittlement of metals [6]. Furthermore, the triaxial stress state created in the vicinity of the notch has a synergistic effect combined with the environmental action, since it accelerates the hydrogen diffusion towards the points of maximum hydrostatic stress.

EIC in the vicinity of cracks and notches is a local phenomenon. The effect of the environment is localized at the crack or notch tip—the place where fracture initiates—and therefore local variables (stress, strain, and strain energy density) must be relevant in such a process. In addition, cracking is time dependent and consequently local kinematic variables (more precisely, the local strain rate at the crack or notch tip) should play a very important role.

The importance of localized transient processes in fracture under aggressive environment has been previously pointed out. It is generally accepted that rupture of oxide film, passivation, or hydrogen diffusion are rate determining steps in environmental cracking [7,8]. Regarding the effect of strain rate, a great research effort has been made in the past [9–17], which has demonstrated that failure load under aggressive environment is a function of the externally applied displacement rate. For stress corrosion cracking (SCC) phenomena, the balance between oxide film rupture and growth of the passivation film makes the dependence nonmonotonic [2,18]: when the displacement rate is very slow (in the limit constant load test) the specimen becomes passivated, and when this rate is very fast, the dissolution does not have time to progress. Between both limits a minimum value of the fracture load is reached. For hydrogen embrittlement processes, fracture load is a monotonic increasing function of the displacement rate [2,18,19]: the higher the displacement rate, the shorter the time for the hydrogen diffusion.

However, the displacement rate is not the most suitable variable and it allows the establishment of only qualitative phenomenological relations. To obtain quantitative relations and objective results one needs to know the local strain rate at the crack or notch tip, because at that point the environmental attack is localized, and the crack (or notch) tip strain rate controls the EIC process [20–21]. Local strain rate, and not applied displacement rate, has to be compared with the dissolution (or film rupture) and passivation rates, or with the hydrogen diffusion rate, depending on the considered process.

Previous research on this subject refers to the computation of (local) strain rate at a crack tip. Many difficulties arise in determining the strain distribution and the spreading of the plastic zone in the vicinity of a crack tip [22]. Lidbury [23] offers several expressions of the crack tip strain rate under conditions of cyclic loading and small scale yielding, and under conditions of monotonic loading and general yielding; in the latter case, which would correspond to slow strain rate tests, the crack tip (of effective) strain rate can be 10 to 20 times the nominal or applied strain rate. Maiya [24,25] and Maiya and Shack [26] propose a definition of the crack tip strain rate associated with a fracture criterion on the basis of the *J*-integral. In Ref 27, Congleton et al. offer an expression of the crack tip strain rate on the basis of the crack tip opening mechanism proposed by Rice and Sorensen [28] for an ideally plastic solid under plane strain and fully plastic conditions. Such an expression is based on

the assumption that the specimen is multicroaked and that global displacement of the specimen ends can be computed by adding the contributions of the cracked and the noncracked parts; it is clearly applicable to anodic dissolution (or pure SCC) processes and has been used by Parkins [29–31] to study the kinetics of EIC. Finally, emphasizing the difficulty of a correct determination of the local strain rate at a crack tip, Andresen and Ford [32] proposed recently an empirical value of the crack tip strain rate coincident with the applied strain rate for transgranular cracking, and five times the applied strain rate for intergranular cracking. An inherent limitation of all these expressions for local strain rate at the crack tip is that they do not take into account the constitutive equation of the material (*work hardening effect*), whose incidence in the local strain rate is not negligible, as is demonstrated in the present paper for notches and outlined previously for cracks [3]. The main consequence of that simplification is the prediction of a constant local strain rate at the crack tip if the typical condition of constant extension rate is achieved during the EIC test.

This paper deals with the concept of local strain rate at a notch tip as a function of the global strain rate or, more precisely, the displacement rate. The first, *local or effective strain rate*, is associated with a reference length short enough to guarantee the convergence of the mathematical method, although greater than the grain size of the material (to preserve the congruence of the continuum mechanics model); the latter, *global, nominal or applied strain rate*, is associated with a reference length long enough to permit uniaxial stress state at its ends. It can be controlled during the test using the appropriate experimental device.

Emphasis is focused on the application of these results to the modeling of EIC growth, in particular SCC and hydrogen assisted cracking (HAC). Results from SSRT of a wide range of notched geometries tested in a hydrogen environment are compared, thus showing the interest of presenting the results as a function of the local strain rate in the vicinity of the notch tip.

### Definitions of Local and Global Strain Rates

In order to define the concepts of local and global strain rates, which are directly applicable to SSRT with precracked and notched specimens, the reference geometries shown in Fig. 1 will be used, where  $L$  is the specimen length;  $D$  the specimen diameter in axisymmetric specimens;  $B$  the thickness in specimens that are not axisymmetric;  $a$  the crack depth (in cracked geometries);  $R$  and  $A$  the notch radius and notch depth, respectively (in notched geometries);  $r$  the radial coordinate;  $z$  the axial coordinate; and  $x$  the distance from the crack or notch tip.

Local strain  $\epsilon_L$  is defined as the strain associated with a local reference length  $L_L$  (small enough to guarantee the convergence of the method) parallel to the bar axis ( $z$ ) and placed next to the crack or notch tip. The local reference length is simply called  $B$  throughout this paper, i.e.

$$\epsilon_L = \frac{\Delta L_L}{L_L} = \frac{\Delta B}{B} = \frac{u_L}{B} \quad (1)$$

where the enlargement  $\Delta B$  of the local reference length  $B$  is the relative displacement between its ends (local displacement  $u_L$ ). The hypothesis of small strains is included in definition (1), which will be used throughout this paper, and it is frequently valid for notched specimens of high-strength steel (or similar brittle material) under SCC or hydrogen em-

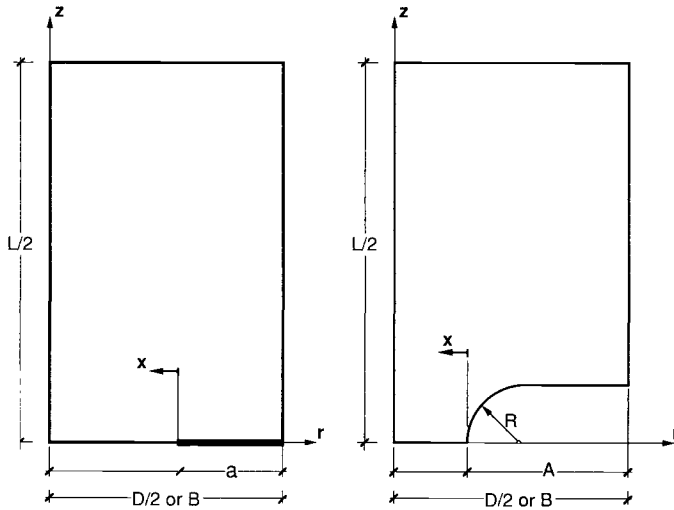


FIG. 1—Precracked and notched slow strain rate specimens ( $L$ : sample length,  $D$ : sample diameter in axisymmetric specimens,  $B$ : sample thickness in specimens that are not axisymmetric,  $a$ : crack depth,  $R$ : notch radius,  $A$ : notch depth,  $r$ : radial coordinate,  $z$ : axial coordinate,  $x$ : distance from the crack or notch tip).

brittlement conditions. However, for cracked specimens of ductile materials, it is necessary to use the logarithmic strain to define local strain as follows

$$d\epsilon_L = \frac{dL_L}{L_L} = \frac{dB}{B} \tag{2}$$

which has to be integrated throughout the loading process to obtain the local strain at any time.

Local reference length  $B$  is always at  $z = 0$  (minimum section of the notched specimen), although it can be placed at a variable distance  $r$  (see Fig. 1). The crack or notch tip ( $x = 0$ ) and its vicinity are the most representative locations.

Global strain  $\epsilon_G$  is defined as the relative displacement between the ends of a specimen of length  $L$  (global displacement  $u_G$ ), divided by a characteristic length of the geometry (diameter  $D$ ) to obtain a dimensionless variable

$$\epsilon_G = \frac{u_G}{D} \tag{3}$$

where  $D$  can be substituted by the thickness  $B$  in plain specimens.

It must be noticed that the global strain is a dimensionless displacement, and unlike local strain, it is not a strain in the Continuum Mechanics sense, since in a notched geometry the strain is nonuniform along the axial direction. Strictly speaking, therefore, it should be called *dimensionless global displacement*.

It is also worth noting that the selection of  $D$  has a fundamental advantage, which is that global strain rate increases as the global reference length  $L$  increases. On choosing the specimen length  $L$  for the dimensionless procedure, the global strain rate decreases as  $L$

increases, since the strain concentration in the vicinity of the crack or notch is attenuated by the lower strain far from that region.

Local and global strain rates can be obtained by time-derivation of expressions (1) and (3).

$$\dot{\epsilon}_L = \frac{u_L^{i+1} - u_L^i}{B\Delta t} \quad (4)$$

$$\dot{\epsilon}_G = \frac{u_G^{i+1} - u_G^i}{D\Delta t} \quad (5)$$

where superscripts  $i$  and  $i + 1$  mean a loading step and the next one respectively. The value  $\Delta t$  represents the time interval between two loading steps, which can be constant or variable between one step and another.

However, parameter  $\Delta t$  can be easily eliminated by calculating the relationship between local and global strain rates

$$\frac{\dot{\epsilon}_L}{\dot{\epsilon}_G} = \frac{\frac{u_L^{i+1} - u_L^i}{B}}{\frac{u_G^{i+1} - u_G^i}{D}} \quad (6)$$

### Relationship Between Local and Global Strain Rates for Notched Geometries

In this section, the concepts previously established are developed for notched geometries, and the relationship between local and global strain rates is numerically computed. In order to make the results more general, a set of four notched geometries of maximum and minimum notch depths and radii were chosen (Fig. 2), with the following dimensions

Sample	$R/D$	$A/D$
A	0.03	0.10
B	0.05	0.39
C	0.36	0.10
D	0.40	0.39

where  $R$  is the notch radius,  $A$  the notch depth, and  $D$  the specimen diameter. These geometries produce very different triaxial stress states in the vicinity of the notch.

The material is modeled as strain hardening according to the Ramberg-Osgood expression

$$\epsilon = \frac{\sigma}{E} + \left(\frac{\sigma}{P}\right)^n \quad (7)$$

where  $E = 199$  GPa,  $P = 2100$  MPa, and  $n = 4.9$  are the values corresponding to the high-strength steel chosen for the SSRT program described in the next section of this paper.

This analysis was carried out under the conceptual framework of the Continuum Mechanics theory by using incremental Plasticity. The finite element method with an elastic-plastic code was used in the computations. The material was considered homogeneous and isotropic.

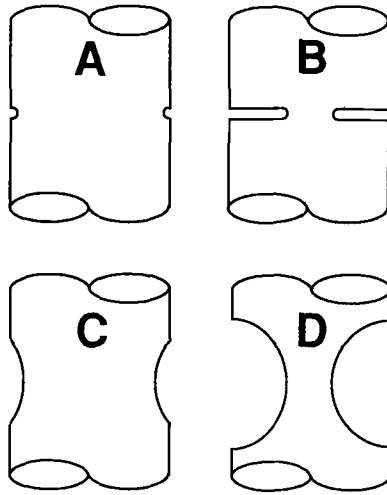


FIG. 2—Notched geometries used to produce different triaxial stress state in the vicinity of the notch.

In practice, it is necessary to choose reference lengths for local and global strain rates. Local reference length ( $B$ ) must be short enough to guarantee the convergence of the computing procedure, and greater than the relevant microstructural characteristic parameter (usually the material grain size), to assure the validity of the assumption of a homogeneous continuum approach, that is, the agreement between the mechanical model and the microphysical reality of the material. As shown in Fig. 3, local reference length ( $B_{\min}$ ), must be greater than—or at least equal to—the characteristic microstructural size of the material ( $x_p$ ).

Mathematical convergence is automatically guaranteed, since the axial displacement distribution is continuous. The objective then is to check from which local reference lengths the solution is accurate enough, however keeping the chosen reference length higher than the material grain size or similar characteristic size of the material microstructure. From the numerical computations, it is possible to conclude that approach to solution is faster when the stress concentration is lower, the convergence being better for geometry  $C$  (maximum radius, minimum depth), and worse for geometry  $B$  (minimum radius, maximum depth). Considering geometry  $B$  as the least convergent, the accuracy is excellent for a local reference length  $B/D = 0.01$ . In this case, the relative error of local strain rate is below 1%. Adopting  $D = 10$  mm as a minimum value of the specimen diameter results in  $B = 100$   $\mu\text{m}$ , clearly greater than the characteristic microstructural size of many materials (e.g., high-strength pearlitic steel, average pearlite colony size: 15  $\mu\text{m}$ ), material for which the research presented here has a special interest. The mathematical model, therefore, agrees fairly well with the microphysical reality of the material.

Global reference length ( $L$ ) should be long enough to permit uniaxial stress state at its ends, so the influence of the notch on the stress state at the ends of the reference length becomes negligible. A value  $L = 4D$  is enough for this purpose, according to the numerical computations.

With these local and global reference lengths, the expressions (4) and (5) for the strain rates become

$$\dot{\epsilon}_L = \frac{u_L^{t+\Delta t}(0.01D) - u_L^t(0.01D)}{0.01 D \Delta t} \quad (8)$$

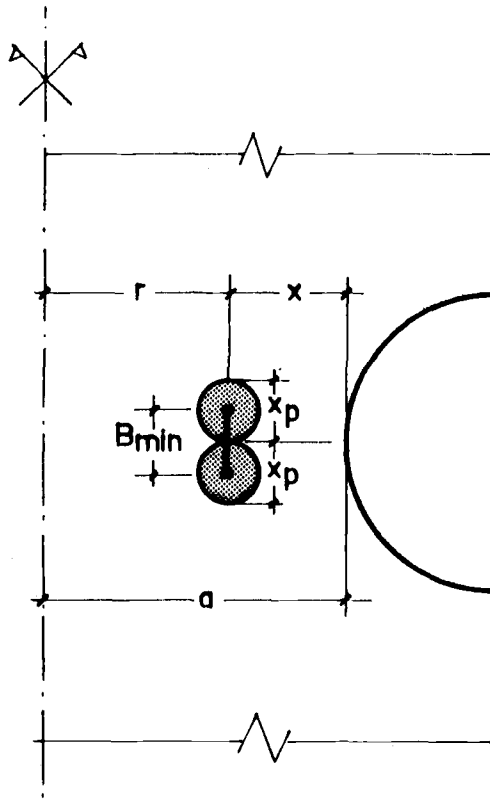


FIG. 3—Minimum local reference length ( $B_{\min}$ ), greater than, or at least equal to, the characteristic microstructural size of the material ( $x_p$ ).

$$\dot{\epsilon}_G = \frac{u_G^{j+1}(4D) - u_G^j(4D)}{D\Delta t} \quad (9)$$

where the variables between parentheses are the local ( $0.01D$ ) and global ( $4D$ ) reference lengths, distances on which the relative displacements between the ends are measured to compute the local and global strains.

A general plot of  $\dot{\epsilon}_L/\dot{\epsilon}_G$  as a function of the global strain  $\epsilon_G$  for all geometries is given in Fig. 4, where local strain rate is computed just at the notch tip. The relationship between local and global strain rates changes with time, as the plastic zone spreads or the global strain (or more properly the dimensionless global displacement) increases. For the wide range of geometries analyzed in this paper, the curve has always the same general aspect, and three regions can be distinguished, each representing a phase of the process. Region I (elastic phase) is horizontal; the whole specimen is in elastic regime, and plastification has not yet begun. Region II (transition phase) has a very pronounced slope; plastification starts at the notch tip and spreads progressively. Region III (plastic phase) is slightly increasing or quasi-horizontal, and plastification reaches the specimen axis.

Notch depth directly influences the length of the transition phase (II). Both notch depth and radius influence the numerical value of the relationship between local and global strain

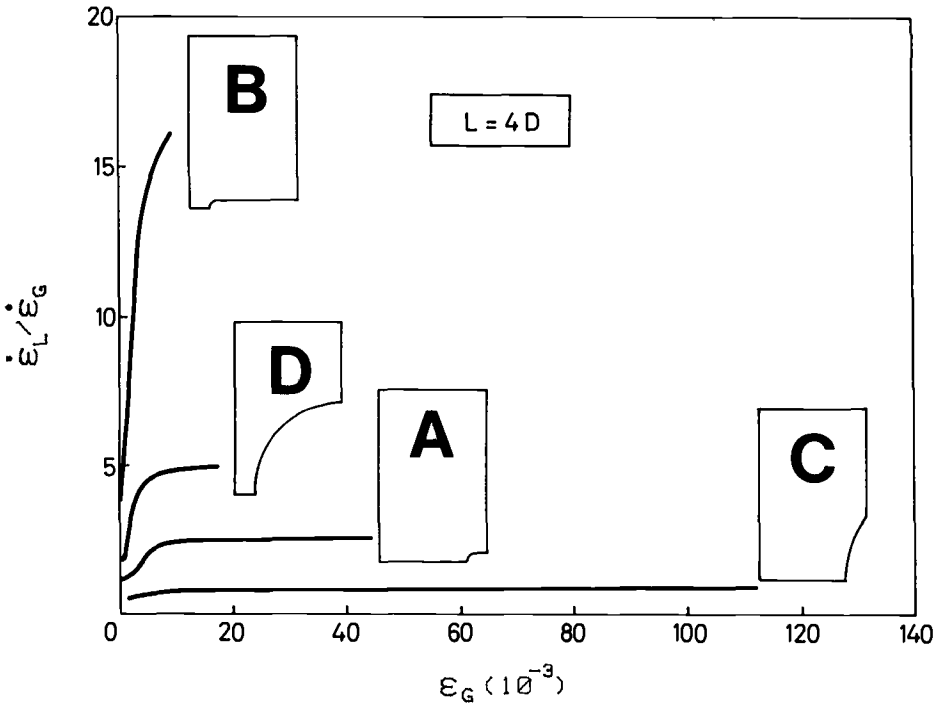


FIG. 4—Relationship between local and global strain rates as a function of global strain (general results at the notch tip).

rates during elastic (I) and plastic (III) phases. The more severe the notch (the lower the radius and the greater the depth), the higher the stress concentration and, therefore, the local strain rate. In all cases the elastic phase is a small percentage of the loading process. The length of the elastic region is a function of the yield strength of the material, increasing with it.

From dimensional analysis, the relationship between the local strain rate at the notch tip and the global strain rate at the specimen ends is

$$\dot{\epsilon}_L / \dot{\epsilon}_G = f(\nu, n, P/E; R/D, A/D, L/D; \epsilon_G) \tag{10}$$

where  $f$  is a function of seven dimensionless variables referring to material properties ( $\nu, n, P/E$ ), geometry ( $R/D, A/D, L/D$ ) and level of loading ( $\epsilon_G$ ). Consideration should be given to the influence of external action  $\epsilon_G$ , which makes the local strain rate  $\dot{\epsilon}_L$  change as the test proceeds, even keeping constant the global strain rate, as usually occurs in slow strain rate tests, in which a constant displacement rate is externally applied on the specimen. Such a variation is not considered in previous calculations of local strain rate at crack tips [23–27,29–32], and is a consequence of the influence of the constitutive equation of the material, and particularly the strain hardening capacity.

To gain insight into this result, the influence of the position of the local reference length (local basis) was analyzed. Such local length is always parallel to  $z$  axis, and will be placed at a variable distance from that axis. Results are shown in Fig. 5 and agree fairly well with previous considerations. Since plastification always begins at the notch tip and spreads

towards the inside, local strain rate is lower as the local basis approaches the specimen axis. The notch produces a stress magnification (and therefore a strain rate magnification) which increases as the notch radius decreases, being maximum in geometry  $A$ .

### Application to SSRT of Notched Bars

When the results presented in this paper are applied to model fracture under aggressive environments and, in particular, when eutectoid pearlitic steels are considered, it is convenient to distinguish between the two regimes associated with EIC phenomena: anodic and cathodic. In the anodic regime the aggressive mechanism is mainly anodic dissolution (or pure SCC) of the metal, oxide film creation (passivation), and film rupture. In the cathodic regime the main mechanism is hydrogen embrittlement (or HAC) [11,18,19].

A standard representation of results from SSRT is in the form of fracture load or reduction in area as a function of externally applied displacement rate. As mentioned in the introductory paragraph, the curve for the anodic regime (SCC) is not monotonic [2,18], but it frequently has a characteristic value of displacement rate for which the aggressiveness of the environment is maximum; for higher values of displacement rate, the solution does not have enough time to corrode the metal surface; for lower values of displacement rate, the passivation takes place and balances the film rupture. The curve for the cathodic regime (HAC), on the other hand, is monotonic [2,18,19]: the higher the displacement rate, the lower the environmental effect, since it is a process of hydrogen diffusion from the solution into the metal.

Modeling anodic dissolution is a complex problem. Apart from the fact that a hydrogen embrittlement mechanism could exist, due to the local electrochemical conditions at the crack or notch tip [33–35], dissolution involves loss of material and geometric changes, which are very difficult to model from the Continuum Mechanics point of view. On the other hand, values obtained for the local strain rate just at the notch tip are truly representative, since chemical attack, passivation, and film rupture are localized in this region, it thus being unnecessary to compute space average values. Finally, time average values are not representative due to the nature of the phenomenon, which depends on the instantaneous local strain rate.

In cathodic regimes, where the main environmental mechanism is hydrogen embrittlement, geometry remains constant since there is no material dissolution. It can thus be perfectly modeled according to Continuum Mechanics. On the other hand, there is an extended process zone or hydrogen affected area, which is the region damaged by hydrogen, which diffuses from the boundary to the internal part of the specimen. Local strain rate, therefore, must be computed at different depths from the notch tip, as is shown in Fig. 5, and throughout the test duration. Here, space-time averages are representative, as will be shown in the next section of this paper.

A space average of the local strain rate may be defined as

$$\langle \dot{\epsilon}_L \rangle = \frac{1}{\pi(a^2 - r_c^2)} \int_0^{2\pi} \int_{r_c}^a \dot{\epsilon}_L(r) r dr d\theta \quad (11)$$

where  $\langle \rangle$  represents space average. According to Fig. 6,  $a$  is the radius of the net section,  $r_c$  the radial coordinate that defines the end of the critical zone or hydrogen affected area, and  $\dot{\epsilon}_L(r)$  the local strain rate at distance  $r$  from the bar axis. It should be noticed that the local strain rate distribution does not depend on the hoop coordinate  $\theta$  because the problem is axisymmetric.

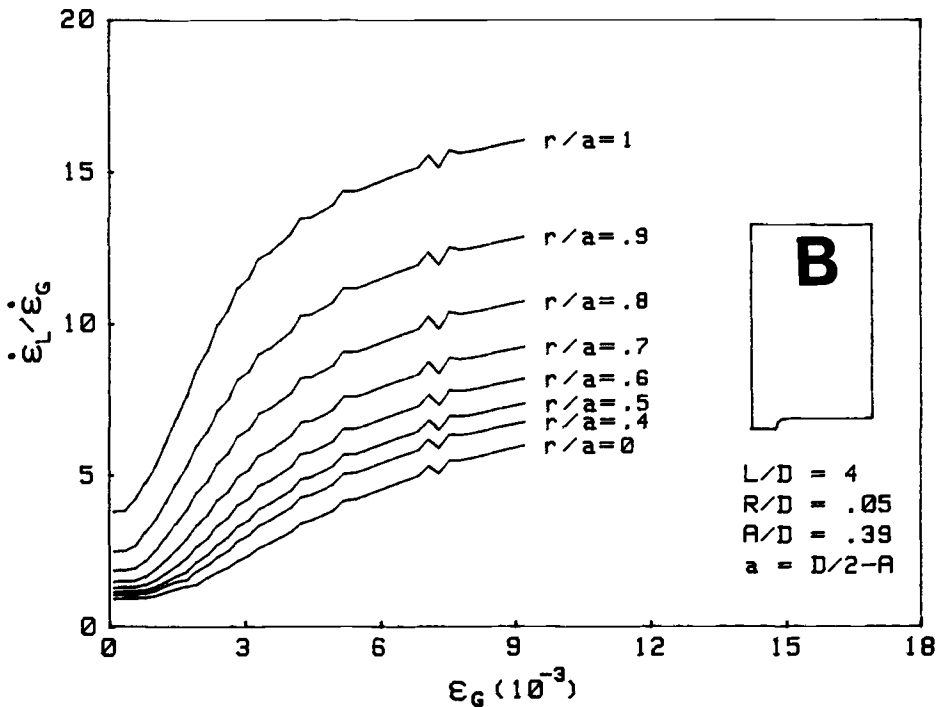
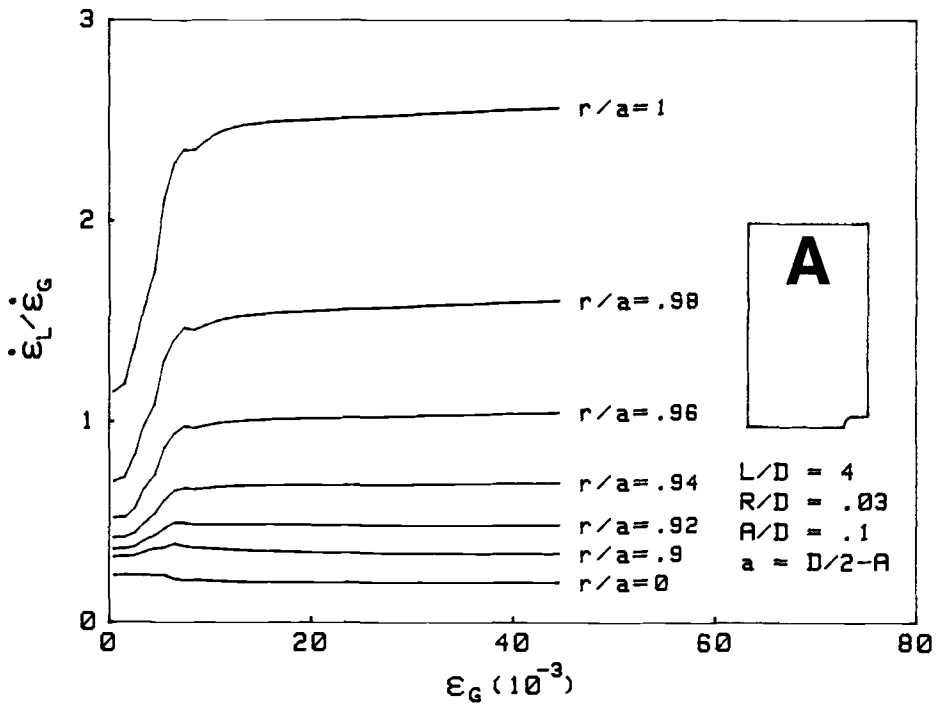
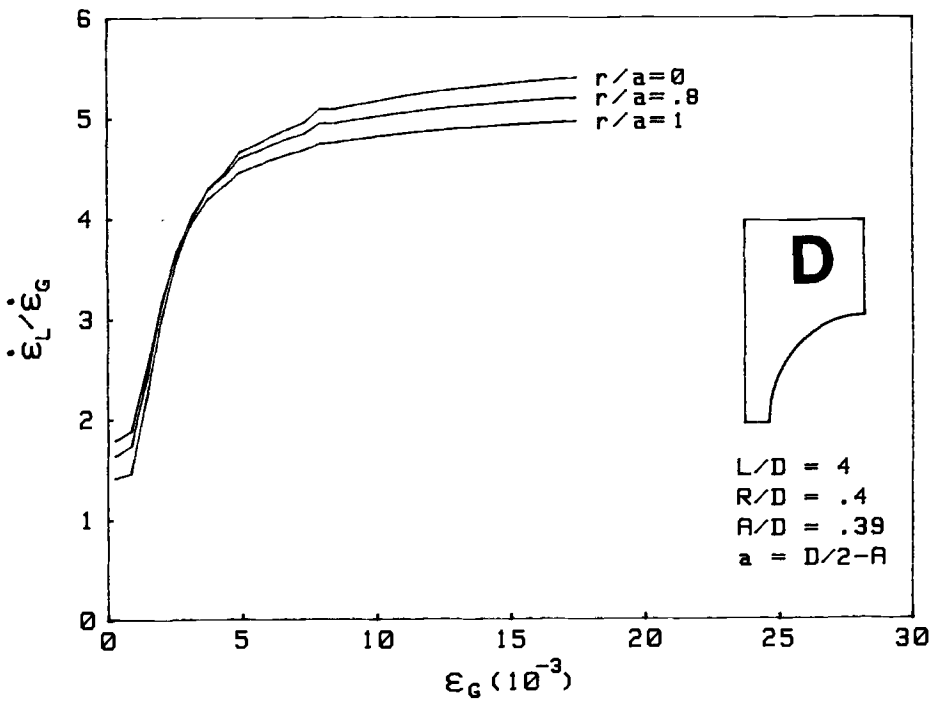
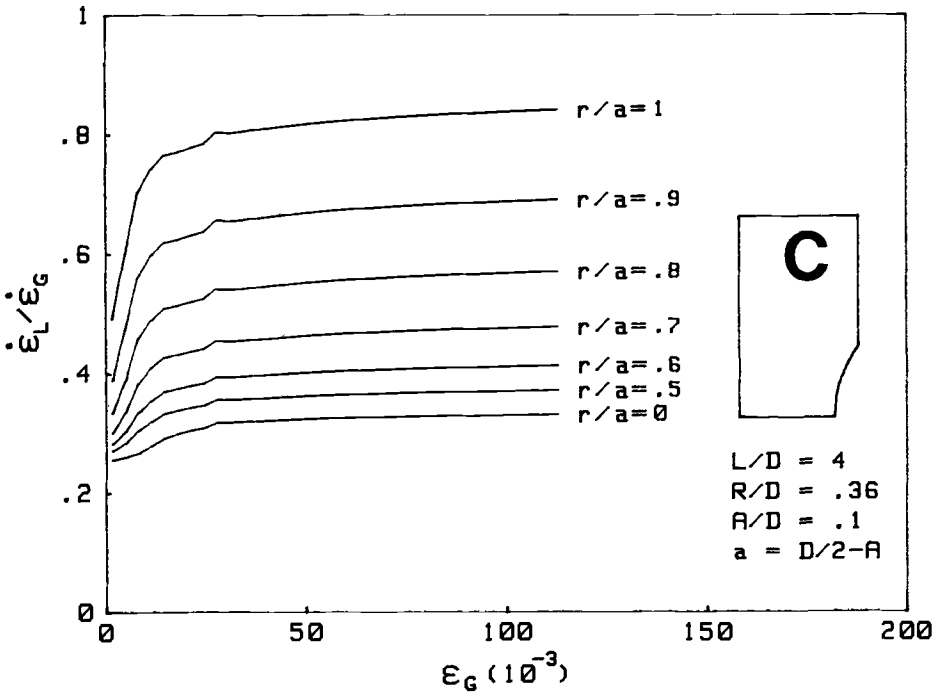


FIG. 5—Relationship between local and global strain rates as a function of global strain, at different points of the net section.



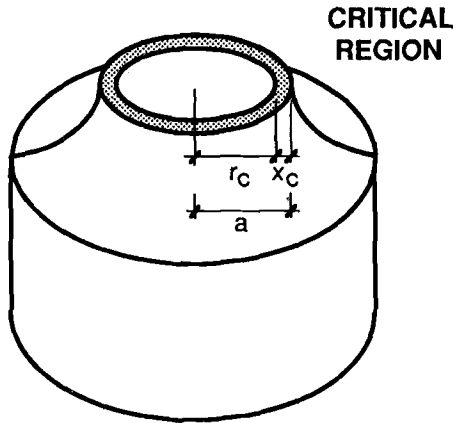


FIG. 6—Critical region for the hydrogen embrittlement criterion.

If, as is frequent, the hydrogen affected region is small enough to have a quasi-linear radial distribution of variables, an approximate expression can be used to compute the space average

$$\langle \dot{\epsilon}_L \rangle = \dot{\epsilon}_L \left( a - \frac{x_c}{2} \right) \tag{12}$$

where  $x_c$  is the depth of the critical region, measured from the notch tip ( $x_c = a - r_c$ , Fig. 6).

To account for the dependence on the global strain throughout the test period, a time average may be carried out from the beginning to the end of the embrittlement tests (i.e., from  $t = 0$  to  $t_c$ , which is the time to failure)

$$\langle\langle \dot{\epsilon}_L \rangle\rangle = \frac{1}{t_c} \int_0^{t_c} \langle \dot{\epsilon}_L \rangle dt \tag{13}$$

where the symbol  $\langle\langle \rangle\rangle$  means space-time average.

In general, fracture criteria in aggressive environments are written as a relation among failure load  $F_C$ , global strain rate  $\dot{\epsilon}_G$  (or global displacement rate  $\dot{u}_G$ ) and specimen geometry, i.e.

$$F(F_C, \dot{\epsilon}_G, \text{geometry}) = 0 \tag{14}$$

Following previous considerations, an improved fracture criteria can be obtained when local strain rate  $\dot{\epsilon}_L$  is considered instead of global strain rate  $\dot{\epsilon}_G$ , i.e.

$$F[F_C, \dot{\epsilon}_L(\dot{\epsilon}_G, \epsilon_G), \text{geometry}] = 0 \tag{15}$$

The application of these results to corrosion-fatigue is clearly beyond the scope of this paper. Nevertheless, some comments can be made about this topic. The synergistic effect of both cyclic loading and environmental effect is greatly influenced by local kinematic variables, since the process is localized at the crack or notch tip (when such a defect actually

exists) and is transient or time-dependent (cf. anodic dissolution and hydrogen embrittlement). Accordingly, it can be suspected that local strain rate at the crack or notch tip plays a relevant role in governing the corrosion-fatigue phenomenon.

**Application to Hydrogen Embrittlement of Round-Notched Specimens**

This paper provides a way to compute  $\dot{\epsilon}_L$  values as a function of  $\dot{\epsilon}_G$  and  $\epsilon_G$  (apart from the dependence on specimen geometry and material properties). These results were applied to the modeling of SSRT on notched specimens of high-strength pearlitic steel in the cathodic regime (hydrogen embrittlement environmental conditions). To this end, slow strain rate tests were performed on round-notched specimens with the four notched geometries sketched in Fig. 2, the specimen diameter being  $D = 11.25$  mm. The electrochemical conditions were  $\text{pH} = 12.5$  and  $E = -1200$  mV SCE, as described elsewhere [36].

Experimental results appear in Fig. 7, which shows the fracture load in the SSRT (divided by fracture load in air), as a function of the cross head speed (or external displacement rate) applied by the testing machine during the tests. The hydrogen embrittlement results plotted in Fig. 7 show quite clearly that although performed at the same global displacement rate  $\dot{u}_G$  (i.e., carried out at the same global strain rate  $\dot{\epsilon}_G = \dot{u}_G/D$ ), the failure load in a hydrogen environment depended on the notch geometry. If, as is suspected, local strain at the notch tip is a more relevant variable, a plot of failure loads versus local strain rate  $\dot{\epsilon}_L$  should give a single curve.

Because fracture loads are also influenced by stress triaxiality—a function of notch geometry—it would be better to apply a more general fracture criterion on the basis of the stress tensor. A simple general criterion can be formulated on the effective or equivalent stress in the Von Mises sense, as previously established [37], applied over the region microscopically affected by the hydrogen ingress: Tearing Topography Surface or TTS, described in previous works [38–40]. Therefore, fracture will take place when the following condition is achieved

$$\langle \bar{\sigma} \rangle = \bar{\sigma}_c \text{ over } x_{\text{TTS}} \tag{16}$$

where  $\bar{\sigma}$  is the equivalent stress (in the Von Mises sense) at any point of the specimen at the fracture instant,  $\bar{\sigma}_c$  is the critical equivalent stress of the material in hydrogen environ-

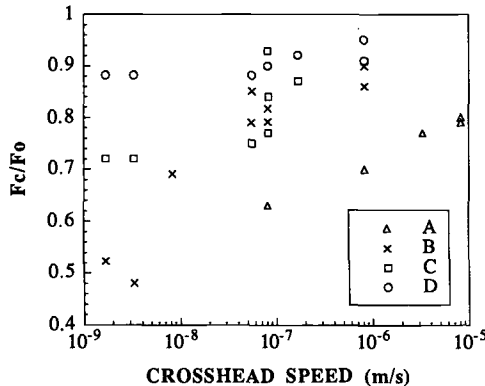


FIG. 7—Fracture load in the SSRT (divided by fracture load in air), as a function of the crosshead speed, or external displacement rate, applied by the testing machine during the tests.

ment, and  $x_{\text{TTS}}$  the depth of the TTS region;  $\langle \rangle$  means in this case the average value over the TTS region, which has to be computed taking into account the cylindrical symmetry of the problem, i.e.

$$\langle \bar{\sigma} \rangle = \frac{1}{\pi(a^2 - r_{\text{TTS}}^2)} \int_0^{2\pi} \int_{r_{\text{TTS}}}^a \bar{\sigma}(r) r dr d\theta \quad (17)$$

where  $r_{\text{TTS}}$  is the radial coordinate that defines the end of the TTS region ( $r_{\text{TTS}} = a - x_{\text{TTS}}$ ) and the other symbols have the same meaning as in Eq 11.

A new step to unify the results from different geometries is the change from  $\dot{\epsilon}_G$  (*global, nominal, or applied strain rate*) to  $\dot{\epsilon}_L$  (*local or effective strain rate*). According to Eq 10, local strain rate  $\dot{\epsilon}_L$  depends—apart from material properties, which are constant in this research—on notch geometry ( $R/D$ ,  $A/D$ ,  $L/D$ ) and global strain  $\epsilon_G$ , the latter being the variable that indicates the level of loading on the specimen and so the extension of the plastic zone. To account for the geometry dependence, a space average of the local strain rate can be made over the TTS zone (microscopically affected region)

$$\langle \dot{\epsilon}_L \rangle = \frac{1}{\pi(a^2 - r_{\text{TTS}}^2)} \int_0^{2\pi} \int_{r_{\text{TTS}}}^a \dot{\epsilon}_L(r) r dr d\theta \quad (18)$$

where  $\langle \rangle$  represents the space average,  $\dot{\epsilon}_L(r)$  is the local strain rate at a distance  $r$  from the bar axis, and the other variables have the same meaning as in Eq 11.

The time average must be computed throughout the SSRT, i.e.

$$\langle \langle \dot{\epsilon}_L \rangle \rangle = \frac{1}{t_c} \int_0^{t_c} \langle \dot{\epsilon}_L \rangle dt \quad (19)$$

where the symbol  $\langle \langle \rangle \rangle$  means space and time average.

Definitions (17) and (19) lead to the following dimensionless relationship

$$F(\bar{\sigma}_c/\bar{\sigma}_o, \langle \langle \dot{\epsilon}_L \rangle \rangle x_s^2/D^*) = 0 \quad (20)$$

where  $\bar{\sigma}_c$  is the critical equivalent stress in hydrogen environment,  $\bar{\sigma}_o$  the same variable in air environment,  $\langle \langle \dot{\epsilon}_L \rangle \rangle$  the space-time average of the local strain rate at the notch tip,  $x_s$  the depth of the maximum hydrostatic stress point in each geometry, and  $D^*$  the diffusion coefficient of hydrogen in steel. It should be noticed that the geometry is represented by only one variable  $x_s$ , the depth of the maximum hydrostatic stress point (measured from the notch tip). This point is a characteristic of each geometry, independent of the loading process, as was previously demonstrated [36]. Its role in hydrogen embrittlement processes is so relevant that the depth of the TTS region in the quasi-static tests reaches exactly the position of the maximum hydrostatic stress point [39,40].

The following data were used in the computations [37]:

$$\bar{\sigma}_o = 1260 \text{ MPa}$$

$$x_s(\text{A}) = 0.3 \text{ mm}$$

$$x_s(\text{B}) = 1.2 \text{ mm}$$

$$x,(C) = 0.8 \text{ mm}$$

$$x,(D) = 1.2 \text{ mm}$$

$$D^* = 5 \times 10^{-11} \text{ m}^2/\text{s}$$

The relationship between the two dimensionless variables of Eq 20 is shown in Fig. 8. It can be observed that some of the results for all geometries fit in the same curve (open and crossed symbols), which demonstrates the role of local strain rate in hydrogen embrittlement of axisymmetric notched specimens. This common curve represents the functional relationship between the critical equivalent stress of the material in hydrogen environment and the local strain rate in the vicinity of the notch tip. In the quasi-static tests (horizontal dashed lines in the left part of Fig. 8, corresponding to the full symbols) the critical equivalent stress in hydrogen environment reaches an asymptotic value different for each geometry. This value limits the range of applicability of the kinematic formulation of the fracture criterion in aggressive environment: for local strain rates higher than those for the quasi-static test of each geometry, the critical equivalent stress of the material in hydrogen environment is a *universal function* (independent of geometry) of the local strain rate.

The local strain rate in the vicinity of the notch tip is so important that, even simply representing failure loads in the SSRT as a function of the space-time average of the local strain rate, all results fit in the same band, as shown in Fig. 9, where it should be noticed that full symbols corresponding to the asymptotic situation (quasi-static tests of each geometry). Given the roughness of this approach (failure load is a single test parameter directly measurable at the end of the test, it being unnecessary to compute the real stress state in the vicinity of the notch tip at the fracture instant), the local strain rate at the notch tip is seen to be a real relevant parameter in SSRT.

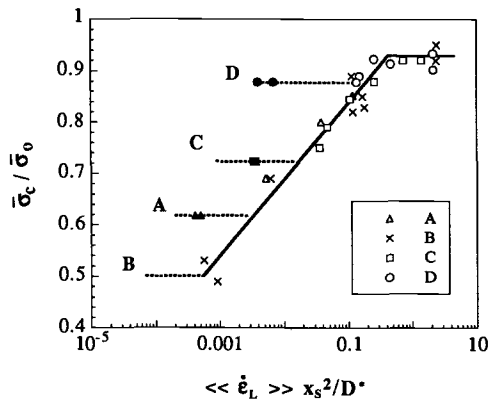


FIG. 8—Critical equivalent stress in the SSRT expressed as a function of the local strain rate in the vicinity of the notch tip ( $\bar{\sigma}_c$ : critical equivalent stress in hydrogen environment;  $\bar{\sigma}_0$ : critical equivalent stress in air;  $\langle \dot{\epsilon}_L \rangle$ : space-time average of the local strain rate in the vicinity of the notch tip,  $x_s$ : depth of the maximum hydrostatic stress point in each geometry,  $D^*$ : diffusion coefficient of hydrogen in steel). Open and crossed symbols represent the kinematic dependence of the results on the local strain rate; full symbols correspond to the quasi-static tests.

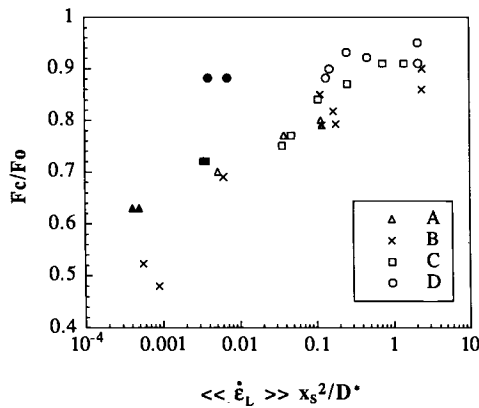


FIG. 9—Fracture load in the SSRT (divided by fracture load in air), as a function of the average local strain rate in the vicinity of the notch tip. Horizontal axis with the same meanings as Fig. 8.

## Conclusions

- (1) In SSRT with precracked and notched specimens, local strain rate at the crack or notch tip—and not externally applied displacement rate—is the variable that controls the EIC.
- (2) This paper provides definitions of the local and global strain rates in cracked and notched geometries, by considering both the mathematical convergence of the method and the agreement between the model and the microphysical reality of the material.
- (3) Local strain rate at the crack or notch tip depends not only on the material properties and specimen geometry, but also on the loading process; that is, on the global strain rate externally applied on the specimen ends. Therefore, the relationship between local and global strain rates is not constant but increases with time, even for constant global strain rate.
- (4) Development of the plastic zone is relevant for the evolution of local strain rate. The importance of the specimen geometry and the constitutive equation, particularly the strain hardening capacity, of the material is thus emphasized.
- (5) Local strain rate results are directly applicable to the modeling of EIC. Usual fracture criteria under aggressive environments can be improved by replacing global strain rates by local ones. For pure SCC, instantaneous values at the notch tip must be used; for HAC, space-time averages of local strain rate are representative.
- (6) Results of SSRT on notched specimens of high-strength pearlitic steel under hydrogen embrittlement environmental conditions can be plotted as a single curve (geometry-independent) by expressing the critical fracture parameter of the material as a function of the local strain rate in the vicinity of the notch tip.
- (7) The importance of local strain rate in the vicinity of the notch tip is emphasized on representing failure loads in the SSRT of different notched geometries as a function of the local strain rate in the vicinity of the notch tip, because the results for all geometries fit in the same band.

## Acknowledgments

This work was supported by the Spanish Office for Science and Technological Research (CICYT) under Grant MAT91-0113-CE. The author would like to thank Professor M. Elices,

Head of the Material Science Department of the Polytechnical University of Madrid, for his encouragement and assistance, and Mr. J. Monar, Nueva Montaña Quijano Company, Santander, Spain, for providing the steel used in the experimental program. In addition, the author wishes to express his gratitude to the Colegio de Ingenieros de Caminos, Canales y Puertos, Demarcación de Galicia, Spain, for the financial support of technical trips during the final stages of this work.

## References

- [1] Parkins, R. N., "Development of Strain-Rate Testing and Its Implications," *Stress Corrosion Cracking: The Slow Strain Rate Technique, ASTM STP 665*, G. M. Ugiansky and J. H. Payer, Eds., American Society for Testing and Materials, Philadelphia, 1979, pp. 5–25.
- [2] Kim, C. D. and Wilde, B. E., "A Review of the Constant Strain-Rate Stress Corrosion Cracking Test," *Stress Corrosion Cracking: The Slow Strain Rate Technique, ASTM STP 665*, G. M. Ugiansky and J. H. Payer, Eds., American Society for Testing and Materials, Philadelphia, 1979, pp. 97–112.
- [3] Scully, J. C., "Propagation of Stress Corrosion Cracks Under Constant Strain-Rate Conditions," *Stress Corrosion Cracking: The Slow Strain Rate Technique, ASTM STP 665*, G. M. Ugiansky and J. H. Payer, Eds., American Society for Testing and Materials, Philadelphia, 1979, pp. 237–253.
- [4] Puiggali, M., Desjardins, D., and Ajana, L., "A Critical Study of Stress Corrosion Cracking Testing Methods for Stainless Steels in Hot Chloride Media," *Corrosion Science*, Vol. 27, 1987, pp. 585–594.
- [5] Caballero, L., García-Cordovilla, C., Pamies, A., Louis, E., and Elices, M., "Advantages of Notched Specimens in SSR Tests," *Fracture Behaviour and Design of Materials and Structures-ECF8*, D. Firrao, Ed., EMAS, West Midlands, U.K., 1990, pp. 492–495.
- [6] Thompson, A. W., "Hydrogen-Assisted Fracture at Notches," *Materials Science and Technology*, Vol. 1, 1985, pp. 711–718.
- [7] Scully, J. C., "The Interaction of Strain-Rate and Repassivation Rate in Stress Corrosion Crack Propagation," *Corrosion Science*, Vol. 20, 1980, pp. 997–1016.
- [8] Ford, F. P., "Stress Corrosion Cracking," *Corrosion Processes*, R. N. Parkins, Ed., Applied Science Publishers, London, 1982, pp. 271–309.
- [9] Takano, M., "Relationship Between Stress Corrosion Cracking and Strain Rates," *Proceedings, 5th International Congress Metallic Corrosion*, Tokyo, 1972, National Association of Corrosion Engineers, Houston, TX, 1972.
- [10] Ford, F. P. and Silverman, M., "Effect of Loading Rate on Environmentally Controlled Cracking of Sensitized 304 Stainless Steel in High Purity Water," *Corrosion*, Vol. 36, 1980, pp. 597–603.
- [11] Parkins, R. N., Elices, M., Sánchez-Gálvez, V., and Caballero, L., "Environment Sensitive Cracking of Pre-Stressing Steels," *Corrosion Science*, Vol. 22, 1982, pp. 379–405.
- [12] Hinton, B. R. W. and Procter, R. P. M., "The Effect of Strain-Rate and Cathodic Potential on the Tensile Ductility of X-65 Pipeline Steel," *Corrosion Science*, Vol. 23, 1983, pp. 101–123.
- [13] Abramson, G., Evans, J. T., and Parkins, R. N., "Investigation of Stress Corrosion Crack Growth in Mg Alloys Using *J*-Integral Estimations," *Metallurgical Transactions A*, Vol. 16A, 1985, pp. 101–108.
- [14] Herbsleb, G. and Schwenk, W., "The Influence of Dynamic Mechanical Parameters on Stress Corrosion Cracking of Steel—A Review," *Corrosion*, Vol. 41, 1985, pp. 431–437.
- [15] Mayville, R. A., Warren, T. J., and Hilton, P. D., "The Influence of Displacement Rate on Environmentally Assisted Cracking of Pre-cracked Ductile Steel Specimens," *Journal of Engineering Materials and Technology*, Vol. 109, 1987, pp. 188–193.
- [16] Mayville, R. A., Warren, T. J., and Hilton, P. D., "Determination of the Loading Rate Needed to Obtain Environmentally Assisted Cracking in Rising Load Tests," *Journal of Testing and Evaluation*, Vol. 17, 1989, pp. 203–211.
- [17] Magnin, T., Chieragatti, R., and Oltra, R., "Mechanism of Brittle Fracture in a Ductile 316 Alloy During Stress Corrosion," *Acta Metallurgica et Materialia*, Vol. 38, 1990, pp. 1313–1319.
- [18] Sánchez-Gálvez, V., Caballero, L., and Elices, M., "The Effect of Strain Rate on the Stress Corrosion Cracking of Steels for Prestressing Concrete," *Laboratory Corrosion Tests and Standards, ASTM STP 866*, G. Haynes and R. Baboian, Eds., American Society for Testing and Materials, Philadelphia, 1985, pp. 428–436.

- [19] Burnell, G., Hardie, D., and Parkins, R. N., "Stress Corrosion and Hydrogen Embrittlement of Two Precipitation Hardening Stainless Steels," *British Corrosion Journal*, Vol. 22, 1987, pp. 229–237.
- [20] Scully, J. R. and Moran, P. J., "Influence of Strain on the Environmental Hydrogen-Assisted Cracking of a High-Strength Steel in Sodium Chloride Solution," *Corrosion*, Vol. 44, 1988, pp. 176–185.
- [21] Rieck, R. M., Atrens, A., and Smith, I. O., "The Role of Crack Tip Strain Rate in the Stress Corrosion Cracking of High Strength Steels in Water," *Metallurgical Transactions A*, Vol. 20A, 1989, pp. 889–895.
- [22] Patel, P. S. and Jarman, R. A., "Strain Distribution Around a Stress Corrosion Crack Tip," *British Corrosion Journal*, Vol. 20, 1985, pp. 23–27.
- [23] Lidbury, D. P. G., "The Estimation of Crack Tip Strain Rate Parameters Characterizing Environment Assisted Crack Growth Data," *Embrittlement by the Localized Crack Environment*, R. P. Gangloff, Ed., AIME, New York, 1983, pp. 149–172.
- [24] Maiya, P. S., "Quantitative Description of Strain Rate Effects on Susceptibility to Intergranular Stress Corrosion Cracking," *Advances in Fracture Research—ICF6*, S. R. Valluri et al., Eds., Pergamon Press, Oxford, 1984, pp. 2335–2343.
- [25] Maiya, P. S., "Prediction of Environmental and Strain-Rate Effects on the Stress Corrosion Cracking of Austenitic Stainless Steels," *Journal of Pressure Vessel Technology*, Vol. 109, 1987, pp. 116–123.
- [26] Maiya, P. S. and Shack, W. J., "Stress Corrosion Cracking Susceptibility of AISI 316 NG and 316 Stainless Steel in an Impurity Environment," *Corrosion*, Vol. 41, 1985, pp. 630–634.
- [27] Congleton, J., Shoji, T., and Parkins, R. N., "The Stress Corrosion Cracking of Reactor Pressure Vessel Steel in High Temperature Water," *Corrosion Science*, Vol. 25, 1985, pp. 633–650.
- [28] Rice, J. R. and Sorensen, E. P., "Continuing Crack-Tip Deformation and Fracture for Plane-Strain Crack Growth in Elastic-Plastic Solids," *Journal of Mechanics and Physics of Solids*, Vol. 26, 1978, pp. 163–186.
- [29] Parkins, R. N., "Factors Influencing Stress Corrosion Crack Growth Kinetics," *Corrosion*, Vol. 43, 1987, pp. 130–139.
- [30] Parkins, R. N., "The Application of Stress Corrosion Crack Growth Kinetics to Predicting Lifetimes of Structures," *Corrosion Science*, Vol. 29, 1989, pp. 1019–1038.
- [31] Parkins, R. N., "Strain Rate Effects in Stress Corrosion Cracking," *Corrosion*, Vol. 46, 1990, pp. 178–189.
- [32] Andresen, P. L. and Ford, F. P., "Life Prediction by Mechanistic Modeling and System Monitoring of Environmental Cracking of Iron and Nickel Alloys in Aqueous Systems," *Materials Science and Engineering A*, Vol. A103, 1988, pp. 167–184.
- [33] Brown, B. F., Fujii, C. T., and Dahlberg, E. P., "Methods for Studying the Solution Chemistry Within Stress Corrosion Cracks," *Journal of the Electrochemical Society*, Vol. 116, 1969, pp. 218–219.
- [34] Barth, C. F., Steigerwald, E. A., and Troiano, A. R., "Hydrogen Permeability and Delayed Failure of Polarized Martensitic Steels," *Corrosion-NACE*, Vol. 25, 1969, pp. 353–358.
- [35] Turnbull, A., "The Solution Composition and Electrode Potential in Pits, Crevices and Cracks," *Corrosion Science*, Vol. 23, 1983, pp. 833–870.
- [36] Toribio, J., Lancha, A. M., and Elices, M., "Macroscopic Variables Governing the Microscopic Fracture of Pearlitic Steels," *Materials Science and Engineering A*, Vol. A145, 1991, pp. 167–177.
- [37] Toribio, J., *Fractura Elasto-Plástica de Alambres Entallados*, Ph.D. thesis, Polytechnical University of Madrid, Spain, 1987.
- [38] Toribio, J., Lancha, A. M., and Elices, M., "Characteristics of the New Tearing Topography Surface," *Scripta Metallurgica et Materialia*, Vol. 25, 1991, pp. 2239–2244.
- [39] Toribio, J., Lancha, A. M., and Elices, M., "Hydrogen Embrittlement of Pearlitic Steels: Phenomenological Study on Notched and Pre-cracked Specimens," *Corrosion*, Vol. 47, 1991, pp. 781–791.
- [40] Toribio, J., Lancha, A. M., and Elices, M., "The Tearing Topography Surface as the Zone Associated with Hydrogen Embrittlement Processes in Pearlitic Steel," *Metallurgical Transactions A*, Vol. 23A, 1992, pp. 1573–1584.

M. G. Vassilaros,<sup>1</sup> R. L. Juers,<sup>1</sup> M. E. Natishan,<sup>1</sup> and  
A. K. Vasudevan<sup>2</sup>

## Environmental Slow Strain Rate *J*-Integral Testing of Ni-Cu Alloy K-500

---

**REFERENCE:** Vassilaros, M. G., Juers, R. L., Natishan, M. E., and Vasudevan, A. K., "Environmental Slow Strain Rate *J*-Integral Testing of Ni-Cu Alloy K-500," *Slow Strain Rate Testing for the Evaluation of Environmentally Induced Cracking: Research and Engineering Applications*, ASTM STP 1210, R. D. Kane, Ed., American Society for Testing and Materials, Philadelphia, 1993, pp. 123–133.

**ABSTRACT:** An investigation of the combined effects of slow strain rate testing and cathodic protection of Ni-Cu Alloy K-500 forgings was performed. The *J*-integral fracture toughness tests were performed in a modified screw-driven Instron testing machine with measured cross head travel speeds of 0.1, 0.013, and 0.001 mm/min (0.004, 0.0005, and 0.000 04 in./min). The 1T compact specimens used were modified for use with direct current potential drop (DCPD) measurement of the crack lengths. Specimens tested at 0.1, 0.013, and 0.001 mm/min were in an air environment. Additional specimens were tested at 0.001 mm/min in a 3.5% NaCl solution with an applied cathodic potential of  $-1.0$  V (SCE). The tests were monitored with a desk top computer data acquisition system that recorded load, load-line opening displacement (COD), DCPD, applied cathodic potential, and impressed current. These data were used to construct *J*-integral resistance (*J*-*R*) curves for all the samples. The *J*-*R* curves for all the specimens tested in air had appeared similar. The specimens tested in salt water with cathodic protection had significant reduction in *J*-integral toughness ( $J_{ic}$ ) to less than half the air value. Examination of the specimens' fracture surfaces revealed that the cathodic protection caused the fracture mode to change from dimpled rupture to intergranular fracture.

**KEYWORDS:** *J*-integral fracture, Monel K-500, slow strain rate, hydrogen embrittlement

The nickel-copper alloy K-500 (K-500) is a high-strength, high-toughness alloy with excellent corrosion resistance. The normal fracture mode of this material is transgranular ductile microvoid growth and coalescence. However, it has been reported that this material has shown a susceptibility to intergranular, brittle fracture in the presence of hydrogen [1,2]. The use of this material in marine environments with steel, which requires cathodic protection, will require the K-500 to have resistance to any deleterious effects of hydrogen. The possible reduction in toughness resulting from a change in fracture mode should be evaluated in order to quantify the effects of hydrogen. This change in toughness could be measured using *J*-integral techniques which would measure the response of the material to hydrogen produced by cathodic protection.

The hydrogen effects must be measured at rates that are slow enough to allow for the diffusion of hydrogen to the deformation zone. The purpose of the research reported here was to establish a *J*-integral test technique for evaluating the effect of hydrogen resulting from cathodic protection and to initiate a study of these effects on K-500.

---

<sup>1</sup> David Taylor Research Center, Annapolis, MD 21402.

<sup>2</sup> Office of Naval Research, Washington, D.C. 22217.

TABLE 1—Chemical composition of Monel K-500 Materials.

Element	Air Melted, wt. %	Electro-Slag Remelted, wt. %
Nickel	64.9	64.9
Copper	28.8	29.3
Cobalt	0.006	0.011
Silicon	0.13	0.18
Sulfur	0.001	0.002
Phosphorus	<0.004	<0.004
Carbon	0.16	0.141
Iron	0.99	0.62
Titanium	0.53	0.48
Zirconium	0.024	0.026
Niobium	0.047	0.045
Aluminum	3.01	2.89
Manganese	0.76	0.77
Oxygen	0.0007	0.00125
Nitrogen	0.0003	0.0008

### Material

Two Ni-Cu alloy K-500 materials in the forged condition were used in this study. The materials were produced by using an electro-slag remelt (ESR) process, and the other by using an air melt process. The specimens produced from these materials had identification codes HJ-xx for electro-slag remelted material and EJ-xx for the air melted material. The chemical composition and room temperature mechanical properties are shown in Tables 1 and 2.

### Experimental

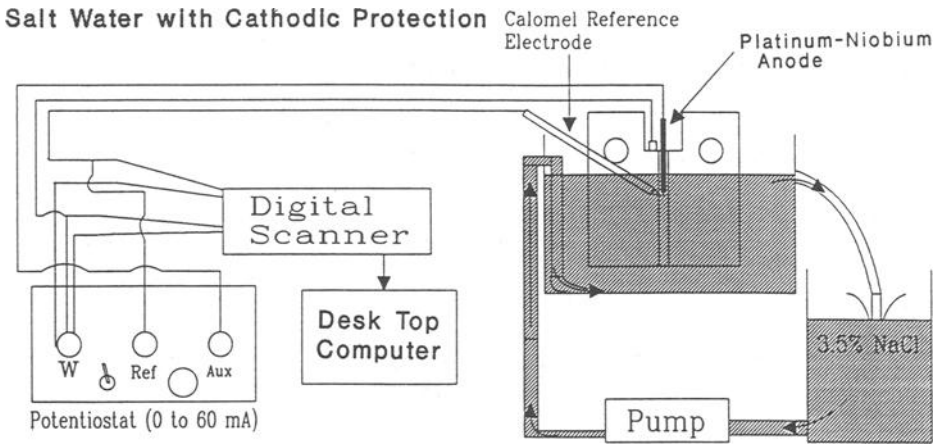
The  $J$ -integral fracture toughness tests were performed using a direct current potential drop (DCPD) technique applied to 1T compact specimens as described by Vassilaros and Hackett [3]. This technique, shown schematically in Fig. 1, measures the crack length in a specimen that has a constant current flowing through the remaining ligament, by monitoring the change in potential drop across the crack mouth. The crack length from DCPD, load, and change in load line opening displacement data were acquired with a desktop computer and used to calculate the applied  $J$ -integral value throughout the test as described in ASTM E 1152, Test Method for Determining  $J$ - $R$  Curves. The  $J$ -integral resistance ( $J$ - $R$ ) curves were used to calculate the fracture toughness initiation value  $J_{Ic}$  as described in ASTM E 813 Test Method for  $J_{Ic}$ , A Measure of Fracture Toughness. The slope of the  $J$ - $R$  curve beyond the initiation point ( $J_{Ic}$ ) is an indication of the residual toughness remaining in the

TABLE 2—Room temperature mechanical properties.

	Air Melted (EJ)	Electro-Slag Remelted (HJ)
Yield Strength, 0.2%	669 MPa	634 MPa
Ultimate Tensile Strength	1089 MPa	1007 MPa
% Elongation	27	31

Reported values are the average of three tests.

Tensile specimen had 13-mm diameter and 51-mm gage length.



**Direct Current Potential Drop**

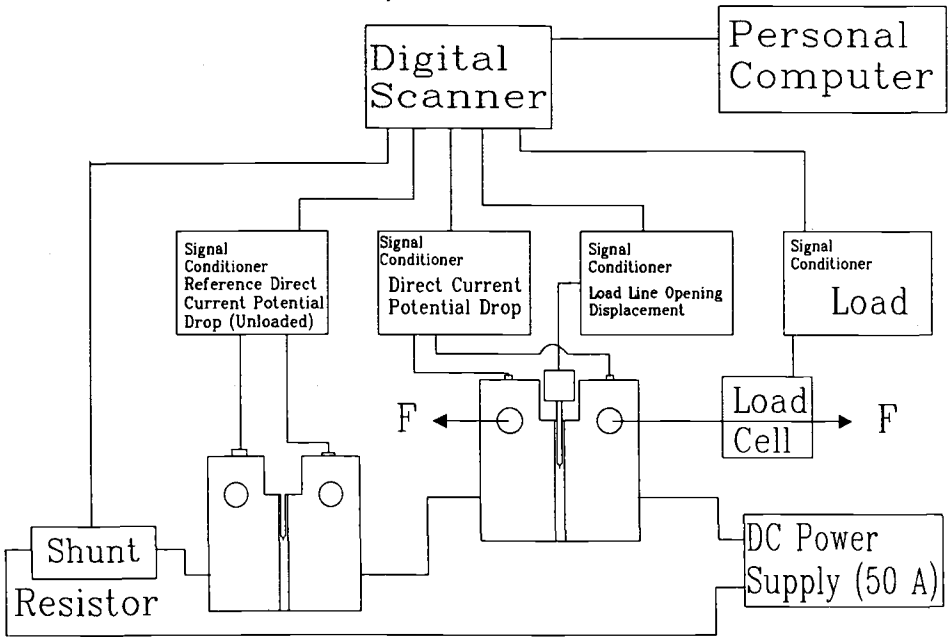


FIG. 1—Schematic of test setup.

material. It can be quantified by the Paris "Tearing Modulus," ( $T$ ) as described by Paris and co-workers [4]. The tearing modulus for these tests was calculated using the normalized slope of the  $J$ - $R$  curve calculated between initiation ( $\Delta a \approx 0.1$  mm) and a crack extension of 1.5 mm. The slope values were normalized using the Paris equation as follows

$$T = (J\text{-}R \text{ curve slope } dJ/da) * E/(\text{Flow stress})^2$$

where

$$\text{Flow stress} = (\text{yield stress} + \text{ultimate tensile stress})/2, \text{ and} \\ E = \text{elastic modulus.}$$

The specimens were precracked to crack length to specimen width ratios ( $a/W$ ) of 0.65 to 0.70. The specimens were tested at a series of cross head rates from 0.100 to 0.001 mm/min. The specimens were unloaded after a crack mouth opening displacement (CMOD) at the load line of  $\approx 6$  mm was achieved. Each specimen was then heat tinted and fatigued open. The fracture surfaces were photographed and used as input data (via a digitizing tablet) for a desktop computer program that measured the initial and final crack lengths. These crack lengths were used in the  $J$ -integral DCPD technique to correct for any material variability or set-up effects of the initial dc potential [3]. The test specimens were then sectioned to remove the fracture surface which was examined in a scanning electron microscope.

The specimens were tested in a 45-kN screw-driven testing machine that had been modified to run with cross head rates from 1 to .001 mm/min while mounted horizontally. The horizontal loading position was desired to minimize difficulties resulting from testing specimens in a 3.5% NaCl solution with cathodic protection of  $-1.0$  V measured with a saturated calomel reference electrode (SCE). This setup is shown schematically in Fig. 1. The entire specimen was painted with a Micro Stop-Off Lacquer to provide isolation from the environment and the notch tip was then sanded to expose the base surface of the K-500 to the environment. The current needed to provide cathodic protection for the entire specimen was beyond the capacity of the 60 mA potentiostat. The reference electrode was placed in the salt water as close as possible to the notch tip. The anode for the cathodic potential was an expanded metal screen of platinum-niobium alloy that was covered with a fine nylon mesh to isolate it from the test specimen. The anode was placed into the specimen notch. The DCPD potential, applied DCPD current, applied cathodic potential, and current were measured with a scanning digital volt meter and input into the desktop computer for data storage with the load line CMOD and load data.

The tests were performed at cross head rates of 0.1 to 0.001 mm/min as listed in Table 3. The 3.5% NaCl solution with cathodic protection environment was used with the specimens tested at a cross head rate 0.001 mm/min. The remaining specimens were tested in an air environment.

TABLE 3—Integral fracture toughness results for nickel-copper alloy K-500.

Spec. ID	Cross Head Rate, mm/min	Test Environ't	$J_{ic}$ kJ/m <sup>2</sup>	$J$ -1.5 mm kJ/m <sup>2</sup>	Tearing Modulus	Crack Extension, mm
EJ	>0.127	AIR	197	—	—	—
EJ	>0.127	AIR	177	—	—	—
ET-54	0.102	AIR	197	385	33	6.04
EJ-45	0.013	AIR	198	385	33	6.29
EJ-55	0.001	AIR	182	368	32	7.20
EJ-56	0.001	SW + CP*	53	175	21	8.27
HJ	>0.127	AIR	242	—	—	—
HJ	>0.127	AIR	247	—	—	—
HJ-52	0.013	AIR	228	490	53	5.18
HJ-44	0.001	AIR	250	508	52	4.89
HJ-50	0.001	SW + CP*	64	324	53	6.39

\* SW + CP = 3.5% NaCl with Cathodic Protection  $-1V$  (SCE).

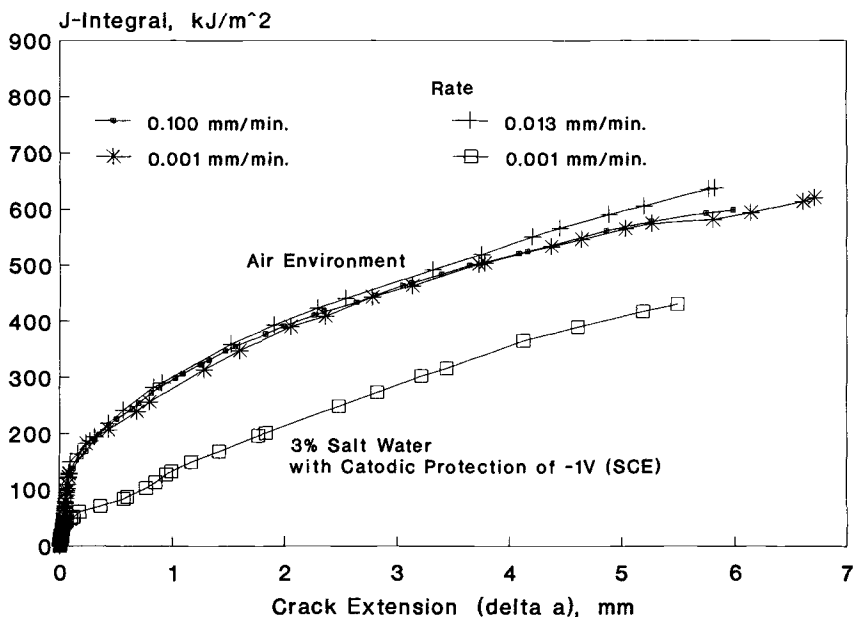


FIG. 2— $J$ - $R$  curves for Ni-Cu alloy Monel K-500, air melted.

## Results and Discussion

The results of the  $J$ -integral test are shown in Table 3 and Figs. 2 and 3 for the air melted and ESR Ni-Cu Alloy K-500 materials. Figure 2 contains the  $J$ - $R$  curves for the air melted K-500 tested at .100 to .001 mm/min in air and 3.5% NaCl with cathodic protection of  $-1.0$

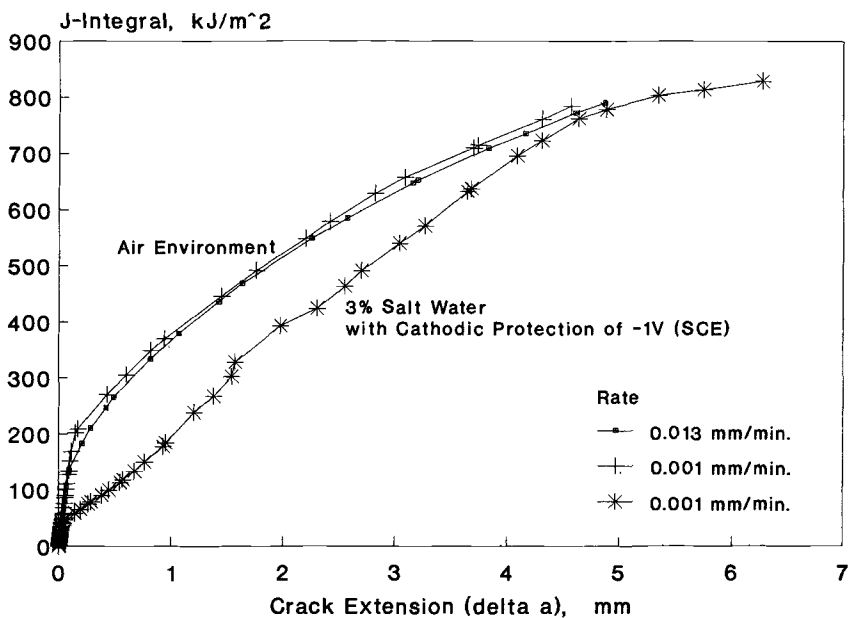


FIG. 3— $J$ - $R$  curves for Ni-Cu alloy Monel K-500, electro-slag remelted (ESR).

V (SCE). Figure 3 contains the  $J$ - $R$  curve results for the electro-slag remelted (ESR) K-500. The two figures show the effects of cathodic potential on the fracture toughness of the two K-500 materials. In both cases  $J$ - $R$  curves for the tests performed in an air environment were higher than the results from the tests performed in a salt water with cathodic protection environment. The fracture toughness  $J_{Ic}$  for the test specimens is listed in Table 3 along with some previous but unpublished results from Natishan on the same materials. The  $J_{Ic}$  results clearly show a reduction in initiation toughness resulting from the hydrogen generated by the cathodic protection of  $-1$  V (SCE). The fracture toughness in air was approximately five times higher than the specimens with hydrogen generated at the crack. The  $J_{Ic}$  values versus cross head rate for K-500 are shown in Fig. 4 which clearly shows the effect.

The fracture surfaces of the Ni-Cu Alloy K-500 specimens indicated a change in fracture mode resulting from the salt water with cathodic protection. Figure 5 has the scanning electron microscope (SEM) fractographs of the crack tip regions for specimens EJ-55 and HJ-44 which were tested with a cross head rate of 0.001 mm/min in an air environment. Both fracture surfaces can be described as dimpled rupture. The SEM fractographs for the air melted and ESR melted K-500 specimens EJ-56 and HJ-50 tested at 0.001 mm/min in a salt water with cathodic protection environment are in Fig. 6. The fractographs of the fracture surface near the crack tip indicate that the specimens failed in an intergranular type fracture mode. The effects of hydrogen on the mechanical properties of K-500 has been reported by Harris and co-workers [5], which included a 40 to 80% reduction in ductility in hydrogen precharged smooth tensile specimens tested in air. The tensile specimens also displayed an outer layer of intergranular fracture with a depth that was proportional to the hydrogen charging time. The observed intergranular fracture mode caused by the hydrogen produced by cathodic protection has been modeled and reported [6,7]. The hydrogen damage was reported to result from a lattice decohesion mechanism whereby the atomic bond energy is lowered in the presence of hydrogen. The grain boundary damage results from the hy-

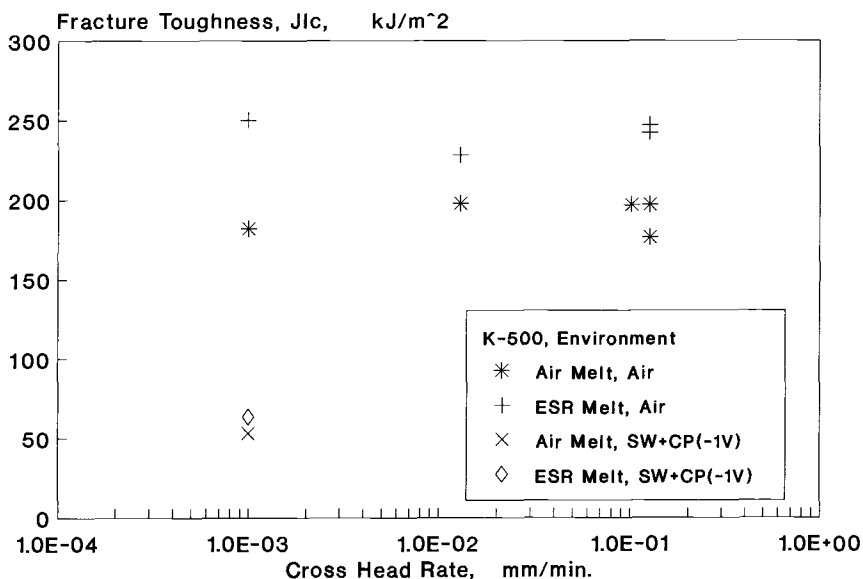
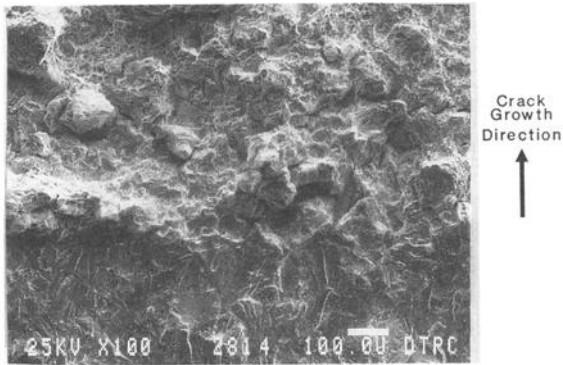
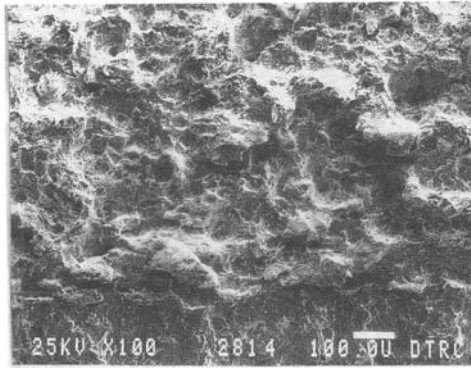


FIG. 4— $J$ -integral results for Ni-Cu Monel K-500.



Specimen EJ-55, Near Center of Fatigue Crack Tip



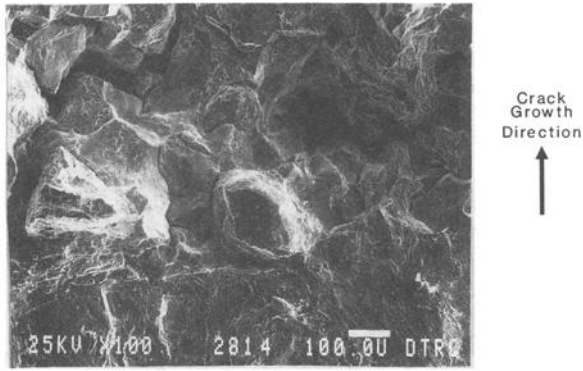
Specimen HJ-44, Near Center of Fatigue Crack Tip

FIG. 5—Fractographs of Monel K-500 tested in air.

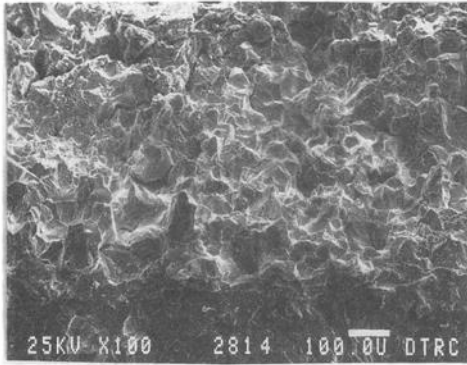
drogen that accumulates at the grain boundaries with the possible assistance of impurity atoms [8]. Monel K-500 has a face-centered cubic structure that has a relatively low rate of hydrogen diffusivity [6]. Although the damage resulting from hydrogen at the crack tip is clear, the behavior of K-500 with crack growth beyond initiation is not as clear.

Since hydrogen has a significant effect on the fracture initiation toughness, why has hydrogen not produced a similar and consistent effect on crack extension? Figure 2 shows that the slope of the  $J$ - $R$  curves beyond crack initiation for the specimen tested in salt water with cathodic protection had a lower value than the slopes of the specimens tested in an air environment for the air melted K-500. Figure 3 indicates that the slope of the  $J$ - $R$  curves did not appear to change with the presence of hydrogen. Figure 7 is a plot of the Tearing Modulus ( $T$ ) versus cross head rate for the K-500 specimens tested. The data indicate that the tearing modulus for the ESR melted K-500 appears to be insensitive to the effects of hydrogen. However, the effect of hydrogen on the air melted K-500 is evident with a 33% reduction in residual toughness measured by  $T$ .

SEM examination of the fracture surfaces of the specimens exposed to hydrogen revealed some differences in fracture mode at some distance below the end of the precrack. Figures 6, 8, and 9 show a series of SEM fractographs from the specimens tested in salt water with cathodic protection (EJ-56 and HJ-50). The fractographs were taken of the areas on the



Specimen EJ-56, Near Center of Fatigue Crack Tip



Specimen HJ-50, Near Center of Fatigue Crack Tip

FIG. 6—Fractographs of Monel K-500 tested in salt water with cathodic protection  $-1\text{ V (SCE)}$ .

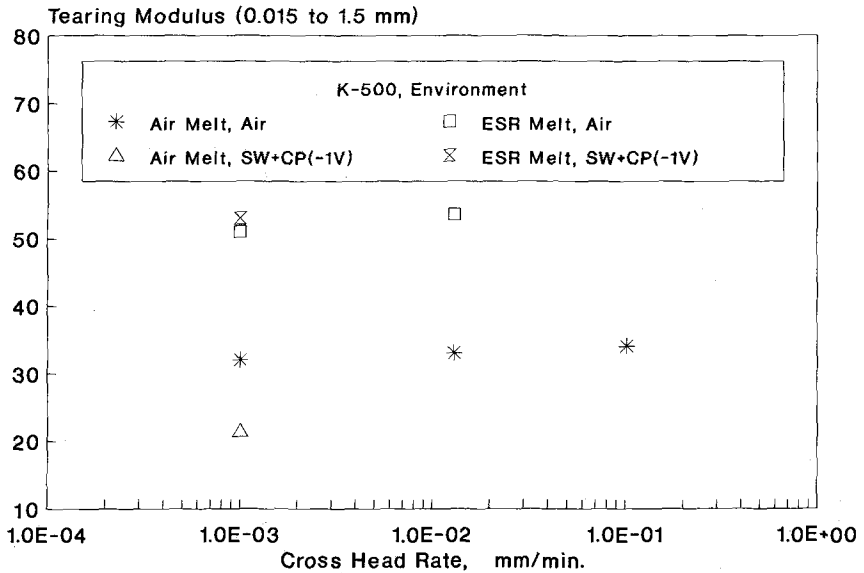
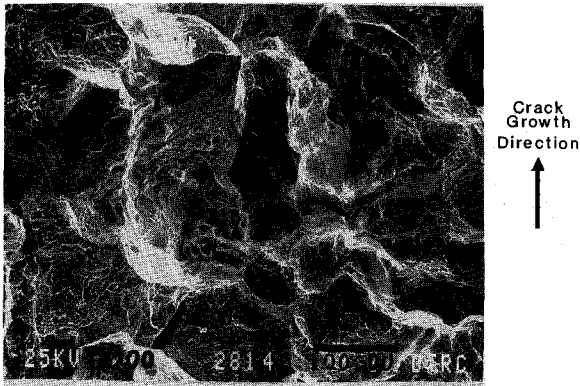


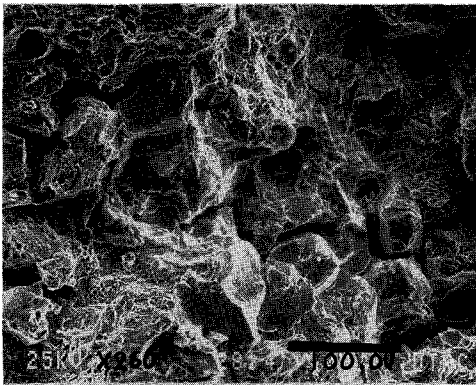
FIG. 7—J-integral tearing modulus results for Monel K-500, 1T compacts.

center line of the fracture surface adjacent to the fatigue crack tip (Fig. 6), 3 mm below the fatigue crack tip (Fig. 8), and 5 mm below the fatigue crack tip (Fig. 9). The fracture surfaces near the fatigue crack are clearly intergranular fracture for both the air melted (EJ) and the ESR K-500 (HJ) shown in Figs. 5 and 6. After 3 mm of crack growth the fracture surface has changed (Fig. 8). Although the air melted (EJ) material is still completely intergranular, some of the grain facets are no longer smooth and featureless but appear to have microvoid fracture on the grain boundaries. The ESR K-500 material (HJ) also appears to have some evidence of microvoid fracture on the surface, but the ductile fracture does not appear to be limited to the grain boundaries. The ductile fracture on the HJ specimen at the 3-mm position appears to be transgranular. The 5-mm positions on the fracture surfaces of the two specimens shown in Fig. 9 appear completely different from each other. The air melted material (EJ) is still mostly intergranular with some microvoid fracture limited to the grain boundary facets while the ESR K-500 (HJ) now appears to be completely transgranular dimpled rupture.

These fractographs indicate that the two Ni-Cu Alloy K-500 materials have a different sensitivity to hydrogen. This may be the result of microstructural differences produced during

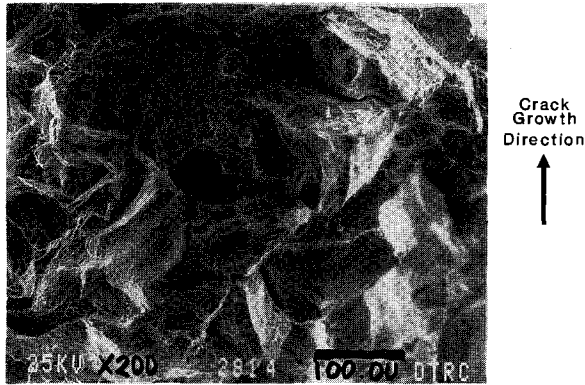


Specimen EJ-56, 3 mm from Fatigue Crack Tip

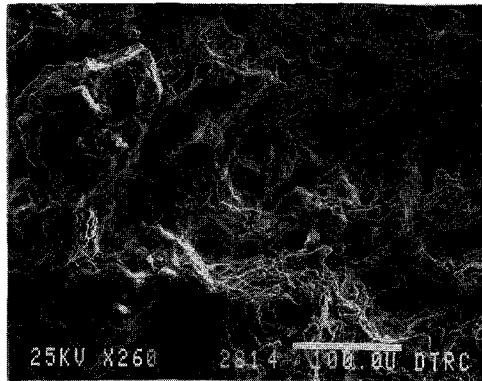


Specimen HJ-50, 3 mm from Fatigue Crack Tip

FIG. 8—Fractographs of Monel K-500 tested at 3 mm from tip.



Specimen EJ-56, 5 mm from Fatigue Crack Tip



Specimen HJ-50, 5 mm from Fatigue Crack Tip

FIG. 9—Fractographs of Monel K-500 tested at 5 mm from tip.

the melting practice. The microstructural effects on  $J$ -integral fracture toughness have been reported [9,10]. These effects are usually related to the level or size distribution of inclusions that affect ductile fracture toughness. The  $J_{Ic}$  results in Table 3 appear to indicate that the inclusion level in the ESR materials is cleaner (lower inclusion level) than the air melted K-500, thus yielding higher initiation toughness values.

**Conclusions**

The purpose of this research was to study the effects of slow loading and environment on the  $J$ -integral fracture toughness of compact specimens of air melted and electro-slag remelted (ESR) Ni-Cu Alloy K-500. The conclusions of the study were:

- (1) The reduction in loading rate from a cross head rate of 0.100 to 0.001 mm/min does not have an effect on the  $J$ -integral resistance curves of K-500 tested in air.
- (2) The air melted K-500 had lower  $J$ - $R$  curves than the ESR Monel K-500.
- (3) The effect of 3.5% NaCl solution and cathodic protection of  $-1$  V (SCE) on the  $J_{Ic}$  value of K-500 was to cause a reduction in toughness and a change in fracture mode from dimpled rupture to intergranular fracture.

## References

- [1] "Effects of Hydrogen on the Engineering Properties of Monel Nickel-Copper Alloy K-500," *Corrosion*, Vol. 28, No. 2, 1972, p. 57.
- [2] Kamdar, M. E., *Hydrogen in Metals, Proceedings of the 2<sup>nd</sup> International Congress, Paris, June 1977*, Pergamon Press, New York, Vol. 2, 2B10.
- [3] Vassilaros, M. G. and Hackett E. M., "*J*-Integral *R*-Curve Testing of High Strength Steels Utilizing the Direct-Current Potential Drop Method," *Fracture Mechanics: Fifteenth Symposium, ASTM STP 833*, R. J. Sanford, Ed., American Society for Testing and Materials, Philadelphia, 1984, pp. 535-552.
- [4] Paris, P. C., Tada, H., Zahoor, A., and Ernst, H., "Initial Experimental Investigation of Tearing Instability Theory," in *Elastic-Plastic Fracture, ASTM STP 668*, J. D. Landes, J. A. Begley, and G. A. Clarke, Eds., American Society for Testing and Materials, Philadelphia, 1979, pp. 251-265.
- [5] Harris, J. A., Scarberry, R. C., and Stephans, C. D., "Effects of Hydrogen on the Engineering Properties of Monel Nickel Copper Alloy K-500," *Corrosion*, Vol. 28, No. 2, 1972, p. 57.
- [6] Smith, C. G., "Effect of Hydrogen on Nickel and Nickel Based Alloys," *Proceedings of Effects on Hydrogen in Metals*, ASM, Champion, PA, Sept. 1973, p. 485.
- [7] Tetelman, A. S., "Recent Developments in Classical (Internal) Hydrogen Embrittlement," *Proceedings of Effects on Hydrogen in Metals*, ASM, Champion, PA, Sept. 1973, p. 17.
- [8] Latanision, R. M., Kurkela, M., and Lee, F., "The Role of Grain Boundary Chemistry and Environment on Intergranular Fracture," *Proceedings of 3<sup>rd</sup> International Conference on Effects of Hydrogen on Behavior of Materials*, AIME, 26-31 Aug. 1980.
- [9] Klassen, R. J., Bassim, M. N., and Bayoumi, M. R., "The Effects of Alloying Elements on the Fracture Toughness of High Strength, Low Alloy Steels," *Materials Science and Engineering*, Vol. 80, 1986, pp. 25-35.
- [10] Garrison, W. M. Jr. and Moody, N. R. "The Influence of Inclusions and Microstructure on the Fracture Toughness of Secondary Hardening Steel AF-1410," *Metallurgical Transactions A*, Vol. 18A, July 1987, pp. 1257-1263.

## Application of the Rising Displacement Test to SCC Investigations

---

**REFERENCE:** Dietzel, W. and Schwalbe, K.-H., "Application of the Rising Displacement Test to SCC Investigations," *Slow Strain Rate Testing for the Evaluation of Environmentally Induced Cracking: Research and Engineering Applications*, ASTM STP 1210, R. D. Kane, Ed., American Society for Testing and Materials, Philadelphia, 1993, pp. 134–148.

**ABSTRACT:** The stress corrosion cracking (SCC) behavior of two metallic materials in sodium chloride containing solutions has been investigated using precracked specimens and a rising displacement test procedure. The tests were evaluated according to linear elastic fracture mechanics, i.e., in terms of  $K_{I,SCC}$  and  $da/dt$  versus  $K$ , and, in addition, by applying elastic-plastic fracture parameters such as the  $J$ -integral and the crack tip opening displacement (CTOD). From the results of these tests conclusions are drawn concerning an accelerated SCC test procedure that might be based on a combination of the rising displacement test on precracked specimens and the conventional slow strain rate test using smooth specimens.

**KEYWORDS:** stress corrosion cracking (SCC), rising displacement test, accelerated SCC test procedure, linear elastic fracture mechanics (LEFM), elastic-plastic fracture mechanics,  $J$ -integral, crack tip opening displacement (CTOD)

### The Fracture Mechanics Approach to SCC

Current approaches to structural design, and to the selection of materials to avoid SCC, grossly fall into two categories, i.e.,

- the **safe life** approach
- the **damage tolerance** approach.

The safe life approach assumes that a structure is fabricated free from defects and cracks and that it will operate for a finite service during which cracking will not initiate. Here designing against SCC is adequately supported by laboratory tests on smooth or mildly notched specimens like in the classical Slow Strain Rate Test [ $I$ ]. The damage tolerance approach accounts for the possibility of cracks or flaws already existing in a structure. Damage-tolerant designing makes use of fracture mechanics analysis, which in turn requires test data from precracked specimens. These data include both the commencement of crack growth from an initial crack or defect and the kinetics of the crack growth process.

The fracture mechanics assessment of the material's susceptibility to SCC is usually based on linear elastic fracture mechanics (LEFM). Hence the elastic stress intensity factor for the opening mode (Mode I),  $K_I$ , is used to characterize the mechanical driving force for the initiation and the subsequent propagation of environmentally assisted cracking. The parameters determined from this LEFM approach are the threshold value of the stress intensity factor,  $K_{I,SCC}$  (or  $K_{IEAC}$ ), below which environmentally assisted cracking in a precracked specimen should not occur, and the velocity of the subcritical crack growth,  $da/dt$ , as a function of  $K_I$ .

---

<sup>1</sup> Senior research engineer and head of Institute of Materials Research, respectively, GKSS-Forschungszentrum Geesthacht GmbH., D-2054 Geesthacht, Germany.

## Fracture Mechanics Based SCC Test Methods

Although a number of fracture mechanics based test methods for the evaluation of these two parameters exist, only a few have achieved the status of a generally accepted standard. Most of the fracture mechanics based SCC tests favor static loading techniques such as the constant load or the constant deflection (or displacement) test.

Both the constant load and the constant deflection technique have their merits, particularly because they are easy to carry out and they require a minimum amount of laboratory equipment. On the other hand, their disadvantage lies in the determination of the necessary test duration, i.e., in the question of how long a test should last, before the data evaluated from this test represent the looked-for threshold value for the investigated material/environment system.

One of the standards for the determination of  $K_{I,SCC}$  is the ISO Standard 7539-Part 6 [2]. In this standard, minimum test durations are recommended for the determination of  $K_{I,SCC}$  by crack initiation in a constant load test, which range from 100 h for titanium alloys to 10 000 h for lower-strength steels, high-alloy steels of the maraging type, and for aluminum alloys. Similar test durations are proposed in a recent draft for a new ASTM standard related to the same field of application.

Apart from the problem of determining a suitable test duration, another shortcoming of the existing LEFM approaches to SCC lies in the fact that the crack tip stress intensity factor  $K_I$  is used to characterize the mechanical driving force and that in most of these approaches plane-strain conditions are demanded. The result of this is a disparity of the crack size requirements for fracture mechanics based SCC testing on the one hand, and the size of cracks typical of practical problems of SCC on the other hand. In practice, SCC can occur under conditions that deviate significantly from plane-strain conditions.

Furthermore, the applicability of LEFM to SCC is based on the assumption of small scale yielding which, for lower-strength alloys with high resistance to SCC, is not justified. Instead, sufficient plasticity may occur so that neither plane-strain nor linear elastic conditions are satisfied. In these cases LEFM cannot be applied and  $K$  is no longer a meaningful parameter. Therefore, elastic-plastic approaches such as the  $J$ -integral or crack tip opening displacement (CTOD) have to be used as the crack driving force in these cases [3-9].

In order to overcome the problem of test durations and to abandon the limitations of the LEFM approach, a test series was conducted that was based on a dynamic test procedure, i.e., the rising displacement technique. This test technique merges the classical Slow Strain Rate Test and the Rising Load  $K_{I,SCC}$  Test [10,11]. It comprises tests at increasing loads or displacements on precracked specimens which, at the same time, are exposed to a corrosive environment. With this test technique the SCC behavior of two metallic materials in sodium chloride containing solutions has been investigated.

## Experimental Technique

### *Test Procedure*

The tests were performed in computer-controlled screw-driven tensile test machines that were horizontally arranged to ease the handling of the environment. The measuring equipment allowed continuous monitoring of load  $F$ , the load-line displacement  $v_{LL}$ , the crack length  $a$  and the crack tip opening displacement  $\delta$ . Details of this experimental setup are given elsewhere [12]. The crack length was measured by a modified version of the dc potential drop technique using a pulsed current with a reversal of the polarity during each measuring cycle and taking additional readings at a reference specimen [13]. The CTOD was either directly measured with a specially designed clip-on gage [14] which is shown in Fig. 1 or it

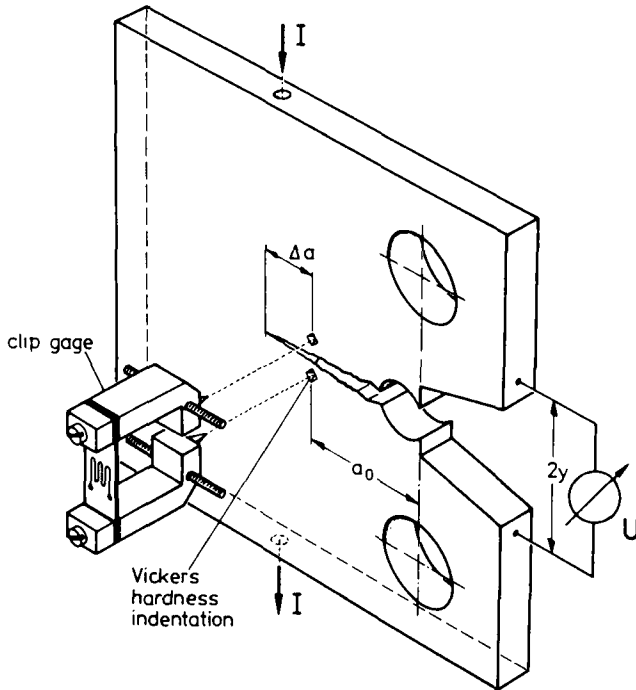


FIG. 1—Experimental setup for measuring the crack tip opening displacement [14].

was calculated from the load line displacement using a modification [14] of the British Standard 5762 [15] which accounts for crack growth. As the experiments showed, the CTOD values obtained with these two methods were in good agreement with each other.

The test machines were run under displacement control with the load line displacement  $v_{LL}$  serving as the controlling parameter. The range of displacement rates that could be covered in the tests reached from  $0.1 \mu\text{m/h}$  to  $30 \text{ mm/h}$ .

To compare the results obtained in the rising displacement tests with data from more conventional fracture mechanics based SCC test methods, additional constant load and constant displacement tests were performed for the same material/environment systems. In addition to this, constant load and slow strain rate tests were conducted on smooth tensile specimens of the aluminum alloy.

#### Materials and Specimen Preparation

The materials investigated were

- (1) high-strength aluminum alloy 2024 in the T351 temper condition, and
- (2) a low-alloy fine-grained structural steel with the European designation FeE 690 T.

The chemical compositions and the mechanical properties of these materials are given in Tables 1–3.

The materials were provided in sheets with thicknesses of 50 mm in the case of the steel and of 100 mm in the case of the aluminum alloy. From these materials the following specimen types were machined (Fig. 2):

- compact type tension (CT) specimens for rising displacement and constant load tests,
- double cantilever beam (DCB) specimens for constant displacement tests,

TABLE 1—*Chemical composition of aluminum 2024 (percent by weight).*

Copper	Magnes.	Zinc	Iron	Silicon	Mangan.	Chrom.	Others
3.56	0.94	0.043	0.15	0.11	0.28	0.0047	<0.15

- surface crack tension (SC) specimens for rising displacement tests (for aluminum only), and
- smooth tensile specimens for constant load and slow strain rate tests.

The CT and DCB specimens had a thickness,  $B$ , of 20 mm. The width,  $W$ , of the CT specimens was 40 mm (steel) and 50 mm (aluminum), respectively. The height,  $H$ , of the DCB specimens was 35 mm. The aluminum specimens were machined in the S-L orientation of the rolled plates, the steel specimens in the L-T orientation.

### Test Environments

For the aluminum alloy the test environment consisted of a 3.5% aqueous sodium chloride solution, modified by an addition of 0.5% sodium chromate/bichromate as an inhibitor against pitting corrosion [16]. For the steel the corrosive environment was prepared according to ASTM D 1141, Specification for Substitute Ocean Water. In this latter case a cathodic potential of  $-900$  mV versus Ag/AgCl electrode was applied to achieve hydrogen charging of the material. Additional tests were conducted in laboratory air and, for the aluminum alloy, in ultra-high vacuum ( $p < 10^{-5}$  Pa) as reference environments.

### Testing Procedure

Prior to the SCC tests the specimens were fatigue precracked at  $R$ -ratios between 0.1 and 0.2 to crack lengths corresponding to initial  $a/W$  values in the order of 0.5 to 0.65, where  $a$  is the overall crack length. The fatigue precracking was carried out under conditions of decreasing  $\Delta K$  using stepped load shedding. Thus it is ensured that the final  $\Delta K$  was close to the material's  $\Delta K_{th}$ -value. For the tests in the corrosive environment the specimens were brought into the solution for approximately 24 h prior to testing and were kept under a low mechanical pre-load (typically, 0.5 kN). After testing, the specimens were again fatigued, this time at  $R$ -ratios of about 0.5 in order to mark the total crack extension on the fracture surface, and then broken.

The fracture surfaces were investigated under an optical microscope for measuring the initial and final crack length. In addition to this, some of the specimens were investigated in a scanning electron microscope for further examination of the fracture surface morphology.

TABLE 2—*Chemical composition of the steel FeE 690 T (percent by weight).*

Carbon	Silicon	Mangan.	Phosphor.	Sulphur	Chrom.	Molybden.
0.18	0.67	1.02	0.009	0.003	0.85	0.48

TABLE 3—Mechanical properties (room temperature).

Material	$\sigma_{0.2}$ , MPa	$\sigma_{UTS}$ , MPa	$\epsilon_f$ , %
Al 2024*	286	421	10.6
FeE 690T	693	820	15

\* Tested in the short transverse direction.

Data Evaluation

From the fracture surfaces, average values of the initial and final crack length were evaluated using a nine-point average method [17]. These values were then used to adjust the crack length values monitored during the test by a linear fit. From the corrected crack length values the crack growth velocity was calculated following the seven-point incremental polynomial method according to ASTM E 647, Test Method for Measurements of Fatigue Crack Growth Rates. From the measured crack length values and the corresponding load readings, the stress intensity factors were derived using [18]

$$K_I = \frac{F}{B\sqrt{W}} \frac{(2 + a/W)}{(1 - a/W)^{1.5}}$$

$$\times [0.886 + 4.64a/W - 13.32(a/W)^2 + 14.72(a/W)^3 - 5.6(a/W)^4]$$

where  $F$  = load and  $B$  = specimen thickness for CT specimens and [19]

$$K_I = \frac{E'v_{LL}H}{8} \sqrt{\frac{1.5H(a + 0.3H)^2 + (H/2)^3}{(a + 0.3H)^3 + (H/2)^2}}$$

for DCB specimens with a load line displacement  $v_{LL}$  ( $H$  = specimen height).

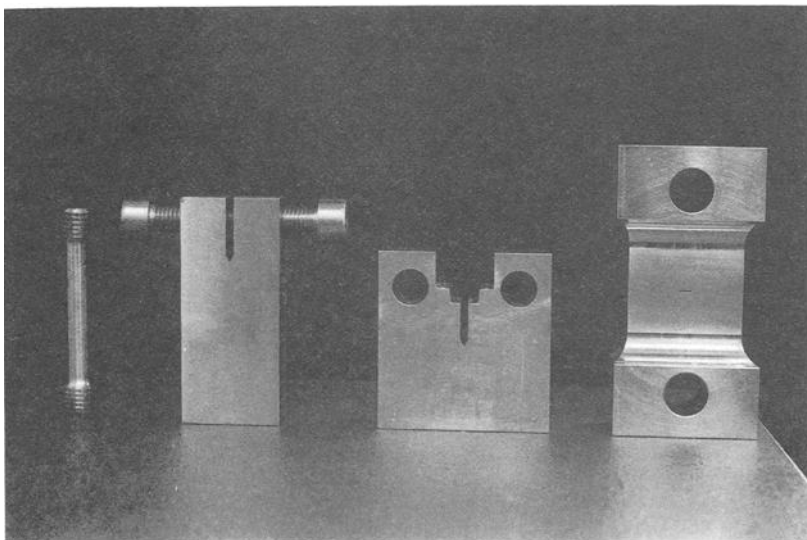


FIG. 2—Specimen types used for testing (material Al 2024 T351).

The  $J$ -integral was determined by [20]

$$J = \frac{U}{B(W-a)} f\left(\frac{a}{W}\right)$$

where

$$f\left(\frac{a}{W}\right) = 2 \frac{1 + \alpha}{(a + \alpha)^2} \text{ and } \alpha = \sqrt{\left(\frac{2a}{W-a}\right)^2 + 2 \frac{2a}{W-a} + 2} - \left(2 \frac{a}{W-a} + 1\right).$$

## Experimental Results

### Aluminum 2024 T351

In this test series the results from three different techniques for evaluating  $K_{Isc}$  and  $da/dt = f(K)$ , i.e., constant load, constant displacement, and rising displacement, were compared. The properties  $K_{Isc}$  and  $da/dt$  obtained from these three test methods are compiled in Figs. 3–5.

From the tests under constant load only the threshold value  $K_{Isc}$  was deduced which, according to Fig. 3, was in the order of  $6 \text{ MPa}\sqrt{\text{m}}$ . The tests under constant displacement yielded information about the complete  $da/dt$  versus  $K$  curve in the range between  $K_{Isc}$  and  $K_{Ic}$  (Fig. 4). The curve shows a plateau region at a crack propagation rate of about  $3$  to  $8 \times 10^{-6} \text{ mm/s}$  and drops to rates below  $10^{-7} \text{ mm/s}$  at a stress intensity level of about  $4$  to  $5 \text{ MPa}\sqrt{\text{m}}$ . This stress intensity was taken as the system's threshold value  $K_{Isc}$ . Figure 4 also contains the results of conventional slow strain rate tests conducted at strain rates of  $1 \times 10^{-9} \text{ s}^{-1}$ . In these tests an average crack growth velocity  $(da/dt)_{av}$  was calculated by dividing the depth of the stress corrosion crack measured after the specimen had failed by

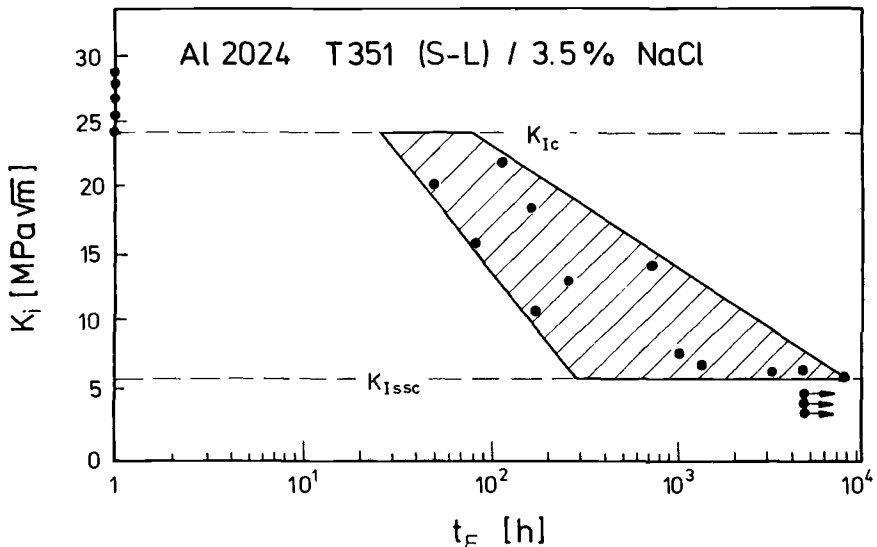


FIG. 3—Dependence of the time-to-failure on the initial stress intensity factor (precracked CT specimens, Al 2024 T351).

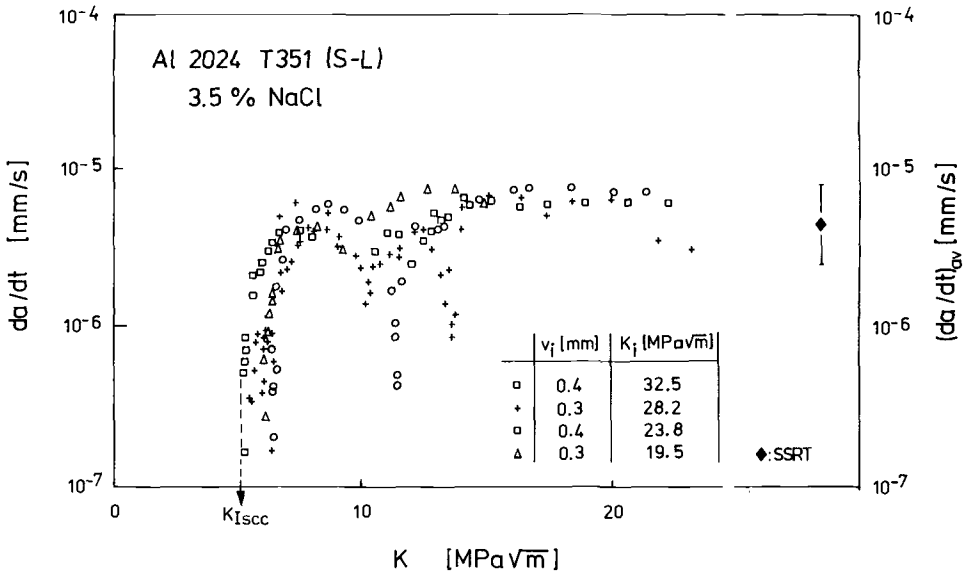


FIG. 4—V-K curve obtained using bolt-loaded DCB specimens with different displacements for aluminum 2024 T351; the symbol on the right-hand part of the diagram represents the average crack growth velocity measured in slow strain rate tests on smooth specimens ( $\dot{\epsilon} = 1 \times 10^{-9} s^{-1}$ ).

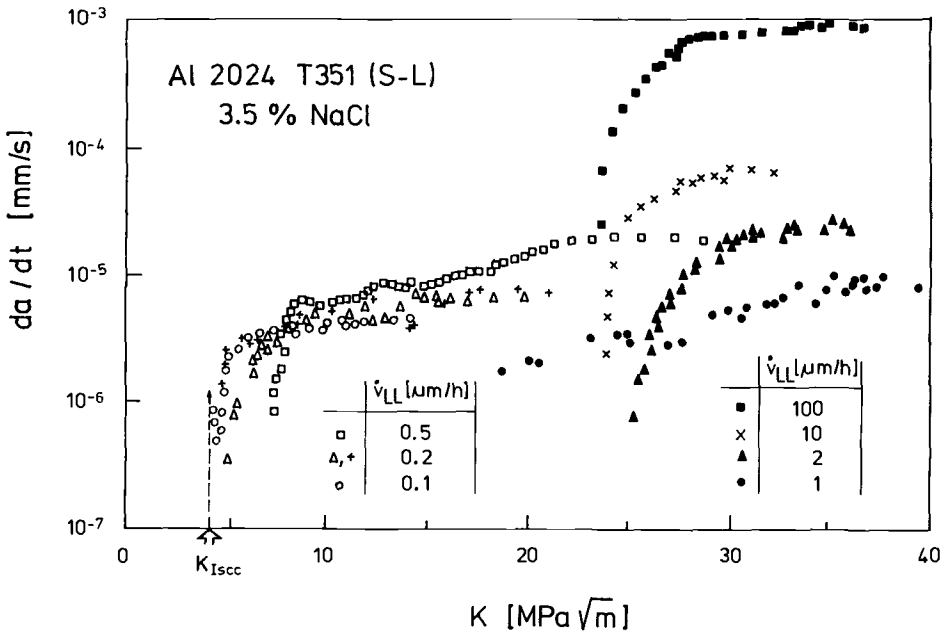


FIG. 5—V-K curve for aluminum 2024 T351 obtained from tests at different rising displacements.

the total time of crack growth. Here the starting point for the time measurement was taken from a slight change in the dc potential drop signal which was continuously monitored in these tests on smooth specimens, too. The point in Fig. 4 represents the mean value from three tests.

Two different types of curves were obtained from the tests under rising displacement conditions (Fig. 5): At displacement rates above  $1 \mu\text{m}/\text{h}$  the curves start at  $K_I$  levels between 25 and  $28 \text{ MPa}\sqrt{\text{m}}$ . This corresponds to the initiation values that were obtained from testing the same material in laboratory air and in ultra-high vacuum using displacement rates between  $1 \text{ mm}/\text{h}$  and  $0.2 \mu\text{m}/\text{h}$ . The crack growth rates measured in these tests are directly proportional to the applied displacement rates (cf. the right hand part of this diagram).

For environmental testing at displacement rates below about  $1 \mu\text{m}/\text{h}$ , no significant further drop of the crack propagation rate in the plateau region could be observed. The curves on the left-hand part of Fig. 5 and the data shown in Fig. 4 fall into the same scatter band. This implies that the threshold values  $K_{I\text{sc}}$  are virtually the same for both testing procedures.

Since the  $K_{I\text{sc}}$  value obtained from the constant load tests is in the same range (Fig. 3), it can be stated that for the Al 2024 T351 tested in 3.5% NaCl solution, all three test types yield a  $K_{I\text{sc}}$  value between 4 and  $6 \text{ MPa}\sqrt{\text{m}}$ .

Metallographic evidence from the fracture profiles in the crack tip region indicates that in all test types intergranular SCC was the mechanism responsible for crack propagation. This is confirmed by scanning electron micrographs from the fracture surfaces. As an example, Fig. 6a shows the fracture surface of a CT specimen tested at a low displacement rate ( $0.1 \mu\text{m}/\text{h}$ ) in the corrosive environment. For comparison, in Fig. 6b the fracture surface of a CT specimen of the same material also tested in the NaCl solution but at a higher displacement rate ( $1 \text{ mm}/\text{h}$ ) is shown. Here the cracking was due to mechanical failure, and the corresponding fracture surface shows items of microductility and glide band fracture.

From Fig. 5 the influence of the displacement rate  $\dot{v}_{LL}$  on the initiation value of the stress intensity factor,  $K_{II}$ , measured in the corrosive environment can be deduced. This leads to a curve with a sigmoidal shape (Fig. 7). At the upper bound of this curve, i.e., at high displacement rates, initiation values are the same as those obtained in air, where the displacement rate has little or no effect on the threshold value. After a steep decrease in the mid-range, at displacement rates around  $1 \mu\text{m}/\text{h}$ , the curve attains its lower bound value for displacement rates at or below  $0.5 \mu\text{m}/\text{h}$ . Here the threshold value corresponds to the results from the static tests. In the experiments no evidence could be found that, at still

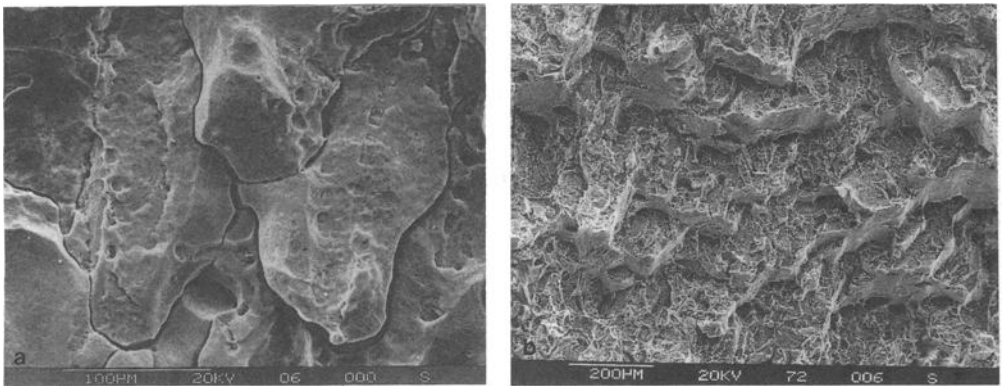


FIG. 6—Fracture surfaces (SEM) of aluminum specimens tested in 3.5% sodium chloride solution; (a) at  $0.1 \mu\text{m}/\text{h}$ ; (b) at  $1 \text{ mm}/\text{h}$ .

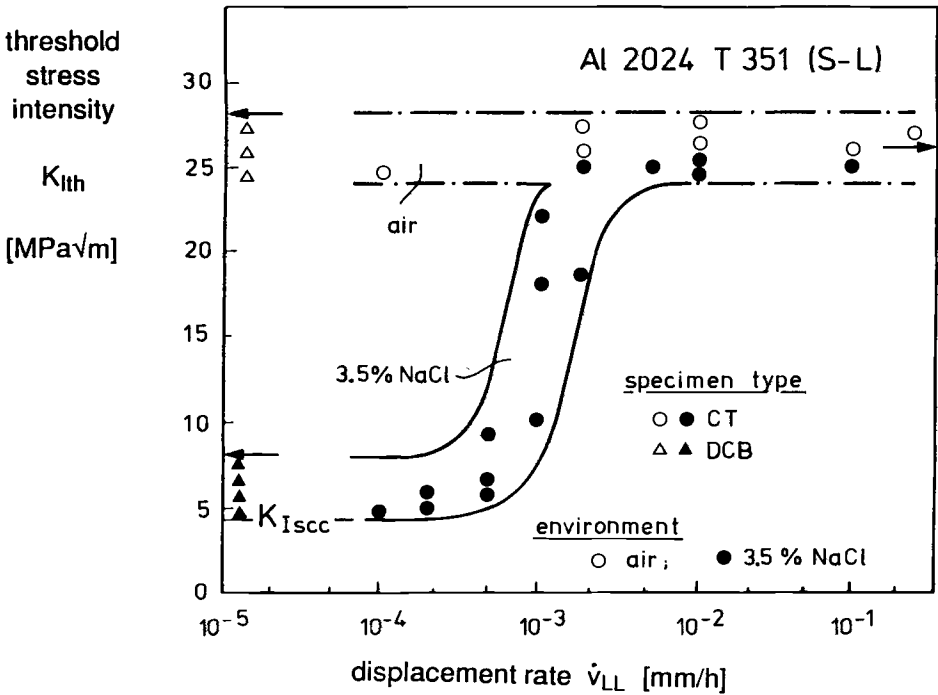


FIG. 7—Influence of the displacement rate ( $dv_{LL}/dt$ ) on the threshold stress intensity  $K_{Ith}$  (aluminum 2024 T351).

lower displacement rates, the threshold values might go up again as would in principle be expected for a repassivating system.

In order to include the regime of small cracks in the investigations, where the LEFM approach does not seem to be applicable, threshold nominal stresses  $\sigma_{th}$  were measured in constant load experiments on initially smooth specimens of the same material and in the same corrosive environment. Together with the results from conventional tensile tests, the  $K_{Isc}$  value from CT and DCB specimens, and the results of fracture toughness tests in air, according to [21] a range of sensitivity to SCC was determined for this material/environment system. This range is plotted in Fig. 8 for a specimen with a semi-elliptical surface crack. In this graph the results from rising displacement tests on surface cracked panels conducted at three different displacement rates are also plotted. Even though crack initiation in these panels did not occur immediately after reaching the “border line” of the SCC sensitive area, the correspondence between the prediction derived from tests on laboratory specimens (CT, DCB, tensile specimens) and the more “realistic” defect represented by a surface cracked specimen appears remarkable.

Finally, Fig. 9 proves that for this material and orientation the requirements for applying LEFM methods were satisfied. In this graph the line drawn under  $45^\circ$  represents the relationship

$$J = K^2/E' \quad \text{with} \quad E' = E/(1 - \nu^2)$$

where  $E$  is Young’s modulus and  $\nu$  is Poisson’s ratio. This relationship is valid only in the linear elastic regime and may thus be taken as a criterion for the applicability of LEFM

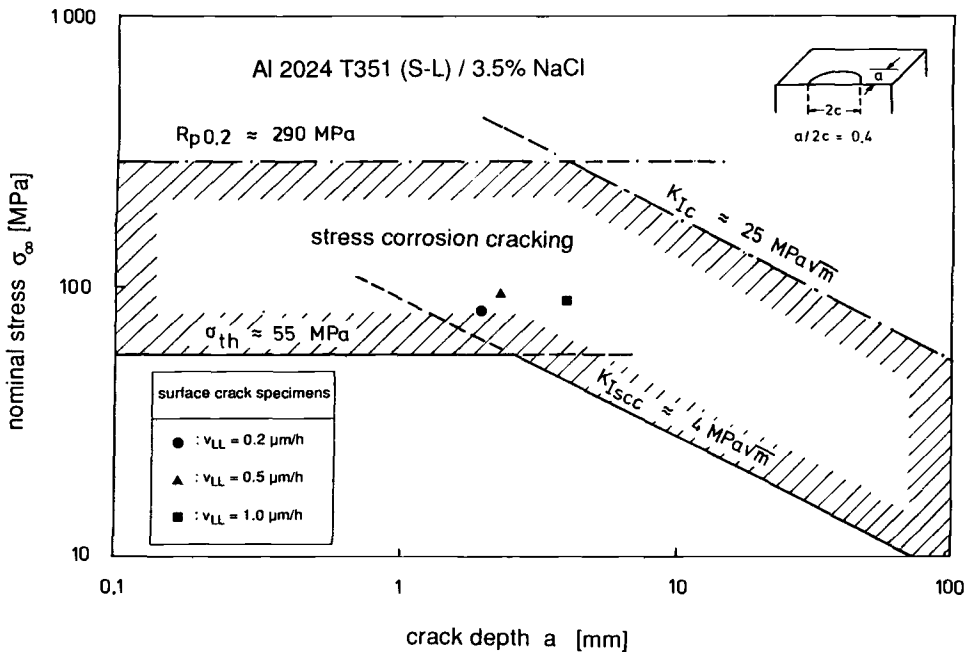


FIG. 8—Combined stress - stress intensity factor versus flaw size diagram predicting the SCC susceptible zone for aluminum 2024 T351; comparison with results from three tests on surface crack specimens.

formalisms in the tests. According to Fig. 9, virtually all curves, even those obtained from testing in air, start in the vicinity of this 45° line. This indicates that in all cases at least the initial cracking occurred under LEFM conditions.

#### Steel FeE 690 T

For the higher-strength steel FeE 690 T, it was doubtful whether LEFM methodologies could be used. Therefore, the formalisms of elastic-plastic fracture mechanics (EPFM) were applied to the data evaluation. From the tests, data crack growth resistance curves ( $R$ -curves) for the  $J$ -integral as well as for the CTOD were generated. Figure 10 shows the  $J$ - $R$  curves obtained in tests at various displacement rates spanning more than four orders of magnitude. The graph contains  $R$ -curves measured in air as well as  $R$ -curves from tests under hydrogen-charging conditions.

According to this graph, the material's resistance against further extension of a pre-existing crack decreases drastically at lower displacement rates when being exposed to the corrosive environment. The critical  $J$ -value taken from these  $J$ - $R$  curves at 0.2 mm of ductile tearing after crack tip blunting and designated  $J_{0.2BL}$  [17] drops from about 300 N/mm measured at a displacement rate of 30 mm/h to less than 30 N/mm at 1  $\mu\text{m/h}$ . Taking into account that for low displacement rates no considerable blunting was detected on the fracture surface, the starting value  $J_i$  for the  $J$ -integral ( $\Delta a=0$ ) can be used to calculate the stress intensity factor  $K_{Isc}$  for the initiation of environmentally enhanced cracking via

$$K_{Isc} = \sqrt{(J * E')}$$

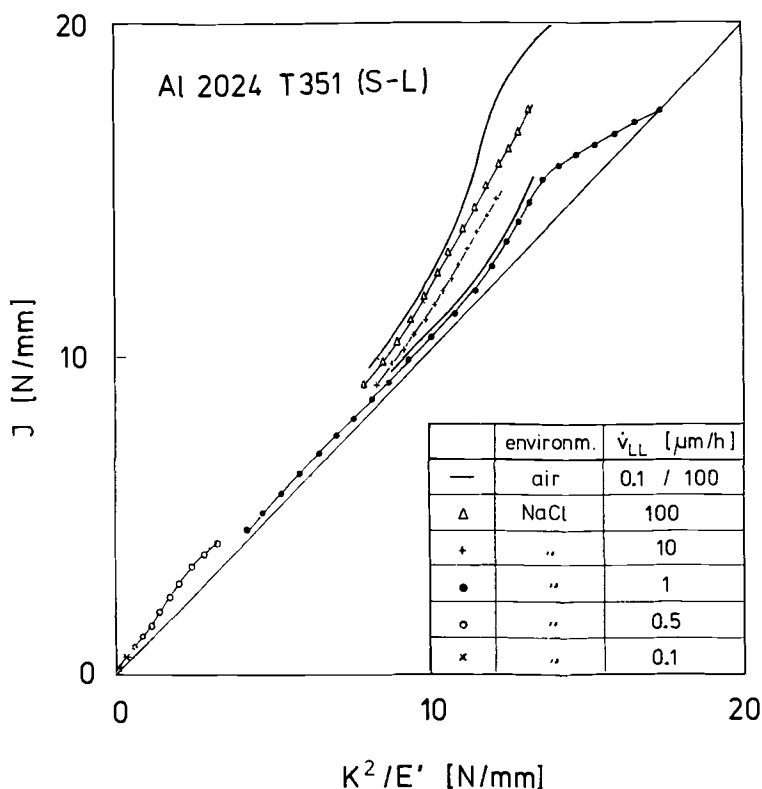


FIG. 9—Plot of  $J$ -integral versus  $K^2/E'$  for aluminum 2024 T351.

Since the lowest initiation value measured in the tests was in the order of  $J_i = 10 \text{ N/mm}$ , the corresponding threshold value should be as low as

$$K_{Jsc} = 50 \text{ MPa}\sqrt{\text{m}}$$

Such low initiation values were found only in rising displacement tests. So far, they could not be verified in tests for the same corrosion system when constant load or constant displacement were applied.

### Fractography

A fractographic examination of the fracture surface of specimens tested in the corrosive environment at the lowest and the highest displacement rate applied in the investigations reveals the different fracture modes occurring under various loading conditions (Figs. 11a,b). The scanning electron micrograph taken from the specimen fractured at 30 mm/h (Fig. 11b) corresponds to a ductile rupture by microvoid coalescence showing dimples of various size with no indication of secondary cracking. For the specimen tested at 1 mm/h the fracture surface is dominated by items of a brittle failure, i.e., quasi-cleavage facets and numerous secondary cracks (Fig. 11a). Hence, the fracture morphology confirms the assumption that

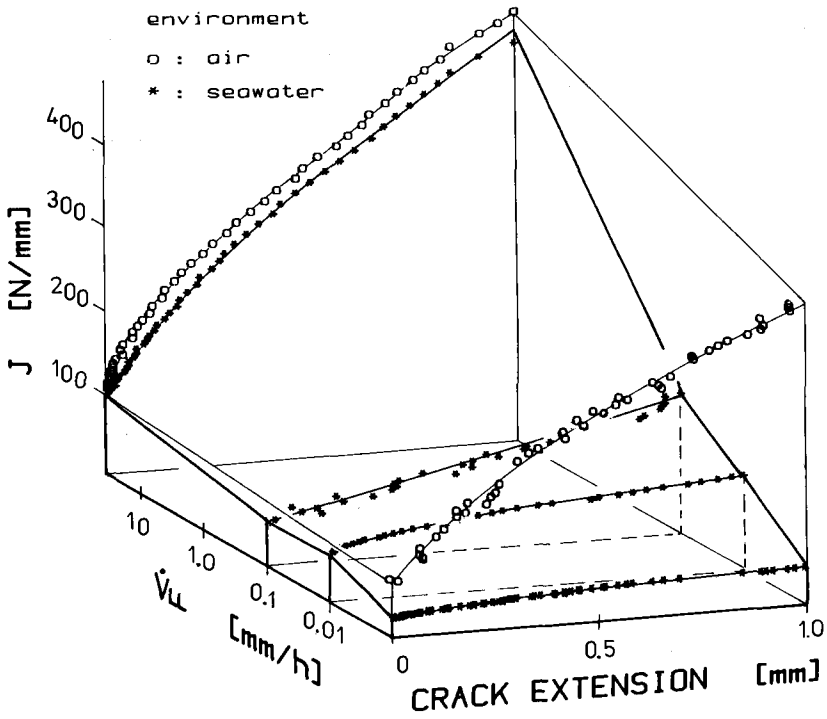


FIG. 10—Influence of the displacement rate on the J-R curves for the steel FeE 690 T.

embrittlement due to the uptake of atomic hydrogen from the aqueous environment has caused the subcritical cracking in this system.

### Discussion

The results show that a rising displacement test can in principle be used for SCC investigations based on the fracture mechanics approach. How testing under these conditions has

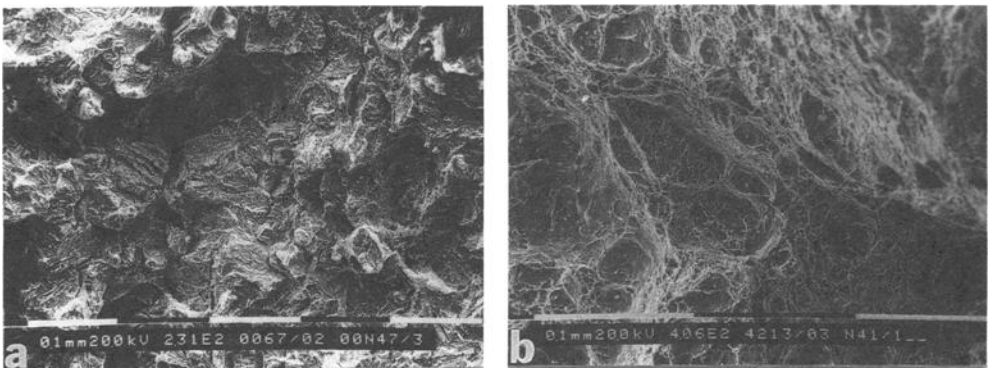


FIG. 11—Fracture surfaces (SEM) of specimens of the steel FeE 690 T tested in ASTM substitute ocean water under cathodic polarization; (a) at  $1 \mu\text{m/h}$ ; (b) at  $30 \text{ mm/h}$ .

to be carried out in order to obtain values that are representative for a given material/environment system has yet to be defined. Here, the major problem is the determination of a suitable displacement rate for tests in the corrosive environment. This rate must be low enough to ensure that the crack growth is truly related to SCC and does not arise from pure mechanical rupture. On the other hand, the rate should not be too low in order to avoid erroneously high threshold values due to possible repassivation effects occurring in some systems [6].

The Technical Committee 10 of the European Structural Integrity Society (ESIS) has made an attempt to elaborate recommendations for SCC testing using precracked specimens [22]. These recommendations are based on the test experiences reported here and also gained in other laboratories applying similar experimental techniques [23]. In a first draft a procedure is proposed that starts off from the assumption that the displacement rate,  $(dv_{LL}/dt)_{sc}$ , at which a test in the corrosive environment should be performed in order to evaluate the  $K_{Isc}$  value of a system can be estimated from the ratio of measured crack growth velocity in an inert environment,  $(da/dt)_{inert}$ , when applying the displacement rate  $(dv_{LL}/dt)_{inert}$ , and the crack growth velocity in the plateau region for environmentally induced cracking,  $(da/dt)_{sc}$ . According to this approach the required displacement rate can be determined by using the formula

$$(dv_{LL}/dt)_{sc} < 0.5 (da/dt)_{sc}/(da/dt)_{inert} * (dv_{LL}/dt)_{inert}.$$

Hence, the basic requirement is the knowledge of the crack growth velocity for environmentally induced cracking,  $(da/dt)_{sc}$ . This information may be obtained within a reasonable amount of time from test techniques that avoid long incubation periods by applying high stress intensity levels. These can be constant displacement tests using compact tension, DCB or WOL specimens or a step-loading procedure [24]. As the results shown in Fig. 4 indicate even average crack velocity data obtained from slow strain rate tests on smooth specimens may serve as a lower bound value for the calculation.

The main argument against this approach arises from the fact that the cracking mechanisms in air or in an inert environment can be completely different from the SCC mechanism. Crack growth velocities derived from tests in air should therefore not be used to calculate the suitable displacement rate for a rising displacement test in a corrosive environment aiming at the determination of the parameters  $K_{Isc}$  and  $(da/dt)$ .

Alternatively a series of SCC tests at different displacement rates would have to be conducted leading to the type of curve shown in Fig. 7. From this curve the lower bound or minimum value in the  $K_{th}$  versus  $(dv_{LL}/dt)$  plot could be taken as the threshold value for a corrosion system. This would help to increase the reliability of the test results but, necessarily, would also increase the number of tests to be conducted and would thus counteract the possible accelerating nature of a rising displacement or rising load SCC test procedure as compared to static tests. In any case, a verification of the recommended procedure by an interlaboratory test program seems to be the necessary next step to take.

## Conclusions

Rising displacement tests at displacement rates between 0.1  $\mu\text{m/h}$  and 30 mm/h have been conducted in air and in sodium chloride containing aqueous solutions using precracked specimens from two metallic materials. The test data were analyzed using formalisms of linear elastic and elastic-plastic fracture mechanics. Additional tests were performed using constant load, constant displacement, and slow strain rate techniques. For the high-strength aluminum alloy Al 2024 T351 the threshold values  $K_{Isc}$  obtained from the different test

methods were in good agreement. In the case of a low-alloyed structural steel charged with hydrogen the data obtained from rising displacement tests yielded lower initiation values than were observed with other test techniques. A proposal for an SCC test procedure based on a rising displacement procedure is reported in which the results from slow strain rate tests on smooth specimens can be used to determine the suitable displacement rate for testing precracked specimens in the corrosive environment to evaluate the parameters characterizing the SCC susceptibility of a material/environment system.

## References

- [1] Parkins, R. N., "Development of Strain-Rate Testing and Its Implications," *Stress Corrosion Cracking: The Slow Strain-Rate Technique*, ASTM STP 665, G. M. Ugiansky and J. H. Payer, Eds., American Society for Testing and Materials, Philadelphia, 1979, pp. 5–25.
- [2] International Standard ISO 7539, "Corrosion of Metals and Alloys—Stress Corrosion Testing"—Part 6: "Pre-Cracked Specimens," International Organization for Standardization, Geneva, 1989.
- [3] Landes, J. D. and McCabe, D. E., "The Effect of Hydrogen Exposure on Fracture Toughness," *Hydrogen Effects in Metals*, I. M. Bernstein and A. W. Thompson, Eds., The Metallurgical Society of AIME, Warrendale, PA, American Institute of Mining, Metallurgical, and Petroleum Engineers, Inc., New York, 1980, pp. 933–941.
- [4] Dietrich, M. R., Caskey, G. R., and Donovan, J. A., "J-Controlled Crack Growth as an Indicator of Hydrogen-Stainless Steel Compatibility," *Hydrogen Effects in Metals*, I. M. Bernstein and A. W. Thompson, Eds., The Metallurgical Society of AIME, Warrendale, PA, American Institute of Mining, Metallurgical, and Petroleum Engineers, Inc., New York, 1980, pp. 634–643.
- [5] Anderson, D. R. and Gudas, J. P., "Stress Corrosion Evaluation of Titanium Alloys Using Ductile Fracture Mechanics Technology," *Environment-Sensitive Fracture: Evaluation and Comparison of Tests Methods*, ASTM STP 821, S. W. Dean, E. N. Pugh, and G. M. Ugiansky, Eds., American Society for Testing and Materials, Philadelphia, 1984, pp. 98–113.
- [6] Abramson, G., Evans, J. T., and Parkins, R. N., "Investigation of Stress Corrosion Crack Growth in Mg Alloys Using J-Integral Estimations," *Metallurgical Transactions*, Vol. 16A, Oct. 1985, pp. 101–108.
- [7] Kawakubo, T. and Hishida, M., "Elastic-Plastic Fracture Mechanics Analysis on Environmentally Accelerated Cracking of Stainless Steel in High Temperature Water," *Transactions of the A.S.M.E.*, Vol. 107, July 1985, pp. 240–245.
- [8] Kumar, A. N. and Pandey, R. K., "Process and Mechanism of Fracture in a Pipeline Material in Chloride and Sulphide Environments," *Engineering Fracture Mechanics*, Vol. 22, No. 4, 1985, pp. 625–633.
- [9] Dietzel, W. and Schwalbe, K.-H., "Influence of Environment on Crack Propagation Under (Monotonic) Tensile Loading," (in German) GKSS Report 87/E/46, GKSS-Forschungszentrum Geesthacht GmbH, Geesthacht, 1987.
- [10] McIntyre, P. and Priest, A. H., "Accelerated Test Technique for the Determination of  $K_{Isc}$  in Steels," British Steel Corporation Report MG/31/71, London, 1972.
- [11] Clark, W. G., Jr. and Landes, J. D., "An Evaluation of Rising Load  $K_{Isc}$  Testing," *Stress Corrosion—New Approaches*, ASTM STP 610, H. L. Craig, Jr., Ed., American Society for Testing and Materials, Philadelphia, 1976, pp. 108–127.
- [12] Dietzel, W., Schwalbe, K.-H., and Wu, D., "Application of Fracture Mechanics Techniques to the Environmentally Assisted Cracking of Aluminum 2024," *Fatigue and Fracture of Engineering Materials and Structures*, Vol. 12, No. 6, 1989, pp. 495–510.
- [13] Dietzel, W. and Schwalbe, K.-H., "Monitoring Stable Crack Growth Using a Combined AC/DC Potential Drop Technique," *Zeitschrift für Materialprüfung/Materials Testing*, Vol. 28, No. 11, 1986, pp. 368–372.
- [14] Hellmann, D. and Schwalbe, K.-H., "On the Experimental Determination of CTOD Based R-Curves," *The Crack Tip Opening Displacement in Elastic-Plastic Fracture Mechanics, Proceedings of the Workshop on the CTOD Methodology*, GKSS-Forschungszentrum Geesthacht GmbH, Geesthacht, 1985, pp. 115–132.
- [15] British Standard BS 5762, "Methods of Tests for Crack Opening Displacement (COD) Testing," British Standards Institution (Gr. 6), London, 1979.
- [16] Lemaitre, C., Baroux, B., and Beranger, G., "Chromate as a Pitting Corrosion Inhibitor: Stochastic Study," *Werkstoffe und Korrosion*, Vol. 40, 1989, pp. 229–236.

- [17] EGF P1-90, "Recommendations for Determining the Fracture Resistance of Ductile Materials," European Structural Integrity Society, Delft, 1990.
- [18] Srawley, J. E., "Wide Range Stress Intensity Factor Expressions for ASTM E 399 Standard Fracture Toughness Specimens," *International Journal of Fracture*, Vol. 12, 1976, pp. 475-476.
- [19] Mostovoy, S., Crosley, P. B., and Ripling, E. J., "Use of Crackline Loaded Specimens for Measuring Plane-Strain Fracture Toughness," *Journal of Materials*, Vol. 2, 1967, pp. 661-681.
- [20] Merkle, J. G. and Corten, H. T., "A  $J$ -Integral Analysis for the Compact Specimen Considering Axial Force as well as Bending Effects," *Journal of Pressure Vessel Technology, Transactions of the A.S.M.E.*, Vol. 96, 1974, pp. 286-292.
- [21] Kaufmann, J. G., "Stress-Corrosion—Tradition vs Fractured Mechanics," *Corrosion—NACE* 35, 1979, i.
- [22] ESIS P4-92 D, "Recommendations for Stress Corrosion Testing Using Pre-Cracked Specimens" (First Draft), European Structural Integrity Society, Delft, 1992.
- [23] Mayville, R. A., Warren, T. J., and Hilton, P. D., "Determination of the Loading Rate Needed to Obtain Environmentally Assisted Cracking in Rising Load Tests," *Journal of Testing and Evaluation*, Vol. 17, No. 4, 1989, pp. 203-211.
- [24] Raymond, L. and Crumly, W. R., "Accelerated Low-Cost Test Method for Measuring the Susceptibility of HY-Steels to Hydrogen Embrittlement," *Proceedings First Hydrogen Problem in Steel, Washington, D.C.*, A.S.M.E., OH, 1982, pp. 477-480.

Duy T. Nguyen,<sup>1</sup> David E. Nichols,<sup>1</sup> and Raymond D. Daniels<sup>2</sup>

## Slow Strain Rate Fracture of High-Strength Steel at Controlled Electrochemical Potentials in Ammonium Chloride, Potassium Chloride, and Ammonium Nitrate Solutions

---

**REFERENCE:** Nguyen, D. T., Nichols, D. E., and Daniels, R. D., "Slow Strain Rate Fracture of High-Strength Steel at Controlled Electrochemical Potentials in Ammonium Chloride, Potassium Chloride, and Ammonium Nitrate Solutions," *Slow Strain Rate Testing for the Evaluation of Environmentally Induced Cracking: Research and Engineering Applications*, ASTM STP 1210, R. D. Kane, Ed., American Society for Testing and Materials, Philadelphia, 1993, pp. 149–157.

**ABSTRACT:** Earlier investigations using slow strain rate fracture tests at controlled electrochemical potentials demonstrated the susceptibility of AISI 4340 high-strength steel to stress corrosion cracking (SCC) in the combustion product residues of jet engine cartridge ignition starters. X-ray diffraction analyses of the residues revealed significant concentrations of ammonium chloride, potassium chloride, and ammonium nitrate. In the present investigation, slow strain rate testing was conducted to determine the effects of each of these chemical compounds on the fracture process. Test environments included ammonium chloride, potassium chloride, and ammonium nitrate solutions at concentrations of 100, 1000, and 10 000 parts per million by weight and at a pH of 5. The tests were performed at a constant extension rate of  $1 \times 10^{-7}$  m/s (strain rate of approximately  $2.7 \times 10^{-6}$ /s). Tests were performed at controlled electrochemical potentials, both anodic and cathodic with respect to the open-circuit corrosion potential, to delineate the potential ranges for SCC and hydrogen-induced cracking.

Of the three compounds studied, only ammonium chloride caused SCC of the AISI 4340 high-strength steel. The corrosion potential of about  $-620$  mV versus saturated calomel electrode (SCE) is at the brink of the potential range for stress corrosion cracking. The most severe embrittlement was observed at a potential of  $-450$  mV and at a solution concentration of 1000 ppm ammonium chloride. Hydrogen-induced cracking was observed at  $-850$  mV in the ammonium chloride and ammonium nitrate solutions, but not in the potassium chloride solutions.

**KEYWORDS:** AISI 4340 high-strength steel, slow strain rate testing, ammonium chloride, potassium chloride, ammonium nitrate

Previous failure analyses of cartridge ignition starter systems of jet aircraft have identified combustion product residues as the corrosive agents responsible for pitting and eventual rupture of starter breech chambers constructed of high-strength steel [1]. Combustion product residues collected from failed breech chambers were used in a moistened condition as

---

<sup>1</sup> Metallurgical engineer and chemical engineer, respectively, National Fertilizer and Environmental Research Center, Tennessee Valley Authority, Muscle Shoals, AL 35660.

<sup>2</sup> Professor, School of Chemical Engineering and Materials Science, The University of Oklahoma, Norman, OK 73019.

an environment in slow strain rate tests (SSRTs). SSRT results confirmed the susceptibility of the breech chamber steel to environmentally induced cracking [2].

SSRTs have also been performed using combustion product residues taken from used, but still serviceable, breech chambers. These tests, which were conducted at controlled electrochemical potentials, demonstrated that the corrosion potential is at the brink of the stress corrosion cracking potential range for steels in this environment [3]. X-ray diffraction analyses of residues collected from failed and used breech chambers yielded detectable amounts of ammonium chloride ( $\text{NH}_4\text{Cl}$ ), potassium chloride (KCl), and ammonium nitrate ( $\text{NH}_4\text{NO}_3$ ), in addition to iron oxides [2,3]. The present study was undertaken to determine the individual contributions of each of these chemical compounds to the fracture process in AISI 4340 high-strength steel in slow strain rate tensile tests. To assess the electrochemical potential effects on the fracture process, the tests were conducted at controlled potentials. The environments consisted of solutions containing 100, 1000, and 10 000 ppm by weight of  $\text{NH}_4\text{Cl}$ , KCl, and  $\text{NH}_4\text{NO}_3$  adjusted to a pH of 5. The tests were conducted at ambient room temperature.

## Materials, Equipment, and Procedures

### *Steel Specimens*

The tensile test specimens were AISI 4340 high-strength steel heat-treated to a Rockwell C 38-42 hardness, corresponding to a tensile strength of 1170 to 1240 MPa (170 000 to 180 000 lb/in<sup>2</sup>). The test specimens were fabricated from 6.35-mm-diameter rod stock to a gage length of approximately 38 mm and a gage diameter of 1.5 mm in accordance with ASTM Test Methods and Definitions for Mechanical Testing of Steel Products (A 370). After heat treatment, the gage length of the test specimens was ground and polished to a 600-grit surface finish.

### *Testing Machine*

The SSRTs were conducted using a universal tensile test machine with a load capacity of 20 000 lb (89 000 N). The tests were performed at a constant extension rate of  $1 \times 10^{-7}$  m/s ( $4 \times 10^{-6}$  in/s), corresponding to a strain rate of approximately  $2.7 \times 10^{-6}$ /s.

### *Corrosion Test Cell*

The corrosion test cell consisted of a 1-L plexiglass cylinder containing specimen holders, a graphite counter electrode, and a reference saturated calomel electrode (SCE). About 750 mL of test solution was used for each test. The solution was neither agitated nor aerated during the test. A fresh solution was used for each test. The tensile test specimen was installed in the test cell so that the entire gage length of the specimen was immersed in the solution. In the tests at controlled potentials, the specimen was polarized either anodically or cathodically using a potentiostat/galvanostat. The potential of the test specimen was controlled within plus or minus 1 mV. A digital voltmeter was used to continuously monitor the specimen potential during the SSRTs. Figure 1 is a sketch of the test apparatus and the electrical connections between the test specimen and potentiostat/galvanostat.

### *Test Solutions*

Test solutions were prepared by adding 100, 1000, or 10 000 mg of reagent-grade  $\text{NH}_4\text{Cl}$ , KCl, or  $\text{NH}_4\text{NO}_3$  to distilled water to make one liter of test solution. These solutions are

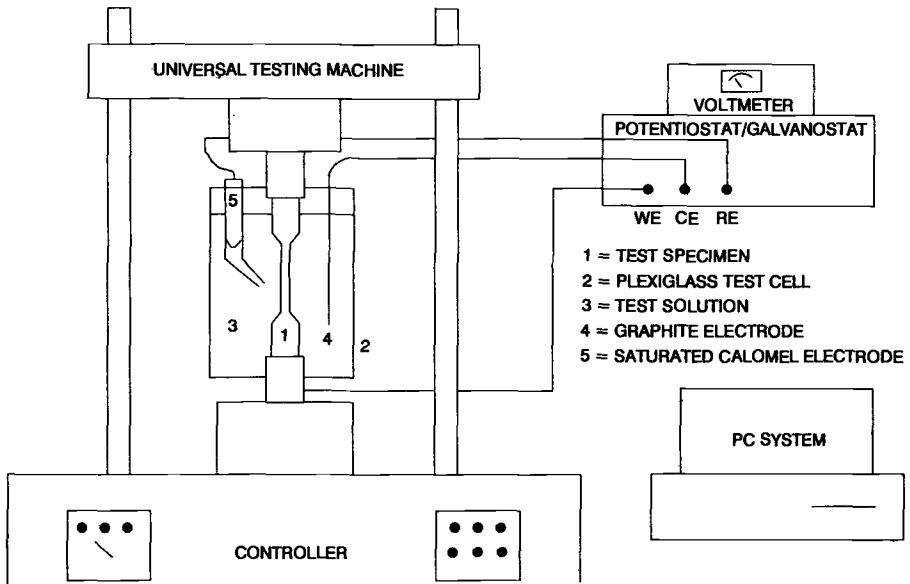


FIG. 1—Test equipment and electrical connections in controlled potential, SSRTs.

equivalent to concentrations of 100, 1000, and 10 000 ppm by weight. The pH of the test solutions was adjusted to the value of 5 using hydrochloric acid (HCl) for the chloride solutions and nitric acid (HNO<sub>3</sub>) for the nitrate solution.

*Test Procedures*

After the apparatus was prepared and the steel specimen was installed, the test solution was poured into the test cell. The counter and reference electrodes were then positioned in the cell. The specimen potential was measured and, where appropriate, controlled during the course of the test. A tension load of 100 lb (450 N) was applied manually to ensure proper seating and alignment of the specimen in the test machine grips. Test data, load versus displacement, were recorded at 25 lb (111 N) increments by computer.

When the SSRT was completed, the failed specimen was immediately removed from the test cell to prevent further corrosion. It was then ultrasonically cleaned in acetone for approximately five minutes to remove loose corrosion products on the surface. The gage length of failed specimens showing some degree of brittleness was examined under a stereo microscope for evidence of pitting and crack initiation. Specimens were examined using a scanning electron microscope for evidence of corrosion cracking.

Embrittlement and cracking susceptibility were evaluated by comparing time-to-failure (*t<sub>f</sub>*), percentage reduction in area (*RA*), percentage elongation (*EI*), and ultimate tensile strength (*UTS*) of the specimens tested in the corrosive environments with data obtained on a specimen tested in an inert environment (vegetable oil). Normalized data for *t<sub>f</sub>*, *RA*, and *UTS* were determined using ratios of the values obtained in the various solutions to the values obtained in the inert environment.

**Results**

SSRT results are presented in Tables 1 through 3. Normalized results are presented in Table 4.

TABLE 1—Slow strain rate<sup>a</sup> tests of AISI 4340 high-strength steel exposed to NH<sub>4</sub>Cl solutions<sup>b</sup>.

Conc., <sup>c</sup> ppm	<i>E</i> , mV vs SCE <sup>b</sup>	<i>t<sub>f</sub></i> , <sup>d</sup> hrs	<i>El</i> , <sup>e</sup> %	<i>RA</i> , <sup>f</sup> %	<i>UTS</i> , <sup>g</sup> MPa	Type of Fracture
Inert env. <sup>1</sup>	...	7.80	36	60	1207	Ductile
100	−350	7.86	30	52	1210	Ductile
	−450	7.41	31	58	1186	Ductile
	−623 <sup>1</sup>	8.10	32	56	1227	Ductile
	−650	7.80	30	58	1172	Ductile
	−850	6.84	24	35	1158	Cracks
1000	−350	5.56	23	47	1110	Cracks
	−450	4.49	19	0	1065	Brittle, cracks
	−621 <sup>1</sup>	7.63	31	30	1227	Cracks
	−650	7.44	29	56	1172	Ductile
	−850	4.94	20	0	1103	Brittle
10 000	−350	6.40	26	44	1125	Ductile
	−450	7.76	31	46	1230	Cracks
	−613 <sup>1</sup>	7.76	31	43	1225	Cracks
	−650	7.62	34	55	1189	Ductile
	−850	5.53	21	0	1043	Brittle

<sup>a</sup> Tested at strain rate of  $2.7 \times 10^{-6}$ /s.

<sup>b</sup> The pH of test solutions was adjusted to a value of 5, and the tests were conducted at ambient temperature.

<sup>c</sup> Test solution concentrations.

<sup>d</sup> Time to failure.

<sup>e</sup> Elongation of test specimens based on 38-mm gage length.

<sup>f</sup> Reduction of cross-sectional area of test specimens.

<sup>g</sup> Ultimate tensile strength of test specimens.

<sup>h</sup> Controlled potential in millivolts versus saturated calomel electrode (SCE).

<sup>1</sup> Test conducted in vegetable oil.

<sup>1</sup> *E*<sub>corr</sub> (corrosion potential) measured versus SCE.

### Tests in NH<sub>4</sub>Cl

The results of the tests in NH<sub>4</sub>Cl solutions are presented in Table 1. Figure 2 shows plots of the normalized *t<sub>f</sub>*, *RA*, and *UTS* versus electrode potentials. The normalized plots show that *t<sub>f</sub>* and *UTS* are not as sensitive as indicators of embrittlement as *RA*. At the controlled potential of −650 mV, there was no embrittlement at any of the three NH<sub>4</sub>Cl concentrations; the SSRT fractures were cup-and-cone-type fractures.

In the 100-ppm solution, only the fracture at −850 mV exhibited some degree of embrittlement. Although the fracture was cup-and-cone, there were numerous circumferential hairline secondary cracks in the gage section near the fracture.

At 1000 ppm NH<sub>4</sub>Cl, the specimens tested at −850 and −450 mV were brittle. There were numerous secondary cracks in the gage length of the specimen tested at −450 mV. Secondary cracking was also observed at the corrosion potential, −621 mV, and at −350 mV, but *RA* was not seriously reduced. There was no secondary cracking at −850 mV.

At 10 000 ppm NH<sub>4</sub>Cl, there was no embrittlement at −650 mV or at the more anodic potentials. The specimen at −850 mV exhibited nearly zero reduction in area at the fracture. No secondary cracking was observed.

TABLE 2—Slow strain rate<sup>a</sup> tests of AISI 4340 high-strength steel exposed to KCl solutions<sup>b</sup>.

Conc., <sup>c</sup> ppm	$E$ , mV vs SCE <sup>b</sup>	$t_f$ , <sup>d</sup> hrs	$EL$ , <sup>e</sup> %	$RA$ , <sup>f</sup> %	$UTS$ , <sup>g</sup> MPa	Type of Fracture
Inert env. <sup>1</sup>	...	7.80	36	60	1207	Ductile
100	-350	7.95	32	52	1172	Ductile
	-450	7.32	29	57	1185	Ductile
	-597 <sup>1</sup>	7.61	33	56	1230	Ductile
	-650	7.61	31	58	1224	Ductile
	-850	7.27	29	56	1185	Ductile
1000	-350	7.30	29	51	1158	Ductile
	-450	7.65	31	55	1193	Ductile
	-585 <sup>1</sup>	8.20	34	56	1225	Ductile
	-650	7.62	31	55	1202	Ductile
	-850	7.90	30	56	1197	Ductile
10 000	-350	7.27	29	50	1116	Ductile
	-450	7.79	31	55	1172	Ductile
	-573 <sup>1</sup>	8.20	33	58	1220	Ductile
	-650	7.71	31	56	1213	Ductile
	-850	7.50	29	54	1179	Ductile

<sup>a</sup> Tested at strain rate of  $2.7 \times 10^{-6}$ /s.

<sup>b</sup> The pH of test solutions was adjusted to a value of 5, and the tests were conducted at ambient temperature.

<sup>c</sup> Test solution concentrations.

<sup>d</sup> Time to failure.

<sup>e</sup> Elongation of test specimens based on 38-mm gage length.

<sup>f</sup> Reduction of cross-sectional area of test specimens.

<sup>g</sup> Ultimate tensile strength of test specimens.

<sup>h</sup> Controlled potential in millivolts versus saturated calomel electrode (SCE).

<sup>1</sup> Test conducted in vegetable oil.

<sup>l</sup>  $E_{corr}$  (corrosion potential) measured versus SCE.

*Tests in KCl*

Table 2 shows the results of the tests in the KCl solutions. Normalized  $t_f$ ,  $RA$ , and  $UTS$  as a function of electrode potentials are shown in Fig. 3. No significant embrittlement was found in any of the three tests with KCl concentrations at any of the controlled potentials. The typical fracture was ductile cup-and-cone. No secondary cracking was observed.

*Tests in NH<sub>4</sub>NO<sub>3</sub>*

Table 3 shows the results of the tests in the NH<sub>4</sub>NO<sub>3</sub> solutions. Normalized  $t_f$ ,  $RA$ , and  $UTS$  as function of electrochemical potentials are presented in Fig. 4.

There was no embrittlement at any of the controlled potentials in the 100-ppm NH<sub>4</sub>NO<sub>3</sub> solution. At 1000 and 10 000 ppm, the fractures were brittle at the -850 mV potential, but not at the more anodic potentials. At 1000 ppm, the  $RA$  was reduced from 56% at -650 mV to 28% at -850 mV. In the 10 000 ppm solution, the  $RA$  was reduced to near zero at -850 mV.

No secondary cracking was observed with these brittle fractures. However,  $t_f$  at -850 mV in the 10 000 ppm solution was greatly reduced (Fig. 4), indicating that cracking initiated early in the test. Such behavior was not observed in other tests.

TABLE 3—Slow strain rate<sup>a</sup> tests of AISI 4340 high-strength steel exposed to NH<sub>4</sub>NO<sub>3</sub> solutions<sup>b</sup>.

Conc., <sup>c</sup> ppm	<i>E</i> , mV vs SCE <sup>b</sup>	<i>t<sub>f</sub></i> , <sup>d</sup> hrs	<i>El</i> , <sup>e</sup> %	RA, <sup>f</sup> %	UTS, <sup>g</sup> MPa	Type of Fracture
Inert env. <sup>1</sup>	...	7.80	36	60	1207	Ductile
100	–350	7.94	31	58	1250	Ductile
	–450	7.75	30	55	1256	Ductile
	–639 <sup>1</sup>	7.45	29	52	1206	Ductile
	–650	7.02	30	53	1207	Ductile
	–850	7.31	29	55	1229	Ductile
1000	–350	7.74	31	51	1207	Ductile
	–450	7.89	32	54	1276	Ductile
	–629 <sup>1</sup>	7.61	27	56	1186	Ductile
	–650	7.21	29	56	1165	Ductile
	–850	7.14	29	28	1179	Brittle
						+ ductile
10 000	–350	7.20	29	50	1165	Ductile
	–450	7.52	30	55	1186	Ductile
	–627 <sup>1</sup>	8.12	32	58	1158	Ductile
	–650	7.32	30	56	1178	Ductile
	–850	1.63	6	0	1074	Brittle

<sup>a</sup> Tested at strain rate of  $2.7 \times 10^{-6}$ /s.

<sup>b</sup> The pH of test solutions was adjusted to a value of 5, and the tests were conducted at ambient temperature.

<sup>c</sup> Test solution concentrations.

<sup>d</sup> Time to failure.

<sup>e</sup> Elongation of test specimens based on 38-mm gage length.

<sup>f</sup> Reduction of cross-sectional area of test specimens.

<sup>g</sup> Ultimate tensile strength of test specimens.

<sup>h</sup> Controlled potential in millivolts versus saturated calomel electrode (SCE).

<sup>1</sup> Test conducted in vegetable oil.

<sup>j</sup>  $E_{\text{corr}}$  (corrosion potential) measured versus SCE.

## Discussion

The embrittlement observed in these solutions at an electrochemical potential of –850 mV versus SCE is consistent with a process of hydrogen embrittlement (hydrogen-induced cracking). In a solution of pH = 5.0, hydrogen will be reduced on the metal surface at potentials more negative than –536 mV versus SCE. Embrittlement occurred in the NH<sub>4</sub>Cl and NH<sub>4</sub>NO<sub>3</sub> solutions at the higher concentrations, but not in KCl even at the highest concentration. Also, there was no appearance of corrosion on the surface of any of the steel specimens tested at this potential.

Secondary cracking at –850 mV was observed only in the 100 ppm NH<sub>4</sub>Cl solution. Conditions for hydrogen-induced crack initiation can differ from those for crack propagation [4,5]. It is possible that the conditions for crack propagation were not favorable in the 100-ppm solution. In contrast, the short *t<sub>f</sub>* in the 10 000 ppm NH<sub>4</sub>NO<sub>3</sub> solution indicates rapid crack growth.

A potential of –650 mV versus SCE, which is slightly cathodic to the corrosion potential in all three solutions, appears to prevent embrittlement in SSRTs. Anodic polarization to –450 and –350 mV promoted general corrosion of the steel, but not necessarily embrittlement. Severe embrittlement occurred only in the NH<sub>4</sub>Cl solution at the intermediate concentration (1000 ppm). This is stress corrosion cracking (SCC). At a more active potential

TABLE 4—Slow strain rate<sup>a</sup> tests, normalized data<sup>b</sup>.

E, mV vs SCE <sup>c</sup>	100 ppm			1000 ppm			10 000 ppm		
	$t_{fN}^d$	$RA_N^e$	$UTS_N^f$	$t_{fN}^d$	$RA_N^e$	$UTS_N^f$	$t_{fN}^d$	$RA_N^e$	$UTS_N^f$
<b>Ammonium Chloride</b>									
-350	1.01	0.87	1.00	0.71	0.78	0.92	0.82	0.73	0.93
-450	0.95	0.97	0.98	0.58	0.00	0.88	0.99	0.77	1.02
$E_{corr}$	1.04	0.93	1.02	0.98	0.50	1.02	0.99	0.72	1.01
-650	1.00	0.97	0.97	0.95	0.93	0.97	0.98	0.92	0.99
-850	0.85	0.58	0.96	0.63	0.00	0.91	0.71	0.00	0.86
<b>Potassium Chloride</b>									
-350	1.02	0.87	0.97	0.94	0.85	0.96	0.93	0.83	0.97
-450	0.94	0.95	0.98	0.98	0.92	0.99	1.00	0.92	0.97
$E_{corr}$	0.98	0.93	1.02	1.05	0.93	1.01	1.05	0.97	1.01
-650	0.98	0.97	1.01	0.98	0.92	1.00	0.99	0.93	1.00
-850	0.93	0.95	0.98	1.01	0.93	0.99	0.96	0.90	0.98
<b>Ammonium Nitrate</b>									
-350	1.02	0.97	1.04	0.99	0.85	1.00	0.92	0.83	0.97
-450	0.98	0.92	0.98	1.01	0.90	1.06	0.96	0.92	0.98
$E_{corr}$	0.96	0.87	1.04	0.98	0.93	0.98	1.04	0.97	0.96
-650	0.90	0.88	1.00	0.92	0.93	0.97	0.94	0.93	0.98
-850	0.94	0.92	1.02	0.92	0.47	0.98	0.21	0.00	0.89

<sup>a</sup> Tested at strain rate of  $2.7 \times 10^{-6}$ /s. The pH of test solutions was adjusted to a value of 5, and the tests were conducted at ambient temperature.

<sup>b</sup> Normalized data determined using ratios of values obtained in the various solutions to values obtained in an inert environment (oil).

<sup>c</sup> Controlled potential in millivolts versus saturated calomel electrode (SCE).

<sup>d</sup> Normalized time to failure.

<sup>e</sup> Normalized reduction of cross-sectional area of test specimens.

<sup>f</sup> Normalized ultimate tensile strength of specimens.

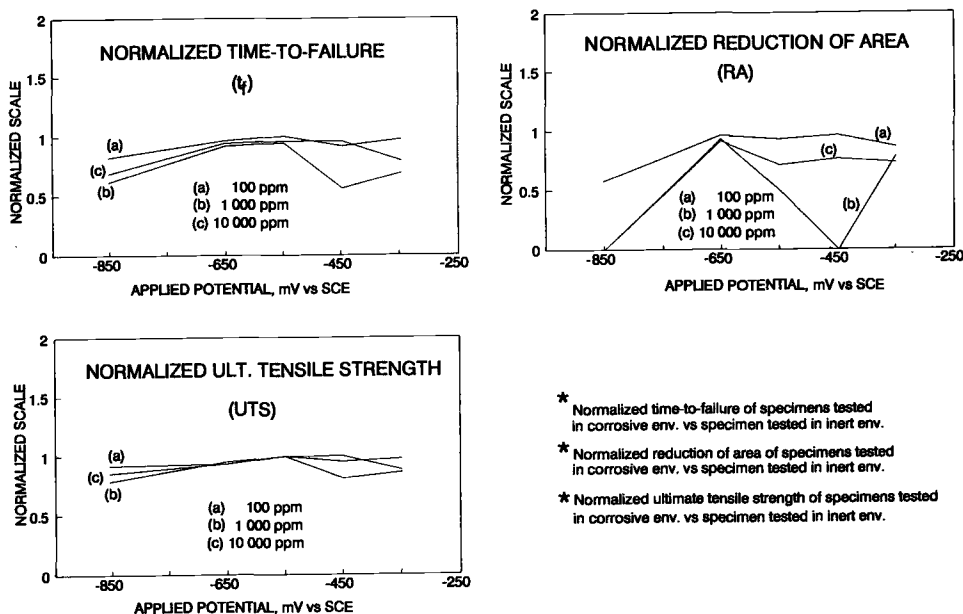
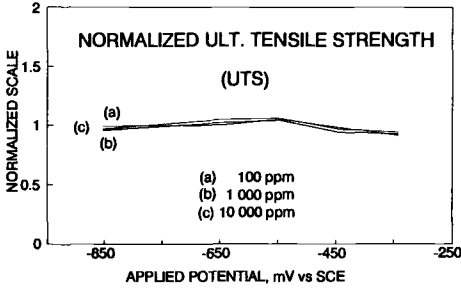
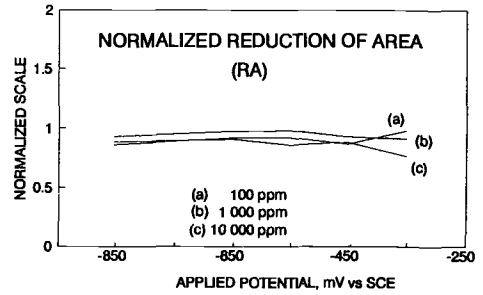
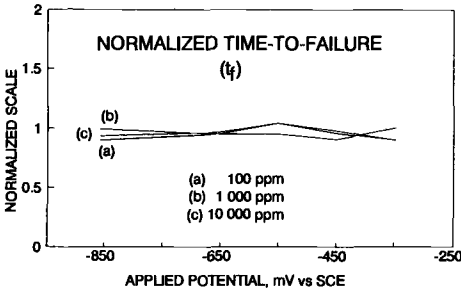
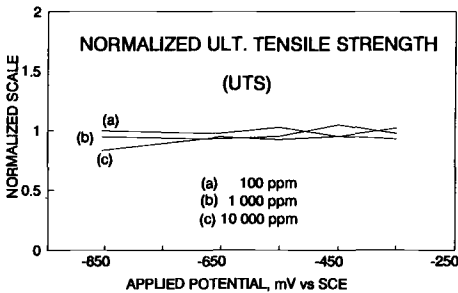
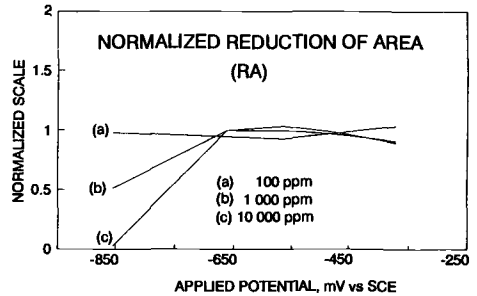
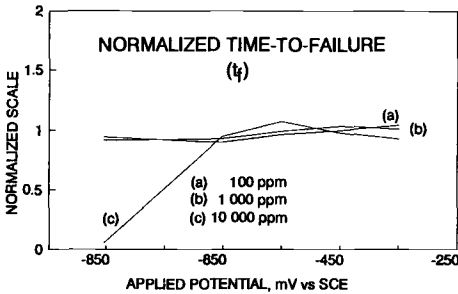


FIG. 2—Normalized time-to-failure, reduction of area, and ultimate tensile strength of specimens tested in solutions containing 100, 1000, and 10 000 ppm of ammonium chloride at ambient temperature (strain rate of  $2.7 \times 10^{-6}$ /s).



- \* Normalized time-to-failure of specimens tested in corrosive env. vs specimen tested in inert env.
- \* Normalized reduction of area of specimens tested in corrosive env. vs specimen tested in inert env.
- \* Normalized ultimate tensile strength of specimens tested in corrosive env. vs specimen tested in inert env.

FIG. 3—Normalized time-to-failure, reduction of area, and ultimate tensile strength of specimens tested in solutions containing 100, 1000, and 10 000 ppm of potassium chloride at ambient temperature (strain rate of  $2.7 \times 10^{-6}/s$ ).



- \* Normalized time-to-failure of specimens tested in corrosive env. vs specimen tested in inert env.
- \* Normalized reduction of area of specimens tested in corrosive env. vs specimen tested in inert env.
- \* Normalized ultimate tensile strength of specimens tested in corrosive env. vs specimen tested in inert env.

FIG. 4—Normalized time-to-failure, reduction of area, and ultimate tensile strength of specimens tested in solutions containing 100, 1000, and 10 000 ppm of ammonium nitrate at ambient temperature (strain rate of  $2.7 \times 10^{-6}/s$ ).

( $-350$  mV), the general dissolution rate of the steel was high and the secondary cracks observed were blunt. A similar argument can be made for even lesser embrittlement at the highest  $\text{NH}_4\text{Cl}$  concentration. In the 10 000 ppm solution at  $-350$  mV, the increased general corrosion must have obviated secondary surface cracking since none was observed. If the presence of secondary cracking is an indicator, the electrochemical potential range for SCC in  $\text{NH}_4\text{Cl}$  extends from about the corrosion potential ( $-613$  to  $-623$  mV) to about  $-350$  mV in the intermediate and highest concentration solutions.

The lack of sensitivity of UTS to the failure mode can partially be explained by the ratio of high yield strength to tensile strength in the steel, but it also indicates that crack initiation does not occur until after some substantial uniform elongation has occurred.

### Conclusions

Of the three compounds studied using SSRT at controlled electrochemical potentials, only ammonium chloride caused SCC in AISI 4340 high-strength steel. The corrosion potential of about  $-620$  mV versus SCE is at the brink of the potential range for SCC. The most severe embrittlement was observed at  $-450$  mV in the intermediate solution concentration of 1000 ppm  $\text{NH}_4\text{Cl}$ . Hydrogen-induced cracking was observed at  $-850$  mV in the  $\text{NH}_4\text{Cl}$  and  $\text{NH}_4\text{NO}_3$  solutions, but not in the KCl solutions.

### Acknowledgments

Special thanks to Myra L. Stults and Cedric P. McCloud who performed the tensile tests in the corrosion laboratory at the National Fertilizer and Environmental Research Center, Tennessee Valley Authority, Muscle Shoals, Alabama.

### References

- [1] Perkins, P. C., Daniels, R. D., and Gillies, A. B., "Failure Analyses of Steel Breech Chambers Used with Aircraft Cartridge-Ignition Starters," *Analyzing Failures*, V. S. Goel, Ed., American Society for Metals, Metals Park, OH, 1986, pp. 143-150.
- [2] Kennelley, K. J. and Daniels, R. D., "Stress Corrosion Cracking of 4340 Steel in Aircraft Ignition Starter Residues," *Journal of Materials Engineering*, Vol. 9, No. 1, 1987, pp. 35-40.
- [3] Daniels, R. D., Sadarangani, A. P., Magner, M. P., and Kennelley, K. J., "Effects of Electrochemical Potential on the Slow Strain Rate Fracture of 4340 Steel in a Combustion Product Residue," *Environmentally Assisted Cracking: Science and Engineering*, ASTM STP 1049, W. B. Lisagor, T. W. Crooker, and B. N. Leis, Eds., American Society for Testing and Materials, Philadelphia, 1990, pp. 103-116.
- [4] Bernstein, I. M., Garber, R., and Pressouyre, G. M., "Effect of Dissolved Hydrogen on Mechanical Behavior of Metals," *Effect of Hydrogen on Behavior of Metals*, A. W. Thompson and I. M. Bernstein, Eds., Metallurgical Society, AIME, New York, 1976, pp. 37-58.
- [5] Parkins, R. N., "Development of Strain-Rate Testing and Its Implications," *Stress Corrosion Cracking: The Slow Strain-Rate Technique*, ASTM STP 665, G. M. Ugiansky and J. H. Payer, Eds., American Society for Testing and Materials, Philadelphia, 1979, pp. 5-24.

D. A. Meyn<sup>1</sup> and P. S. Pao<sup>1</sup>

## Slow Strain Rate Testing of Precracked Titanium Alloys in Salt Water and Inert Environments

---

**REFERENCE:** Meyn, D. A. and Pao, P. S., "Slow Strain Rate Testing of Precracked Titanium Alloys in Salt Water and Inert Environments," *Slow Strain Rate Testing for the Evaluation of Environmentally Induced Cracking: Research and Engineering Applications, ASTM STP 1210*, R. D. Kane, Ed., American Society for Testing and Materials, Philadelphia, 1993, pp. 158–169.

**ABSTRACT:** The stress corrosion cracking (SCC) propagation kinetics of fatigue-precracked Ti-6Al-4V (an  $\alpha$ - $\beta$  alloy) and Ti-15V-3Al-3Cr-3Sn (a  $\beta$ - $\alpha$  alloy) were studied in neutral 3.5% NaCl solution and in inert environments. The slow strain rate method was used instead of the constant load method. This was pursued in an effort to minimize the number of specimens normally required and reduce the time required to determine the stress intensity threshold for SCC. The results were encouraging, but some anomalies in the crack growth kinetics were noted. At a relatively low extension rate, crack rates in both alloys alternated between high Stage II rates and very low rates during the test. At a higher extension rate, crack rates in the Ti-15-3 alloy behaved as previously described, whereas in the Ti-6-4 alloy crack growth remained at Stage II rates continuously above the threshold. No traces of crack arrest could be found on the fracture surfaces.

**KEYWORDS:** stress corrosion cracking (SCC), environmental cracking, discontinuous cracking, slow strain rate, titanium alloy

Aqueous stress corrosion cracking (SCC) of titanium alloys has traditionally been performed by loading fatigue-precracked fracture mechanics specimens up to or above an estimated threshold stress intensity factor  $K_{Ith}$ , then maintaining that load until fracture ensued or the time allotted for the experiment was reached [1]. Several such specimens are usually required to bracket  $K_{Ith}$ , unless one uses step loading, wherein the load on a single specimen is increased after some lengthy wait at each previous load, until crack growth occurs. Such a test can provide not only an estimate of  $K_{Ith}$ , but also the kinetics of SCC propagation by monitoring crack depth as well as load during the test. The classic three-stage propagation kinetics [1,2] is normally observed when titanium alloys are tested in neutral salt solution, except that the strongly  $K_I$ -dependent Stage I behavior is not observed. No SCC propagation is observed until  $K_{Ith}$  is reached, whereupon cracking suddenly jumps into Stage IIa and subsequently rises to Stage II [2]. This paper describes some data obtained while using the slow strain rate method to obtain threshold and kinetics data for an  $\alpha$ - $\beta$  alloy, Ti-6-4, and a  $\beta$ - $\alpha$  alloy, Ti-15-3. The classic Stage IIa-Stage II kinetics behavior described was expected to occur. However, the results to be presented will show that this was not the case. Even though  $K_I$  increased continuously or remained constant during crack propagation, cracking occurred discontinuously under certain conditions in these alloys.

---

<sup>1</sup> Code 6320, Naval Research Laboratory, Washington, DC 20375-5000.

TABLE 1—Composition and properties (wt%).

Material	Al	Cr	V	Sn	O	H	0.2% YS, MPa	$K_{Ic}$ , MPa $\sqrt{m}$
Ti-6-4	6.7	—	4.3	—	0.20	0.006	869	87
Ti-15-3	2.83	2.5	14.1	2.4	0.13	0.015	1137	—

### Materials and Methods

The compositions and properties of the two titanium alloys are given in Table 1. The Ti-6-4 alloy was obtained as 25.4-mm-thick hot-rolled plate, in the beta STA condition (1038°C 0.5 h, air cooled to ambient, aged at 732°C 2 h, air cooled). The Ti-15-3 alloy was obtained as 25.4-mm-thick hot-rolled plate, hot isostatic pressed at 954°C/103 MPa 2 h, cooled directly to 524°C and aged 12 h at that temperature. Specimens were of the pin-loaded WOL configuration [3], with  $W = 64.8$  mm. Ti-6-4 specimens were 25.4-mm-thick with no side grooves, whereas the Ti-15-3 specimens were 10-mm-thick with 0.5 mm deep, 90° V-shaped side grooves on each side. Specimens were precracked in fatigue under zero-tension loading according to specifications of ASTM E 399, Test Method for Plane-Strain Fracture Toughness of Metallic Materials. Knife edges were cemented to the front edges of the specimens on either side of the notch mouth in order to attach a displacement gage and record crack mouth opening displacement (CMOD) [3]. Load was measured with a load cell, and crack depths,  $a$ , were calculated from CMOD and load [3]. Stress intensity factors,  $K_I$ , were calculated using the calibration in ASTM E 399, and crack growth rates were calculated by finite differentials, i.e., the increment of crack growth,  $\Delta a$ , was divided by the corresponding increment of time,  $\Delta t$ .

Tests in 3.5% (wt.) NaCl solution were carried out with the specimen tensile axis horizontal and the crack growth direction vertical, so that the back end of the specimen dipped into the environment in a loosely covered glass container (Fig. 1). The fatigue crack was about 26-mm-long, so that the tip of the crack was immersed. Except for one experiment, the solution was neither changed nor aerated during the test, and evaporated water was periodically replaced by additions of distilled water. The solution volume was about 650 mL. Tests in unmodified laboratory air were conducted in the same configuration. Tests in vacuum were conducted in a stainless steel chamber under a pressure less than  $1 \times 10^{-4}$  Pa, with the tension axis vertical. The test was of the extension-controlled type, with constantly

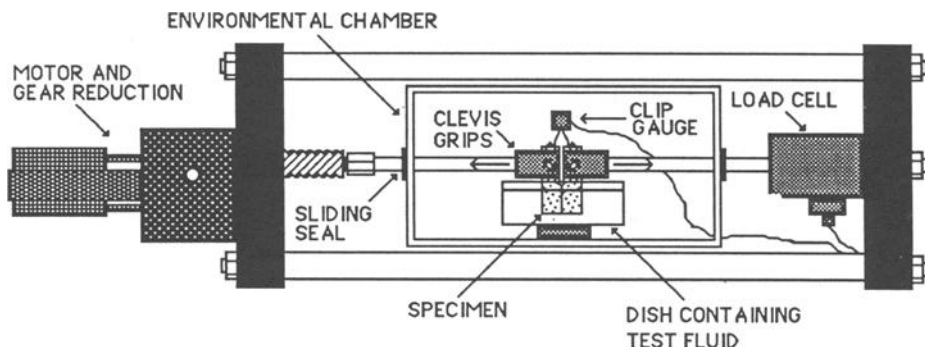


FIG. 1—Slow strain rate testing apparatus.

increasing applied extension, resulting in constantly increasing CMOD, by means of a lead screw. The "slow" extension rate (measured with no load) was approximately  $0.015 \mu\text{m/s}$ , resulting in actual loading rates of 0.6 to  $0.8 \text{ kPa}\sqrt{\text{m/s}}$  under load, before the onset of rapid crack propagation. The "fast" extension rate was about  $0.15 \mu\text{m/s}$ , with the resulting loading rate of 6 to  $8 \text{ kPa}\sqrt{\text{m/s}}$ . Extension rates for the Ti-6-4 specimens in air and vacuum were approximately  $0.004 \mu\text{m/s}$  producing loading rates of  $0.2 \text{ kPa}\sqrt{\text{m/s}}$ . The stress intensity factor rates are those under elastic conditions before the onset of fast crack growth; they increase markedly during Stage II crack propagation.

## Results

Table 2 summarizes the experimental conditions and results. The SCC growth rates are shown in Figs. 2 and 3 as functions of the stress intensity factor for Ti-6-4 and Ti-15-3, respectively. It is useful in interpreting these plots to remember that the vertical  $\Delta a/\Delta t$  axis is logarithmic, so that small variations in the low growth rate regimes are greatly exaggerated relative to variations in the higher growth rate regimes. It is probable that the apparent crack growth below the threshold  $K_{Ith}$  is mostly caused by local yielding at the crack tip which is detected by the CMOD gage, and does not represent real crack propagation. All the growth rate plots are truncated at the point where  $K_I$  begins to decrease at large crack depth to avoid confusion in interpretation. The decrease in  $K_I$  at large crack depth is a consequence of the stiffness of the loading arrangement under extension control. When crack growth is rapid, relaxation due to crack opening outpaces the applied extension to such an extent that  $K_I$  begins to decrease. Figure 4 shows typical behavior, the curve wrapping back on itself, with crack growth arresting at a low value of  $K_{Iarr}$  near the threshold value  $K_{Ith}$ . Large crack depths can not be precisely calculated from CMOD and load without unusual precautions because of frictional effects in the grips. This accounts for some of the discrepancy between  $K_{Ith}$  and  $K_{Iarr}$ , although there may also be a true physical difference.

Ti-6-4 in salt water (Fig. 2a) shows no Stage I behavior at the low extension rate ( $0.015 \mu\text{m/s}$ ). The crack rate jumps to Stage II SCC at about  $55 \text{ MPa}\sqrt{\text{m}}$ , then drops to a virtual halt, until at  $78 \text{ MPa}\sqrt{\text{m}}$  the crack rate again jumps to Stage II, remaining there until  $K_I$ ,

TABLE 2—Results of SSR tests.

Alloy	Ext. Rate, $\mu\text{m/s}$	Environment	$K_{Ith}$ , $\text{MPa}\sqrt{\text{m}}$	Stg. II Rate, $\mu\text{m/s}$	Discontinuous Cracking?
Ti-6-4	0.015	3.5% NaCl	55 <sup>a</sup>	10–23	Yes
	0.15	3.5% NaCl	65	10–23	No
	0.003	Air	91 <sup>b</sup>	N/A <sup>c</sup>	No
	0.0045	Vacuum	69 <sup>b</sup>	N/A <sup>c</sup>	No
Ti-15-3	0.015	3.5% NaCl (aer.)	63 <sup>a</sup>	100–1500 <sup>d</sup>	Yes
	0.15	3.5% NaCl	58 <sup>a</sup>	100–1500 <sup>d</sup>	Yes
	0.015	Air	48 <sup>a</sup>	300–1000 <sup>d</sup>	Yes
	0.015	Air	55 <sup>a</sup>	1000 <sup>d</sup>	Yes
	0.015	Vacuum	66 <sup>a</sup>	1000 <sup>d</sup>	? <sup>e</sup>

<sup>a</sup> Start of initial spike.

<sup>b</sup> Onset of significant crack growth.

<sup>c</sup> No Stage II.

<sup>d</sup> Possibly quasi-stable mechanical fracture, rather than Stage II.

<sup>e</sup> Similar behavior except only one large spike.

(Data based on 1 test per material/condition).

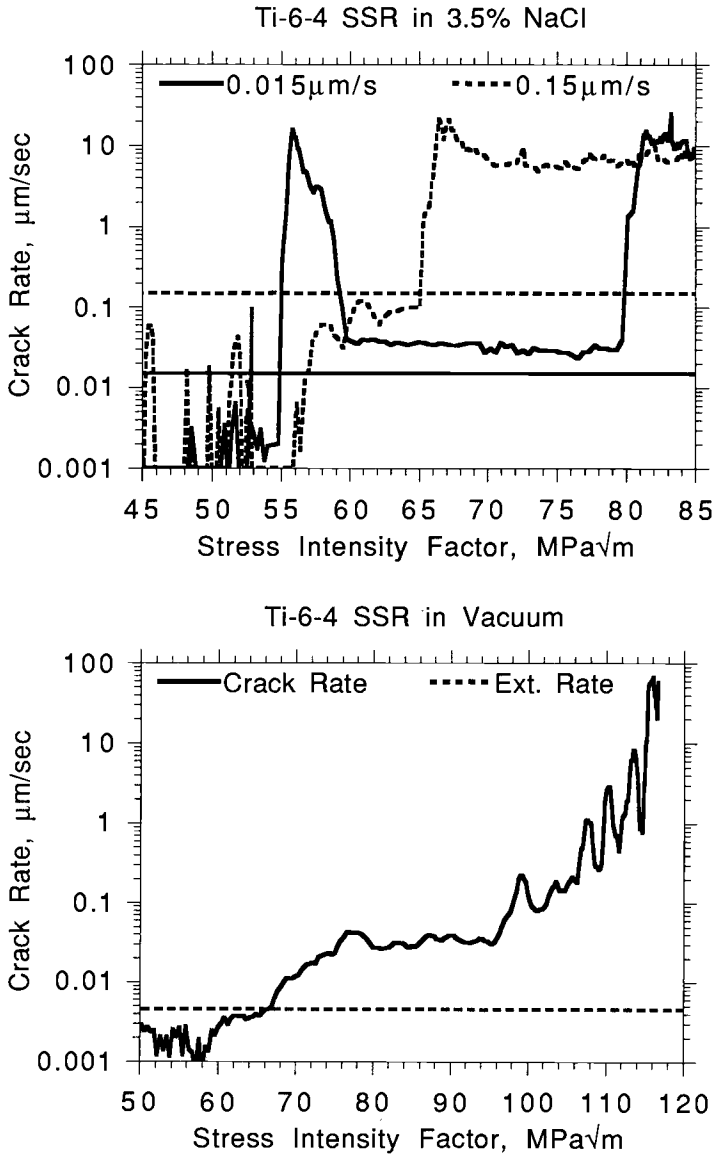


FIG. 2—Cracking kinetics versus stress intensity factor for the Ti-6-4 alloy. The matching horizontal lines are the corresponding extension rates for visual comparison. (a) Salt water environment. (b) Vacuum environment. Results similar in air.

having reached a peak value, decreases to  $K_{Icr}$ , whereupon crack growth slows to a halt. The decreasing  $K_I$  regime is not shown. At the higher extension rate ( $0.15 \mu\text{m/s}$ ), apparent crack growth at a very low rate, possibly inert-environment sustained load cracking SLC caused by internal hydrogen [4], begins at about  $56 \text{ MPa}\sqrt{\text{m}}$ , then the rate jumps to Stage II SCC at  $65 \text{ MPa}\sqrt{\text{m}}$  which continues until  $K_I$  decreases below threshold. No conventional static load threshold measurements have been made on this particular plate. However, these

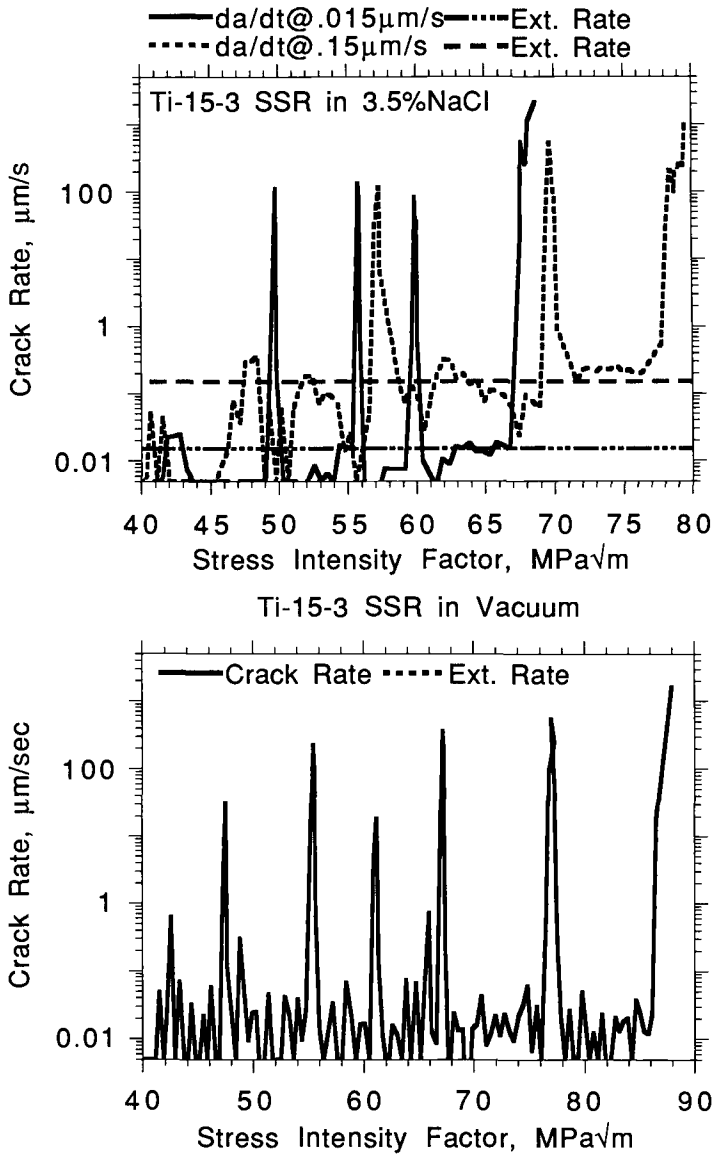


FIG. 3—Cracking kinetics versus stress intensity factor for the Ti-15-3 alloy. The matching horizontal lines are the corresponding extension rates for visual comparison. (a) Salt water environment. (b) Air environment. Vacuum similar except only one large spike.

initial threshold values are in approximate agreement with other data for  $\beta$ -annealed Ti-6-4 [2]. The appearance of the fracture surfaces is identical for both cases, consisting of typical cleavage and flutes [5] in the SCC regions, Fig. 5. No traces of the hiatus in Stage II cracking for the low extension rate, such as an arrest mark or a stain, could be found in the fracture surface. Kinetics in both air and vacuum (Fig. 2b) differed greatly from those in salt water. No distinct onset of rapid crack growth nor any true Stage II cracking occurred. The crack

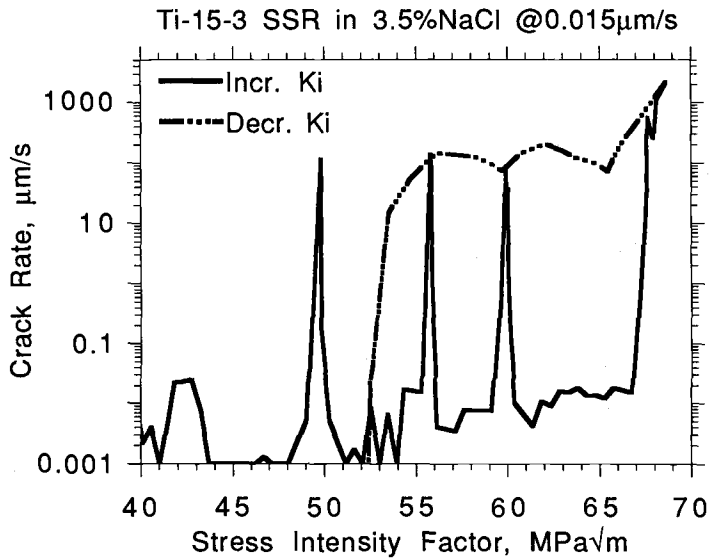


FIG. 4—Cracking kinetics for the Ti-15-3 alloy at 0.015  $\mu\text{m/s}$  showing the decreasing  $K_I$  behavior.

rate increased continuously although somewhat irregularly with  $K_I$ , above an indistinct threshold which was in the range 69 to 97  $\text{MPa}\sqrt{\text{m}}$ . The fracture surfaces consisted of microvoid coalescence and quasicleavage, similar to overload fracture. This behavior is consistent with prior studies of sustained load cracking in inert environments under static loading conditions for Ti-6-4 alloys [4].

Ti-15-3 in salt water (Fig. 3a), shows discontinuous crack propagation at both extension rates, with spikes of very rapid propagation starting at 63  $\text{MPa}\sqrt{\text{m}}$  under 0.015  $\mu\text{m/s}$  extension rate, and at 58  $\text{MPa}\sqrt{\text{m}}$  under 0.15  $\mu\text{m/s}$ . Steady apparent Stage II growth takes

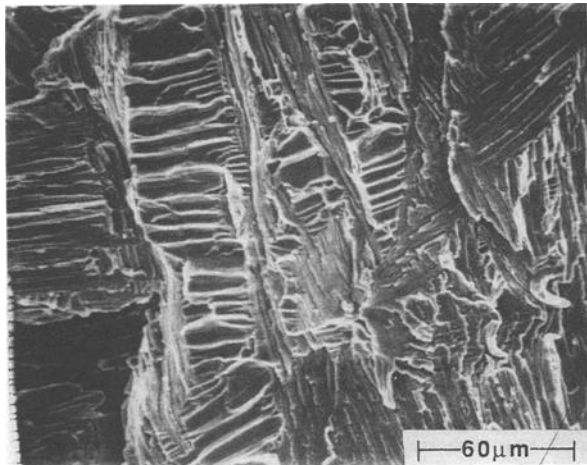


FIG. 5—Scanning electron micrograph of Ti-6-4 Stage II SCC fracture area, showing typical cleavage plus flutes morphology.

over in the later stages of the test. No effect of extension rate on the spikey nature of propagation seems evident, nor did aeration have any measurable effect. The fracture surfaces (Fig. 6) consisted of mixed intergranular and transgranular microvoid coalescence MVC [6]. No arrest marks or other traces of the abrupt transitions between crack stagnation and rapid propagation could be found on the fracture surfaces. Tests in air environment showed similar results (Fig. 3b). A test in vacuum was also similar, except only one large spike occurred. Fracture features were identical to those of the salt water specimens.

The extension rates are also plotted on Figs. 2 and 3 in order to show how that parameter relates to the crack growth rates. The crack rates for Ti-6-4 show no obvious influence of

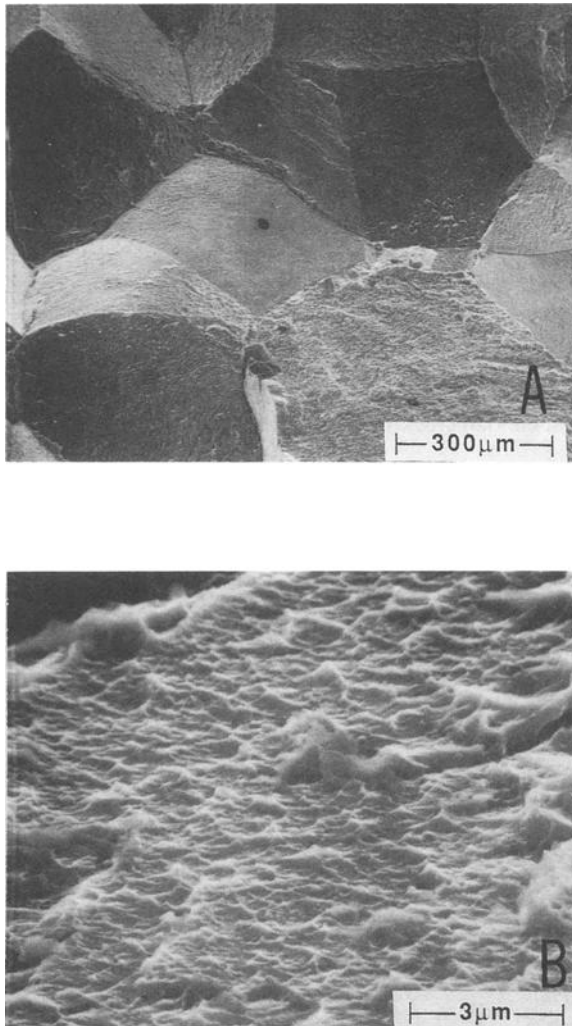


FIG. 6—Scanning electron micrograph of Ti-15-3 fracture area, showing typical mixed intergranular and transgranular cracking. Salt water fracture shown, vacuum and air fractures similar. (a) General view. (b) Apparently smooth intergranular facet at high magnification, showing extensive microplasticity (MVC).

the applied extension rates. However, the stagnation crack growth rates for Ti-15-3 between high growth rate spikes, and to a lesser extent the crack rates during the spikes, do seem to be influenced by the extension rate.

Figure 7 shows crack rates together with the corresponding stress intensity factors for the two alloys at the slower extension rate,  $0.015 \mu\text{m/s}$ , on a crack depth basis. These show that although the crack growth rate spikes in Fig. 3 look rather brief, they cause a significant portion of the total crack propagation. Discontinuous cracking (spikes) is a feature of the early period of crack propagation. During most of the crack propagation life of these experiments, crack growth is continuous at the high, Stage II-like, rate. Much of this continuous cracking occurred while the nominal value of  $K_I$ , having reached a peak and decreased, was within the range wherein discontinuous cracking occurred at smaller crack depths.

Figures 8 and 9 are expanded plots of the discontinuous crack growth part of Fig. 7. Additional curves of crack growth rate and stress intensity factor are shown, calculated by assuming that the crack rate jumps immediately to Stage II and remains constant under constant load. These calculated curves are intended to simulate behavior under constant load, for comparison with the constant extension rate experimental results.  $K_I$  under constant extension rate conditions remains nearly constant or rises only a little during the Stage II, high growth rate, episodes. The crack grows so fast as to outrun the slow increase in extension, so that the load drops rapidly enough to counteract the effect of increasing crack depth on the  $K$ -factor. Most of the increase in  $K_I$  during the test takes place during the periods of crack growth stagnation between Stage II episodes.  $K_I$  under constant load, on the other hand, increases rapidly during Stage II cracking, and approximately maintains pace with the long term average increase in  $K_I$  resulting from the discontinuous crack growth under constant extension rate cracking. Figure 10 shows data for Ti-6-4 at the higher extension rate. The rate of increase of  $K_I$  with crack depth under constant extension rate

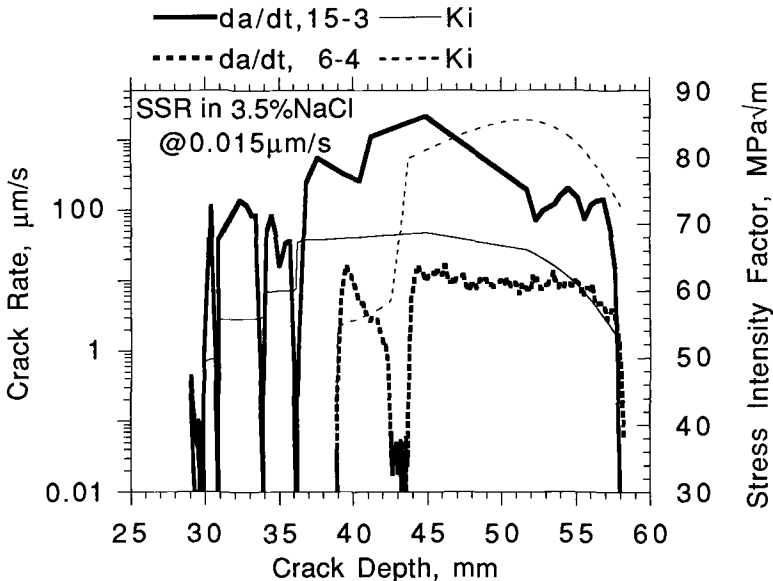


FIG. 7—Cracking kinetics together with stress intensity factors for both alloys at  $0.015 \mu\text{m/s}$  as a function of crack depth.

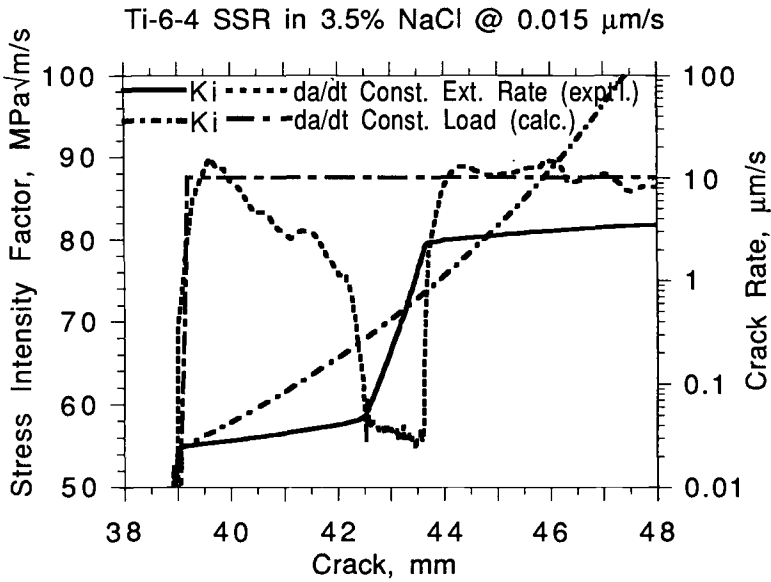


FIG. 8—Cracking kinetics and stress intensity factor for Ti-6-4 at 0.015  $\mu\text{m/s}$ , comparing constant extension rate behavior (experimental) with that under constant load (calculated).

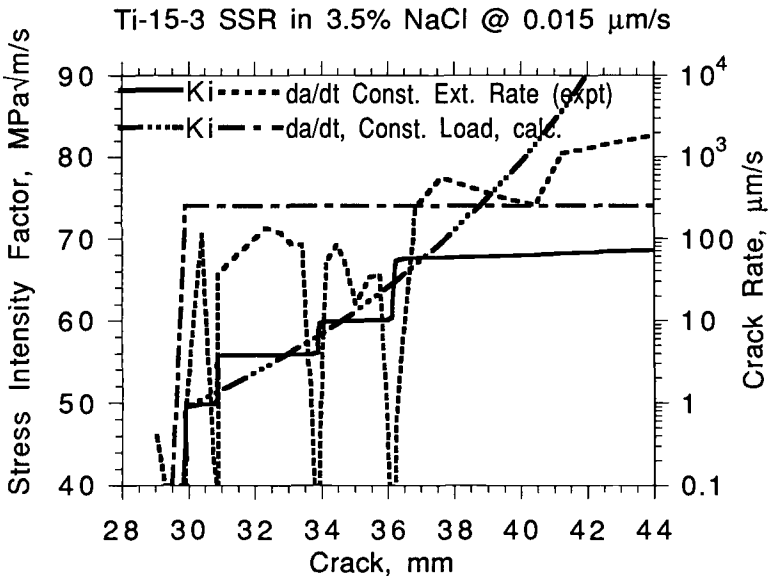


FIG. 9—Cracking kinetics and stress intensity factor for Ti-15-3 at 0.015  $\mu\text{m/s}$ , comparing constant extension rate behavior (experimental) with that under constant load (calculated).

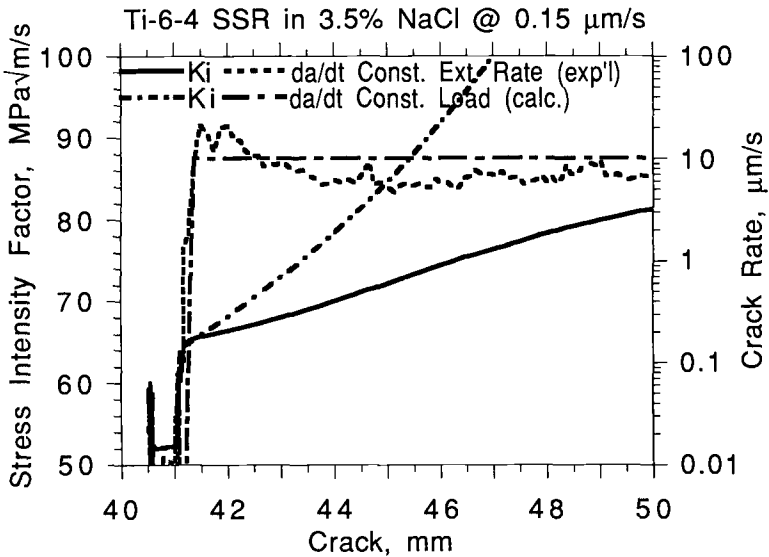


FIG. 10—Cracking kinetics and stress intensity factor for Ti-6-4 at 0.15  $\mu\text{m/s}$ , comparing constant extension rate behavior (experimental) with that under constant load.

loading is somewhat greater at the higher extension rate, compared with that shown in Fig. 8 for the lower extension rate.

## Discussion

It is apparent that the behaviors of these two alloys are quite different. The Ti-6-4 alloy displays true SCC with the expected Stage II regime (albeit interrupted in the low extension rate case), and a radical difference between salt water on one hand and air or vacuum environment on the other. The Ti-15-3 alloy shows no SCC effect of the salt water, the behavior in air and vacuum being substantially the same. There is some question whether the high crack rates in this alloy signify Stage II cracking as usually understood, or if they are caused by quasi-stable mechanical overload cracking.

Turning first to the Ti-6-4 alloy, it appears that discontinuous cracking is extension rate dependent, that is, it does not occur at the higher of the two extension rates used. One can speculate that discontinuous cracking is controlled by the crack tip strain rate, which, if sufficiently high, will maintain conditions conducive to Stage II crack growth. Figures 8 and 9 show that  $K_I$  under constant extension rate conditions does not increase as rapidly during Stage II episodes as under constant load conditions, and discontinuous cracking has not been reported under constant load conditions. It is as if some minimum rate of increase in  $K_I$  is required to sustain Stage II, at least until some critical value of  $K_I$  is reached for which the strain rate necessary can be maintained without further increases in  $K_I$ . Figure 10 supports this view; both  $K_{I,II}$  and the rate of increase in  $K_I$  with crack depth during Stage II are significantly higher than for the lower extension rate case, and discontinuous cracking is not observed.

A number of current models for SCC involve a passive film at the crack tip interacting with localized deformation and crack tip electrochemistry [7]. The potential for repassivation may be such that when a critical crack tip strain rate is reached, complete passivation is not

maintained at the tip, and rapid embrittling reactions occur. This critical crack tip strain rate is a function of the applied extension rate and the level of  $K_I$  as well as the electrochemical environment. Ordinarily, once begun this process would be expected to continue until fracture or until  $K_I$  dropped below  $K_{I,irr}$ . However, in the present case for some reason the embrittling process, after causing some initial rapid cracking, stagnates, not resuming again until a  $K_I$  value far above the initial  $K_{I,th}$  is reached. Stagnation could occur when a change in conditions in the crack brought on by rapid crack propagation facilitates repassivation, for example, a change in the electrolyte composition, or a drop in  $K_I$ . The former should happen even at the higher extension rate, where no stagnation was observed. The latter does not seem to occur (Figs. 8 through 10), although  $K_I$  does remain constant or rise more slowly with increasing crack growth under extension rate control than under constant load. However,  $K_I$  does increase more rapidly with crack growth at the higher extension rate than at the lower extension rate (compare Fig. 10 with Fig. 8). This provides some evidence that the local crack tip strain rate (which is proportional both to  $K_I$  and to  $dK_I/dt$ ) controls the onset of stagnation.

The Ti-15-3 alloy did not display any influence of environment nor of extension rate on the slow strain rate cracking behavior. It did, however, display discontinuous crack growth. There were no signs of arrest marks on the fracture surfaces, and because it occurred in an inert as well as an active environment, no argument of the kind advanced for Ti-6-4 above applies. Gerberich [8] has developed a model based on the formation of a microcracked process zone at the crack tip to explain similar behavior during inert environment sustained load cracking of 4340 steel and Ti-30Mo, a beta titanium alloy. The model assumes that the material ahead of the crack tip becomes discontinuously microcracked, so that neither any one such microcrack nor the ultimate crack tip (comprising really the distribution of microcracks penetrating furthest into the material) bears the brunt of the stress distribution. Therefore, until the local distribution of microcracks links up to produce a uniform crack front, the effective stress intensity factor is reduced below that necessary to maintain Stage II cracking, i.e., below  $K_{I,th}$ . The repetition of this process of Stage II cracking, its stifling by formation of multiple microcracks, their final linkage and resumption of Stage II, etc., give rise to discontinuous cracking behavior. He was able to show that cracking occurred in 4340 steel by mixed modes, suggesting the existence of such an obstructive process zone, and that the Ti-30Mo alloy had microbranched crack tip regions. He was also able to show that the intensity of plastic deformation in cleavage facets in the Ti-30Mo indicated that they were forming well ahead of the nominal crack tip, and that the effective stress intensity factor where cracking was occurring was considerably lower than the nominal value. This analysis has promise, and it is planned to attempt further experimental and analytical investigation of this phenomenon.

The purpose of aerating the solution for the Ti-15-3 alloy test at low strain rate was to test the passivation/depassivation hypothesis set forth for the Ti-6-4 alloy to some extent. It was considered that a marginal passivating potential might exist at the higher strain rate, and that cracking might be suppressed at a lower strain rate with excess aeration and more time for passivation. It is apparent that this concept was not borne out by the results, and that the alloy was not affected by the salt water environment in any case.

Discontinuous crack growth could be caused by alternating periods of hydrogen absorption and hydride growth [9]. Below  $K_{I,th}$  hydrogen generated at the crack tip by local cathodic reactions could enter the metal and diffuse along the high-diffusivity beta phase. At some point the hydrided volume cracks at the Stage II rate, arresting when entering uncontaminated metal, the process repeating. However, Ti-15-3 is a beta alloy, and these alloys do not easily form hydrides, even at extremely high hydrogen levels [10]. Furthermore, crack propagation occurs entirely by microvoid coalescence and there is no evidence of an envi-

ronmental effect. Hydride precipitation would occur more easily in the Ti-6-4 alloy. However, the cracking mode in Ti-6-4 is identical to SCC in nonhydrogenous environments, such as  $\text{CCl}_4$ , with no intergranular or  $\alpha$ - $\beta$  interfacial component such as would be expected if cracking involved hydrogen absorption and hydride formation on a large scale [11].

## Conclusions

Both an  $\alpha$ - $\beta$  alloy, Ti-6-4, and a  $\beta$ - $\alpha$  alloy, Ti-15-3, were subjected to slow strain rate loading as precracked fracture mechanics specimens. The  $K_{Ith}$  values measured were in the range expected from published results obtained by conventional techniques. Ti-6-4 displayed normal continuous Stage II SCC at the higher of two extension rates used, but cracked discontinuously at the lower rate. Behavior in air and vacuum was similar to prior work done under static load conditions. Ti-15-3 displayed interrupted growth at all rates and in all environments. No markings corresponding to the Stage II growth interruptions could be found on the fracture surfaces of specimens which underwent discontinuous cracking. The mechanisms for this behavior have not been identified, and further studies of the phenomenon and analysis of the micromechanical state at the crack tips during interrupted growth are planned.

## References

- [1] Sedriks, A. J., *Stress Corrosion Cracking Test Methods (Corrosion Testing Made Easy, Vol. 1)* National Association of Corrosion Engineers, Houston, TX, 1990.
- [2] Blackburn, M. J., Smyrl, W. H., and Feeney, J. A., "Titanium Alloys," *Stress Corrosion Cracking in High Strength Steels and in Titanium and Aluminum Alloys*, B. F. Brown, Ed., Naval Research Laboratory, Washington, DC 20375-5000, 1972, p. 275.
- [3] Saxena, A. and Hudak, S. J. Jr., "Review and Extension of Compliance Information for Common Crack Growth Specimens," *International Journal of Fracture*, Vol. 14, No. 5, 1978, pp. 453-468.
- [4] Meyn, D. A., "Effect of Hydrogen Content on Inert Environment Sustained Load Crack Propagation Mechanisms of Ti-6Al-4V," *Environmental Degradation of Engineering Materials in Hydrogen: Proceedings of Conference on Environmental Degradation of Engineering Materials, Part II*, Sisson, Louthan, and McNitt, Eds., Virginia Polytechnic Institute and State University, Blacksburg, VA, 1981, pp. 383-392.
- [5] Meyn, D. A. and Brooks, E. J., "Microstructural Origin of Flutes and Their Use in Distinguishing Striationless Fatigue Cleavage from Stress-Corrosion Cracking in Titanium Alloys," *Fractography and Materials Science, ASTM STP 733*, L. N. Gilbertson and R. D. Zipp, Eds., American Society for Testing and Materials, Philadelphia, 1981, pp. 5-31.
- [6] Boyer, R. R. and Barta, E. R., "High Strength Titanium Castings," *Report BMT-SR-7790*, Boeing Materials Technology Div., Renton, WA, Jan. 31, 1990.
- [7] Diegle, R. B. and Boyd, W. K., "The Role of Film Rupture during Slow Strain-Rate Stress Corrosion Cracking Testing," *Stress Corrosion Cracking: The Slow Strain-Rate Technique, STP 665*, G. M. Ugiansky and J. H. Payer, Eds., American Society for Testing and Materials, Philadelphia, 1979, pp. 26-46.
- [8] Gerberich, W. W., "The Micromechanics and Kinetics of Environmentally Induced Fractures," *Fracture Mechanics: Microstructure and Micromechanisms*, Nair, Tien, Bates, and Buck, Eds., ASM International, 1989, pp. 201-228.
- [9] Birnbaum, H. K., Private communication, Feb. 19, 1992 (see also: Grossbeck, M. L., Birnbaum, H. K., "Low Temperature Hydrogen Embrittlement in Niobium," *Technical Report to Office of Naval Research*, June 1975, Contract N00014-67-A-0305-0020 (M. L. Grossbeck, Ph.D. thesis, 1975, University of Illinois at Urbana-Champaign).
- [10] Costa, J. E., Banerjee, D., and Williams, J. C., "The Effect of Hydrogen on Microstructure and Properties of Ti-10V-2Fe-3Al," *Titanium—Science and Technology*, Lütjering, Zwicker, and Bunk, Eds., Deutsche Gesellschaft für Metallkunde e.V., Oberursel, Germany, 1985, pp. 2479-86.
- [11] Meyn, D. A. and Bayles R. A., "Role of Hydrogen-Assisted Mechanisms in Sustained Load Cracking and Stress Corrosion Cracking of Ti Alloys," *Hydrogen and Materials—4th Conference*, Chen and Azou, Eds., HYMAT-Institut Supérieur des Matériaux et de la Construction Mécanique, Saint Ouen, France, 1989, pp. 455-462.

**Industrial Applications of Slow Strain  
Rate Testing to Evaluate Environmentally  
Induced Cracking**

## Case Histories Using the Slow Strain Rate Test

---

**REFERENCE:** Baumert, K. L. and Watkins, W. R., Jr., "Case Histories Using the Slow Strain Rate Test," *Slow Strain Rate Testing for the Evaluation of Environmentally Induced Cracking: Research and Engineering Applications, ASTM STP 1210*, R. D. Kane, Ed., American Society for Testing and Materials, Philadelphia, 1993, pp. 173–180.

**ABSTRACT:** The slow strain rate test (SSRT) has been used at Air Products and Chemicals for a number of different environments. It was used to estimate the propensity of various amines to stress crack storage tanks; it was used to determine if existing equipment could be used in amine manufacture. Several tests were conducted to duplicate conditions that produced cracking in process equipment. The results of some tests were inconclusive.

**KEYWORDS:** slow strain rate test (SSRT), amines/stress corrosion cracking, mercury/stress corrosion cracking, chloride/stress corrosion cracking, caustic/stress corrosion cracking

The slow strain rate test (SSRT) was first used in the 1960s although it was not widely used until recently [1]. Its original intent was to be an improvement on existing laboratory techniques for determining the susceptibility of alloys to stress corrosion cracking (SCC). One of its most notable features is the speed in which test results can be acquired. Test results can be achieved in a matter of days versus weeks, months, and, in some cases, never for static stress specimens. This is because there is a definite end to the SSRT when the specimen fractures while there is always uncertainty in U-bend tests when the experiment is terminated after a reasonable period of time. The nagging question is: Would cracking have occurred if the test were run one day longer?

In recent years, the SSRT has become more widely used and accepted. Many companies [2] use this test to screen materials for processes especially if existing equipment is proposed for the process. Some organizations consider this test to be a standard for SCC susceptibility. It has been found that results from the SSRT sometimes differ from those produced by other techniques [2]. In some cases, the SSRT does not produce cracking when it is known to have occurred in the field.

To address this issue, the Materials Technology Institute (MTI) commissioned a study to determine why anomalous results sometimes occur with SSRT. Their results [3] indicate one important variable cannot be overlooked; that is, the potential of the specimen during the test. This should be monitored during the test and compared to the anticipated potential of the material in service. If it is not known, a range of potentials can be used during the tests. With the critical potential known, an effort can be made to keep a given alloy at a safe potential in an actual piece of equipment.

This paper reports several case histories of SSRTs conducted to qualify existing equipment for a new process. An attempt was also made to use the SSRT method to determine

---

<sup>1</sup> Senior Engineering Associate-Materials, Air Products and Chemicals, Inc. and <sup>2</sup> lead research engineer, Air Products and Chemicals, Inc., Allentown, PA 18195-1501.

conditions that resulted in cracking in some existing equipment. Finally, the test was used to determine if existing products or contaminants could produce cracking in carbon steel equipment.

## Experimental Procedure

### Materials

Carbon steel plate, ASTM A516-Gr70 was welded to itself and used for testing in amines. Type 304 and 316 Stainless Steel specimens, ASTM A240, were taken from annealed and cold-worked plate. Alloy 2205 and Nitronic 50® samples were machined from as-received plate.

### Specimens

Sample blanks were machined to 0.250-in. (0.635 cm). A 1-in. (2.54 cm) gage length by 0.150 ± 0.001-in. (0.381 cm) diameter was machined from the blank. The carbon steel specimens contained a weld in the gage length orientated perpendicular to the axis of the specimen.

### Alkyl Amines/Carbon Steel

Approximately seven years ago, an effort was made to determine if alkyl amines would stress crack carbon steel. Since some of the products produced by Air Products and Chemicals were similar to ammonia, there was a question about the safety of carbon steel storage tanks. The products in question were monomethylamine (MMA), dimethylamine (DMA), trimethylamine (TMA), monoethylamine (MEA), and monoisopropylamine (MIPA).

The first set of tests were carried out in liquid monomethylamine, in the presence of both oxygen and nitrogen. The partial pressure of air present during the test was not controlled but was probably in the vicinity of 1 atmosphere. Temperature was held at 120°F (49°C) which was the highest we would anticipate during storage. The test chamber was first purged and filled with nitrogen or zero grade air. Test results, Table 1, indicated no tendency towards SCC with monomethylamine on ASTM A516 Gr70 steel. Similar tests were conducted on carbon steel using dimethylamine and trimethylamine. Table 2 gives the results of these tests. These higher amines showed no tendency to stress crack A516-70 in an air or an inert environment.

TABLE 1—SSRT in monomethylamine.

Environment <sup>a</sup>	Fracture Time	Max Load, lb (N)
Blank - Zero Air <sup>b</sup>	18 h 15 min	1530 (6805)
	17 h 29 min	1405 (6250)
MMA + N <sub>2</sub>	20 h 45 min	1466 (6520)
	18 h 40 min	1495 (6649)
MMA + O <sub>2</sub>	20 h 23 min	1667 (7415)
	19 h 28 min	1438 (6396)

<sup>a</sup> Material ASTM A516 Gr70  
 Extension Rate  $2.8 \times 10^{-6} \text{ s}^{-1}$   
 Temperature 120°F (49°C)  
 Pressure 100 psi (689 KPa)

<sup>b</sup> CO<sub>2</sub> scrubbed from air.

TABLE 2—SSRT in dimethylamine and triethylamine.

Environment <sup>a</sup>	Time Fracture	Max Load, lb (N)
Blank - Zero Air <sup>b</sup>	18 h 15 min	1530 (6805)
	17 h 29 min	1405 (6249)
DMA + N <sub>2</sub>	17 h 49 min	1452 (6458)
	23 h 17 min	1771 (7877)
DMA + O <sub>2</sub>	21 h 10 min	1514 (6734)
	22 h 56 min	1567 (6970)
	18 h 15 min	1530 (6805)
Blank Zero Air <sup>b</sup>	17 h 29 min	1405 (6249)
	29 h 29 min	1771 (7877)
TMA + N <sub>2</sub>	18 h 55 min	1545 (6872)
	18 h 34 min	1732 (7704)
<sup>a</sup> Material	ASTM A516 Gr70	
Extension Rate	$2.8 \times 10^{-6} \text{ s}^{-1}$	
Temperature	120°F (49°C)	
Pressure	15 psi (1 bar)	
<sup>b</sup> CO <sub>2</sub> scrubbed from air.		

The final set of tests were conducted in monoethylamine and monoisopropylamine. Table 3 gives the results of the SSRTs. There was one disparity in that a test in monoisopropylamine plus air took approximately twice as long to fracture as the other tests. The reduction in area, however, was similar to the other tests.

The positive results of these tests increased our level of confidence in the safety of storing and shipping these chemicals in carbon steel.

### Polyamines/Existing Plant Materials

In the laboratory a process was developed for the manufacture of polyamines. Part of the development program involved corrosion testing to determine suitable materials of con-

TABLE 3—SSRTs in monoethylamine and monoisopropylamine.

Environment <sup>*</sup>	Time Fracture	R.A., %
Blank-Air	18 h 15 min	50.7
ER = $2.8 \times 10^{-6} \text{ s}^{-1}$		
MEA-no oxygen	22 h 01 min	50.3
ER = $2.8 \times 10^{-6} \text{ s}^{-1}$		
MEA-air added	19 h 24 min	51.1
ER = $2.8 \times 10^{-6} \text{ s}^{-1}$		
MEA-air added	Not recorded	48.9
ER = $1.4 \times 10^{-6} \text{ s}^{-1}$		
MIPA-no oxygen	19 h 31 min	49.6
ER = $2.8 \times 10^{-6} \text{ s}^{-1}$		
MIPA-air added	18 h 19 min	48.9
ER = $2.8 \times 10^{-6} \text{ s}^{-1}$		
MIPA-air added	39 h 16 min	50.7
ER = $1.4 \times 10^{-6} \text{ s}^{-1}$		
<sup>*</sup> Material	ASTM A516 Gr70	
Extension Rate	$2.8 \text{ and } 1.4 \times 10^{-6} \text{ s}^{-1}$	
Temperature	120°F (49°C)	
Pressure	cylinder pressure	

struction for a commercial plant. The two concerns were general corrosion and SCC, both of which would occur in the various chemicals used in the process.

Immersion tests were conducted on carbon and stainless steel coupons and U-bend specimens. Both types of coupons were exposed in a pilot plant also. A series of SSRTs was also conducted on carbon steel in the various precursor chemicals.

SSRT results indicated that carbon steel would stress crack in several streams at temperatures of about 440°F (227°C). Testing also revealed that incipient cracking occurred at about 420°F (216°C). Using these results along with the general corrosion data, minor modifications were made to an existing plant to avoid SCC and minimize the effects of general corrosion.

### Chloride/Stainless Steel

It has been reported by several investigators [2] that some SSRT results have produced anomalous behavior. Specifically, chloride cracking of stainless steel was not correctly predicted by slow strain rate testing. Since the SSRT was becoming widely used and accepted, it was important to understand why specific tests did not predict cracking in stainless steel when it was known to occur in both the field and also with U-bend test coupons.

A proposal was made to Materials Technology Institute (MTI) to fund a project which would study the SSRT method and attempt to explain the anomalous results. Several laboratory tests were conducted to support the need for the MTI project. Tests were conducted on annealed Type 304 stainless steel in 15% NaCl at 210°F (99°C). The three tests, Table 4, did not produce cracking even though parallel tests with U-bends did produce cracking.

The solution for both tests was made up in a common container and then divided so it was not a variable. Apparently the potential of the U-bend was different from that in the SSRT. Perhaps this was caused by a different amount of dissolved oxygen in the two solutions.

### Caustic/Stainless Steel

After extensive corrosion testing, Nitronic 50 was chosen as a material of construction for one alkyl amines plant tower. Caustic additions were metered into the feed so that acidic compound buildup could be controlled in the tower. After operating in this mode for a period of time, a process upset resulted in caustic cracking of the vessel. It was important to understand the conditions that lead up to the failure so that it would not be repeated.

To help understand the process conditions better, slow strain rate tests were initiated in an attempt to define the caustic concentration needed to crack Nitronic 50. Table 5 lists the

TABLE 4—SSRT annealed 304SS in 15% NaCl.

	Test			
	Blank	#1	#2	#3
Time to Failure	163 h 42 min	132 h 18 min	129 h 04 min	132 h 26 min
% Elongation	49.6	41.5	41.3	40.9
% Reduction in Area	56.7	55.0	54.4	55.7
Temperature	70°F (21°C)	210°F (99°C)	210°F (99°C)	210°F (99°C)
Atmosphere	Air	Air	Air	Air
Pressure	1 atm (1 bar)	1 atm (1 bar)	100 psi (689 kPa)	100 psi (689 kPa)
Extension Rate	$1.14 \times 10^{-6} \text{ s}^{-1}$			

TABLE 5—*Slow strain rate testing in caustic solutions<sup>a</sup>.*

Test No.	Alloy	NaOH, %	Ext. Rate	Fracture Time	R. A., %	Results
1	Nitronic 5	1	2.8 E-6 s <sup>-1</sup>	30 h 25 min	...	No cracking
2	Nitronic 50	10	2.8 E-6 s <sup>-1</sup>	...	...	No cracking
3	316 (.04C)	10	2.8 E-6 s <sup>-1</sup>	...	59.3	Ductile with side cracks
4	316 (.04C)	15	2.8 E-6 s <sup>-1</sup>	16 h 21 min	59.3	Ductile with side cracks
5	316 (.04C)	20	2.8 E-6 s <sup>-1</sup>	...	55.0	Ductile with side cracks
6	Nitronic 50	20	2.8 E-6 s <sup>-1</sup>	28 h 13 min	55.0	Ductile with side cracks
7	Nitronic 50	25	2.8 E-6 s <sup>-1</sup>	27 h 28 min	56.7	Ductile with side cracks
8	316 (.04C)	25	1.4 E-6 s <sup>-1</sup>	...	51.3	Ductile with side cracks
9	2205	20	2.8 E-6 s <sup>-1</sup>	Reactor leaks—Test aborted	...	
10	316 (.04C)	20	2.8 E-6 s <sup>-1</sup>	6 h 03 min	13.0	IG cracking <sup>b</sup>
11	2205	20	2.8 E-6 s <sup>-1</sup>	29 h 56 min	...	Ductile with side cracks
Blank	316 (.04C) at 70°F (21°C)	in air	2.8 E-6 s <sup>-1</sup>	41 h 32 min	75.7	...

<sup>a</sup> Temperature 350°F (177°C)  
 Pressure 350 psi (2.41 MPa)  
 Atmosphere Nitrogen  
 Solution Reagent NaOH with 100 ppm Na<sub>2</sub>SO<sub>3</sub> added  
 Specimen Gage Length—1.0 in. (2.54 × 10<sup>-2</sup> m) Diameter—0.150 in. (3.81 × 10<sup>-3</sup> m)

<sup>b</sup> Reactor leaks causing concentration of solution to unknown level.

tests that were conducted on various alloys. Since Nitronic 50 did not crack in conditions that were thought to be severe, Type 316 was exposed to the same conditions. No cracking was observed on Type 316 in 20% NaOH at 350°F (177°C). Testing then reverted back to the Nitronic materials; however, it did not crack in 25% caustic at 350°F (177°C). The same held true for alloy 2205 when it was exposed to 20% NaOH at 350°F (177°C). The only cracking occurred when an upset in the test resulted in Type 316 being exposed to concentrated caustic.

### Mercury/Stainless Steel

Equipment used to liquify natural gas must operate at temperatures to about -260°F (-162°C). The standard material of construction is aluminum or stainless steel, both of which remain ductile at the low temperatures.

A known contaminant in some natural gas sources is mercury. At cryogenic temperatures this does not present a corrosion problem to aluminum or stainless steel because mercury is a solid. However, it is well-known that mercury will stress crack aluminum alloys at room temperature under certain conditions. There was some question as to what effect mercury would have on stainless steel at room temperature.

Table 6 gives the results of a series of slow strain rate tests on Type 304 stainless steel in

TABLE 6—*Slow strain rate testing in Mercury*<sup>a</sup>.

Environment	Condition	Ult. Strength, ksi (MPa)	Elong., %	R.A., %	Failure Time, h	Failure Mode
Air	Cold-Worked <sup>1</sup>	114 (786)	34	56	32	Ductile
Hg	Cold-Worked <sup>1</sup>	109 (752)	29	24	28	Brittle
Hg <sup>h</sup>	Lab Annealed <sup>1</sup>	88 (606)	72	64	75	Ductile
Hg	Lab Annealed <sup>1</sup>	95 (655)	63	35	60	Brittle
Air	Fac. Annealed <sup>2</sup>	114 (786)	80	56	76	Ductile
Hg	Fac. Annealed <sup>2</sup>	101 (696)	78	30	74	Brittle
Hg	Cold-Worked <sup>3</sup>	112 (772)	58	19	60	Brittle

<sup>a</sup> Temperature

Ambient

Extension Rate  $2.8 \times 10^{-6} \text{ s}^{-1}$ <sup>b</sup> Since this test resulted in a completely ductile failure, it was used for comparison purposes as an "in-air" test.<sup>1</sup> Heat #D642<sup>2</sup> Heat #D799<sup>3</sup> Heat #D711

mercury. All tests were conducted at a strain rate of  $2.8 \times 10^{-6} \text{ s}^{-1}$ . Load versus time was continuously recorded on an x-y recorder. All "in air" tests were performed by slowly purging compressed air through the test chamber. Mercury tests were performed in an equivalent environment using triple distilled mercury in a polyethylene retaining cup attached to the specimen. The entire specimen gage length was exposed to mercury.

Up to the point of necking, the mechanical properties of Type 304 stainless steel were not adversely affected by mercury. Mercury embrittles Type 304 stainless steel once necking has been initiated. The resultant fracture was primarily brittle and was characterized by intergranular and transgranular cracking. The results indicated that Type 304SS could safely be used in a mercury environment. Under normal conditions the equipment would not be in a stress state where necking down and failure was imminent.

## Discussion

Testing was conducted in two mediums; namely, aqueous and nonaqueous using carbon and stainless steel materials. Conditions for the nonaqueous tests should have closely duplicated field conditions inasmuch as the primary variable was temperature. Another test parameter, namely oxygen content of the fluid was generally controlled during the tests. The oxygen content in nonaqueous solutions is not expected to alter the potential of the specimen appreciably like it could in an aqueous solution.

For the amines, cracking of carbon steel could possibly occur above 440°F (227°C) in polyamines. The process was designed such that the temperature was avoided and stress cracking of carbon steel components has not occurred in plant components to date. Likewise, no stress corrosion was ever reported for the other amines that were tested.

The test results of stainless steel in mercury showed that cracking would occur only when the specimen was severely deformed. From a practical standpoint, stainless equipment in this state of deformation has already failed and any embrittlement would be incidental.

The tests in aqueous solutions using stainless steel specimens are a different matter as potential comes into play. The chloride/stainless steel test was done to provide data in support of a larger test program. This program was conducted by MTI and showed that potential control was important in aqueous solutions. Obviously, the free corrosion potential of the SSRT was different from that of the U-bends. A somewhat different oxygen content could account for this.

The test results of the stainless steel in caustic environments were inconclusive. Tests were conducted in conditions where cracking had been reported previously. Likewise, it was felt that conditions in the tower were also duplicated, yet no cracking was produced. A likely reason for this difference could be the potential of the test specimens versus that in the tower. One variable that could affect this is the oxygen content of the different systems.

## Conclusions

The SSRT has been used at Air Products and Chemicals in various different ways. It was employed as a tool to design a polyamines process around existing equipment. It was used to assess the propensity of alkyl amines to stress crack carbon steel containment vessels. The results of tests where stainless steel was exposed to caustic and chlorides were inconclusive. Finally, tests showed that mercury did not stress crack stainless steel unless it is severely plastically deformed.

**References**

- [1] Parkins, R. N., "Development of Strain Rate Testing and Its Implications," *Stress Corrosion Cracking: The Slow Strain Rate Technique*, ASTM STP 665. G. M. Ugiansky and J. H. Payer, Eds., American Society for Testing and Materials, Philadelphia, 1979.
- [2] The Materials Technology Institute, Technical Advisory Committee Meeting, Clearwater Beach, FL, February 1988.
- [3] Materials Technology Institute Project No. 61, Draft, Limitations of the Slow Strain Test for Stress Corrosion Cracking Testing, October 1990.

R. D. Kane,<sup>1</sup> D. Wu,<sup>1</sup> and S. M. Wilhelm<sup>1</sup>

# Use of Slow Strain Rate Tests to Evaluate the Embrittlement of Aluminum and Stainless Alloys in Process Environments Containing Mercury

---

**REFERENCE:** Kane, R. D., Wu, D., and Wilhelm, S. M., "Use of Slow Strain Rate Tests to Evaluate the Embrittlement of Aluminum and Stainless Alloys in Process Environments Containing Mercury," *Slow Strain Rate Testing for the Evaluation of Environmentally Induced Cracking: Research and Engineering Applications*, ASTM STP 1210, R. D. Kane, Ed., American Society for Testing and Materials, Philadelphia, 1993, pp. 181–192.

**ABSTRACT:** As a process contaminant, mercury is a significant problem due to its ability to induce liquid metal attack (LMA) and embrittlement (LME) in some alloys of construction. Aluminum alloys are particularly susceptible to LME. Several test methods (i.e., constant load tensile tests, fracture mechanics crack growth tests, and slow strain rate tests) were used to evaluate LME in aluminum alloys along with AISI 304 stainless steel. Additionally, the effect of various surface treatments on LME of aluminum alloys was also examined. This paper evaluates the effectiveness of the various testing techniques and results obtained in laboratory studies conducted in elemental mercury.

**KEYWORDS:** slow strain rate tests, embrittlement, aluminum alloys, mercury, liquid metal attack (LMA)

## Background

In circumstances where mercury (Hg) condenses in cryogenic gas processing equipment, exposure of the materials of construction to mercury can lead to equipment failures by mercury attack. The common source of mercury is its presence as a contaminant in natural gas feedstocks from several reservoirs around the world (see Table 1) [1]. As shown in Fig. 1, mercury is found to cause liquid metal embrittlement (LME) in several metallic systems; the most predominant systems from an engineering significance are aluminum alloys, copper, ferrous and stainless alloys which are common to gas processing equipment [2]. LME is one of four mechanisms of Hg-attack with the other three consisting of (1) amalgamation, (2) amalgam corrosion, and (3) galvanic corrosion [3]. LME is distinct from the other forms of Hg-attack in that it can produce rapid brittle fracture which can lead to catastrophic failure of these materials under some service conditions.

Many of the characteristics of LME are similar to other forms of environmentally induced cracking phenomena in metals and alloys such as hydrogen embrittlement cracking and stress corrosion cracking (SCC). Chemical, electrochemical, and mechanical processes can result in the initiation of a crack (or cracks) of subcritical dimensions. These can subsequently propagate until they reach a critical size and thereby cause fracture of the material. In LME as in SCC, breakdown of the protective surface film (typically oxide) can be a critical stage

---

<sup>1</sup> Cortest Laboratories, Inc., Houston, TX 77269.

TABLE 1—Elemental mercury concentrations in natural gas.

Location	$\mu\text{g}/\text{Nm}^3$
Algeria (wellhead)	50 - 80
Algeria (pipeline entrance)	0.1 - 89
Algeria (Skikda plant inlet)	0.001 - 0.65
Groningen (wellhead)	180
Groningen (to pipeline)	12
North Germany (wellhead)	15 - 450
South Germany (wellhead)	<0.1 - 0.3
South America	69 - 119
Far East (Pakistan)	3 - 20
Far East	58 - 193
Far East	0.02 - 0.16
Africa (Angola)	0.3 - 130
Middle East (Iran)	1 - 9
Eastern U.S. Pipeline	0.019 - 0.44
Midwestern U.S. Pipeline	0.001 - 0.10
North America	0.005 - 0.040
Sumatra, Indonesia	200 - 300

in this process. Electrochemical impedance data have shown that the surface oxide of untreated Al-alloy 5083-O has low electrical resistance with mercury. By comparison, anodized surfaces show both high resistance (600 mV DC potential) and high capacitance [4]. Experiments have shown that under certain circumstances, these surface films can be quite protective in environments containing mercury from the standpoint of Hg-attack.

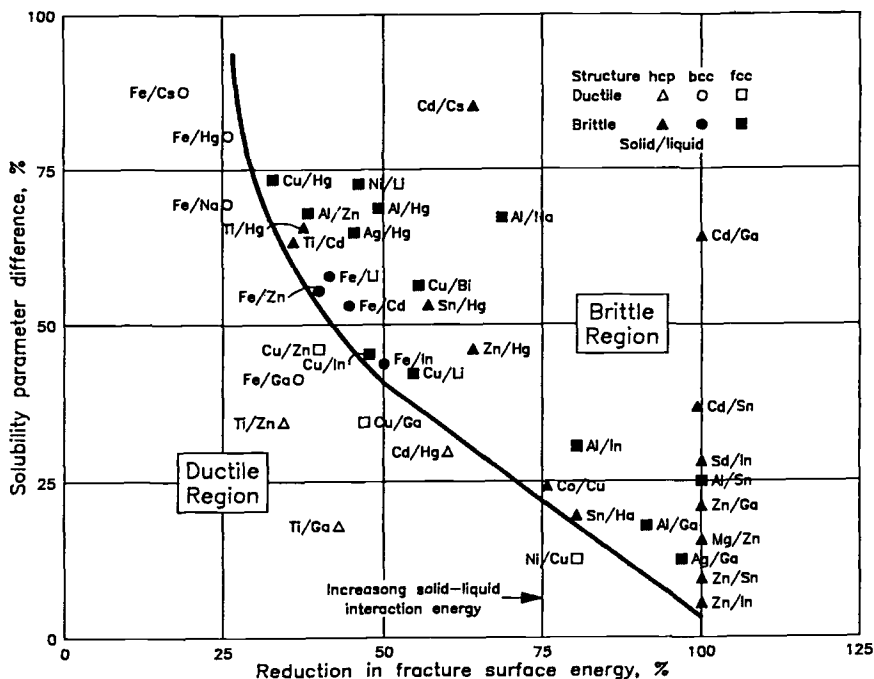


FIG. 1—Embrittlement and nonembrittlement couples in solid/liquid metal systems.

It is also known that LME is primarily driven by physical dissolution of the susceptible alloy in mercury rather than by an oxidation/reduction process as is common for SCC. The rate and preference of dissolution can be highly specific to grain boundaries and particular microstructures. Aluminum welds are preferentially attacked by mercury because of the reduced protective properties of surface oxides in the area of the weld and because of the higher degree of susceptibility of the weld microstructure.

### Technical Approach

In the present study, mercury exposure tests were conducted on materials typically used in gas processing applications. The mercury exposure tests consisted of the following:

- (1) Static load direct tension tests.
- (2) Fracture mechanics crack growth tests.
- (3) Slow strain rate (SSR) tests.

Initially, all three test methods were compared to reveal the extent of LME using the various testing techniques. Following this investigation, the SSR tests were used to evaluate several environmental and metallurgical parameters to show their effects on LME.

### Experimental Procedure

#### Materials and Specimens

Al-alloy 5083-O (UNS A95083) plate and 3003-O (UNS A93003) wrought bar stock were used in this program. For comparative purposes, AISI 304 (UNS S30400) wrought bar stock was also included in the study. Specimens of these materials were prepared in both wrought form and welded form. Nominal compositions and mechanical properties for the aforementioned materials are given in Table 2.

The direct tension and fracture mechanics specimens are shown in Fig. 2*a* and *b*. The direct tension specimens were of round cross-section with a gage section of 25.4-mm-long by 6.4-mm-diameter. The tensile axis was parallel to the rolling direction. In the case of welded specimens, the specimen was machined perpendicular to the welding direction so as to contain base metal, heat affected zone (HAZ), and weld metal.

TABLE 2—Nominal chemical composition and tensile properties for alloys tested.

	Composition						
	Mn	Mg	Cu	Al	Cr	Ni	Fe
Al-Alloy 5083-O	0.7	4.4	0.10*	Bal	0.15	—	—
Al-Alloy 3003-O	1.2	—	0.13	Bal	—	—	—
AISI 304	2.0*	—	—	—	19	10	Bal

\* Maximum.

	Tensile Properties			
	Y.S. (MPa)	UTS (MPa)	Elong (%)	RA (%)
Al-Alloy 3083-O	175	312	20	11
Al-Alloy 3003-O	46	114	24	63
AISI 304	310	581	45	63

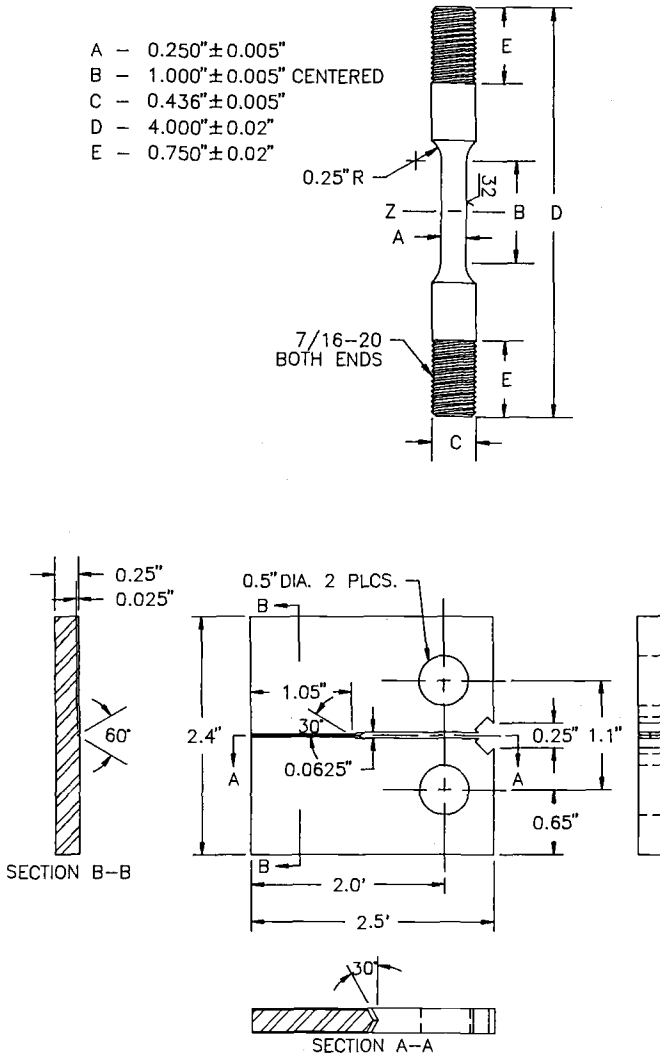


FIG. 2—(a) Direct tension specimen. (b) Fracture mechanics crack growth specimen.

The SSR specimens were also of round cross-section with a 25.4-mm-long by either 6.4-mm- or 3.8-mm-diameter depending on the starting size of the material. Orientations were the same as defined for the direct tension specimens. These specimens were used to evaluate LME in wrought and welded alloy 5083, wrought and base metal alloy 3003, and wrought AISI 304 stainless steel.

Fracture mechanics specimens were prepared per ASTM E 399, Test Method for Plane-Strain Fracture Toughness of Metallic Materials, in the TL orientation with a 3.8 ligament thickness. Side grooves with a depth of 0.63 mm were used to promote planar crack growth. These specimens were precracked by fatigue using 9 Hz and a 1780 N (400 lb) peak load prior to testing.

### *Test Environment*

In all environmental tests, the media used were triple distilled mercury. In the case of the tension specimens, the mercury was held in contact with the gage section of the specimens using a section of plastic tubing clamped to the shoulder of the specimens. The mercury was loaded into the tubing by use of a syringe.

For the crack growth tests the mercury was placed directly in the notch area of the specimen at the initiation point of the fatigue pre-crack. To ensure adequate wetting of the crack with mercury, a surface activating agent consisting of a weak solution of  $\text{HNO}_3$  was used [5]. SSR tests were also conducted in a gaseous environment above a liquid pool of mercury using alloy C-276 autoclaves fixtured to conduct SSR tests. These environments were simulations of plant environments containing mercury vapor with  $\text{H}_2$  and hydrocarbons.

### *Static Load Direct Tension Tests*

These tests were conducted using proof ring fixtures per ASTM G 49, Recommended Practice for Preparation and Use of Direct Tension Stress Corrosion Test Specimens. Specimens were tested at constant load for periods up to 30 days. Time-to-failure was monitored using electrical timers which were deactivated when the proof ring relaxed upon specimen failure.

### *Slow Strain Rate Tests*

SSR tests were conducted using an electrically driven tensile machine capable of producing a constant cross-head displacement. All tests were conducted at an initial strain rate of  $4 \times 10^{-6} \text{ s}^{-1}$ . Load on the specimen versus time was monitored using a strip chart recorder.

All of the SSR tests performed in mercury were conducted in duplicate with a corresponding single specimen tested in air. The test in air was used as a basis of comparison using specimen time-to-failure. Fractured specimens were then visually examined for brittle fracture and the ratio of time-to-failure ( $t_r$  Ratio = Hg test/Air test) was calculated.

### *Fracture Mechanics and Crack Growth Rate Tests*

These tests were conducted using the apparatus shown in Fig. 3. After applying the wetting solution and the mercury to the specimen, the specimen was placed in the test apparatus. The crack growth test was conducted per ASTM E 647, Test Method for Measurements of Fatigue Crack Growth Rates, using specimen compliance and crack tip opening displacement as measured using a clip gage on the specimens. An initial load of 800 N (180 lb) was placed on the specimen. This load was increased in increments of 222 N (50 lb) until crack growth was initiated. During crack growth, the load was kept constant using the dead weight loading arrangement shown in Fig. 3.

Similar tests were also conducted to determine the  $K_{\text{ILME}}$  versus temperature. In this case, the load was applied and increased in increments of 222 N (50 lb) until cracking was initiated. The load value at the onset of cracking was used to determine the  $K_{\text{ILME}}$  value (i.e., plane strain threshold fracture toughness for LME).

## **Results and Discussion**

### *Constant Load Tests*

As shown in Fig. 4, the threshold stress (in 720 h) for LME in welded alloy 5083 was approximately 10% of its tensile yield strength at room temperature. This is a very low

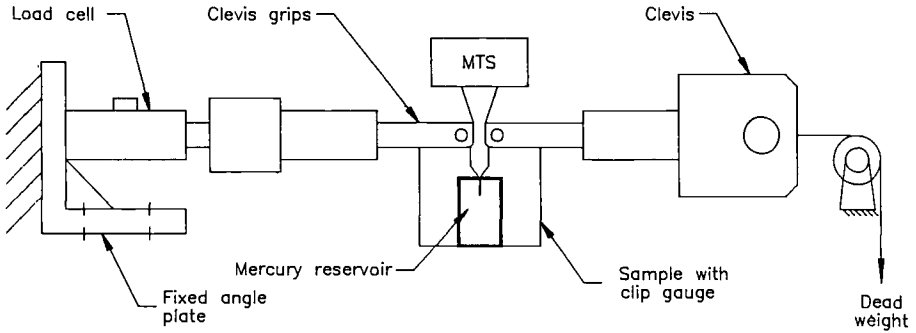


FIG. 3—Crack growth test apparatus.

value which indicates very high susceptibility to cracking. The nature of the cracking indicated several modes of attack. These included LME (both perpendicular and longitudinal to the applied load), general dissolution, intergranular attack, and pitting. Other alloys tested showed greater resistance to LME as a result of their higher threshold stress in mercury. AISI 304 stainless steel did not fail in the constant load tests indicating high LME resistance. Only one of two alloy 3003 specimens failed. The failure site was located at a weld defect. The other specimen went the entire 720 h without failure but exhibited deep pits in the weld, HAZ, and base metal.

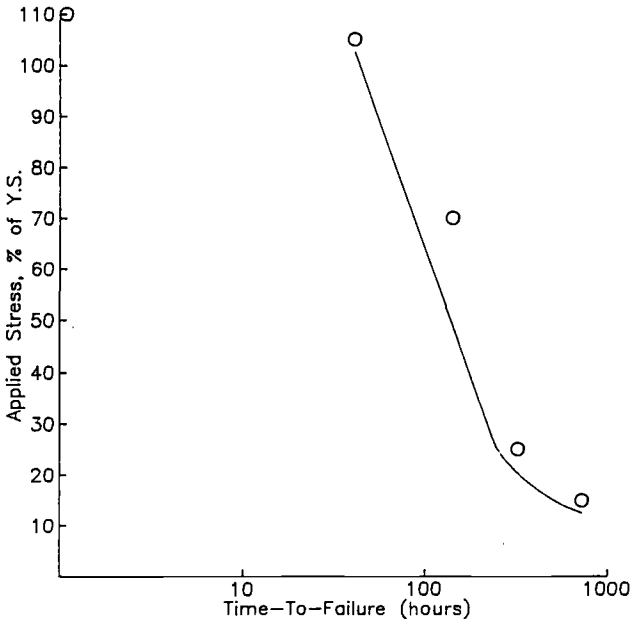


FIG. 4—Stress versus time-to-failure for constant load specimens of alloy 5083 in mercury at room temperature.

*Fracture Mechanics Tests*

Likewise, fracture mechanics tests conducted at room temperature for this alloy also showed threshold stress intensity values of between 5.5 to 8.8 MPa M<sup>1/2</sup> (5 to 8 ksi/in.) (see Fig. 5). This test method also shows very high susceptibility to LME in alloy 5083. As the temperature is reduced as shown in Fig. 6, the threshold stress intensity for LME increases to a point where below -72°C, no cracking is observed.

Under susceptible conditions, crack growth rates in alloy 5083 for LME in mercury were very rapid. As shown in Fig. 5, *da/dt* increase very rapidly with increasing stress intensity. It appears from the data in Fig. 4 that the threshold for LME may be slightly lower in welded material than in the wrought alloy. However, crack growth rates in the wrought material increase more rapidly than in the welded material. Therefore, it is probably difficult to say that one condition is actually more susceptible to cracking than the other.

*Slow Strain Rate Tests*

The results from several slow strain rate tests are given in Figs. 7 through 9. Respectively, these figures show (1) the general susceptibility to LME of various alloys, (2) the effect of temperature on cracking, and (3) the effect of liquid or gaseous mercury environments on cracking.

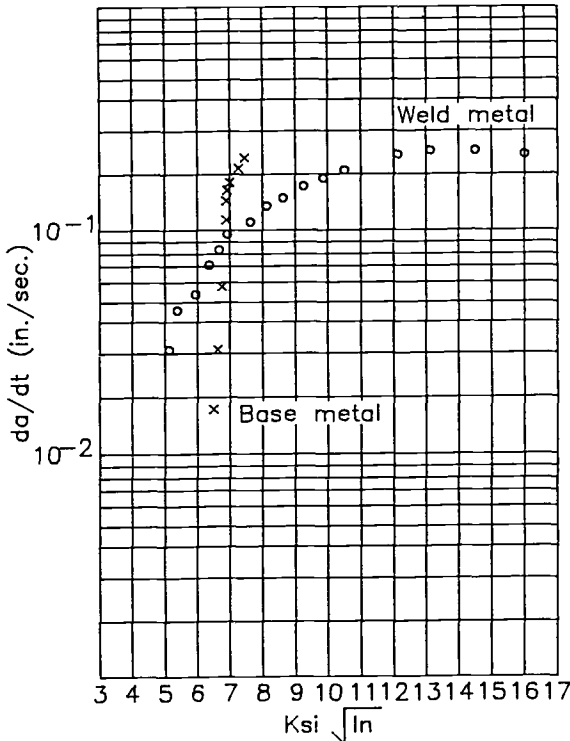


FIG. 5—Crack growth rate (*da/dt*) versus *K* value for welded and nonwelded alloy 5083.

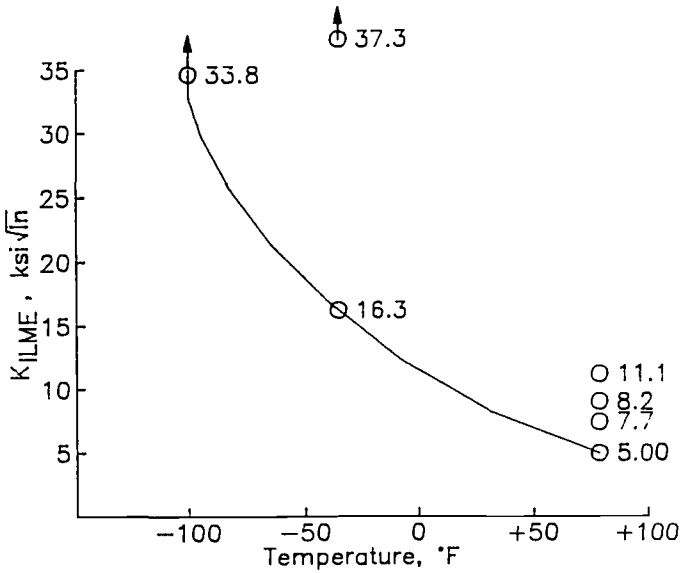


FIG. 6—Critical threshold stress intensity ( $K_{IL,ML}$ ) for wrought alloy 5083 versus test temperature.

As shown in Fig. 7, both wrought and welded alloy 5083 exhibit similar susceptibilities to LME. The level of LME susceptibility appears to be very high as manifested from the very low ratios of time-to-failure ( $t_f$  ratio < 0.20). The other materials show varying susceptibilities to LME.

Alloy 3003 had widely varying susceptibility depending on the conditions (i.e., wrought, vacuum brazed, or salt brazed) with  $t_f$  ratios of 0.48, 0.80, and 1.03, respectively. The nature of the attack on the alloy 3003 specimens which produced the widely varying  $t_f$  ratios was completely different than that found on the alloy 5083 SSR specimens. Very little evidence

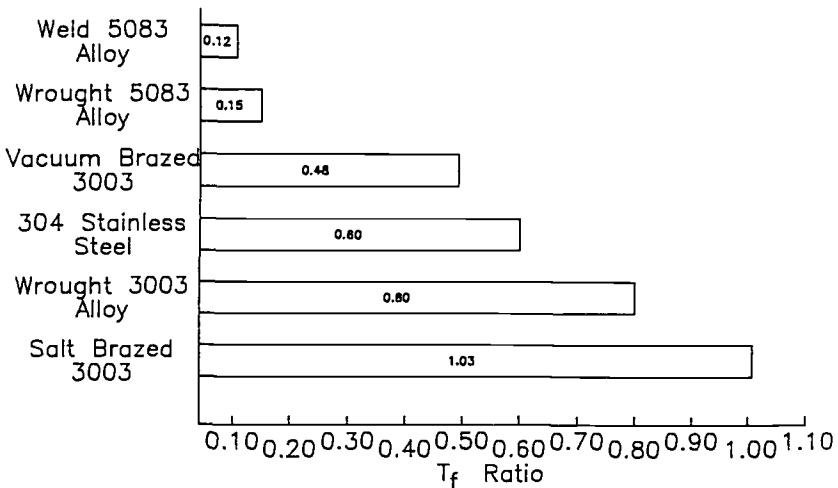


FIG. 7—SSR time-to-failure ratio for various alloys in mercury.

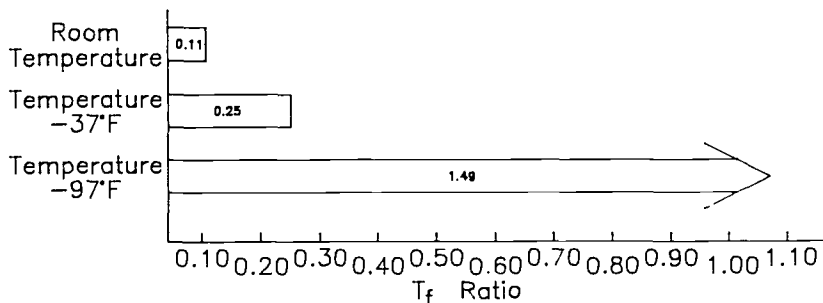


FIG. 8—Effect of temperature on  $t_f$  ratio in SSR test for alloy 5083.

of LME and only limited surface attack was found on the alloy 3003 specimens. This surface attack which consisted of a small amount of fissuring or fine cracking was located only in the highly cold-worked material in the necked region on the specimen immediately adjacent to the final fracture surface. The variation in these SSR tests was similar to the variability observed in the constant load tests which was related to localized attack with only little contribution from susceptibility to LME.

The AISI 304 showed an intermediate value of  $t_f$  ratio (0.60). This result was somewhat surprising since AISI 304 was not expected to exhibit cracking based on the constant load results. Metallographic examination revealed that SSR specimens of this material had small short cracking on the surface of the gage section which were limited to about 0.13 mm around the surface. Most likely, the imposition of the constant extension on the specimen resulted in cracks in the passive oxide layer on the surface of AISI 304 that did not occur in the constant load tests. Once this passive layer was damaged in the SSR tests, LME could proceed to a limited degree. Similar action could occur in service if AISI 304 stainless steel components are subject to plastic strain or surface wear which could damage the normally passive oxide layer on this material.

The effect of SSR test temperature is shown in Fig. 8. These tests show that LME in alloy 5082 is very temperature dependent. SSR tests conducted at room temperature and  $-38^\circ\text{C}$  with mercury revealed  $t_f$  ratios in the range of 0.11 and 0.25, respectively. Tests conducted at  $-72^\circ\text{C}$  showed a  $t_f$  ratio of greater than 1.0 indicating no evidence of LME under these

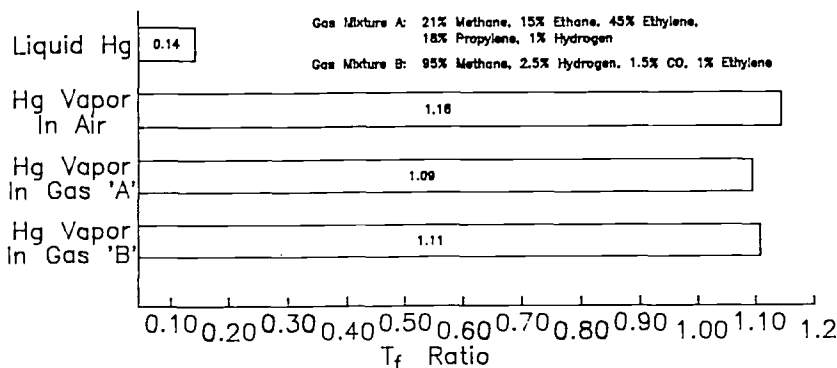


FIG. 9—Effect of mercury environment on  $t_f$  ratio in SSR test for alloy 5083.

conditions. These data show very similar trends to those obtained from the fracture mechanics tests that were previously discussed. At a temperature of  $-72^{\circ}\text{C}$ , threshold stress intensity values for alloy 5083 were  $37.2 \text{ MPa (m)}^{1/2}$  ( $33.8 \text{ ksi}\sqrt{\text{in.}}$ ) which is very close to the value determined in air at room temperature of  $48.0 \text{ MPa (m)}^{1/2}$  ( $43.6 \text{ ksi}\sqrt{\text{in.}}$ ). The lower value is probably the result of the lower test temperature and not due to LME. In the SSR tests, no surface activating (wetting) agent was needed. The application of the slow constant extension rate was sufficient to initiate cracking.

Finally, SSR tests were employed to assess the effect of varying environmental conditions on LME of alloy 5083. Specifically, four environments were evaluated: (1) liquid mercury, (2) mercury vapor in air, (3) mercury vapor in Gas Mixture 1 (21% methane, 15% ethane 45% ethylene, 18% propylene, 1% hydrogen), and (4) mercury vapor in Gas Mixture 2 (95% methane, 2.5% hydrogen, 1.5% carbon monoxide, and 1% ethylene). The two gas mixtures were selected as being representative of gas processing environments where mercury contamination is commonly involved. In Environment 1, the gage section of the specimen was directly exposed to liquid mercury. In Environments 2 through 4, the gage section of the SSR specimens were above the pool of mercury and only exposed to the gaseous environment with mercury vapors.

The results from the aforementioned SSR tests are given in Fig. 9. As can be seen in this figure, the only case where LME was observed in highly susceptible alloy 5083 was in the direct exposure to liquid mercury. These results are significant in terms of actual service because it reveals that only conditions of direct exposure to liquid mercury will result in cracking. This limits the areas of concern in processing equipment and consequently allows for a prioritization of required inspection. Typically, areas of greatest concern are those where mercury can pool or in crevices that can contain liquid mercury.

### Relevance of SSR Tests

As shown in this study, SSR testing can be of great value in the study of LME. Similar to studies of SCC relevant to other alloy/environment systems, LME from mercury exposure was found to produce reduction in time to failure of SSR test specimens in susceptible alloys. Similar results were found using this test method as were found in constant load tests and fracture mechanics tests.

Additionally, in some cases it was found that SSR testing was somewhat more aggressive than similarly tested specimens using constant load. AISI 304 stainless steels tested in liquid mercury is a good example for such behavior. In constant load tests, it was found that this material did not exhibit LME. In contrast, in the SSR test, AISI 304 stainless steel was found to show an intermediate degree of susceptibility to LME. This cracking was limited to the highly strained material in the necked region of the tension specimen. Such behavior in the SSR test can be an indication of potential susceptibility to cracking in (1) cold-worked materials, (2) wrought material that has been highly strained in service, or (3) under conditions of wear or abrasion where the passive layer has been disrupted.

SSR testing was also able to differentiate between two aluminum alloys with significantly different response to the liquid mercury environment. In the case of alloy 5083, the material exhibited both corrosive degradation and susceptibility to cracking. Consequently, it showed very limited cracking resistance (i.e., low  $t_f$  ratio) under conditions of an externally imposed constant extension rate. By comparison, alloy 3003 showed a somewhat inconsistent response to liquid mercury in the SSR test. It was very susceptible to localized corrosive attack with only limited susceptibility to cracking. Therefore, there was substantial scatter in both the constant load and SSR test data as a result of the localized corrosion behavior of this alloy in mercury.

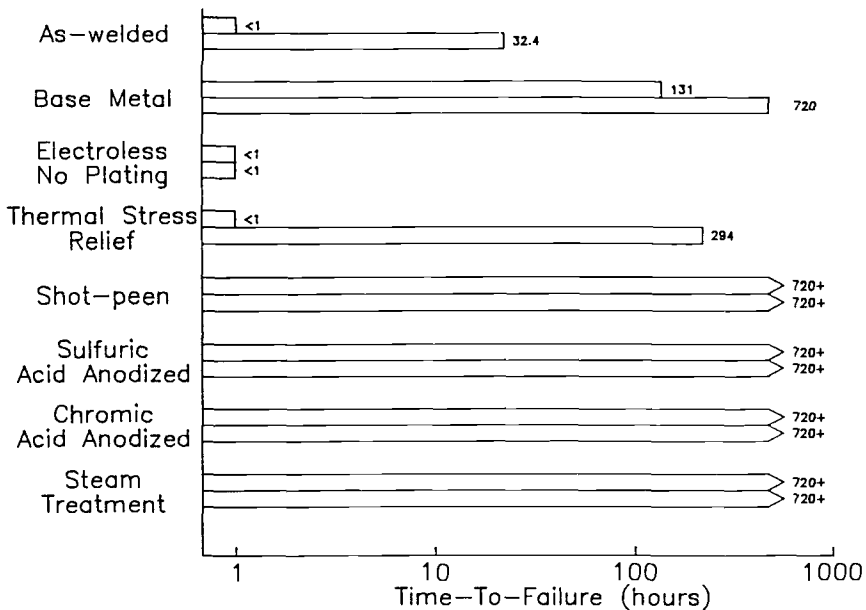


FIG. 10—Effectiveness of surface treatments on time-to-failure of alloy 5083 in liquid mercury at room temperature.

The comparison of the behavior between the two aluminum alloys and AISI 304 reveal the importance of physical examination of the test specimens. It is clear that a minor amount of cracking ( $\leq 0.13$  mm in the case of AISI 304) can substantially reduce the tensile performance of materials tested by the SSR technique. Therefore, post-test characterization of the nature of the corrosion and cracking greatly aids in the interpretation of the test results. Additionally, the post-test evaluation confirmed that the mode of Hg-attack in alloy 3003 was not LME, but actually a form of localized corrosion in the area of the weld.

Figure 10 shows the results of a study conducted on the effect of surface treatments on LME in alloy 5083 which was found to be very susceptible to cracking. These tests were conducted with the constant load test. As can be seen, some methods were very effective in protecting this material from LME under conditions of exposure to liquid mercury. It was decided not to use SSR test methods for this evaluation due to the high degree of plastic straining of the specimen that takes place in the test method. Under conditions of plastic strain, the beneficial effects of shot peening (i.e., compressive residual stresses on surface), electroless nickel, and thickening of the oxide layer by anodizing were considered to be of limited value. It was anticipated that the plastic strain in the SSR tests would produce cracking of these surface layers and allow penetration of mercury to the substrate.

## Conclusions

Based on the results of the research program described herein, the following conclusions were made:

- (1) Mercury attack was manifested in aluminum and stainless alloys in the form of general and localized corrosion and as brittle cracking (i.e., LME).
- (2) Both forms of attack can produce premature failures in stressed specimens.

(3) Al-alloy 5083 showed greatest susceptibility to LME of the alloys tested. This was confirmed by both constant load and SSR tests.

(4) Al-alloy 3003 exhibited failures and scattered results in stressed tests resulting from its susceptibility to localized corrosive degradation in liquid mercury. However, this alloy did not show susceptibility to LME in either constant load or SSR tests.

(5) AISI 304 stainless steel did not exhibit failures in constant load tests, but did show LME and reduced failure times in SSR tests. Cracking in this alloy was limited to the highly strained necked region in the SSR specimen.

(6) SSR tests and fracture mechanics tests showed similar trends in terms of temperature effects on LME. Both test methods revealed that at temperature of  $-72^{\circ}\text{C}$ , LME did not occur in alloy 5083.

(7) The SSR test was found to be a valuable tool in the examination of LME in aluminum and stainless alloys.

#### *Acknowledgments*

The authors of this paper would like to thank the contributions of Mr. Dale R. McIntyre (Saudi ARAMCO; formerly Cortest Laboratories, Inc.) in the project management and technical supervision of the experimental program. The creative and precise laboratory work of Mr. Felix Lopez and Mr. Keith Benoit of Cortest Laboratories greatly contributed to the quality of this study. In addition, the authors would like to acknowledge the support of Cain Chemical (currently Occidental Chemical) and E.I. DuPont de Nemours & Company.

#### **References**

- [1] Bodle, W. W. and Serauskas, R., "Considerations for Mercury in LNG Operations," Institute of Gas Technology, 6th International Conference on Liquefied Natural Gas, Kyoto, Japan, April 1980.
- [2] Kamdar, N. M., "Liquid Metal Embrittlement," *Metals Handbook*, 9th ed., Vol. 13: *Corrosion*, 1988, pp. 171–189.
- [3] Wilhelm, S. M., "The Effect of Elemental Mercury on Engineering Materials Used in Ammonia Plants," *Plant Operations Progress*, Vol. 1, No. 4, October 1991, pp. 189–193.
- [4] McIntyre, D. R. and Oldfield, J. W., "Environmental Attack of Ethylene Plant Alloys by Mercury," NACE, *Symposium Proceedings of Corrosion Prevention in the Process Industries*, Amsterdam, The Netherlands, November 1988, pp. 239–252.
- [5] Kapp, J. A. et al., "Crack Growth of Aluminum Alloys Tested in Liquid Hg," *Journal of Engineering Materials Technology*, Transactions ASME, Vol. 108, No. 1, 1986, pp. 37–43.

## Effect of Heat Treatment on Liquid Metal-Induced Cracking of Austenitic Alloys

---

**REFERENCE:** Krupowicz, J. J., "Effect of Heat Treatment on Liquid Metal-Induced Cracking of Austenitic Alloys," *Slow Strain Rate Testing for the Evaluation of Environmentally Induced Cracking: Research and Engineering Applications*, ASTM STP 1210, R. D. Kane, Ed., American Society for Testing and Materials, Philadelphia, 1993, pp. 193–201.

**ABSTRACT:** Slow strain rate tests were used to rank the liquid metal embrittlement (LME) susceptibility of Types 304 (UNS S30400), 304L (UNS S30403), 316 (UNS S31600), 316L (UNS S31603), and 321 (UNS S32100) stainless steel, as well as alloys 600 (UNS N06600) and 800 (UNS N08800). Testing revealed that LME susceptibility was influenced significantly by heat-treated condition. Sensitized materials were consistently more susceptible to cracking in liquid mercury at ambient conditions. Cracking was predominantly intergranular for the sensitized materials and was analogous to stress corrosion cracking in high temperature aqueous solutions. These results suggest that low-carbon or stabilized materials are inherently more resistant to LME and are preferable for applications in environments where mercury may exist.

**KEYWORDS:** environmental cracking, liquid metal embrittlement, stress corrosion cracking, mercury-induced cracking, stainless steels, nickel alloys, slow strain rate tests

Brittle fracture of structural materials is a concern in process streams where liquid metal contaminants exist in the feedstocks. Mercury-induced cracking of aluminum alloys and highly stressed mild steels is well-known [1,2]. More recently, mercury LME data on stainless steels [3–5] and nickel alloys [6–8] have become available. In none of the studies was any effort made to discriminate the effects of sensitizing heat treatments. Since interest has focused on replacement of various aluminum alloy process stream components with stainless steel, a study was undertaken to compare the mercury LME resistance of different stainless steels and nickel-base alloys in various heat-treated conditions. Heat treatments were used to simulate the heat affected zone (HAZ) in welded structures since such regions are typically susceptible to environmentally-assisted cracking.

### Experimental

Chemical compositions and mechanical properties of the materials used in this study are given in Tables 1 and 2, respectively. Stainless steels were obtained as bar stock in the solution-annealed and cold-finished condition; bar stock for alloys 600 and 800 was in the mill-annealed condition. Specimens were machined according to Fig. 1 with gage sections ground and polished to a final diameter of 2.54 mm. Sensitization heat treatments were performed by heating in vacuum to 650°C, holding for four hours, and water quenching. The gage sections of heat-treated specimens subsequently were repolished to remove thin oxide films.

---

<sup>1</sup> Engineering associate, Mobil Research and Development Corporation, Materials Engineering Section, Paulsboro, NJ 08066.

TABLE 1—Chemical compositions of alloys tested (percent by weight).

Alloy	C	Mn	P	S	Si	Fe	Cr	Ni	Cu	Mo	Ti	Al
Type 304 (Heat A033)	0.06	1.39	0.030	0.024	0.50	Bal.	18.58	8.30	0.31	...	...	...
Type 304L (Heat D343)	0.02	1.55	0.024	0.025	0.63	Bal.	18.31	9.26	0.46	0.36	...	...
Type 316 (Heat D744)	0.05	1.47	0.026	0.026	0.33	Bal.	16.28	11.17	0.22	2.84	...	...
Type 316L (Heat 321)	0.02	1.71	0.033	0.027	0.51	Bal.	17.25	12.90	...	2.05	...	...
Type 321 (Heat 886)	0.05	1.68	0.026	0.030	0.65	Bal.	17.29	10.34	0.25	0.30	0.59	...
Alloy 600 (Heat 752)	0.07	0.35	...	0.003	0.10	9.62	14.80	Bal.	0.40	...	...	...
Alloy 800 (Heat 727)	0.07	0.88	...	0.008	0.21	44.61	21.92	31.15	0.50	...	0.36	0.29

Acrylic/polyvinyl chloride test cells were used to immerse the specimen gage sections in the test fluids. Control tests were conducted in air or mineral oil. Pure (triple distilled) mercury was used for the LME tests. All tests were performed at room temperature (21°C) by uniaxially loading the specimens at a constant strain rate of  $5.0 \times 10^{-6} \text{ s}^{-1}$ . Load versus time (strain) was monitored continuously by *x-y* recorder during the tests. After testing, specimens were measured and examined by stereo (optical) and scanning electron microscopy.

## Results

Slow strain rate test results comparing as-received and heat-treated (sensitized) specimens are given in Table 3. Both as-received and sensitized Type 304 stainless steel specimens were tested in air for comparison. Resulting load/time (strain) curves were similar for both tests. Since heat-treating did not significantly change the time to failure or reduction in area for the Type 304 stainless steel tests, air tests for other heat-treated materials were deferred.

Time to failure and reduction in area values indicated that alloy 600, and, to a lesser extent, Types 304 and 304L stainless steel were embrittled significantly by mercury, both in the as-received and sensitized conditions. The load/time (displacement) curves were indis-

TABLE 2—Room temperature mechanical properties of materials tested.

Alloy	Condition	Yield Strength		Tensile Strength		Reduction in Area, %
		MPa	ksi	MPa	ksi	
Type 304	As-received	465	67.5	788	114.3	80.9
	Heat-Treated*	439	63.7	791	114.7	79.1
Type 304L	As-received	501	72.7	773	112.1	83.5
Type 316	As-received	364	52.8	649	94.1	79.7
Type 316L	As-received	590	85.5	703	102.0	77.5
Type 321	As-received	527	76.4	689	99.9	78.0
Alloy 600	As-received	282	40.9	643	93.3	71.6
Alloy 800	As-received	401	58.2	606	87.9	77.2

\* Heated to 650°C (1200°F), held for four hours, water-quenched.

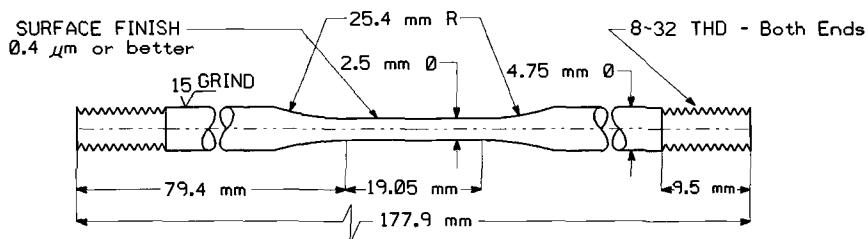


FIG. 1—Slow strain rate test specimen geometry.

tinguishable from the air (control) specimens up to the point of rupture, which always occurred after yielding. Mercury LME was less pronounced for the other materials tested.

*Type 304 Stainless Steel*

Reduction in area losses were greater than 50% for both the as-received (annealed and cold-finished) and sensitized Type 304 specimens. Although sensitized Type 304 did not exhibit a significantly lower reduction in area value compared to as-received material tested in mercury, time to failure was lower for the sensitized material. Macroscopic features, illustrated by low magnification scanning electron microscopy (Fig. 2), included a faceted, branched region of brittle fracture across approximately one half the specimen cross-section

TABLE 3—Slow strain rate test results.<sup>a</sup>

Alloy	Condition <sup>b</sup>	Environment	Time to Failure, h	Reduction in Area, %	Secondary (Surface) Cracking
Type 304	As-received	Air	36.2	80.9	N
		Hg	25.5	35.0	LC
	Heat-Treated	Air	38.2	79.1	N
		Hg	16.6	33.6	RC (Traces)
Type 304 L	As-received	Air	32.7	83.5	N
		Hg	28.4	49.4	RC (Traces)
	Heat-Treated	Hg	31.3	54.2	RC
		Air	37.4	79.7	N
Type 316	As-received	Hg	37.7	78.5	N
		Hg	36.1	71.8	N
Type 316 L	As-received	Air	23.2	77.5	N
		Hg	23.2	77.2	N
	Heat-Treated	Hg	23.5	75.9	N
		Air	25.5	78.0	N
Type 321	As-received	Hg	24.3	75.4	RC (Traces)
		Hg	21.6	69.6	RC
Alloy 600	As-received	Air	29.1	71.6	N
		Hg	24.0	58.2	LC/RC
	Heat-Treated	Hg	11.5	25.3	LC/RC
		Air	23.9	77.2	N
Alloy 800	As-received	Hg	26.4	70.9	N
		Hg	25.7	73.1	N

N = No Cracking, LC = Linear Cracking, RC = Random Cracking.

<sup>a</sup> Room temperature tests at  $5 \times 10^{-6} \text{ s}^{-1}$ .

<sup>b</sup> As-received specimens heat-treated by heating to 650°C (1200°F), holding for four hours, and water-quenching.

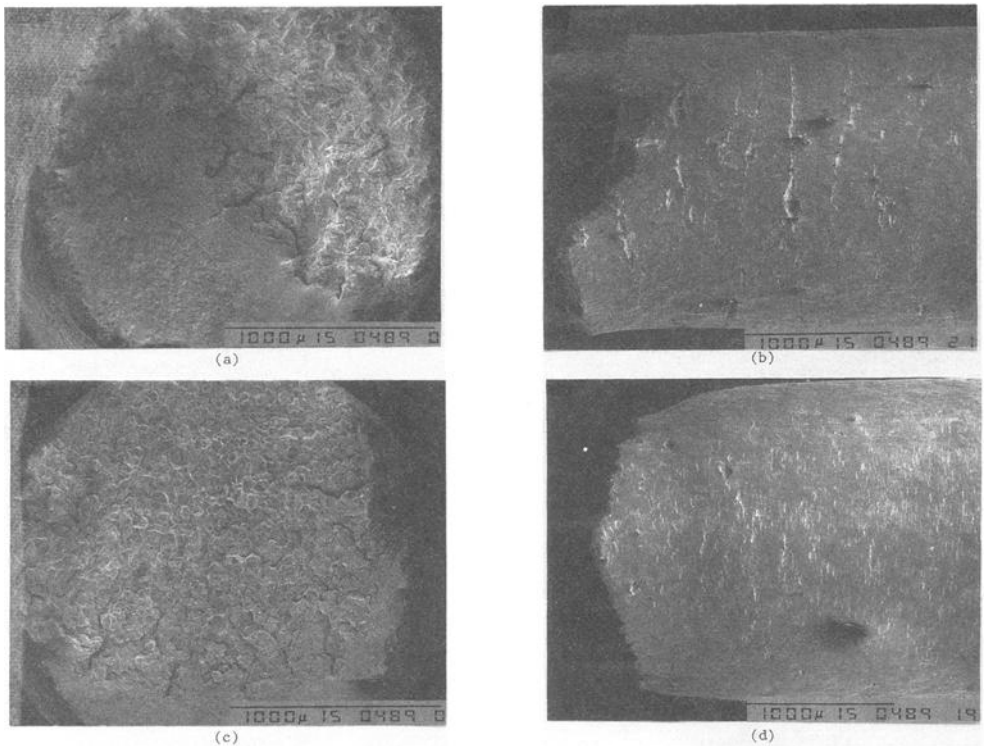


FIG. 2—Type 304 stainless steel SSRT specimen fracture surfaces and gage lengths after testing in mercury. (a),(b) Annealed and cold finished condition, (c),(d) Sensitized condition.

for the as-received material and a similar brittle region extending over most of the surface for the sensitized material. The gage length surface of the as-received material exhibited numerous linear cracks along slip planes perpendicular to or slightly inclined with respect to the axis of the specimen, whereas the sensitized material exhibited a few short, random cracks.

Higher magnification fractography for the as-received material (Fig. 3) tested in mercury revealed that the embrittled region consisted of mixed mode (transgranular and intergran-

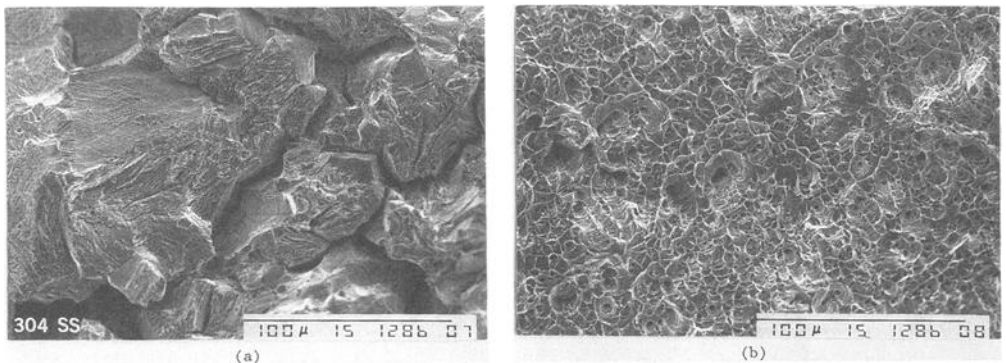


FIG. 3—Fractographic features of annealed and cold-finished Type 304 stainless steel fractured in mercury. (a) Embrittled region, (b) Ductile region.

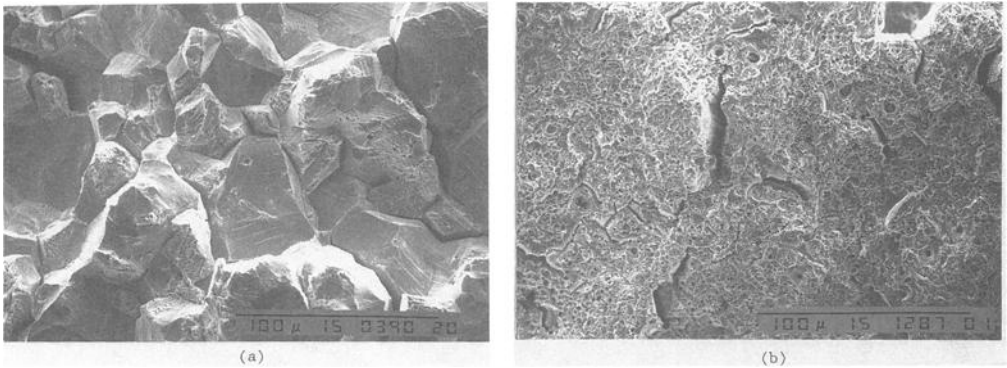


FIG. 4—Fractographic features of sensitized Type 304 stainless steel. (a) Fractured in mercury, (b) Fractured in air.

ular) cracking with delineation of slip planes (slip plane enhancement). The final fracture region exhibited ductile dimples (microvoid coalescence) identical to specimens tested in air. Fractographic features for the sensitized material tested in mercury, Fig. 4a, were significantly more intergranular in the embrittled region. In comparison to as-received material which exhibited purely microvoid coalescence in ductile rupture regions, the fracture surface of the sensitized material tested in air, Fig. 4b, exhibited some grain boundary fissures in addition to microvoid coalescence.

#### *Type 304L Stainless Steel*

Both the as-received (annealed and cold-finished) and heat-treated Type 304L specimen tests exhibited similar results, indicating that sensitization heat treatment did not significantly affect embrittlement. Embrittlement, as measured by time to failure and reduction in area, was more moderate than Type 304 stainless steel, particularly for the heat-treated material. However, embrittled regions of both as-received and heat-treated specimens extended over approximately one half the cross-section (similar to as-received Type 304) and mixed mode fracture morphologies (Fig. 5) were also comparable to as-received Type 304. Random secondary (surface) cracks were observed on both the as-received and heat-treated specimens tested in mercury.

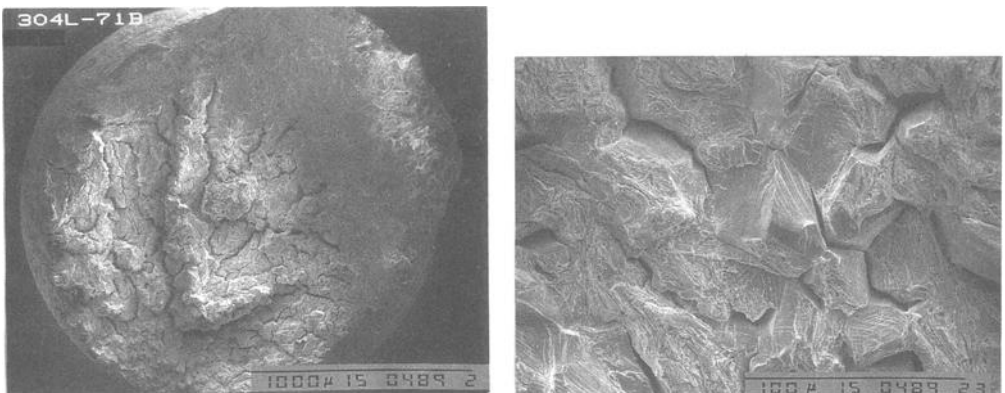


FIG. 5—Fractographic features of Type 304L stainless steel tested in mercury.

### *Type 316 Stainless Steel*

Fracture of the as-received (annealed and cold-finished) specimen tested in mercury did not exhibit time to failure, reduction in area, or macroscopic differences compared to fracture in air. The heat-treated (sensitized) specimen exhibited slight ductility loss. Fractographic examination revealed microvoid coalescence and small, localized regions near the gage length surface where mixed mode fracture was evident (Fig. 6). Secondary (surface) cracks were not observed on any of the test specimens.

### *Type 316L Stainless Steel*

As-received (annealed and cold-finished) and heat-treated specimens tested in mercury did not exhibit time to failure, reduction in area, or fractographic differences compared to fracture in air. Secondary (surface) cracks were not observed on any of the test specimens.

### *Type 321 Stainless Steel*

Differences in time to failure and reduction in area results for the air and mercury tests for as-received (annealed and cold-finished) material were minor; slightly greater decreases in both measures were observed for the heat-treated material. Both as-received and heat-treated materials exhibited regions with mixed mode fracture and traces of secondary (surface) cracking.

### *Alloy 600*

Results for alloy 600 were analogous to Type 304 stainless steel: significant mercury liquid metal embrittlement for the as-received (mill-annealed) material and greater embrittlement for the sensitized condition. The as-received material tested in mercury resulted in small areas of embrittlement near the gage surface (compared to approximately one half of the total cross-sectional area for Type 304), while the sensitized material exhibited embrittlement across the entire fracture surface (Fig. 7). Fracture morphology for the as-received material was predominantly transgranular, and the sensitized material was distinctly intergranular (Fig. 8). Linear and random secondary (surface) cracks were observed on both the as-received and heat-treated specimens tested in mercury.

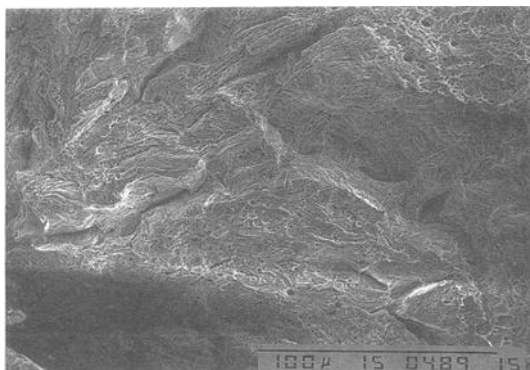


FIG. 6—Traces of mixed mode fracture in heat-treated Type 316 stainless steel.

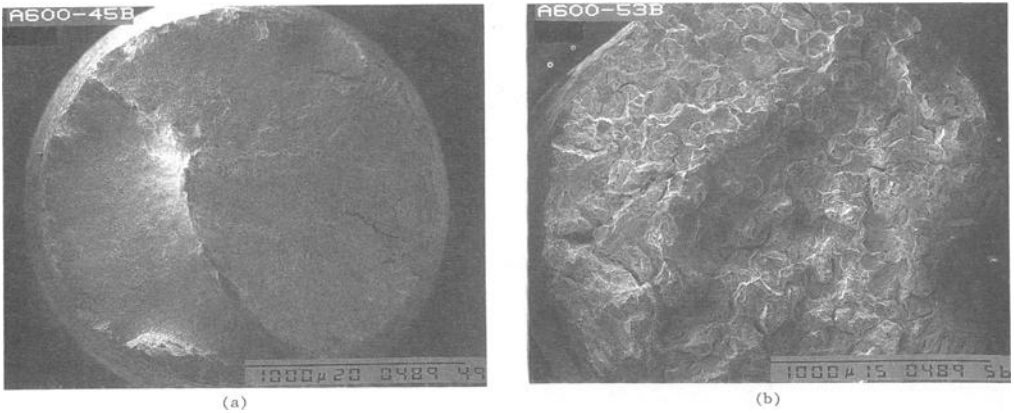


FIG. 7—Alloy 600 tested in mercury. (a) Mill-annealed condition, (b) Sensitized condition.

### Alloy 800

As-received (mill-annealed) and heat-treated specimens tested in mercury exhibited only slightly decreased reduction in areas compared to the air test. Fractographic examination (Fig. 9), revealed predominantly microvoid coalescence with random areas of intergranular and transgranular fracture. Secondary (surface) cracks were not observed on any of the test specimens.

### Discussion

Experimental results demonstrated that mercury liquid metal embrittlement of austenitic materials was influenced significantly by heat-treated condition. Materials which were most prone to sensitization, such as Type 304 stainless steel and alloy 600, also were more readily embrittled by mercury. In the fully sensitized conditions these materials exhibited pronounced intergranular fractures with decreased times to failure and, in the case of alloy 600, lower reduction in area value. Materials which were less prone to sensitization due to low carbon (L-grades) or stabilization (titanium in Type 321 stainless steel and alloy 800) exhibited significantly less mercury LME.

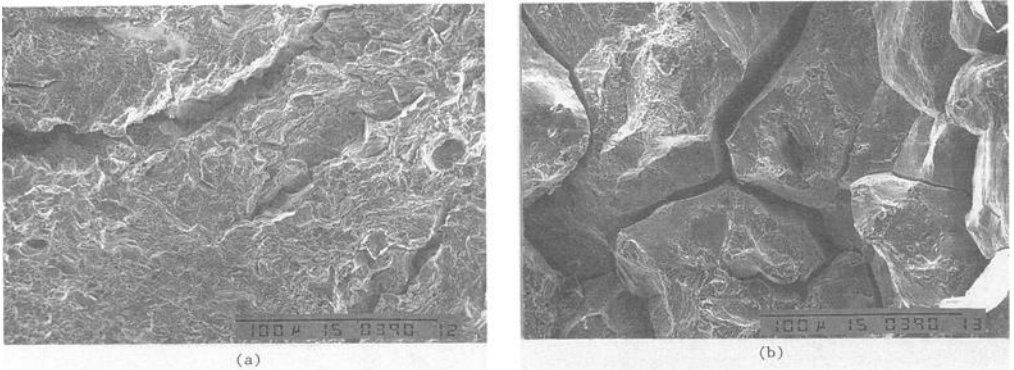


FIG. 8—Fractographic features of alloy 600 tested in mercury. (a) Mill-annealed condition, (b) Sensitized condition.

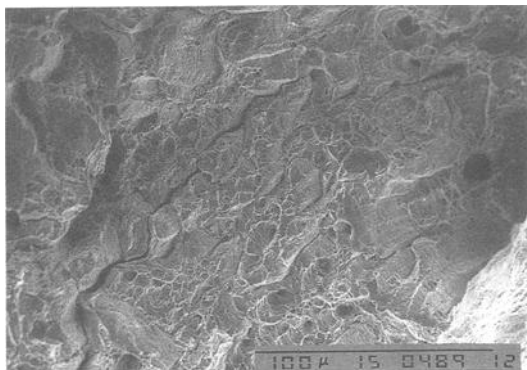


FIG. 9—Fractographic features of heat-treated alloy 800.

The fractographic study revealed similarities between mercury LME and chloride stress corrosion cracking of austenitic stainless steel. Transgranular cracking typically occurs in nonsensitized materials in aqueous chloride environments, but intergranular cracking can occur in sensitized materials exposed at high temperatures. This study revealed a propensity for intergranular cracking in the sensitized materials. Slip plane enhancement in the transgranularly fractured LME regions also was similar to the fracture morphology often observed with transgranular chloride stress corrosion cracking.

Based on time to failure, reduction in area, secondary (surface) cracking, and fractographic examination, a ranking of mercury LME susceptibility, irrespective of heat-treated condition, was as follows:

- Type 316L (Least susceptible)
- Type 316
- Alloy 800
- Type 321
- Type 304L
- Type 304
- Alloy 600 (Most susceptible).

Since most engineering applications involve welds, the low-carbon grades are particularly attractive for minimizing LME susceptibility in heat-affected zones.

It is interesting to note that Types 304 and 304L stainless steels exhibited inherent mercury LME susceptibility in the annealed and cold-finished condition, whereas Types 316 and 316L in a similar condition relatively were unaffected by mercury. The reasons for the poorer performance of Types 304 and 304L can possibly be explained in part by the higher molybdenum content of the Types 316 and 316L grades. It is possible that molybdenum plays a role in mercury LME fracture resistance. However, determination of specific effects of molybdenum additions was beyond the scope of this study.

Strain rate sensitivity also may play a minor role in the LME susceptibility. Only one strain rate,  $5.0 \times 10^{-6} \text{ s}^{-1}$ , was used for all the tests. Previous investigations for Type 304 [3] and Nickel 200 [8] indicated constant embrittlement for strain rates slower than  $5.0 \times 10^{-3} \text{ s}^{-1}$  and  $1.0 \times 10^{-5} \text{ s}^{-1}$ , respectively.

Degree of sensitization for each of the materials also could affect results to a limited degree. All as-received materials except Type 316L exhibited some evidence of intergranular fracture. Even fully annealed (solution-treated) and quenched material can contain some grain boundary carbides which could promote intergranular cracking. Except for the sen-

sitized materials, however, mercury LME fractures were predominantly transgranular in all cases.

The distinct effects of heat treating on the mercury LME fracture present a means for supplementing other sensitization assessment techniques such as electrochemical potentiokinetic reactivation (EPR). A parametric study using various alloys, heat treatments, and sensitization gaging techniques could provide some interesting results.

## Conclusions

(1) Mercury liquid metal embrittlement susceptibility of austenitic materials was influenced significantly by heat-treated condition. Sensitized materials were more susceptible to intergranular cracking in liquid mercury.

(2) Low-carbon or stabilized materials which are less prone to sensitization were more resistant to mercury liquid metal embrittlement and are preferable for applications where mercury may exist.

(3) Slow strain rate testing of austenitic materials in liquid mercury can be used to supplement other test methods, such as EPR, for determining degree of sensitization.

## Acknowledgments

The author acknowledges J. W. Anders, D. S. Hampton, and A. W. Smith for performing the tests and assisting in the post-test examinations. Helpful suggestions from L. R. Scharfstein are also recognized. Permission granted by Mobil Research and Development Corporation, Engineering Department, to publish this work is appreciated.

## References

- [1] W. Rostoker, J. M. McCaughey, and H. Markus, *Embrittlement by Liquid Metals*, Reinhold, New York, 1960.
- [2] M. H. Kamdar, "Liquid Metal Embrittlement," *Metals Handbook*, Ninth ed., Vol. 11, *Failure Analysis and Prevention*, American Society for Metals, Metals Park, OH, p. 236.
- [3] J. J. Krupowicz, Trans. ASME: *Journal of Engineering Materials and Technology*, Vol. 111, 1989, pp. 229–234.
- [4] D. R. McIntyre, J. J. English, and G. Kobrin, "Mercury Attack of Ethylene Plant Alloys," *CORROSION/89*, Paper No. 106, National Association of Corrosion Engineers (NACE), Houston, TX, 1989.
- [5] D. E. Drake, H. Sutanto, J. A. Colwell, and W. N. Stieglmeyer, "Corrosion Resistance of Materials Under Arun Field, Indonesia Conditions—Parts 1 and 2," *CORROSION/90*, Paper Nos. 57 and 58, National Association of Corrosion Engineers (NACE), Houston, TX, 1990.
- [6] C. E. Price and J. K. Good, Trans. ASME: *Journal of Engineering Materials and Technology*, Vol. 106, 1984, pp. 184–191.
- [7] L. B. Traylor and C. E. Price, Trans. ASME: *Journal of Engineering Materials and Technology*, Vol. 108, 1986, pp. 31–36.
- [8] C. E. Price and L. B. Traylor, *Corrosion*, Vol. 43, No. 4, 1987, pp. 229–238.

Paul A. Klein,<sup>1</sup> Richard A. Hays,<sup>2</sup> Patrick J. Moran,<sup>3</sup> and John R. Scully<sup>4</sup>

## Hydrogen Cracking Initiation of a High-Strength Steel Weldment

---

**REFERENCE:** Klein, P. A., Hays, R. A., Moran, P. J., and Scully, J. R., “Hydrogen Cracking Initiation of a High-Strength Steel Weldment,” *Slow Strain Rate Testing for the Evaluation of Environmentally Induced Cracking: Research and Engineering Applications, ASTM STP 1210*, R. D. Kane, Ed., American Society for Testing and Materials, Philadelphia, 1993, pp. 202–222.

**ABSTRACT:** The hydrogen assisted crack initiation susceptibility of 5-Ni-Cr-Mo-V (MIL-S-24371A) quenched and tempered steel plate, weldment, and Gleeble thermal cycled materials representative of tempered and untempered weld metal was investigated in 3.5% NaCl solution. The conjoint role of steady state diffusible hydrogen content and maximum principal stress was quantitatively characterized by: (1) Devanathan-Stachurski hydrogen permeation tests, and (2) slow strain rate tests conducted under various cathodic protection levels.

For the four material conditions studied, the threshold maximum principal stress decreased with increasing hydrogen concentration. The base plate was less susceptible to hydrogen assisted crack initiation than the weld metal and thermal cycled weld metals. The tempered and untempered thermal cycled weld materials defined the upper and lower bounds of the as-welded material cracking susceptibility respectively.

**KEYWORDS:** slow strain rate testing, high-strength steel, 3.5% NaCl solution, hydrogen embrittlement, welds

Demand to improve the performance of U.S. Navy vessels has led to the development of high-strength, tough, weldable structural steels such as the 5Ni-Cr-Mo-V (MIL-S-24371A) alloy system. Associated with the benefit provided by increased strength, however, is an increased susceptibility to stress corrosion cracking (SCC). Stress corrosion cracking may be defined as subcritical cracking which results from the combined action of tensile stress and a specific environment. In the case of high-strength steels in a marine environment under cathodic protection, hydrogen embrittlement is a persistent concern.

During alloy development, tests conducted using smooth, bolt-loaded specimens showed complete resistance to SCC [1,2]. Subsequent testing using precracked specimens revealed susceptibility to SCC in marine environments [3,4]. These tests typically used fatigue-precracked specimens of rectangular cross-section under either constant load or displacement. Recent advancements in test techniques include the use of “ripple” loading (small cyclic load superimposed on a constant static load) [5], and the slow strain rate technique [6].

---

<sup>1</sup> Materials engineer, Baltimore Gas and Electric Company, Calvert Cliffs Nuclear Power Plant, Lusby, MD 20657.

<sup>2</sup> Materials engineer, Naval Surface Warfare Center, Code 613, Annapolis, MD 21402.

<sup>3</sup> Associate professor of Mechanical Engineering, U.S. Naval Academy, Annapolis, MD 21402.

<sup>4</sup> Assistant professor, Center for Electrochemical Sciences and Engineering, Department of Materials Science, University of Virginia, Charlottesville, VA 22901.

These techniques have been used to establish SCC susceptibility limits under conditions more representative of service loading conditions.

The objective of this research was to quantitatively characterize the conjoint role of steady state hydrogen content and maximum principal stress on the hydrogen cracking initiation susceptibility of 5Ni-Cr-Mo-V steel base plate and weldments. The maximum principal stress parameter was selected in order to allow laboratory test data to be applied to service structures. Because previous investigations [7] have determined that weldments in this system are more susceptible to embrittlement than base plate, the present work concentrated on the welds.

## Experimental Procedure

The experimental aspect of this work was divided into two components: (1) measurement of diffusible hydrogen content in the material and (2) slow strain rate tests. Slow strain rate tests were performed on base plate, as-welded material, and thermal cycled weld materials. Thermal cycled materials were used to simulate untempered and tempered regions within a given weld deposit.

### *Materials and Specimen Preparation*

The 5Ni-Cr-Mo steel test specimens were machined from a 38-mm (1.5-in.) thick welded plate fabricated using the gas metal arc process (GMAW) with a double-vee butt weld joint design. Welding parameters, as well as compositions of the Airco AX-140 filler wire, weldments and base plate are provided in Table 1. Hydrogen contents of less than 1 ppm were measured for the base plate, weldments, and heat affected zone by fusion analysis.

Thermal cycles were produced using a Duffer's Gleeble machine [8]. The apparatus heats and cools the specimen to a programmed cycle using electrical resistance heating. Temperatures are controlled by a thermocouple percussion welded at the midlength of the specimen. Heat is extracted through the water cooled copper jaws with quenching available through the use of a liquid nitrogen quench system. Two thermal cycled conditions were produced. The initial Gleeble-produced condition (Gleeble 1), simulates high hardness regions of the weld bead that do not receive tempering from subsequent passes. The rapidly cooled thermal cycle treatment was accomplished by heating the welded specimen to a 1316°C (2400°F) peak temperature with immediate cooling simulating the cooling rate of a weld in a 25-mm (1-in.) thick plate with heat input of 45 kJ/in. The second Gleeble-produced condition (Gleeble 2) simulates the lower hardness "eyebrow" regions of a weld deposit which have received tempering from subsequent weld passes. This condition was produced using an initial thermal cycle identical to that used for Gleeble 1 followed by an additional thermal cycle with a 677°C (1250°F) peak temperature and immediate cooling.

### *Hydrogen Permeation Experiments*

The Devanathan-Stachurski technique [9] was used to study hydrogen permeation in the 5Ni-Cr-Mo-V steel. The details of this aspect of the work have been previously reported [10-13]. Hydrogen is introduced into one side of a steel wafer by cathodically charging at a constant current density in 3.5% NaCl solution (Fig. 1). The cathodic charging current densities ranged from 25 to 1200  $\mu\text{A}/\text{cm}^2$  (161 to 7742  $\mu\text{A}/\text{in.}^2$ ) depending on experiment. The cathodic current densities near the low end of this range are representative of current densities observed per unit area of cathodically protected uncoated steel in seawater [14].

TABLE 1—Weld parameters and compositions of 5Ni-Cr-Mo-V steel weldment and base plate.

Welding Parameters Using 60 Degree Double-Vee Weld Joint									
Weld Wire	Heat #	Wire Size	Preheat Temp.	Interpass Temp.	Voltage	Current	Travel Speed	Heat Input	Shield Gas
Airco AX-140	51252	0.15 cm 1/16 in.	135°C 275°F	150°C 300°F	26 V	330 A	33 CM/PM 13 IPM	102 kJ/cm 40 kJ/in.	Ar-2% O <sub>2</sub>

## Chemical Composition

Material	Weight Percent									
	C	Mn	P	S	Si	Ni	Cr	Mo	V	H (ppm)*
Base Plate	0.11	0.84	0.005	0.005	0.28	4.93	0.61	0.45	0.07	0.9
Heat Affect Zone	0.11	0.84	0.005	0.005	0.27	4.87	0.63	0.45	0.08	0.7
Airco Weld Wire	0.093	1.71	0.006	0.004	0.24	2.1	1.02	0.63	0.01	2.4
Weldment	0.09	1.51	0.012	0.006	0.38	2.54	1.05	0.56	0.04	0.8

\* Hydrogen content obtained from vacuum fusion analysis.

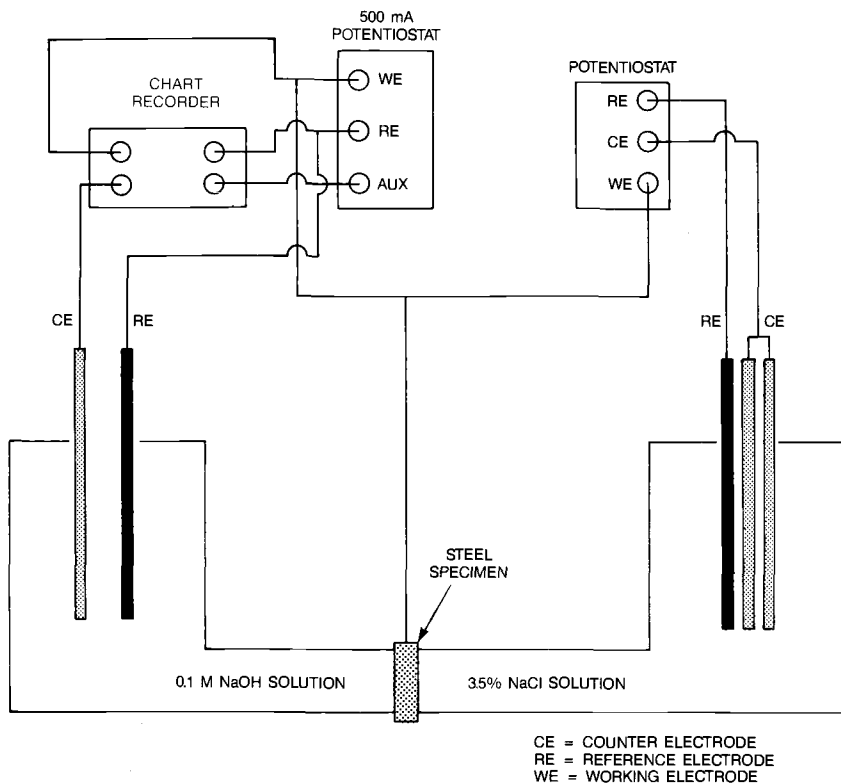


FIG. 1—Schematic of hydrogen permeation apparatus.

Sputter deposited palladium coated the exit (left) side of the steel wafer in all cases. The exit chamber was filled with 0.1 molar sodium hydroxide and polarized to a potential that would ionize any hydrogen permeating through the steel wafer. The anodic reaction for this oxidation of hydrogen is  $H \rightarrow H^+ + e^-$ . Thus, the anodic current of the exit side is a direct measurement of hydrogen permeation through the specimen. Permeation currents were monitored until a steady state current was reached and remained stable for at least one day.

### Slow Strain Rate Tests

Slow strain rate tests were conducted on notched cylindrical specimens shown schematically in Fig. 2. The notched specimen geometry was used to promote localized areas of high stress and strain. All slow strain rate specimens were oriented with the tensile axis perpendicular to the rolling direction of the plate (long transverse orientation). The specimens were masked prior to test by painting on an electronic stop-off lacquer on all areas except the notched region.

Tests were performed using a constant displacement rate of  $2 \times 10^{-5}$  mm/s ( $9 \times 10^{-7}$  in./s). Specimens were tested in air, in the freely corroding (open circuit) condition, and cathodically polarized under potentiostatic control. A saturated calomel reference electrode and high-density graphite counter electrodes were used in the slow strain rate cell, which was deoxygenated with nitrogen during test.

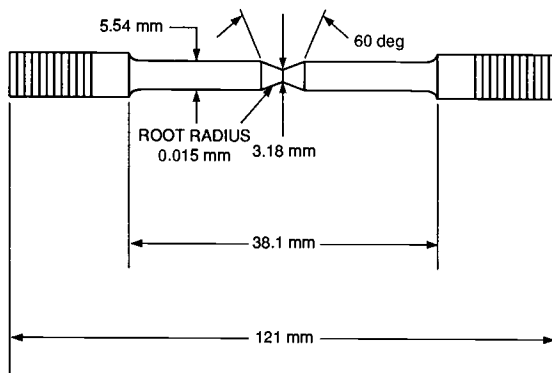


FIG. 2.—Slow strain rate test specimen.

In order to determine a maximum principal stress for this material, an elastic-plastic stress analysis was obtained for the circumferentially notched 5Ni-Cr-Mo-V steel slow strain rate specimen under uniaxial tensile loading conditions using finite element computational analysis [10]. While the analysis performed is only applicable for crack initiation, the similarity between the maximum loads and failure loads observed in the testing indicates that crack propagation is rapid and, therefore, failure is controlled by initiation.

## Results and Discussion

### Material Characterization

Tensile properties for smooth and notched base plate and welded 5Ni-Cr-Mo-V steel specimens are presented in Table 2. Material strength was quite similar for base plate and weldments in both longitudinal and transverse orientations with yield strengths greater than 1000 MPa (145 ksi) and ultimate tensile strengths of 1048 to 1070 MPa (152 to 155 ksi). The base plate exhibited greater elongation than the weldments.

Figure 3 provides Diamond Pyramid Hardness (DPH) measurements of a weld cross-section. The measurements ranged from 305 to 415, using a 1-kg load. Inhomogeneity in the weld deposit is demonstrated by hardness measurements near 400 in the central, untempered region of the weld bead and in the last pass weld bead to measurements in the low 300s in the "eyebrow" regions. For comparison, the hardness values in the base plate averaged about 320. Hardness measurements averaged 397 DPH for the Gleeble 1 material and 323 for the Gleeble 2 material.

### Hydrogen Permeation

Steady state permeation currents were measured for various cathodic charging current densities ranging from 25 to 1200  $\mu\text{A}/\text{cm}^2$  (161 to 7742  $\mu\text{A}/\text{in.}^2$ ). Figure 4 shows permeation transient flux measurements recorded as a function of reciprocal time for transients performed on the base plate material. Using procedures and conditions to satisfy the solution of McBreen [15], a hydrogen diffusivity of  $4.2 \times 10^{-7} \text{ cm}^2/\text{s}$  ( $6.5 \times 10^{-8} \text{ in.}^2/\text{s}$ ) was calculated from the slope of this plot. This value agrees with the literature [15–17]. Having determined the diffusivity ( $D$ ), steady state diffusible hydrogen concentrations were calculated and are shown in Fig. 5, which illustrates the steady state hydrogen concentration versus cathodic overpotential for the base plate.

TABLE 2—Tensile data and notch strength ratios of 5Ni-Cr-Mo-V steel base plate and weldments average of two specimens.

Material	Orientation	Notched or Smooth	Baked 177°C 30 h	Ultimate Tensile,		Yield Strength,		Elongation	Notch Strength Ratio (UTS Notched/UTS Smooth)
				MPa (ksi)	MPa (ksi)	MPa (ksi)	MPa (ksi)		
Base Plate	Longitudinal	Smooth	No	1062 (154)	1013 (147)	1013 (147)	26	—	
Base Plate	Longitudinal	Smooth	Yes	1062 (154)	1013 (147)	1013 (147)	27	—	
Base Plate	Transverse	Smooth	No	1048 (152)	1007 (146)	1007 (146)	26	—	
Base Plate	Transverse	Smooth	Yes	1048 (152)	1000 (145)	1000 (145)	26	—	
Weldment	Transverse	Smooth	No	1069 (155)	1020 (148)	1020 (148)	19	—	
Weldment	Transverse	Smooth	Yes	1069 (155)	1007 (146)	1007 (146)	22	—	
Base Plate	Longitudinal	Notched	No	1668 (242)	—	—	—	1.6	
Base Plate	Longitudinal	Notched	Yes	1744 (253)	—	—	—	1.6	
Base Plate	Transverse	Notched	No	1675 (243)	—	—	—	1.6	
Base Plate	Transverse	Notched	Yes	1675 (243)	—	—	—	1.6	
Weldment	Transverse	Notched	No	1903 (276)	—	—	—	1.8	
Weldment	Transverse	Notched	Yes	1682 (244)	—	—	—	1.6	

DPH AVERAGE HARDNESS  
 LAST PASS BEAD: 377  
 BASE PLATE: 323

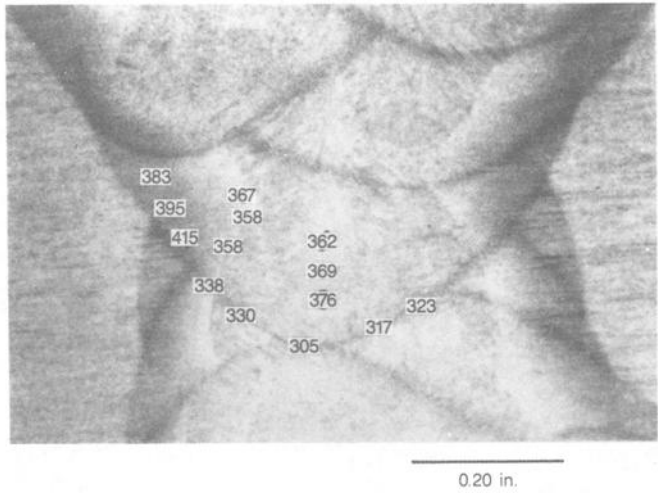


FIG. 3—Macrograph of 5Ni-Cr-Mo-V steel weldment etched to show location of DPH hardness measurements within weld deposit.

Slow Strain Rate Tests

Table 3 summarized the results of slow strain rate testing. While the base plate, as-welded, and Gleeble 2 (tempered weld) materials exhibited similar breaking strengths in air, the Gleeble 1 (untempered weld) material was significantly stronger. Figure 6 compares the

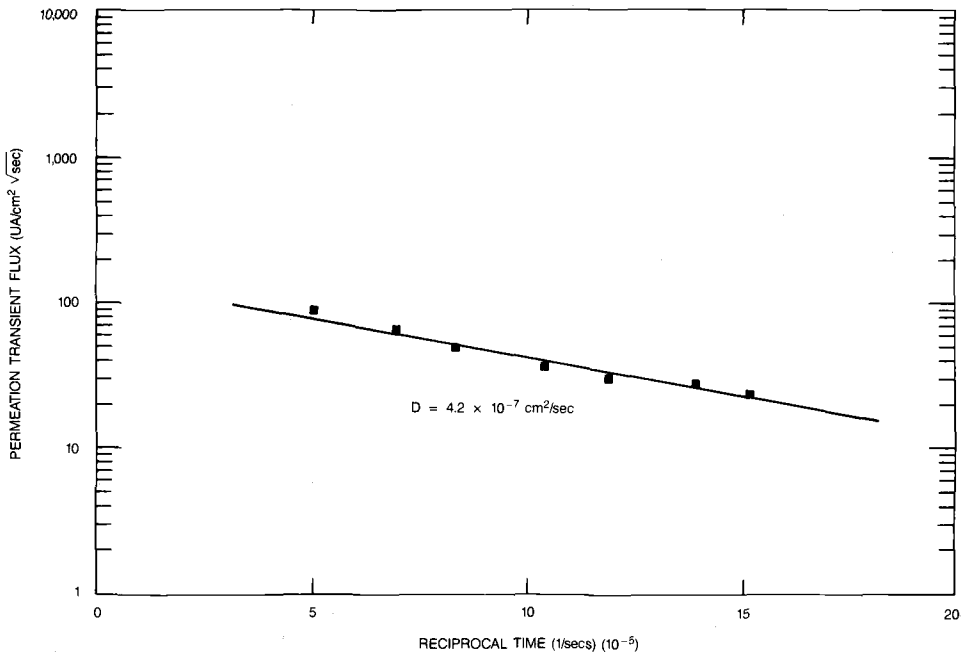


FIG. 4—Hydrogen permeation transient flux versus reciprocal time for 5Ni-Cr-Mo-V steel base plate.

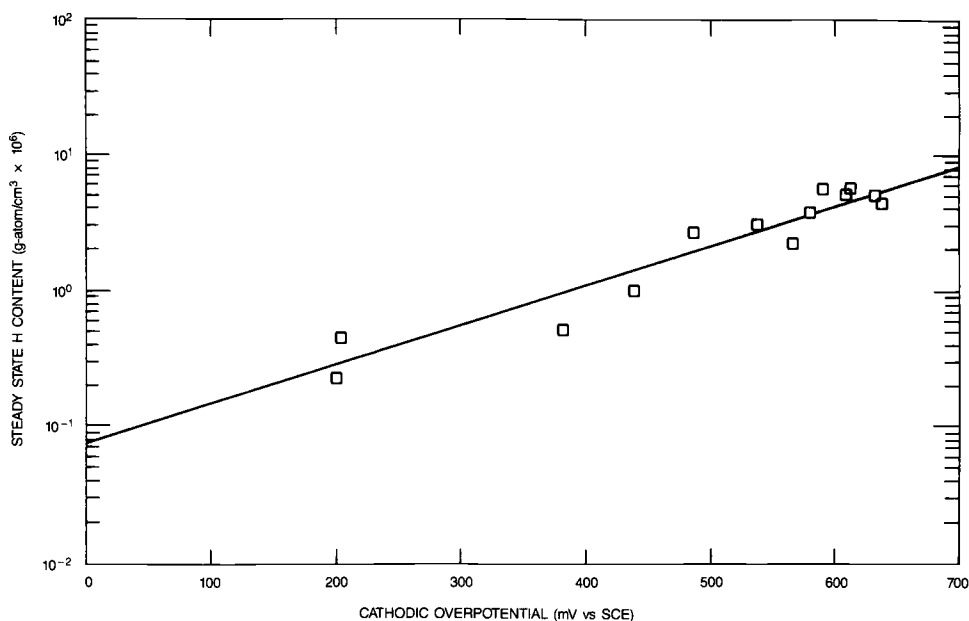


FIG. 5—Steady state diffusible hydrogen versus cathodic overpotential for 5Ni-Cr-Mo-V steel base plate.

average slow strain rate test results as a function of cathodic potential for the four material conditions. All breaking load data were normalized by the average breaking load in air for each material condition, to account for differences in strength.

A deterioration of load carrying capability with increasing cathodic potential is evident for all material conditions. As expected, the base plate exhibited greater resistance to hydrogen cracking than the weld metal, in agreement with previous investigations [3,7]. Although not shown by this figure, the as-welded material exhibited considerably more variability than either of the thermal cycled conditions.

For all material conditions, virtually no loss of load carrying capability was observed between the open circuit potential and  $-0.85$  V versus SCE potential. Unlike the base plate, as-welded, and Gleeble 2 materials, the Gleeble 1 material showed some decrease in load at a  $-0.850$  V potential when compared to air. In seawater, the reversible potential for hydrogen evolution is in the range  $-0.700$  V to  $-0.750$  V versus SCE [16]. Thus, at a  $-0.850$  V versus SCE protection potential, a relatively small overvoltage for hydrogen evolution exists.

When tested at a  $-1.0$  V versus SCE potential, the base plate and Gleeble 2 materials retained approximately 85% of the load carrying capacity in air. However, a significant decrease in breaking load ensued for the as-welded and Gleeble 1 materials at the  $-1.0$  V cathodic protection level. Breaking loads between 49% and 82% compared to air for the as-welded and between 56% and 77% compared to air for the rapid cooled thermal cycled weldment were measured. When breaking loads were averaged at the  $-0.85$  V and  $-1.0$  V potentials, the drops in load between these environments were 33% and 22% for the as-welded and Gleeble 1 materials, respectively. Based on three specimens, the base plate exhibited a 10% reduction in breaking load between  $-0.900$  V and  $-1.0$  V. At the  $-1.50$

TABLE 3—Summary of slow strain rate data.

MATERIAL CONDITION	ENVIRONMENT	CATHODIC POTENTIAL (mV vs. SCE)	LOG DIFF. HYD. CONTENT (g-atoms/cm <sup>3</sup> )	# of TESTS	BREAKING LOAD				MAXIMUM PRINCIPLE STRESS							
					MIN. (kN)	(lb)	AVG. (kN)	(lb)	MAX. (kN)	(lb)	MIN. (kN)	(lb)	AVG. (kN)	(lb)	MAX. (kN)	(lb)
Base Metal	Air	-750	-7.125	1	13.3	2981	13.3	2981	13.3	2981	2117	307	2117	307	2117	307
	3.5% NaCl	-900	-6.580	1	13.3	2980	13.3	2980	13.3	2980	2117	307	2117	307	2117	307
	3.5% NaCl	-1000	-6.332	2	12.6	2823	12.6	2823	12.6	2823	2069	300	2069	300	2069	300
	3.5% NaCl	-1150	-5.845	1	11.1	2489	11.3	2548	11.6	2606	1986	288	2000	290	2013	292
	3.5% NaCl	-1500	-4.928	1	8.8	1988	8.8	1988	8.8	1988	1917	278	1917	278	1917	278
As-Welded	Air	-650	-7.288	4	13.3	2994	13.9	3120	14.4	3230	2117	307	2172	315	2220	322
	3.5% NaCl	-850	-6.695	6	11.4	2551	13.2	2967	15.2	3414	2000	290	2124	308	2324	337
	3.5% NaCl	-1000	-6.333	9	6.8	1527	9.3	2087	12.0	2703	1841	267	1911	306	2186	317
	3.5% NaCl	-1250	-5.677	5	4.7	1050	5.9	1336	8.7	1966	1538	223	1687	245	1910	277
	3.5% NaCl	-1500	-4.971	6	4.7	1058	6.3	1425	8.0	1804	1551	225	1755	255	1882	273
Un-Tempered Weld (Gleeble 1)	Air	-650	-7.092	3	15.6	3506	18.4	4133	21.2	4763	2372	344	2717	394	3068	445
	3.5% NaCl	-850	-6.637	3	13.7	3069	14.7	3296	15.7	3525	2144	311	2262	328	2386	346
	3.5% NaCl	-1000	-6.164	4	9.6	2165	11.7	2621	13.9	3124	1937	281	2031	295	2165	314
	3.5% NaCl	-1250	-5.698	2	5.6	1266	6.5	1468	7.4	1670	1689	245	1775	258	1862	270
	3.5% NaCl	-1500	-5.091	2	4.9	1105	5.3	1190	5.7	1276	1593	231	1644	239	1696	246
Tempered Weld (Gleeble 2)	Air	-650	-7.228	2	13.6	3048	13.6	3052	13.6	3056	2137	310	2137	310	2137	310
	3.5% NaCl	-850	-6.517	4	12.7	2852	13.2	2966	14.5	3254	2075	301	2134	310	2294	324
	3.5% NaCl	-1000	-6.239	6	9.1	2046	11.5	2586	14.2	3182	1924	279	2026	294	2200	319
	3.5% NaCl	-1250	-5.396	5	6.9	1560	7.7	1737	8.6	1942	1848	268	1874	272	1910	277
	3.5% NaCl	-1500	-4.872	4	5.1	1148	6.3	1417	7.0	1562	1613	234	1775	258	1848	268

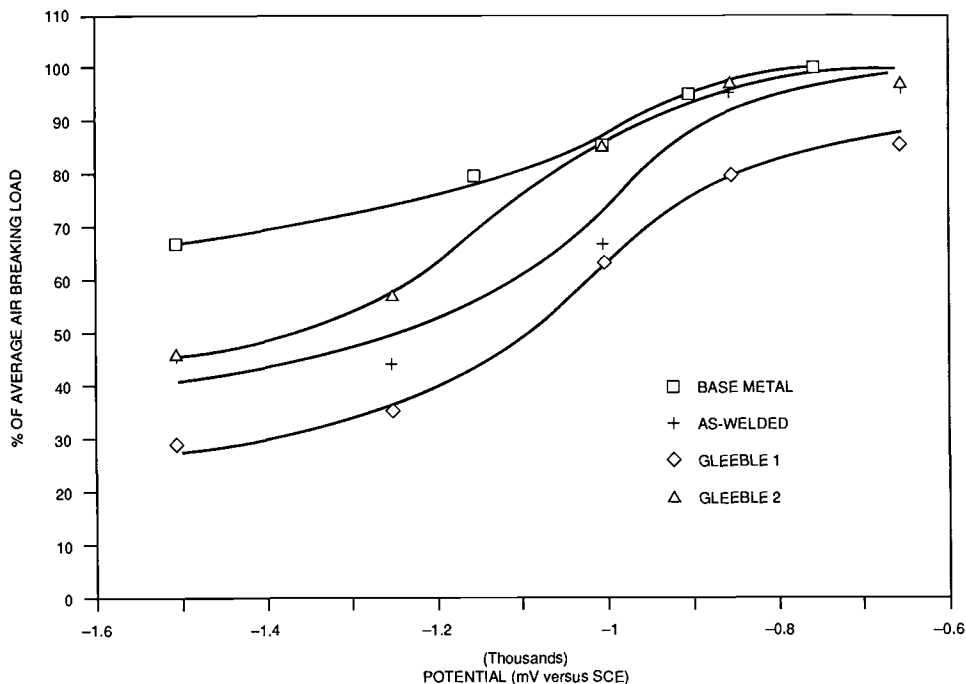


FIG. 6—Normalized breaking load versus cathodic potential for all material conditions.

V versus SCE cathodic protection level, a significant lowering in load carrying capacity occurred in all four material conditions with the as-welded and thermal cycled materials exhibiting the greatest reductions. At potentials in the range of  $-1.00$  V to  $-1.50$  V, the lower bound of weld metal breaking loads was approximately the same as the Gleeble 1 material.

### Fractography and Metallography

Scanning electron microscopy was performed on fracture surfaces of the welded material cathodically charged to different hydrogen contents during the slow strain rate tests. Low and high magnification views of the as-welded steel, tested in air and in the freely corroding condition, are shown in Figs. 7 and 8. In these environments, a completely ductile microvoid coalescence (MVC) fracture was observed. Figures 9 and 10 show typical fracture surfaces of the as-welded and Gleeble 1 material at the  $-0.850$  V versus SCE potential. While some reduced ductility was noted at this potential, the fracture surfaces were dominated by MVC.

Fractographs of the materials at the  $-1.00$  V,  $-1.25$  V, and  $-1.50$  V potentials showed increasing amounts of intergranular fracture and secondary cracking with more electronegative potentials (Figs. 11 through 13). Intergranular fracture due to hydrogen embrittlement has been previously shown for 5Ni-Cr-Mo-V steel [18]. Ductile fracture was observed near the centers of the specimens, where the remaining ligaments failed by ductile overload once hydrogen cracking initiation reduced the cross-section of the specimens.

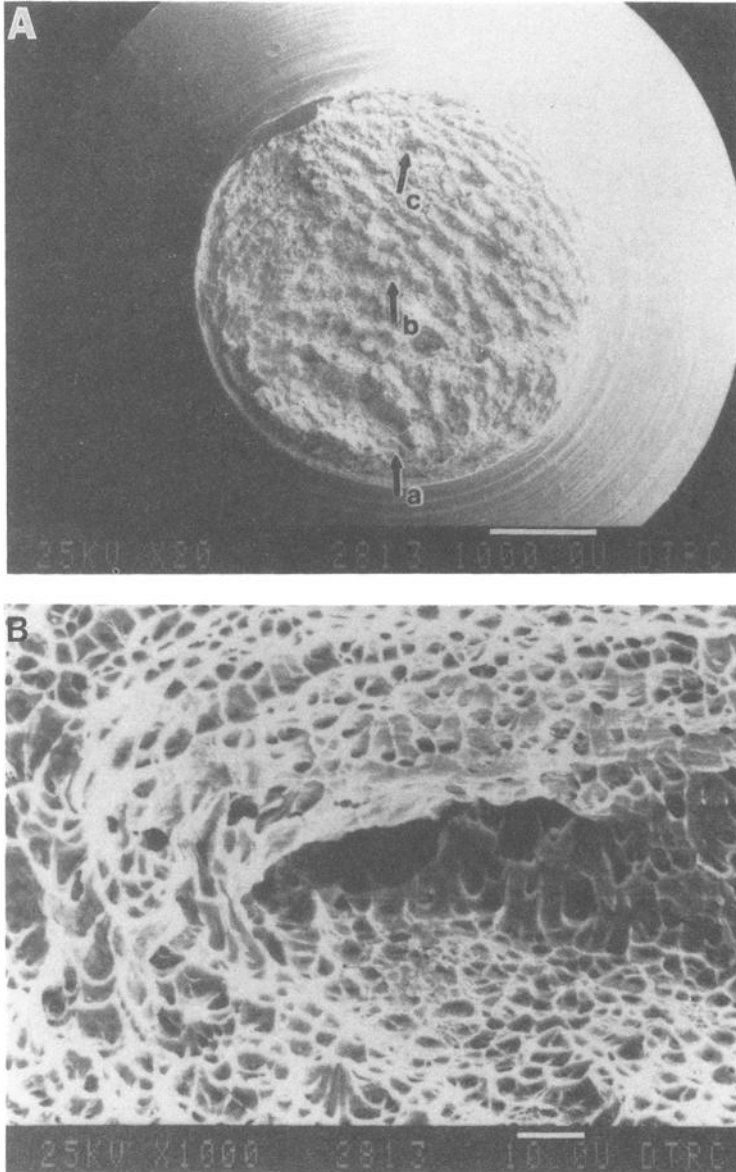


FIG. 7(a)—Macrograph of as-welded 5Ni-Cr-Mo-V steel fracture from air test. (b) Completely ductile fracture surface of as-welded 5Ni-Cr-Mo-V steel from air test (from Area a in Fig. 7a).

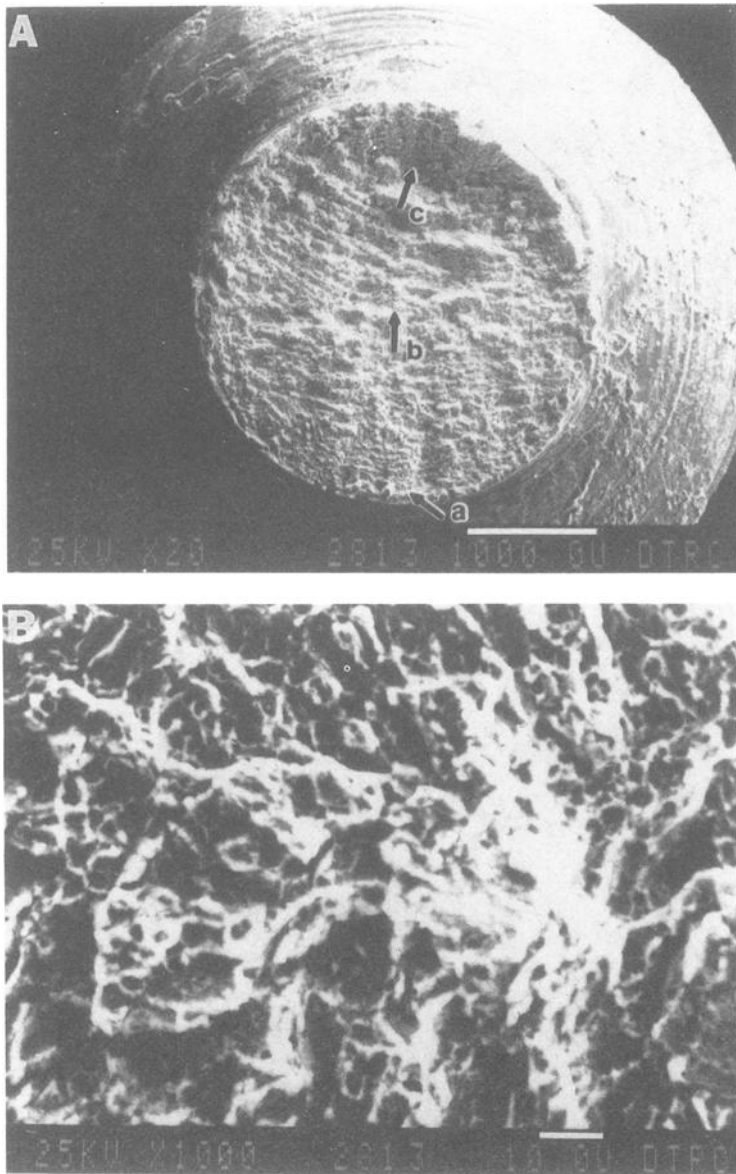


FIG. 8(a)—Micrograph of as-welded 5Ni-Cr-Mo-V steel fracture from open circuit potential test. (b) Ductile fracture surface of as-welded 5Ni-Cr-Mo-V steel from open circuit potential test (from Area a in Fig. 8a).

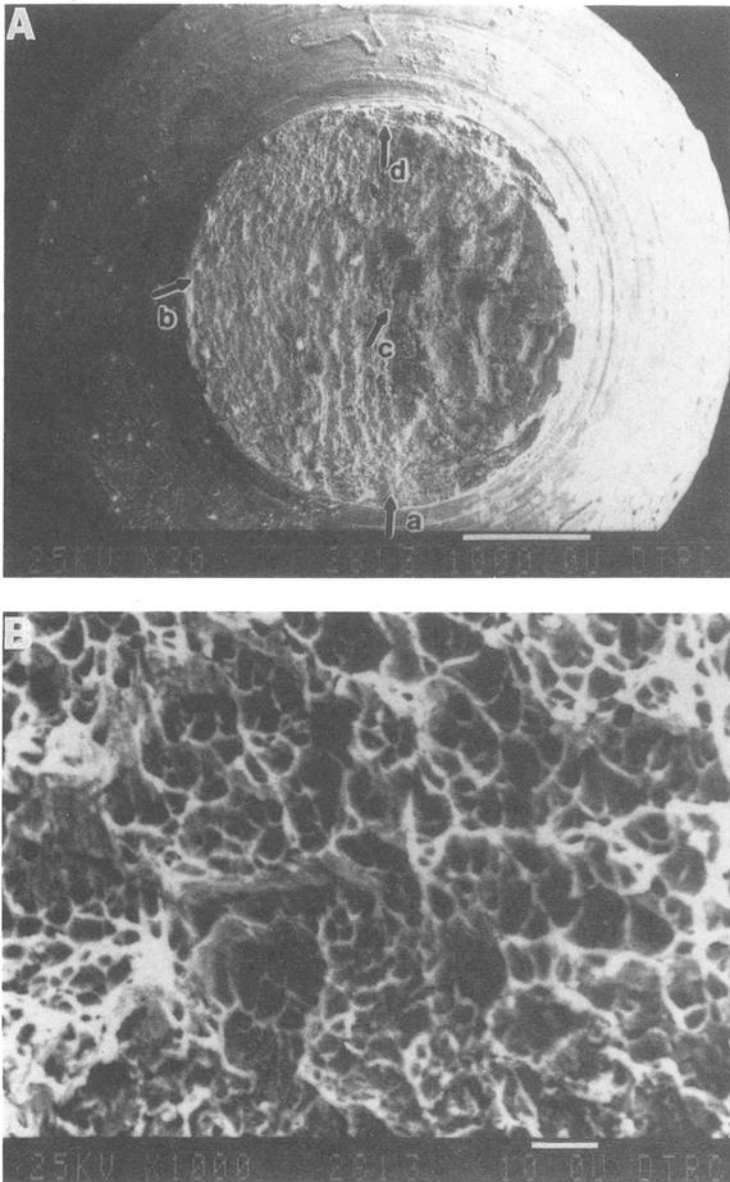


FIG. 9(a)—Macrograph of as-welded 5Ni-Cr-Mo-V steel fracture from  $-0.850$  V SCE test. (b) Representative fracture surface of as-welded 5Ni-Cr-Mo-V steel from  $-0.850$  V SCE test (from Area a in Fig. 9a).

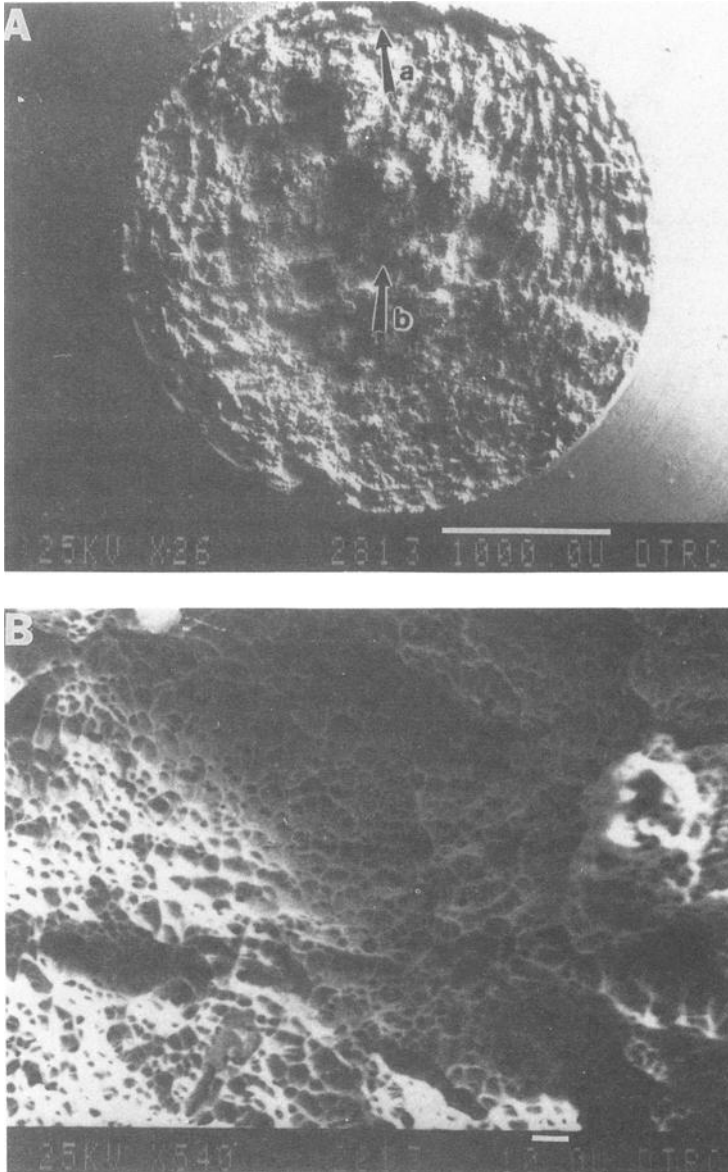


FIG. 10(a)—Macrograph of Gleebly 1 specimen fracture from  $-0.850$  V SCE test. (b) Representative ductile fracture surface of Gleebly 1 specimen from  $-0.850$  V SCE test (from Area a in Fig. 10a).

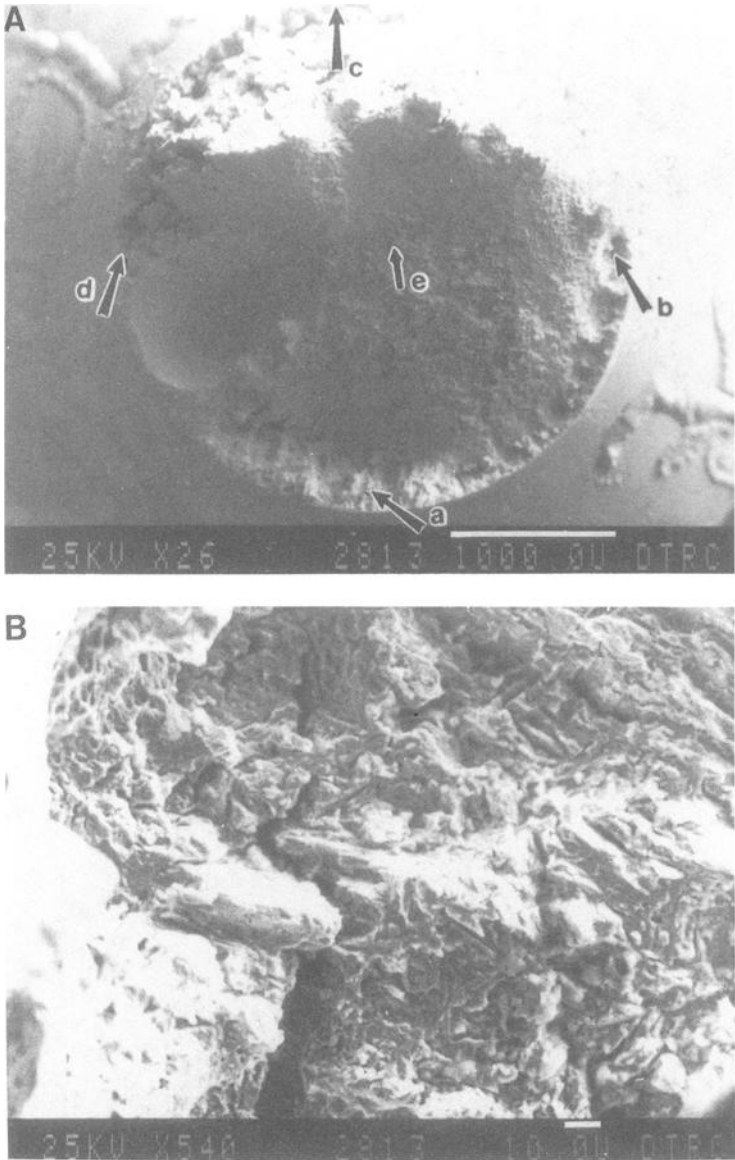


FIG. 11(a)—Macrograph of as-welded 5Ni-Cr-Mo-V steel fracture from  $-1.000$  V SCE test. (b) Fracture surface of as-welded 5Ni-Cr-Mo-V steel from  $-1.000$  V SCE test (from Area b in Fig. 11a).

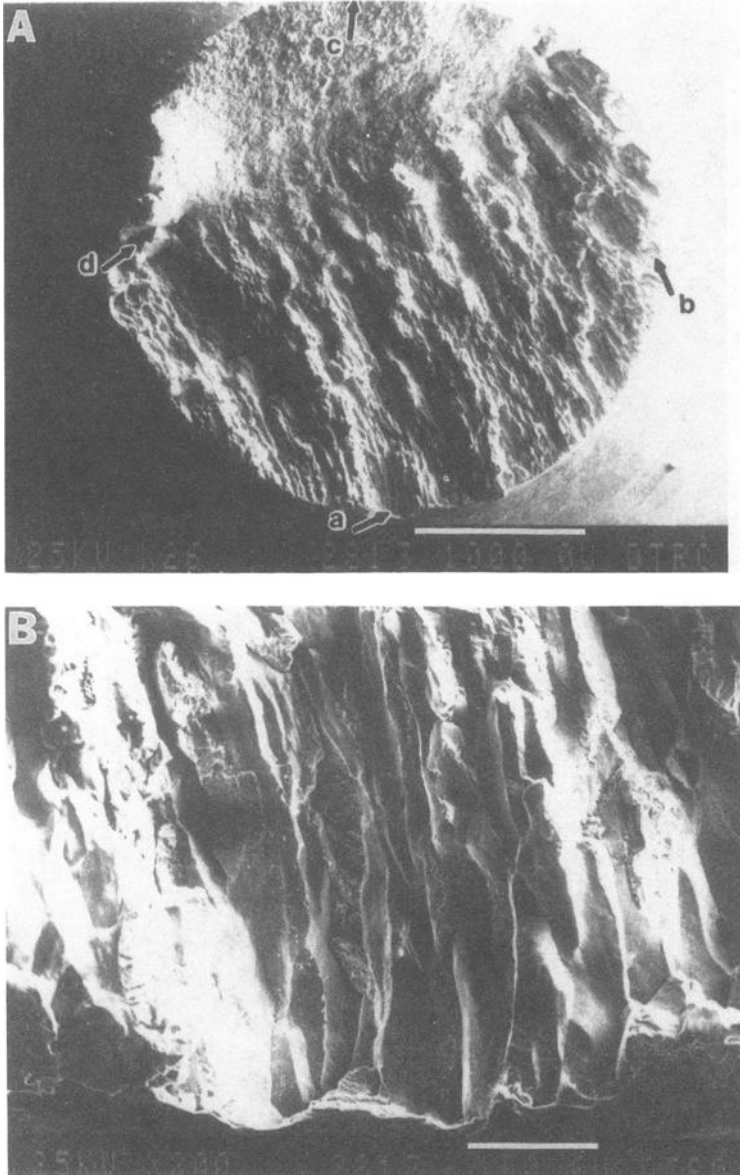


FIG. 12(a)—Macrograph of as-welded 5Ni-Cr-Mo-V steel fracture from  $-1.250$  V SCE test. (b) Fracture surface of as-welded 5Ni-Cr-Mo-V steel from  $-1.250$  V SCE test (from Area a in Fig. 12a).

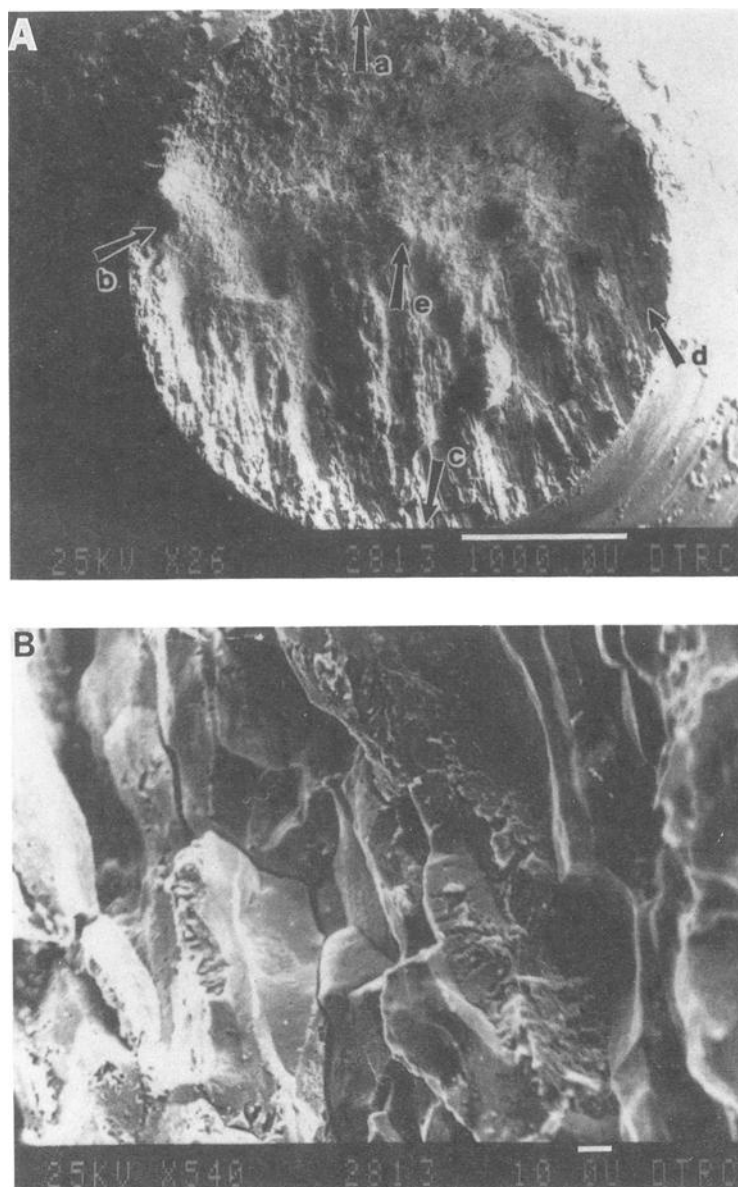


FIG. 13(a)—Macrograph of as-welded 5Ni-Cr-Mo-V steel fracture from  $-1.500$  V SCE test. (b) Fracture surface of as-welded 5Ni-Cr-Mo-V steel from  $-1.500$  V SCE test (from Area d in Fig. 13a).

*Maximum Principal Stress versus Steady State Diffusible Hydrogen Concentration*

Figure 14, which was developed from the elastic-plastic analysis of the specimen geometry, plots the maximum principal stress versus load for the base plate specimens used in this investigation [10]. Using this relationship, along with the hydrogen content versus cathodic overpotential relationship depicted in Fig. 5, it becomes possible to plot maximum principal stress versus steady state diffusible hydrogen concentration for the material conditions tested. Since hydrogen diffusivity measurements for the weld metal were unsuccessful due to microporosity, the hydrogen diffusivity value calculated for the base plate is used to estimate diffusible hydrogen concentrations for all material conditions.

Figure 15 shows the relationship between maximum principal stress and steady state diffusible hydrogen concentration for the four material conditions. These lines represent the threshold maximum stress for fracture at a given hydrogen content. Plotted in this fashion, increasing sensitivity to diffusible hydrogen is represented by a more negative slope. The threshold maximum principal stress for hydrogen cracking initiation decreased as the steady state diffusible hydrogen concentration of the materials was increased. In agreement with earlier work [3,7], the base plate exhibited greater resistance to hydrogen cracking as a function of increasing diffusible hydrogen content than the weld metal conditions. The numerous thermal processing steps used in fabrication of 5Ni-Cr-Mo-V steel plate produce a highly refined, relatively homogenous, tempered martensite grain structure. This type of microstructure provides maximum resistance to hydrogen embrittlement for this material [19].

Figure 16 shows the same data normalized against the maximum principal stress measured in air for each material condition. This figure clearly indicates that the resistance to hydrogen cracking initiation is greatest for plate material and least for the Gleeble 1 (untempered)

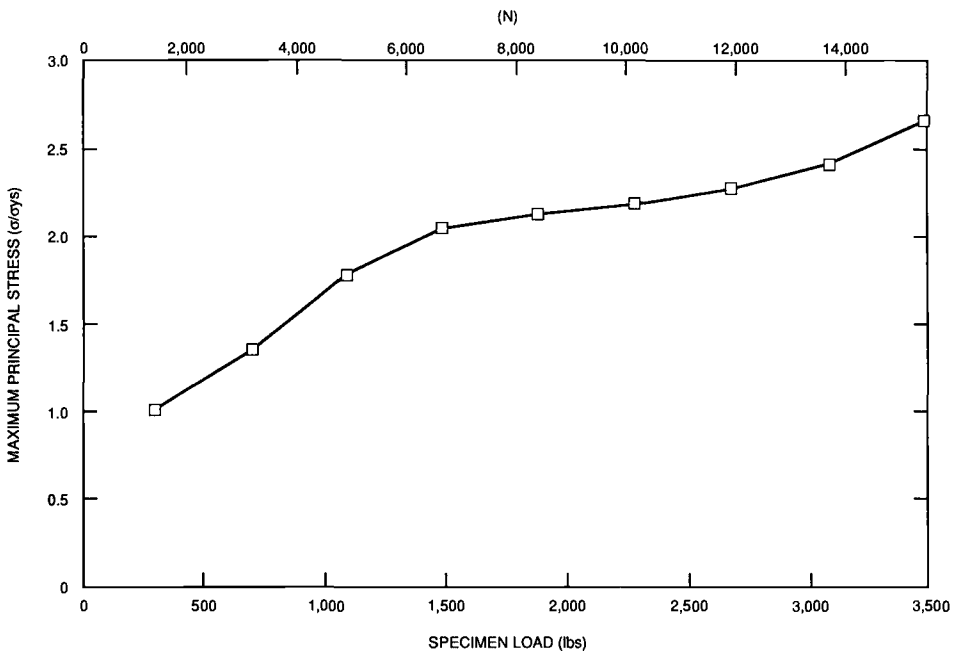


FIG. 14.—Maximum principle stress versus specimen load for cylindrical notched 5Ni-Cr-Mo-V steel slow strain rate specimen.

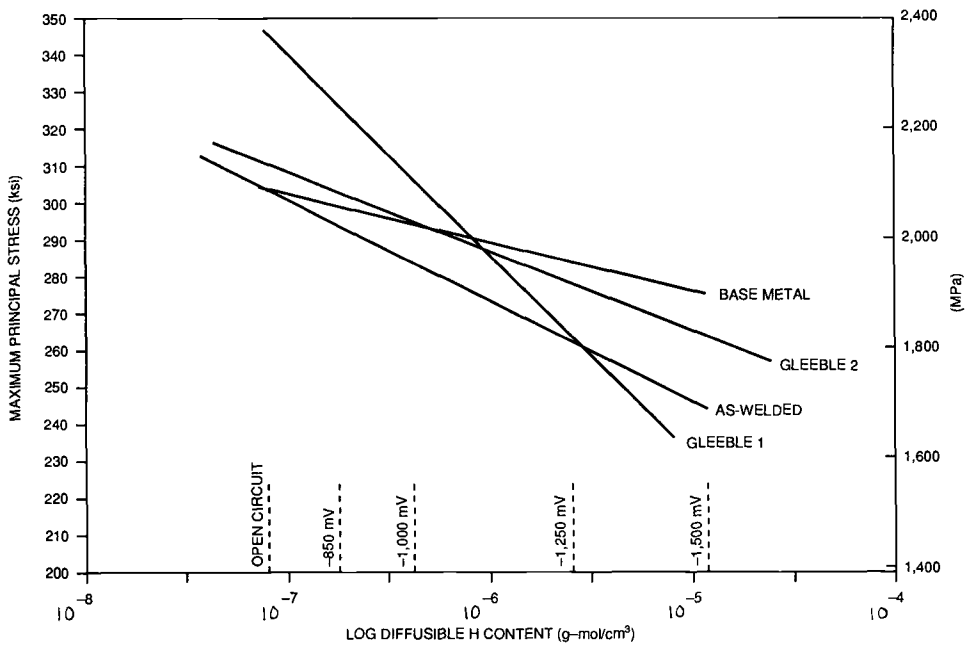


FIG. 15—Maximum principle stress versus diffusible hydrogen content for all material conditions (linear regression fit).

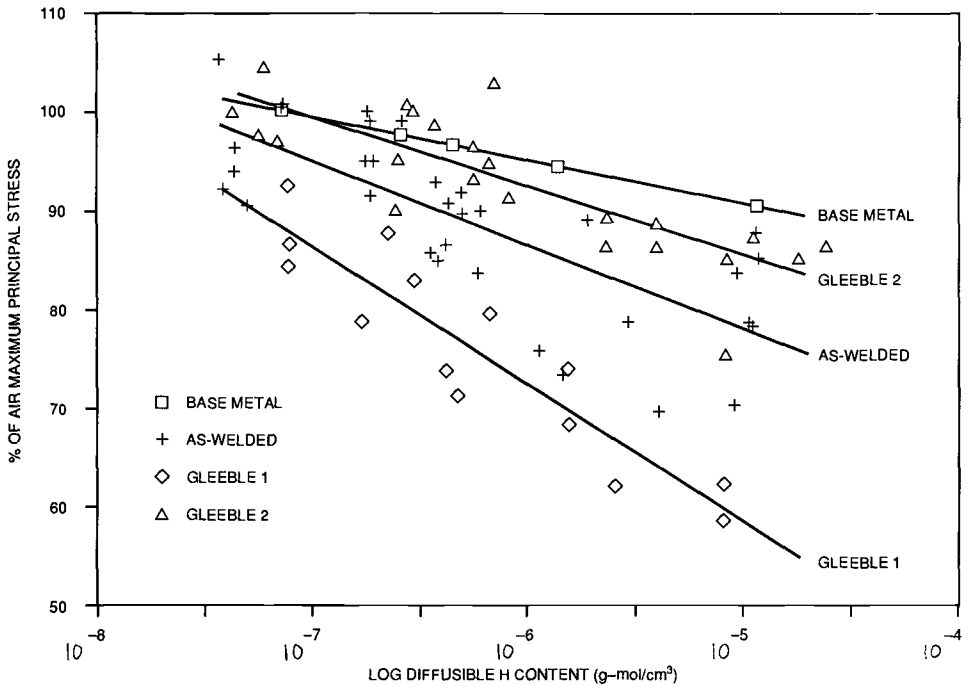


FIG. 16—Normalized maximum principle stress versus diffusible hydrogen content for all specimen conditions (linear regression fit).

weld material. All weld metal conditions exhibited greater susceptibility to hydrogen cracking than the base metal. Both the Gleeble 1 and the as-welded material exhibited significant reductions in maximum stress with increasing hydrogen content.

Also shown in Fig. 16 is the large degree of variability exhibited by the as-welded material compared with all other material conditions. This was not unexpected since the specimens were taken randomly from the weld deposit and therefore are representative of the complex microstructure previously described. This variability is better understood when it is observed that the untempered Gleeble 1 material data describe the lower bound of the as-welded material data and the tempered Gleeble 2 material data describe the upper bound of the as-welded material data.

These results lead to several observations. First, thermal cycling with the Gleeble machine is a viable way to produce a more homogenous specimen representative of certain regions within the weld. More important, the coarse untempered martensitic microstructure present in various regions of a weld deposit seem to be the most susceptible to hydrogen cracking, and the softer, tempered "eyebrow" regions seem to be the most resistant to hydrogen cracking. Finally, the variability in the weld metal data (Table 3) likely results from the inhomogeneity of its microstructure (i.e., it contains a range of microstructures between tempered and untempered martensite as seen in Fig. 3).

## Conclusions

The objective of this research was to quantitatively characterize the conjoint role of steady state hydrogen content and maximum principal stress on the hydrogen cracking initiation susceptibility of 5Ni-Cr-Mo-V steel base plate, weldments, and thermal cycled weldments.

- A correlation of maximum principal stress to steady state diffusible hydrogen content has been developed for 5Ni-Cr-Mo-V steel base plate, weldments, and tempered and untempered weldment regions in 3.5% NaCl solution. For all material conditions, the threshold maximum principal stress for hydrogen cracking initiation decreased as the hydrogen concentration increased.
- The 5Ni-Cr-Mo-V steel base material was shown to be less susceptible to hydrogen embrittlement than any of the welded conditions.
- The variability in as-welded material results is likely attributable to differences in susceptibility to hydrogen assisted cracking between local regions within a given weld deposit. Untempered weld metal was shown to have the greatest susceptibility and tempered weld metal was shown to have the least susceptibility.
- A significant decrease in load carrying capability of the welded materials occurred between a  $-0.85$  V and  $-1.00$  V SCE cathodic protection level. A transition in fracture mode from a ductile, microvoid coalescent fracture to an intergranular fracture was observed between these potentials.

## Acknowledgments

The authors would like to acknowledge the work of T. McClenahan and B. Pearce in the area of slow strain rate testing. We would also like to acknowledge P. Holsberg and J. Blackburn for their assistance in developing and performing the Gleeble thermal cycles, F. Scheffel for her SEM work, and A. Brandemarte for his metallographic assistance.

## References

- [1] Loginow, A. W., "Corrosion and Stress Corrosion of HY-130 (T) Steel and HY-80 Steel in Marine Environments," *U.S. Steel Applied Research Laboratory Report*, July 1967.

- [2] Loginow, A. W., "Four-Year Corrosion Tests of HY-130 and HY-80 Steels in Marine Environments," *U.S. Steel Applied Research Laboratory Report*, July 1969.
- [3] Wacker, G. A., "Effects of Marine Environment on High-Strength Steels," *Materials Performance and the Deep Sea, ASTM STP 445*, American Society for Testing and Materials, Philadelphia, 1969, pp. 68-87.
- [4] Fujii, C. T., "The SCC Properties of Modified High-Strength Steel Plates and Weld Metals," *NRL Report 8325*, Naval Research Laboratory, Washington, DC, July 1979.
- [5] Crooker, T. W., Hauser, J. A. II, and Bayles, R. A., "Ripple-Loading Effects on Stress-Corrosion Cracking in Steels," in *Proceedings of Third International Conference on Environmental Degradation of Engineering Materials—III*, M. R. Louthan, M. R. McNitt, and R. D. Sisson, Jr., Eds., The Pennsylvania State University Press, University Park, PA, 1987.
- [6] Scully, J. R. and Moran, P. J., "The Influence of Strain on Hydrogen Entry, Transport, and Embrittlement of a High-Strength Steel in Aqueous Sodium Chloride Solution," *DTNSRDC/SME-86/109*, March 1987.
- [7] Savage, W. F., Nippes, E. F., and Husa, E. I., "Hydrogen Assisted Cracking in HY-130 Weldments," *Welding Journal Supplement*, s-233, August 1982.
- [8] Savage, W. F., "Apparatus for Studying the Effects of Rapid Thermal Cycles and High Strain Rates on the Elevated Temperature Behavior of Materials," *Journal of Applied Polymer Science*, Vol. 21, No. 6, pp. 303-315.
- [9] Devanathan, M. A. and Stachurski, Z., *Proceedings of the Royal Society*, Vol. A270, 1962, p. 90.
- [10] Klein, P. A., "The Hydrogen Cracking Initiation Susceptibility of High Strength 5Ni-Cr-Mo-V Steel Base Plate and Weldments in Marine Environments," Master's thesis, The Johns Hopkins University, Baltimore, MD, October 1989.
- [11] Scully, J. R. and Moran, P. J., *Corrosion*, Vol. 44, No. 3, 1988, pp. 176-186.
- [12] Scully, J. R. and Moran, P. J., *Environmentally Assisted Cracking: Science and Engineering, ASTM STP 1049*, W. B. Lisagor, T. W. Crooker, and B. N. Leis, Eds., American Society for Testing and Materials, Philadelphia, 1990, pp. 5-29.
- [13] Scully, J. R. and Moran, P. J., *Journal of the Electrochemical Society*, Vol. 135, No. 6, 1988, pp. 1337-1348.
- [14] *Handbook of Corrosion Protection of Steel Structures in Marine Environments*, T. D. Dismuke, S. K. Coburn, and C. M. Hirsch, Eds., AISI, Washington, DC, 1981.
- [15] McBreen, J., Nanis, W., and Beck, W., *Journal of the Electrochemical Society*, Vol. 113, 1966, p. 1218.
- [16] Scully, J. R., Ph.D. thesis, The Johns Hopkins University, Baltimore, MD, 1987.
- [17] Berman, D. A., Beck, W., and Deluccia, J. J., in *Hydrogen in Metals*, I. M. Berstein and A. W. Thompson, Eds., ASM, Metals Park, OH, 1974.
- [18] Challenger, K. D. and Mason, B. J., *Welding Research Supplement to the Welding Journal*, AWS, February 1984.
- [19] Fraser, F. W. and Metzbower, E. A., "Fractographic and Microstructural Analyses of Stress Corrosion Cracking in HY-130 Weldments," *Welding Journal Supplement*, s-112, April 1982.

**Use of Slow Strain Rate Testing for  
Qualification of SCC Resistance of  
Corrosion Resistant Alloys: Case  
Histories in Petroleum Production**

## Problems Associated with Slow Strain Rate Quality Assurance Testing of Nickel-Base Corrosion Resistant Alloy Tubulars in Hydrogen Sulfide Environments

---

**REFERENCE:** Ahluwalia, H. S., "Problems Associated with Slow Strain Rate Quality Assurance Testing of Nickel-Base Corrosion Resistant Alloy Tubulars in Hydrogen Sulfide Environments," *Slow Strain Rate Testing for the Evaluation of Environmentally Induced Cracking: Research and Engineering Applications*, ASTM STP 1210, R. D. Kane, Ed., American Society for Testing and Materials, Philadelphia, 1993, pp. 225–239.

**ABSTRACT:** Slow strain rate testing (SSRT) has been evaluated by the oil and gas industry for investigating anodic chloride/sulfide stress corrosion cracking (SCC). It is used not only as a method of screening nickel-base corrosion resistant alloys (CRA) for downhole use, but also as a quality control test. In this respect a number of end-users are including SSRT as part of the material specification requirements for downhole tubulars. Controversy exists over the suitability and reproducibility of SSRT results in testing nickel-base CRAs. The purpose of this paper is to highlight some of the problems associated with the recent SSRT quality assurance testing of nickel-base CRAs. The effects of surface finish, strain rate, and electrode potential are some of the parameters that should be considered in interpretation of SSRT data. In addition, evaluation criteria and comparison to other test methods will be discussed.

**KEYWORDS:** slow strain rate testing (SSRT), quality assurance, oil and gas, stress corrosion cracking (SCC), nickel-base, corrosion resistant alloys (CRAs), surface finish, strain rate, electrode potential, test methods

Prior to the early 1980s most oil and gas wells were normally completed with low-alloy steel with the use of chemical inhibition to control corrosion. Decreasing reserves and the energy crisis accelerated ventures involving deep hot wells, carbon dioxide (CO<sub>2</sub>) floods, deep-water offshore platforms, and Arctic explorations [1]. The extremely corrosive and deep sour gas wells highlighted issues related to material reliability and safety of operations. Conventional steel tubing and other components rapidly deteriorated by uniform corrosion, localized pitting or crevice corrosion, stress corrosion cracking (SCC), and hydrogen embrittlement (HE) in these hostile environments. Furthermore, the effective use of inhibitors and coatings faced many technical limitations [2].

The inability to inhibit corrosion of conventional steel tubing in deep sour gas production led to the evaluation of nickel-base corrosion resistant alloys (CRAs) [3]. In addition, to the presence of the highly corrosive hydrogen sulfide (H<sub>2</sub>S)/brines and bottom hole temperatures approaching 260°C, the CRA tubulars have to possess the strength capable of handling bottom-hole pressures up to 23 000 psi (159 GPa) at depths more than 15 000 feet (4572 m) [4]. To meet these extreme stress levels, higher yield strengths are achieved by

---

<sup>1</sup> Group leader, Haynes International, Kokomo, IN 46902.

cold-working (750 to 1240 MPa), by precipitation strengthening (960 to 1380 MPa), and cold-working plus aging heat treatments (1240 to 1930 MPa). The selection process of the appropriate material for liners, production tubulars, and accessories is usually dependent on the well environment. Well depth, bottom-hole temperature and pressure, and the presence of hydrogen sulfide/free sulfur (along with other corrosive species: brine, packer fluids, acidizing agents) greatly complicate the material selection process.

Initially, the nickel-base CRAs were thought to be immune to HE based on various laboratory tests. However, further testing showed some high-strength nickel-base CRA tubulars to be susceptible to HE. Specifically, the more corrosion resistant alloys (high molybdenum and low iron, e.g., alloy C-276) in the highly cold-worked and aged conditions were observed to be susceptible to HE. The least corrosion resistant of the nickel-base alloys (containing low to moderate amounts of molybdenum and more iron: e.g., alloys 718 and G-3) are less susceptible to HE. However, these alloys were found to be susceptible to elevated temperature anodic chloride-sulfide SCC. In addition, when evaluating the CRAs for resistance to localized attack in chloride environments, [3,5], alloys G-3 and 718 suffered pitting corrosion.

In view of this, both end-users and manufacturers have conducted extensive programs evaluating the CRAs to determine the suitability for service in sour gas production [6]. The test methods used to qualify and to select high-strength nickel-base CRAs may involve one or more of the test methods listed in NACE standard TM0177-90 [7]. The test methods include standard tensile test, bent-beam test, C-ring test, and double cantilever beam test. Newer test methods such as slow strain rate testing (SSRT) and critical pitting temperature testing are also employed either to obtain additional information for alloy selection or for qualification of production tubulars [8].

The slow strain rate test is being used not only as a method of screening nickel-base CRAs for downhole use, but also as a quality control test. The use as a quality control test has been primarily due to the rapid nature of the test. A number of end-users are including SSRT as part of the material specification requirements for downhole tubulars.

The purpose of this paper is to highlight some of the problems associated with recent quality assurance testing of nickel-base CRAs using the slow strain rate technique.

### **SSRT Material Specification Requirements**

A typical end-user's specification for nickel-base CRA tubulars usually requires the final tubulars to meet certain criteria, such as chemical composition limits, microstructural cleanliness, grain size range, mechanical testing that may involve hardness, tensile and ring flattening properties, and the passing of nondestructive examination and dimensional requirements. In addition, some end-users can require other corrosion or mechanical tests and SSRT before acceptance of the finished tubulars.

The frequency of SSRT is usually different for each end-user. For example, one end-user may require one test per heat while another may require one or more tests per heat treatment lot. Generally one or more specimens are tested in a benign environment, and two or three specimens are tested in the simulated sour environment, which is specified by the end-user. This environment may or may not relate to the actual well environment. An SSRT test specimen passes the acceptance criteria if the reduction in area ratio ( $R_{envir}/R_{air}$ ), elongation ratio ( $E_{envir}/E_{air}$ ) and time to failure ratio ( $T_{f,envir}/T_{f,air}$ ) all exceed a value determined by the end-user (usually 0.8 or 0.9). In addition, there should be no evidence of secondary cracking. In some specifications, scanning electron fractographic examination is required on the failed SSRT specimens. A retest protocol usually also exists. The retest

TABLE 1—Nominal composition of alloys (weight percent).

Common Name	UNS Desig.	Ni	Co	Fe	Cr	Mo	W	Mn	Si	C	Others
C-276	(N10276)	57	2.5 <sup>a</sup>	5	16	16	4	1 <sup>a</sup>	0.08 <sup>a</sup>	0.01 <sup>a</sup>	V = 0.35 <sup>a</sup>
G-50 <sup>(TM)</sup>	(N06950)	50 <sup>b</sup>	2.5 <sup>a</sup>	16	20	9	1 <sup>a</sup>	1 <sup>a</sup>	1 <sup>a</sup>	0.02 <sup>b</sup>	Cu = 0.5 <sup>a</sup>
G-3	(N06985)	44	5 <sup>a</sup>	19.5	22	7	1.5 <sup>a</sup>	1 <sup>a</sup>	1 <sup>a</sup>	0.15 <sup>a</sup>	Cu = 2.5
2550	(N06975)	50		15	25	6		1	1 <sup>a</sup>	0.10	Cu = 1 Ti = 1

<sup>a</sup> Maximum.

<sup>b</sup> Minimum.

G-50 is a trademark of Haynes International, Inc.

provision may require that if the SSRT results do not meet the specification minimum requirements, additional tubulars may be selected for retest. The details of the retest protocol are usually governed by the end-user.

It is important to understand all the parameters and variables that may affect the SSRT test. This is to ensure that the SSRT test is not so severe that it leads to the rejection of a tubular, lot, or heat that would prove acceptable for a particular service condition downhole. At the same time, the SSRT should not be so trivial as to permit the usage of a tubular in circumstances where rapid failure could ensue. The effects of specimen preparatory techniques, discussed in this paper, illustrate how such a variable can have a significant influence on SCC susceptibility or resistance.

### Experimental Procedure

#### Materials

Table 1 summarizes the nominal chemical composition of alloys evaluated in this investigation. These alloys are solid solution strengthened austenitic nickel-base alloys that are cold-worked to achieve the required high yield strengths for downhole use.

#### Environments

The simulated downhole sour environments used in this investigation are outlined in Table 2. The hydrogen sulfide (H<sub>2</sub>S) gas was of 99.5% commercial purity grade. The chemicals used were reagent grade.

TABLE 2—Simulated downhole environments.

Environment A	Environment B
Aqueous Phase NaCl-20% Distilled Water	Aqueous Phase NaCl-25% Distilled Water Acetic acid-0.5%
Gas Phase H <sub>2</sub> S-75 psi (.5 MPa) at RT CO <sub>2</sub> -700 psi (4.8 MPa) at RT	Gas Phase H <sub>2</sub> S-100 psi (.7 MPa) at RT

### SSRT

Details of the test technique have been described by a number of authors [9]. Essentially, the testing procedure outlined in Proposed NACE standard test method T-1F-9 [10] was followed. Specimens machined from tubulars had a nominal gage length of 1 in. (2.54 cm) and a gage diameter of 0.15 in. (0.38 cm). Surface roughness measurements of the specimens were made using a Surfalyzer<sup>®2</sup> 2000 System.

After the specimen has been loaded into the slow strain rate machine and the autoclave cell, an appropriate amount of sodium chloride (NaCl) solution is drawn into the autoclave. The vessel is then deaerated using a cyclic vacuum and nitrogen purge procedure. Several cycles of evacuation (5 min) followed by nitrogen purge (5 min) at 30 psi (207 KPa) are carried out. H<sub>2</sub>S is then introduced at the required pressure and the cell purged for 2 h before final pressurization. Subsequently, the autoclave is heated to the operating temperature. This procedure has been very effective in ensuring complete deaeration and saturation of the solution with H<sub>2</sub>S. It is interesting that the deaeration procedure and the purging procedure can vary from laboratory to laboratory [11].

### Statically Loaded C-Ring

In addition to SSRT, statically loaded C-ring specimens were also tested for comparison purposes. The C-ring specimens were prepared and loaded according to NACE Standard TM0177-90, Methoc C [7]. The deaeration procedure and gas charging procedure are similar to that described for SSRT. Specimens are removed from the autoclave for examination at intervals of 48, 96, 168, 240, 336, 504, 744, and 1008 h. The specimen is considered to have failed at the first sign of cracking. After each time interval, fresh solution is introduced and the deaeration and purging procedure repeated. The bolts for straining are typically made from the same alloy composition or from alloy C-276.

In creviced C-ring tests, a thin strip of the same alloy composition is gas tungsten arc spot welded on the outside diameter of the C-ring. This provides a potential site for crevice corrosion initiation. A typical C-ring sample with a crevice is shown in Fig. 1.

## Results and Discussion

### Effect of Surface Finish

Table 3 shows quality assurance slow strain rate data generated at two approved labs on UNS N06950 in environment A at 218°C and at a strain rate of  $4 \times 10^{-6} \text{ s}^{-1}$ . Tests were initially conducted at Lab A. Data from Lab A indicated that tubulars from six lots failed to meet the specification minimums and were thus deemed to be unsatisfactory for downhole use. The results were surprising because the tubulars exhibited the correct chemical composition, microstructure, and strength. In the selection process the alloy had been extensively evaluated in this test environment. Results such as these can cause significant delays and therefore have cost implications to both the end-user and the manufacturer. However, using the retest protocol, tests were conducted at Lab B on specimens taken from the same tubulars. The results from Lab B showed all the embrittlement ratios to be above the specification minimums. The differences between the two laboratories were too large to be explained on the basis of interlaboratory scatter or differences in type of machines used.

---

<sup>2</sup> Surfalyzer, trademark of Federal Products Corp.

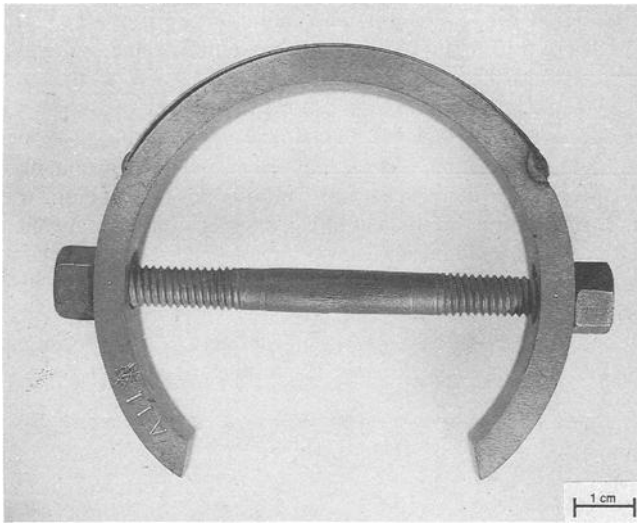


FIG. 1—Artificially creviced C-ring specimen. Note that the alloy strip is spot welded onto the outside diameter of the C-ring to create a crevice.

Detailed evaluation of the testing procedures and test specimens indicated that the main difference between the results from the two laboratories appeared to be the surface quality of the SSRT specimens. Lab A used a vendor that machined the specimens using a turning tool whereas specimens used by Lab B were manufactured by grinding. Following surface polishing, the average roughness of specimens from Lab A was 41  $\mu\text{in}$ . (1.03  $\mu\text{m}$ ) with the

TABLE 3—Quality assurance slow strain rate testing UNS N06950 tubulars.

Tubular Number	Time to Failure Ratio*		Elongation Ratio*		Reduction in Area Ratio*	
	Lab A	Lab B	Lab A	Lab B	Lab A	Lab B
1	0.83	0.96	0.70	1.13	0.20	1.05
	0.96	0.83	0.92	0.95	0.96	1.06
2	0.83	0.83	0.74	1.02	0.45	1.03
	1.08	0.83	1.03	1.02	1.00	1.03
3	1.03	0.85	1.02	0.89	0.79	0.93
	0.95	0.91	0.95	1.01	0.99	0.98
4	1.01	0.84	1.03	0.86	0.72	0.94
	0.78	0.88	0.70	0.91	0.61	0.90
5	0.78	0.84	0.66	0.94	1.23	0.93
	1.08	0.85	1.06	1.00	0.39	1.11
6	0.80	1.05	0.72	1.07	0.73	0.94
	0.66	1.04	0.54	1.00	0.39	1.11
Specification Minimum	0.8		0.8		0.8	

Environment: 20% NaCl + 75 psi (0.5 MPa) H<sub>2</sub>S + 700 psi (4.8 MPa) CO<sub>2</sub> at 218°C.

\* Ratio of test in environment to test in air.

maximum value being 58  $\mu\text{in.}$  ( $1.45 \mu\text{m}$ ) and minimum 25  $\mu\text{in.}$  ( $0.63 \mu\text{m}$ ). The average values from Lab B were 5  $\mu\text{in.}$  ( $0.125 \mu\text{m}$ ) with maximum value being 10  $\mu\text{in.}$  ( $0.25 \mu\text{m}$ ) and minimum being 4  $\mu\text{in.}$  ( $0.1 \mu\text{m}$ ).

The scanning electron micrograph in Fig. 2 shows the surface of an SSRT specimen tested by Lab A in air at 218°C. The yawed mechanical tears in the gage section are clearly visible. Clearly, if a similar specimen was to be tested in a sour environment the susceptibility to SCC could be dramatically increased. This would result in low embrittlement ratios, as illustrated in Fig. 3. In addition, analysis of SSRT data tested in air showed a large variation in reduction in area ratios. Comparing the reduction in area ratios of the air specimens results in reduction in area ratios of 0.78, 0.77, and 0.74. These specimens would therefore fail to meet the specification minimums. Clearly, this is not logical.

To evaluate the influence of specimen surface roughness, SSRT specimens were prepared using the grinding and turning operations. SSRT tests were conducted in environment B at

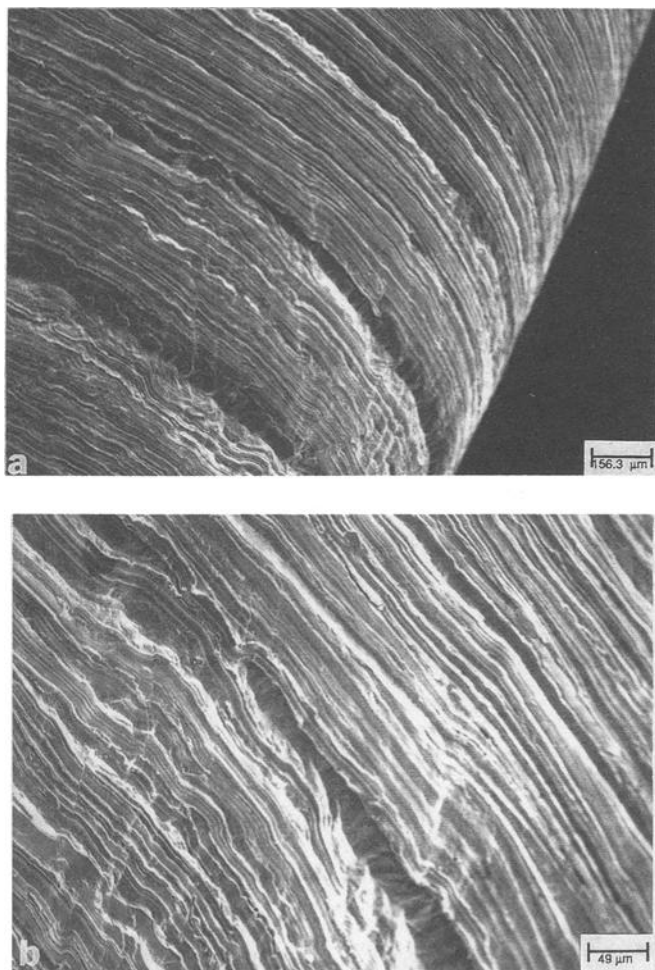


FIG. 2—(a) Scanning electron micrograph showing yawed turning marks near the fracture surface on the gage section of UNS N06950 SSRT specimen tested in air at 218°C by Lab A. (b) Higher magnification of (a) showing crack initiation and coalescence at a turning mark.

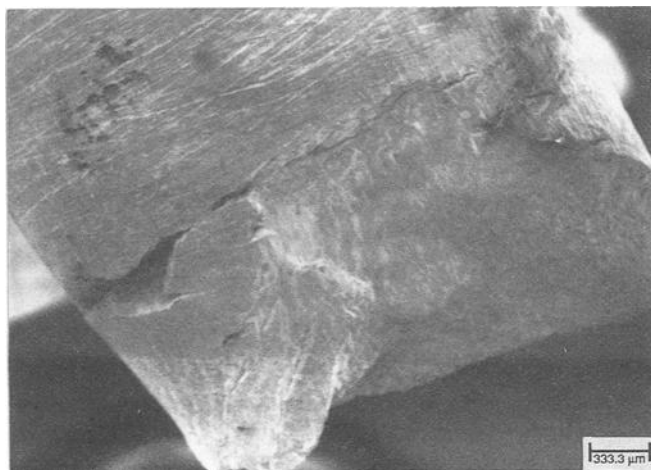


FIG. 3—Scanning electron micrograph showing tearing in the vicinity of the fracture surface in a UNS N06950 specimen tested in environment A at 218°C by test Lab A. Ductility ratios:  $T_{envir}/T_{air}$ : 0.66,  $E_{envir}/E_{air}$ : 0.54,  $R_{envir}/R_{air}$ : 0.39.

204°C at a strain rate of  $4 \times 10^{-6} \text{ s}^{-1}$ . The reduction in area to fracture, in specimens that were ground, was on average 70%, and for turned specimens was 50%. Figure 4 shows the typical gage section surface characteristics of ground and turned specimens before and after testing in the test environment. Specimens prepared by the turning operation had secondary cracks visible that were associated with turning marks. The ground specimens showed no evidence of cracking.

Operations such as grinding and turning inevitably affect the subsurface layers of a specimen and this in turn can influence crack initiation. Cracks are likely to initiate at stress concentrators such as the troughs of turning marks where the net tensile stress is highest. Abusive machining operations can also create high tensile residual stresses as a result of inhomogeneous plastic deformation at the subsurface. It is well-known that bulk residual stresses can markedly affect SCC initiation. The residual stresses decrease with increasing distance below the surface [12]. Although the deleterious effect of stress concentrators and, therefore, surface finish on crack initiation is well known, little attention has been given to its significance on SSRT results [13]. Clearly, in the case of cold-worked, high-strength CRAs, specimen surface characteristics significantly affect the susceptibility or resistance to cracking. To avoid erroneous results and conclusions, nickel-base SSRT specimens must be prepared by machining and polishing techniques that do not create stress concentrators and high tensile residual stresses. Ensuring a surface finish of 10 μin. (0.25 μm) or less and specimen preparation using low-stress grinding techniques are ways of eliminating errors due to surface effects.

#### *Effect of Strain Rate*

Where film formation conditions exist, the crack tip will remain bare only if the rate of film formation is exceeded by the rate at which clean metal is formed by straining. Varying the strain rate may be expected to result in SCC being at a maximum at intermediate strain rates but not being observed at relatively high or low rates [14–16].

For every alloy and environment combination it is prudent to determine the critical strain rate range for maximum susceptibility to SCC. Most of the SSRT tests in simulated sour

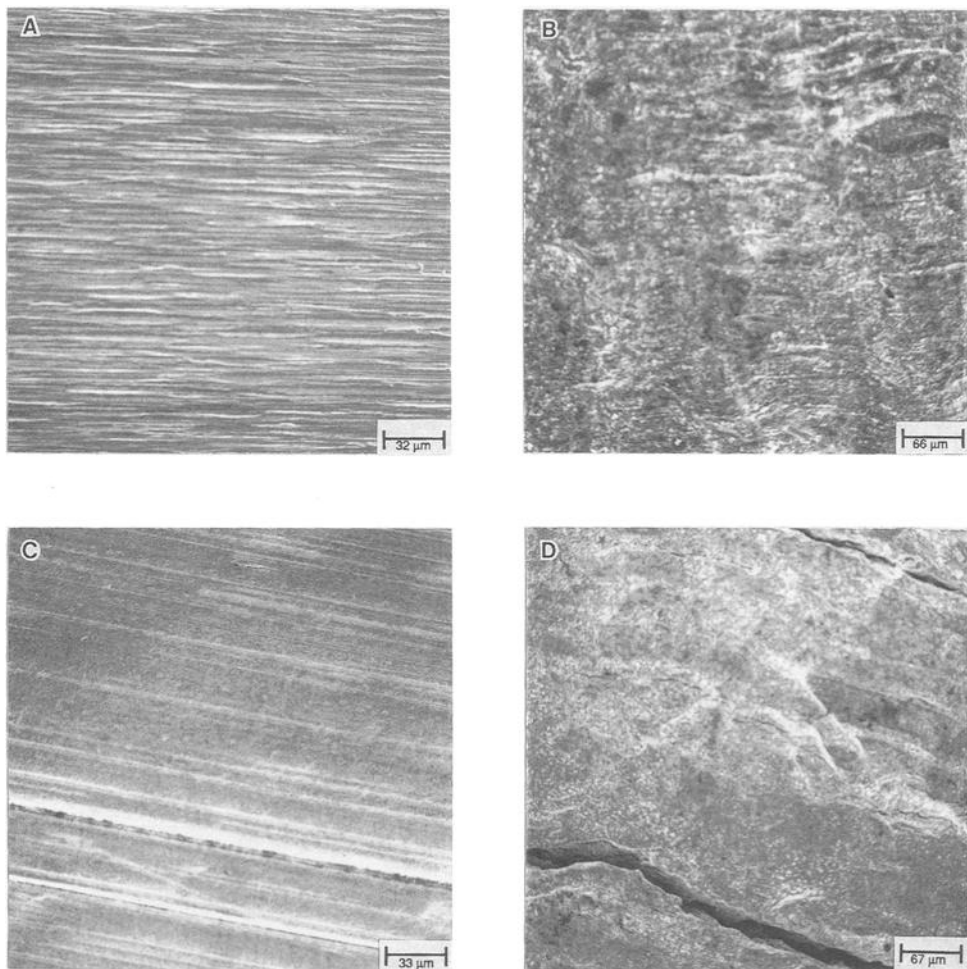


FIG. 4—Micrograph of UNS N06950 SSRT specimens. (a, b) Ground specimen surface before and after testing, respectively. (c, d) Turned specimen surface before and after testing, respectively. Note that the cracks in micrograph (d) are associated with turning marks.

gas environments have generally been conducted at a strain rate of  $4 \times 10^{-6} \text{ s}^{-1}$ . In the present investigation the effect of strain rate on SCC susceptibility was evaluated above the critical cracking temperature for UNS N06985. Figure 5 shows the reduction in area to fracture as a function of strain rate on UNS N06985 tested in environment B. Cracking was confirmed by fractographic examination. The width of the optimum strain rate range increases as the temperature and therefore the severity of the environment increases. Since SCC is related to film fracture, corrosion reactions rather than stress have a greater influence on the kinetics of film fracture in aggressive environments. The critical strain rate is a function of alloy, environment, and temperature.

A wide range of alloys exists within the nickel-base CRA family having varying resistance to SCC. Clearly, using one strain rate, environment, and temperature can result in erroneous conclusions when evaluating various CRAs for ranking purposes.

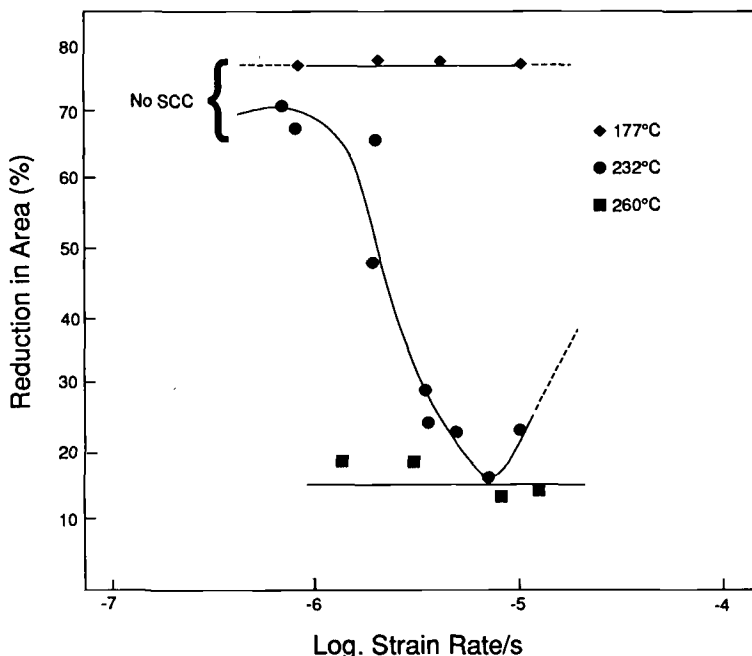


FIG. 5—Reduction in area to fracture as a function of strain rate on UNS N06985 in environment B at various temperatures.

*Effect of Electrode Potential*

In any particular alloy-environment system SCC occurs within a specific electrode potential range [17–19]. Essentially, crack formation and propagation depends on a critical balance between activity and passivity at the crack tip; that is, film rupture must produce sufficient dissolution to advance the crack, yet the crack sides must remain relatively passive. Only in a certain range of potential will this balance between electrochemical activity on fresh surface and relative passivity on crack walls be achieved. This range is the critical potential range.

Ueda and Kudo [20] have shown that UNS N08825 exhibits greater susceptibility to SCC in sour brine environment at 50 mv more noble than the open circuit potential. In situations where there is a loss of electrical isolation in the autoclave during testing, the potential has been shown to shift into the cracking range. The presence of oxygen, due to leaks or improper deaeration procedure, can also lead to changes in potential that can accelerate SCC. In the present investigation a sample of UNS N06950 was tested in environment B. During the test a leak in the seal introduced oxygen into the cell, resulting in severe cracking in an alloy and environment system expected to be immune. This is illustrated in Fig. 6.

Similarly, introduction of elemental sulfur to the test solution has been shown to change the open circuit potential and move the potential within the cracking range [21]. The accelerating effect of sulfur is dependent on whether it is in solution or undissolved as a separate solid or liquid phase. When sulphur is in solution, in the form of hydrogen polysulfides, the cathodic reaction is diffusion controlled, similar to the oxygen corrosion mechanism [21–25]. Under these conditions, susceptibility to SCC is only moderate. If, however, elemental sulfur particles are in direct contact with the sulfide covered metal surface, then

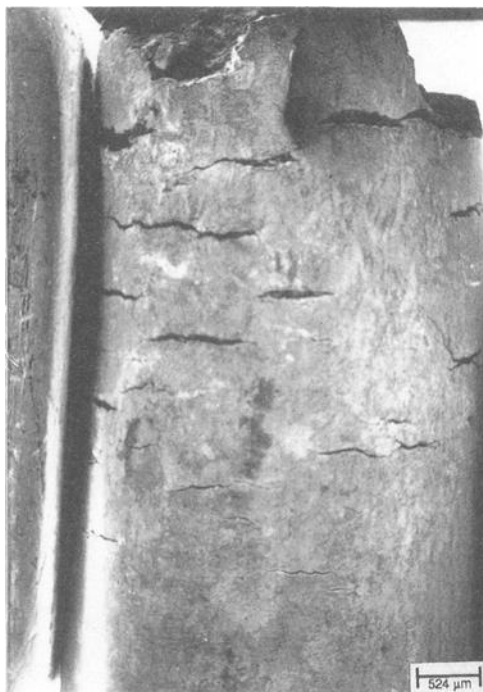


FIG. 6—Fracture characteristics of UNS N06950 specimen tested in environment B at 230°C in the presence of oxygen.

susceptibility to SCC is dramatically increased. Sulfur is unlikely to deposit on tubulars downhole since the high pressures and temperatures' downhole increase the solubility of sulfur and thus decrease the susceptibility to SCC. It is interesting that test environments required by some specifications include elemental sulfur. Choi [26] has reported that the way sulfur is charged into an SSRT autoclave greatly affects the susceptibility to SCC. The methods investigated included dry charging, charging by using a sleeve around the specimen, and charging sulfur in a capsule in the autoclave away from the specimen but allowing any sulfur reactions to occur.

#### *SSRT Evaluation Criteria for Tubulars*

Most specifications for SSRT employ the measurement of specimen ductility to determine cracking susceptibility. Time to failure, elongation, and reduction in area are the parameters used. The ductility measurements in a benign environment are compared to those in the simulated downhole environment. A critical value is assigned to the ductility ratio and test specimens with a ratio above this value are assessed to be SCC resistant. Test specimens with ratios below the critical value are judged to be susceptible.

A wide statistical scatter exists in measuring time to failure ratios. Small differences in specimen diameter can cause time to failure ratios to vary. In some commercially available SSRT equipment the cross-head speed has been shown to vary from test to test and, as pointed out by McIntyre [27], the difference between  $3.5$  and  $4.0 \times 10^{-6} \text{ s}^{-1}$  in cross-head speed can result in a 14% decrease in time to failure. Such a difference may be significant

in relationship to specification minimums. Further, the initiation process for SCC is somewhat random and therefore the initiation time can vary significantly. It is also difficult to decide whether a particular tubular, that has a longer time to failure, has better crack initiation resistance or slower crack propagation compared to one with a shorter time to failure.

Elongation measurements are also prone to wide scatter. Ikeda [28] has shown a wide scatter in elongation measurements of alloy UNS N06985 tested in environment B at 177°C. The scatter is thought to be due to the homogeneous plastic deformation of the gage section. General corrosion and pitting in the gage section will also affect the elongation ratios.

The only reliable and acceptable methods of confirming SCC is by metallographic or fractographic examination. Once information is obtained by either of these techniques, then reduction in area ratios can be used to quantify the susceptibility. Metallographic measurements of crack length and therefore, crack velocity from secondary cracks along the gage section is also a useful parameter that can be used.

Distinction between different tubulars from the same alloy based upon ductility specification minimums is difficult to achieve without good quality control and a knowledge of the test apparatus used.

#### *Comparison with Other Test Methods*

In the present investigation tubular samples from UNS N06950 aged at 870°C for 15 min were tested using the slow strain rate and constant strain (C-ring) techniques. The aging treatment generated gross precipitation in the grain boundaries and the matrix. This microstructure would be expected to lead to SCC. The tests were conducted in environment B at 204°C. Analysis of the SSRT specimen after testing showed the fracture surface to be ductile in nature, and no secondary cracks were visible in the gage section. In contrast, a C-ring test statically loaded to 100% of yield showed severe cracking after 96 h. The precipitated grain boundaries and intergranular SCC in the C-ring specimen is illustrated in Fig. 7. These preliminary results clearly show the insensitivity of the SSRT test to an aged microstructure.

Watkins et al. [29] tested alloy 2550 using the constant strain test (C-ring) and SSRT in 25% NaCl pressurized with 2.4 MPa H<sub>2</sub>S and 1.7 MPa CO<sub>2</sub> at 232°C. SSRT showed the material to be susceptible to SCC whereas the six-month C-ring test showed no susceptibility.

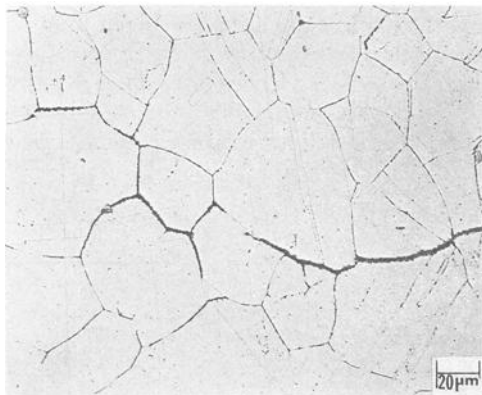


FIG. 7—Intergranular SCC in UNS N06950 C-ring specimen aged at 870°C for 15 min, tested in environment B at 204°C.

The same authors also used SSRT to evaluate alloy UNS N06975 and some other less corrosion resistant alloys in environment B [30]. The SSRT results showed alloy N06975 to be more susceptible to SCC than lesser alloyed samples. Previously, alloy N06975 had been shown to have the best SCC resistance of all the specimens tested using the C-ring test.

Craig et al. [31] evaluated a large number of alloys for the Madden Deep Unit in Wyoming using SSRT and statically loaded C-rings. The environment used was 5% NaCl 0.5 acetic acid with 100 ppm sulfur at H<sub>2</sub>S pressure of 6.2 MPa and CO<sub>2</sub> pressure of 6.9 MPa. The results showed alloy 825 (UNS N08825) not to be susceptible to SCC in this environment although other investigators have observed cracking under essentially similar conditions with 25% NaCl using C-ring. It is thought that the reason for this discrepancy may be related to chloride content.

Ueda and Kudo [20] evaluated alloy C-276 in a sulfur containing sour brine environment at 260°C. The SSRT showed no susceptibility, whereas C-ring tests showed susceptibility to SCC. The reason for this difference is likely to be the effect of the method of charging sulfur into the autoclave. However, they also report that for ranking purposes SSRT results compared favorably with C-ring tests in various sour brine environments.

Clearly, the SSRT is subject to great variability in test results. In some situations SSRT indicates susceptibility when long-term statically loaded C-ring specimens have shown immunity. In other instances, SSRT results have indicated immunity when statically loaded specimens have failed.

### Alternative Accelerated Test Method

#### *Crevice C-Ring*

SSRT has been advocated because long times are required for crack initiation in statically loaded C-ring tests resulting in test duration of 1000 h or longer.

One way of shortening test times is to conduct C-ring tests with a crevice, (Fig. 1). A thin strip of the same alloy is gas tungsten arc spot welded onto the outside diameter of the C-ring to provide a potential site for crevice corrosion initiation. This test method has been advocated by Place et al. [6]. The gap formed between the C-ring surface and the strip is, of course, variable. This is intentional, since the optimum gap dimensions to promote SCC initiation is alloy and test dependent and therefore not known.

In the present investigation, statically loaded artificially creviced C-ring tests were conducted on UNS N06975, N06985, and N06950 in environment B at 204°C and on UNS N10276 at 232°C. Table 4 summarizes the results obtained from the creviced C-ring tests. Figure 8 shows the cracks observed at the apex of the specimens under the crevice. Some crevice corrosion was also observed under the alloy strip. Clearly, with the severe test conditions used in these tests, crack initiation is promoted and thereby shortens the test times. C-ring tests without crevice did not fail under the same environmental conditions

TABLE 4—Statically loaded C-rings. Artificially creviced 25% NaCl + 0.5 acetic acid + 0.7 MPa H<sub>2</sub>S.

Alloy	Yield Strength, MPa	Temperature, °C	Approx. No. of Cracks	Time to Failure, h
2550	862	204	>100	48
G-3	750	204	60	240
G-50	951	204	50	168
C-276	938	232	15	504

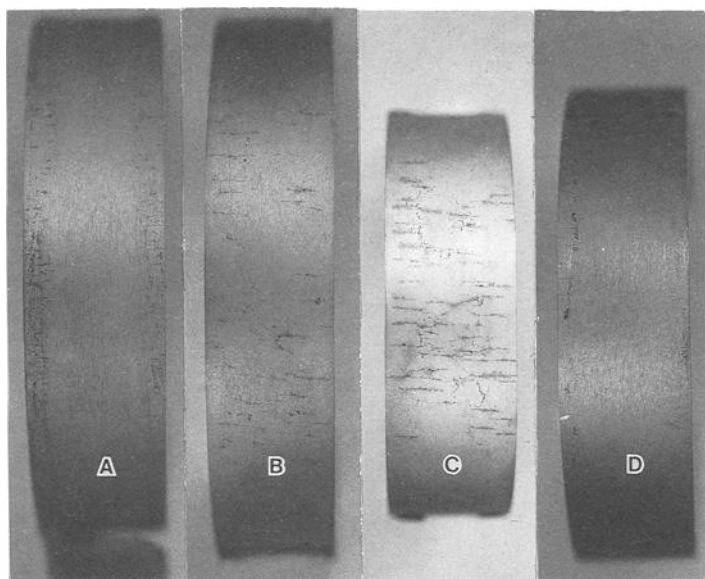


FIG. 8—Photomicrograph of the apex of artificially creviced C-ring specimens tested in environment B. (a) UNS N06950, (b) UNS N06985, (c) UNS N06950, (d) UNS N10276.

after 1000 h. These results raise the question on the value and use of accelerated test methods, such as SSRT and creviced C-ring test. In one application UNS N10276 has had three years of successful service in a deep sour gas well with 10% H<sub>2</sub>S and 5% chloride brine [32], whereas in the accelerated test method previously discussed, UNS N10276 has been shown to be susceptible to SCC.

Better control of the crevice gap and optimization of the stress level would make this method a more reliable and rapid method for ranking alloys.

## Conclusions

- (1) Slow strain rate testing permits a rapid method for ranking alloys for material selection purposes. However, it is subject to great variability in test results and further evaluation of the test method is required before it can be successfully used as a quality control test method.
- (2) Variances in specimen surface preparation can lead to erroneous results and conclusions. Nickel-base SSRT specimens must be prepared by machining and polishing techniques that avoid creating stress concentrators and high tensile residual stresses. Ensuring a surface finish of 10  $\mu\text{in.}$  (0.25  $\mu\text{m}$ ) or less and specimen preparation using low stress grinding techniques are ways of eliminating errors due to surface effects.
- (3) The critical strain rate range for maximum susceptibility to SCC for every alloy and environment combination should be determined.
- (4) The only reliable and acceptable methods of confirming SCC is by metallographic or fractographic examination. Once confirmation is obtained by either of these techniques, then reduction in area ratios can be used to quantify the susceptibility.

### Acknowledgments

The author wishes to acknowledge D. C. LaCluyse for his assistance in performing the experiments. Appreciation is also extended to D. S. Acuncius and L. H. Flasche for their helpful discussions during the preparation of the manuscript.

### References

- [1] Hamby, T. W., Broussard, C. P., and Taylor, D. B., *Journal of Petroleum Technology*, June 1976, p. 629.
- [2] Ahluwalia, H. S., Ishwar, V. R., and Petersen, G. J., NACE CORROSION/91, Paper No. 119, Cincinnati, OH, March 1991.
- [3] Watkins, M. and Greer, J. B., *Journal of Petroleum Technology*, Vol. 28, 1976, p. 698.
- [4] Tuttle, R. N., *Journal of Petroleum Technology*, July 1987, p. 756.
- [5] Asphahani, A. I., "High Performance Alloys for Deep Sour Gas Wells," *Proceedings of the 7th International Congress on Metallic Corrosion*, Rio de Janeiro, 1978, p. 976.
- [6] Place, M. C., Rhodes, P. R., and Mack, R. D., CORROSION/91, Paper No. 1, Cincinnati, OH, March 1991.
- [7] NACE Standard Test Method TM0177-90 "Laboratory Testing of Metals for Resistance to Sulfide Stress Cracking in H<sub>2</sub>S Environments," NACE, Houston, TX.
- [8] Wilhelm, S. M. and Currie, D. M., Production Operations Symposium, Society of Petroleum Engineers, OK, April 1991.
- [9] *Stress Corrosion Cracking: The Slow Strain Rate Technique*, ASTM STP 665, G. M. Ugiansky and J. H. Payer, Eds., American Society for Testing and Materials, Philadelphia, 1979.
- [10] T-1F-9 Proposed NACE Standard Test Method, "Slow Strain Rate Test Method for Screening Corrosion Resistant Alloys for Stress Corrosion Cracking in Sour Oilfield Service," NACE, Houston, TX, 1989.
- [11] Discussion at NACE'92, T-1F-9 Committee Meeting, Nashville, TN, April 1992.
- [12] Koster, W. P. and Kohls, J. B., Society of Manufacturing Engineers, SMP Paper No. IQ 72-207, 1972.
- [13] Paxton, H. W. and Procter, R. P. M., Paper No. EM 68-520, presented at American Society of Tool and Manufacturing Engineers Symposium, Pittsburgh, PA, 1968.
- [14] Ahluwalia, H. S., Ph.D. thesis, University of Newcastle upon Tyne, U.K., 1987.
- [15] Parkins, R. N., *Stress Corrosion Cracking: The Slow Strain Rate Technique*, ASTM STP 665, G. M. Ugiansky and J. H. Payer, Eds., American Society for Testing and Materials, Philadelphia, 1979, pp. 5-25.
- [16] Kim, C. D. and Wilde, B. E., *Stress Corrosion Cracking: The Slow Strain Rate Technique*, ASTM STP 665, G. M. Ugiansky and J. H. Payer, Eds., American Society for Testing and Materials, Philadelphia, 1979, pp. 97-112.
- [17] Diegle, R. B. and Boyd, W. K., *Stress Corrosion Cracking: The Slow Strain Rate Technique*, ASTM STP 665, G. M. Ugiansky and J. H. Payer, Eds., American Society for Testing and Materials, Philadelphia, 1979, pp. 26-46.
- [18] Payer, J. H., Berry, W. E., and Boyd, W. K., *Stress Corrosion—New Approaches*, ASTM STP 610, H. L. Craig, Ed., American Society for Testing and Materials, Philadelphia, 1976, pp. 82-93.
- [19] Theory of Stress Corrosion Cracking in Alloys, J. C. Scully, Ed., NATO, Brussels, March, 1971.
- [20] Ueda, M. and Kudo, T., NACE CORROSION/91, Paper No. 2, Cincinnati, OH, 1991.
- [21] Miyasaka, A., Denpo, K., and Ogawa, H., NACE, CORROSION/88, Paper No. 70, St. Louis, MO, 1988.
- [22] Schmitt, G., NACE CORROSION/90, Paper No. 39, Las Vegas, 1990.
- [23] Sridhar, N. and Corey, S. M., NACE CORROSION/89, Paper No. 12, New Orleans, LA, 1988.
- [24] Rhodes, P. R., NACE CORROSION/86, Paper No. 322, Houston, TX, 1986.
- [25] Wilhelm, S. M., NACE CORROSION/88, Paper No. 77, New Orleans, LA, 1988.
- [26] Choi, H. J., ASTM Committee G-1 Workshop, San Antonio, TX, 1990.
- [27] McIntyre, D. R., *Hydrogen Embrittlement: Prevention and Control*, ASTM STP 962, L. Raymond, Ed., American Society for Testing and Materials, Philadelphia, 1988, pp. 178-189.
- [28] Ikeda, A., Ueda, M., and Okamoto, Y. E., NACE CORROSION/90, Paper No. 272, Las Vegas, 1990.

- [29] Watkins, M., Chaung, H. E., and Vaughn, G. A., NACE CORROSION/87, Paper No. 283, San Francisco, CA, 1987.
- [30] Chaung, H. E., Watkins, M., and Vaughn, G. A., NACE CORROSION/85, Paper No. 227, Houston, 1985.
- [31] Craig, B. D., Collins, J. C., Patrick, P., and Gilbert, T., *Materials Performance*, Vol. 30, No. 12, 1991, p. 51.
- [32] NACE Publication 1F192, Item No. 54290, "Use of Corrosion Resistant Alloys for Resistance to Environmental Cracking in Oilfield Environments," NACE 1992.

Akio Ikeda,<sup>1</sup> Masakatsu Ueda,<sup>2</sup> and Hiroshi Okamoto,<sup>2</sup>

## The Role of Slow Strain Rate Testing on Evaluation of Corrosion Resistant Alloys for Hostile Hot Sour Gas Production

---

**REFERENCE:** Ikeda, A., Ueda, M., and Okamoto, H., "The Role of Slow Strain Rate Testing and Evaluation of Corrosion Resistant Alloys for Hostile Hot Sour Gas Production," *Slow Strain Rate Testing for the Evaluation of Environmentally Induced Cracking: Research and Engineering Applications, ASTM STP 1210*, R. D. Kane, Ed., American Society for Testing and Materials, Philadelphia, 1993, pp. 240–262.

**ABSTRACT:** The slow strain test is an effective technique for evaluating the application of high-nickel corrosion resistant alloy tubulars for hostile deep sour wells. To increase that effectiveness, it is important that maximum exchangeability among various data from different laboratories be established. In order to accomplish this, it is necessary to minimize data scattering and maximize the consistency of phenomena by controlling test methods, i.e., specimen dimensions, test machine characteristics including strain rate control, test procedures, and degradation indices. Effect of strain rate on the SCC susceptibility of CRA in such hostile environments tends to be the highest at  $1 \times 10^{-6}$  to  $10 \times 10^{-6} \text{ s}^{-1}$ , similar to the active pass SCC of carbon steels reported so far. The use of SSRT to assess the contribution of environmental factors on SCC and corrosion is objective and mostly consistent with the results from the other SCC test methods. The effect of electrical insulation between specimen and test equipment and application of anodic polarization on the SSRT is analyzed in this paper. From the engineering viewpoint for material selection, it is recommended that such a galvanic effect should be avoided. It is also recommended that SCC data at the off-gage section should be eliminated and vacuum evacuation in the deaeration process should be used. A test machine that minimizes fluctuation of strain rate control has been developed and used at one of our mills for corrosion resistance quality assurance of mass-produced CRA tubulars. Results are discussed in this paper.

**KEYWORDS:** slow strain rate testing (SSRT) SCC corrosion resistant alloys (CRAs), Cr-Ni-Mo alloys, active pass corrosion, APC, sour gas, deep well, tubular products, OCTG, line pipe,  $\text{H}_2\text{S}$ ,  $\text{CO}_2$ ,  $\text{Cl}^-$

Slow strain rate testing (SSRT) has been widely used to aid the selection of corrosion resistant alloys (CRAs) for use in hostile environments such as deep sour gas wells. In order to effectively use various data from different sources, it is necessary to define simply the physical meaning of SSRT data and to clarify most of the factors affecting variability in reported SSRT results. For this purpose, it is essential to minimize data variation resulting from test procedures, equipment differences, and differing measures of evaluation. This means that a standardization of the SSRT method is essential. As for test equipment, various SSRT instruments have been installed and used in different laboratories. There are many variations even in the tensile test machine, which is an essential constituent of SSRT tools.

---

<sup>1</sup> Osaka Head Office, Sumitomo Metal Industries, Ltd., Osaka 541, Japan.

<sup>2</sup> Iron and Steel Research Laboratories, and Pipe and Tube Works, respectively, Sumitomo Metal Industries, Ltd., Hyogo 660, Japan.

In the attempt to standardize the test method, it must be taken into account that different tensile machines will be used even in the future. Recently, standardization of SSRT has been discussed in the National Association of Corrosion Engineers [1]. This discussion generally contributes to a mutual understanding of SSRT techniques.

The authors have investigated the application of SSRT techniques for the evaluation of CRA tubulars for hostile deep sour gas wells. In this paper, information concerning the SSRT method and procedure, stress corrosion cracking (SCC) criteria, and effect of environmental factors and effect of anodic polarization on SSRT are reviewed, mainly on the basis of the authors' experience. Finally, a case study of application of SSRT for quality assurance of mass-produced CRA tubulars is presented.

**Discussion**

Materials discussed in this paper are shown in Table 1.

*Concept of SCC Evaluation of CRAs by SSRT*

A concept of evaluation of high-nickel CRAs using SSRT is shown in Fig. 1 [2]. The objective is to evaluate the environmental degradation, particularly SCC susceptibility, in hostile deep sour gas conditions, which have various chemicals such as H<sub>2</sub>S, CO<sub>2</sub>, S, Cl<sup>-</sup>, acetate ion, etc., affecting corrosivity. In SSRT, a tensile deformation is continuously introduced into the material. As the mechanical effect of this deformation increases, the passive film on the surface of CRAs is artificially destroyed, unless a repairing reaction occurs. In an open air environment, a passive film similar to the original one is reformed instantly. It is noted that corrosion itself plays an essential role in both film destruction and subsequent reformation. In the hostile environment, corrosion resistance of high-nickel CRAs such as UNS N10276 is brought about by the double-layer film structure, which is composed of an upper layer of Ni-S<sub>x</sub> and an under layer of Cr-oxide. This film structure is completely different from a passivation film formed in open air [3,4]. In the hostile environment, at the area where the passivation film is destroyed during the continuous extension in SSRT, a dissolution reaction of the matrix occurs. If dissolved metallic ions repair the passivation film

TABLE 1—Materials referred to in this paper.

Mark*	UNS No.	Chemical Composition (wt.%)			
		Ni	Cr	Mo	Others
316L	S31653	10/13	17/19	2.5/3.5	
22Cr D.S.	S31803	4.5/6	21/23	2.5/3.5	0.12N
25Cr D.S.	S31260	5.5/7	24/26	2.5/3.5	0.14N(Cu, W)
SM2030	N08135	28/32	20/25	3.5/4.5	
SM2535	N08534	30/40	24/28	3.0/4.0	
SM2242	N08825	38/46	20/23	3.0/4.0	1Ti, 2Cu
SM2550	N06975	48/53	24/27	5.0/7.0	Cu
SM2060Mo	N06060	54/58	20/23	12/14	Nb, W, Cu
Alloy G3	N06985	48/53	20/23	6.0/7.5	1W, 1Nb
Alloy 625	N06625	60/67	20/23	8.0/10	3Nb
SM-C276	N10276	58/65	14/17	15/17	3W, 5Fe, 1Co

\*NOTE: An expression of SM2535-110, for example, means the SM2535 alloy with specified minimum yield strength of 110 ksi (759 MPa).

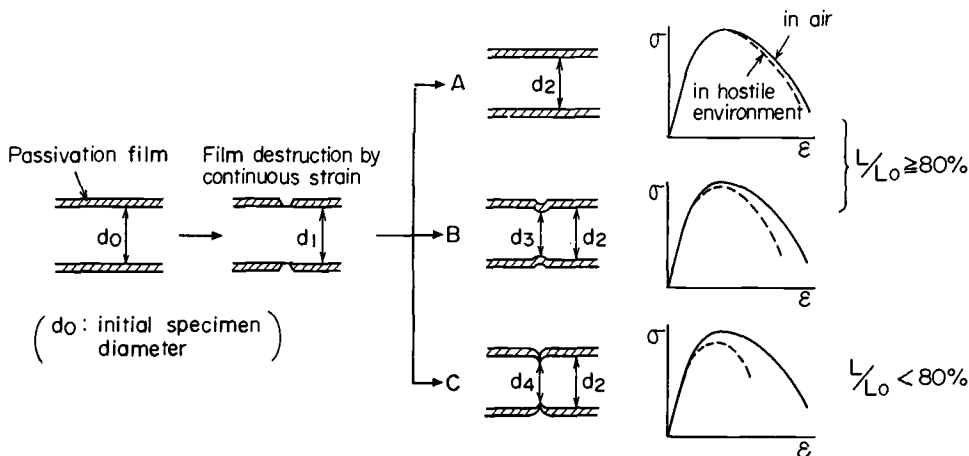


FIG. 1—Schematic illustration of environmental cracking behavior of CRAs in hostile well environment by SSRT after Ikeda et al. [2]. NOTE: Specimen diameter during SSRT,  $d_0$ : Initial;  $d_1$ ,  $d_2$ : in deforming homogeneously;  $d_3$ : in initiating shallow pits; and  $d_4$ : in initiating deep pits and SCC.

instantly and completely, degradation of the tensile properties would not be observed in the materials at all. This means that the corrosion resistance of the material is excellent in the specific environment. If the repair of passivation film is delayed or incomplete, any degradation of the tensile properties due to a general corrosion or a localized corrosion is observable as a function of the corrosion resistance of materials. Hence, the localized corrosion is more serious in SSRT, because the dynamic strain resulting from the continuous tensile deformation tends to concentrate at the area of localized corrosion and accelerate the pitting propagation rate. If the passive film is not formed in the pit, the growth of pit depth would be stopped due to the release of the stress concentration. On the other hand, if conditions allowing formation of a passive film in the pits are sustained, deep and sharp pittings would be nucleated, followed by the initiation of SCC. Thus, the principal SCC initiation mechanism of CRAs in SSRT is closely related to the destruction and reformation behavior of passive film. Generally speaking, both the effect of changes of media in the pits, e.g., pH change or  $\text{Cl}^-$  increase, and changes of surface conditions of the material, i.e., crevice formation, composition change underneath the thick corrosion products, or long-time aging, cannot be evaluated by means of the SCC mechanism of SSRT. The environmental degradation of materials in SSRT is assessed by the existence of secondary cracks at the gage section and by the value of ductility loss. It is noted that any degradation in the final stage of the tensile test is not realistic for assessing SCC susceptibility of material because a material that has suffered a heavy plastic deformation is not the same as the original one. It is noted, therefore, that the secondary cracks on the main fracture surface where a heavy plastic deformation has occurred should not be considered in the assessment of SCC susceptibility from the engineering standpoint.

#### Effects of Temperature and Strain Rate on Mechanical Properties

Testing temperature affects tensile properties of most of the iron base alloys and nickel base alloys used in the oil field as well as other physical properties such as elasticity, thermal properties, and so on. Generally speaking, in the tensile test, an elongation of these materials at the elevated temperature range between 373 K (100°C) and 573 K (200°C) decreases as

temperature increases [5]. An example of the effect of temperature on tensile properties in the conventional tensile test is shown in Fig. 2. In this case, the elongation of SM2535-110 alloy at 450 K (177°C) is about 76% of that at the ambient temperature. In addition, as shown in Fig. 2, a low strain rate also contributes to a lower elongation in the tensile test. In this case, the elongation with a slow strain rate of  $4 \times 10^{-6} \text{ s}^{-1}$  is about 92% of that with the conventional strain rate of  $8.3 \times 10^{-4} \text{ s}^{-1}$ . In SSRT, effect of environmental degradation is assessed by the ductility loss previously described. Therefore, in order to distinguish between a contribution of environmental factors and of tensile test conditions on the change in ductility, it is suggested that tensile test data in the hostile environment be compared with data from the inert environment at the same temperature and strain rate conditions.

*Effect of Test Specimen Dimensions on Tensile Test Data*

In the tensile test in general, it is desirable that the fracture occurs at the gage section of specimens. If not, elongation value is abnormally low even in the inert environment. It is also important that any notch effect on the specimen be avoided because the notch would contribute to a remarkable decrease of homogeneous plastic elongation, particularly in the hostile environment. In spite of showing no secondary crack and having a good reduction in area, poor elongation values are frequently obtained. In machining specimens, undercutting of specimen tends to occur at the transition area between the parallel-machining section and the curvature-machining section. Thus, in the SSRT in hostile environment, off-

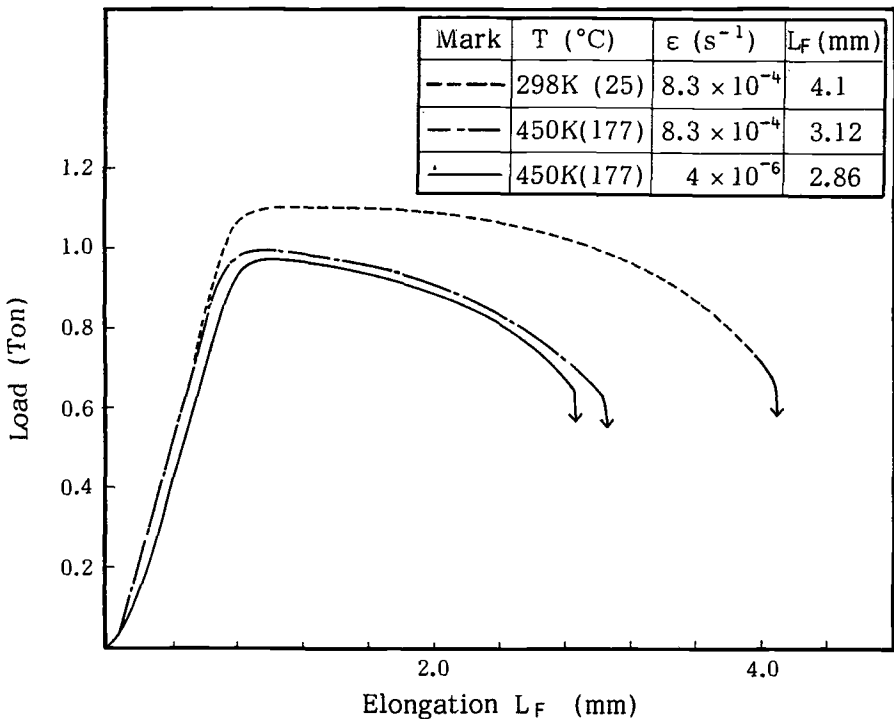


FIG. 2—Effect of temperature and strain rate on tensile properties in the open air (Material: SM2535-110, Test specimen: 4 mm  $\phi$   $\times$  G. L. 30 mm).

gage fractures occur frequently, resulting in the stress concentration in this area. Although it is important, of course, to avoid the undercut in machining in order to eliminate the off-gage fractures, it is recommended, from practical point of view, that the specimen diameter at the gage section be machined slightly smaller in that range of precision than that at off-gage section to decrease the possibility of off-gage fracture [2].

Ikeda et al. have shown that both environmental degradation indices of time-to-fracture and plastic elongation depend upon specimen dimensions such as gage length and diameter. Figure 3 shows the relationship between time-to-fracture, in other words time-to-failure, and  $\log \sqrt{A_0}/L_0$ , where each  $A_0$  and  $L_0$  is a cross-sectional area and gage length of specimen, respectively. Time-to-fracture is virtually equivalent to elongation, and  $\log \sqrt{A_0}/L_0$  is a measure of true strain. Thus, Fig. 3 shows that the value of elongation is proportional to the true strain introduced during the tensile deformation [2]. Ikeda et al. also showed that a ratio of plastic elongation in hostile environment to elongation in an inert environment ( $L/L_0$ ) which is an index of environmental degradation does not depend upon the dimension of the specimen [2]. Thus, the  $L/L_0$  value is recommended for SSRT assessment, since test data from specimens with different dimensions can be compared objectively.

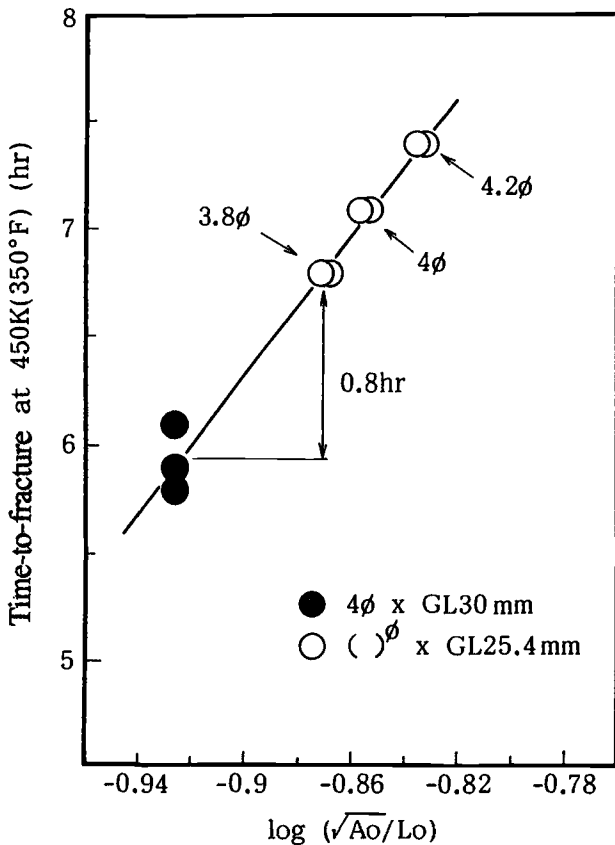


FIG. 3—Effect of specimen dimension on time-to-fracture (or elongation), where each  $A_0$  and  $L_0$  is area of cross-section and length at gage section, respectively.

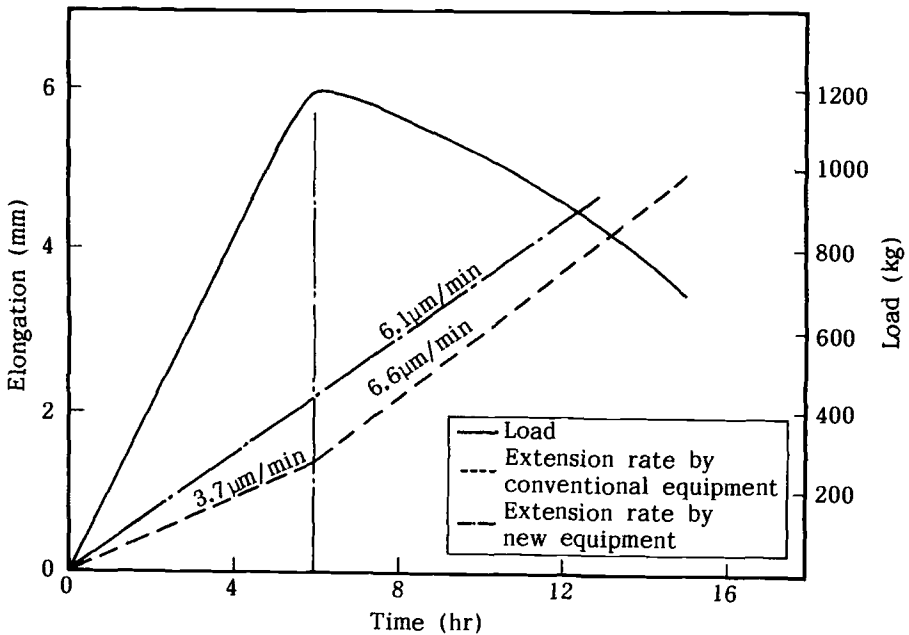


FIG. 4—Effect of test equipment on extension rate control (ambient temperature).

#### Effect of Tensile Test Machine Characteristics on Tensile Test Data

D. R. McIntyre et al. pointed out that the stiffness of the frame of tensile equipment could affect time-to-fracture index [6]. However, the deflection behavior of the load train system including stiffness of frame is more important because it is related to a variation of extension rate, which essentially affects the SCC mechanism in SSRT because the extension rate is directly related to the strain rate at the gage section of the specimen. Therefore, in 1991, the authors developed a SSR testing machine with a combination of feedback controlled system and load train facilities with high stiffness. As a result, a rigid extension rate was obtained. Figure 4 compares extension rate data from the new equipment to data from the conventional equipment. The material used is UNS N08825 alloy with a yield strength of 989 MPa (138 000 psi) and a diameter of 3.82 mm at gage section. The extension rate in the former was controlled in the error range of  $\pm 5\%$  of setting rate, i.e.,  $6.1 \times 10^{-6}$  m/min, while the extension rate in the latter was  $3.7 \times 10^{-6}$  m/min until the maximum load and  $6.6 \times 10^{-6}$  m/min after the maximum load. Thus, the characteristics of equipment significantly affect the extension rate in the stage of elastic deformation of the specimen because the deflection of frame is proportional to the applied load. By the same token, equipment characteristics affect the extension rate in the stage of final necking deformation, where the load decrease is significant and rapid. On the other hand, in the stage of homogeneous plastic deformation, the influence of equipment on the extension rate is relatively small. In Fig. 4, the fluctuation of extension rate is about  $5 \times 10^{-7}$  m/s, which corresponds to a fluctuation of strain rate of about  $3 \times 10^{-7}$  s $^{-1}$ . Thus, when the environmental degradation behavior by SSRT is discussed in relation to the initial and intermediate stage behaviors of plastic deformation as described in the previous section, the effect of equipment characteristics on SSRT would be minimized. On the contrary, if the phenomena related to the final

necking deformation, for examples, fracture mode, secondary cracking at fracture surface, and so on, are discussed in the SSRT, it must be taken into consideration that they would inevitably have some test equipment dependence in addition to the complexity in fracture phenomena. Thus, these data should not be used for practical purposes unless fracture mechanism would be scientifically clarified.

The difference between extension rate and strain rate must be discussed because the latter depends more or less on both test equipment and dimensions of the specimen even when the setting extension rate is constant. In SSRT of CRAs in a hostile environment, the extension rate of the specimen as it is extracted is controlled on the pull rod located above and outside of the autoclave. Even if a testing machine is calibrated to ensure the constant extension rate, i.e., a constant cross-head speed and the stiffness of the machine frame, etc., deflection of pull rod would occur and this would affect the strain rate at the gage section of the specimen, as shown in the following equations

$$\Delta l_0 = \Delta l_1 + \Delta l_3 - \Delta l_2 \quad (1)$$

$$\Delta l_3 \ll \Delta l_1 \text{ and } \Delta l_2 \text{ in the rigid control of extension rate} \quad (2)$$

$$\varepsilon = \Delta l_0 / l_0 \quad (3)$$

$$d\varepsilon/dt = d(\Delta l_0 / l_0) / dt = (d\Delta l_1 / dt + d\Delta l_3 / dt - d\Delta l_2 / dt) / l_0 \quad (4)$$

where  $\Delta l_0$ ,  $\Delta l_1$ ,  $\Delta l_2$ , and  $\Delta l_3$  are the deflection of the gage section, of the cross-head, of the pull rod, and of the frame, respectively, and  $l_0$  is gage length,  $\varepsilon$  is strain, and  $t$  is time. In the tensile machine with the frame of high stiffness,  $d\Delta l_3 / dt$  is nearly equal to zero. Therefore, Eq 4 becomes Eq 5.

$$d\varepsilon/dt = (d\Delta l_1 / dt - d\Delta l_2 / dt) / l_0 \quad (5)$$

In the load train system of the SSRT equipment used for CRA evaluation, generally, the ratio of diameter of pull rod to a specimen diameter at the gage section ranges from approximately 5 to 8 and the ratio of length of pull rod to gage length of specimen ranges from approximately 20 to 25. As shown in Eq 5, the extension rate due only to the pull rod is virtually comparable to the extension rate of the gage section in the elastic deformation, when the ratios of diameter and length are 5 and 25, respectively. Therefore, the strain rate at the gage section is about half of its initial setting. However, the true strain rate can be calculated from the extension rate given, dimensions of pull rod, and specimen. When the specimen is plastically deformed, deflection of the specimen accounts for virtually all of the cross-head extension rate, because  $d\Delta l_1 / dt$  is nearly 0, when there is no load variation. When the maximum tensile load has been achieved,  $d\Delta l_2 / dt$  changes to a negative value. This results in slightly higher extension rate in the specimen than in the cross-head. This suggests that a stress-strain ( $S$ - $S$ ) curve itself could slightly affect the actual strain rate. At present, most of engineering data do not take this effect into account, because it is assumed that the fluctuation due to  $S$ - $S$  curve is sufficiently smaller than the strain rate allowance for the degradation measurement of CRA.

#### *Investigation of Environmental Factors and Alloy Systems by SSRT*

Ikeda et al. systematically studied the influence of environmental factors on corrosion and SCC behavior of CRAs by the constant strain SCC tests [4,7-9]. The result is summarized

in Table 2. A concept of SCC initiation is also presented in Fig. 5. When the long duration constant strain test was used, the effect of alloys and environmental factors on SCC was similar to that found when the SSRT was used [2,12]. In general, the SSRT evaluation was severer than the other tests; however, under specific critical alloy-environmental conditions such as C276 alloy (UNS N10276) in 0.7 MPa H<sub>2</sub>S-5%CH<sub>3</sub>COOH-25%NaCl in the vicinity of 423 K (250°C), the SSRT was less severe than the other test. In the actual SCC process, localized corrosion such as pitting corrosion and crevice corrosion occurs and, in these areas, become SCC sites if the pH of solution decreases and the corrosivity of environment increases. In SSRT, the influence of environmental change on SCC cannot be assessed.

*Effect of Strain Rate*—C. D. Kim et al. showed that a SCC phenomenon of carbon steel for pressure vessels in air-contaminated ammonia was dependent on strain rate and was the most susceptible when the strain rate was in the vicinity of 1 to 2 × 10<sup>-6</sup>s<sup>-1</sup> [10]. W. E. Berry showed that CO<sub>3</sub><sup>2-</sup>-HCO<sub>3</sub><sup>-</sup> SCC of line pipe steel at -680 mV versus SCE was also the most susceptible when the strain rate is in the vicinity of 1 to 2 × 10<sup>-6</sup>s<sup>-1</sup> [11]. Thus, as for active pass corrosion type SCC of carbon steel, a strain rate in the vicinity of 1 × 10<sup>-6</sup>s<sup>-1</sup> seems to be the most susceptible to SCC. It is now generally accepted that the mechanism of SCC is as follows: first, localized film destruction, followed by dissolution of matrices, film reformation, and then stress concentration, leading to initiation of pitting, and, finally, SCC.

In the case of high-nickel CRAs in H<sub>2</sub>S-CO<sub>2</sub>-Cl<sup>-</sup>, critical strain rate for SCC was also found in the vicinity of 4 to 10 × 10<sup>-6</sup>s<sup>-1</sup>, as can be seen in Fig. 6 [12]. As regarding the strain rate in the stage of homogeneous plastic deformation, this range (e.g., about 6 × 10<sup>-6</sup>s<sup>-1</sup>) is sufficiently wider than the fluctuation of strain rate (e.g., 1.5 × 10<sup>-7</sup>s<sup>-1</sup>) resulting from the difference of equipment as mentioned in the previous section. This means that SSRT data from the different sources could be effectively discussed on the common base, as long as discussing the phenomena in the plastic deformation. When the alloys were resistant in some specific environment, the effect of strain rate on SCC was not observed, as can be seen in Fig. 7 [2]. In the future, more data must be accumulated to discuss the effect of strain rate more clearly.

*Effect of Temperature and Alloy*—Figure 8 shows a relationship between testing temperature and molybdenum content on SCC of CRA due to SSRT in 25%NaCl-0.5%CH<sub>3</sub>COOH-0.7MPa H<sub>2</sub>S [2]. The strain rate was 4 × 10<sup>-6</sup>s<sup>-1</sup>. This result was obtained without electrical

TABLE 2—*Influence of environmental factors on corrosion behavior of high-nickel corrosion resistant alloys after Ikeda et al. [4,7-9].*

Factors	Contribution	Phenomena
Temperature pH Drop Free Sulfur H <sub>2</sub> S O <sub>2</sub> Contamination	Large	Corrosion rate accelerated. SCC susceptibility increased. Localized corrosion and SCC accelerated by S-deposition. Corrosion prevention effectiveness increased by Mo ≥ 10% addition.
H <sub>2</sub> S Cl <sup>-</sup> SO <sub>4</sub> <sup>2-</sup>	Intermediate	Corrosion rate, SCC susceptibility accelerated. Localized corrosion accelerated. Corrosion rate and SCC decelerated.
CO <sub>2</sub> Cation Species	Small	Little effect observed.

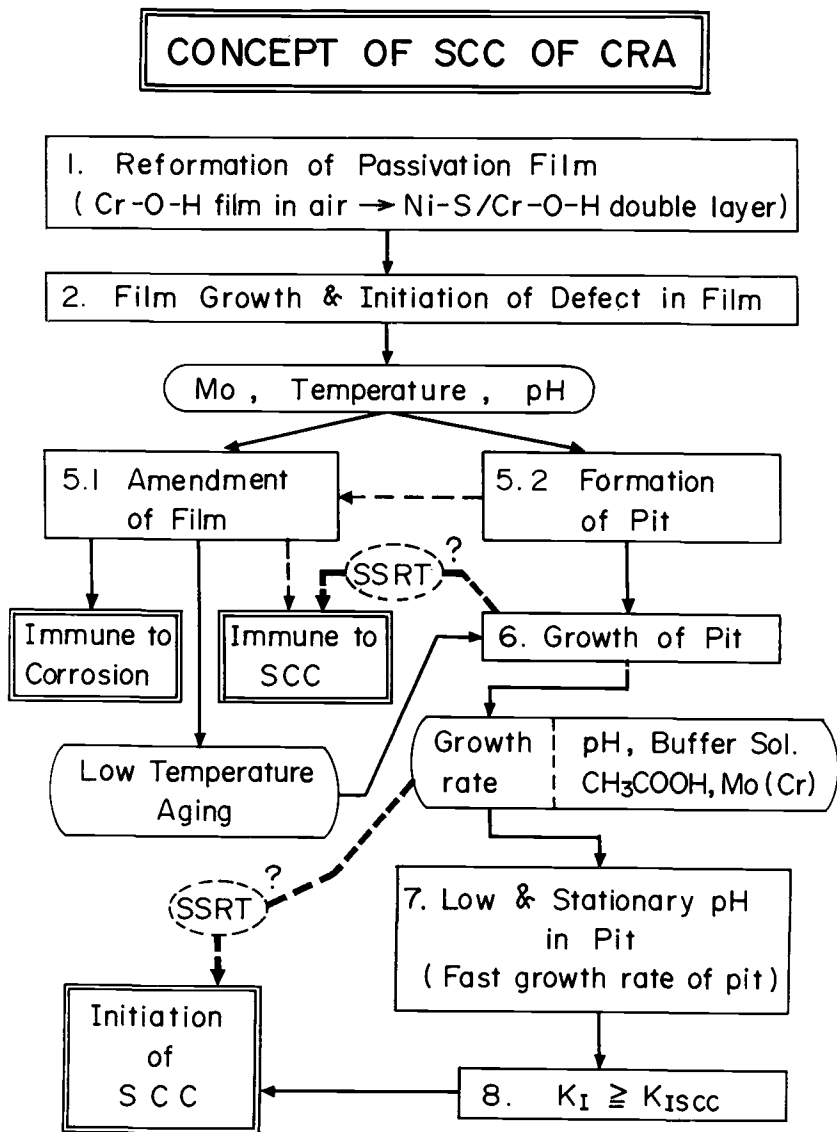


FIG. 5—A concept of SCC initiation and propagation of CRA in the hostile condition after Ikeda et al. [2].

insulation between the specimen and the test equipment, which was made of CRA material, SM2550 (UNS N06975, 25Cr-50Ni-6Mo). Thus, a galvanic effect might have affected the result to some degree. Although this effect is precisely discussed in the later section, it is noted here that the critical line for SCC or no SCC as can be seen in Fig. 8 tends to shift to the left side in the condition with the electrical insulation, when secondary crack initiation at the gage section outside of the necking area is used as the SCC criterion.

The result shown in Fig. 8 is similar to the corrosion and SCC behaviors of CRA obtained by other constant strain test methods both in the brine-H<sub>2</sub>S-CO<sub>2</sub>-free sulfur condition and

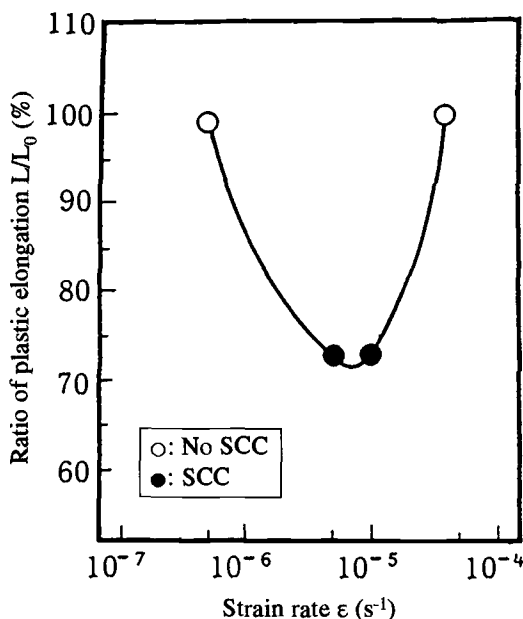


FIG. 6—Effect of strain rate on SCC susceptibility by SSRT after Ueda et al. [12] (SM2030-110, 423 K, 25%NaCl-0.5%CH<sub>3</sub>COOH, 1.0 MPa H<sub>2</sub>S-1.0 MPa CO<sub>2</sub>).

the brine-H<sub>2</sub>S-CO<sub>2</sub> acidized to low pH condition. It is noted that these conditions are severer than the environmental conditions tested in Fig. 8 [4,7,8]. This consistency of result might be explained by the following analogy of film destruction: The passivation film is artificially destroyed in SSRT and it is similarly destroyed by the severer corrosion reaction in the constant strain tests. Although the chromium content enhances corrosion resistance of CRA as temperature increases in the constant strain test in the conventional hostile environment [4], molybdenum content plays the primary role in the severe corrosion conditions previously described.

*Addition of Acetic Acid in Brine*—Ikeda et al. showed in the four-point bent beam test that the addition of 0.5%CH<sub>3</sub>COOH in 25%NaCl-1.0MPaH<sub>2</sub>S-1.0MPaCO<sub>2</sub>-1 g/L free sulfur aqueous solution extremely increased corrosion rate and SCC susceptibility of 20Cr-50Ni alloy with molybdenum content less than 10% [7]. They also showed in SSR test that the addition of 0.5%CH<sub>3</sub>COOH in brine increases a SCC susceptibility of UNS N08825 alloy [2]. In another test, it was also clarified that the addition of acetic acid generally increases the corrosive effect of environment on CRAs by lowering the pH value of corrosion media.

*Partial Pressure of H<sub>2</sub>S (P<sub>H<sub>2</sub>S</sub>)*—A typical effect of P<sub>H<sub>2</sub>S</sub> on SCC in SSRT is shown in Fig. 9 [2]. It shows that the higher P<sub>H<sub>2</sub>S</sub> makes CRAs more corrosive in a critical environmental condition. This effect of P<sub>H<sub>2</sub>S</sub> on corrosion behavior is usual and is consistent with the results in Table 2 clarified by the constant strain test result. However, the effect of P<sub>H<sub>2</sub>S</sub> on SCC behavior is not always simple. Ikeda et al. showed that there was a complex contribution of P<sub>H<sub>2</sub>S</sub> on SCC behavior in the SSRT as can be seen in Table 3 [13]. In the case of the test condition without vacuum deaeration, UNS N06975 alloys were more susceptible to SCC in the lower P<sub>H<sub>2</sub>S</sub> than in the higher P<sub>H<sub>2</sub>S</sub>. It is presumed that the solubility of elemental sulfur, which was produced by the reaction of H<sub>2</sub>S and O<sub>2</sub> was low in the brine with the lower P<sub>H<sub>2</sub>S</sub>, and a free sulfur that was produced locally on the specimen contributed to

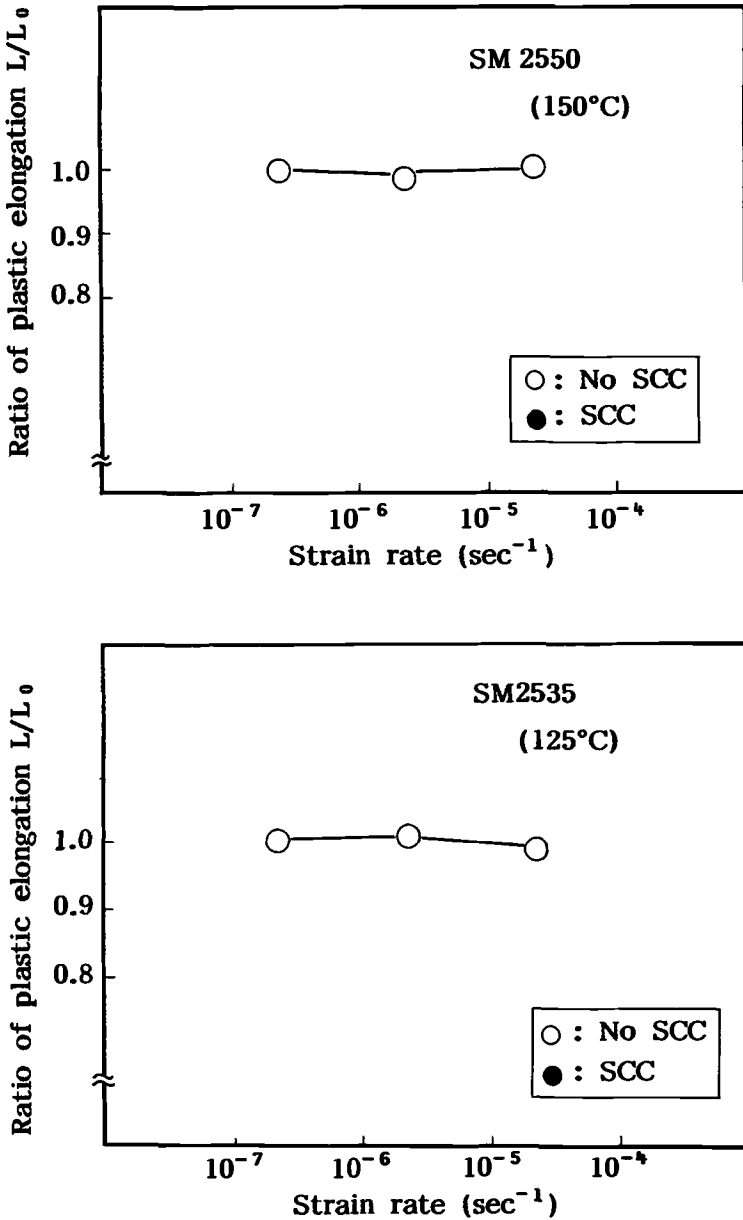


FIG. 7—Effect of strain rate on environmental cracking susceptibility of CRAs at the safety temperature, i.e., 423 K (150°C) for SM2550 and 398 K for SM2535 (125°C) after Ikeda et al. [2] (25%NaCl-0.5%CH<sub>3</sub>COOH, 0.7 MPa H<sub>2</sub>S).

initiation of SCC in the SSRT through the formation of stress concentration sites due to pitting corrosion. This study was originally carried out to standardize the test procedure, and particularly to stress the necessity of vacuum deaeration, because O<sub>2</sub> in the air, which was trapped in the dead space between specimen and specimen holder gradually diffused

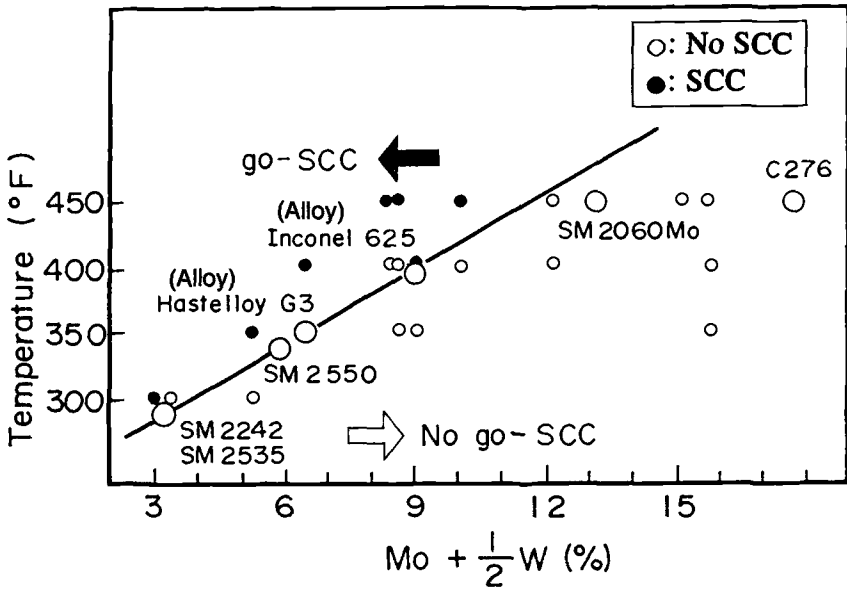


FIG. 8—A relationship between testing temperature and  $(Mo + 0.5 W)$  contents on SCC occurrence in SSRT of CRAs in  $H_2S-Cl^-$  environment after Ikeda et al. [2] ( $4 \times 10^{-6}s^{-1}$ , 25%NaCl-0.5% $CH_3COOH$ , 0.7 MPa  $H_2S$ ).

out into the brine, yielding elemental sulfur in the reaction with  $H_2S$  in the brine, and this elemental sulfur worked as a strong oxidant in the corrosion reaction during the SSRT.

Therefore, because the SSRT is an aggressive acceleration test and is also sensitive to test conditions, specific phenomena or problems, or both, could emerge in the SSRT.

*Chloride Ion Concentration*—A typical result of effect of  $Cl^-$  on SCC in SSRT is shown in Fig. 10 [2]. It clearly shows that a higher concentration of  $Cl^-$  drastically degrades corrosion

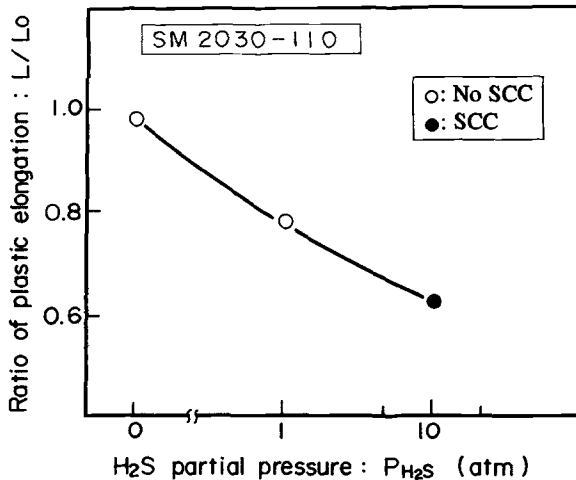


FIG. 9—Effect of partial pressure of  $H_2S$  on SCC susceptibility of SM2030-110 alloy by SSRT after Ikeda et al. [2] ( $4 \times 10^{-6}s^{-1}$ , 423 K, 25%NaCl-0.5% $CH_3COOH$ , 1.0 MPa  $CO_2-H_2S$ ).

TABLE 3—Effect of deaeration and environmental conditions on SSRT after Ikeda et al. [13].

Environmental Condition			Ratio				Secondary Crack
Environment*	Deaeration Process	Material**	TTF (%)	L/L <sub>0</sub>		RA/RA <sub>0</sub> (%)	
				(%)	Average		
1	Vacuum	E	98	99	100	98	No
			99	101		101	
		70	112	106		95	
1	Non vacuum	50	99	91	86	100	No
			90	80		87	Yes
		R	91	83	75	90	Yes
			78	67		70	Yes
			70	91		(82)	83
2	Non vacuum	R	99	93	94	97	No
			99	94		99	

\*Environment 1: 25% NaCl-0.5% CH<sub>3</sub>COOH, H<sub>2</sub>S 1.42 psi-CO<sub>2</sub> 14.2 psi, 149°C.

Environment 2: 25% NaCl-0.5% CH<sub>3</sub>COOH, H<sub>2</sub>S 100 psi 149°C.

(Strain rate  $\dot{\epsilon} = 4 \times 10^{-6} \text{ s}^{-1}$ ).

\*\*All of E, 70, 50, and R are SM2550 alloy produced from different heats.

NOTE: 1 psi = 6.9 kPa.

resistance of CRAs under critical conditions. Thus, the SSRT technique is more effective than the other SCC test methods in determining the contribution of factors.

An example of a useful application of SSRT is a chart shown in Fig. 11, where the effect of  $P_{H_2S}$  and  $Cl^-$  on application limits of duplex stainless steels and 316L austenitic stainless steels is shown. This chart actually has been used for determining the safest application criteria in the design of facilities for oil and gas production [15].

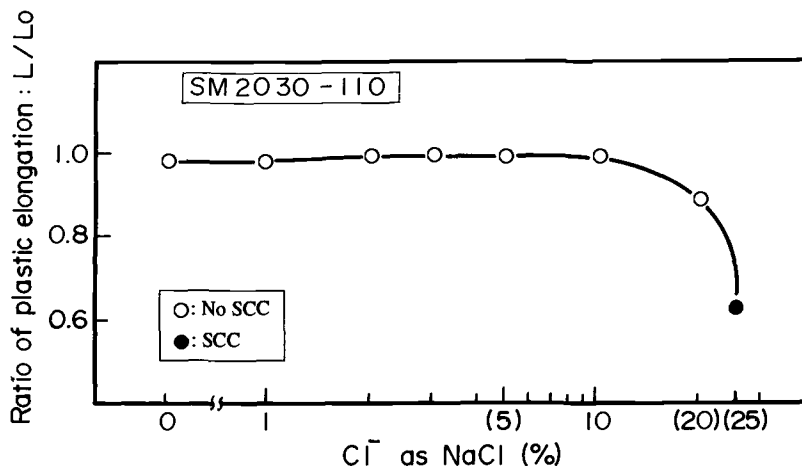


FIG. 10—Effect of chloride ion on SCC susceptibility of SM2030-110 alloy by SSRT after Ikeda et al. [2] ( $4 \times 10^{-6} \text{ s}^{-1}$ , 423 K, NaCl-0.5%CH<sub>3</sub>COOH, 1.0 MPa CO<sub>2</sub>-1.0 MPa H<sub>2</sub>S).

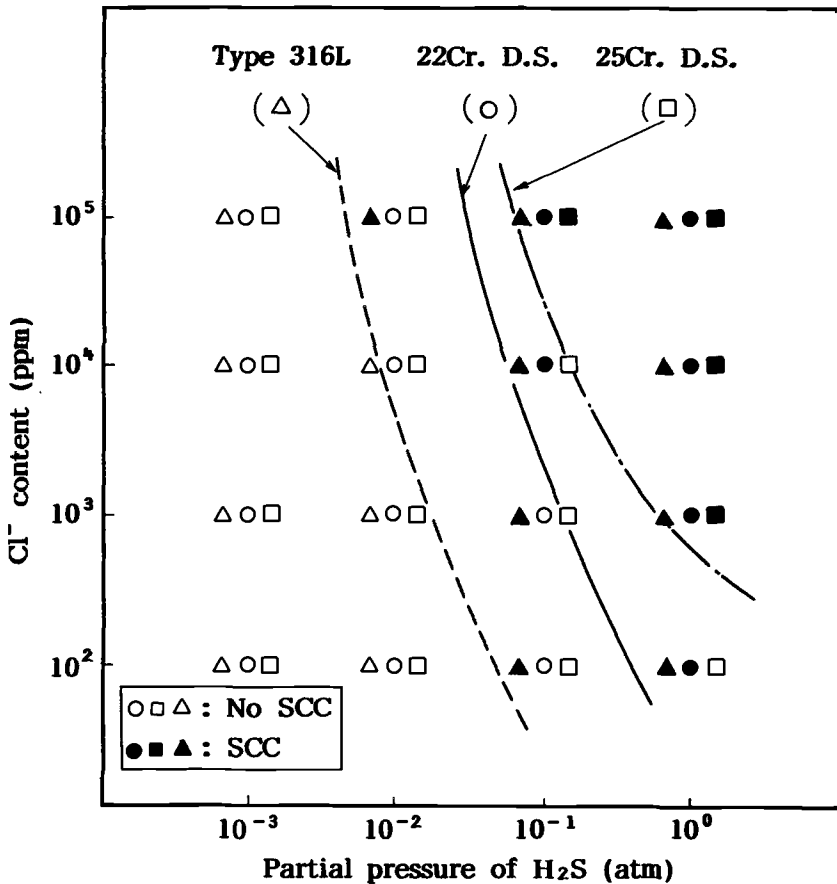


FIG. 11—SCC susceptibility of 316 stainless steel (SS) and 22Cr- and 25Cr-duplex SSs by SSRT in NaCl-H<sub>2</sub>S environment after Tsuge [15] ( $4 \times 10^{-6}$ s<sup>-1</sup>, 353 K, Annealed material).

#### Effect of Electrochemical Polarization

Ueda et al. showed that the electrochemical polarization significantly affected SSRT measurement of corrosion resistance of UNS N08825 alloy in a marginal environment [12]. Their data are rearranged in Figs. 12 and 13 by means of slightly changing the assessment criteria of SCC. This is done by discounting as SCC criteria any secondary cracks that originated on the primary fracture surface.

In Fig. 12 [12], the corrosion potential ( $E_{\text{corr}}$ ) of the specimen is slightly shifted to the noble side, when the specimen of N08825 alloy is in contact with equipment made of UNS N10276 alloy. This means that the specimen contacted with the equipment in the SSRT is anodically polarized about 40 to 50 mV more than  $E_{\text{corr}}$  of the specimen electrically insulated from the equipment, and suffers SCC in the SSRT. It is also shown in Fig. 12 that the addition of elemental sulfur in the test solution in the SSRT results in SCC and the shifting of  $E_{\text{corr}}$  of this alloy to a noble potential of 40 to 50 mV more than  $E_{\text{corr}}$  when there is no free sulfur and the specimen is insulated electrically from the equipment. This means that the free sulfur acts as the oxidant in the corrosion reaction and raises  $E_{\text{corr}}$ . This effect is similar to the aforementioned electrochemical polarization due to the galvanic effect.

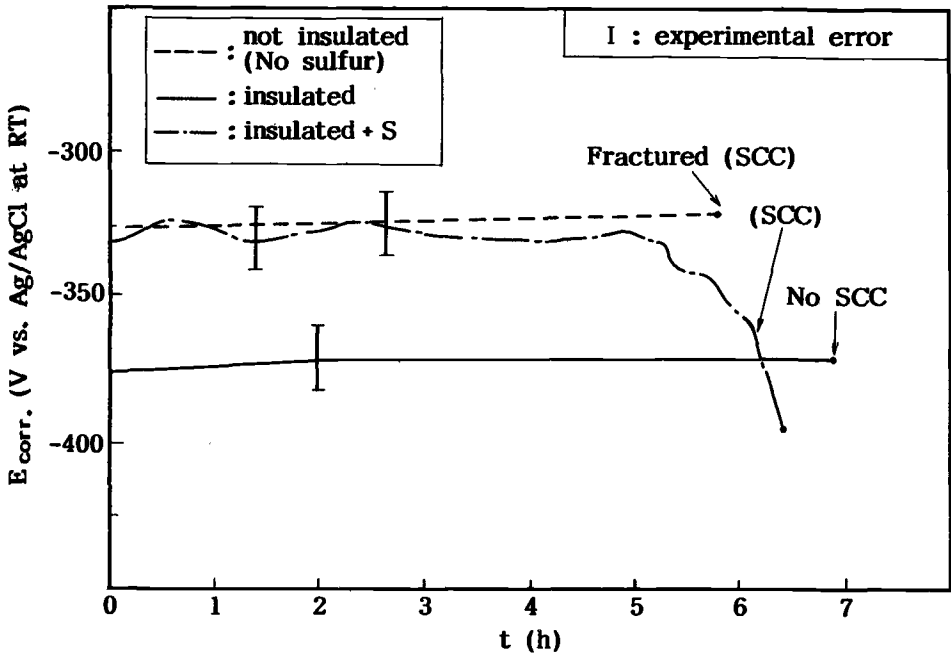


FIG. 12—Effect of electrical insulation and elemental sulfur on corrosion potential ( $E_{\text{corr}}$ ) and SCC behavior of SM2242 (UNS N08825) alloy in SSRT after Ueda et al. [12] ( $4 \times 10^{-6} \text{s}^{-1}$ , 423 K, 0.7 MPa  $\text{H}_2\text{S}$ , 25% NaCl-0.5%  $\text{CH}_3\text{COOH}$ ).

In Fig. 13, the effect of electrochemical polarization on SSRT is more systematically shown. At the  $E_{\text{corr}}$  and in the cathodic polarization to a potential of 20 mV less than  $E_{\text{corr}}$ , a degradation is not observed. At the slightly anodic polarization of 20 mV, a tendency of degradation at the main fracture surface is observed, but no secondary crack is observed on the other gage section. In the anodic polarization of 40 to 50 mV more than  $E_{\text{corr}}$ , SCC occurred. This is consistent with the results in Fig. 12 previously described. The anodic polarization of up to 80 to 100 mV more than  $E_{\text{corr}}$  results in the transpassivity of the specimen. As a result, a thinning effect of specimen diameter occurs. The formation of many deep pits and secondary cracks is observed as well as the weight loss corrosion. It is noted that transpassive potential is less noble in the SSR test than in the constant load test, which is less noble than in no load condition [14].

In summary, the corrosion resistance of CRAs in the hostile sour environment is achieved by the formation of stable passivation film with the double layer structure [3,4]. As described in the previous section, the SSRT assesses a corrosion resistance by means of evaluating the ability of alloys to repair the passive film. However, the application of anodic polarization in the SSRT results in an artificial disturbance of the ability to repair itself the artificially destroyed film. Therefore, as long as the relationship between the SSRT under the anodic polarization and any concrete practical phenomenon cannot be physically clarified, the anodic polarization in SSRT should not be used easily.

#### SCC Criteria

In order to accomplish maximum exchangeability of data obtained in the different laboratories, it is necessary to define adequate indices for the assessment of environmental

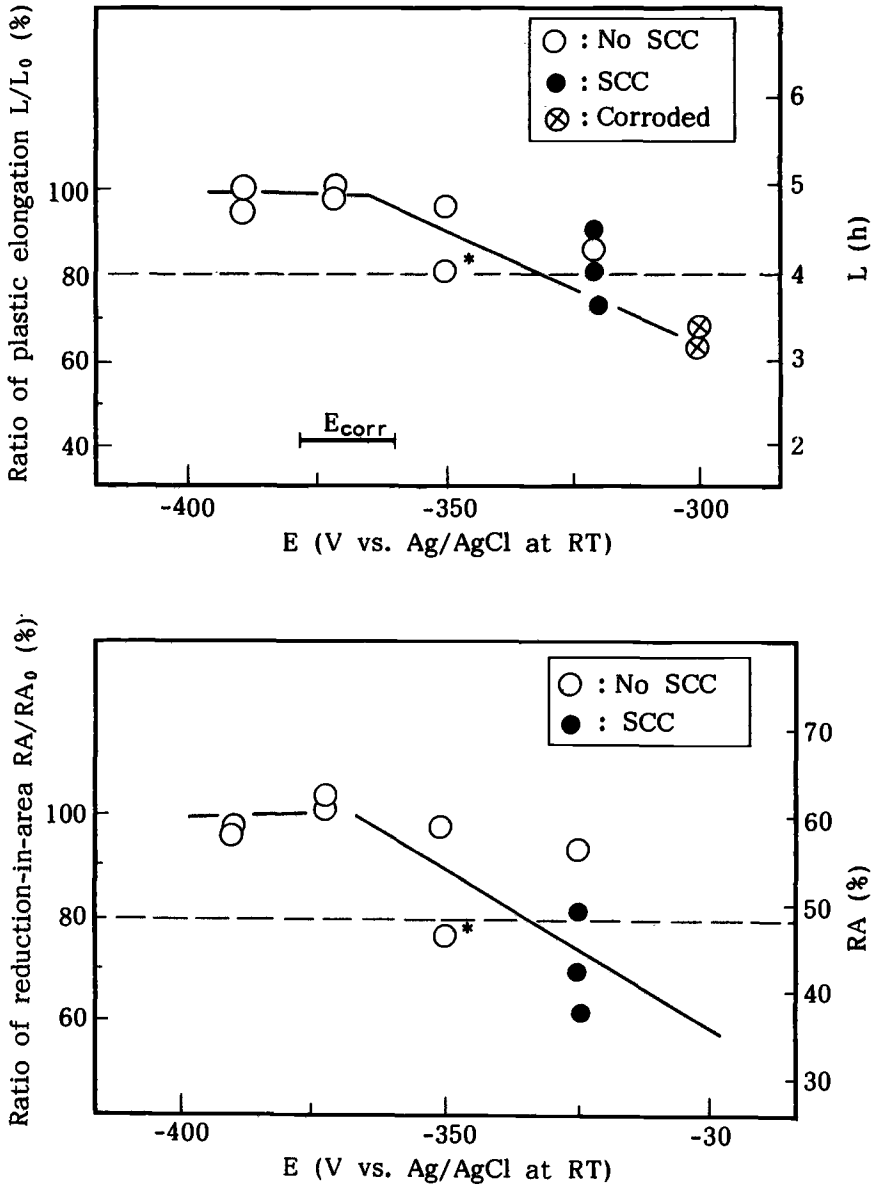


FIG. 13—Effect of controlled potential (E) on SCC behavior of SM2242 (UNS N08825) alloy in SSRT after Ueda et al. [12] ( $4 \times 10^{-6} \text{ s}^{-1}$ , 423 K, 25%NaCl-0.5%CH<sub>3</sub>COOH, 0.7 MPa H<sub>2</sub>S). NOTE: Secondary cracking is observed only on the primary fracture surface.

degradation. A ratio of time-to-fracture  $T_f/T_{F_0}$  is frequently used, where  $T_f$  is time-to-fracture in hostile environment and  $T_{F_0}$  is time-to-fracture in inert environment [6]. If the equipment itself were rigidly standardized in the SSRT, this ratio could be used as a common index. However, many different types of tensile machines are presently being used for the SSRT in the world. It is likely that new machines will continue to be developed in the future

for various purposes. Since this is the case, it is essential that the SSRT establish its position as a more useful testing tool for the assessment of environmental degradation of CRAs.

It was shown in the previous sections that the ratio of plastic elongation  $L/L_0$  is one of the most convenient indices in the previous section, where  $L$  is a plastic elongation in hostile environment and  $L_0$  is one in inert environment. The reasons are summarized as follows:

- (1) The environmental degradation of CRAs is closely related to the behavior of plastic deformation, and the value of  $L/L_0$  is directly related to ductility loss.
- (2) As long as the discussion considers only the stage of plastic deformation and not the stage of heavy necking formation, a dependence of strain rate on the characteristics of the test equipment is minimal. It is important that the fluctuation of strain rate be minimal, because it essentially affects the mechanism of SCC.
- (3) The value of  $L/L_0$  is largely unaffected by the dimensions of the test specimen, as long as the degradation of CRAs in the SSRT is mainly considered on the basis of the behavior of homogeneous plastic deformation.
- (4) The effect of heavy necking on elongation could be minimized by the use of the  $L/L_0$  index.

Ikeda et al. proposed that whether the value of  $L/L_0$  was less than 80% or not should be a criterion for determining SCC initiation of CRAs [9]. So far, this criterion is consistent with the occurrence of secondary cracks.

It has been the consensus of past research concerning SCC of stainless steels and CRAs in the SSRT that the existence of secondary cracks was evidence of SCC occurrence. From the view point of an engineering application, however, there are two methods of evaluating secondary cracks. One method is to consider only the secondary cracks on the gage section, excluding cracks on the primary fracture surface, as evidence of SCC occurrence in CRAs. The other method considers any observation of the secondary cracks as evidence of SCC occurrence. The present paper points out that the phenomena at the necked portion, i.e., the occurrence of secondary cracks on the fracture surface, etc., depend upon the characteristics of the test equipment. It is also pointed out that it is useless from the engineering view point to consider the degradation in the necking stage, since it is not clear that the area such as the necked portion which has suffered a heavy plastic deformation has the same metallurgical characteristics as the original material. The authors propose, therefore, that the former method of assessment of secondary cracks is adequate for the objective and practical judgment of SCC.

In addition to use of this method of the assessment of secondary cracks and of the proposed adjustment of the  $L/L_0$  value, it is recommended that both information about the reduction-in-area and the fracture surface of the specimen be reported as references in order to better understand the SCC phenomena.

#### *Application to Quality Assurance*

This section reports a case in which the SSRT was used for corrosion resistance quality assurance of mass-produced high-nickel CRA tubulars. The newly developed SSRT testing machine was used, because a criterion of time-to-fracture was required and an accurate control of strain rate was required, as shown in Fig. 4. The characteristics of the new equipment were precisely described in the previous section. The following conditions were used in the SSRT:

Material: SM2550 (UNS N06975) with specified minimum yield strength of 758 MPa (110 ksi) and 862 MPa (125 ksi), a variance of yield strength; 138 MPa (20 ksi).

## SSRT testing conditions:

Strain rate:  $4 \times 10^{-6} \text{ s}^{-1}$  [cross-head speed:  $6.1 \times 10^{-6} \text{ m/min}$ ]Hostile environment: Solution 25%NaCl-0.5%CH<sub>3</sub>COOHGas 0.7 MPa H<sub>2</sub>SRatio of solution volume to gage section:  $700 \times 10^{-6} \text{ m}^3/\text{cm}^2$ Temperature: 422 K ( $149 \pm 2.5^\circ\text{C}$ )

## Criteria:

Time-to-fracture:  $T_F, T_{F_0} \geq 6 \text{ h}$ Ratio of time-to-fracture:  $T_F/T_{F_0} \geq 80\%$ Reduction-in-area:  $RA, RA_0 \geq 25\%$ Ratio of reduction-in-area:  $RA/RA_0 \geq 80\%$ 

No secondary cracking

where each  $T_{F_0}$  and  $RA_0$  is time-to-fracture and reduction-in-area in the inert environment and each  $T_F$  and  $RA$  is the corresponding value in the hostile environment.

When SM2550 alloy has been produced in accordance with the material production specifications, it has been our experience for the past ten years that SM2550 alloy does not show any environmental degradation by the SSRT in this environment, and it satisfies with the aforementioned criteria [2,4,7,13]. Therefore, if the material showed any evidence of degradation in the SSRT, it must be that some metallurgical factor is affecting the degradation of corrosion resistance. Corrosion resistance has been one of the most critical properties leading to the selection of SM2550 alloy, and as the SSRT requires only a short time for evaluation, it allows a faster delivery time. Thus, the SSRT was used for the quality assurance in the commercial production.

The evaluation method is as follows: From each one tubular of different heat, two specimens are taken. They are tested in both hostile and inert environments. The values of time-to-fracture and reduction-in-area are evaluated. Next, whether there is a presence or absence of secondary cracks is noted.

All tubulars tested by this method satisfied the testing criteria. Even in the primary fracture surfaces, no secondary cracks were observed at all. Next, all data have been statistically analyzed in order to clarify the relationship among tensile test characteristics both in the inert and hostile environments. Figures 14 through 17 show the relationship between time-to-fracture  $T_{F_0}$  and  $T_F$ , between reduction-in-area  $RA_0$  and  $RA$ , between yield strength and  $T_F$  and between yield strength (YS) and  $RA$ , respectively. The following four linear equations have been obtained by regression analysis of data.

$$T_{F_0} = 0.95 T_F + 0.35 \quad (6)$$

$$RA_0 = 0.30 RA + 47.9 \quad (7)$$

$$T_F = -0.22 \text{ YS} + 37.6 \quad (8)$$

$$RA = -0.12 \text{ YS} + 83.4 \quad (9)$$

where each expression of time-to-fracture ( $T_{F_0}$ ,  $T_F$ ), reduction-in-area ( $RA_0$ ,  $RA$ ) and yield strength (YS), is hours, percent, and 1000 psi (6.9 MPa), respectively. A virtual one-to-one correspondence between  $T_{F_0}$  and  $T_F$  can be seen, while the correspondence between  $RA_0$  and  $RA$  is low. Therefore, Eq 7 is insignificant. This means that other factors such as yield strength and microstructure rather than the corrosion probably contributed to an increase in the variance of reduction-in-area in this SSRT. Although a comparison of properties in

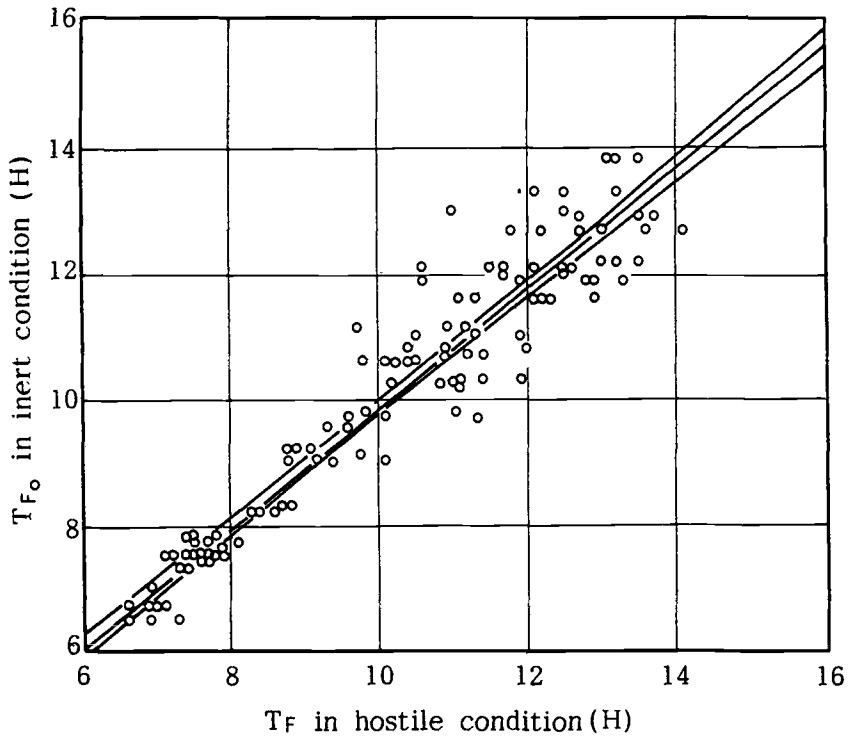


FIG. 14—Relationship between time-to-fracture in hostile environment ( $T_F$ ) and in inert environment ( $T_{F_0}$ ) in SSRT results for mass-produced SM2550 alloy [No SCC; Total sampling frequency, 138].

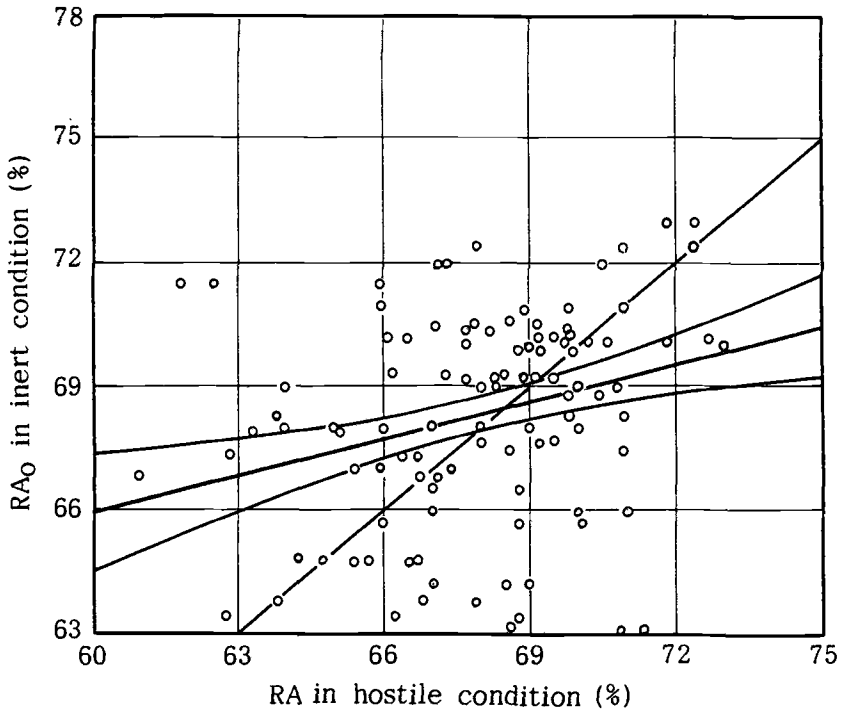


FIG. 15—Relationship between reduction-in-area in hostile environment (RA) and in inert environment ( $RA_0$ ) in SSRT results for mass-produced SM2550 alloy [No SCC, Total sampling frequency, 138].

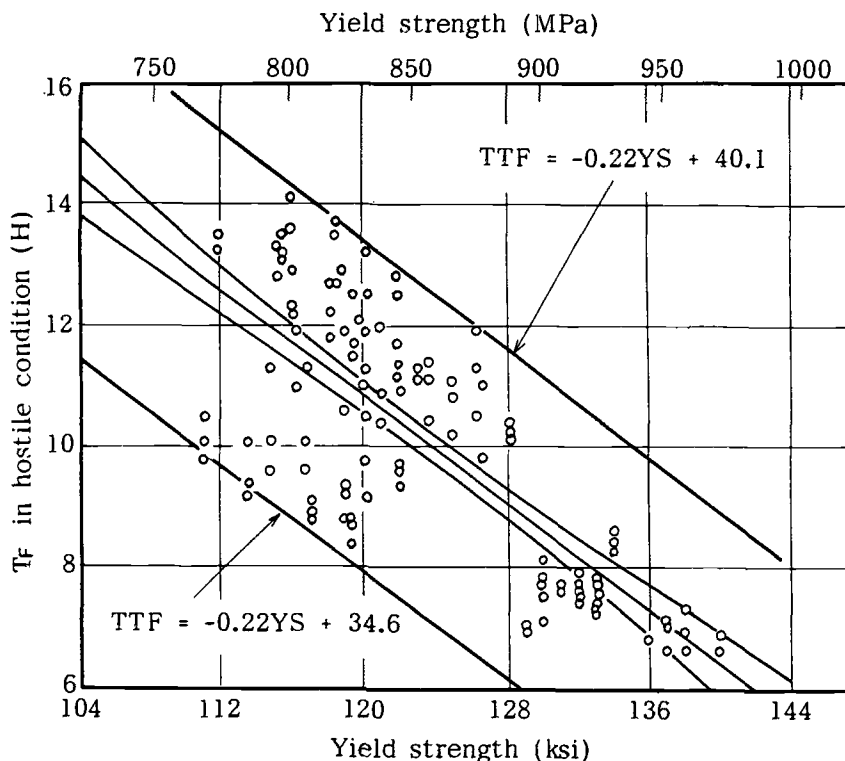


FIG. 16—Relationship between yield strength and time-to-fracture in hostile environment ( $T_f$ ) in SSRT results for mass-produced SM2550 alloy [No SCC, Total sampling frequency, 144].

a hostile environment with those inert is essential, the degradation information from the hostile environment is more essential than that from the inert environment. Thus, the information in Figs. 16 and 17 be used to assure the quality of future heat of SM2550 alloy, if a reduction in the frequency in the SSRT in the inert condition is required according to the various reason, e.g., problems with the SSR testing capacity, short delivery time, or need for cost saving.

The constitution of such data base for each alloy could be achieved by means of the standardization of the SSRT in the future.

#### Deaeration Process by Evacuation

Ikeda et al. showed that vacuum deaeration is necessary for the SSRT procedure in the hostile environment which contains  $H_2S$  [13]. As shown in Fig. 18, a dead space is inevitably formed between specimen and specimen holder. After the specimen is installed in the specimen holder, the autoclave is closed, the test solution is poured into the autoclave, and a conventional deaeration is conducted two or more times by bubbling  $N_2$ , pressurizing and purging it. The air trapped in the dead space can not be purged by the conventional deaeration. As the result, it diffuses out to the test solution during the SSRT, reacts with the  $H_2S$ , producing elemental sulfur which is deposited on the specimens and contributes to the corrosion reaction [13]. An example of curious corrosion behavior resulting from the differences in the deaeration process has already been described in this paper. In order to

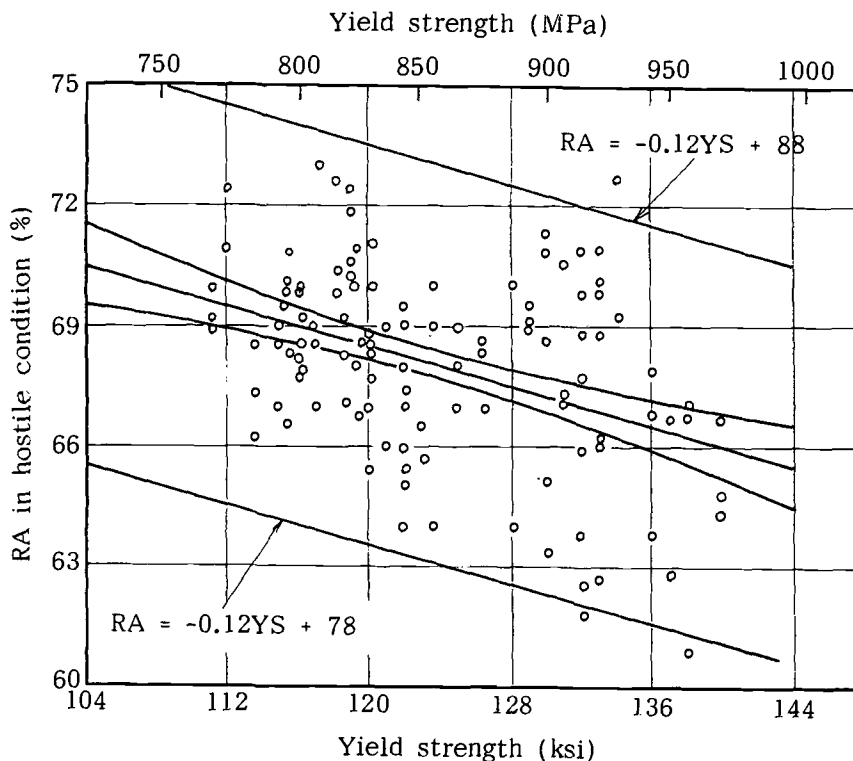


FIG. 17—Relationship between yield strength and reduction-in-area in hostile environment (RA) in SSRT results for mass-produced SM2550 alloy [No SCC, Total sampling frequency, 144].

avoid such a situation, it is strongly recommended that the autoclave be thoroughly evacuated after it is closed and before solution is poured.

## Conclusion

- (1) The SSRT testing technique is useful in assessing the environmental degradation of corrosion resistant alloys.
- (2) The results of evaluations by the SSRT are mostly consistent with the data obtained by other evaluation method. Furthermore, the effect of environmental factors and metallurgical factors on SCC can be clearly assessed in critical condition. Particularly, the effect on SSRT of temperature,  $Cl^-$ ,  $P_{H_2S}$ , addition of acetic acid has been further clarified.
- (3) As a result, environmental degradation should be assessed by the ratio of ductility in a hostile condition to that in an inert condition at the same strain rate and temperature.
- (4) The ratio of plastic elongation  $L/L_0$  is recommended as an index of degradation in SSRT which would permit maximum exchangeability of data from different laboratories. As the criteria of SCC occurrence, it is proposed that a value of  $L/L_0$  be lower than 80% and the presence of secondary cracks be noted. From the view point of engineering applications, it is proposed that secondary cracks on the primary fracture surface be omitted from consideration in the evaluating process.

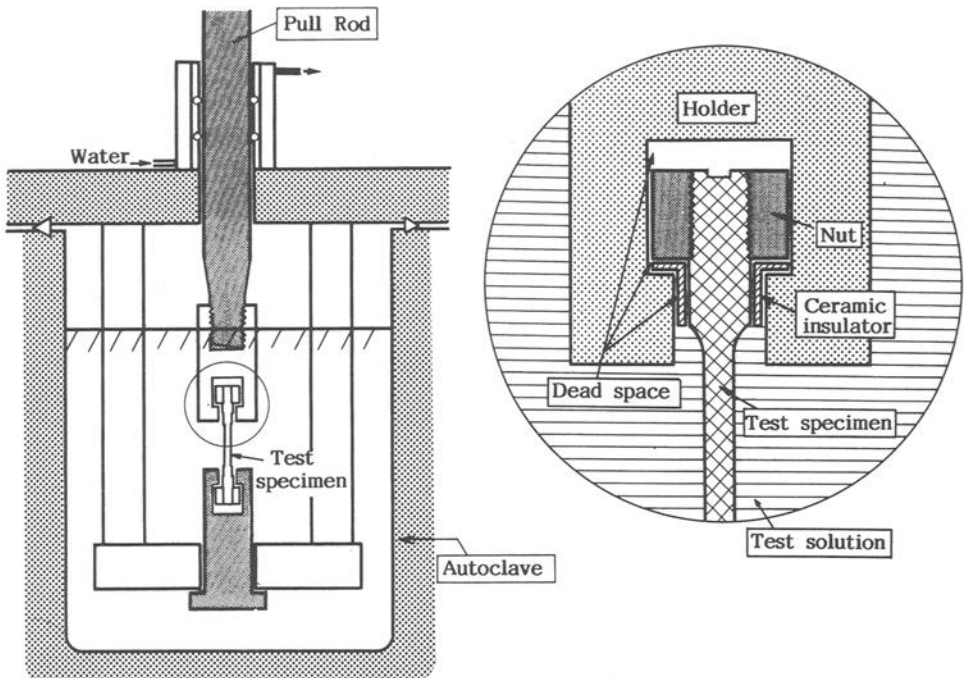


FIG. 18—Schematic illustration of specimen holder, pull rod and specimen installation method in SSRT using autoclave tester.

- (5) A SSR testing technique has successfully been used for a quality assurance of mass-produced CRA tubulars.
- (6) In order to reduce data scattering, the vacuum deaeration process is strongly recommended. Nonelectrical insulation between specimen and test equipment tends to accelerate the degradation of CRAs in the SSRT. The anodic polarization also accelerates the degradation of CRAs in the SSRT. These galvanic effects tend to make it more difficult to clarify the physical meaning of SSRT result of CRAs. In order to reduce a data scattering, these galvanic effects should be avoided in the engineering application of SSRT.
- (7) The SCC susceptibility of CRA tends to maximize at a strain rate of  $4 \times 10^{-6}$  to  $10 \times 10^{-6} \text{ s}^{-1}$ .
- (8) As long as the phenomena of SSRT are discussed in relation to homogeneous plastic deformation and not heavy plastic deformation, the effect of equipment difference on the test result is minimized, including the effect of the fluctuation of strain rate.

## References

- [1] NACE/T-1F-9: Draft #9 of "Proposed NACE Standard Test Method," NACE, Feb. 1992.
- [2] Ikeda, A., Ueda, M., and Tsuge, H., *Corrosion '89*, Paper No. 7, NACE, 1989.
- [3] Murayama, J., Miyuki, H., Kudo, T., Fujino, N., and Terasaki, F., TMS of AIME Meeting, Paper No. A 84-45, 1984.
- [4] Ikeda, A., Kudo, T., Okada, Y., Mukai, S., and Terasaki, F., *Corrosion '84*, Paper No. 206, NACE, 1984.
- [5] Maeda, G., Maeda, M., Yoshikawa, J., and Ohta, T., *Tetsu-to-Hagane*, 36, 1950, 18.
- [6] McIntyre, D. R., Kane, R. D., and Wilhelm, S. M., *Corrosion* 44, 920, 1988.

- [7] Ikeda, A., Igarashi, M., Ueda, M., Okada, Y., and Tsuge, H., *Corrosion* 45, NACE, 1989, pp. 838–847.
- [8] Ueda, M., Tsuge, H., and Ikeda, A., *Corrosion '89*, Paper No. 8, NACE, 1989.
- [9] Ikeda, A., "Steel and Alloys for Oil and Gas Production," *The Advance of Strengthening Technology in Steel Products*, Ch. 3, ISIJ, 1992, p. 90.
- [10] Kim, C. D. and Wilde, B. E., *Stress Corrosion Cracking: The Slow Strain Rate Technique*, ASTM STP 665, G. M. Ugiansky and J. H. Payer, Eds., American Society for Testing and Materials, Philadelphia, 1979, pp. 97–112.
- [11] Berry, W. E., *Proceedings of the Fifth Symposium on Line Pipe Research*, Vol. 1, AGA, Houston, TX, 20–22 Nov. 1974.
- [12] Ueda, M. and Kudo, T., *Corrosion '91*, Paper No. 2, NACE, 1991.
- [13] Ikeda, A., Ueda, M., Okamoto, H., and Yamamoto, E., *Corrosion '90*, Paper No. 272, NACE, 1990.
- [14] Ikeda, A., Miura, M., Mukai, S., Ueda, M., and Koso, K., *Corrosion '86*, Paper No. 333, NACE.
- [15] Tsuge, H., *Sumitomo Search*, No. 36, Sumitomo Metal Industries, Ltd., 1988, p. 65.

S. M. Wilhelm<sup>1</sup> and D. M. Currie<sup>2</sup>

## Relationship of Localized Corrosion and SCC in Oil and Gas Production Environments

---

**REFERENCE:** Wilhelm, S. M. and Currie, D. M., “**Relationship of Localized Corrosion and SCC in Oil and Gas Production Environments,**” *Slow Strain Rate Testing for the Evaluation of Environmentally Induced Cracking: Research and Engineering Applications*, ASTM STP 1210, R. D. Kane, Ed., American Society for Testing and Materials, Philadelphia, 1993, pp. 263–289.

**ABSTRACT:** Laboratory corrosion tests consisting of electrochemical cyclic polarization, critical pitting temperature (CPT), and slow strain rate (SSR) tests were performed on a group of candidate nickel base alloys. The objective of the test program was to predict service performance in deep sour gas well applications. Of particular interest were localized corrosion resistance and stress corrosion cracking (SCC).

The test data indicated that localized corrosion can occur at intermediate temperatures (110 to 170°C) and that SCC may also occur in this temperature region. The temperature region of susceptibility coincides with the transition from a stable chromium oxide surface film to a predominantly sulfide surface film. The localized loss of chromium oxide protectiveness at 150 to 180°C is manifested by crevice corrosion, pitting, and ductility loss. Elemental sulfur in the test environment lowers the region of susceptibility to 100 to 150°C.

From the information provided by this experimental program (and others), procedures and criteria were established for purchase specifications for tubular products. SSR test methods were used to predict service performance.

**KEYWORDS:** slow strain rate (SSR) testing, stress corrosion cracking (SCC), nickel base alloys, critical pitting temperature (CPT) tests, natural gas production, petroleum, localized corrosion, pitting

It is now a prevalent practice to complete deep sour gas wells with highly alloyed corrosion resistant materials that contain substantial amounts of chromium, nickel, and molybdenum [1]. Production tubing is typically furnished in the cold-worked condition at a high strength level (120 to 170 ksi [827.4 to 1172 MPa] minimum yield). The use of such materials allows higher production rates, reduces the frequency of workovers, eliminates the necessity for treatment chemicals, and maintains a high degree of reliability.

Corrosion resistant alloys (CRA) are expensive (10 to 20 times steel) and their price is a strong function of alloy content. Therefore, there is a need to match the capabilities of the tubing alloy exactly to its requirements. Furthermore, in a competitive market, several proprietary products are available in an alloy class. The material selection engineering then involves making a determination of the “best” product. This latter determination involves cost as only a secondary consideration because the minor price difference from alloy to alloy within a generic class is usually insignificant when considering delivery, quality, uniformity, and performance.

---

<sup>1</sup> Cortest Laboratories, Inc., Cypress, TX 74429.

<sup>2</sup> Mobil Exploration and Production U.S., Inc., New Orleans, LA 70113.

CRA tubing products that are generally equivalent in composition can exhibit substantial variation in performance. Performance means the ability to withstand a hostile well environment for possibly 20 to 30 years or more. The long term reliability is a critical issue and is often complicated by numerous uncertainties in the understanding of the well fluid composition at the time completion systems are selected.

The principal failure modes for CRA tubing are stress corrosion cracking [2], localized corrosion [3], and hydrogen embrittlement [4] that result from contact with sour produced fluids containing brine as a separate phase. Corrosive attack that produces cracking or pitting is facilitated by high temperature, increasing chloride content in the brine, lower pH, and sulfur activity. Sulfur can originate as dissolved  $H_2S$  (and its ionic forms) or as elemental sulfur present as a discrete phase, or both.

The empirical determination of an alloy's ability to resist cracking downhole includes exposing test specimens to a simulated environment and assessing damage after a period of time. This requires long exposure times (on the order of six months or more). Evaluation programs also employ tests that apply dynamic strain simultaneous with exposure to a simulated environment. These slow strain rate (SSR) tests diagnose cracking susceptibility in a short time period (2 days).

Localized corrosion can be diagnosed using electrochemical techniques and by exposure of coupons having an occluded cell geometry. Localized corrosion typically is slow to initiate; hence, accelerated tests are preferred.

Hydrogen embrittlement of nickel base alloys is sometimes difficult to distinguish from stress corrosion cracking when viewing crack morphology. When testing in the laboratory for an alloy's susceptibility to hydrogen embrittlement, the material of interest is coupled to carbon steel or artificially charged with a power supply to accelerate the cathodic reaction. Atomic hydrogen, produced by the corrosion reaction, causes damage (fracture) under the appropriate combinations of stress, temperature, and environment.

There is a significant interdependence of the localized corrosion process and the SCC mechanism. Both involve occluded cells (surface areas in which diffusion or convection is the rate limiting step for corrosion). Often crevice corrosion or pitting is prerequisite for the initiation of SCC. Localized corrosion, in turn, is intimately sensitive to alloy composition and to microstructural factors such as inclusions and grain boundary chemistry. The difference in performance of alloys that have the same generic bulk chemistry is therefore determined by subtle microstructural and compositional differences. The exposition of performance then requires specialized electrochemical tests (critical pitting temperature [CPT] tests) to delineate the abilities of proprietary products to resist corrosive attack.

This paper deals with differentiation of the performance of a group of proprietary alloys (Alloy G-type, 20–25 Cr, 45–50 Ni) having the same generic chemistry. The performance differences of interest relate to their ability to withstand degradation caused by produced fluids. The engineering protocol required measuring resistance to hydrogen embrittlement, localized corrosion and SCC, and the influence of environmental parameters (temperature, sulfur, brine chemistry) on each degradation mechanism.

## Experimental

Eight candidate materials from four manufacturers were considered, as outlined in Table 1. The material chemistries are set forth in Table 2. Nominally these materials contain 20 to 25% chromium, 42 to 55% nickel, and 3 to 7% molybdenum in addition to other alloying elements. Mechanical properties are described in Table 3. Yield strengths for these materials ranged from 139 to 169 ksi (958 to 1165 MPa). Microstructural differences were rigorously documented but are not included in this paper. The materials examined covered the entire

TABLE 1—*Candidate materials.*

Code	Manufacturer	Form	Avg Lng Yield. ksi	Dimensions
502	A	Pipe*	139	4.27 OD 0.75 wall
1029	B	Pipe*	156	4.25 OD 0.75 wall
1031	C	Pipe*	151	4.25 OD 0.75 wall
1032	A	Pipe*	169	4.25 OD 0.75 wall
1034	D	Pipe*	151	4.25 OD 0.75 wall
1035	D	Pipe*	137	4.25 OD 0.75 wall
1217	A	Pipe	139	3.5 OD 0.375 wall
1216	A	Pipe	141	5.0 OD 0.422 wall

\* coupling stock

NOTE: 1 ksi = 6.9 MPa.

range of products available in the time period in which the evaluating process took place (1986–1989) but do not necessarily reflect the properties of products now being produced. The test data should not be considered, nor are they intended to be, indicative of the quality of one manufacturer as opposed to another.

TABLE 2—*Material chemical analysis.*

Code	A502	B1028	C1021	A1032	D1034	D1035	A1217	A1216
Yield Strength, ksi	139	156	151	169	151	137	139	141
Element								
C	0.007	0.011	0.014	0.010	0.027	0.022	0.010	0.012
Mn	0.86	0.21	0.76	0.85	0.67	0.70	0.75	0.071
Si	0.19	0.20	0.60	0.80	0.60	0.66	0.65	0.060
Cr	24.27	21.50	21.82	22.42	24.74	24.40	22.4	20.0
Ni	44.58	39.73	44.70	42.00	48.0	48.57	44.8	54.4
Co	2.76							
Mo	6.92	2.86	6.97	6.97	6.0	6.05	6.95	9.00
W	1.01							
Fe	17.43						19.1	15.0
Cu	1.42							
Ti	0.10							
Nb	0.31							
P		0.014	0.018	0.023	0.016	0.011	0.016	0.01
S		0.002	0.001	0.001	0.004	0.002	0.005	0.007

NOTE: 1 ksi = 6.9 MPa.

TABLE 3—Material mechanical properties.

Material Code	Avg Lng. Yield, ksi	UTS, ksi	Avg Lng. Charpy, ft-lbs	Avg MW Hardness, RC
A502	139	148	220	30
B1029	156	166	93	35
C1031	151	156	182	34
A1032	169	173	156	37
D1034	151	168	188	37
A1217	139	151		32
A1216	141	149		37

NOTE: 1 ksi = 6.9 MPa. 1 ft-lb = 1.35 J.

### Test Methods

Susceptibility of production tubing samples to environmental cracking was measured by the SSR test method [5]. The method employs subsize tensile specimen (2.54 cm-long, 0.38 cm-diameter gage section) that is machined parallel to the longitudinal dimension of the pipe. The specimen is evaluated by exposing it to a simulated environment simultaneous with application of loading that produces an initial strain rate of  $4.0 \times 10^{-6}$  in./in./s ( $10.16 \times 10^{-6}$  cm/cm/s.).

Low-temperature (20 to 120°C) SSR tests were designed to measure susceptibility to hydrogen embrittlement. The hydrogen generation reaction was accelerated by attacking a small steel (API N-80) coupon adjacent to the SSR test specimen gage section such that the specimen and steel couple were in electrical contact. The surface area of the coupon was the same as the exposed specimen surface area (10 cm<sup>2</sup>).

Cracking susceptibility and localized corrosion susceptibility were verified using autoclave exposures of 30-day duration. C-ring specimens, DCB specimens, and coupons with serrated washers were used to make these determinations. The environmental simulation was identical to SSR simulations (see the following) with the exception of duration and size of autoclave. Autoclave test procedures and specimens are discussed in detail by Mack et al. [6].

Environmental simulations were accomplished using autoclaves (HC 276 construction) that were charged with brine and gas to reproduce the well water cut chemistry and the corrosive gas partial pressures. Hydrocarbon components were omitted. The chemical components in the brine phase reproduced the produced brine chloride content with NaCl and the produced fluid pH using acetic acid. Elemental sulfur was added in some tests as a discrete phase. The gas phase partial pressures were duplicated in proportions that simulate the well equilibrium at temperature. The environmental components are listed in Table 4.

TABLE 4—Test environments.

Environment Designation	NaCl, %	H <sub>2</sub> S (psia)	CO <sub>2</sub> (psia)	S (g/L)
823 <sup>a</sup>	20	75	700	—
823-S <sup>b</sup>	20	75	700	1
823-SC <sup>c</sup>	20	75	700	—

<sup>a</sup> Simulated moderately sour brine.

<sup>b</sup> 823 plus elemental sulfur.

<sup>c</sup> 823-SC specimen coupled to steel—no sulfur.

Electrochemical tests for localized corrosion included cyclic polarization (ASTM G 61, Test Method for Conducting Cyclic Potentiodynamic Polarization Measurements for Localized Corrosion susceptibility of Iron-, Nickel-, or Cobalt-Based Alloys) and CPT tests. The CPT tests measured the temperature at which localized corrosion initiated for a given combination of chloride, sulfide temperature, and potential. The test apparatus for CPT tests consisted of a high-temperature and pressure electrochemical cell that employed cylindrical (0.635 cm-diameter, 10.16 cm-long) electrodes. The simulated 823 environment was the same as described for SSR tests.

The CPT test method [7] applied an oxidizing potential using a potentiostat to a sample electrode that was exposed to the simulated environment. Electrode current was measured versus time. The electrode current/time function is recorded at temperatures that increase incrementally. The onset of localized corrosion (pitting) was observed by a sudden increase in current above the background level.

*Test Matrices*

The initial SSR test matrix was a screening study (Table 5) designed to examine a variety of material compositions and strengths. From this initial set of experiment, two materials were selected having a particular performance characteristic which were subsequently ex-

TABLE 5—Alloy screening test matrix.

Material	Environment	Temperature, C (F)							
		22 (75)	65 (150)	93 (200)	120 (250)	150 (300)	175 (350)	200 (400)	225 (450)
A502	Air 823-SC 823	1	1	1	2		2		
						2	2	2	2
B1029	Air 823-SC 823	1						1	
		1	1	1	1	2	2	2	2
C1031	Air 823-SC 823	1						1	
		1	1	1	1	2	2	2	2
A1032	Air 823-SC 823	1						1	
		1	1	1	1	2	2	2	2
D1034	Air 823-SC 823	1						1	
		1	1	1	1	2	2	2	2
D1035	Air 823-SC 823	1						1	
		1	1	1	1	2	2	2	2
A1217	Air 823-SC 823	1				2			2
A1216	Air 823-SC 823	1				2			2

NOTE: Numbers indicate test frequency.

TABLE 6—*Focused SSR test matrix.*

Material	Environment	Temperature, C (F)							
		38 (100)	65 (150)	93 (200)	120 (250)	150 (300)	175 (350)	200 (400)	225 (450)
A502	Air		2			2		2	
D1035	Air	2				2		2	
A502	823-SC <sup>a</sup>	2	2	2	2	2			
D1035	823-SC	2	2	2	2	2			
A502	823 <sup>b</sup>			2	2	2		2	
D1035	823-S <sup>c</sup>			2	2	2	2	2	
A1217	Air	1				2		2	
A1216	Air				2		2		
A1217	823			2	2	2	2	2	2
A1216	823			2	2	2	2	2	2
A1217	823-SC	1	1	1	1	1			
A1216	823-SC	1							
A1217	823-S			2	2	2	2	2	2
A1216	823-S			2	2	2	2	2	2

<sup>a</sup> Specimen coupled to steel.  
<sup>b</sup> 823 = 20% NaCl, 75 psi H<sub>2</sub>S, 700 psi CO<sub>2</sub>.  
<sup>c</sup> 823 plus 1 g/L elemental sulfur.

NOTE: 1 psi = 6.9 kPa.

aminated in detail as described in Table 6. Two additional materials from manufacturer A (see Table 1) were examined in the test matrix also shown in Table 6 which was concerned with the influence of elemental sulfur. Autoclave and electrochemical test matrices are provided in Table 7.

*Evaluation of Susceptibility to SCC and Localized Corrosion*

The relative performance of the sample alloys were differentiated on the basis of SSR parameters set forth in Table 8. Primarily, this assessment compares elongation and reduction

TABLE 7—*CPT test matrix.*

Material	H <sub>2</sub> S (psia)	CO <sub>2</sub> (psia)	Environment	
			NaCl, %	S (g/L)
A502	75	700	5	0
D1035	75	700	5	0
A502	75	700	20	0
D1035	75	700	20	0
A502	75	700	10	1
D1035	75	700	10	1

Autoclave Test Matrix

Environment	Temperature,		C-ring	Specimen	
	F	C		DCB	Coupon
823	300	150	2	2	2
823	450	225	2	2	2

TABLE 8—SSR parameters.

Time to Failure ( $t_f$ ) = $t_f - t_0$ where $t_f$ is the time to fracture from zero load ( $L$ ). NOTE: $t_0$ is the time derived from extrapolation of the elastic portion of the $L/\epsilon$ curve to zero load.
Elongation ( $E\%$ ) = $(t_f - t_c) 100/\epsilon$ where $t_c$ = time to yield defined as the time at which the $L/\epsilon$ curve becomes nonlinear.
Reduction in Area ( $R\%$ ) = $100 - (100D_f^2)/D_o^2$ where $D_f$ is the fracture diameter and $D_o$ is the diameter of the original gage length of the specimen.
Strain Rate ( $\epsilon$ ) = $4.0 \times 10^{-6}$ in./in./s
$E/E_a$ = ratio of environmental elongation in air (at test temperature)
$R/R_a$ = ratio of reduction in area to reduction in area in air
UTS = tensile strength from SSR curve
SC = secondary cracks defined as cracks outside the necked region of the gage diameter.

in fracture surface area. Secondary cracking was examined by inspection using a microscope. The criteria for cracking susceptibility are set forth in Table 9.

Localized corrosion performance was evaluated using coupons having serrated washers per ASTM G 78, Guide for Crevice Corrosion Testing of Iron Base and Nickel Base Stainless Alloys in Seawater and Other Chloride-Containing Aqueous Environments. The designation of localized corrosion is semiquantitative.

Cyclic polarization experiments (ASTM G 61) yield characteristic potential values that were used to diagnose pitting/crevice corrosion susceptibility. The criterion for localized attack was hysteresis in the  $i/V$  plot. The potential was ramped in the positive direction from  $E_{corr}$ . The potential at which the current increases suddenly was designated  $E_p$  ( $p$  = pitting). When the current density increased past a certain value ( $5 \times 10^{-3}$  A/cm<sup>2</sup>), the potential ramp was reversed. The potential at which the current on the reverse ramp was

TABLE 9—Criteria for cracking susceptibility.

	$E/E_a$	$R/R_a$	SC
Pass (nonsusceptibility)	>0.8 (and)	>0.8 (and)	No
Fail (clear susceptibility)	<0.8 (or) <0.5 (or) <0.6 (and)	<0.8 (and) <0.5 (and) <0.6 (and)	Yes No No
Gray area (requires further testing)	>0.6 < 0.8 (and) >0.8 (and)	>0.6 < 0.8 (and) >0.8 (and)	No Yes

NOTE: gray area requires SEM analysis.

TABLE 10—*Electrochemical criteria for localized corrosion susceptibility (ASTM G 61).*

Pass	No Hysteresis $E_{rp} - E_{cor} > 300 \text{ mV}$ $E_p - E_{con} > 500 \text{ mV}$
Fail	$E_{rp} < E_{con}$ $E_p - E_{con} < 100 \text{ mV}$
Gray area	$100 \text{ mV} < E_p - E_{con} < 500 \text{ mV}$ $0 < E_{rp} - E_{con} < 300 \text{ mV}$

equal to the current measured in the forward potential ramp was designated  $E_{rp}$  ( $rp$  = repassivation). The criteria for localized corrosion susceptibility based on these measured parameters are set forth in Table 10.

CPT tests employed a temperature step and applied potential to diagnose localized corrosion susceptibility. The potential of the sample alloy was held constant at  $E_{cpt} = E_{con} + E_a$  ( $E_a = 100 - 500 \text{ mV}$ ) while the temperature is increased in 10-degree (C) increments. At each temperature, the current of the alloy sample is measured versus time. An increase in current denoted localized corrosion and that temperature, therefore, is labeled the CPT. Alloys with lower CPT have a greater susceptibility to localized corrosion.

## Results

SSR data from the initial SSR screening experiments are compiled in Tables 11 and 12. Table 11 provides low-temperature (20 to 120°C) hydrogen embrittlement data and Table 12 provides high-temperature (150 to 225°C) SCC data. These data indicate ductility loss for alloys in low-temperature experiments at 93°C when coupled to carbon steel and in high-temperature experiments at temperatures that depend on sample material. Autoclave experiments were conducted to further define localized corrosion and cracking susceptibility. These data are essentially pass/fail and are summarized in Table 13.

Based on the screening experiments, two materials (A502, D1035) were selected for further evaluation with respect to localized corrosion and cracking susceptibility. SSR cracking data for these two materials are compiled in Tables 14 and 15 for hydrocarbon embrittlement (low temperature) and SCC (high temperature), respectively.

SSR data for materials A1216 and A1217 are compiled in Tables 16 and 17. The studies on these two materials were directed at determination of hydrogen embrittlement and high temperature SCC, specifically the effect of elemental sulfur on the latter mechanism. Materials A1216 and A1217 were new products commercialized after the original materials were selected.

Electrochemical cyclic polarization data are compiled in Tables 18 through 20. CPT tests data are summarized in Tables 21 through 23.

## Discussion

### Screening Experiments

SSR screening data Tables 11 and 12 identified three possible types of ductility loss.

Low temperature ductility loss (LTDL)—Materials C1031, A1032, and D1035 exhibited lower fracture area reduction ( $R$ ) and reduced elongation ( $E$ ) at 93°C. The mechanism is thought to involve hydrogen generated by the steel couple. Figures 1 through 3 plot elon-

TABLE 11—SSR test data, low-temperature experiments.

Material	Test Temp (C)	Test Temp (F)	Environment	T <sub>f</sub> (hours)	E (%)	E/E <sub>a</sub>	R (%)	R/R <sub>a</sub>	UTS (ksi)	SC
A502	22	75	823-SC	9.8	11.0	1.06	63.3	1.00	159.5	NO
A502	65	150	823-SC	8.5	9.3	0.90	59.6	0.94	149.6	NO
A502	93	200	823-SC	7.8	8.3	0.81	59.6	0.94	138.9	NO
A502	120	250	823-SC	7.7	8.1	0.78	67.7	1.07	157.3	NO
B1029	22	75	823-SC	6.5	5.8	0.97	62.4	0.98	151.2	NO
B1029	65	150	823-SC	5.9	5.4	0.90	58.0	0.91	137.5	NO
B1029	93	200	823-SC	5.7	5.3	0.88	58.2	0.91	136.4	NO
B1029	120	250	823-SC	6.0	5.8	0.97	65.0	1.02	127.6	NO
C1031	22	75	823-SC	10.0	10.6	0.83	60.0	0.80	146.8	NO
C1031	65	150	823-SC	9.8	10.5	0.82	75.7	1.01	145.8	NO
C1031	93	200	823-SC	8.2	8.1	0.63	44.2	0.59	144.6	NO
C1031	120	250	823	8.8	9.5	0.74	71.6	0.95	144.6	NO
A1032	22	75	823-SC	8.4	8.2	0.95	58.2	0.93	165.0	NO
A1032	65	150	823-SC	7.0	6.5	0.75	52.8	0.85	150.7	NO
A1032	93	200	823-SC	6.6	5.8	0.67	37.1	0.59	152.9	NO
A1032	120	250	823	7.1	6.6	0.77	59.0	0.95	143.0	NO
D1034	22	75	823-SC	11.6	13.2	0.82	57.3	0.80	162.2	NO
D1034	65	150	823-SC	11.9	13.7	0.85	50.0	0.70	143.6	NO
D1034	93	200	823-SC	11.6	13.5	0.84	53.8	0.75	137.5	NO
D1034	120	250	823	11.9	14.0	0.87	67.9	0.95	149.7	NO
D1035	22	75	823-SC	16.7	20.4	0.88	58.2	0.77	132.0	NO
D1035	65	150	823-SC	16.6	20.7	0.89	59.0	0.78	140.2	NO
D1035	93	200	823-SC	15.4	19.0	0.82	42.2	0.56	121.0	NO
D1035	120	250	823	16.4	21.0	0.91	69.4	0.92	113.3	NO

TABLE 12—SSR test data, high-temperature experiments.

Material	Test Temp (C)	Test Temp (F)	Environment	Tf (hours)	E (%)	E/Ea	R (%)	R/Ra	UTS (ksi)	SC
A502	150	300	823	8.6	9.1	0.88	70.8	1.11	155.1	NO
A502	175	350	823	7.6	7.5	0.73	66.3	1.04	149.7	NO
A502	200	400	823	8.2	8.4	0.81	63.6	1.00	135.6	NO
A502	225	450	823	7.7	7.9	0.77	67.3	1.06	149.3	NO
B1029	150	300	823	5.0	3.8	0.78	41.9	0.68	131.6	NO
B1029	175	350	823	4.6	3.2	0.66	29.5	0.48	135.3	NO
B1029	200	400	823	3.8	2.0	0.41	29.3	0.47	125.2	YES
B1029	225	450	823	4.5	3.0	0.62	31.5	0.51	133.5	YES
C1031	150	300	823	7.9	7.7	0.86	66.8	1.13	147.0	NO
C1031	175	350	823	6.7	7.2	0.81	46.2	0.78	137.8	YES
C1031	200	400	823	7.2	7.4	0.83	46.4	0.79	140.3	NO
C1031	225	450	823	8.0	8.5	0.95	51.9	0.88	141.1	NO
A1032	150	300	823	6.5	6.1	0.92	58.4	1.35	152.4	NO
A1032	175	350	823	5.4	4.4	0.66	42.0	0.97	156.2	NO
A1032	200	400	823	5.0	3.8	0.57	38.9	0.90	152.9	YES
A1032	225	450	823	3.7	2.0	0.31	13.5	0.31	137.0	YES
1034	150	300	823	7.5	7.6	0.68	56.0	0.76	147.4	NO
D1034	175	350	823	5.0	3.9	0.35	17.2	0.24	151.5	YES
D1034	200	400	823	8.4	6.4	0.57	41.9	0.57	151.8	NO
D1034	225	450	823	8.0	8.6	0.76	65.6	0.89	146.3	NO
D1035	150	300	823	6.9	7.2	0.49	27.0	0.41	119.7	YES
D1035	175	350	823	5.4	4.9	0.35	21.9	0.33	117.7	YES
D1035	200	400	823	13.1	15.8	1.08	68.3	1.04	125.7	NO
D1035	225	450	823	14.7	18.3	1.24	56.9	0.87	113.7	NO

NOTE \*\* Data are averages of duplicate tests.

TABLE 13—Summary table: Autoclave tests.

Material	Crevice Corrosion		SSR Cracking		C-ring/DCB Cracking	
	150°C	225°C	150°C	225°C	150°C	225°C
1029-9	X	—	X	X	—	X <sup>a</sup>
1031-11	X	—	X	—	—	X <sup>a</sup>
1032-3	—	—	—	X	—	X <sup>a</sup>
1033-13	X	—	—	X	—	XX <sup>b</sup>
1034-8	X	—	X	—	—	—
1035-7	X	—	X	—	—	—

<sup>a</sup> DCB cracking only.<sup>b</sup> DCB and C-ring cracking.

TABLE 14—Slow strain rate test data; low-temperature experiments, steel couple.

Material	Test Temp, C	Test Temp, F	Environment	Tf, hours	E(%)	E/Ea	R(%)	R/Ra	UTS (ksi)	SC
A502	38	100	823-SC	7.2	7.1	0.93	57.4	0.84	136.8	NO
	65	150	823-SC	7.5	7.5	1.00	63.6	0.93	140.4	NO
	93	200	823-SC	7.1	6.8	0.91	53.3	0.78	135.4	NO
	120	250	823-SC	6.6	6.4	0.84	48.8	0.71	127.1	NO
	150	300	823-SC	6.8	6.7	0.89	59.3	0.86	128.3	NO
D1035	38	100	823-SC	13.0	15.8	1.01	49.1	0.7	143.2	NO
	65	150	823-SC	12.9	15.4	0.99	48.7	0.69	132.8	NO
	93	200	823-SC	12.0	14.1	0.93	41.2	0.59	134.6	NO
	120	250	823-SC	12.4	14.7	0.95	46.1	0.66	129.1	NO
	150	300	823-SC	11.6	13.7	0.89	50.8	0.72	121.3	NO

NOTE: Data are averages of duplicate tests.

TABLE 15—Slow strain rate test data; high-temperature experiments.

Material	Test Temp, C	Test Temp, F	Environment	Tf, hours	E(%)	E/Ea	R(%)	R/Ra	UTS (ksi)	SC
A502	93	200	823	7.4	7.4	1.00	69.6	1.04	134.6	NO
	120	250	823	7.5	7.8	1.05	66.0	0.99	133.0	NO
	150	300	823	7.5	7.7	1.05	69.4	1.04	134.5	NO
	175	350	823	7.0	7.1	0.96	66.9	1.00	124.6	NO
	200	400	823	5.3	4.5	0.58	55.1	0.82	115.1	NO
D1035	93	200	823-S	13.6	16.4	1.19	72.9	1.05	135.8	NO
	120	250	823-S	6.9	7.0	0.54	27.7	0.40	137.0	YES
	150	300	823-S	7.8	8.2	0.67	43.3	0.64	129.9	NO
	175	350	823-S	4.8	3.9	0.30	12.9	0.19	124.7	YES
	200	400	823-S	4.3	3.5	0.26	11.6	0.17	102.8	YES

NOTE: Data are averages of duplicate tests.

TABLE 16—*Slow strain rate test data; low-temperature experiments.*

Material	Test Temp, C	Test Temp, F	Environment	Tf, hours	E(%)	E/Ea	R(%)	R/Ra	UTS (ksi)	SC
A1217	38	100	823-SC	8.0	8.2	0.98	51.9	0.91	129.1	NO
	65	150	823-SC	8.6	9.1	1.09	49.1	0.86	122.1	NO
	93	200	823-SC	7.6	7.6	0.91	59.9	1.05	119.3	NO
	120	250	823-SC	7.8	8.4	1.01	50.1	0.88	117.6	NO
	150	300	823-SC	6.7	6.5	0.78	48.2	0.84	117.0	NO
A1216	93	200	823	8.9	9.2	0.91	55.6	1.06	153.7	NO
	120	250	823	9.1	10.0	0.98	58.6	1.12	130.2	NO
	150	300	823	9.1	9.7	0.95	55.5	1.06	143.6	NO
	175	350	823	8.7	9.4	0.93	52.4	1.00	139.3	NO
	200	400	823	10.7	12.4	1.22	49.1	0.94	131.0	NO
	225	450	823	10.2	11.5	1.13	45.3	0.87	132.9	NO

NOTE: Data are averages of duplicate tests.

gation ratio and reduction in area ratio as a function of temperature. There is a clear minimum at 93°C.

Intermediate temperature SSC (ITSCC)—Materials B1029, D1034, and D1035 exhibited loss of ductility and evidence of secondary cracking at 150 to 175°C. This observation is unique in that this susceptibility to cracking *did not* persist with increasing temperature. Figures 4 through 6 illustrate loss of ductility associated with SCC at intermediate temperature.

High temperature SSC (HTSCC)—Materials B1029 and A1032 exhibited susceptibility SSC that increased with increasing test temperature. This type of behavior is typical for nickel base alloys in that elevated temperature is known to accelerate SCC. Figure 7 illustrates HTSCC.

The SSR screening data are of interest because they identify possible degradation mechanisms heretofore unacknowledged in the literature. Kane [8] identified hydrogen embrittlement (HE) of nickel base alloys at room temperature as a possible failure mode in long-term charging experiment of alloy C-276. HE has not been identified as a mode of degradation of Alloy G (20–25 Cr and 45–50 Ni) type materials at nominal strength levels.

The LTDL measured in SSR experiments do not equate with cracking *per se*. No independent verification of fracture in statically stressed specimens was achieved (see autoclave data in Table 13 and discussion in paragraphs to follow). LTDL, however, is thought to involve hydrogen absorption and transport which is a strong function of temperature. Hydrogen diffusivity is very low in nickel base alloys at 22°C but increases rapidly with temperature. It is feasible, therefore, that the 93°C ductility loss reflects an increasing amount of absorbed hydrogen. At temperatures greater than 93°C, increased dislocation mobility may account for the restoration of ductility.

ITSCC has not been reported previously in the literature for Alloy G type materials. It results from localized corrosion that is peculiar to the identified temperature range (120 to 175°C). ITSCC in SSR specimens is accompanied by substantial amounts of surface corrosion adjacent to the fracture. The alloy surface appearance is otherwise pristine. The mechanism of ITSCC involves initiation of localized corrosion at surface striations resulting from specimen machining. Highly polished surfaces do not demonstrate ITSCC as readily.

ITSCC is distinguished from HTSCC by surface appearance. At higher temperatures (175 to 225°C) G-type alloys form sulfide corrosion products, the thicknesses of which increase with temperature. At lower temperatures, the film is primarily Cr<sub>2</sub>O<sub>3</sub> which acts as a galvanic

TABLE 17—Slow strain rate test data; HISSC experiments.

Material	Test Temp (C)	Test Temp (F)	Environment	Tf (hours)	E (%)	E/Ea	R (%)	R/Ra	UTS (ksi)	SC
A1216	93	200	823	8.9	9.2	0.91	55.6	1.06	153.7	NO
A1216	120	250	823	9.1	10.0	0.98	58.6	1.12	130.2	NO
A1216	150	300	823	9.1	9.7	0.95	55.5	1.06	143.6	NO
A1216	175	350	823	8.7	9.4	0.93	52.4	1.00	139.3	NO
A1216	200	400	823	10.7	12.4	1.22	49.1	0.94	131.0	NO
A1216	225	450	823	10.2	11.5	1.13	45.7	0.87	132.9	NO
A1216	93	200	823-S	9.2	9.9	0.98	62.8	1.20	138.1	NO
A1216	120	250	823-S	8.1	8.5	0.84	60.3	1.15	135.6	NO
A1216	150	300	823-S	7.6	7.6	0.75	42.2	0.80	138.7	NO
A1216	175	350	823-S	5.2	4.1	0.41	17.7	0.34	137.8	YES
A1216	200	400	823-S	4.0	2.6	0.26	18.2	0.35	126.8	YES
A1216	225	450	823-S	3.6	2.2	0.22	17.8	0.34	123.4	YES
A1217	93	200	823	7.5	7.5	0.93	58.9	1.10	112.1	YES
A1217	120	250	823	7.7	8.0	1.00	52.3	0.97	103.6	NO
A1217	150	300	823	7.3	7.4	0.92	50.5	0.94	108.1	NO
A1217	175	350	823	7.3	7.4	0.91	47.2	0.88	101.4	NO
A1217	200	400	823	8.2	8.7	1.07	52.6	0.98	109.0	NO
A1217	225	450	823	10.0	11.5	1.43	50.1	0.93	108.1	NO
A1217	93	200	823-S	7.8	7.9	0.98	62.6	1.16	110.2	NO
A1217	120	250	823-S	6.6	6.0	0.74	40.4	0.75	122.1	NO
A1217	150	300	823-S	6.0	5.5	0.68	36.8	0.68	104.0	NO
A1217	175	350	823-S	4.0	2.5	0.31	15.4	0.29	105.1	YES
A1217	200	400	823-S	3.2	1.4	0.18	10.4	0.19	92.0	YES
A1217	225	450	823-S	3.6	2.4	0.30	17.8	0.33	86.1	YES

NOTE \*\* Data are averages of duplicate tests.

TABLE 18—Pitting scan results of alloy D1035 and alloy A502 in 5% NaCl solution.

Temperature		$E_p$ (V)	$E_{pp}$ (V)	$E_{corr}$ (V)	$E_p - E_{corr}$ (V)	$E_{pp} - E_{corr}$ (V)
C	F					
D1035						
65	150	*	0.240	-0.224	—	0.464
93	200	*	0.250	-0.122	—	0.372
120	250	*	-0.050	-0.124	—	0.074
150	300	*	—	-0.464	—	—
175	350	*	-0.200	-0.428	—	0.228
A502						
65	150	*	-0.120	-0.372	—	0.252
93	200	*	—	-0.178	—	—
120	250	*	—	-0.104	—	—
150	300	*	—	-0.378	—	—
175	350	*	-0.150	-0.468	—	0.318

\* No hysteresis.

cathode driving the anodic corrosion reaction. Dynamic strains produced by the SSR test are necessary for ITSCC initiation.

HTSCC of G-type alloys in sour environments is well-documented in the literature. HTSCC coincides with corrosion that produced primarily sulfide films and is accentuated by elevated temperature, chloride content in the aqueous phase, lower pH, and high sulfur activity. The mechanistic discussion is of importance because the alloys under scrutiny exhibit varying degrees of susceptibility to LTDL, ITSCC, and HTSCC. It is, therefore, highly advantageous to understand the implications of test results on materials performance in service not only as a means of ranking performance, but also in an effort to understand ramifications for end use.

TABLE 19—Pitting scan results of alloy D1035 and alloy A502 in 20% NaCl solution.

Temperature		$E_p$ (V)	$E_{pp}$ (V)	$E_{corr}$ (V)	$E_p - E_{corr}$ (V)	$E_{pp} - E_{corr}$ (V)
C	F					
D1035						
65	150	0.150	-0.050	-0.314	0.464	0.264
93	200	0.250	0.020	-0.260	0.510	0.280
120	250	—	-0.170	-0.272	—	0.102
175	350	-0.030	—	-0.152	0.122	—
A502						
65	150	0.150	0.000	-0.278	0.428	0.278
93	200	0.250	0.010	-0.266	0.516	0.366
120	250	—	-0.130	-0.244	—	0.114
175	350	—	-0.200	-0.492	—	0.292

TABLE 20—Pitting scan results of alloy D1035 and alloy A502 in 20% + 1 g/L sulfur solution.

Temperature		$E_p$ (V)	$E_{pp}$ (V)	$E_{corr}$ (V)	$E_p - E_{corr}$ (V)	$E_{pp} - E_{corr}$ (V)
C	F					
D1035						
65	150	0.400	0.170	-0.006	0.406	0.176
93	200	0.400	0.040	-0.068	0.468	0.108
120	250	—	—	0.196	—	—
150	300	—	—	0.056	—	—
175	350	—	—	-0.102	—	—
A502						
65	150	0.520	0.130	-0.012	0.532	0.142
93	200	0.420	0.140	-0.102	0.522	0.242
120	250	0.680	0.600	0.244	0.704	0.376
150	300	—	—	0.070	—	—
175	350	—	—	-0.086	—	—

TABLE 21—Critical pitting temperature test of D1025 and alloy A502 in 5% NaCl solution.

Temperature		$E_{con}$ (V)	$E_a$ (V)	$I_i$ (mA/cm <sup>2</sup> )	$I_l$ (mA/cm <sup>2</sup> )
C	F				
D1035					
65	150	-0.110	0	0.67	0.39
93	200	-0.110	0	1.20	0.36
120	250	-0.124	0	2.45	0.94
150	300	-0.407	-0.300	0.089	0.089
175	350	-0.450	-0.350	0.16	0.083
175	350	-0.476	-0.000	12.2	8.12
175	350	-0.451	+0.100	29.3	17.9
A502					
65	150	-0.108	0	0.67	0.47
93	200	-0.117	0	1.49	0.30
120	250	-0.104	0	3.77	0.90
150	300	-0.385	-0.285	0.10	0.010
175	350	-0.478	-0.378	0.035	0
175	350	-0.492	0.000	16.2	6.01
175	350	-0.373	+0.100	29.3	11.4

$E_{E_{corr}}$  = Open Circuit Potential.

$E_a$  = Applied Potential.

$I_i$  = Initial Current Density.

$I_l$  = Current Density after 15 min.

TABLE 22—Critical pitting temperature test of D1025 and alloy A502 in 20% NaCl solution.

Temperature		$E_{\text{corr}}$ (V)	$E_a$ (V)	$I_i$ (mA/cm <sup>2</sup> )	$I_f$ (mA/cm <sup>2</sup> )
C	F				
D1035					
65	150	-0.236	0.0	1.56	1.07
93	200	-0.248	0.0	1.58	0.82
120	250	-0.240	0.0	2.9	1.74
175	350	-0.328	0.0	10.8	108 <sup>a</sup>
A502					
65	150	-0.211	0.0	1.67	1.27
93	200	-0.261	0.0	1.67	0.88
120	250	-0.230	0.0	3.19	0.72
175	300	-0.340	0.0	10.8	108 <sup>b</sup>

<sup>a</sup> In 80 seconds.<sup>b</sup> In 300 seconds.

Autoclave exposures were used to verify the SSR test results and to gain further insight into the various mechanisms. Data from statically stressed specimens (C-rings, DCBs) did not discover any incidence of ITSCC; however, localized corrosion susceptibility was confirmed for all materials that exhibit ITSCC using coupons having artificial crevices. HTSCC of susceptible alloys was also confirmed using C-ring specimens and DCB specimens.

### ITSCC Experiments

Two alloys from two different manufacturers were selected for further investigation of the ITSCC mechanism. SSR tests were conducted at low temperature and high temperature.

TABLE 23—Critical pitting temperature test of D1025 and alloy A502 in 10% NaCl + 1 g/L sulfur solution 75 psia H<sub>2</sub>S, 700 psia CO<sub>2</sub>.

Temperature		$E_{\text{corr}}$ (V)	$E_a$ (V)	$I_i$ (mA/cm <sup>2</sup> )	$I_f$ (mA/cm <sup>2</sup> )
C	F				
D1035					
65	150	-0.052	0.200	1.0	0.12
93	200	-0.062	0.200	1.6	0.26
120	250	-0.203	0.400	4.29	0.74
150	300	-0.130	0.330	6.7	17.8
175	350	-0.161	0.100	8.0	13.0
A502					
65	150	-0.063	0.200	0.75	0.075
93	200	-0.075	0.200	1.8	0.1
120	250	-0.190	0.330	4.7	0.63
150	300	-0.119	0.330	10.0	2.89
175	350	-0.115	0.115	5.0	10.0

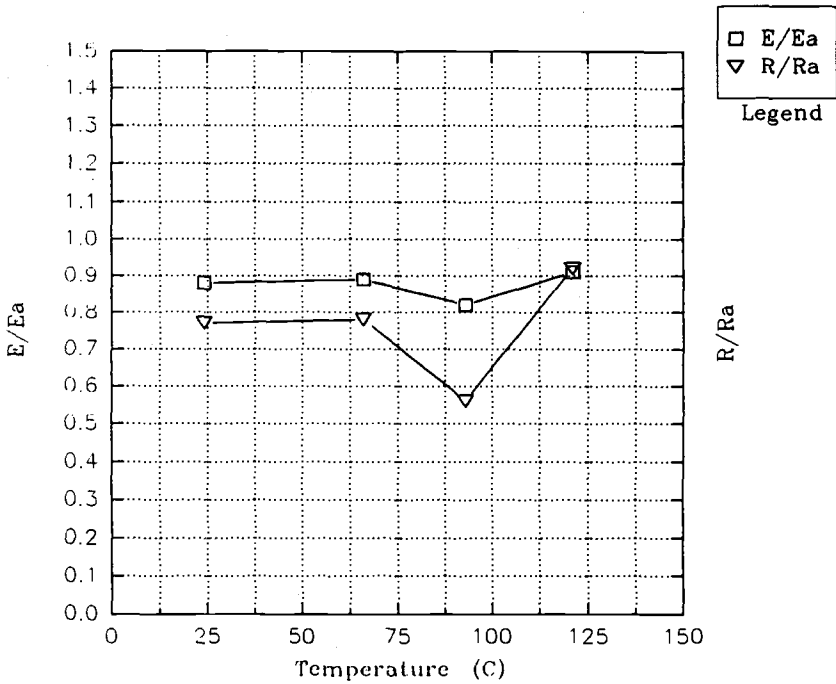


FIG. 1—Ductility ratios versus temperature D1035, screening experiments.

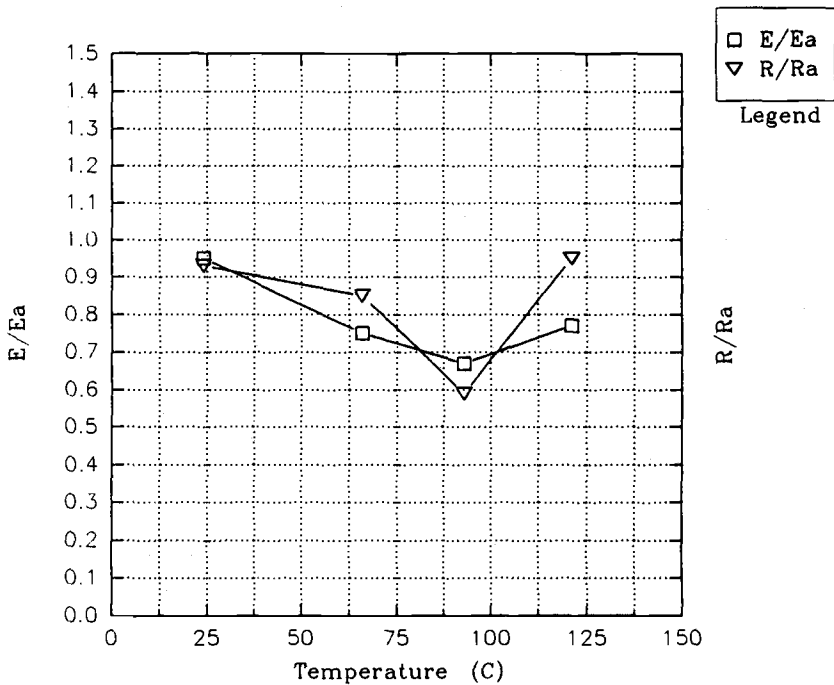


FIG. 2—Ductility ratios versus temperature A1032, screening experiments.

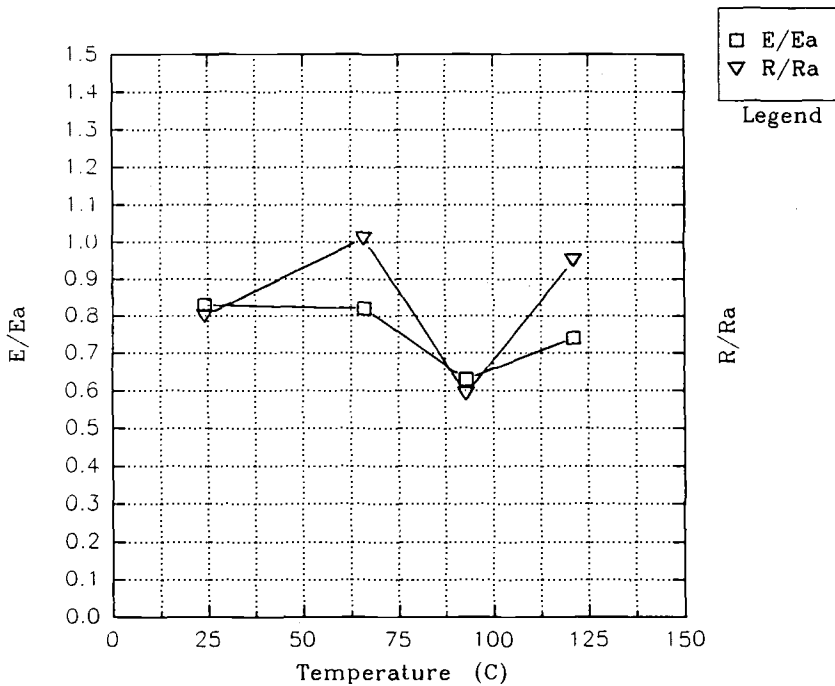


FIG. 3—Ductility ratios versus temperature C1031, screening experiments.

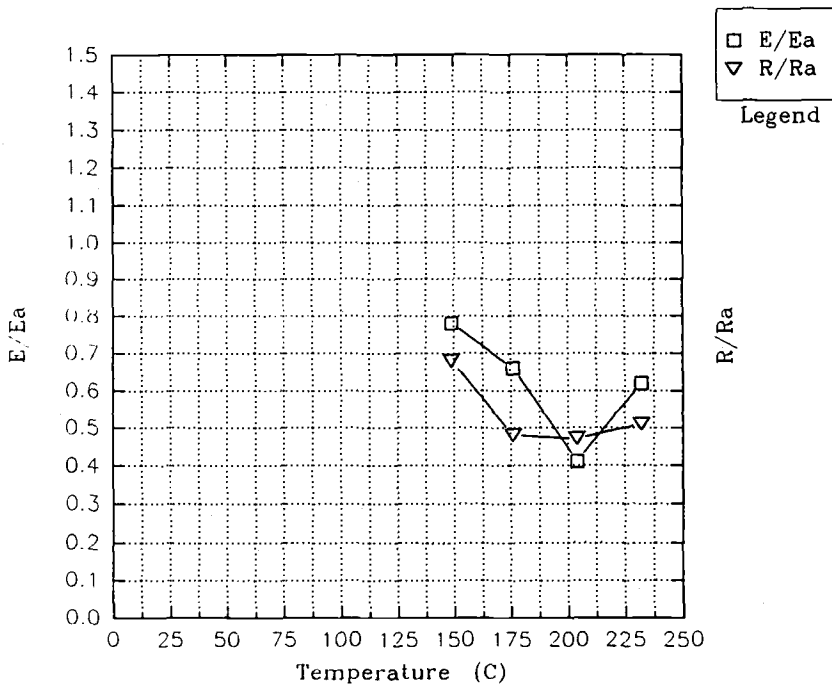


FIG. 4—Ductility ratios versus temperature B1029, screening experiments, elemental sulfur.

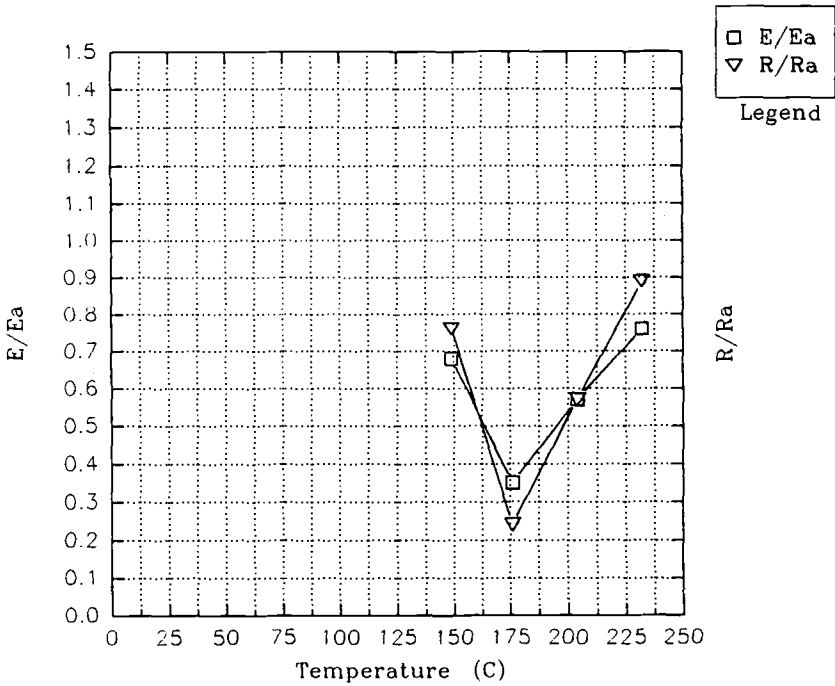


FIG. 5—Ductility ratios versus temperature D1034, screening experiments.

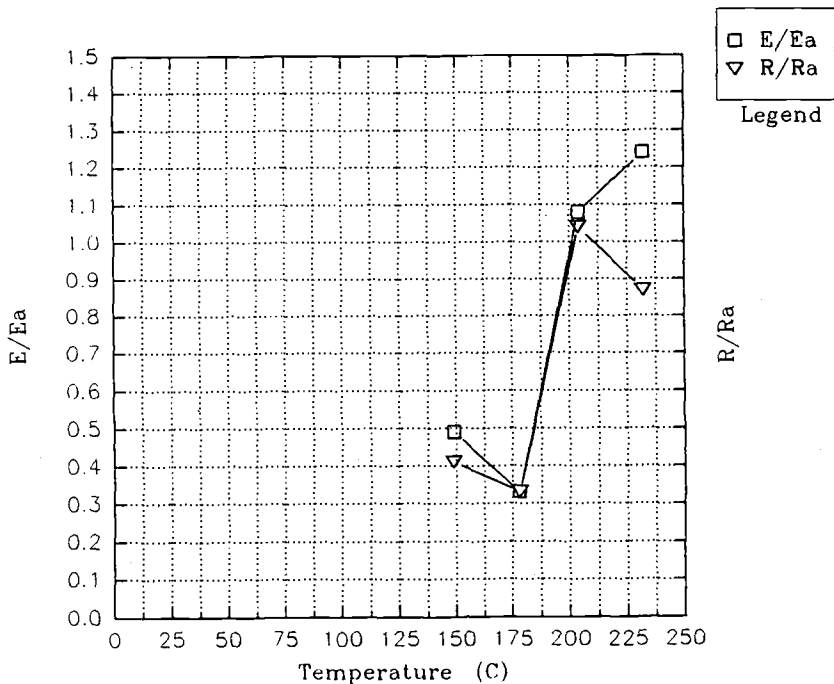


FIG. 6—Ductility ratios versus temperature D1035, screening experiments.

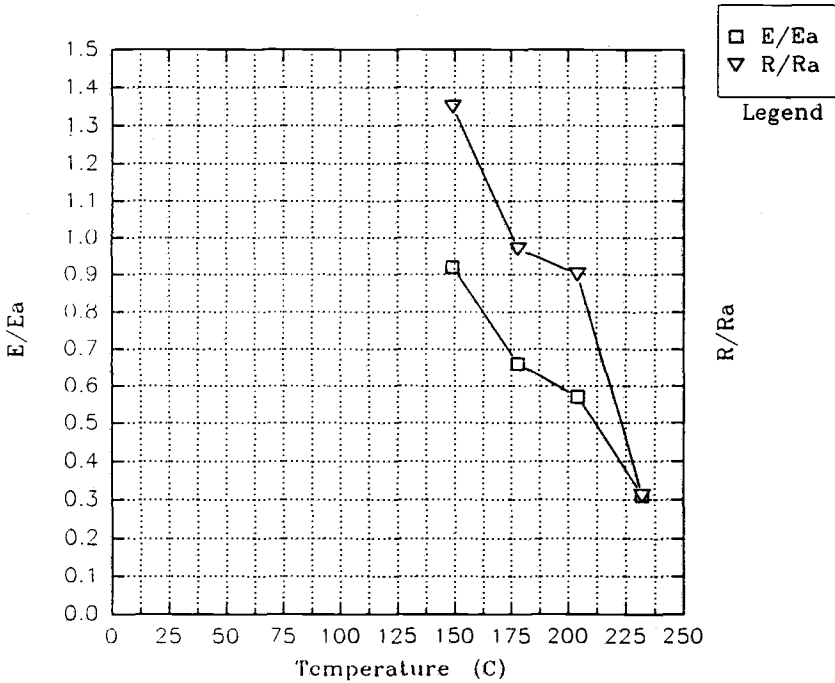


FIG. 7—Ductility ratios versus temperature A1032, screening experiments.

The low-temperature experiments (Table 14) verified that alloy A502 was not sensitive to LTDL or to ITSCC. Alloy D1035 was verified as sensitive to LTDL and HTSCC in the presence of elemental sulfur (see Figs. 8 and 9).

The elemental sulfur question results from uncertainty in the well composition. Well test data had suggested that elemental sulfur was possible in produced gas. Previous research on this subject [9] had indicated the pronounced detrimental effect of elemental sulfur on SCC susceptibility. At grossly exaggerated levels (1 g/L) employed in SSR tests, elemental sulfur produces SCC when present in combination with brine, H<sub>2</sub>S, and low pH (CO<sub>2</sub>). The loss of ductility is evident at 150°C and all higher temperatures for alloy D1035.

### HTSCC Experiments

Two proprietary alloys from manufacturer A (A1216 and A1217) were selected for scrutiny of their relative abilities to resist HTSCC as complicated by elemental sulfur. The data are graphically depicted in Figs. 10 and 11 which demonstrate the pronounced loss of performance at temperatures above 120°C. These data allow the conclusion that G-type alloys cannot withstand situations in which copious amounts of elemental sulfur are produced. Luckily, however, this is not the case for the 823 field.

### Electrochemical Experiments

The performance of G-type materials was concluded to depend intimately with localized corrosion resistance. Two materials were selected for intensive investigation based on the results of SSR tests which showed material A506 resistant to ITSCC while alloy D1035

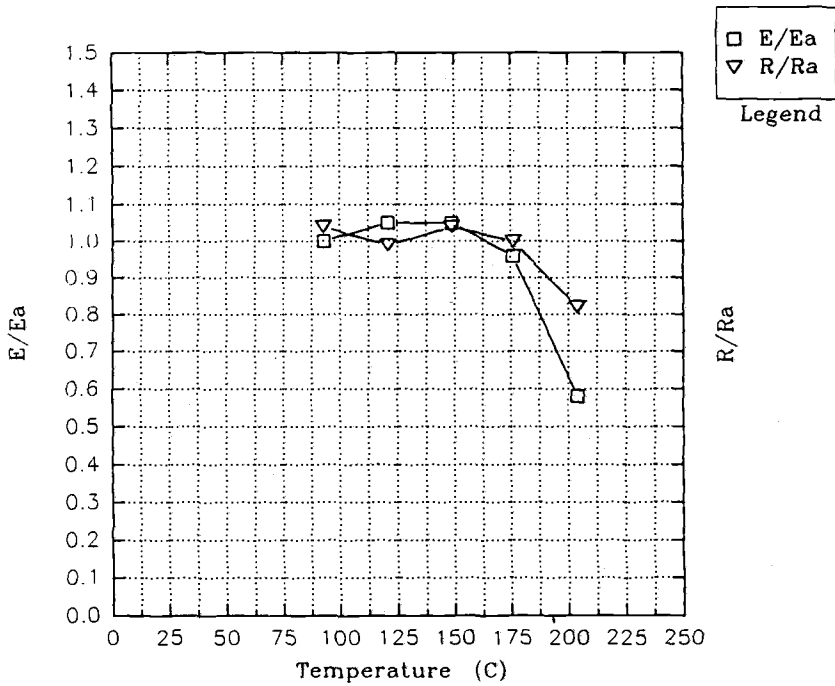


FIG. 8—Ductility ratios versus temperature, A502.

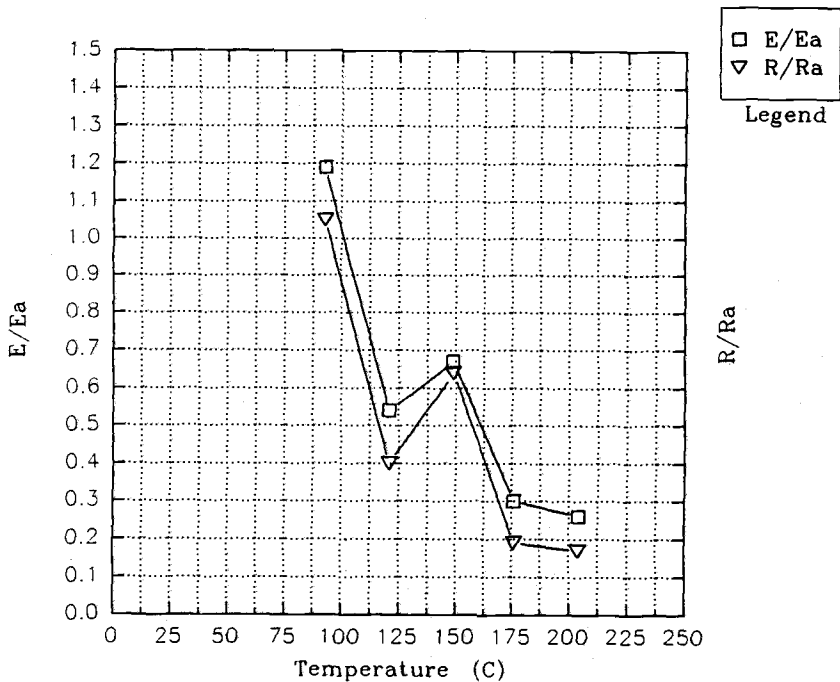


FIG. 9—Ductility ratios versus temperature, D1035, elemental sulfur.

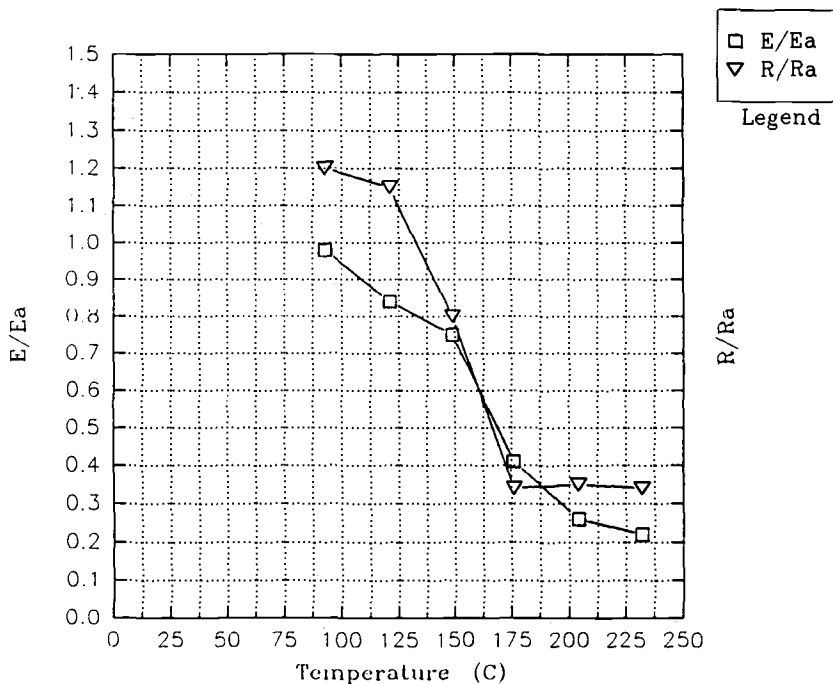


FIG. 10—Ductility ratios versus temperature, A1216, elemental sulfur.

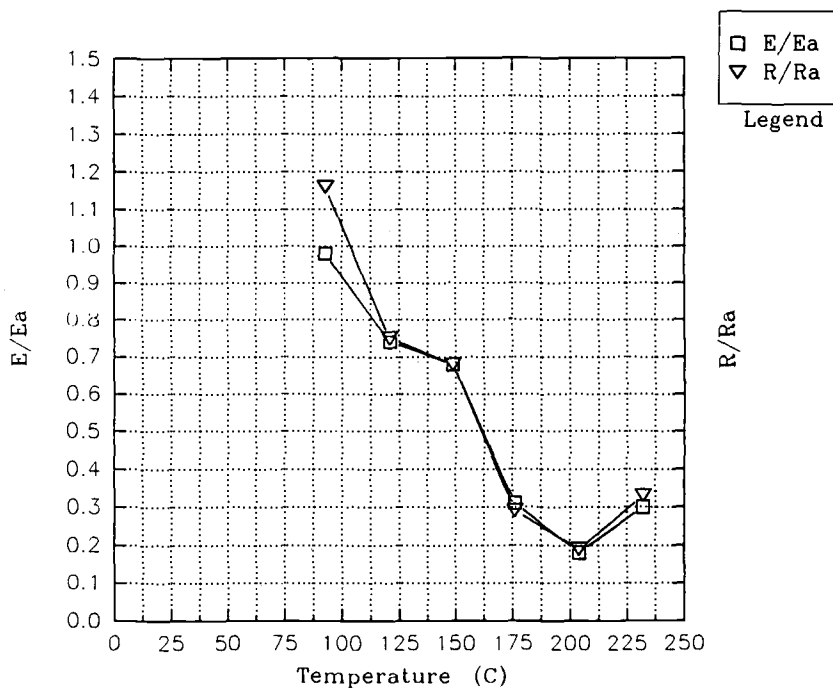


FIG. 11—Ductility ratios versus temperature, A1217, elemental sulfur.

susceptible. The chosen alloys were subjected to electrochemical tests at various temperatures and in brines having differing amounts of chloride and in some cases elemental sulfur.

Typical polarization scans to measure pitting resistance are shown in Figs. 12 through 14 for materials A502 and D1035. The three parameters used to diagnose localized corrosion from pitting scans are corrosion potential ( $E_{corr}$ ), pitting potential ( $E_p$ ), and repassivation potential ( $E_{rp}$ ).  $E_{corr}$  is the open circuit potential before the scan,  $E_p$  is the potential where a sharp current increase occurs, and  $E_{rp}$  is the potential where the reverse scan intersects the forward scan. The difference between  $E_{corr}$  and  $E_p$  ( $E_p - E_{corr}$ ) quantifies the resistance to pit initiation; the larger the difference the more difficult for pitting corrosion to initiate. The difference between  $E_{rp}$  and  $E_{corr}$  ( $E_{rp} - E_{corr}$ ) is related to pit propagation: the smaller the difference the easier for existing pits to propagate. Existing pits will not repassivate (or heal) if  $E_{rp} < E_{corr}$ . Hysteresis on the pitting scan (current density on the reverse scan is higher than that on the forward scan) means that localized corrosion (pitting) is a component of the corrosion mechanism.

Data on both electrodes in three solutions are compiled in Tables 18 through 20. In 5% NaCl solution, the pitting scan curves of alloys D1035 and A502 at the same temperatures are similar. No hysteresis was found on A506 or on D1035 at 175°C indicating resistance to pitting. The difference between ( $E_{rp} - E_{corr}$ ) of the two materials is not significant. Both materials are immune to pitting corrosion in 5% NaCl solution which is the least aggressive solution tested.

In 20% NaCl solution, both materials behaved similarly at every temperature except at 175°C. The repassivation potential,  $E_{rp}$ , for D1035 at 175°C is less than  $E_{corr}$ , while  $E_{rp}$  for A502 is 0.292 V above  $E_{corr}$ . This suggests that A502 is substantially more resistant to pitting than D1035 at 175°C in 20% NaCl. In 10% NaCl plus 1 g/L sulfur solution, similar pitting scans and pitting resistances were found for both materials below 120°C. At 120°C, A502 is more pitting resistant as indicated by  $E_{rp} - E_{corr}$ .

Pitting corrosion scans, therefore, indicate that A502 is significantly more resistant to pitting corrosion at intermediate temperatures.

In CPT tests, the electrodes were polarized to potentials more noble than the open circuit potential and the anodic current of the electrode was recorded for 15 min. The initial current

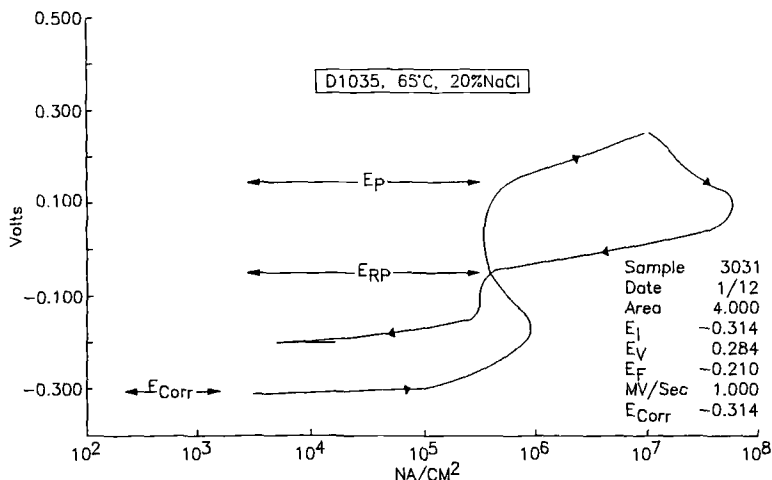


FIG. 12—Electrochemical cyclic polarization scan, D1035, 65°C, 20% NaCl.

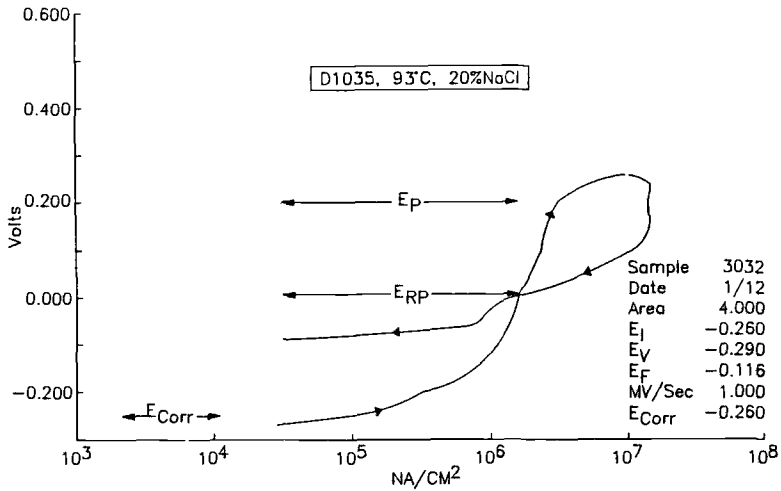


FIG. 13—Electrochemical cyclic polarization scan, D1035, 93°C, 20% NaCl.

density (current density immediately after potential was applied) and the final current density (current density after 15 min at applied potential) were used to diagnose localized corrosion. A final current density ( $I_f$ ) that is substantially greater than the initial current density ( $I_i$ ) signifies that pitting corrosion has initiated. If  $I_f$  is less than (or equal to)  $I_i$ , pitting corrosion has not initiated. The critical pitting temperature is defined as the lowest temperature for which  $I_f$  is substantially greater than  $I_i$ .

Initial and final current densities of CPT tests are listed in Tables 21 through 23. For 5% NaCl solution, the final current densities were always lower than the initial current densities

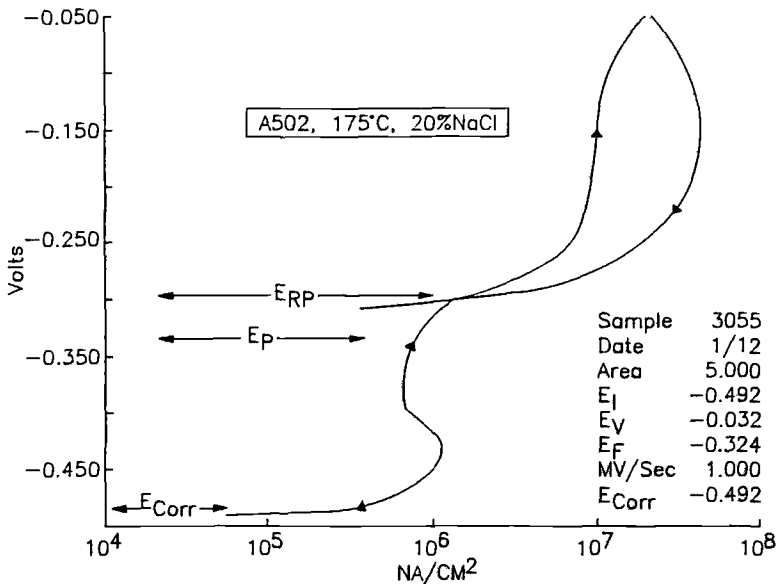


FIG. 14—Electrochemical cyclic polarization scan, A502, 175°C, 20% NaCl.

for both D1035 and A502. This means no initiation of pitting during the fifteen-minute-periods up to and including 175°C. The pitting resistances of D1035 and A502 in the 5% NaCl solution are good and cannot be differentiated.

In 20% NaCl solution and at temperatures below 120°C, no current increases were observed. At 175°C, however, the current increased rapidly indicating localized corrosion had initiated (Fig. 15). This observation suggests pitting corrosion of D1035 and A502 is likely to occur between 120 and 175°C. The current density of A502 increased at a slower rate than D1035, suggesting that it takes a longer time for pitting corrosion to initiate on A502. Hence, the CPT tests indicate that A502 is more resistant to pitting than D1035 in 20% NaCl solution. The critical pitting temperatures for both alloys are 120°C in 20% NaCl (75 psi H<sub>2</sub>S, 750 psi CO<sub>2</sub>).

In 10% NaCl solution with 1 g/L sulfur (75 psi H<sub>2</sub>S, 750 CO<sub>2</sub>), no current increases were found on either material at temperatures below 120°C. The current-time curves of both alloys at 120°C and 150°C are shown in Fig. 16. Current increases were found on D1035 and A502 at 150°C suggesting that both materials undergo localized corrosion. Again, the current increase being faster on D1035 than on A502 suggests D1035 is less resistant to pitting in the environment at 150°C. The CPT for both alloys is 120°C.

The CPT test is an accelerated test and indicates relative performance and the possibility of localized corrosion. It is concluded that A502 is more resistant to localized corrosion than D1035 in the test environments. Pitting corrosion may occur on both materials in high chloride or sulfur containing solutions at a temperature range of 120 to 175°C, which should be confirmed by autoclave tests.

In sum, the pitting scans and CPT tests suggest alloys D1035 and A502 are potentially susceptible to localized corrosion in 10% NaCl with 1 g/L sulfur and in 20% NaCl environments at 120 to 175°C. This finding coincides with the fact that D1035 suffered stress corrosion cracking at intermediate temperatures as indicated by SSR tests. It can be reasonably inferred that medium-temperature stress cracking found in SSR tests is initiated by localized corrosion. Alloy A502 is found to be more resistant to pitting corrosion and hence more resistant to stress cracking under such conditions.

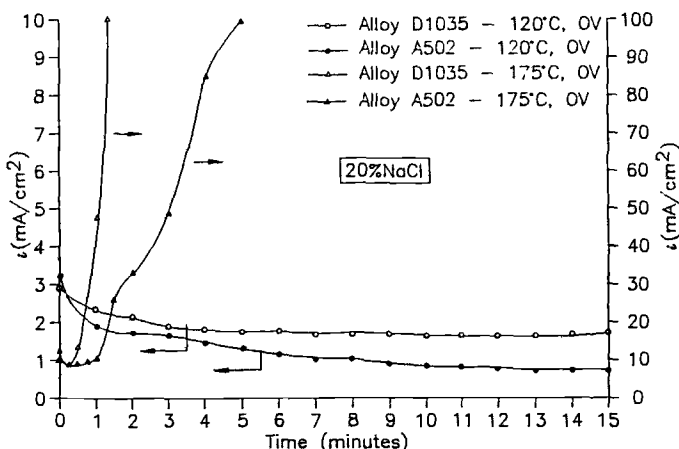


FIG. 15—Critical pitting temperature test, current versus time.

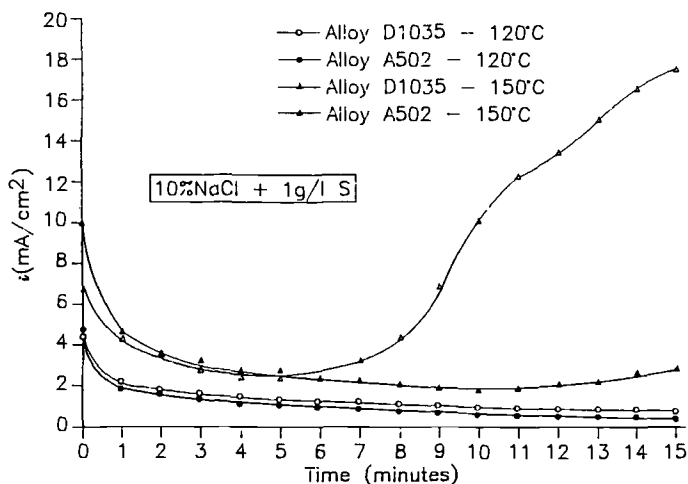


FIG. 16—Critical pitting temperature test, current versus time.

## Conclusions

Alloy G-type (nominally 20–25 Cr, 45–55 Ni) materials are potentially susceptible to localized corrosion at temperatures between 120 and 175°C. Alloy performance is a subtle function of compositional and microstructural differences. Under conditions of dynamic strain, localized corrosion can result in SCC; however, the observation of SCC in SSR tests may be an artifact of testing related to strain rate and surface finish and may not indicate a likelihood of service degradation.

Resistance to localized corrosion in G-type materials is alloy-specific. A range of performance can be measured using coupon exposures, electrochemical tests, and SSR experiments.

At low temperature ( $T < 120^\circ\text{C}$ ), and under conditions of hydrogen charging, some alloy G-type materials can experience slight ductility loss caused by hydrogen absorption. The ductility minimum is specific to 93°C and likely results from a kinetic balance between rate of hydrogen generation, hydrogen diffusion, and dislocation mobility.

SSR tests at temperatures between 120 and 175°C predict cracking susceptibility (ITSCC) that is initiated by localized corrosion. The observation of ITSCC depends on surface roughness in that machining striations provide sites for localized corrosion initiation under conditions of dynamic strain.

SCC of G-type materials is greatly affected by elemental sulfur. When elemental sulfur is present in gross excess, all G-type materials exhibit SCC susceptibility that increases with temperature.

It is possible to rank localized corrosion susceptibility of alloys using electrochemical CPS and CPT tests so as to predict service performance. The performance prediction agree with autoclave tests and SSR tests to provide a clear differentiation of alloy capability.

## References

- [1] Wilhelm, S. M. and Kane, R. D., "Selection of Materials for Sour Service in Petroleum Production," *Journal of Petroleum Technology*, Society of Petroleum Engineers, October 1986.
- [2] Rhodes, P. R., "Stress Cracking Risks in Corrosive Oil and Gas Wells," *Corrosion/86*, Paper No. 322, National Association of Corrosion Engineers, March 1986.

- [3] Tuttle, R. N., "Corrosion in Oil and Gas Production," *Journal of Petroleum Technology*, Society of Petroleum Engineers, July 1987.
- [4] Coyle, R. J., Kargol, J. A., and Fiore, N. F., "The Effect of Aging on Hydrogen Embrittlement of a Nickel Alloy," *Metallurgical Transactions A*, Vol. 12A, April 1981.
- [5] McIntyre, D. R., Kane, R. D., and Wilhelm, S. M., "Slow Strain Rate Testing for Materials Evaluation in High Pressure H<sub>2</sub>S Environments," *Corrosion/86, Paper 149*, National Association of Corrosion Engineers, 1986.
- [6] Mack, R. D., Wilhelm, S. M., and Steinberg, B. G., "Laboratory Corrosion Testing of Metals and Alloys in Environments Containing Hydrogen Sulfide," *Laboratory Corrosion Tests and Standards, ASTM STP 866*, G. S. Haynes, Ed., American Society for Testing and Materials, Philadelphia, 1985, pp. 245-259.
- [7] Kane, R. D., Wilhelm, S. M., and McIntyre, D. R., "Application of the Critical Pitting Temperature Test to the Evaluation of Duplex Stainless Steels," *Corrosion Testing and Evaluation, Silver Anniversary Volume, ASTM STP 1000*, R. Baboian, Ed., American Society for Testing and Materials, Philadelphia, 1990.
- [8] Kane, R. D. and Greer, J. B., "Embrittlement of High Strength High Alloy Tubular Materials in Sour Environments," *Journal of Petroleum Engineers*, Society of Petroleum Engineers, October 1977.
- [9] Wilhelm, S. M., "Effect of Elemental Sulfur on Stress Corrosion Cracking of Nickel Base Alloys in Deep Sour Gas Well Production," *Corrosion/88, Paper No. 77*, March 21-25, 1988.

## Improved SSR Test for Lot Acceptance Criterion

---

**REFERENCE:** Hibner, E. L., "Improved SSR Test for Lot Acceptance Criterion," *Slow Strain Rate Testing for the Evaluation of Environmentally Induced Cracking: Research and Engineering Applications*, ASTM STP 1210, R. D. Kane, Ed., American Society for Testing and Materials, Philadelphia, 1993, pp. 290–294.

**ABSTRACT:** For quite some time now, the Slow Strain Rate (SSR) test has been used in the Oil Patch as a Lot Acceptance Criterion. The most common pass/fail criteria for SSR testing is the ratio of Time to Failure (TTF), Percent Reduction of Area (%RA), or Percent Elongation (%El), or a combination thereof, measured in an environment relative to the same parameter in an inert environment (air or nitrogen). Specimens are typically examined for secondary cracking away from the main fracture surface. However, there are many innate problems associated with the SSR test that complicate its use as a lot acceptance criterion. The nature of these problems is discussed, along with corrective actions.

**KEYWORDS:** slow strain rate (SSR), test, time to failure, percent reduction of area, percent elongation, environments, strain rate, surface preparation, deaeration, machining, machine compliance, calibration

Historically in materials selection, corrosion has been a more or less add-on property with the primary consideration being given to strength and fabricability. This approach emphasized general composition and the ability to manufacture product shapes and forms. If corrosion was of real concern, it could be overcome by conservative, but costly, over-alloying. The chance of failure was usually small.

In the 1960s and 1970s, another factor, internal alloy structure control, began to emerge as a critical component for success. Thermomechanical processing history was precisely controlled in addition to general composition. Cost also began to play a major role as end users wanted to pay for only enough corrosion resistance to survive the application.

These different approaches to material selection and usage can be visualized with the aid of some simple figures. The historic, over-alloying situation is similar to a box (the alloy) on a step (the application) (see Fig. 1). It is very difficult for the box to fall from the step without some extreme outside interference.

The common situation of alloys which are pushed to their limits is more like a ball on a step (see Fig. 2). In this precarious situation, minor changes in either the ball or the support can cause it to fail. Under these critical conditions, the SSR test has been used in the Oil Patch on a go-no-go basis [*J*] for Corrosion Resistant Alloys (CRAs). As Murphy's Law (what can go wrong, will go wrong) governs the SSR test, it is very critical to make an intensive effort to provide the best SSR results possible.

This paper discusses what can go wrong, how it may adversely affect SSR test results, and describes how to improve the SSR test for Lot Acceptance Criterion.

---

<sup>1</sup> Senior metallurgist, Inco Alloys International, Inc., Huntington, WV 25720.

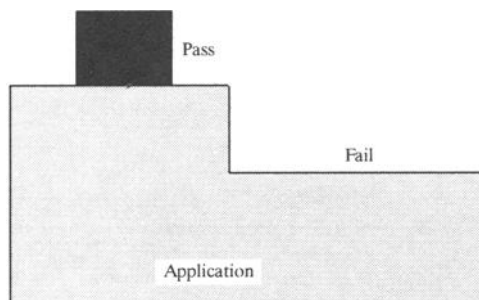


FIG. 1—Over-allying approach to material selection.

### Pass/Fail Criteria

In review, the most common pass/fail criteria for SSR testing is a ratio of Time to Failure, % Reduction of Area, or %Elongation, or a combination thereof, measured in a simulated oil patch environment relative to the same parameter in an inert environment (air or nitrogen). Passing is frequently defined by a ratio of 0.90 or greater, depending on the alloy and the environment. If the ratio is between 0.80 and 0.90, the specimen is examined under the Scanning Electron Microscope (SEM) for evidence of ductile or brittle fracture of the primary fracture surface. A ratio below 0.80 typically fails. All specimens are examined for secondary cracking in the gage length, away from the primary fracture. The absence of secondary cracking in specimens with acceptable ratios is indicative of good stress corrosion cracking (SCC) resistance and passes. The presence of secondary cracks fails. In most cases, one inert SSR test is conducted along with three environmental SSR tests for each acceptance lot. To account for data scatter, two inert SSR tests are sometimes conducted along with two environmental SSR tests. If all the environmental tests pass the TTF, %RA, or %EI ratios, or a combination thereof, (as required by specification) and exhibit no secondary cracking, the test lot of material passes and is released. Attention to details and the testing procedure improvements suggested in the following will help ensure the credibility of the SSR test as a lot acceptance criterion.

### NACE Test Procedure

The National Association of Corrosion Engineers (NACE) under its Technical Activities Committee, T-1F-9, is developing a standard "Slow Strain Rate Test Method for Screening

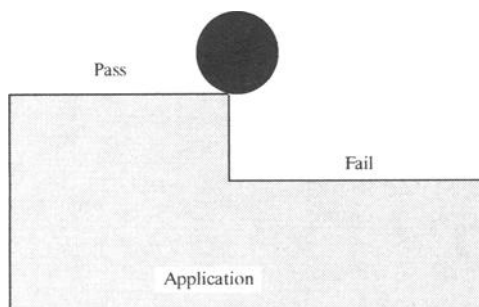


FIG. 2—Just enough corrosion resistance to survive an application.

Corrosion Resistant Alloys (CRAs) for Stress Corrosion Cracking in Sour Oil Field Service.” When completed, this document in combination with the recommendations made in the following discussion will provide a good basis for an SSR lot acceptance test.

### Testing Problems Associated with the SSR Test

In the development of a lot acceptance test, the first step should be to evaluate precision through an interlaboratory test program (round robin). Precision, by definition, is the closeness of agreement between randomly selected individual measurements or test results (see ASTM E 456, Terminology Relating to Quality and Statistics), or simply, repeatability within a laboratory and reproducibility between laboratories. Without an understanding of what the precision should be under the best conditions, it is possible to pass or fail material irrespective of its true condition. Bias, by definition, is a systematic error that contributes to the difference between a population mean of the measurements or test results and an accepted reference value (see ASTM E 456). Bias is probably not an issue because there is no reference value.

The only known, organized interlaboratory round robin test program on SSR testing is that currently being conducted by NACE Technical Activities Committee, T-1F-9. Alloy N08825 is being evaluated in sour oil field environments at varied temperatures and strain rates. S. M. Wilhelm [2], T-1F-9 Committee Chairman, stated that testing to date indicates that the participating laboratories are in general agreement as to pass or fail. Significant differences exist, however, between laboratories in actual values obtained for measured parameters. Interlaboratory reproducibility is good when tests are conducted on the same machine.

When the NACE round robin is completed, it should provide a good perspective on the precision of the SSR test as a lot acceptance criterion. Irrespective of that, here are some problems affecting precision that can be addressed:

Before beginning SSR testing for a lot acceptance criteria, data scatter of the inert (air or nitrogen) test should be examined to determine if one inert test is representative enough for determination of TTF ratios or if the average of two inert tests is required to determine the TTF ratio. This is affected by the alloy type and condition, for example cold-drawn, or aged corrosion resistant alloys may show different scatter in replicate inert environmental tensile tests.

A slow, constant extension rate is imposed on the SSR test specimen for the duration of the test. The SSR results are a function of the cross-head rate [3,4]. The effect of the extension rate should be evaluated over several orders of magnitude of extension rate. For Oil Patch applications of CRAs, the standard extension rate is  $4.0 \times 10^{-6} \text{ s}^{-1}$  [5,6]. To ensure an accurate cross-head speed, the extension rate is typically calibrated every 30 days, minimum.

A load train which is out of compliance can result in a dog-legged or twisted specimen as seen in Fig. 3. Mechanical testing machines and alignment devices used for SSR testing should be calibrated to ensure load train compliance to avoid torsional or bending loads on the specimen. Compliance calibration is usually done semiannually or when dog-legging or twisting of the test specimen is observed. Cortest Laboratories has recently developed an excellent procedure for compliance calibration [2]. A NACE Technical Activities Committee under T-1F is considering the development of a similar procedure.

Improper machining of the SSR test specimen can result in an invalid test. Either twisting of a specimen while being machined, or selection of a nonflat blank for machining can result in dog-legging of the specimen during the test. An example of a nonflat blank cut from a

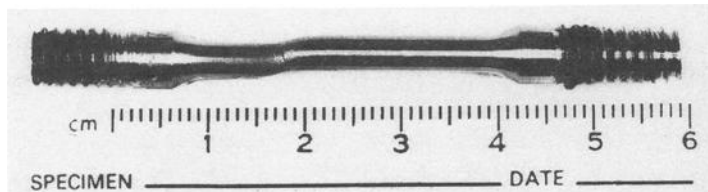


FIG. 3—A dog-legged SSR test specimen.

longitudinal strip of cold-drawn, as-drawn tubing which bowed due to longitudinal stress is illustrated in Fig. 4. Extreme care should be taken to avoid these problems.

Machining of a test specimen must be performed carefully so as to avoid overheating and unnecessary cold-working of the gage section. Wet grinding of the specimen would help accomplish this. The final two passes should remove a total of about 0.002 in. (0.05 mm) of metal, maximum [6].

Specimen surface finish during testing has a major influence on the SSR test results. Polishing of the specimen after machining results in less susceptibility to SCC [7]. NACE [6] recommends the test specimen be finished to a surface roughness of 32  $\mu\text{in.}$  (80  $\mu\text{m}$ ) or finer. Personal experience over many years of testing has shown that a final surface finish of 500 to 1200 grit from dry  $\text{Al}_2\text{O}_3$  paper is sufficient for optimum SSR test results. Choi was successful using an 800 grit SiC finish [7]. No beneficial effect of diamond polishing the specimen gage as opposed to using  $\text{Al}_2\text{O}_3$  or SiC paper has been observed or documented in the current literature search. Further, three lots of alloy G-3 (UNS N06985) were SSR tested in 25% NaCl + 100 psig  $\text{H}_2\text{S}$  + 0.5% acetic acid at 300°F with two surface finishes, first polished to a 500 grit surface finish with  $\text{Al}_2\text{O}_3$  paper and second polished to a 1 micron surface finish with diamond paste. No effect of surface finish on SSR test results was observed.

Experience has shown that a deep scratch on one side of the specimen gage, caused by either a jump of the cutting tool during machining or by point micrometers scratching the gage area, can also cause the specimen to dog-leg during the test. A test specimen of alloy G-3 (UNS N06985) was observed to have a scratch on the polished gage, caused by point calipers. The scratch was observable with the naked eye and went approximately one third of the way around the gage diameter. Location of the scratch was noted and, after testing in 25% NaCl + 100 psig  $\text{H}_2\text{S}$  + 0.5% acetic acid at 300°F, the specimen was observed to dog-leg at the location of the scratch. This phenomenon occurred in three or four tests in a series of 219 environmental SSR tests. This phenomenon has also been observed by Wilhelm and Currie [8]. To avoid this problem, the machined test specimen should be examined under 20 to 30 $\times$  magnification before polishing. If deep gouges exist, another specimen should be prepared. After polishing and measuring the gage, the test specimen should again be examined under 20 to 30 $\times$  magnification for scratches. If scratches are too deep to remove by polishing, another test specimen should be prepared. Measuring the

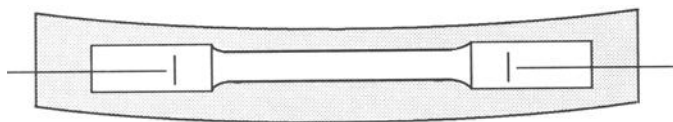


FIG. 4—SSR test specimen being machined from a nonflat section of tube wall, bowed due to longitudinal stress.

specimen gage before testing with a straight edge caliper instead of with point micrometers will help avoid scratching the final polished surface of the test specimen.

### Conclusion

The NACE "Slow Strain Rate Test Method for Screening Corrosion Resistant Alloys (CRAs) for Stress Corrosion Cracking in Sour Oil Field Service" in combination with the recommendations made in the discussion will provide a good basis for a SSR lot acceptance test.

The recommendations from this paper are:

- (1) Evaluate data scatter of the inert test to determine the number of inert tests required for determination of TTF ratios.
- (2) The effect of the extension rate on SCC resistance should be evaluated over several orders of magnitude.
- (3) The extension rate should be calibrated every 30 days, minimum.
- (4) Compliance calibration of the load train should be done semiannually or when dog-legging or twisting of the test specimen is observed.
- (5) Avoid twisting, gouges, unnecessary cold work, or overheating of a test specimen during machining.
- (6) The final surface finish of the test specimen should be 500 grit or finer.
- (7) Test specimens should be examined under 20 to 30 $\times$  magnification for gouges after polishing. Gouged specimens should not be tested.
- (8) Measure the specimen gage before testing with a straight edge caliper instead of with point micrometers to help avoid scratching the final polished surface of the test specimen.

### References

- [1] Kim, C. D. and Wilde, B. E., "A Review of the Constant Strain-Rate Stress Corrosion Cracking Test," *Stress Corrosion Cracking: The Slow Strain-Rate Technique*, ASTM STP 665, G. M. Ugiasky and J. H. Payer, Eds., American Society for Testing and Materials, Philadelphia, 1979, p. 97.
- [2] Wilhelm, S. M., Cortest Laboratories, 11115 Mills Rd., Suite 102, Cypress, TX 77429, Private communication.
- [3] Solomon, H. D., Povich, M. J., and Devine, T. M., "Slow Strain-Rate Testing in High Temperature Waters," *Stress Corrosion Cracking: The Slow Strain Rate Technique*, ASTM STP 665, G. M. Ugiasky and J. H. Payer, Eds., American Society for Testing and Materials, Philadelphia, 1979.
- [4] Beavers, J. A. and Koch, G. H., "Limitations of the Slow Strain Rate Test for Stress Corrosion Cracking Testing," NACE CORROSION/91 Meeting, March 11-15, 1991, Cincinnati, OH, Paper No. 477.
- [5] Vaughn, G. A. and Greer, J. B., "High-Strength Nickel Alloy Tubulars for Deep, Sour Gas Well Applications," 1980 SPE-AIME Annual Meeting, Paper No. 9240 (Richardson, TX: Society of Petroleum Engineers and New York, NY: American Institute of Mining, Metallurgy and Petroleum Engineers, 1980).
- [6] National Association of Corrosion Engineers, T-1F-9, Proposed NACE Standard Test Method, "Slow Strain Rate Test Method for Screening Corrosion Resistant Alloys (CRAs) for Stress Corrosion Cracking in Sour Oil Field Service."
- [7] Choi, H. J., "The Effect of Elemental Sulfur and Surface Condition on Stress Corrosion Cracking of High Nickel Alloys Under Hot Sour Environments," NACE CORROSION/92 Meeting, April 27-May 1, 1992, Nashville, TN, Paper No. 59.
- [8] Wilhelm, S. M. and Currie, D. M., "Selection of High-Alloy Tubulars for the 823 Field (Mobile Bay)," Society of Petroleum Engineers, Production Operations Symposium, April 7-9, 1991, Oklahoma City, OK, Paper No. SPE 21738, pp. 943-957.

## Author Index

### A-B

Ahluwalia, H. S., 225  
 Alter, D., 83  
 Baumert, K. L., 173  
 Beavers, J. A., 22

### C-D

Currie, D. M., 263  
 Daniels, R. D., 149  
 Dewes, P., 83  
 Dietzel, W., 134

### G-H

Garzarolli, F., 83  
 Hahn, R., 83  
 Hays, R. A., 202  
 Hibner, E. L., 290

### I-J

Ikeda, A., 240  
 Indig, M. E., 51  
 Juers, R. L., 123

### K

Kane, R. D., 1, 40, 181  
 Klein, P. A., 202  
 Koch, G. H., 22  
 Krupowicz, J. J., 193

### M

Meyn, D. A., 158  
 Miglin, B. P., 65  
 Miglin, M. T., 65  
 Moran, P. J., 202

### N

Natishan, M. E., 123  
 Nelson, J. L., 83  
 Nguyen, D. T., 149  
 Nichols, D. E., 149

### O-P

Okamoto, H., 240  
 Pao, P. S., 158  
 Parkins, R. N., 7

### S-T

Schwalbe, K-H., 134  
 Scully, J. R., 202  
 Toribio, J., 105

### U-V

Ueda, M., 240  
 Vassilaros, M. G., 123  
 Vasudevan, A. K., 123

### W

Watkins, W. R. Jr., 173  
 Wilhelm, S. M., 40, 181, 263  
 Wu, D., 181

# Subject Index

## A

- AISI 4340 high-strength steel, SSR testing, 149
- Alkyl amines, stress cracking of carbon steel, 173
- Aluminum alloys, embrittlement in mercury environments, 181
- Amines, stress cracking of carbon steel, 173
- Ammonium chloride, in residues from breech chambers, 149
- Ammonium nitrate, in residues from breech chambers, 149
- Anodic polarization, effect on SSR testing, 240
- ASTM Committee G-1.06.05, 40
- ASTM standards
  - E 456, 292
  - E 647, 134

## B

- Boiling water reactors
  - deformability of stainless steels and nickel-base alloys, 83
  - SSR test applications, 65
  - SSR test for IGSCC, 51
- Breech chamber residues, X-ray diffraction analyses, 149
- BWRs (*see* Boiling water reactors)

## C

- Calibration
  - extension rate, 290
  - load train, 290
- Carbon steels
  - amine cracking, 173
  - polyamine cracking, 173
  - SSR test limitations, 22
- Cathodic protection, effects on Ni-Cu alloy K-500, 123
- Caustic cracking, of stainless steel, 173

- Chemical process industry, SSR test methods, 22
- Chromium-nickel-molybdenum alloys, in hot sour gas production, SSR testing, 240
- Compliance calibration, of load train, 290
- Constant extension rate test, 65
- Copper alloys, SSR test limitations, 22
- Corrosion resistant alloys
  - in hot sour gas production, 240
  - SSR testing in hydrogen sulfide environments, 225
- Crack tip opening displacement, 134
- CRA's (*see* Corrosion resistant alloys)
- Critical pitting temperature, nickel-base alloys, 263
- Cyclic loading, 7

## E

- Elastic-plastic fracture mechanics, material susceptibility to SSC, 134
- Electrical insulation, effects on SSR testing, 240
- Electrochemical polarization, effects on SSR testing, 240
- Electrochemical potential
  - controlled, SSR testing of high-strength steel, 149
  - hydrogen addition effects in BWRs, 51
  - inadequate measurement, 22
- Electrode potential, effects on SSR testing results, 225
- Embrittlement, aluminum and stainless steel in mercury environments, 181
- Extension rate, calibration, 290

## G

- Global strain rate, 105

**H**

- Heat effects, on LME of austenitic alloys, 193
- High-strength steels
  - SSR testing at controlled electrochemical potentials, 149
  - weldments, hydrogen embrittlement, 202
- Hydrogen
  - effects on electrochemical potential in BWRs, 51
  - water chemistry in BWRs, 51
- Hydrogen assisted cracking, 105
- Hydrogen embrittlement
  - cathodic protection-related, 123
  - high-strength steel weldment, 202
  - SSR testing, 40
- Hydrogen sulfide environments, SSR testing of nickel-base CRAs, 225

**I**

- IGSCC (*see* Intergranular stress corrosion cracking)
- In-pile tests
  - nickel-base alloys, 83
  - stainless steels, 83
- Insulation, electrical, effects on SSR testing, 240
- Intergranular stress corrosion cracking
  - in boiling water reactors, 51
  - nickel-base alloys, heat treatment effects, 83
- Interrupted SSR testing, 7
- Irradiation Assisted Stress Corrosion Cracking, 83
- Irradiation effects, on in-pile behavior of stainless steels, 83
- ISO 7539 Part 7: Method for SSR Testing, 40

**J**

- J*-integral test
  - Ni-Cu alloy K-500, 123
  - precracked specimens with rising displacement, 134

**L**

- Light water reactors
  - deformability of stainless steels and nickel-base alloys, 83
  - SSR testing, 65

- Linear elastic fracture mechanics, material susceptibility to SCC, 134
- Liquid metal attack, aluminum and stainless steel in mercury environments, 181
- Liquid metal embrittlement
  - aluminum and stainless steel in mercury environments, 181
  - SSR testing standardization activities, 40
  - stainless steels and nickel alloys, 193
- LMA (*see* Liquid metal attack)
- LME (*see* Liquid metal embrittlement)
- Load train, calibration, 290
- Localized corrosion, nickel-base alloys, 263
- Local strain rate, 105
- Lot acceptance criterion, 290

**M**

- Machining, of specimens, 290
- Mercury, LME and LMA in aluminum alloys and stainless steel, 181
- Mercury cracking
  - nickel alloys, 193
  - stainless steel, 173, 193
- Monotonic SSR testing, 7

**N**

- NACE Task Group T-1F-9, 40, 290
- Natural gas production, localized corrosion and SSC of nickel-base alloys, 263
- Nickel-base alloys
  - corrosion resistant, SSR testing, 225
  - deformability in light water reactors, 83
  - liquid metal embrittlement, 193
  - localized corrosion and SSC, 263
  - reactor core, 65
  - SSR test limitations, 22
- Nickel-copper alloys, K-500, effects of SSR testing and cathodic protection, 123
- Notched specimens, 105
- Nuclear power industry
  - boiling water reactors, 65
  - BWRs, SSR testing, 51
  - light water reactors, 65
  - pressurized water reactors, 65
  - SSR test applications, 65

## O

Oxygen levels, for SSC prevention, 65

## P

Percent elongation, in SSR testing, 290  
 Percent reduction of area, in SSR testing, 290  
 Petroleum production, localized corrosion and SCC of nickel-base alloys, 263  
 Pitting, nickel-base alloys, 263  
 Polyamines, cracking of stainless and carbon steels, 173  
 Potassium chloride, in residues from breech chambers, 149  
 Precracked specimens  
   SSC behavior, rising displacement test, 134  
   in SSR testing, 105  
   titanium alloys, 158  
 Pressure vessel steels, SSR tests, 65  
 Pressure water reactors, deformability of stainless steels and nickel-base alloys, 83  
 Pressurized water reactors, SSR testing, 65

## Q

Quality assurance, nickel-base corrosion resistant alloys, 225

## R

Rising displacement tests, 134

## S

Salt water, SSR testing of precracked titanium alloys, 158  
 Slow strain rate testing  
   aluminum and stainless steel embrittlement in mercury environments, 181  
   anomalous behavior survey, 22  
   for cracking conditions in existing equipment, 173  
   for CRAs in host sour gas production, 240  
   development, review, 7  
   effects of  $H_2S$ ,  $Cl^-$ ,  $CO_2$ , 240

for existing materials qualification, 173  
 high-strength steel at controlled electrochemical potentials, 149  
 hydrogen embrittlement of steel weldments, 202  
 for IGSCC in BWRs, 51  
 interrupted, 7  
 in light water reactor cores, 83  
 limitations, 22  
 LME of stainless steels and nickel alloys, 193  
 lot acceptance criterion, 290  
 monotonic, 7  
 nickel-base alloys in gas production applications, 263  
 Ni-Cu alloy K-500, 123  
 notched specimens for, 105  
 precracked specimens for, 105  
 precracked titanium alloys, 158  
 standardization activities, 40  
 survey, 22  
 Sour gas production  
   Cr-Ni-Mo alloy SSR testing, 240  
   NACE T-1F-9, 40, 290  
   nickel-base alloys, localized corrosion and SCC, 263  
 Specimens  
   machining, 290  
   notched specimens, 105  
   precracked specimens, 105, 134  
   surface finish, 290  
   tapered, 7  
 SSR testing (*see* Slow strain rate testing)  
 Stainless steel  
   alloys, embrittlement in mercury environments, 181  
   austenitic  
     deformability in light water reactors, 83  
     IGSCC, SSR testing, 51  
   deformability in light water reactors, 83  
   in-pile behavior, 83  
   liquid metal embrittlement, 193  
   mercury cracking, 173  
   polyamine cracking, 173  
   SSR testing, 65  
   SSR test limitations, 22  
 Standardization, ASTM Committee G-1.06.05 and NACE Task Group T-1F-9, 40, 290  
 Steam generators  
   SSR testing, 65  
   thin-wall tubing, 65

## Steels

- AISI 4340 high-strength SSR testing, 149
  - 5Ni-Cr-Mo high-strength weldments, 202
  - stainless (*see* Stainless steel)
- Storage tanks, carbon steel, amine cracking, 173
- Strain rate
- appropriate, 7
  - CRA SCC susceptibility in hot sour gas environments, 240
  - effects on SSR testing results, 225, 240
  - global, 105
  - inadequate measurement, 22
  - local, 105
  - slow, 22
- Stress corrosion cracking
- accelerated test procedure, 134
  - amine-related, 173
  - in BWRs, SSR testing, 51
  - caustic solution-related, 173
  - chloride-related, 173
  - CRAs in hot sour gas production, 240
  - CRAs in hydrogen sulfide environments, 225
  - irradiation-assisted, 83
  - limitation of SSR testing, 22
  - LME of stainless steels and nickel alloys, 193
  - mercury-related, 173
  - nickel-base alloys in gas production environments, 263
  - notched specimens for SSR testing, 105
  - in reactor cooler environments, 65
  - rising displacement test, 134
  - standardization activities, 40
  - strain rate determination, 7
  - titanium alloys in salt water and inert environments, 158

## Surface finish

- effects on SSR testing results, 225
- of specimens, 290

**T**

- Tapered specimen tests, 7
- Temperature, effects on SSR testing, 240
- Tensile bars, for testing nickel-base alloys, 65
- Three-point-bend loading, for material resistance to cracking, 65
- Threshold stresses, determination, 7
- Time to failure, in SSR testing, 290
- Titanium alloys
  - SSR testing in salt water and inert environments, 158
  - SSR test limitations, 22
- Tubular products
  - CRAs in hydrogen sulfide environments, 225
  - high-nicked CRAs, SSR testing, 240

**W**

- Water environments, in BWRs, electrochemical potential effects, 51
- Welds, high-strength steel, SSR testing, 202

**X**

- X-ray diffraction, residues from breech chambers, 149

**Z**

- Zirconium alloys, SSR test limitations, 22

ISBN 0-8031-1870-8